UNIVERSITY OF ADELAIDE LIBRARY
23.1.90

Nature and Formation of Supergene Manganese Deposits on Groote Eylandt, N.T., Australia

Dipl.-Min. Bernhard Pracejus
Department of Geology and Geophysics
The University of Adelaide
P.O.Box 498, Adelaide
Australia 5001



September 1989

A thesis submitted to the University of Adelaide in the fulfilment of the requirements for the degree of Doctor of Philosophy

DEN Menschen will ich wohl, allein betrübt,
Daß sie mißbrauchen was man Gutes gibt,
Versteck' ich Gold an schmaler Klüfte Wand,
Als Staub zerstreu' ich's breit in Fluß und Sand;
Und wenn sie's dann mit Müh und Fleiß erhascht,
Wird es sogleich vergeudet und vernascht,
Mit vollen Händen wird es ausgestreut
Und niemand häuft den Schatz für künft'ge Zeit ...

"Gnome", Johann Wolfgang von Goethe (1830)

Contents

Page

Abstract ..... IX.

Statement ..... X.

Acknowledgments ..... XI.

1. General Introduction

1.1 Aims of the Project 1
1.2 Geologic Setting 2
1.3 Previous Work 5
1.4 Terminology of Primary and Secondary Materials 7
1.5 Methods 7

2. Stratigraphy

2.1 Introduction 9
2.2 Sampling Locations 10
2.3 Distribution of Ores and Rocks 12
2.3.1 F1-Quarry 13
2.3.2 F2-Quarry 14
2.3.3 F3-Quarry (orebody) 15
2.3.4 F3-Quarry (laterite) 17
2.3.5 Costean 138 18
2.3.6 A-South-Quarry 20
2.3.7 G-Quarry 21
2.3.8 G-South-Quarry 23
2.4 Discussion 24

3. Petrology and Mineralogy

3.1 Introduction 26
3.2 Description of Samples 27
3.2.1 Uncemented ("soft") Oolite/Pisolite 27
3.2.2 Cemented Mangcrete (oolitic/pisolitic) 29
3.2.3 Fe-Oolite/Pisolite 30
3.2.4 Massive Mangcrete 32
3.2.5 Massive Ferricrete 33
3.2.6 Hardground 33
3.2.7 Envelope Grain 34
3.2.8 Laminar Mangcrete 35
3.2.9 Manganese Cave Pearl 36
3.2.10 Spherulite (manganiferous) 37
3.2.11 Fe-Pipe Wall 37
3.2.12 Radial Pyrolusite 38
3.2.13 Siliceous Ore 39
3.2.14 Concretions (surface) 40
3.2.15 Digital Concretion (below ore) 41
3.2.16 Laterite (ferruginous/manganiferous) 41
3.2.17 Chocolate Ore 43
3.2.18 Clay 43
3.2.19 Soil 43
3.2.20 Sand 44
3.2.21 Conglomerate 44
3.2.22 Quartzite/Sandstone 44

Page

3.3 Mineralogy....48
3.3.1 X-Ray Diffraction (XRD)....48
3.3.2 Fourier Transform Infrared Spectrometry (FTIR)....55
3.4 Discussion....58

4. Geochemistry

4.1 Introduction....61
4.2 Chemical Characterization of Ores and Rocks....62
4.2.1 Inter-Element Correlations....62
4.2.2 Composition of Ores and Rocks....64
4.2.2.1 Major and Minor Elements....65
4.2.2.2 Trace Elements....68
4.2.2.3 Rare Earth Elements....73
4.3 Elements in the Vertical Sequence....77
4.3.1 Single Element Distributions....78
4.3.2 Shale-normalized Rare Earth Patterns....81
4.3 Discussion....83
4.3.1 Relationships between Trace Elements and REEs in Different Materials....83
4.3.2 Stratigraphy-controlled Element Variations....85
4.3.3 Comparison of REE Patterns from Groote Eylandt and Other Mn Oxide Deposits....86

5. Application and Interpretation of Normative Mineralogy

5.1 Introduction....90
5.2 Method of Norm Calculation....91
5.3 Norm Minerals in the Vertical Geological Profile....103
5.3.1 Costean 138....103
5.3.2 F3-Quarry....105
5.3.3 G- and G-South-Quarry....105
5.3.4 D-Quarry Laterite....110
5.4 Characterization of Ores and Rocks....112
5.4.1 Normative Composition of Ores....112
5.4.2 Relationships between Ore Types....115
5.4.3 Major and Trace Element Composition of Ore Minerals....118
5.4.4 Normative Composition of Associated Rocks....120
5.4.5 Relationships between Rock Types....122
5.4.6 Major and Trace Element Composition of Gangue Minerals....124
5.5 Normative Ore Minerals and Microbiological Leaching....125
5.6 Normative Ore Minerals and Battery-activity Tests....128
5.7 Discussion....129

6. Hydrochemistry

6.1 Introduction....134
6.2 Environmental Influences on Dissolved Species....136
6.2.1 Rainfall, Tides, Chlorine and pH....136
6.2.2 Temperature, Oxygen Saturation....140
6.2.3 Organic Complexes, Phosphoru....141
6.3 Characterization of Water Types....141
6.3.1 Mine Water....141
6.3.2 River Water (Angurugu River)....144
6.3.2.1 pH, Cl, Oxygen Saturation, P and C....144
6.3.2.2 Mn, Fe, Si and Al....146

Page

6.3.2.3 Rare Earth Elements ... 149
6.3.2.4 Further Stream Load and Tidal Interaction ... 150
6.3.2.5 Diurnal Fluctuations ... 151
6.3.3 Coastal Seawater ... 153
6.3.3.1 General Composition Pattern ... 153
6.3.3.2 Rare Earth Elements ... 155
6.4 Discussion ... 156

7. Experimental Work

7.1 Introduction ... 159
7.2 Design of Experiments ... 160
7.3 Results ... 162
7.3.1 Fresh Water Experiments ... 162
7.3.1.1 Electro-Chemical Data ... 162
7.3.1.2 Hydrochemistry ... 164
7.3.1.3 Mineralogical Investigations ... 164
7.3.1.3.1 FTIR-Characterization ... 165
7.3.1.3.2 XRD-Characterization ... 167
7.3.2 Salt Water Experiment, General Observations ... 168
7.4 Discussion ... 169

8. Origin of Supergene Manganese Oxide Deposits

8.1 Introduction ... 172
8.2 Evidence of Supergene Activity ... 173
8.3 Mobilization Processes ... 176
8.3.1 Dissolution of Quartz, Kaolinite, and Gibbsite ... 176
8.3.1.1 Thermodynamics of Si-Al-H_2O Systems ... 177
8.3.1.2 Complexation of Quartz by Fe and Mn ... 180
8.3.1.3 Organically Induced Kaolinite Dissolution ... 180
8.3.2 Dissolution of Iron Oxyhydroxides ... 181
8.3.2.1 Thermodynamics of the Fe-H_2O System ... 181
8.3.2.2 Dependency of Fe Minerals upon Kaolinite Stability ... 183
8.3.2.3 Biological Reduction of Fe Phases ... 184
8.3.3 Dissolution of Manganese Oxides ... 184
8.3.3.1 Thermodynamics of the Mn-H_2O System ... 185
8.3.3.2 Redox Reactions Between Iron Phases and Manganese Oxides ... 187
8.3.3.3 Dependency of Mn Minerals upon Kaolinite Stability ... 190
8.3.3.4 Pedogenic Conditions ... 190
8.3.3.5 Biological Activities ... 191
8.3.3.6 Electrolytic Weathering ... 193
8.3.3.7 Pressure Solution ... 193
8.3.3.8 Disproportionation and Protonation Reactions ... 194
8.4 Transport of Dissolved Manganese ... 195
8.5 Fixation Processes ... 198
8.5.1 Precipitation of Si-Al Minerals ... 199
8.5.2 Precipitation of Fe Minerals ... 200
8.5.2.1 Precipitation of Fe During Redox Reaction with Mn ... 200
8.5.2.2 Influence of Foreign Ions on Initial Fe Precipitates ... 201
8.5.2.3 Further Oxidation of Goethite ... 202
8.5.2.4 Microbial Influences on Fe Precipitation ... 202
8.5.2.5 Precipitation of Iron Phases in Seawater ... 203
8.5.3 Precipitation of Mn Minerals ... 203
8.5.3.1 Pedogenic Oxidation of Mn ... 203
8.5.3.2 Microbial Mn Oxidation ... 204

Page

8.5.3.3 Mn Precipitation During Disproportionation Reactions 205
8.5.3.4 Precipitate Dependency upon Mineralogy of Substrate Rocks 205
8.5.3.5 Grainsize Variation of Substrate 206
8.5.3.6 Mn Precipitation in Seawater 207
8.6 Discussion 207

9. The Mangcrete Model

9.1 Introduction 210
9.2 Cyclic Mobility of Supergene Ores and Rocks 210
9.3 The Mangcrete Profile 213
9.4 Review of Supergene Influenced Mn Deposits 216
9.4.1 Moanda, Gabon 217
9.4.2 Janggun Mine, South Korea 218
9.4.3 Nikopol/Chiatura, USSR 219
9.4.4 Úrkút Basin, Hungary 219
9.4.5 General Comparison of Supergene Products in Different Areas 220
9.5 Discussion 221

10. Résumé and Conclusions 222

References 225

Appendix I. (methods)*

1 Rock Samples
1.1 Sampling Technique ..... A I. - 1
1.2 Equipment and Sample Preparation ..... A I. - 1
1.3 Rock Analyses ..... A I. - 2
1.3.1 X-Ray Fluorescence (XRF) ..... A I. - 2
1.3.1.1 Analytical Background ..... A I. - 2
1.3.1.2 Equipment and Method ..... A I. - 2
1.3.1.3 Sample Preparation for Fusion Beads ..... A I. - 2
1.3.1.4 Sample Preparation for Pressed Powder Buttons ..... A I. - 2
1.3.2 X-Ray Diffraction (XRD) ..... A I. - 3
1.3.2.1 Analytical Background ..... A I. - 3
1.3.2.2 Equipment and Sample Preparation ..... A I. - 3
1.3.3 Fourier Transform Infrared Spectroscopy (FTIR) ..... A I. - 3
1.3.3.1 Analytical Background ..... A I. - 3
1.3.3.2 Equipment and Method ..... A I. - 4
1.3.3.3 Sample Preparation ..... A I. - 4
1.3.3.4 Further Computerized Handling ..... A I. - 4
1.3.4 Inductive Coupled Plasma Spectroscopy (ICP) ..... A I. - 5
1.3.4.1 Analytical Background ..... A I. - 5
1.3.4.2 Equipment and Method ..... A I. - 5
1.3.4.3 Calibration Standards ..... A I. - 6
1.3.4.4 Calibration Curves ..... A I. - 7
1.3.4.5 Instrument Setting ..... A I. - 8
1.3.4.6 Sample Preparation ..... A I. - 8
1.3.5 Atomic Absorption (AA) ..... A I. - 9
1.3.5.1 Analytical Background ..... A I. - 9
1.3.5.2 Equipment and Method ..... A I. - 9
1.3.5.3 Sample Preparation ..... A I. - 9

* The Appendix number corresponds to the respective chapter.

Page

1.3.6 K/Ar-Age Determinations ..... A I. - 9
1.3.6.1 Analytical Background ..... A I. - 9
1.3.6.2 Equipment, Sample Preparation, and Method ..... A I. - 10
2 Water Samples
2.1 Sampling ..... A I. - 10
2.1.1 Equipment ..... A I. - 10
2.1.2 Sampling Procedures ..... A I. - 10
2.2 Field Tests ..... A I. - 11
2.2.1 Temperature ..... A I. - 11
2.2.2 pH ..... A I. - 11
2.2.3 Flux Rate of Springs and Seepages ..... A I. - 11
2.2.4 Total Manganese ..... A I. - 11
2.2.4.1 Analytical Background ..... A I. - 11
2.2.4.2 Method and Equipment ..... A I. - 12
2.2.5 Total Iron ..... A I. - 12
2.2.5.1 Analytical Background ..... A I. - 12
2.2.5.2 Method and Equipment ..... A I. - 12
2.2.6 Oxygen Saturation ..... A I. - 13
2.2.6.1 Analytical Background ..... A I. - 13
2.2.6.2 Method and Equipment ..... A I. - 13
2.3 Laboratory Analyses ..... A I. - 13
2.3.1 Chlorine ..... A I. - 13
2.3.2 Total Organic Carbon (TOC) ..... A I. - 14
2.3.2.1 Application ..... A I. - 14
2.3.2.2 Equipment and Method ..... A I. - 14
2.3.2.3 Procedure ..... A I. - 14
2.3.3 Bulk Chemical Analysis by ICP ..... A I. - 15
3 Experimental Work
3.1 Investigations on Redox Reaction ..... A I. - 15
3.1.1 Equipment ..... A I. - 15
3.1.2 Test Vessel Specifications ..... A I. - 15
3.2 Biological Leaching of Mn-oxides ..... A I. - 16
3.3 Battery-activity Tests ..... A I. - 16

Appendix II. (Stratigraphy)

II.1 Sample Localities, Sampling Position in Vertical Section; Grainsize ..... A II.1, 1-3

Appendix III. (Petrology and Mineralogy)

III.1 Ore and Rock Types ..... A III.1, 1-3

Appendix IV. (Geochemistry)

IV.1 XRF/AA Major and Minor Element Analyses ..... A IV.1, 1-12
IV.2 ICP Trace Element Analyses of Ores and Rocks ..... A IV.2, 1-12
IV.3 XRF Trace Element Analyses of Ores and Rocks ..... A IV.3, 1-1
IV.4 INAA Analyses of Selected Ore Samples ..... A IV.4, 1-1
IV.5 Element Correlation Matrix for Ore and Rock Samples ..... A IV.5, 1-3

Page

Appendix V. (Normative Mineralogy)

V.1 Mineral Normalization Results from Ores and Rocks....A V.1, 1-12
V.2 Microbiological Leaching of Mn Ores from Groote Eylandt....A V.2, 1-2
V.3 Battery-activity Data and Mineral Norm of Samples....A V.3, 1-3

Appendix VI. (Hydrochemistry)

VI.1 Sampling Locations....A VI.1, 1-1
VI.2 Field Test Data....A VI.2, 1-2
VI.3 Chemical Analyses of Water Samples....A VI.3, 1-8
VI.4 Rainfall Data....A VI.4, 1-1
VI.5 Correlation Matrix for Water Analyses....A VI.5, 1-2

Appendix VII. (Experimental Work)

VII.1 pH and mV Data....A VII.1, 1-2
VII.2 Hydrochemical Analyses of Experiments....A VII.2, 1-1
VII.3 Geochemical Analyses of Solids from Experiments....A VII.3, 1-1

Abstract

During three field sessions in 1985 and 1986, ore, rock, and water samples were collected from the manganese oxide deposit on Groote Eylandt in the Northern Territory of Australia. Detailed geological sampling of open mine cuts allowed an exact survey of the stratigraphy of the respective sections and a determination of relationships between ore and rock units. Additionally, water samples were taken from mine seepages, rivers, and the sea. Until recently, very limited data on secondary manganese deposits existed, and the available studies illustrated only single aspects of such residual ores. Thus, the mineralogical/petrological examination of the solids and the geochemical analysis of both solids and waters provides the basis for a better understanding of the formation conditions for supergene materials dominating the Groote Eylandt deposit. An improved knowledge about upgrading of low-grade manganese ores is vital for mine management and for exploration projects in target areas.

The ores generally indicate that todorokite and cryptomelane occur more commonly in higher parts of the stratigraphic profile, that pyrolusite dominates at the base, and that cryptomelane is often the latest in the sequence of supergene minerals. The broad stratification is also reflected by many trace elements depicting higher concentrations near the top of the orebody. A normalization technique developed to assist in the mineralogical quantification of samples demonstrates that elements with atomic radii >1Å are mainly incorporated in pyrolusite. Elements with radii <1Å occur in cryptomelane and todorokite. The same method also shows that supergene horizons within the ore can be traced laterally and that the formation of these units is generally independent of the protore.

The study of water samples reveals that at present, manganese oxides are being dissolved, transported, and precipitated by supergene processes. Therefore, the deposit is altered constantly. The availability of water and Fe^{2+} is the main factor for the reduction of Mn^{4+} at Groote Eylandt. Evidence for the importance of this process was detected in the field where goethite and/or kaolinite commonly replace manganese oxides. The redox reaction was duplicated successfully in experiments. Seasonal geochemical variations result in alteration cycles mobilizing or precipitating the respective ore and gangue minerals. A comparison with other supergene influenced Mn deposits demonstrates similar secondary products and thus, supergene alteration processes described for Groote Eylandt are generally applicable for comparable ores.

Statement

To the best of the writer's knowledge, and except where referenced, this thesis contains no copy or paraphrase of previously published material nor any material that has been accepted for the award of any other degree or diploma in any university.

September 1989, Bernhard Pracejus

Acknowledgements

This thesis greatly benefitted from the help and guidance of numerous people and institutions. I therefore, wish to express my appreciation and thankfulness to all those who contributed to this study in one way or the other. Thank you to:

my dear family for tolerating a massive disruption of our daily life and for moral support;

Prof. L.A. Frakes and *Mr. B.R. Bolton* for their friendly advice and supervision (Department of Geology and Geophysics, The University of Adelaide (UA));

Dr. M. Abbott (Flinders University, Adelaide; ICP), *Dr. P. Hannaker* (Melbourne University; ICP), *Dr. B. Hart* and *Mr. M. Jones* (Chisholm Institute of Technology, Melbourne; TOC), *Dr. J. Madgwick* and *Mrs. R. Varga* (University of New South Wales, Sydney; Microbiological Leaching), *Dr. A. Giblin* (CSIRO, Sydney; borehole water sampling device), *Mr. T. Ryan* (La Trobe University, Melbourne; battery cell), for scientific co-operation and advice;

staff members of the department (UA) for technical assistance; in particular: *Dr. K. Turnbull* and *Mr. P. McDuie* (chemistry), *Mr. J. Stanley* and *Mrs. C. Badcock* (XRD, XRF), *Mr. W. Mussared* and *Mr. G. Trevelyan* (sectioning), *Mr. J. Willoughby* (computing), *Mr. R. Barrett* and *Mr. E. Bleys* (photography);

reviewers for critically reading manuscripts contributing to this study (in alphabetical order): *Prof. H. de Baar* (Nederlands Instituut voor Onderzoek der Zee), *Dr. R. Burns* (Massachusetts Institute of Technology); *Dr. E. De Carlo* (University of Hawaii), *Dr. G. Glasby* (New Zealand Oceanographic Institute), *Prof. R. Giovanoli* (ETH Zürich), *Dr. J. Hein* (U.S. Geological Survey, Menlo Park), *Dr. A. Kleyenstüber* (Mintek, Republic of South Africa), *Prof. D. Nahon* (Université d'Aix-Marseille);

staff members of B.H.P.Ltd.Co. and Groote Eylandt Mining Company (GEMCO) for practical help and discussion; in particular: *Dr. J. Ostwald* (Central Research Laboratories Canberra, B.H.P.), *Mr. G. Alcott* and *Mr. H. Berents* (GEMCO);

institutions for providing financial assistence: B.H.P.Ltd.Co. and GEMCO (scholarship, travel allowance, field accommodation), IGCP-Project 226 (UNESCO; travel allowance), Australian IGCP Committee Grant-in-Aid 1988 (conference allowance), Department of Geology and Geophysics (UA; travel allowance);

and, last but not least, to my dear wife *Ramona* for typing (too) many data and for preparing a large reference collection.

UNIVERSITY OF ADELAIDE LIBRARY

1. General Introduction

1.1 Aims of the Project

The present study examines the giant sedimentary manganese oxide deposit of Groote Eylandt in the Northern Territory of Australia, to determine the geochemical environment which results in the mobilization of ores and rocks, and which leads to the reprecipitation of extensive secondary Mn oxide units (Fig. 1.1). Until recently, very little was known about the type and strength of individual mechanisms involved in the redistribution of supergene manganese ores. Thus, an improved understanding of residual Mn deposits is potentially of great benefit for mine management and exploration projects that look for metallurgical and battery-active ores. A model that can be applied to other manganese deposits is of particular interest, because it assists in the comparison and evaluation of different secondary processes elsewhere. However, it is also demonstrated that the knowledge of alteration conditions at Groote Eylandt contributes to the understanding of bauxite and laterite development.

Supergene processes generated some of the world's largest manganese ore deposits (Roy, 1981). For example, the highest grade ores at the giant Moanda deposit in Gabon include supergene manganite, pyrolusite and cryptomelane derived from the dissolution and re-deposition of Mn from underlying manganese-bearing, carbonaceous shale protore (Leclerc and Weber, 1980). Supergene processes also seem to have been important in a number of other deposits, such as the Rio das Velhas Series and Minas Gerais deposits in Brazil (Dorr et al.,1956), the Janggun deposits in South-Korea (Kim, 1980), the Iron Ore Group deposits in India (Fermor, 1909), and many more. Elsewhere, supergene alteration of primary carbonate ores led to the formation of battery active manganese oxide ores, which are especially valuable for the mining industry. Examples include the Molango deposit in Mexico (Alexandri et al., 1985) and the Nsuta deposit of Ghana (Perseil and Grandin, 1978).

To dissolve manganese under any condition, water is the most essential component. Therefore, the mild tropical or subtropical conditions at Groote Eylandt are especially favourable environments for weathering and alteration processes which upgrade low-quality primary ores. Sufficient water for these processes is supplied from rainfall and perennial streams. Recent studies on Groote Eylandt have demonstrated that supergene overprinting has played a significant role in the development of the contemporary orebody (Ellis, 1978; Ostwald, 1980; Slee, 1980; Bolton, 1982; Varentsov, 1982; McHugh, 1983; Pracejus, et al. 1988). Therefore, this project was initiated to examine the Groote Eylandt orebody and to obtain information for the development of a genetic model for supergene Mn enrichment. The main aspects of this research work are presented below to give an overview of the project:

- stratigraphy, detailed sampling of selected vertical sections,
- petrography / mineralogy (ores and associated rocks),
- chemistry of ores and rocks (major and trace elements),
- theoretical mineralogy (mineral composition of samples)
- chemistry of fresh and salt water samples (major and trace elements),
- experimental work (redox reactions between ore and gangue minerals),
- thermodynamics and other physico-chemical processes (reduction/transport/precipitation),
- development of a genetic model for supergene manganese deposits.

1.2 Geologic Setting

Occurrences of manganese oxides on Australias northern coast were first noted in 1814 by early explorer Captain Matthew Flinders. Nearly 100 years later, Brown (1908) described manganese samples from a beach site on Groote Eylandt, and it took another 50 years until the Bureau of Mineral Resources started more intense investigations on the deposits, which led to the current mining activities (Dunn, 1962). The oxidic manganese ore body on Groote Eylandt is one of the largest sedimentary deposits in the world, having reserves in excess of 400 million tonnes. Similar to Chiatura and Nikopol in the U.S.S.R., the Groote Eylandt ores probably formed in shallow marine environments and occur mainly as primary Mn-oxide oolites, pisolites and small amounts of hardgrounds, associated with various secondary ores.

Groote Eylandt lies on the eastern margin of the Proterozoic McArthur Basin (Frakes and Bolton, 1984). The feldspathic sandstone/quartzite basement of the island is largely subhorizontal and it is essentially undeformed, although Cretaceous or post-Cretaceous fault block movements have occurred in the region (Frakes, 1979). These "Groote Eylandt Beds" are of middle Proterozoic age and they are equivalent to other sandstones in eastern Arnhem Land (Plumb et al., 1980). The basement is overlain unconformably by shallow-marine, glauconitic sands (Albian); Upper Cambrian to Jurassic sediments are apparently absent (Fig. 1.2). This time gap could either be related to an erosion of existing sediments or to tectonically very stable

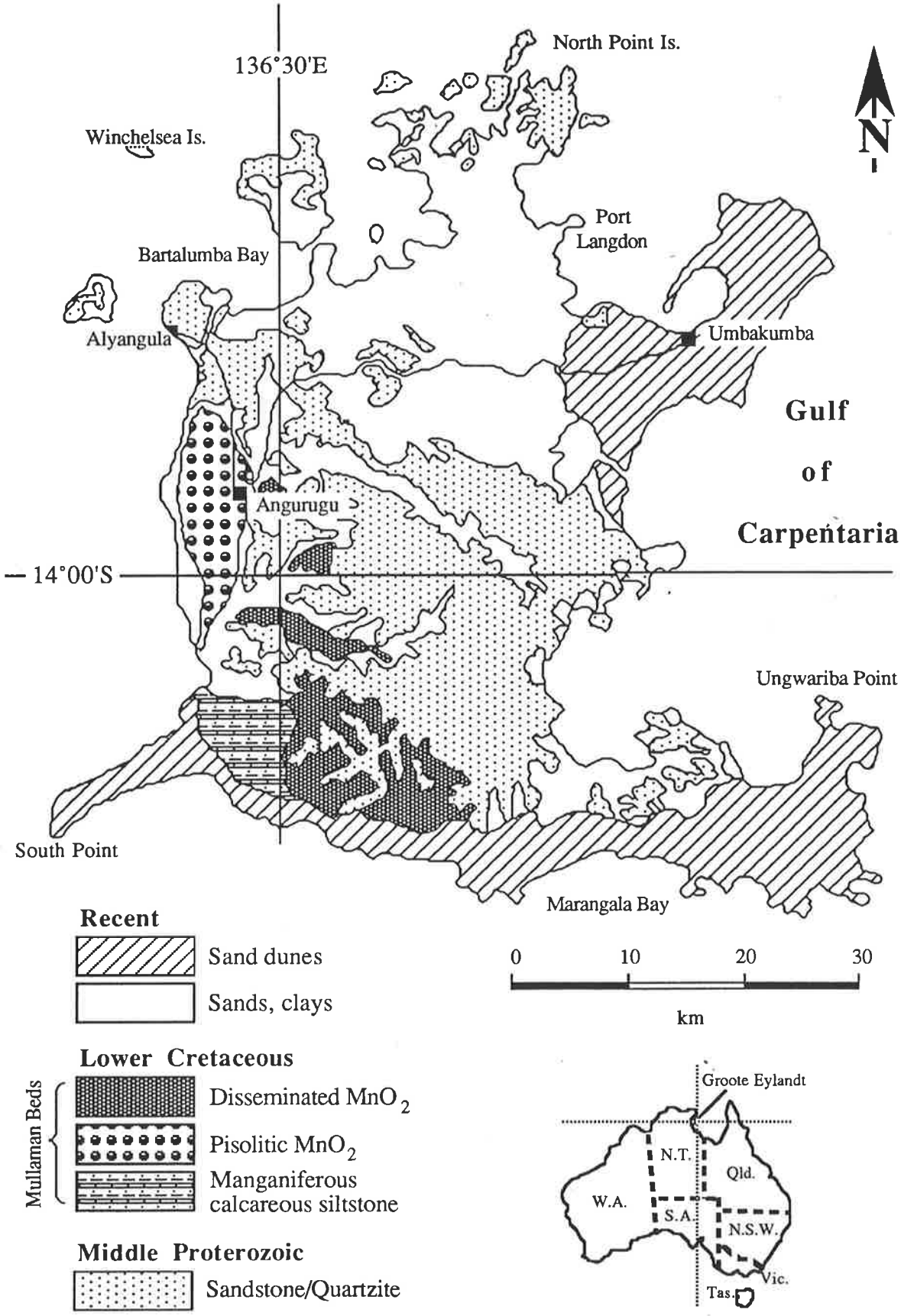


Fig. 1.1: Geologic Map of Groote Eylandt, Northern Territory, Australia; modified after Pracejus et al., 1988.

conditions with negligible sedimentation. Lower and Middle Cretaceous glauconitic clays amd sands overlie the Albian sands. The manganiferous strata, with a maximum thickness of about 9 m, occur in the upper parts of this sequence, which can reach up to 100 m in thickness. Oxidic manganese oolites and pisolites exhibit several cycles of normal and inverse grading, the latter generally to be found in the lower parts of the deposit. Size grading of the pisolites often ranges between 2 and 25 mm over an interval of 1 to 2 meters.

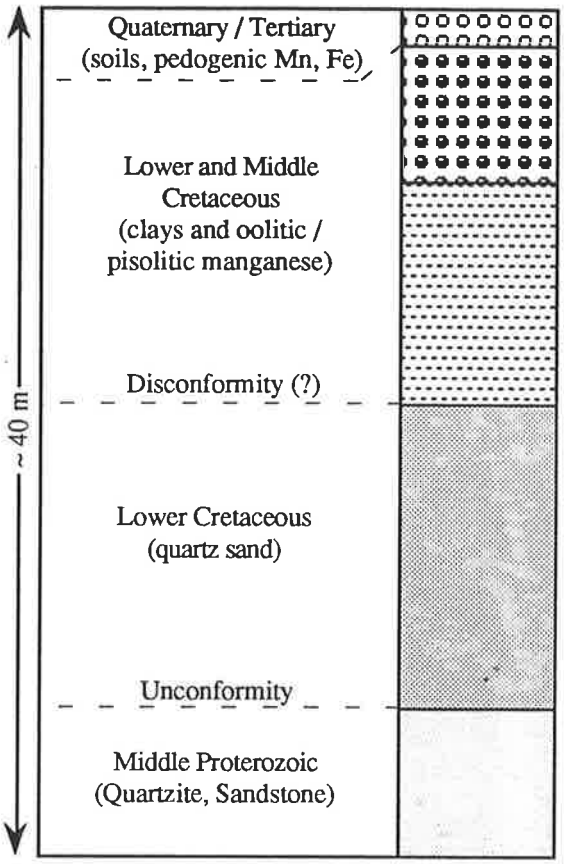


Fig. 1.2: Stratigraphic section at Groote Eylandt (after Bolton et al., 1988).

Straddling the western part of the island, the manganiferous sediments occupy two sub-basins separated by basement sandstones (Fig. 1.3). The northern deposit consists of Mn-oxides, which are presently being mined, whereas the southern occurrences are dominantly composed of a manganiferous calcareous siltstone, containing rhodochrosite and manganocalcite as the main Mn minerals.

Frakes and Bolton (1984) relate the formation of the primary manganese ores on Groote Eylandt to the existence of a partly anoxic intracratonic basin that acted as a trap for dissolved manganese. Such basins with restricted exchange with the open sea can lead to an accumulation of dissolved manganese. When the geochemical environment changes, that is, becomes more oxic, the concentrated manganese can precipitate either as oxide or carbonate. Frakes and Bolton demonstrated that sea-level changes(e.g. regressions) lead to a variation of a number of physico-chemical parameters including oxygen concentration and energy level, which in turn can produce conditions that favour precipitation. The two sub-basins reflect some of these variations through their mineralogy and their position in the vertical sequence. The northern oxide deposit formed in an oxidizing environment and at relatively shallow depths (15 - 50m), whereas the southern carbonate-dominated deposit developed under less oxidizing or even slightly reducing conditions and at greater depths (≤ 90m).

Recent K/Ar-dating of glauconite grains (Amdel, 1981) from clay units immediately underlying the ores, shows that the beds yielding the Mn, as well as those underlying the orebody are of Lower to mid-Cretaceous age (~ 95 Ma). This finding is supported by paleontologic data, which also show that the faunal assemblages associated with the sediments developed in a

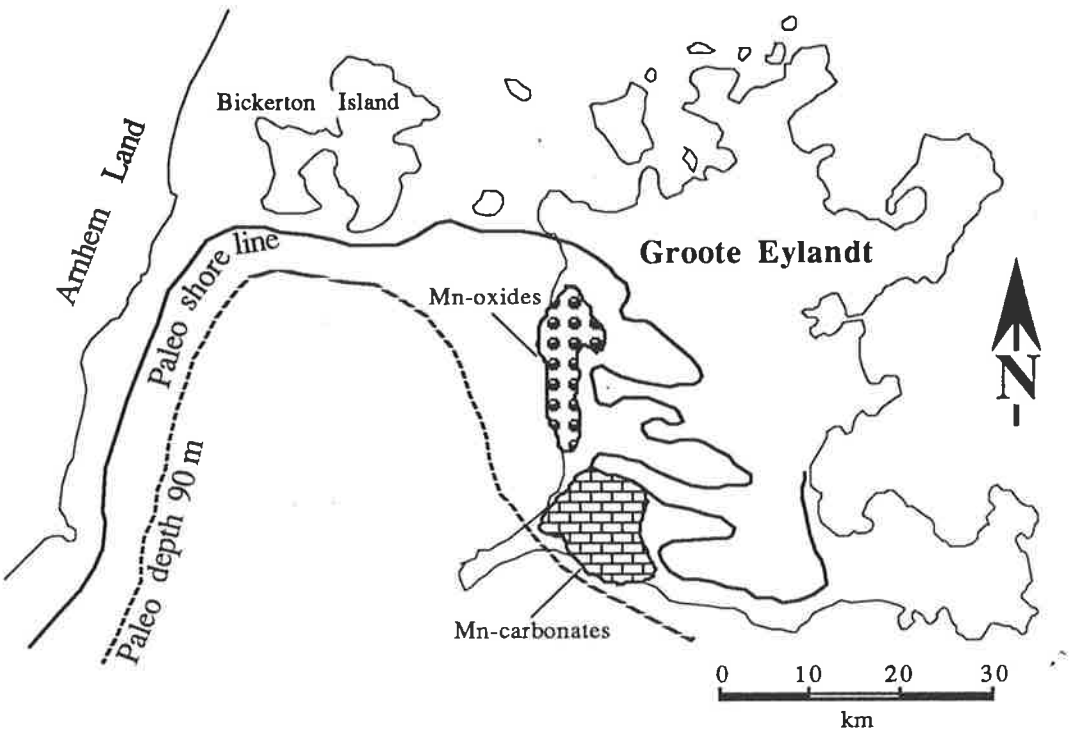


Fig 1.3: Paleogeography of Groote Eylandt, showing the shoreline of an intracratonic basin and its relationships to the manganese deposits on the present island (after Frakes and Bolton, 1984).

shallow marine, inner sublittoral environment (Smith et al., 1965; Taylor, 1979, 1981). The poorly preserved fauna (*Haplophragmoides spp., Radiolaria spp., Ammodiscus cf cretaceus*) indicates a mid-Cretaceous age. New results from K/Ar-datings of a number of cryptomelane samples seem to provide "secondary" ages of supergene overprinted rocks (Amdel, 1986, 1987; see also 8.2).

1.3 Previous Work

Until recently, supergene rocks on Groote Eylandt and their formation processes have not been examined systematically (Bolton, 1981; McHugh, 1983; Ostwald, 1988). Although most investigators acknowledge the existence of secondary lithologies, emphasis commonly focuses on primary sedimentary features and rock types. It is demonstrated later that this provides only a small part of the overall picture of the deposit. However, all previous studies agree that supergene overprints are probably of Tertiary to Recent age.

Smith and Gebert (1969) attributed little importance to secondary processes. Their explanation of the different textures involves deposition of manganese oxides in different localities of a shallow marine environment. They concluded, for example, that cemented rock types were deposited on substrates composed of permeable material such as sand or loose pisoliths, from

which the clay matrix had been washed by wave action. Loose pisolites are thought to have been deposited on an impermeable bottom such as clay or cemented pisolites. Other textures are attributed to different localities or mechanisms.

In contrast to this view, Ostwald (1976) considered secondary processes to be responsible for the development of some of the ore textures. He suggested that concretionary and massive rock types developed by colloidal processes acting within and replacing manganiferous clays and sandy clays. Cementation is attributed to diagenetic processes, and laterization was shown to produce manganese minerals such as todorokite and lithiophorite.

A slightly different idea was presented by Ellis (1978). He stated that there had been two types of post-depositional environments, which altered both the physical and chemical character of the mineralization. The first of the processes recognized is diagenesis, which is said to be responsible for compaction, shrinkage, cementation, recrystallization and replacement. These processes are thought to have been active throughout the entire deposit. In contrast, Ellis suggests that laterization, the second post-depositional process, has affected only the upper part of the section.

Slee (1980) concluded that many secondary processes are active on Groote Eylandt and that they produce textureless and concretionary rock types. These processes include crystallization, cementation, syneresis fracturing, veining, mineralogical changes, concretionary and septarian nodule development, replacement of quartz and argillaceous sediments, leaching of pisoliths and the destruction of pisolitic texture. However, Slee also acknowledged the primary sedimentary origin of both oolites and pisolites.

Varentsov (1982) presentd a totally different model for the ore formation. He suggested that the deposit resulted from reworking of a pre-existing weathering crust. The source of this crust is thought to be a manganiferous marl, which, according to Slee (1980), may exist at depth in the Cretaceous sediments. Cryptomelane is the major mineral to have been deposited by this mechanism. Alteration to pyrolusite, followed by formation of laterite, producing lithiophorite, todorokite, nsutite and romanechite, were later processes. Varentsov concluded that this formation mechanism makes Groote Eylandt an analogue of the Moanda deposit in Gabon.

The importance of supergene processes is emphasized by Bolton (1982). He stated that secondary processes were significant in the development of the sequence, in that they led to the formation of secondary lithotypes superimposed on the primary sediments, frequently obliterating original textures. He characterized the typical profile formed by secondary mechanisms as mangcrete profile, consisting of an unconsolidated surface layer composed mainly of pisoliths of pedogenic origin (spheruliths), an underlying laminar mangcrete, a massive mangcrete, and a lowermost mottled zone, all of which overlie unaltered parent rock.

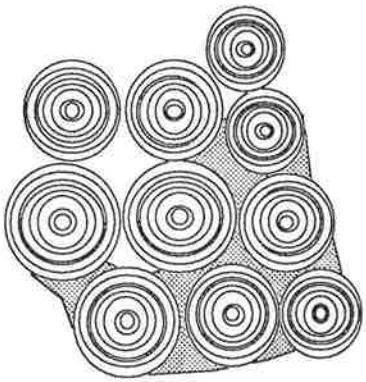
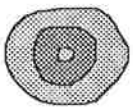
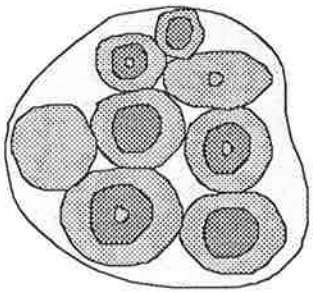
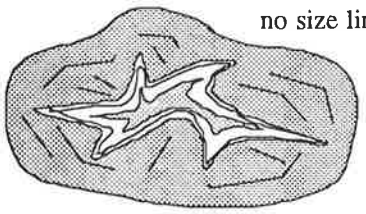
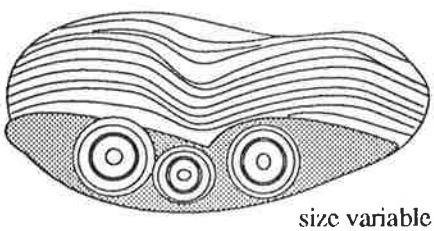
1.4 Terminology of Primary and Secondary Materials

The terminology used in this study was proposed by Pracejus et al. (1988). However, a brief definition of the main terms and generalized sketches are repeated here, because of the somewhat confusing descriptions found in the literature (Table 1.1). The terminology is considered to be important for many deposits and individual terms are thought to provide descriptions with a common applicability. Nonetheless, it is necessary to explain and describe further supergene ore and rock types, which are probably limited to a specific type of deposit and alteration environment. This is done in chapter 3 which in detail examines primary and secondary materials identified at Groote Eylandt.

1.5 Methods

A number of analytical techniques were employed for rock and water analyses. The equipment, sample preparation and analytical background are described in Appendix I. For further information see also Table of Contents.

Table 1.1: Terminology for primary and secondary ores and rocks, including sketches of the most common materials; pl.* = plural of individual types; modified after Pracejus et al., 1988.

Grain	Rock	Terminology, Description
 < 2 mm		Oolith (pl.* ooliths) separate ovoid to spherical grain, concentrically laminated, primary origin Oolite (pl. oolites) rock composed of ooliths, grain- or matrix- supported
 ≥ 2 mm		Pisolith (pl. pisoliths) separate ovoid to spherical grain, concentrically laminated, primary origin Pisolite (pl. pisolites) rock composed of pisoliths, grain- or matrix-supported
 ~ 3 - 50 mm		Spherulith (pl. spheruliths) separate ovoid to spherical grain, crudely laminated, secondary origin in soils Spherulite (pl. spherulites) mass of spheruliths, matrix supported
no size limit		Concretion separate and/or intergrown particles, rounded shapes, dense, occasionally dehydration features, centers commonly hollow or filled with detrital materials, secondary origin
size variable		Mangcrete The term mangcrete is applied in the same sense as calcrete (Read, 1974), silcrete, and ferricrete, and it is specified by additional descriptions; as example see left figure: cemented mangcrete (pisolitic) with upper contact to laminar mangcrete. Mangcrete is used as a modification of "manganocrete", which is the original definition by Netterberg (1967) for superficial manganese oxides.

2. Stratigraphy

2.1 Introduction

The general stratigraphy of the area is outlined in the previous chapter and thus, emphasis focuses on individual vertical geological profiles. Since a number of authors have examined the sedimentology of the Groote Eylandt ores and have prepared detailed geological sections (Slee, 1976; Bolton, 1982; McHugh, 1983; Frakes and Bolton, 1984), descriptions were kept brief (localities, stratigraphic positions, and grainsize data are given in Appendix II., Table 1). The main concern of this study is to provide background information supporting interpretations drawn from field observations. Most of the localities discussed here were subjected to a small-scale sampling procedure (see Appendix I.1) to allow a stratigraphy-oriented geochemical analysis of the materials.

Three vertical profiles (2 ore sections, 1 laterite log) were examined in D-Quarry in the south of the deposit. However, D-Quarry is not discussed in this chapter as it was not possible to match the profiles. These were obtained from locations 15 - 20 m apart, but are affected by extreme interruptions of the orebody. In many aspects however, the ore types of D-Quarry are similar to materials of the F-area (F1-F4). The laterite of D-Quarry is also comparable to that of F3-Quarry and thus, D-Quarry materials are broadly known. All other sections discussed below are typical representatives for the respective localities and most ore/rock types are laterally continuous over larger distances (tens to hundreds of meters), except for lensoid intercalations and very thin units. Some of the vertical sections may initially prove to be difficult to interpret, for instance units with a clay dominance may show grainsizes of several millimeters. Since this study primarily deals with manganese oxides, the grainsize of these minerals (plus Fe-phases) is emphasized. This way, it is possible to illustrate grainsize gradients of ore components within strongly altered and/or replaced materials, as are laterites (e.g. Fig. 2.7).

2.2 Sampling Locations

An overview over the Groote Eylandt geology is given in the previous chapter (Fig. 1.1), the locations of mining areas in the northern basin and the boundaries with outcropping basement rocks are presented in Fig. 2.1. The quarries are named with letters and numbers such as F3 or G-South. Plates 2.1-2 (Figs. 2a-h) briefly present the main oolites and pisolites ore units and two large-scale alteration features that are representative for many parts of the deposit.

An aerial view of F3-Quarry depicts the large open cut operations typical for mining activities at Groote Eylandt (Plate 2.1, Fig. 2a). The thick laterite cover can also be distinguished by brown colours which contrast with the black Mn ores. Where present, the laterite is stripped away to allow direct access to the ore.

Detailed photos of the pisolitic orebody and the extensive laterite overlying the ore show vertical pipe systems which are of particular importance for the geochemical alteration of the ore (Figs. 2b-d). Dark columns outline these pipes within the laterite (Fig. 2c), the light clay materials filling the pipes also stand out in the black ore. Such drainage systems are common throughout the deposit. Other features important for the interpretation of sedimentary processes and geochemical reactions are seen on Plate 2.2 (Fig. 2e); primary and secondary structures of the orebody are depicted in Figs. 2f-h .

Plate 2.1

Fig. 2a: Aerial view of F3-Quarry, showing open-cut mining of manganese oxide ores.

Fig. 2b: Overview of F3-Quarry ore and laterite.

Fig. 2c: Columnar relics of pisolite units in laterite of F3-Quarry (after Pracejus et al., 1988).

Fig. 2d: Overview of D-Quarry.

Plate 2.2

Fig. 2e: Goethitic replacements of manganese oxide ores in costean C-138 near F3-Quarry.

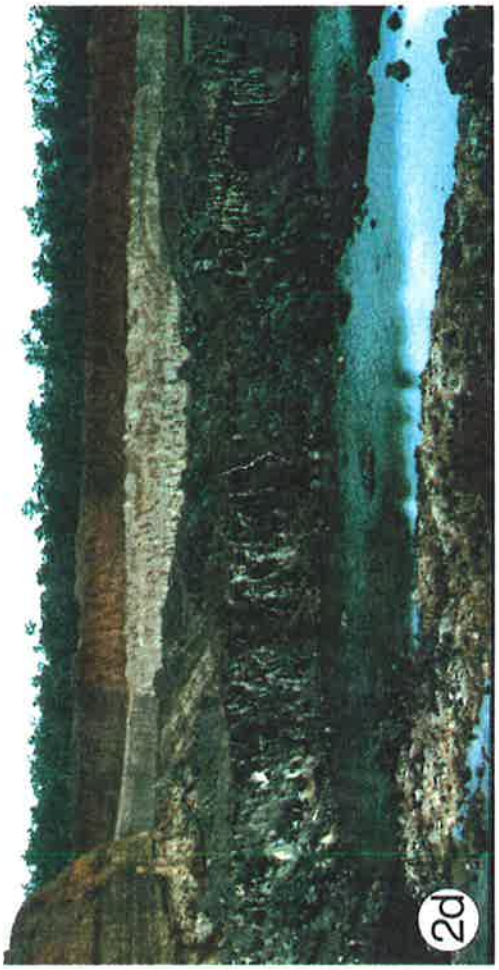
Fig. 2f: Overview of G-South Quarry.

Fig. 2g: Clay bands in G-South Quarry oolite.

Fig. 2h: Inversely graded pisolite in G-Quarry.

Plate 2.1







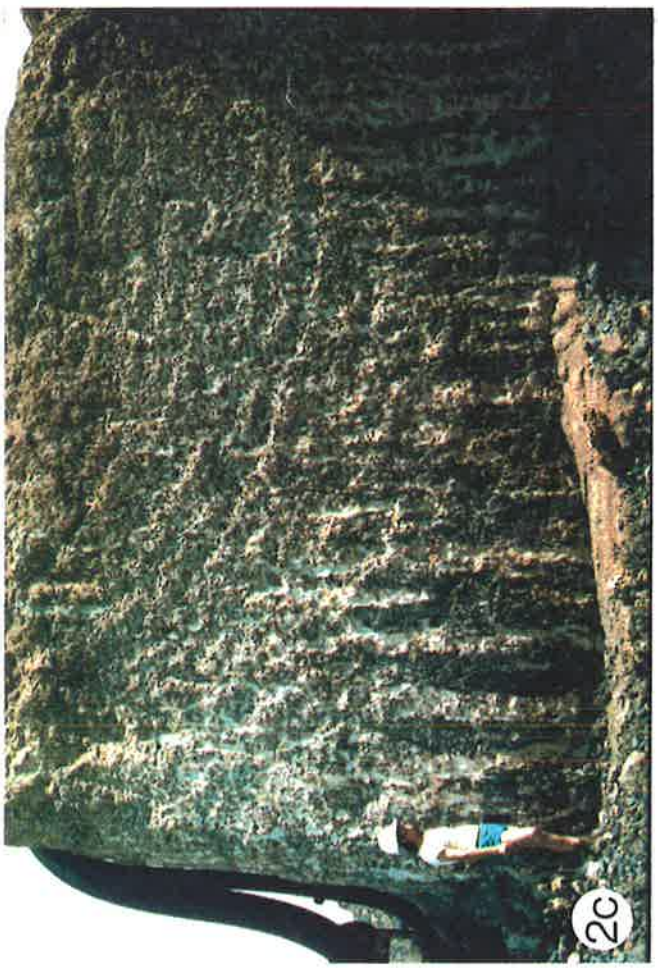
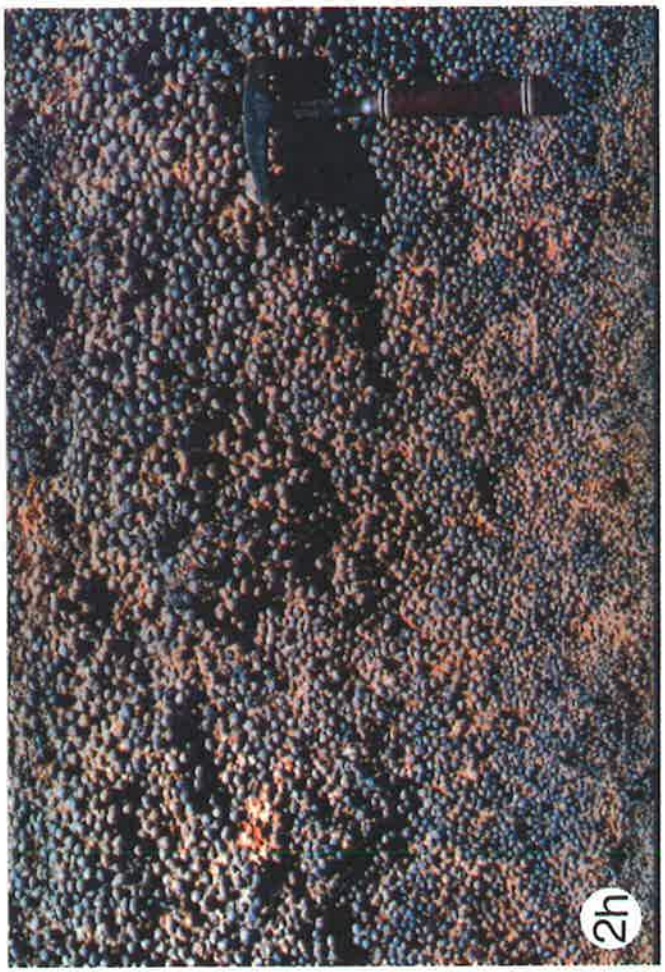
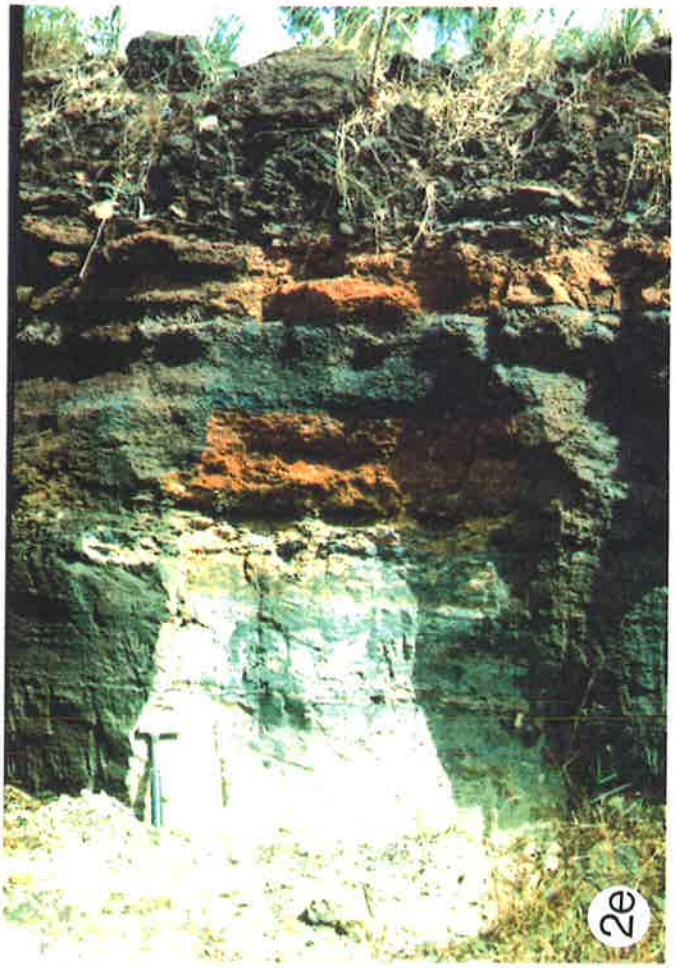


Plate 2.2









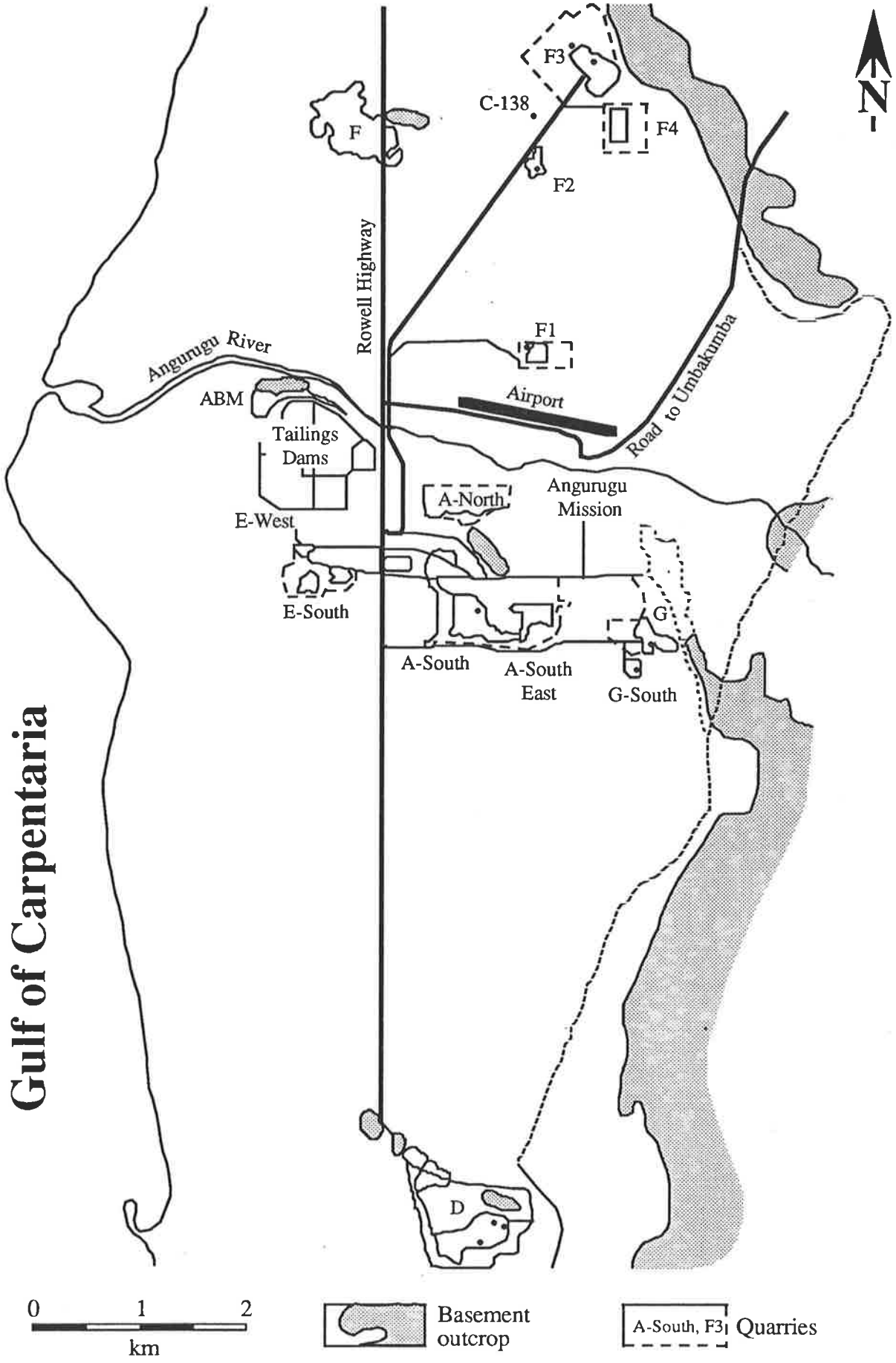


Fig. 2.1: Location map of mining areas at Groote Eylandt; • indicates stratigraphic section (some are not discussed).

2.3 Distribution of Ores and Rocks

The common legend for all stratigraphic sections of this chapter (Fig. 2.3) shows the lithology of the main ore and rock types, demonstrates the possible combinations of ores with gangues and supergene features (e.g. pipe systems), and provides structural information.

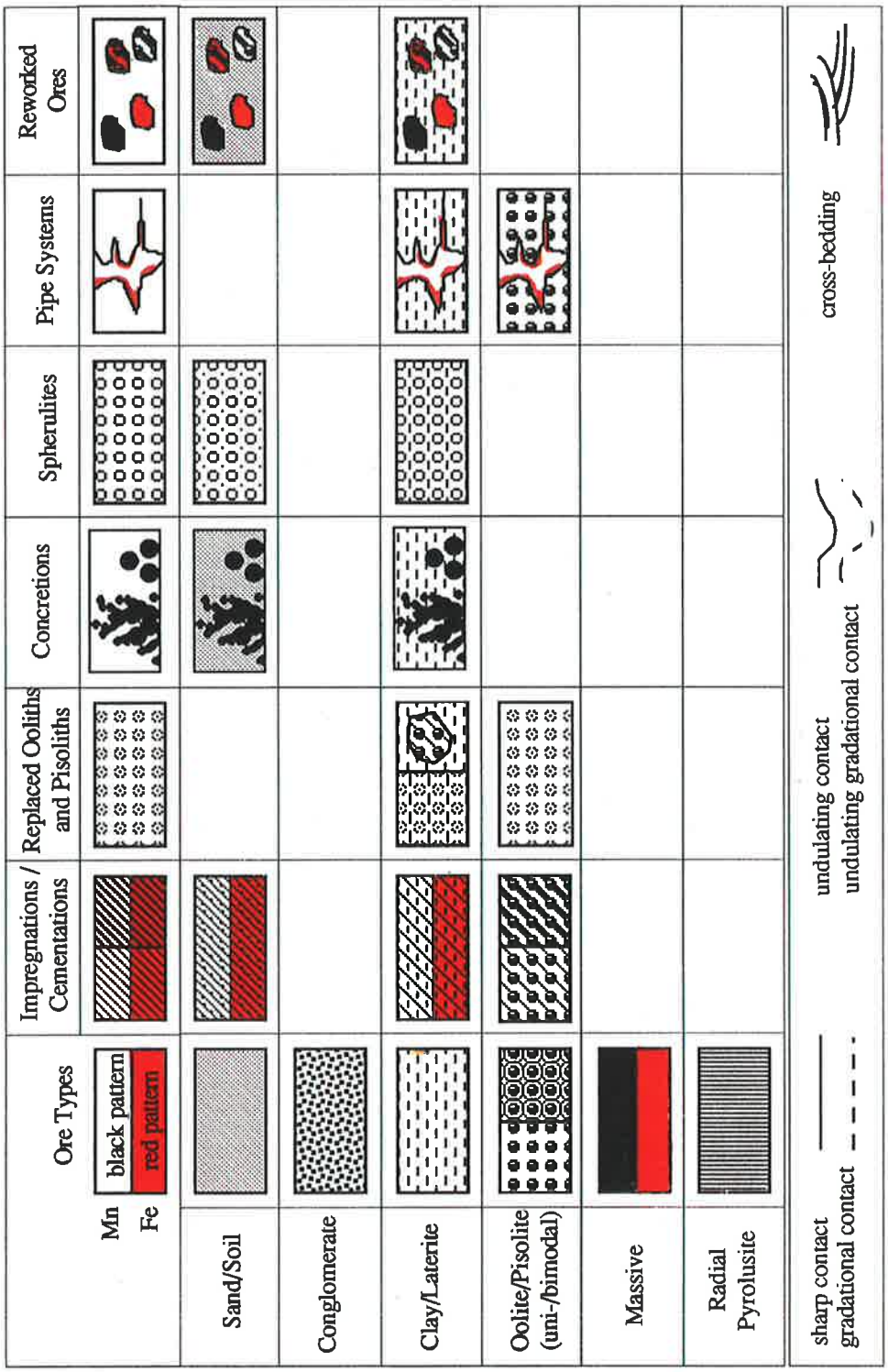


Fig. 2.3: Legend for stratigraphic sections, lithological combinations and structural features.

2.3.1 F1-Quarry

The stratigraphy of F1-Quarry was examined at the northwestern face (Fig. 2.4; location see Fig. 2.1). The ores are covered by a relatively thin manganiferous laterite containing reworked Mn oxides. In contrast to most other areas of the deposit, here the clay fillings of pipe systems are often washed out, leaving open drainage channels.

Most units can be traced throughout the deposit, but unlike other ores, large parts of the ore-body exhibit strongly undulating features with oscillations of 10 - 20m. Two inversely graded manganese oxide horizons overly Mn- and Fe-impregnated quartz sands. The upper unit consists of a pisolite with a large grainsize gradient. The top of this unit is strongly cemented by Mn and, in places, the material grades into a massive mangcrete with relic pisolith outlines. Commonly, the relic pisoliths, but not the surrounding matrix, are replaced by ferruginous phases such as goethite.

Although a small grainsize gap exists at the contact to the underlying pisolite, the boundary is difficult to detect in the field. However, the lower pisolite unit contains clay lenses and pipes, which are not observed above. The grainsize distribution is uniform and occasionally, mottled

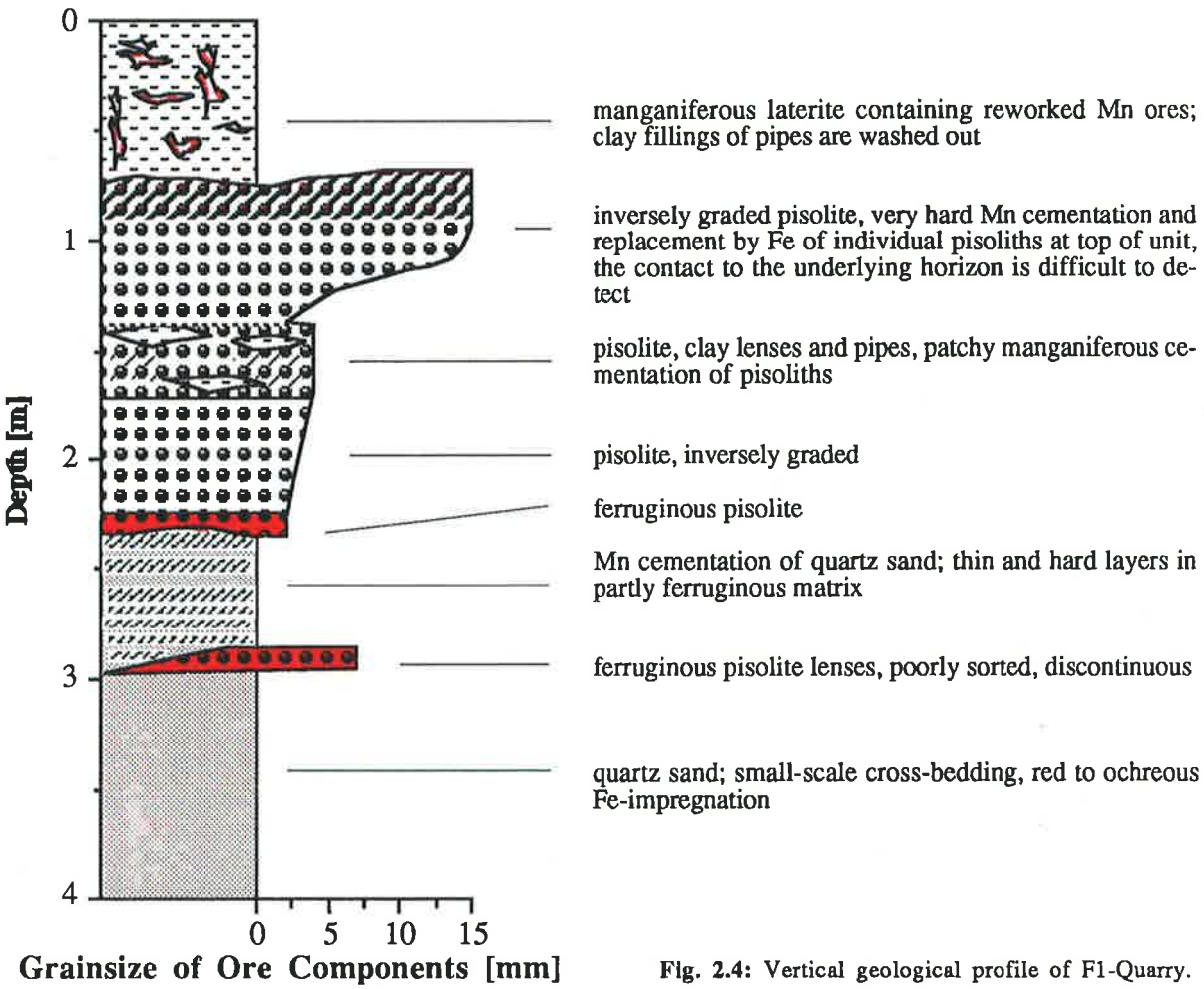


Fig. 2.4: Vertical geological profile of F1-Quarry.

Mn cementations of pisoliths are found. Below this unit, the second inversely graded Mn pisolite occurs. A sharp boundary separates it from the underlying ferruginous pisolite. This latter unit seems to cut across primary Mn structures, such as pisolith grains, indicating replacement processes.

The underlying medium grained quartz sand shows ferruginous impregnations. Throughout the upper 70cm of this sand unit, thin but very hard siliceous Mn oxide layers occur in regular intervals. The sand grains incorporated in these layers illustrate the seconday nature of this material, which cemented the primary sediment (sand) with remobilized manganese. Discontinuous lenses of ferruginous pisolite with variable size seem to mark the lower limit of the cemented layers. Below these lensoid bodies, no significant Mn cementation is observed. The ferruginous sand underlying this material possesses a small-scale cross-bedding.

2.3.2 F2-Quarry

This section was examined at the eastern side of F2-Quarry, where additional excavation provided an entire profile through the orebody. The cover at this location is much thicker (~ 4m) than in the previous section (< 1m) (Fig. 2.5) and the soil contains dense, probably reworked Mn oxides. Small pipe systems are developed, where Fe impregnations are partly remobilized (bleached). Pipes in the laterite below are larger than those within soils and they appear throughout the rock. The laterite also shows varying degrees of Fe cementation forming mottles and horizons of increased Fe concentration; occasionally, manganese oxide stains are seen. In deeper parts of this unit, a bleached (white) Mn- and Fe-free clay horizon occurs.

The base of the laterite contains large grains (16mm) of pisoliths replaced by kaolinite. The log demonstrates that the grainsize of these replacement products extends from the inversely graded sedimentary sequence of the underlying ore. This particular interval of the laterite thus strongly suggests that lateritic products remobilize and replace parts of the orebody. Other observations made in deeper parts of this section support this interpretation, although these findings are less evident. However, with the exception of the lowermost interval of the laterite, other parts of this profile do not possess oolith or pisolith relics which could indicate the replacement of a former orebody.

The inversely graded pisolite unit below the laterite is strongly cemented by Mn at the top and it grades into more clay-rich materials deeper down. Relatively thin inversely (2) and normally (1) graded horizons underlying this sequence often show Mn cementation at respective boundaries. These ores also contain relics of cemented pisolitic ores. Near the base of the orebody clays and goethitic/hematitic minerals increasingly dominate the matrix of these materials; occasionally, the ores are totally replaced.

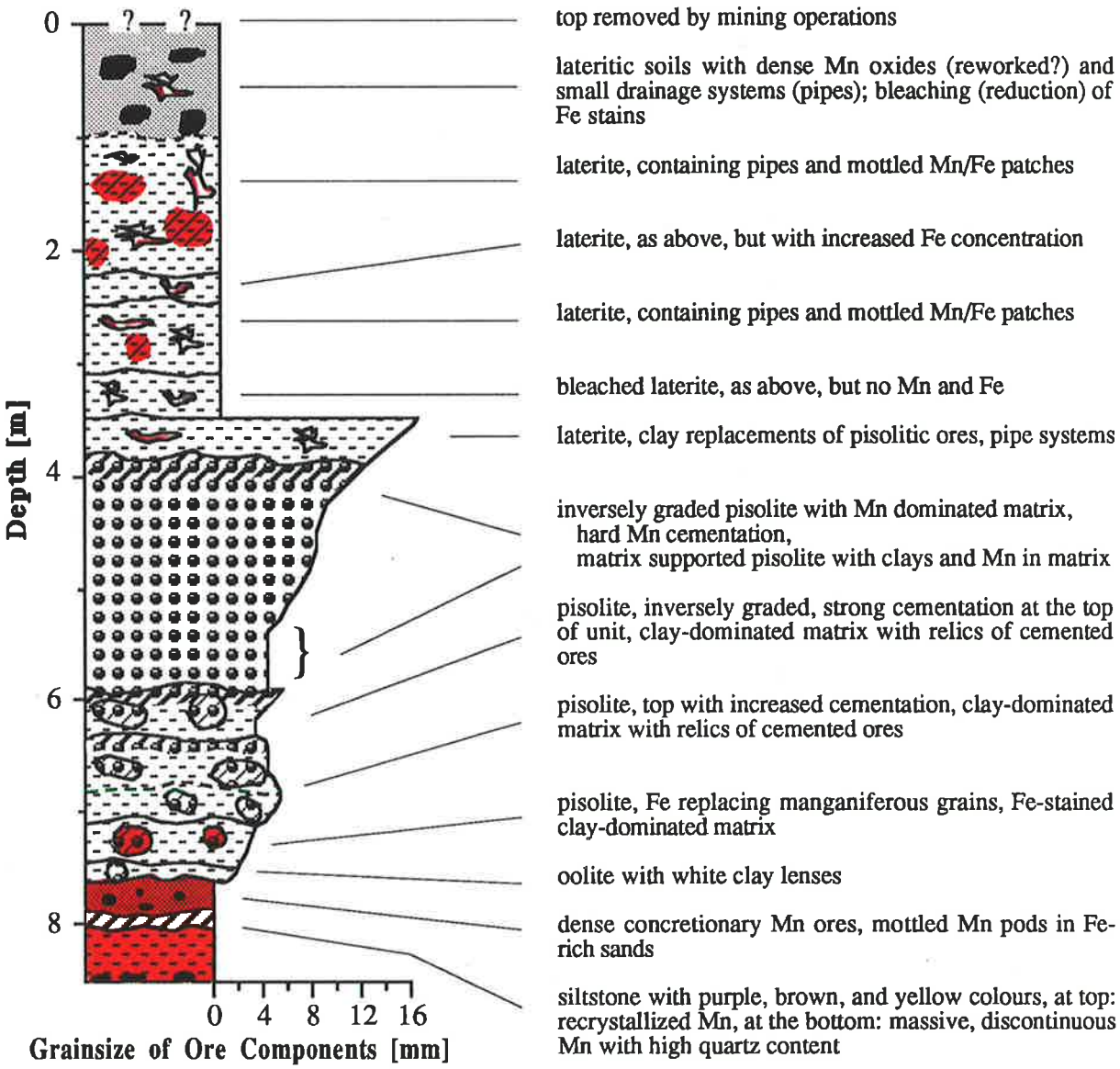


Fig. 2.5: Vertical geological profile of F2-Quarry.

2.3.3 F3-Quarry (orebody)

The examination of orebody and laterite in F3-Quarry was separated into two sections to allow an independent discussion, because the laterite depicts features essential to understanding geochemical alteration processes in the deposit.

Dipping at about 10° to the southwest, the orebed is generally flat and undisturbed. In places, however, the quartzite basement interrupts the sequence with irregular domal or pillar-like relics (erosional features). These structures occasionally occur within the laterite and thus, ore sedimentation in these locations appears to have been disrupted.

F3-Quarry displays pisolites which are mostly well cemented, very hard, and uniform in appearance (Fig. 2.6). Several sedimentation sequences are observed through normally and inversely graded units. Individual horizons generally possess the highest cementation near or at the contact between adjoining sedimentation units. Due to the uniformity of the cemented pisolites it is often difficult to discern the boundaries of sedimentation units. At the base of the main orebody relics of cemented pisolitic ores are embedded in a clay matrix and a dense, structureless Mn cementation is observed to be continuous over tens of meters.

Pipe systems appear throughout the orebody, although they concentrate in the middle part of the section, where an inversely and a normally graded unit meet (grainsize limits of both horizons). This zone shows older, horizontal pipes, and younger, vertical pipe systems crosscutting the older structures. Possibly, the horizontal pipes represent a sequence of primary clays formed during sedimentation; lateritic pipes are predominantly vertically aligned.

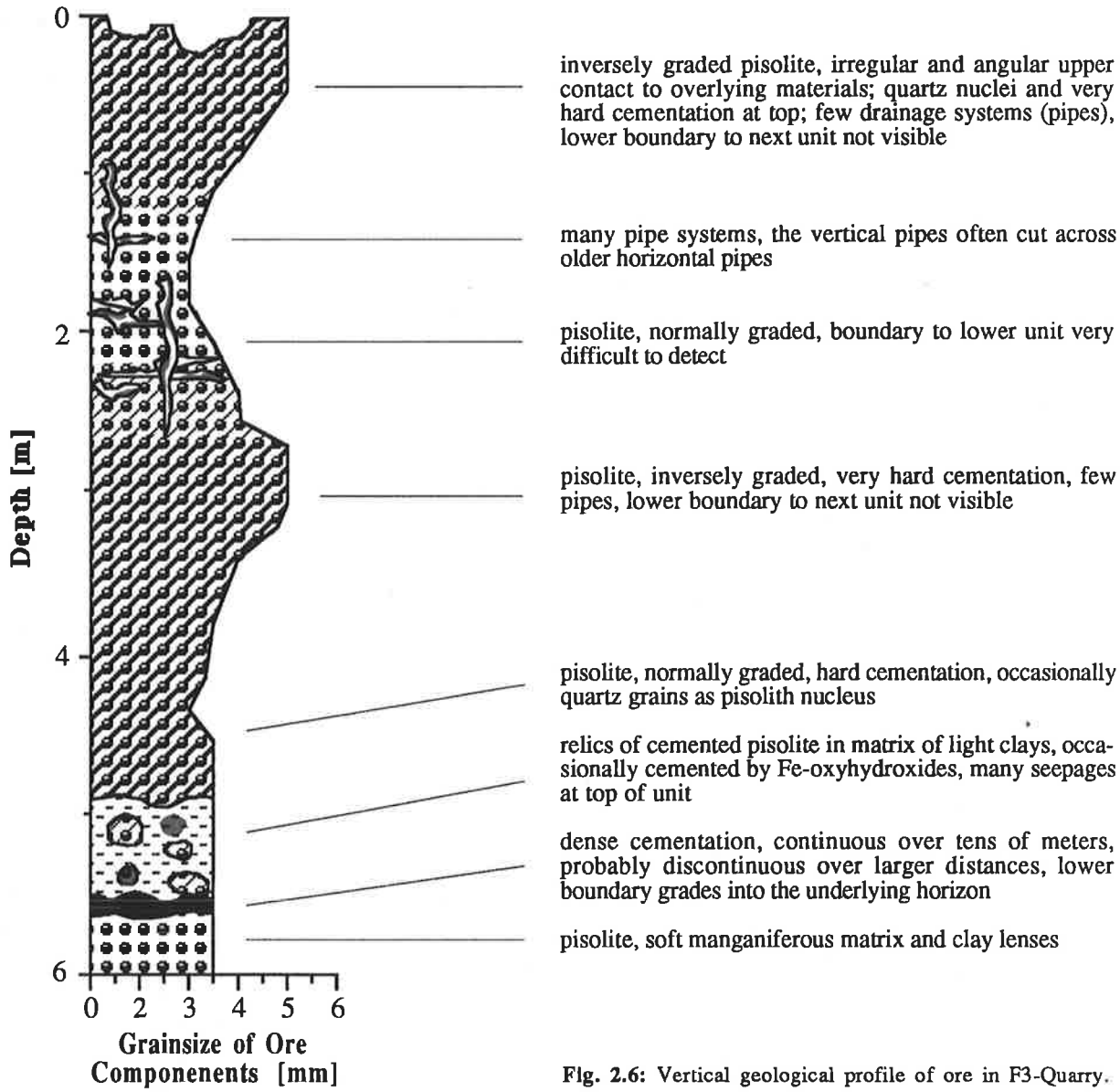


Fig. 2.6: Vertical geological profile of ore in F3-Quarry.

Geological features of pipes are later discussed in detail (chapter 7), since the association of distinctive secondary ores and rocks is used to model electrochemical alteration processes occurring in ores and laterites. Nevertheless, observations of three stratigraphic sections consistently indicate that laminar mangcretes, lining the outer boundary of pipes (not plotted for simplicity), are up to 5 cm thick near the surface. Deeper down the section these ores become considerably thinner or disappear. This suggests that oxygen availability plays a significant role in the precipitation of laminar mangcretes (and other ores?).

2.3.4 F3-Quarry (laterite)

Relic pisoliths found in the F3-laterite (but also elsewhere; compare 2.3.2) indicate former orebodies that were chemically remobilized to a large extent. These preserved grains enable the description of primary sedimentation units containing normally and inversely graded manganiferous horizons (Fig. 2.7). Such "relic grainsize profiles" can be compared with stratigraphic ore/laterite sections from other parts of the deposit.

The laterite is covered by spherulitic soils which occasionally fill vertical pipes or collapse structures. Generally, spherulites show normal grading, at depth the grains commonly form larger, accretionary particles with concretion-like shape. Below the spherulite, a dark brown zone occurs where the laterite is cemented by evenly disseminated ferruginous phases. A relatively sharp boundary separates this unit from the underlying light laterite. Intercalated in this material is a relatively thin horizon containing conglomerates (cemented and massive Mn oxides, quartzite, and other detrital materials) in a matrix of Fe-stained clay. Deeper down the section, dark columnar structures appear in lighter coloured materials. These columns are enriched in relic pisolitic Mn ores and Fe oxyhydroxides, whereas kaolinite dominates the light materials between the columns.

Near the base of the laterite, large lenticular bodies of conglomerates occur, which possess strongly undulating erosional surfaces and sub-horizontal bases. These conglomerates were initially interpreted to reflect both the end of Mn sedimentation and, together with this event, a time boundary. However, the findings above show that the precipitation of manganese oxides and the formation of oolitic/pisolitic orebodies must have continued over considerable geological time spans, after the conglomerates were deposited. Otherwise, the presence of relic ores within 10m of laterite would be difficult to explain. The observation of "clean", continuous grainsize gradients over 2 to 4 meter also supporte this view.

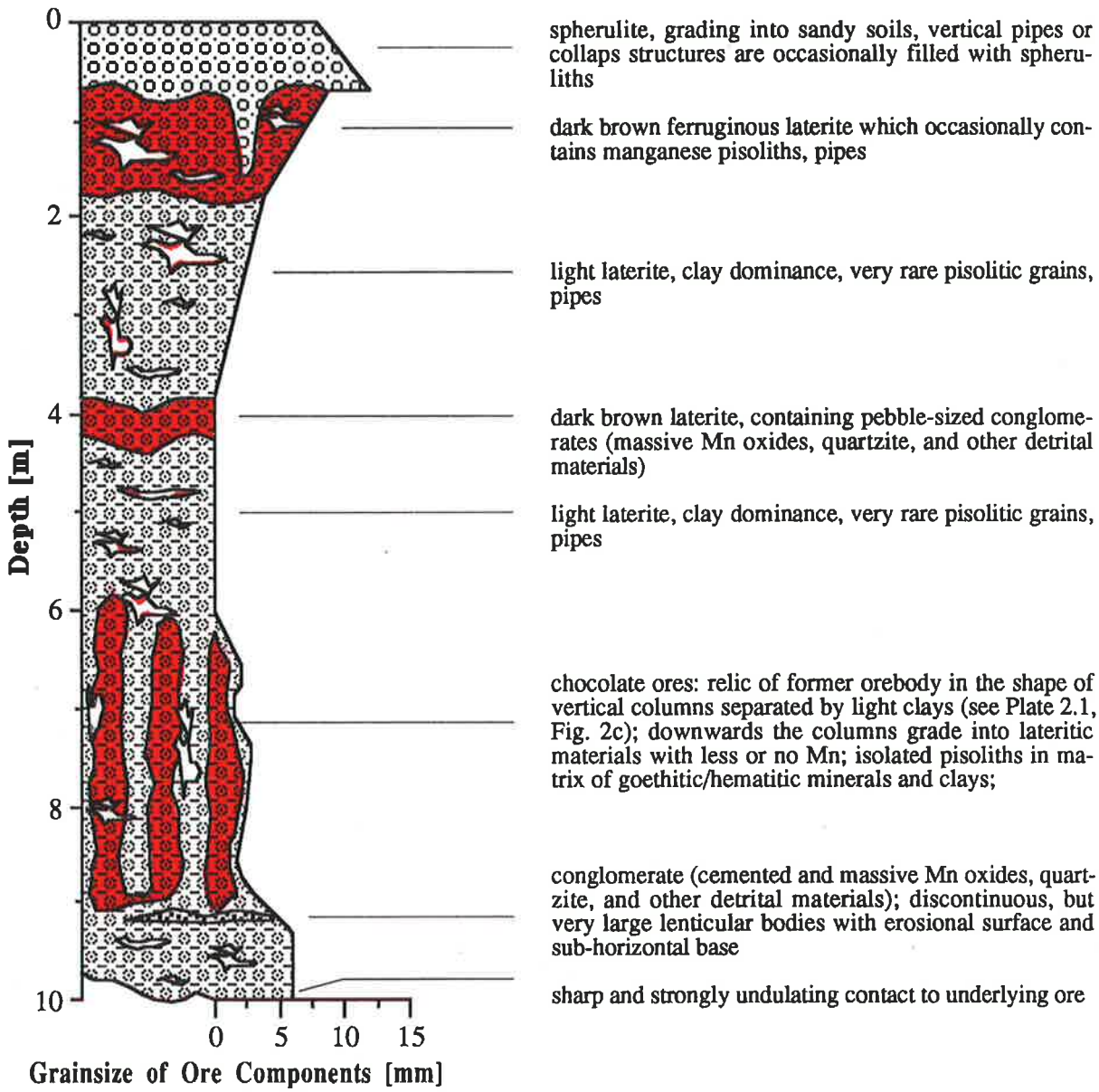


Fig. 2.7: Vertical geological profile of laterite covering the ore in F3-Quarry (compare also Fig. 2. 5).

2.3.5 Costean C-138

Costean C-138 is located in the center of the F-Quarries area but contains only a relatively thin sequence of two inversely graded pisolite units (Fig. 2.8). The ore is covered by lateritic and reworked materials and is separated from these rocks by massive bands of manganese and iron minerals. The manganese pisolite itself shows a distinct replacement by goethitic and hematitic phases at the top and at the bottom of the sedimentation units (see also Plate 2.2, Fig. 2e), the center of this "sandwich" structure appears to be mostly unaltered. The medium grained quartz sands below the ores are mainly impregnated with manganese oxides, upper parts are also stained by Fe phases. Small quartzite pebbles occur at the top of the sand unit and are partially cemented by manganese oxides. The profile of this location bears strong similarities with the

section at F1-Quarry. Although the replacement features are much more prominent at C-138, comparable replacements are observed in F1. The lithology of both areas is also very similar, as both locations possess two inversely graded pisolites with an abrupt change of grainsize between the respective units, the laterite cover is relatively thin, and the underlying sands show Mn-impregnations.

The ores of costean C-138 are of particular interest to the geological history of the deposit in several aspects. First, an extensive overburden separates the underlying orebody of the F3 area (the ore dips at ~ 10° towards C-138; see 2.3.3) from this thin pisolitic unit. This supports previous conclusions that showed a continuation of manganese sedimentation after the establishment of the presently "visible" main orebody. Secondly, although insignificant in thickness when compared with other locations, this unit is only partially replaced by iron minerals. This contrasts strongly with several meters of former ores chemically remobilized and removed from sections, where extensive laterites are apparent (compare 2.3.4); the laterite cover here is negligible. Obviously, the abundance of lateritic phases, such as kaolinite or goethite, is essential for the destruction of manganese oxides. On the other hand, associated quarts sand seems to act as a sink, and dissolved manganese is removed more easily.

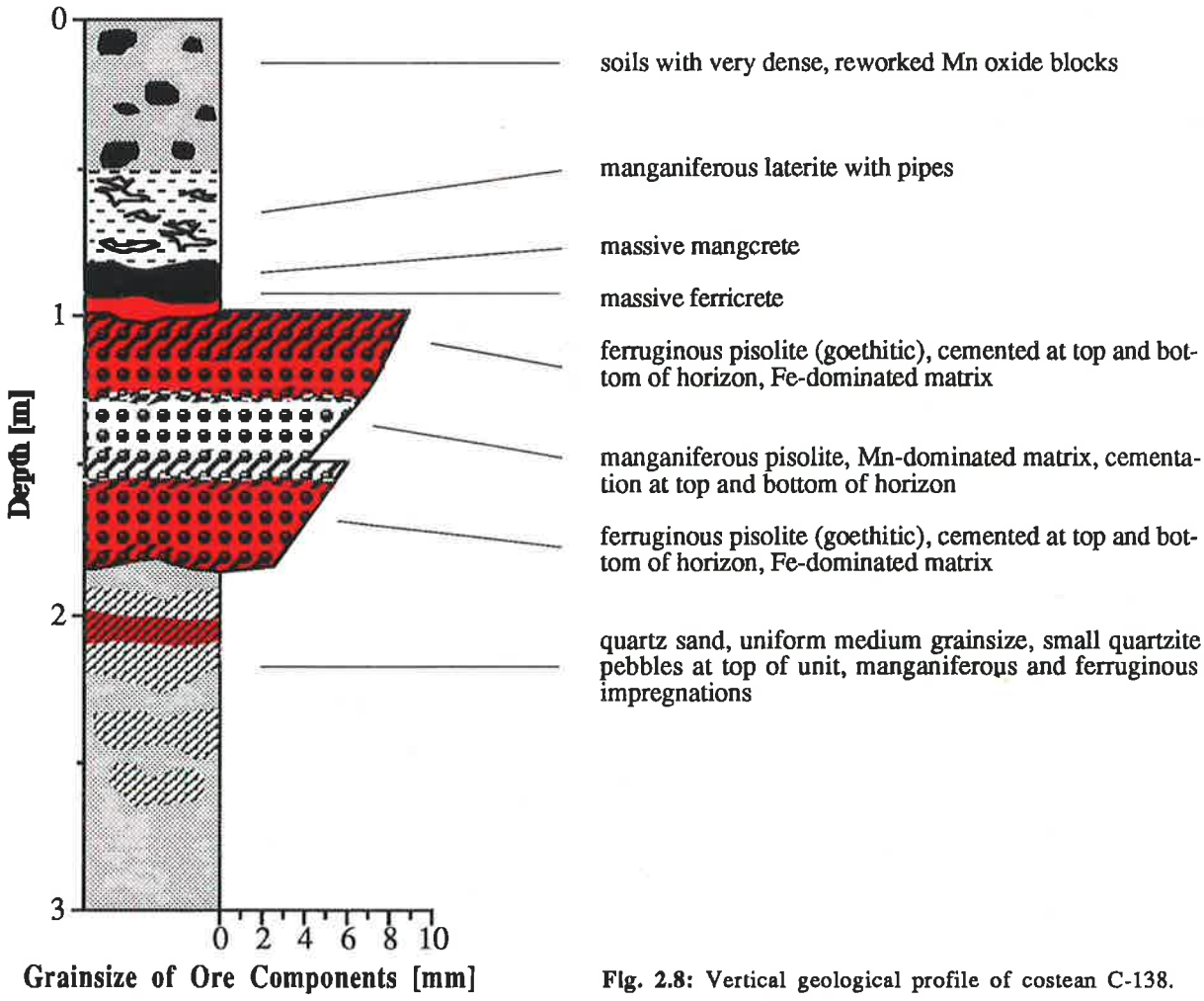
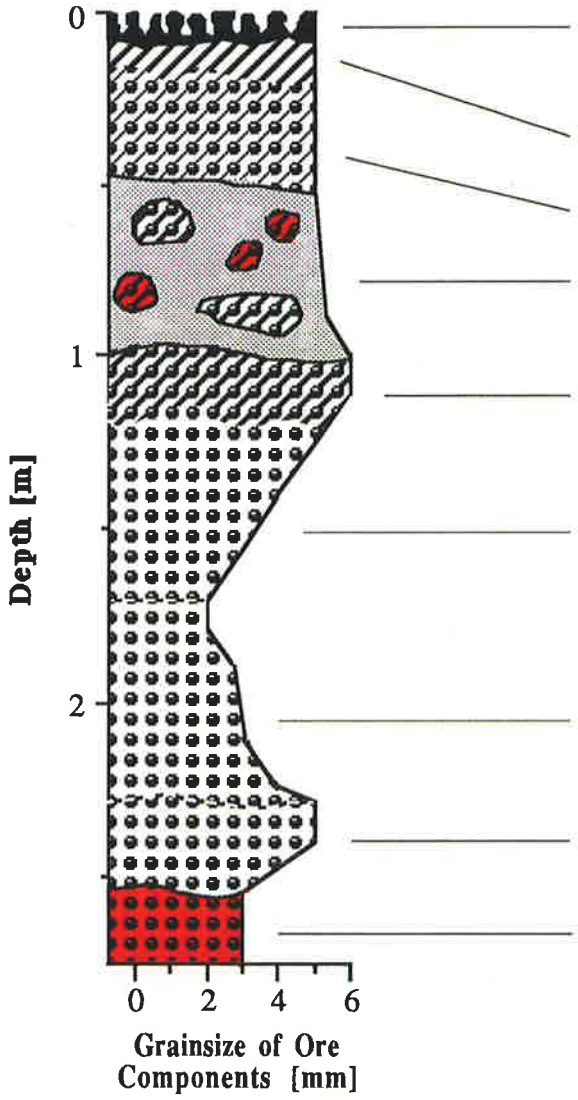


Fig. 2.8: Vertical geological profile of costean C-138.

2.3.6 A-South Quarry

Refilling operations with waste materials hindered the examination of an entire section. However, parts of the orebody were exposed during the field session and are presented (Fig. 2.9). Large concretions occur at the top of the ore and are surrounded by white clay minerals; in many cases these clays are washed out. The concretions show an upwards oriented growth and, occasionally, fill sinkholes. The materials at the base of this unit grade into cemented pisolitic ores, via an intermittent development of massive mangcrete. The contact to the underlying sandy horizon is relatively sharp. The medium grained quartz sand contains relics of probably reworked cemented pisolite; in places manganese is replaced by ferruginous minerals. Below this unit, an inversely graded massive mangcrete (pisolith relics) grades into a cemented pisolite; deeper down the section the ore becomes less well cemented. This part of the section is generally well sorted. A contact to the underlying normally graded pisolite is very difficult to detect. Here, the ore is not very well sorted, has a sandy matrix, and shows a gradational lower contact. The inversely graded pisolite below appears to be reworked, contains many platy fragments and a sandy matrix, and is poorly sorted; its base undulates but is sharp. The following sequence, a ferruginous pisolite, is well sorted and possesses uniform grainsizes.



concretions with upwards oriented growth; grading into the underlying cemented mangcrete; upper parts of concretions are in contact with white clays (mostly washed out); concretions occasionally fill sinkholes

massive mangcrete, few pisoliths recognizable; at lower parts grading into cemented pisolite

cemented pisolite, relative sharp boundary to lower unit

relics (reworked?) of cemented pisolite in sand matrix; in places the Mn pisolite is replaced by goethitic minerals

very hard massive/cemented mangcrete with relic outlines of pisoliths; grading downwards into pisolite; sharp upper contact

pisolite, inversely graded, well sorted

pisolite, normal grading; upper boundary very difficult to detect, lower contact gradational; medium sorting; sandy matrix

pisolite, inversely graded; reworked; often platy, poor sorting, sandy matrix

ferruginous pisolite, sharp upper contact, well sorted

Fig. 2.9: Vertical geological profile of A-South Quarry.

2.3.7 G-Quarry

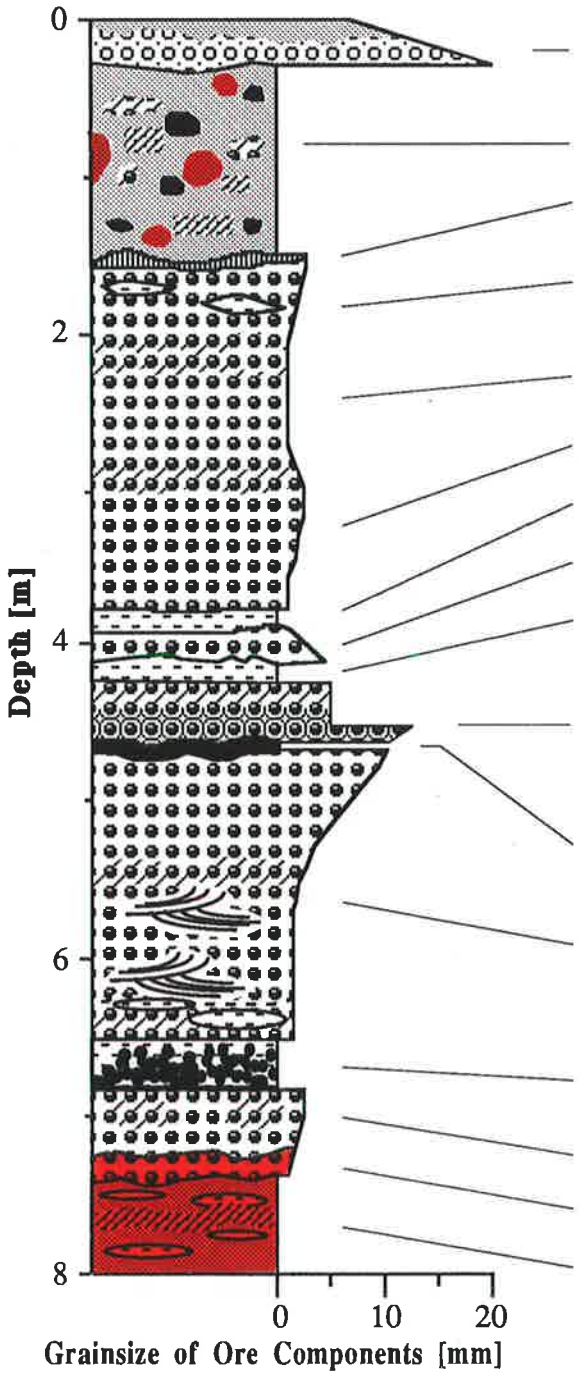
The ores of the G- and G-South Quarries are unique in the deposit, mineralogically and petrologically, because they possess a pronounced battery-activity. The Mn oxides are mostly soft and friable, with the exception of hardgrounds and large pisoliths, and strong grainsize variations exist within both normally and inversely graded units (Fig. 2.10).

The soil covering the deposit contains spheruliths which incorporate ooliths in the core, indicating erosional processes. Since the orebody here is almost at the highest level above sea, it can be assumed that the reworked ooliths were physically transported to the present location. Thus, ores must have existed at elevations above the eastern boundaries (inland) of the deposit. Fe-rich quartz sand below the soil also shows angular, reworked products (massive manganiferous and ferruginous materials).

Oolitic ores underlying this sand are capped by a recrystallized Mn oxide band (a few centimeters thick), depicting a strongly undulating erosional surface and a sub-horizontal base. The uppermost inversely graded oolite is relatively thin and contains clay lenses in irregular intervals. Although the lower boundary to the underlying normally graded oolite is hard to detect, it is assumed here that it is reflected through zones of increased Mn cementation. The same observation applies to the following sedimentation sequence, which consists of an inversely graded oolite.

Underlying these ores, two clay- and Fe-rich horizons border a thin oolite unit. These layers are subhorizontal and, in places, they cross-cut neighbouring ore units. The oolite depicts a normal grading and has fair sorting. Deeper down the section a bi-modal oolite/pisolite occurs which is cemented at the top. The ore is poorly sorted, shows ripple cross-lamination and occasionally contains tabular Mn intraclasts. Commonly, large pisoliths are accumulated in depressions of the underlying hardground. This ore type is discontinuous over larger distances, but well developed in places. Occasionally, envelope grains (thick laminae around relic ores), up to some 20cm in length, seem to take the place of the hardground.

A prominent inversely graded pisolite/oolite unit occurs below the hardground. The ore is generally well sorted. A manganiferous cementation of the oolite is observed in association with sandy clays lenses near the base; trough cross-bedding occurs in the lower half of the unit. A siltstone abruptly interrupts the ore sequence. This rock contains digital, upwards oriented concretions originating from a fine sand layer, through which Mn carrying solutions can move more easily. Below the siltstone a relatively thin manganiferous oolite, partly replaced by ferruginous materials, overlies Fe-rich sand. The sand also contains clay lenses and thin layers of recrystallized manganese oxides.



spherulitic soil; occasionally ooliths in core; normal grading

Fe-rich sand containing massive (reworked?) Mn and Fe ores and Mn cementations

recrystallized Mn oxide layer at top of oolite unit

oolite with clay lenses in upper part of unit; cemented patches and layers in irregular intervals; inverse grading

normally graded oolite; boundary to upper unit not recognizable

inversely graded oolite, cemented at the top

clay-rich horizon with Fe cementation

normally graded oolite, fair sorting

clay-rich horizon with Fe cementation, discontinuous, but prominent in places

bi-modal oolite/pisolite (plotted are the large pisoliths); poorly sorted; cemented at the top; pisoliths are often accumulated in depressions of the underlying horizon; ripple cross lamination; tabular Mn intraclasts; occasionally composite grains

hardground, discontinuous, but well developed in places; occasionally replaced by large composite grains

inversely graded pisolite/oolite; well sorted; cemented parts in the middle (sedimentation boundary?) and at the bottom of the unit, together with lenses of sandy clays; trough cross-bedding

white, yellow, and pink siltstone with sand layers at the bottom of the horizon; digital concretions with upwards oriented growth (coral-like)

Mn oolite, mottled cementation

Fe oolite

Fe-rich quartz sand with clay lenses, containing layers of recrystallized manganese oxides

Fig. 2.10: Vertical geological profile of G-Quarry.

2.3.8 G-South Quarry

In many aspects, the materials of G-South Quarry are very similar to the ores in G-Quarry (Fig. 2.11; compare Fig. 2.10). The ore is covered by lateritic and reworked materials, but, when compared with the extensive laterites of other mining areas in the deposit, this cover although coarser, is of minor importance. The massive reworked ore components within this part of the section may have their origin in the karstic ores nearby (outcrop of orebody) or they may derive from eroded former orebodies that could have existed at higher elevations.

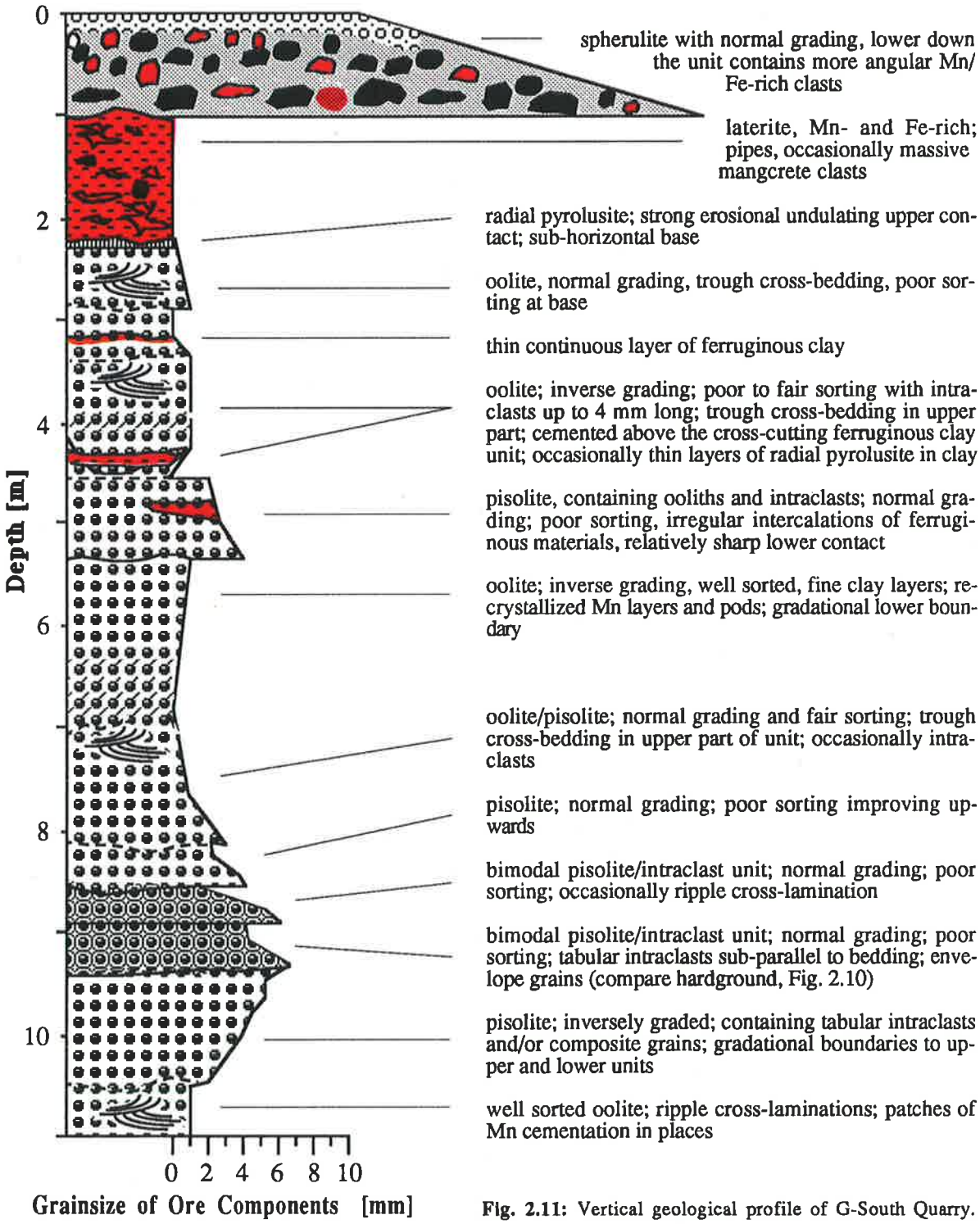


Fig. 2.11: Vertical geological profile of G-South Quarry.

The oolites and pisolites show a number of normally and inversely graded units with abrupt changes of the grainsize at the boundary. Several ore horizons are bimodal and contain reworked tabular intraclasts. Generally, the ores of this locality are very soft and friable and they possess a low density, with the exception of occasional composite grains and the larger pisoliths deeper down the section. Trough cross-bedding and ripple cross-lamination are observed frequently. Ferruginous, subhorizontal clay layers, commonly only a few millimeters thick, appear in many ore units (compare also Plate 2.2, Figs. 2f,g). These clays sometimes cut across the original ore bedding and are thus of secondary origin.

Comparable to the previous section, the top of the ore is marked by a characteristic thin but dense Mn oxide layer. Continuous hardgrounds, such as those found in G-Quarry, are not developed, but envelope grains occur in the respective stratigraphical position. Digital concretions below the ore were not observed due to inaccessibility.

2.4 Discussion

The information in the eight stratigraphical profiles can be used to generalize some primary and supergene features. Commonly, grainsize gaps between neighbouring ore units are observed which probably are indicative of short erosional events during sedimentation or an interruption of the manganese input. Such variations of the grainsize are preferred sites for increased cementation of the larger grains near the contact of two units. This fact is emphasized by the weathering profile of "softer" vertical sections in the field (e.g. G-South Quarry). Here, the cemented parts of the profile resist the erosional forces longer than the less cemented ores and as a result, cemented bands stand out and act as an aid for the detection of unit boundaries, which might otherwise be difficult to detect. Similarly, cemented and massive mangcretes are often bound to positions adjacent to sedimentation boundaries. Thus, the secondary cementation of ores by manganese oxides (also Fe phases?) is strongly controlled by grainsizes and by grainsize gaps between different units.

Other genetic information for the development of ores is found, when concretions below and above the ore and their host materials are examined. Concretionary ores are always associated with clay-rich units, either in siltstone (e.g. G), in clays (e.g. A-South), or in clayey sands near the surface elsewhere. Obviously, this type of ore does not form in "pure" sands, as is indicated by many Mn-impregnated or cemented sands which do not show the development of concretions (e.g. F1, C-138).

Open drainage systems (clay-pipes) create a similar type of geochemical environment. They are partly filled with clays and they act as conduits for fast moving oxygenated surface waters that percolate downwards. Thin layers of manganese oxides (laminar mangcrete) line these

pipes. Compared with concretionary materials, this very fine grained ore type encloses detrital products such as sand grains. The importance of oxygen in the formation of laminar mangcrete is demonstrated by the fact that the thickness of the entire unit decreases significantly down the section. The association of laminar mangcrete with kaolinitic, K-bearing clays may already point to the formation of cryptomelane, which is the dominant manganese mineral in this ore, and which is also the main K-carrier of the Mn oxides.

Ferruginous minerals such as goethite or hematite often replace manganese ores partly or totally, as seen particularly well in ores and laterites of F3- and D-Quarry and costean C-138. In many cases this replacement is found either near the orebody-laterite interface or in the lowest parts of the ore section, where clays and sands dominate. The same replacement structures exist near clay pipes and in the vicinity of clay/Fe-rich units. This finding will be discussed in following chapters on the interpretation of supergene processes which liberate manganese oxides and replace them with Fe-phases and clays.

3. Petrology and Mineralogy

3.1 Introduction

The previous chapter presented an overview over the stratigraphy of those parts of the deposit, which had been selected for detailed sampling. Below, the materials from these vertical geological profiles are examined to provide further descriptive and analytical information to assist in the interpretation of supergene mobilization and precipitation processes. Therefore, emphasis concentrates on features of secondary products supporting conclusions drawn from field observations. Detailed work by Frakes and Bolton (1984) and Bolton et al. (1988) focused on primary sedimentary aspects in the deposit.

Although it has been demonstrated that a large number of superficial ores and gangues are associated with the deposit, additional types of ores and rocks exist, which could not be incorporated into the geological profiles for technical reasons (e.g. supergene materials in pipes). Therefore, the stratigraphic setting for each material is briefly outlined or repeated in the following handspecimen descriptions. Observations on handspecimens and petrological descriptions illustrate the general appearance of ores and rocks; the discriptions are ordered in such a way that similar ore and rock types are discussed in succession. The terminology used here follows that of section 1.4.

As mentioned before, oolitic and pisolitic ores predominate over all other ore types at Groote Eylandt and laterites are the main rocks associated with the deposit. Although other ores and rocks discussed below are of minor importance in quantity, many of them are important indicators for alteration processes. Therefore, it is also necessary to examine those supergene products, which might otherwise be excluded from the description because of their scarcity.

It must also be said that though oolites and pisolites can be grouped into uncemented and cemented ores, transitional stages between both types commonly occur, so that an unambiguous description is sometimes difficult to make. The same applies for a number of other combinations of ores and gangues. Therefore, it must be kept in mind that only endmembers are discussed here to depict individual types. Relationships to other materials are mentioned where appropriate. A summary of the examined ores and rocks is presented in Tables 3.1a-c.

The X-Ray diffraction (XRD) study that follows the descriptive part of this chapter examines most of the rocks and ores, with the exception of some rocks that are of minor importance for the development of the deposit (e.g. conglomerates or sandstones). With this technique, about 90 samples were scanned for their main components, minor peaks in the spectra were also checked for trace minerals. The study by Fourier Transform Infrared Spectroscopy (FTIR), on the other hand, focuses on a single stratigraphic section (F3-Quarry) which is dominated by cemented mangcrete. With the help of this method relatively uniform ores are investigated to identify stratigraphy controlled mineralogical variations (the same suit of samples was also subject of microbiological leaching tests; see 5.5). A detailed description of the analytical techniques is provided in Appendix I. (XRD: 1.4.2; FTIR: 1.4.3); a listing of the sample specifications (ore/rock types) is given in Appendix III., Table 1.

3.2 Description of Samples

3.2.1 Uncemented ("soft") Oolite/Pisolite

Handspecimen *(Plate 3.1, Figs. 1a, b)*

With the exception of some outcropping parts of the deposit, where previous structures and textures are destroyed, uncemented oolites and pisolites occur as subhorizontal units throughout the deposit, together with their cemented equivalents. Several cycles of normal and inverse grading can be recognized in various locations and small to medium scale cross-bedding can also be identified. Locally, vertical and horizontal pipe systems cross-cut the ore and replace it with manganiferous and ferruginous supergene products and clays.

Although the ore mineralogy is relatively simple in most cases, with pyrolusite, cryptomelane, todorokite, and romanechite (romanechite) being the dominant oxide phases, more complex and structurally less well defined minerals occur in the G/G-South area (e.g. birnessite, nsutite, vernadite). Paragenetic minerals, which are probably not syngenetic, are kaolinitic clay (~ 5 - 15%) and ferruginous impregnations (~ 1 - 5%), both concentrated in the matrix. The relative proportions of these matrix materials result in ores that are black, greyish, or dark brown. The grains are spherical to ovoid, sometimes flattened, and their sizes vary between «1 mm and ~ 25 mm. Locally, the sorting can be poor or good, and occasionally, bimodal units occur.

Generally, the ores are porous, poorly consolidated, and relatively soft. Different types of cementation (Mn, Fe, clay) result in the development of mottled ores that can grade into cemented mangcretes. This type of ore thus contains the products of alteration processes overprinting the primary sedimentary material.

Microscopy *(Plate 3.1, Figs. 1c, d)*

As above, oolites and pisolites are discussed together, because they are only distinguished by an artificial size boundary. Internally, the grains are laminated concentrically and individual laminae, often less than 10µ thick, show radially and/or tangentially oriented crystallites (Bolton et al., 1988). With the exception of the G/G-South Quarry area where a number of poorly crystallized manganese oxides occur (see above), most other localities show a dominance of pyrolusite and romanechite and/or cryptomelane alternating as laminae in ooliths and pisoliths. Generally, the thickness of the laminae seems to increase in outer parts of the grains. Occasionally, abraded and truncated features (micro-unconformities) indicate erosional processes during the growth of the grains. Rarely, silt-sized detrital materials are accommodated between the manganiferous laminae.

Although ooliths and pisoliths generally do not exhibit nuclei, they occasionally contain detrital materials. Commonly, such nuclei consist of poorly rounded to angular quartz grains, reworked Mn ores (abraded ooliths/pisoliths), argillaceous materials, or cellular organic remains. The contours of these materials tend to be levelled out by a few laminae so that the overal morphology of nuclei is mostly not reflected in the shape of the ooliths/pisoliths.

The complex mineralogy of the G/G-South Quarry ores results in friable materials that are easily deformed. Ooliths show sutured contacts and compressed grains have an angular shape, less frequently they are fractured. Thus, the appearance of these ores indicates that the precipitating material must have been very friable during and after deposition. This finding strongly contrasts with the broken and dislocated outer laminae of larger pisoliths observed in other areas. In these cases, a much harder material probably formed initially, which broke under stress.

The matrix of ooliths and pisoliths often consists of extremely fine grained manganese oxides (« 5µ) of varying hardness and cementation, diffuse kaolinite impregnations, and traces of iron oxyhydroxides. However, ores with almost no matrix have also been observed (Bolton et al., 1988). Locally, quartz sand can become an important matrix component. The angular shape of these quartz grains indicates a short distance of transport, and they are also poorly sorted (size ranging between ~50 and 500µ).

3.2.2 Cemented Mangcrete (oolitic/pisolitic)

Handspecimen *(Plate 3.1, Fig. 2a)*

Cemented mangcretes are found throughout the deposit, overprinting the original uncemented oolites/pisolites to a lesser or greater extent. An exception is the mineralogically distinct area of G/G-South, where the ores are mostly unconsolidated. Stratigraphically, cemented mangcretes often develop where abrupt changes in the grainsize occur and are concentrated in the coarser-grained horizon. Primary sedimentary features, such as normal and inverse grading, can easily be distinguished. Depending on the original setting, the ores are generally subhorizontal and they form layers of varying thickness (from a few centimeters to 3 or 4 meters).

Although pyrolusite dominates this ore, the emphasis shifts towards cryptomelane, when compared with the uncemented oolites/pisolites. The crystallinity of the matrix visibly increases (coarser grains) and the samples contain less todorokite and nsutite (G/G-South Quarries). As in the uncemented ores, pipes cross-cut the units, and in places, clay occurs in the matrix. Primary grains are occasionally replaced by manganiferous and ferruginous phases.

These ores are mostly black, dark grey, or silvery grey. Individual grains are spherical to ovoid, in some cases flattened, and occasionally closely fitted polygonal grains are found, suggesting compaction during sedimentation and/or oriented cementation. The sorting is poor to good, depending on the precursor (unconsolidated material). Normally, the ores are hard and dense, but they can also grade into poorly cemented and mottled oolites/pisolites that show composite grains (small-scale cementation of a few primary grains). When wet, micro-pores in the sample matrix quickly absorb water, thus indicating that although difficult to detect in handspecimen, the material is more porous than expected. The description above already demonstrated that the origin of this ore type is secondary and that uncemented units are overprinted. However, the cementation occasionally is superimposed on all primary sedimentary features and the ore grades into a massive mangcrete, which is described below.

Microscopy *(Plate 3.1, Figs. 2b-d)*

Oolitic and pisolitic structures and textures were examined in the previous section, therefore, emphasis here is put on the manganiferous cement. The dominant mineral of the matrix is cryptomelane. Its slightly darker grey colour (brownish tint) helps to distinguish it from the bright silvery grey of the pyrolusite in the adjacent ooliths/pisoliths. Often extremely fine grained (<5μ), matrix cryptomelane tends to crystallize into larger idiomorphous crystals (200μ or more), when vacuoles are available.

Plate 3.1

Fig. 1a: Bimodal poorly cemented oolite/pisolite from G-South Quarry; sample 903-101; the scale equals 2cm.

Fig. 1b: Mottled manganiferous cementation of otherwise uncemented pisolite; matrix contains kaolinite; G-South Quarry; sample 903-77b; the scale equals 2cm.

Fig. 1c: Uncemented oolite with strongly deformed grains; G-South Quarry; darker colour: vernadite; sample 903-102; polished section; parallel polarizers; the bar equals 200µ.

Fig. 1d: Mainly uncemented pisolite; the large pisolith depicts an angular quartz grain as nucleus; the matrix contains also quartz grains, clay minerals, and minor amounts of Fe-oxyhydroxides; F3-Quarry; sample 903-10; polished section; crossed polarizers, the bar equals 200µ.

Fig. 2a: Cemented mangcrete (pisolitic) with closely fitted polygonal grains; F1-Quarry; sample 66161 courtesy of B.R. Bolton; the scale equals 2cm.

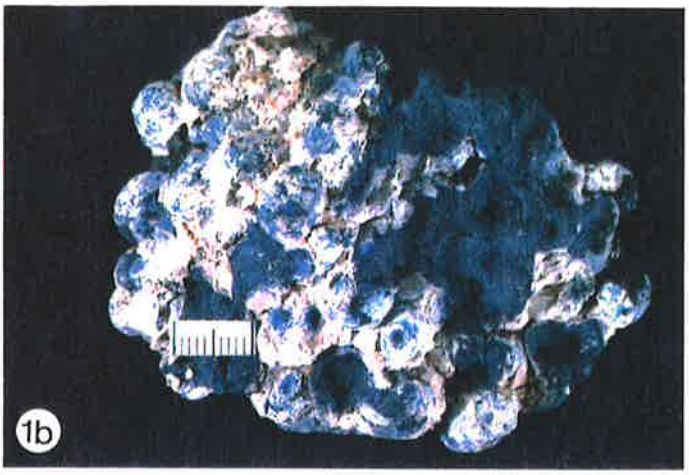
Fig. 2b: Different generations of manganese oxide cement in largely uncemented pisolite; light: pyrolusite, darker gray: cryptomelane; F3-Quarry; sample 903-6; polished section; crossed polarizers; the bar equals 200µ.

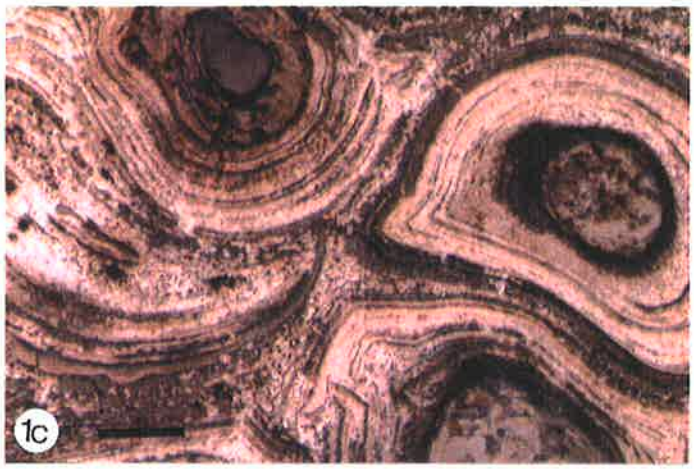
Fig. 2c: Cemented oolite; G-South Quarry; sample 903-38; polished section; parallel polarizers; the bar equals 200µ.

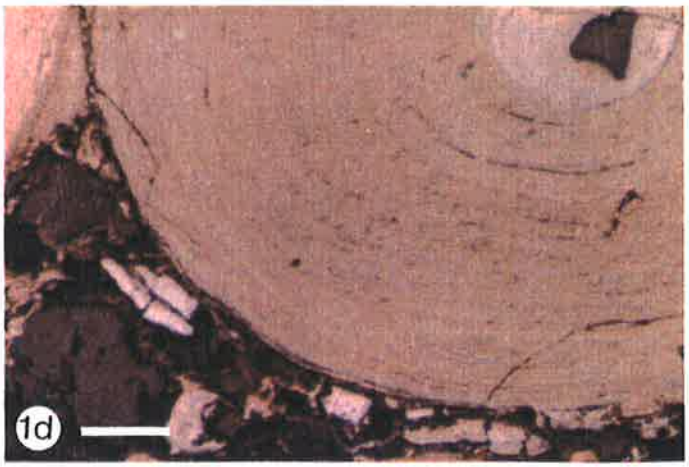
Fig. 2d: Strongly cemented oolite grading towards massive mangcrete; recrystallized ore with relic laminae of primary grain; G-South Quarry; sample 903-38; polished section; crossed polarizers; the bar equals 30µ.

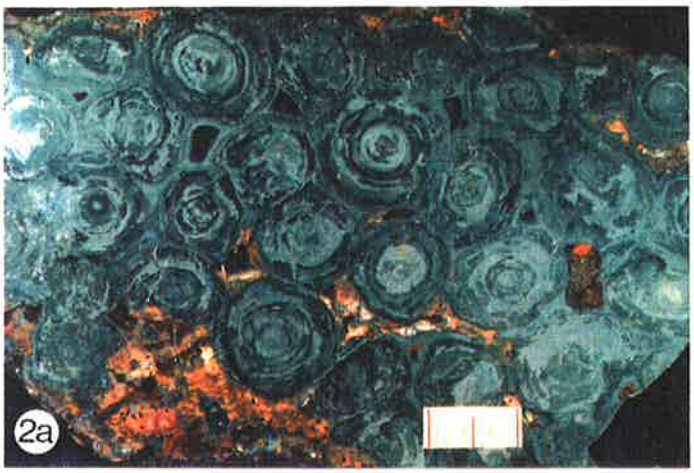
Plate 3.1

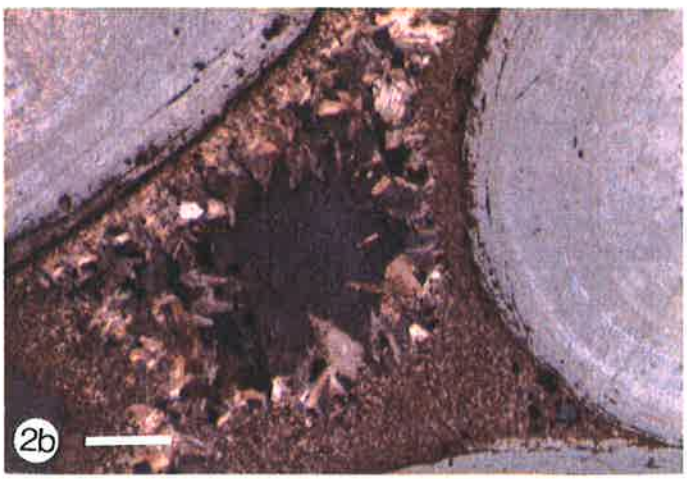


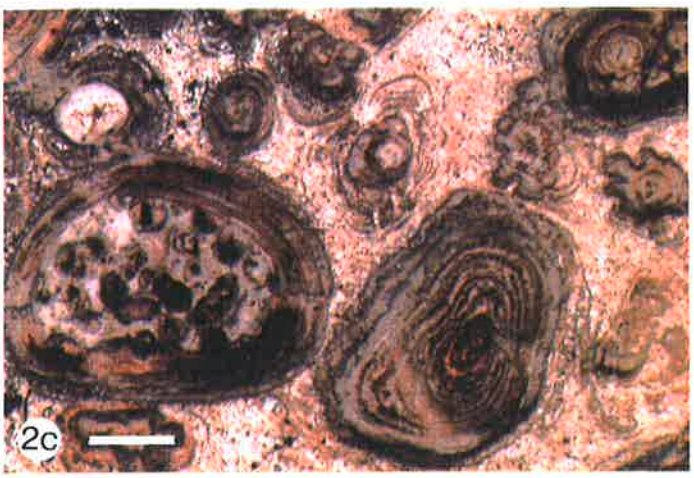


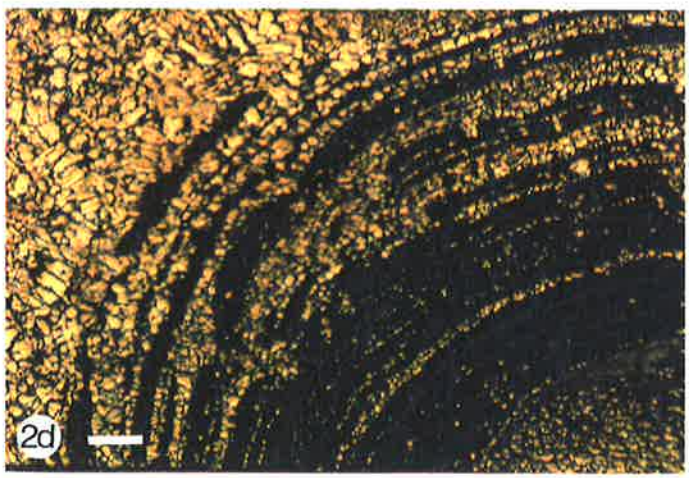












In ores influenced by supergene mobilization processes (selective removal) parallel to a strong zone of cementation, first the pores between the primary grains are filled, and later ooliths and pisoliths themselves are replaced by fine-grained matrix type cryptomelane. This leads to a massive, structureless ore, which only contains relic outlines of primary laminae.

Rarely, the matrix seems to enhance textural deformation structures, such as those of closely fitted polygonal grains. Pressure solution at contacts between grains leads to partial dissolution of ooliths/pisoliths and to successive cementation in adjoining open pore spaces. Thus, grains appear to fit closely with their neighbours.The amount of detrital material such as quartz, kaolinite, or goethite varies from sample to sample (≤ 10%). However, gangues generally do not play a vital role in cemented mangcretes. This ore type is strongly dominated by manganese oxides, both in ooliths/pisoliths and in the matrix.

3.2.3 Fe-Oolite/Pisolite

Handspecimen *(Plate 3.2, Figs. 3a,b)*

Ferruginous oolites and pisolites are observed throughout the F area and also around G- and G-South Quarry. Commonly, this rock occurs directly below the Mn orebody at the boundary with underlying kaolinitic clays, but in some cases it appears within or on top of the ore (C-138). The rock forms laterally extensive bodies and only occasionally it is found in lenses and thin layers. Generally, Fe-oolites/pisolites cut across manganiferous units and replace these partially or totally.

Ferruginous oolite/pisolite exhibits ochreous colours which are darkened by hematite. Most structures and textures observed in this rock, such as the fine lamination of ooliths/pisoliths, are identical to those found in the initial ore which is replaced. Thus, the characteristics of both uncemented and cemented Mn oolites and pisolites apply to this gangue material. Individual grains are spherical to ovoid, occasionally elongated and flattened; sorting and grading also depend upon the precursor. Grainsizes vary between 1mm and about 20mm; the full size range detected in Mn ores was not found, because these materials are rarer than their manganiferous equivalents. Bimodal units were not observed for the same reason. As with the cemented mangcretes, a harder and more dense cementation seems to concentrate where grainsize changes occur. Whether this directly reflects the initial material or whether the effect relates to actual Fe precipitation independently of the precursor, is unknown.

Normally, the material is porous and relatively soft. The mostly fine-grained matrix is relatively soft, kaolinite occurs less frequent when compared with the manganese ores. Near the surface, hematite occasionally forms a hard cement between ooliths and/or pisoliths. However,

the predominant mineral of this rock is goethite; hematite is generally much rarer. Fine secondary quartz crystals and supergene Mn phases are rarely associated with vacuoles; here, quartz shows idiomorphous crystals covering secondary manganese oxides.

Intermediate replacement stages between manganese ores and ferruginous rocks occur commonly in association with cemented mangcretes, where pyrolusite-rich ooliths/pisoliths are replaced by ferruginous materials. The cryptomelane-dominated matrix remains relatively unchanged. Such replacements can vary between negligible amounts of Fe minerals in Mn ores and a total destruction of the manganese oxides.

Microscopy *(Plate 3.2, Figs. 3c,d)*

Though ferruginous oolites and pisolites appear to be supergene replacement products, they nonetheless exhibit all primary features such as grainsize, shape, and laminae, recognizable in handspecimens and polished sections. Surprisingly, this rock type seems to enhance primary structures and textures that may have been overprinted intermittently by a prior manganiferous cementation of the material. As an example for such successive overprints a pisolith is shown which is cross-cut by ferruginous replacement products. This grain contains very dense and highly reflective manganese oxides (mainly pyrolusite), and although a fine lamination is apparent, it is weak and without much contrast. The replacing material on the other hand regained the strongly visible alternation of the laminae from the primary manganiferous grains.

Contrasting with Mn ooliths/pisoliths, the ferruginous materials do not possess the radially and/or tangentially oriented crystallites commonly observed within laminae of their manganiferous counterparts. These crystals are instead replaced with even finer, disordered particles. Nuclei were not detected in ooliths and pisoliths, but this is probably also due to the lower abundance of this rock type.

Goethite and the much rarer hematite, present in both matrix and ooliths/pisoliths, are very fine grained and individual grains are much smaller than the manganese oxides in the cemented mangcretes. Clay minerals, such as kaolinite, though present in most samples in small quantities, are difficult to discern. They blend into the ferruginous matrix as disseminated and diffuse occurrences.

3.2.4 Massive Mangcrete

Handspecimen *(Plate 3.2, Fig. 4a)*

Massive mangcrete is found in most parts of the deposit, with the exception of the G/G-South area. In places it occurs at the top of the orebody (e.g. C-138), but more frequently it is developed as subhorizontal units at the top of cemented mangcrete at various stratigraphic levels.

Massive mangcrete consists predominantly of cryptomelane and small amounts of todorokite. This ore overprints and replaces various other ores and gangues and thus, its appearance varies according to its precursor. Commonly, massive mangcrete is the final stage in the development of cemented mangcretes (compare Plate 3.1, Fig. 2d), but it was also recognized as a replacement of lateritic soils (see microscopy) or even quartz sands. The ore is dark grey to black, fine grained, and it is very hard and dense. Commonly, it contains thin subparallel horizontal veins of recrystallized cryptomelane which shows crystallites oriented vertically to the elongation of the veins (strongly reflecting in handspecimen). Although Smith and Gebert (1969) interpreted massive mangcretes to be sedimentologically controlled ore types. The gradational development from cemented mangcretes, however, and/or the replacement of various ore and gangue minerals clearly point to a supergene origin.

Microscopy *(Plate 3.2, Figs. 4b,c)*

At first sight, massive mangcretes appear as what the name implies. However, they contain a number of clues on the nature of their precursors, and are thus, valuable to understanding the formation of supergene Mn ores. The material is generally extremely fine grained (~ 1µ or slightly larger) and it contains relic detrital materials, such as quartz grains (~10-30µ) or partly replaced vermiform kaolinite (up to ~200µ long). These minerals are gradually replaced by manganese phases and in some cases only the outlines and/or cleavages are preserved (e.g. kaolinite). Occasionally, cemented mangcretes develop into massive mangcretes, when the ore is strongly overprinted by recrystallization and cementation processes, and the primary structure is partially or completely destroyed (compare Plate1, Fig. 2d).

The reflectance colour of the massive mangcrete indicates a dominance of cryptomelane, other manganese oxides have not been detected but may be present in the matrix. Horizontal dehydration cracks containing secondary Mn minerals show a sub-parallel growth of fibrous cryptomelane that crystallized perpendicular to the orientation of the crack. These fibers are up to about 150µ long and they show a common optical orientation (also in handspecimens). Fine grained and granular cryptomelane containing higher amounts of diffuse gangue minerals successively fills the remaining open spaces in cracks.

3.2.5 Massive Ferricrete

Handspecimen *(Plate 3.2, Fig. 4a)*

Massive ferricretes are much rarer than their manganiferous equivalents and they are also less abundant than ferruginous oolites/pisolites. This rock type was been observed in the F-Quarries area. Generally, massive ferricretes are laterally continuous over at least tens of meters and they are associated with Fe-oolite/pisolite. Normally this rock type consists of structureless, dense, and very fine-grained goethite. Except for occasional Mn oxide impregnations and thin manganiferous veinlets, goethite is predominant. The colour is ochre; red hematitic stains have not been recorded. This rock is of supergene origin.

Microscopy *(Plate 3.2, Fig. 5)*

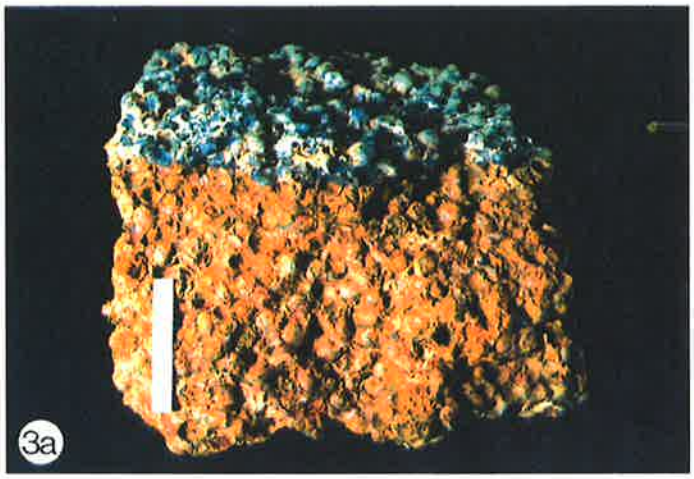
Massive ferricrete is extremely fine grained (~ 1μ or slightly larger). Since this rock does not exhibit a lamination, it appears structureless, massive, and dense. Goethite strongly dominates this material and hematite is absent. Other detrital or primary minerals, such as quartz and kaolinite, are generally subordinate in their abundance, and are easily overlooked. These minerals are finely disseminated in the matrix, they rarely concentrate in vugs. Occasionally, 10μ thick subhorizontal dehydration cracks are filled with fine grained cryptomelane. Next to these fractures, thin rims occur (~ 20 - 30μ thick) where manganiferous phases impregnate and stain the goethitic material. Associated are bleached parts with dendrite-like shapes (~ 150μ long), indicating small-scale Fe mobilization from goethite. The lighter appearance of the bleached materials suggests enrichments in kaolinite and/or other clay minerals, since hydrated or oxidized iron minerals are generally darker in colour.

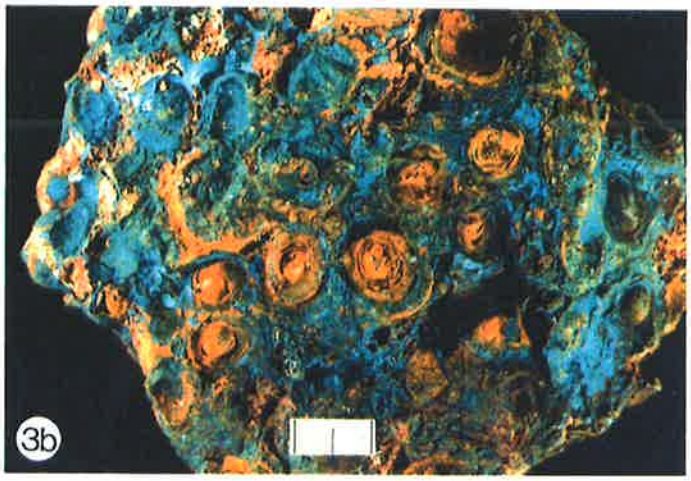
3.2.6 Hardground

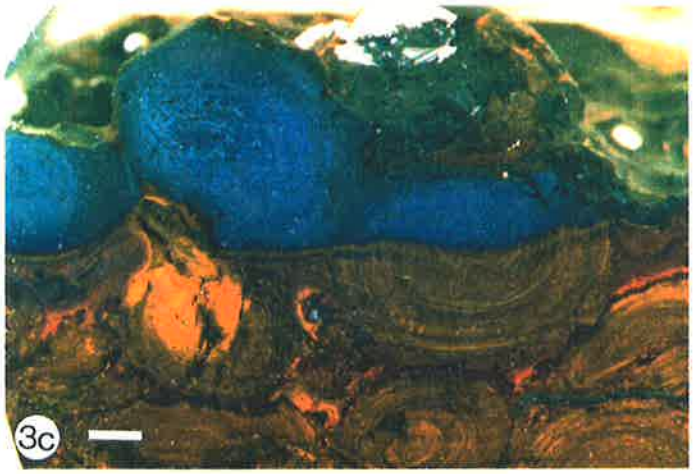
Handspecimen *(Plate 3.3, Fig. 6a)*

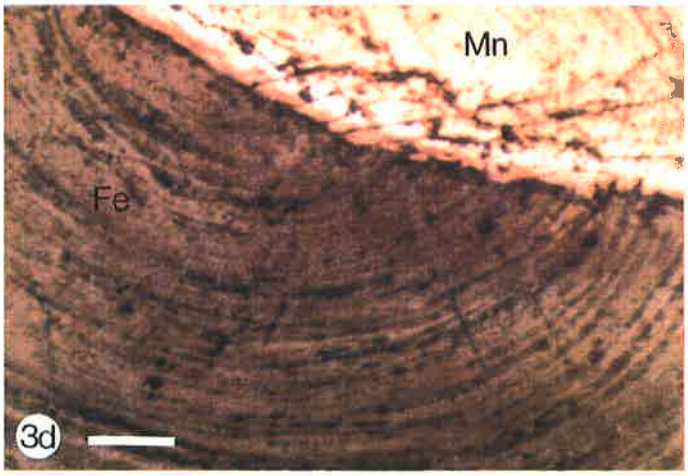
Hardgrounds are locally distributed in the G/G-South, F, and A areas, where they overlie an inversely graded pisolite. Hardgrounds are laterally continuous over tens of meters although some 4-cm-thick. The upper surface is strongly undulating probably due to erosion and exhibits structural features that resemble ripple marks. A broad subhorizontal banding is also visible. Large grains of the overlying bimodal pisolite unit are accumulated in small depressions of the hardground. Occasionally, blocky reworked fragments of Mn-oxides are observed. These characteristics indicate a primary origin. The black colour of the ore indicates that cryptomelane is dominant in the ore and that the concentration of paragenetic minerals, such as kaolinite or Fe-phases, is negligible. The ore is fine grained, hard, and dense.

Plate 3.2

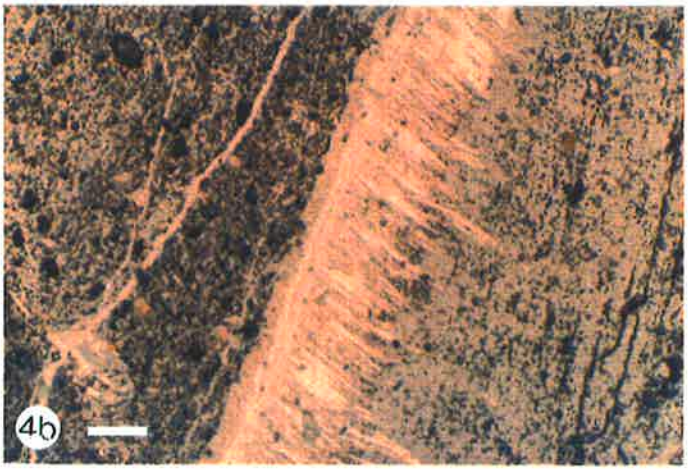


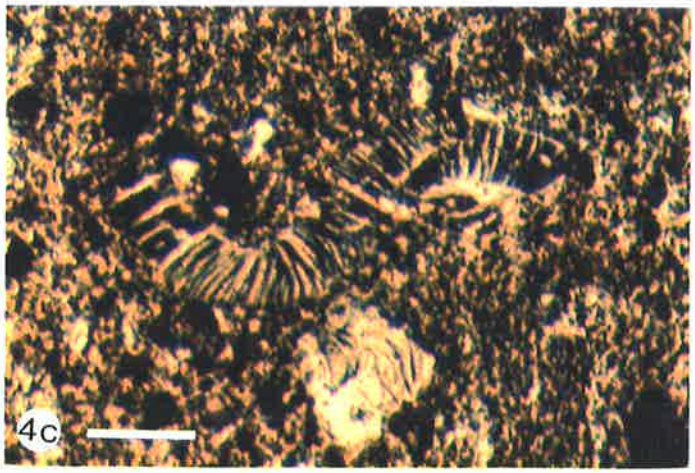


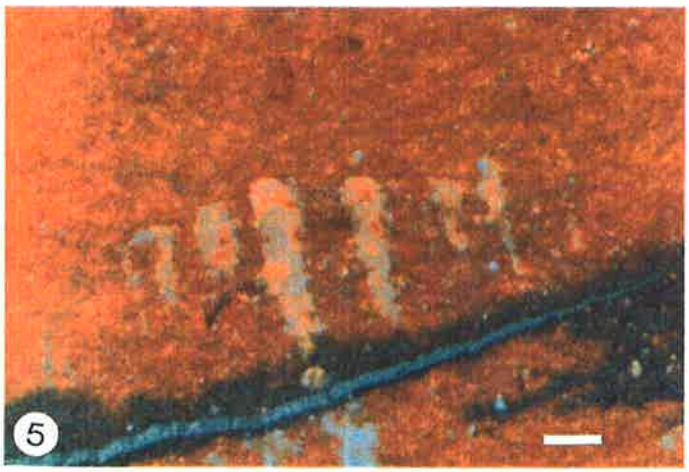












Microscopy *(Plate 3.3, Figs. 6b,c)*

In handspecimen, hardgrounds appear to be massive but show large scale banding (> 1cm). Polished sections illustrate, however, that the upper parts of the hardground possess an undulating fine sub-horizontal lamination, whereas the lower parts become increasingly more massive. Enclosed in the fine matrix (≤ 20µ) are detrital materials, such as quartz grains (~ 70µ) and other unidentified particles (rounded, varying sizes, opaque). Deformed and/or fractured ooliths are also contained in the matrix in irregular intervals. Generally, these grains are replaced to varying degrees by fine-grained manganese phases.

Hardgrounds are dominated by pyrolusite, but cryptomelane increasingly appears to gain importance in patches. The minerals can be distinguished by their reflectance colour (pyrolusite: bright grey, cryptomelane: yellowish grey) and their grainsize. Pyrolusite reaches grainsizes of about 20µ; cryptomelane on the other hand is much finer grained (~ 5µ) and replaces pyrolusite-rich parts of the ore. Thus, cryptomelane overprints and destroys previous minerals, structures, and textures.

3.2.7 Envelope grain

Handspecimen *(Plate 3.3, Fig. 7)*

Envelope grains are restricted in their distribution to the G/G-South area. Stratigraphically, they occur approximately at the same level as the hardground described above, that is, at the top of an inversely graded pisolite unit.

The ore consists of a crudely laminated envelope of fine grained material containing tabular fragments of cemented mangcrete (oolitic/pisolitic). The general appearance of this material is comparable to the hardground, but individual specimens do not exceed a length of some 20 cm. The shape of the envelope grains is round to elongated ovoid, occasionally with angular margins. Apart from cryptomelane, no other ore minerals have been identified. Cryptomelane colours the ore a lustreless black. Envelope laminae are generally dense, whereas spaces between ooliths/pisoliths can partly be empty. Often, the exterior of envelope grains is coated with kaolinite.

Although the features and structures of envelope grains point to primary sedimentary development perhaps initially within hardgrounds, a secondary origin similar to concretionary growth cannot be excluded totally. It has already been demonstrated that the formation of massive mangcrete can result in structureless ores that replace almost any precursor. In such a case, a local geochemical micro-environment (early diagenetic and/or supergene) may well have developed concretion-like ores that enclose existing materials (compare 3.2.13, concretion).

3.2.8 Laminar Mangcrete

Handspecimen *(Plate 3.3, Figs. 8a,b)*

Generally, the distribution of laminar mangcretes is not restricted to specific ore types, and thus, this ore can be identified in almost any locality within the deposit. However, depending on the geochemical environment of the surrounding ores, laminar mangcretes vary in their development and they can be overlooked in places where they consist solely of thin coatings in vugs.

In most cases, however, this ore type lines the outer boundaries of vertical and horizontal pipe systems and is much less apparent in vugs. In pipes, laminar mangcrete decreases strongly with increasing depth. This fact points to an effective geochemical control (oxygen) over the formation of laminar mangcrete, and it is supported by observations from D-Quarry, which exhibits large numbers of vertical pipes that contain little or no laminar mangcretes. Here, the orebody underlies extensive laterites and the abundance of laminar mangcrete is thus negligible.

Thick crudely laminated ores can also be found near or at the surface, where the orebody crops out (e.g. in the east of G-Quarry, K-deposit in the south of the island). Here, environmental factors lead to the development of karst features. In this manganese karst, where open drainage channels (up to 1m wide and ~ 0.5m high) are lined, the higher walls are covered with an extensive layer of laminar mangcrete (cm), whereas the coating at the bottom is relatively thin (mm).

As the name suggests, laminar mangcretes consist of subparallel layers of manganese phases. Individual laminae range from about a centimeter in karst materials to much less than a millimeter in vugs. There is a dominance of cryptomelane over other manganese oxides. Paragenetic minerals are quartz and kaolinite. Goethite and hematite are associated with the laminar mangcrete of pipes, where ferruginous cementations are seen as supergene cements. Often, the ore is fine grained, hard, dense, and well cemented. A description and a generalized model of the entire suite of secondary products of a clay pipe is presented in the experimental section (Figs. 7.1a-d).

Microscopy *(Plate 3.3, Fig. 8c)*

Laminar mangcretes in clay pipes are generally fine grained (≤ 10μ) and they show a thin lamination throughout (20-40μ thick), which outlines the surface of underlying materials. Laminar mangcrete consists mainly of cryptomelane enclosing dispersed detrital materials, such as quartz grains (≤ 200μ, rounded), kaolinite, goethite, and hematite. Occasionally, relic ooliths/pisoliths are also incorporated.

Plate 3.3

Fig. 6a: Hardground below bimodal pisolite unit; undulating surface collects larger grains in depressions; broad banding; G-Quarry; sample 903-78b; the scale equals 3cm.

Fig. 6b: Enlargement of hardground; note oolith partially replaced by Mn oxides; oolith shows deformation structure and fracture; note cryptomelane (very fine grained, yellowish) replacing pyrolusite (coarser, gray); G-Quarry; sample 903-78b; polished section; crossed polarizers; the bar equals 100μ.

Fig. 6c: Contact of hardground to overlying bimodal pisolite unit; quartz grains and kaolinite in matrix; G-Quarry; sample 903-78b; polished section; parallel polarizers; the bar equals 200μ.

Fig. 7: Envelope grain; note cemented pisolite surrounded by dense Mn oxides; G-South Quarry; sample 903-312; the scale equals 2cm.

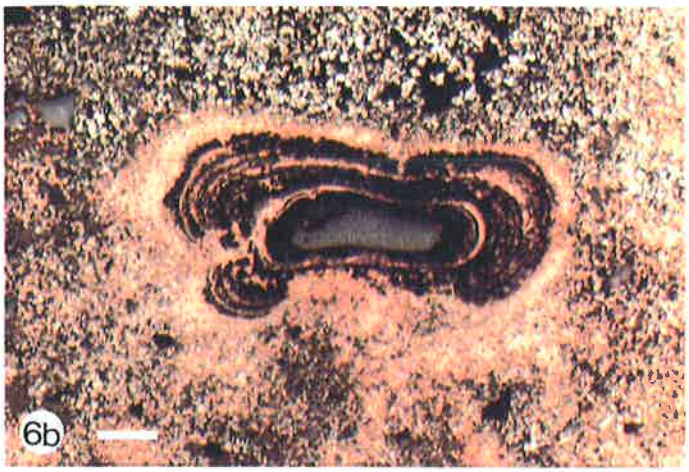
Fig. 8a: Laminar mangcrete developed on cemented pisolite; note thin cover of Fe-pipe wall; F3-Quarry; sample 66167 courtesy of B.R. Bolton; the scale equals 2cm.

Fig. 8b: Outcrop of orebody; development of Mn karst features; east of G-Quarry; the camera cap equals 5cm.

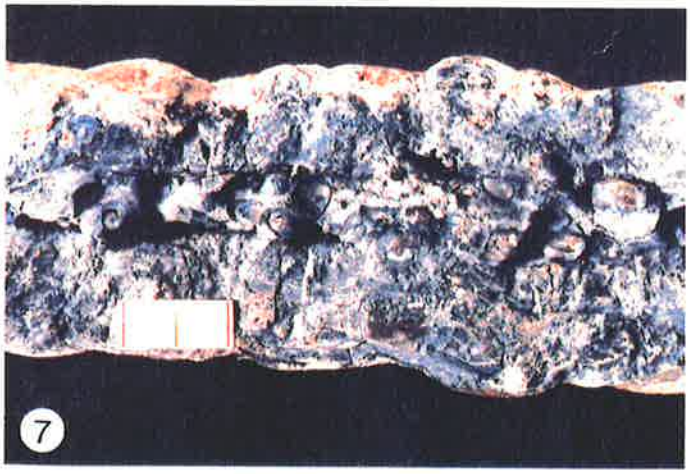
Fig. 8c: Enlargement of laminar mangcrete containing quartz grains;F3-Quarry; sample 903-16; polished section; parallel polarizers; the bar equals 200μ.

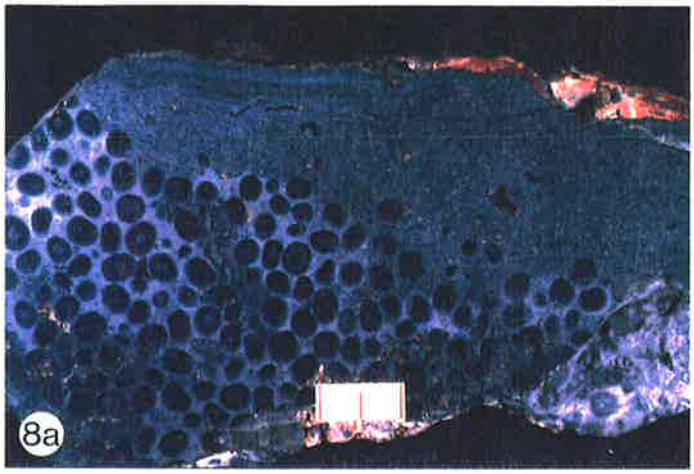
Plate 3.3



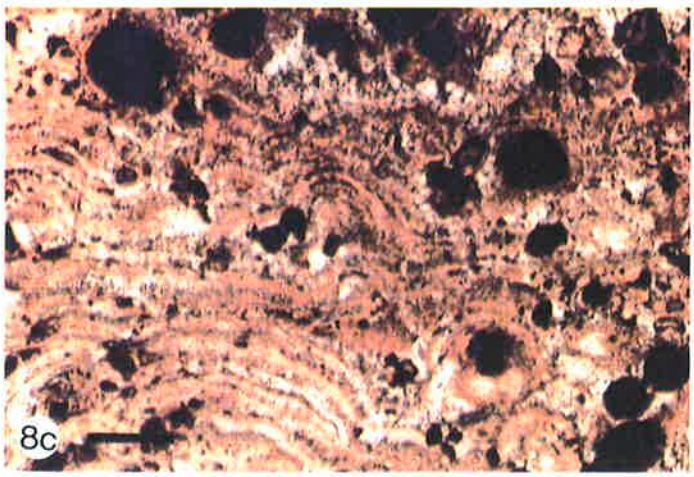












3.2.9 Manganese Cave Pearl

Handspecimen *(Plate 3.4, Fig. 9a)*

The occurrence of manganese cave pearls is limited to solution channels near the surface in the manganiferous karst materials of K-deposit (southern sub-basin; see Fig. 1.1). These channels are irregular open structures that allow a fast water movement. Accumulations of hundreds of of loose cave pearls are found in depressions at the bottom of the channels.

Although cave pearls do not resemble laminar mangcrete at first sight, they are comparable in their internal structure. When opened, a fine concentric lamination is visible outlining the pebble-sized nucleus. All examined samples contain this large nucleus, generally consisting of an Mn-impregnated sandstone or quartzite. The nucleus often comprises about half of the diameter of individual grains. Coarse quartz grains are also embedded in the laminae. The shape of cave pearls varies from round to elongated and flattened, and they reach sizes up to about 8 cm. Generally, the sorting within an accumulation is poor. This ore has a relatively low density. The dull and lustreless black colour of the material indicates that cryptomelane is the main manganese mineral, other Mn-oxides cannot be discerned.

Microscopy *(Plate 3.4, Figs. 9b,c)*

In polished section it becomes even more evident that cave pearls are comparable to laminar mangcrete. Throughout the very fine grained manganiferous matrix, detrital quartz grains are diffusely disseminated. In contrast to laminar mangcrete, however, the concentric laminae outlining the substrate (nucleus) of cave pearls are strongly disrupted by abrasional processes. This indicates a high transport energy; generally angular quartz grains additionally suggest a short transport distance. Obviously, the precipitation processes that are responsible for the formation of manganese cave pearls are physically much more active than processes in the pipes.

The fine grained nature of the manganese phases in cave pearls hinders the determination of the mineralogy, but the reflectance colours of the manganese phases (bright grey, yellowish) indicate that both pyrolusite and cryptomelane are present in approximately equal quantities. Relatively high amounts of other fine grained detrital materials (undetermined) are also evenly distributed within the matrix.

3.2.10 Spherulite (manganiferous)

Handspecimen *(Plate 3.4, Fig. 10a)*

Spherulites occur in laterally continuous beds over large areas throughout the deposit and are found in all places above the deposit where soils exist. The formation of karst seems to inhibit the development of spherulite. This ore type is purely pedogenic (forms only near the surface), although vertical pipes and sinkholes have been observed to introduce spheruliths into deeper parts of the section. The size of the spheruliths ranges between some millimeters and a few centimeters and they are of rounded, irregular shape. Further down the section the grains tend to form concretionary bodies. Poorly crystalline Mn phases together with iron oxyhydroxides colour the spherulite dark brown, thus masking large amounts of cemented detrital materials, such as quartz grains. Mostly, the spheruliths have a low density and they are relatively soft.

Microscopy *(Plate 3.4, Fig. 10b)*

Spheruliths possess a poorly defined colloform concentric banding that varies considerably in thickness. The laminae of spheruliths resemble those of Mn cave pearls or laminar mangcrete, but their spacing is much wider than in those ores. As in cave pearls, large amounts of detrital quartz are incorporated in the matrix. Goethite and hematite are very fine grained and it is often difficult to distinguish individual grains. Quartz grains on the other hand show a large range of sizes from approximately 50µ to some 500µ; reworked manganese ores were observed in sizes up to several centimeters. Clay minerals also appear in small quantities in the matrix, but their distribution is diffuse and they are often hard to detect. All detrital materials, with the exception of kaolinite, are angular to sub-angular, thus indicating short transport distances.

3.2.11 Fe-Pipe Wall

Handspecimen *(Plate 3.3, Fig. 8a; see upper contact of laminar mangcrete)*

Ferruginous pipe walls are distributed throughout the deposit but is limited to places where clay pipes are developed. This rock is structureless and has a fine grained matrix. Its appearance varies from soft and diffuse Fe impregnations to hard and massive goethitic/hematitic cementations of relic ores and gangues. The name of the Fe-pipe walls implies their association with supergene clay pipe systems and thus the rock is also of secondary origin.

Microscopy *(Plate 3.4, Fig. 11)*

In polished section Fe-pipe walls often look similar to spheruliths, but this rock lacks the broad lamination observed in the soil spheruliths. Goethite and hematite are extremely fine grained, and it is often difficult to detect individual hematite grains in the section, although the red and pink colouration of the rock results from an even distribution of very fine grained hematite (it will be shown in chapter 5 that, nevertheless, goethite dominates over hematite). Quartz is much coarser and generally well rounded, but it does not depict the same strong size variations (50 - 200μ) as the spherulite.

3.2.12 Radial Pyrolusite

Handspecimen *(Plate 3.4, Fig. 12a)*

Radial pyrolusite is only observed in the G/G-South area, where it occurs at the top of the ore-body and at a second level approximately 1.5 to 2 m deeper down the section. Its upper surface strongly undulates and thus indicates erosion, its base is subhorizontal. Both boundaries are sharp, and the ore laterally extends over tens of meters.

Perpendicular to the thin horizons (~ 2cm), elongated prisms of silvery pyrolusite are set in a fine grained matrix of dark grey pyrolusite. The paragenetic minerals kaolinite and iron phases are often concentrated directly below the ore unit. Radial pyrolusite is usually well cemented and hard, but it breaks parallel to long axes of the crystals. The upwards oriented growth of pyrolusite that seems to cut across primary materials indicates its secondary origin.

Microscopy *(Plate 3.4, Fig. 12b)*

The large sub-parallel pyrolusite crystals (1-2 cm long) of this ore type are intergrown with each other and thus, they develop irregular feathery shapes. The crystals are strongly pleochroitic and their colours range from a yellowish grey to an intense blue. Throughout this dense ore, detrital materials are evenly distributed. The brown reflections of these small grains (30-70μ) indicate ferruginous minerals such as goethite. Kaolinite is probably also present, but clay minerals are generally hard to determine when they occur as indistinct small grains.

A close examination of radial pyrolusite reveals that the precursor of this ore type is an oolite. Although most ooliths are entirely recrystallized and destroyed, some ghost structures remain. Such relic ooliths contain a fine grained and structureless pyrolusite, which enables a differentiation of the primary shapes from the superimposed acicular pyrolusite. Only the outlines of the

Plate 3.4

Fig. 9a: Mn cave pearls;K deposit; samples 903-344; the scale equals 2cm.

Fig. 9b: Enlargement of cut cave pearl; note large Mn-impregnated sandstone/quartzite nucleus; K deposit; samples 903-344; the bar equals 0.5cm.

Fig. 9c: Enlargement of cave pearl lamination; note detrital quartz grains incorporated in laminae; K deposit; samples 903-344; polished section; parallel polarizers; the bar equals 200μ.

Fig. 10a: Separate spheruliths; G-Quarry; sample 903-327; the scale equals 2cm.

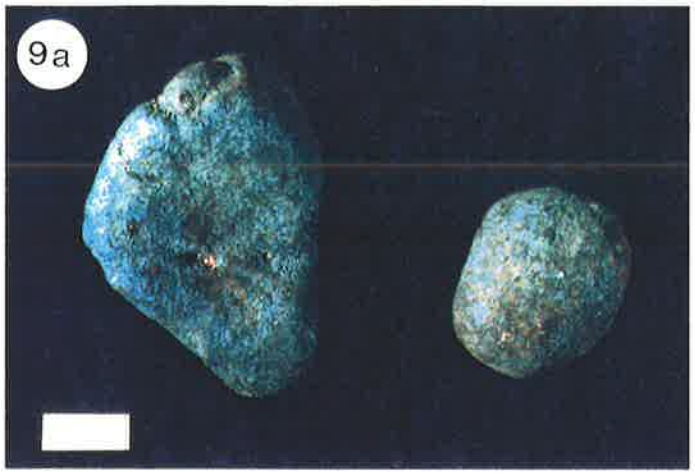
Fig. 10b: Enlargement of cut spherulith; note coarse lamination and the cementation of detrital materials; F3-Quarry; sample 903-30; polished section; partially crossed polarizers; the bar equals 200μ.

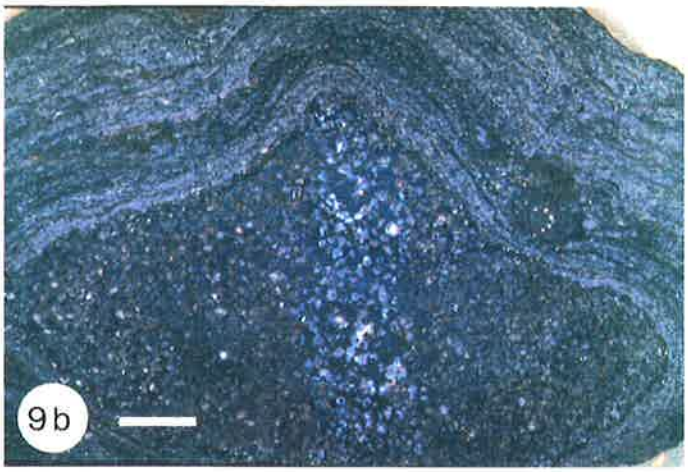
Fig. 11: Contact betweenFe-pipe wall and laminar mangcrete; F3-Quarry; sample 903-16; polished section; partially crossed polarizers; the bar equals 200μ.

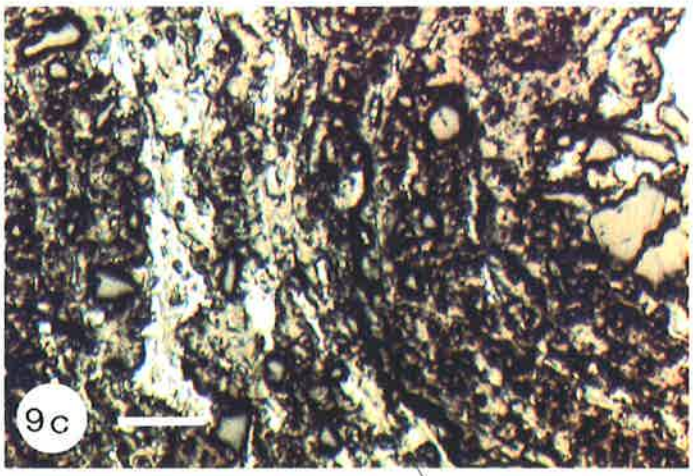
Fig. 12a: Radial pyrolusite; G-South Quarry; sample 903-63; the scale equals 2cm.

Fig. 12b: Enlargement of radial pyrolusite; note relic oolith within sub-parallel pyrolusite crystals; G-South Quarry; sample 903-63; polished section; crossed polarizers; the bar equals 200μ.

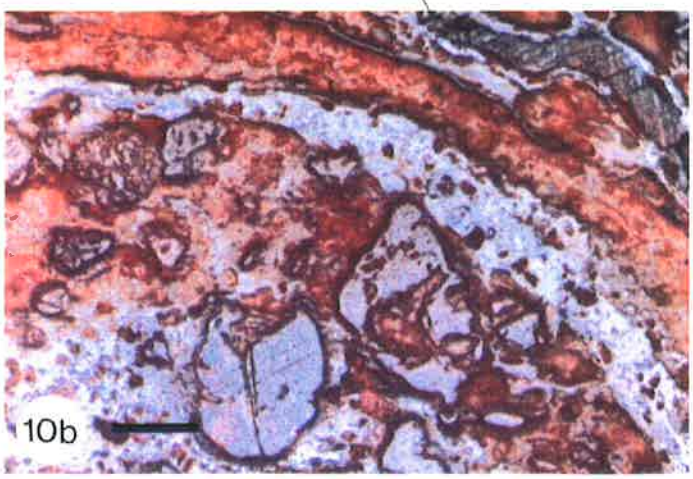
Plate 3.4

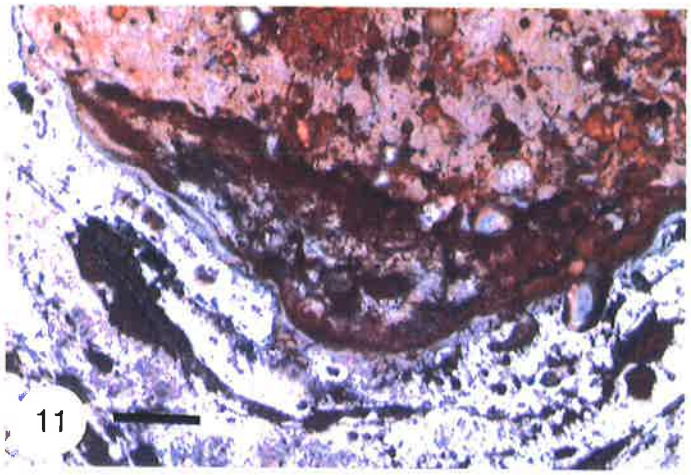


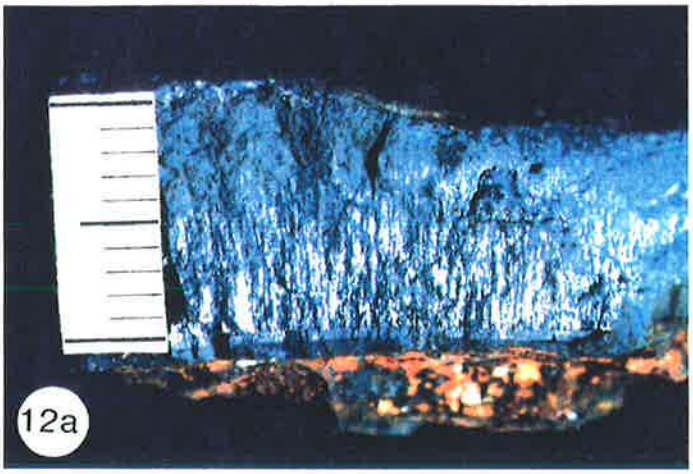


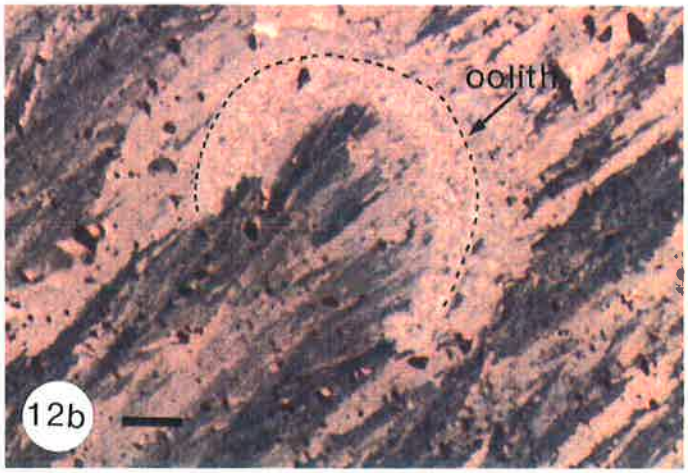












relics are visible and in some cases prismatic pyrolusite "perforates" the ooliths, leaving the shell-like structures of the outer laminae.

3.2.13 Siliceous Ore

Handspecimen *(Plate 3.5, Fig. 13a)*

Siliceous ore is distributed in varying quantities throughout the deposit and is even found in minor amounts in the G/G-South area, although this location generally favours the formation of different types of ore. The units are subhorizontal and often they occur in lower parts of the orebody, sometimes cementing underlying sands. The ores are structureless and massive; occasionally they contain recrystallized Mn phases.

Cryptomelane and pyrolusite dominate the manganese mineralogy, but the dark and mostly lustreless colour probably indicates a higher abundance of cryptomelane. Vugs are filled with kaolinite, quartz sand, and goethite. The matrix of siliceous ore is generally fine grained and dense. In places, the manganiferous cementation can be observed to gradually increase from essentially Mn-free quartz sand to highly cemented siliceous ore.

Microscopy *(Plate 3.5, Fig. 13b)*

Siliceous ore can best be examined in partially cemented quartz sand/sandstone that has not yet undergone a complete recrystallization. Often, sand grains are partially covered with fine prismatic felt-like manganese oxides that radiate into open pores. It is difficult to determine the mineralogy of these needles under the microscope because the crystals are so small (<10µ long, <1µ thick), but XRD determinations show cryptomelane and pyrolusite (see Fig. 3.19a, sample 903-254).

Occasionally, pores of the sand/sandstone are filled with cryptocrystalline manganese phases which possess a high reflectance and which show multiple nuclei (diameter: ~ 50 - 300µ) with radially oriented fibers. These crystallites suggest rapid precipitation from manganiferous gels with many crystallization nuclei. Individual crystallization areas commonly have sharp boundaries with their neighbours and this results in a mosaic-like texture. Slower precipitation rates are indicated on the other hand by the formation of separate crystals, as described above. Depending on the type of sand/sandstone which is cemented by the manganese minerals, the quartz grains vary in their size from 50 to about 500µ in diameter, and they vary from angular to rounded.

3.2.14 Concretions (surface)

Handspecimen *(Plate 3.5, Figs. 14a-c)*

Concretionary ores were identified in numerous localities of the F-, A-South, and G-Quarry areas. However, they seem to be missing in the southern areas which possess extensive laterites covering the orebody (D-Quarry). Concretions occur both on top of the ore and below. Because there are significant differences between these two types, they are discussed separately. In this section, concretions from near the surface are examined.

Stratigraphically, the ore horizons occur above the ore and below the soil, they are also found at the surface. Concretions are generally associated with clay-rich materials and they show an upwards oriented irregular growth. When opened, these ores reveal colloform structures and dehydration cracks that are either open or partially/totally filled with recrystallized manganese minerals. Hollow centers occasionally contain small amounts of clay or sand.

The dull and lustreless colours of these ores indicate cryptomelane as the dominant manganese phase. The concretions usually range in size between a few centimeters to some 30 cm and they become larger with increasing depth. This ore type is very hard and dense. The structural appearance classifies the concretionary ores as supergene materials.

Microscopy *(Plate 3.5, Fig. 14d)*

Concretions that developed near the surface generally possess colloform banding and structures that reflect their formation from metalliferous gels. Generally, the ores are very fine grained (<10μ) and they enclose small to large amounts of detrital materials from the rocks in which they developed, such as sand grains and dispersed clay minerals. However, in most cases the detritus is of minor importance, when compared with the spherulites that are dominated by the incorporated gangues.

As can be expected from ores that originate from gels, the concretions frequently show dehydration cracks containing recrystallized manganese oxides. These thin bands contain much less detrital material than the surrounding material, they are "cleaner", and thus, their reflectance is brighter. Such precipitates probably indicate a small-scale redistribution of Mn within individual concretions. In contrast, wider cracks occasionally accommodate clay-rich or ferruginous products mixed with manganese oxides (contacts to surrounding rocks?). These parts have a lower reflectance than the main matrix. Cryptomelane is the only manganese mineral identified in all examined concretions.

Plate 3.5

Fig. 13a: Siliceous ore; D-Quarry; sample 903-340b; the scale equals 2cm.

Fig. 13b: Mn-impregnated sand; note extremely fine grained matrix and radial fibres; Costean 138; sample 903-190; polished section; crossed polarizers; the bar equals 200µ.

Fig. 13c: Mn-impregnated sand; note free Mn oxide crystals radiating into open pore spaces; Costean 138; sample 903-178; thin section; crossed polarizers; the bar equals 50µ.

Fig. 13d: Mn-impregnated sand; note Mn oxides cementing and partially replacing quartz grains; Costean 138; sample 903-190; polished section; crossed polarizers; the bar equals 50µ.

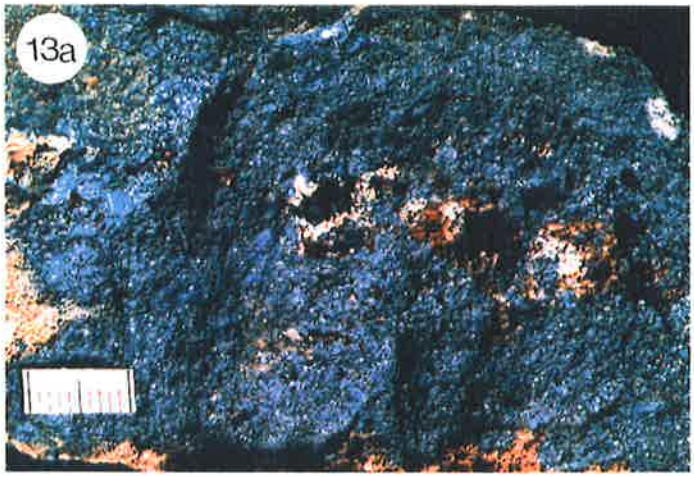
Fig. 14a: Concretion from near the surface; A-South Quarry; sample 903-330; the scale equals 2cm.

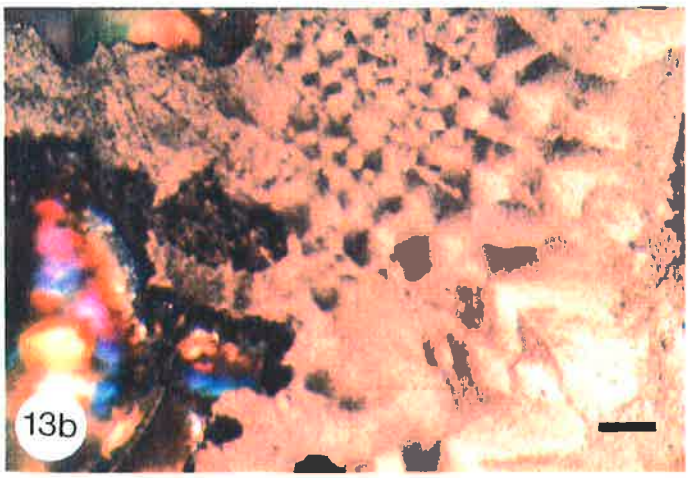
Fig. 14b: Felt-like cryptomelane needles in dehydration crack of concretion; A-South Quarry; sample 903-341c; the bar equals 1mm.

Fig. 14c: Cut concretion (compare Fig. 14a); A-South Quarry; sample 66160 courtesy of B.R. Bolton; the scale equals 2cm.

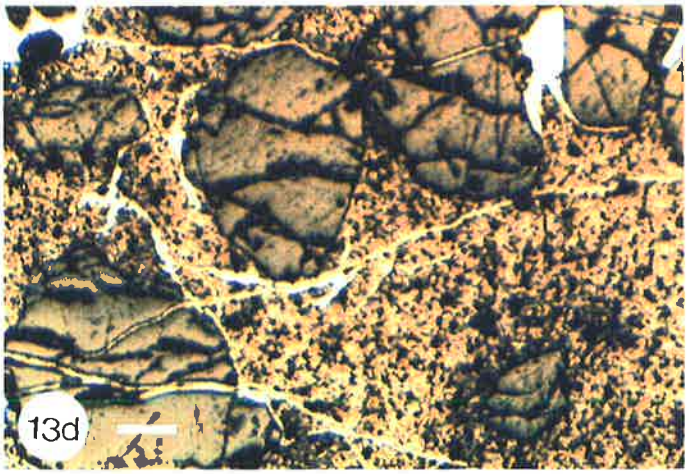
Fig. 14d: Enlargement of concretion from near the surface; note colloform textures; A-South Quarry; sample 66030 courtesy of B.R. Bolton; the bar equals 200µ.

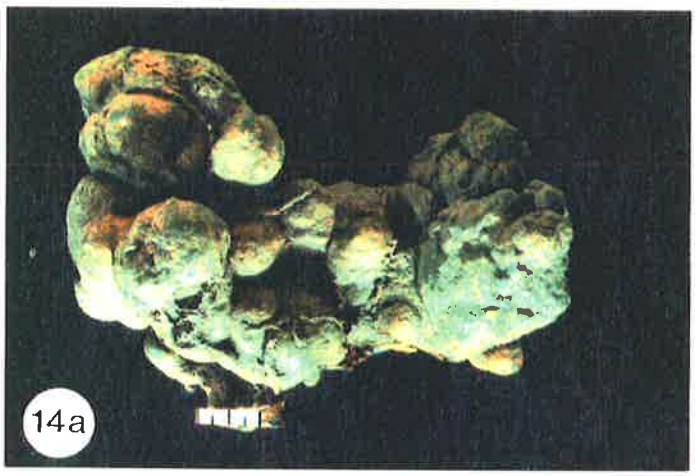
Plate 3.5

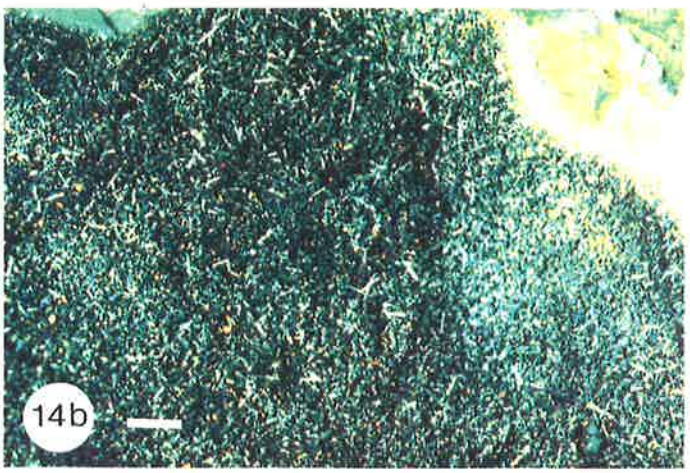


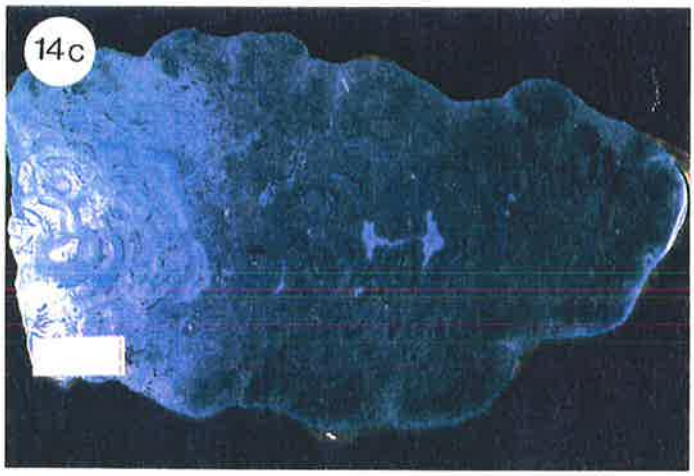


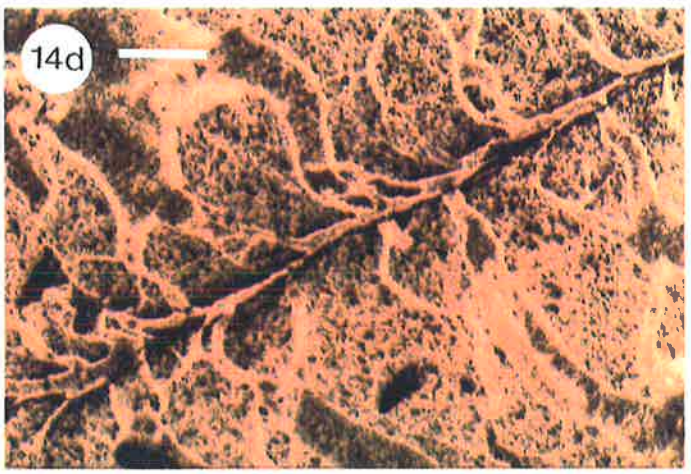












3.2.15 Digital Concretions (below ore)

Handspecimen *(Plate 3.6, Figs. 15a,b)*

Digital concretions are well developed in the G-Quarry area, where they occur below the main orebody, but they are also found in the A and F quarries. The concretions are coral-like, their growth is oriented upwards, and they increase in diameter upwards. When cut along their vertical axis, they resemble manganese dendrites (~ 10 cm long). Digital concretions mainly consist of cryptomelane; they are black, dense and hard.

This ore type originates from thin sand layers within siltstone underlying the orebody. The sand obviously acts as a conduit for solutions carrying manganese, and from here the growth of the Mn digits starts. The siltstone itself seems to be pressed away, thus suggesting supergene formation. Red hematitic stains around the concretions change their mineralogy towards hydrated yellow iron phases (e.g. goethite). Occasionally, dehydration cracks are observed in the thicker parts of the digits.

Microscopy *(Plate 3.6, Fig. 15c)*

In many aspects digital concretions from below the ore are similar to the previously examined concretions that overly the orebody. However, digital concretions contain much less detrital materials and they thus appear homogeneous. The ore is very fine grained and it is often impossible to distinguish boundaries between separate mineral grains. A coarse colloform banding is found in most digits, which seems to have accumulated fine dust-like products (unidentified) between the laminae. Quartz grains (mostly <300μ) that were incorporated during the growth of the concretions occasionally show dissolution and replacement features. Relatively few dehydration cracks can be found and these are mainly unmineralized.

3.2.16 Laterite (ferruginous/manganiferous)

Handspecimen *(Plate 3.6, Figs. 16a,b)*

Laterites cover most areas of the deposit, except for localities with outcropping ores. Depending on the basement topography, the laterites tend to increase in thickness from east to west. The greatest thickness was recorded in D-Quarry (15 - 20m). Laterites generally underly spherulitic soil layers sub-horizontally and they occur in most cases directly above the ore.

Near the surface laterite frequently exhibits diffuse Mn cementation that results in a darker colour than in the underlying material. A common feature that all laterites show to varying

degrees is a small-scale bleaching of the oxidic ferruginous parts of the rock (brown to white/ greenish), which causes a mottled appearance. Horizontal and vertical drainage systems (pipes) are usually well developed in the laterite and they can be up to 0.5 m in diameter. Often, typical laterite minerals, such as kaolinite and Fe-oxyhydroxides, invade the orebody through these pipes. Kaolinite dominates over all other minerals (goethite, hematite), although brown or black colours of the laterite seem to imply a dominance of ferruginous or manganiferous phases. Minor amounts of quartz sand in pockets and conglomerate lenses are also associated with laterites.

In many places laterites replace manganese ores and thus, relics of cemented ores and/or ooliths and pisoliths are still visible. Occasionally, vertical columns of dark materials are observed in a matrix that essentially consists of clay (compare chocolate ore; see also Plate 2.1, Fig. 2c). The degree of cementation and the colour (white, yellow, brown to red-brown, brown-black) depend on the presence of manganese and iron phases. Due to their clay-dominated nature, laterites are generally very fine grained. However, relics of ore precursors may give the rock a coarser appearance. Laterites are of secondary origin.

Microscopy *(Plate 3.6, Fig. 16c)*

The examination of the laterites also includes the chocolate ores, because these rocks are related in their development. The predominantly kaolinitic clays are often stained with extremely fine grained goethite or hematite. These impregnations are irregular in shape and they result in a mottled appearance. Most laterites contain angular to rounded detrital quartz of varying size.

All laterites contain residual manganese oxide ores, although these are difficult to detect in many cases. Commonly, the ores are replaced by goethite/hematite or kaolinite. However, in places ooliths and pisoliths are only partially replaced, or their shape is preserved (see hand-specimen; Plate 3.6, Fig. 16b), and these grains present valuable clues for the understanding of supergene mineral reactions.

Relic manganiferous grains are generally surrounded by ferruginous stains which can themselves be replaced by kaolinite. Because the replacement process does not destroy primary structures, primary concentric laminations are still visible in the kaolinitic material. In the laterites and chocolate ores all stages of this process are manifest. However, the order in which the grains are replaced is vital, and it must be kept in mind that the final step, from iron phases to kaolinite, depends on the first stage, in which manganese oxide are replaced by iron precipitates. A direct mineral reaction of the type manganese oxide to kaolinite has not been detected in the laterites and associated products of the Groote Eylandt deposit.

3.2.17 Chocolate Ore

Handspecimen *(Plate 3.6, Fig. 17)*

Chocolate ores are immediate precursors of laterites and thus, they occur in most places where laterites are developed. However, they appear stratigraphically between the manganese orebody and "pure" laterite as intermediate alteration products of ores. Chocolate ores are normally irregular in their shape, they occur in small patches, larger sub-horizontal bodies, or in vertical columns that can be several meters high. This "ore" represents a heterogeneous mixture of different types of manganese ores, depending on the respective locality, with high amounts of kaolinite and hematite/goethite in the fine grained matrix (compare Plate 3.6, Fig. 16c). The material is dark brown, soft and brittle, and it has a relatively low density. As with laterites, pipes are common (and essential) features of chocolate ores. This material is a supergene product.

3.2.18 Clay

Handspecimen *(Plate 3.6, Fig. 18)*

Next to the manganese ores, clays of different origins are the most common minerals in the deposit. They are laterally continuous over extensive areas, either in the laterites that overlie the orebody, or as thick sub-horizontal layers underlying the ore and capping the bedrock (e.g. as claystone/siltstone in the G-area). Clays are also dominant phases in pipes, where pedogenic features such as subhorizontal layering are occasionally observed.

The main clay mineral is kaolinite. However, small deposits of montmorillonite have been recorded in the A-South area, and nontronite has been described recently (this material was not available during the present work). The rocks are clay to silt sized and show white, greenish, yellow, brown, and pink colours. Secondary kaolinite often impregnates many ore units. Usually, relatively coarse quartz grains are dispersed in the clay matrix or they are accumulated in thin subhorizontal layers. Concretionary manganese oxides frequently develop within claystones and clay-rich horizons. The rocks are generally soft and friable, but occasionally harder cementation by Mn and Fe phases occurs. Clay/claystone units can be of both primary and secondary origin and without additional geological information it is often impossible to discern the mode of their development.

3.2.19 Soil

Soils are encountered in all parts of the deposit, with the exception of areas with outcropping ores and the successive development of Mn karst which is rare. Their distribution is irregular,

Plate 3.6

Fig. 15a: Siltstone containing digital concretions from below the main orebody; note upwards oriented growth, decolouration of hematitic stains next to digits, and porous sand layer from which the concretions start to grow; G-Quarry; sample 903-163; the scale equals 2cm.

Fig. 15b: Concretionary growths from below the main orebody; same stratigraphic level as material from Fig. 15a; G-Quarry; sample 903-288; the scale equals 2cm.

Fig. 15c: Enlargement of digital concretion in siltstone matrix; note colloform banding and occasional quartz crystals; G-Quarry; sample 903-164; the bar equals 2cm.

Fig. 16a: Manganiferous laterite; from near the surface; F3-Quarry; sample 903-29; the scale equals 2cm.

Fig. 16b: Ferruginous laterite below Mn laterite (Fig. 16a); note the various stages of Mn replacement by goethite and kaolinite; D-Quarry; sample 903165a; the scale equals 2cm.

Fig. 16c: Ferruginous laterite; note partially replaced Mn pisolith; D-Quarry; sample 903-166b; polished thin section; the bar equals1mm.

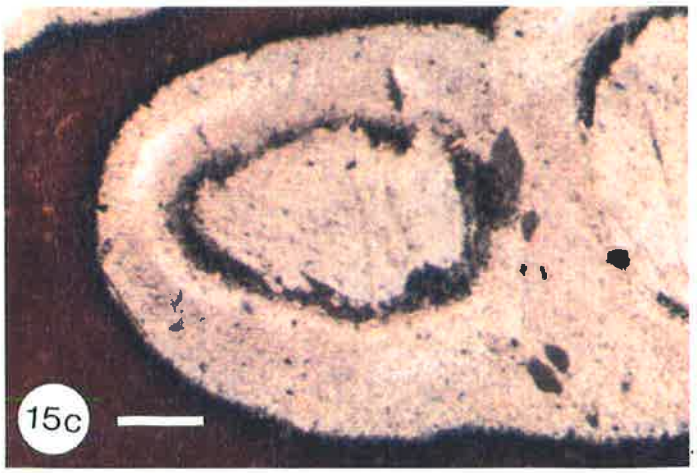
Fig. 17: Chocolate ore with clay pipe in center; D-Quarry; sample 903-166a; the scale equals 2cm.

Fig. 18: Selected clay samples; greenish: Fe^{2+}-carrying and unoxidized; yellow: impregnated with hydrated Fe minerals (goethite); pink: stained with oxidized Fe phases (hematite); D-Quarry; samples 903-141a-c; the scale equals 2cm.

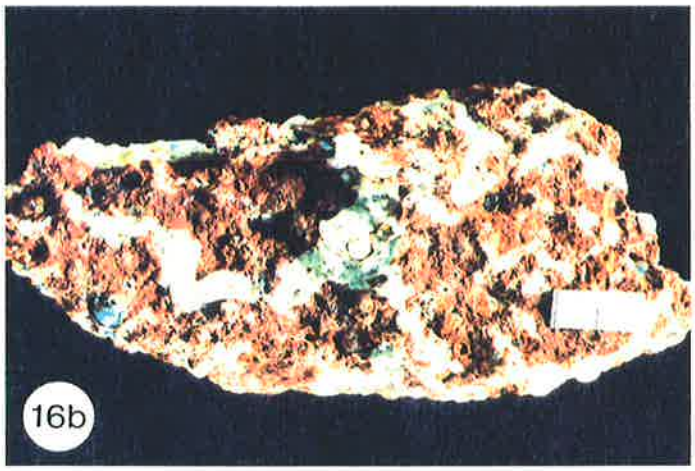
Plate 3.6

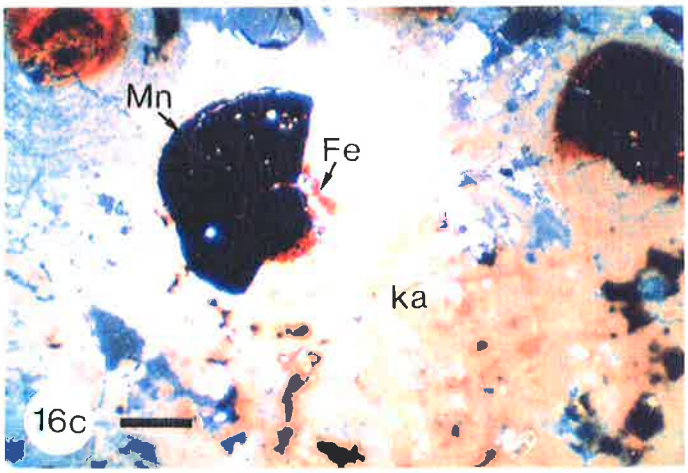
















but they are concentrated in areas of low topography. Soils occur laterally continuous at the surface, only occasionally they fill pipes and channels. They belong to the red tropical soils, which mainly contain quartz sand, clays, ferruginous impregnations, and relatively small amounts of organic material. Iron colours the soils from ochreous to red- or dark brown; the degree of cementation varies considerably. Generally, manganiferous spherulites develop above the deposit.

3.2.20 Sand

Sand generally occurs in soils and stratigraphically in places below the ore (e.g. C-138, A-South); sometimes it accumulates in small pockets within clay pipes and laterites. Occasionally, small to medium scale cross-bedding can be found. The sand associated with the deposit is normally devoid of accessory heavy minerals and it is medium to coarse grained quartz. Mostly well sorted, the grains are generally angular to sub-angular in shape, and they show light grey to brown colours, depending on the type of impregnation. In places, manganiferous cementation of the sand leads to the development of siliceous ore. Although the quartz sand plays only a minor role in the supergene recycling of minerals (replacements in siliceous and massive ores), quartz has been identified in small quantities in idiomorphic crystals within supergene materials. How far this process is applicable to the presence of quartz grains in laterites cannot be established here.

3.2.21 Conglomerate

Irregular lenses and pockets of conglomerate appear mainly in lower parts of laterites in the northern areas of the deposit (F-Quarries). This rock is laterally discontinuous, but large bodies appear occasionally. Generally, the conglomerate consists of pebble to cobble sized quartzite, reworked manganese ores, and iron oxyhydroxides, with a matrix of clayey sand. The material is not well sorted and mostly unconsolidated.

3.2.22 Quartzite/Sandstone

Quartzite and sandstone form the bedrock of the island, and these rocks crop out at the eastern margin of deposit. The material is relatively dense and few sedimentary features other than planar bedding can be discerned. The predominant mineral is quartz, but very small quantities of Mn-impregnations or detrital/reworked other materials are found. The rocks are usually very light in colour, their medium to coarse grains are rounded to sub-angular and they are mostly well sorted. The degree of cementation varies widely.

Table 3.1a: Primary Mn ores (modified after Pracejus et al., 1988).

Name	Structure/geometry	Mineralogy	Secondary overprint
Oolite (uncemented)	Normal and inverse grading, subhorizontal, following the relief of the bedrock, small/ medium scale cross-bedding	Pyrolusite, todorokite, cryptomelane, birnessite, nsutite, romanechite, lithiophorite, vernadite, (manganocalcite); nuclei contain silt, sand grains and reworked Mn-ores	Replacements: Fe, Mn, clays; cementation: Mn, compaction
Pisolite (uncemented)	Normal and inverse grading, subhorizontal, following the relief of the bedrock, small/ medium scale cross-bedding	Pyrolusite, todorokite, cryptomelane, birnessite, nsutite, romanechite, lithiophorite, vernadite; nuclei contain silt, sand grains and reworked Mn-ores	Replacements: Fe, Mn, clays; cementation: Mn, compaction, pressure solution along fractures
Siliceous ore	Massive cementation of sand grains; sand grains in matrix of oolitic/pisolitic ores	Pyrolusite, cryptomelane, todorokite, quartz	
Hardground	Dense, thin layers (cm), occasionally erosional features on surface, laterally continuous over tens of meters; incorporation of reworked oolitic, pisolitic, and massive ores	Cryptomelane, pyrolusite	Infilling of cracks by secondary Mn/Fe-phases; replacement by Fe-oxides and clays; replacement of primary structures and textures by Mn oxides

Table 3.1b: Secondary Mn ores (modified after Pracejus et al., 1988).

Name	Structure/geometry	Mineralogy
Cemented mangcrete (oolitic/pisolitic)	Oolitic/pisolitic ores, massive, very hard, generally subhorizontal	Pyrolusite, cryptomelane, todorokite, nsutite
Massive mangcrete	Massive, hard to very hard cementations in oolites, pisolites, and in other ore types, often relic structures of primary features, horizontal to sub-horizontal	Cryptomelane, pyrolusite, sometimes pisoliths are weathered out
Envelope grain	Laminated envelope containing loose or cemented ooliths or pisoliths, within oolite/pisolite units, round to angular shapes	Cryptomelane, pyrolusite
Laminar mangcrete	Finely laminated on pipe walls, following vertical and horizontal pipes, in outcrops as Mn-karst	Cryptomelane, quartz
Mn cave pearls	Loose, rounded and elongated shapes with concentric layering, comparable to laminar mangcrete, but with much lower density	Cryptomelane, pyrolusite, quartz
Spherulite (manganiferous)	Cementation of different materials (e.g. sand, pebbles) in ovoid masses in soils, laterally continuous horizons	Todorokite, cryptomelane, goethite, hematite, quartz
Radial pyrolusite	Laterally continuous over tens of meters, strongly undulating, erosional upper boundary and flat base, following the top of the orebody (G-South) and within clay units, overprinting oolitic/pisolitic textures	Pyrolusite
Siliceous ore / manganiferous sand	Massive to recrystallized, often horizontal, partly cemented sands	Pyrolusite, todorokite, cryptomelane, quartz
Concretions (near surface)	Varying in size, sometimes dehydration features, laterally continuous horizons, upwards oriented growth	Cryptomelane, goethite
Digital concretions (below ore)	Digital or coral-like growth, increasing upwards in thickness, dehydration features, below main orebody	Cryptomelane
Chocolate-ore	Strongly leached, irregular, brittle matrix with Fe-oxyhydroxides and clays, rare pisoliths/ooliths or cemented fragments	Pyrolusite, cryptomelane, todorokite, kaolinite, Fe-oxyhydroxides

Table 3.1c: Rocks and sediments associated with Mn ores (modified after Pracejus et al., 1988).

Name	Structure/geometry	Lithology/mineralogy	Secondary overprint
Soil	Irregular, laterally extensive, concentrated in low topography, vertical in pipes and channels	Quartz sand, organics, conglomerates, clays	Fe/Mn-spherulites, fining up to the top, Mn-concretions, lateritic alterations
Sand	Laterally extensive, occasionally in pipes, small to medium scale cross-bedding and massive	Mainly quartz, along coast: coral and shell debris	Fe/Mn-impregnations and cementation, rare silification
Laterite (Mn)	Laterally extensive, underneath soils, vugular	Sands, cementations of Mn/Fe-oxyhydroxides, clays	Pipes and sinkholes with spherulites
Laterite (Fe)	Lateral, underneath manganiferous laterite, vugular	Sands, Fe-oxides/oxyhydroxides, clays	Horizons with Fe-enrichment and pipes, replacement of oolites/pisolites
Clay	Planar, regionally up to 50m thick, sometimes layered, mostly irregular in laterites and pipes, rarely layers in vugs, as impregnation in the matrix of ores	Kaolinite, (nontronite, montmorillonite), as clays, silts, claystones, siltstones, and clayey sands	Impregnations of Fe-oxides/oxyhydroxides, Mn-concretions and digital concretions
Fe-oolite / pisolite	Soft to hard cementation, cross-cutting manganiferous units	Goethite, occasionally hematite	
Massive ferricrete	Dense, hard, lateral cementations	Goethite	Occasionally patchy manganese oxide minerals, rarely quartz
Fe-pipe wall	Dense cementation of relic rocks and minerals, following outer boundary of pipes	Hematite, goethite, kaolinite, quartz	
Conglomerate	Irregular pockets and lenses, discontinuous	Sand, quartzite pebbles, reworked Mn-ores, Fe-oxides, clays	
Quartzite / sandstone	Dense, bedrock with erosion features	Quartz	(Mn)-impregnations

3.3 Mineralogy

Below, bulk samples representative for the various ore and rock types are analyzed by X-Ray Diffraction (XRD) to determine the dominant mineralogy of the samples. The specimens, chosen from some 90 spectra, provide information on the full range of ore/rock types in the deposit. Other ore samples were selected from a vertical geological prolfile in F3-Quarry to investigate mineralogical variations within the relatively homogeneous materials of the section. The latter samples were analyzed by Fourier Transform Infrared Spectroscopy (FTIR), because this technique can detect minute compositional changes, even when the ores are poorly crystalline. Generally, minerals occurring in very small quantities were not investigated in detail; this study was undertaken to establish a common basis for general comparison, and an examinations of trace or ultra-trace minerals was not attempted.

The lattice dimensions of many manganese oxides can vary considerably, depending on substitution effects altering the cell structure. Therefore, XRD and FTIR analyses of the samples were mainly based on mineralogical studies from Groote Eylandt to guarantee sample compatibility (Frazer, 1969; Anthony et al., 1983; Fysh and Fredericks, 1983; Fredericks et al., 1984; Dubrawski, 1985). Occasionally, it was necessary to use additional mineral data from other localities for the interpretation of FTIR analyses (Potter and Rossman, 1979), because some spectra of the present study did not match with results of Ostwald (1988).

3.3.1 X-Ray Diffraction (XRD)

The X-ray diffraction patterns of the most common ores of the deposit are illustrated together with some less frequent materials (Fig. 3.19a; oolitic and pisolitic ores, radial pyrolusite and Mn-impregnated sand). The following figure shows the patterns of laminar and massive mangcretes, concretionary ores, and an Mn cave pearl, which are all of supergene origin (Fig. 3.19b). Additionally, another ore is shown which has strongly been overprinted by alteration and/or supergene processes (hardground). Lateritic products such as spherulite, massive ferricrete, and different types of laterite, are examined in the final plot of this section to investigate the mineralogy of the main gangue minerals (Fig. 3.19c). The d-spacings of the discussed diffractograms are listed in Table 3.2.

Radial pyrolusite was selected to be shown first, because the sample is almost monomineralic (Fig. 3.19a). Only small quantities of kaolinite are detected in addition to the high pyrolusite contents. For this reason, the XRD-trace can be used for comparison with other ore samples. Similarly, uncemented oolite contains insignificant amounts of kaolinite together with abundant pyrolusite. However, this ore type exhibits the highest concentrations of todorokite, when compared with all other ores and rocks (at ~10.9 °2ϑ). Loose, but hard and recrystallized pisoliths

sampled from the same geological section as the previous ore types possess a comparable Mn oxide composition with slightly less todorokite, but the pattern shows larger quantities of kaolinite and quartz, and the presence of goethite is indicated. These gangue minerals form the matrix between the grains.

In the pattern of cemented pisolite, cryptomelane gains importance although pyrolusite is still the dominant mineral. Todorokite appears in small amounts and with the exception of a small quartz peak no other ore and gangue minerals can be identified. Uncemented pisolite shows less well crystallized Mn oxides than the cemented pisolite; the major peaks of pyrolusite and cryptomelane are smaller. Small amounts of todorokite, quartz and kaolinite are also seen. The manganese oxides of manganiferous sand exhibit similar, but relatively low, pyrolusite and cryptomelane concentrations. The small broad peak for the main todorokite line at ~10.9 °2ϑ indicates this mineral. However, when compared with the other Mn phases of this sample it is an important component, because the quantities of all manganese minerals are generally low and still the todorokite peak is visible. Even under "normal" conditions, in cases when the ore minerals dominate, the latter line does not become very large (see previous XRD-traces).

The XRD-pattern of the hardground closely resembles the diagrams of uncemented oolitic and pisolitic ores of the previous plot (Fig.19b). In the field, this ore type is found within mostly uncemented oolitic/pisolitic units of the G-Quarry area and the mineralogical similarities are therefore not surprising. Pyrolusite dominates largely over small amounts of todorokite, less cryptomelane and insignificant kaolinite concentrations. Laminar mangcrete, which lines the walls of clay pipes, is mainly composed of cryptomelane, although pyrolusite is present. Small amounts of todorokite, quartz, and kaolinite are also apparent.

The manganese oxides of massive mangcrete seem to have a low crystallinity, which is illustrated by the low intensities of the reflections. Cryptomelane is the main ore mineral and todorokite shows comparably high concentrations, although its dominant peak overlaps with a kaolinite line. Goethite, kaolinite, and quartz all exhibit relatively small peaks. The mineralogy of concretionary ores appears to be very simple as only cryptomelane lines can be identified, with the exception of a minimal indication for kaolinite. Digital concretions from below the orebody are similar in their mineralogical composition to the concretions from the top of the ore. Cryptomelane dominates in the sample and small pyrolusite peaks are recognized. However, strong lines are observed for quartz and less important peaks show kaolinite. These two gangue minerals form the matrix between the digital masses of this ore type. The last example of this figure is the Mn cave pearl. Though this type of ore is very rare, it is shown for comparison. The crystallinity of the manganese oxides is very low, pyrolusite seems to dominate over cryptomelane, quartz is one of the main constituents of the sample, and kaolinite is of minor importance.

The secondary rocks associated with the deposit are mainly composed of kaolinite, quartz, goethite, and small amounts of hematite (Fig. 3.19c). Depending on the rock type, one or the other mineral dominates over the other phases. Commonly, remnants of the precursor of the present rocks, such as manganiferous pisoliths in laterite, can still be recognized.

The Fe-pipe wall constitutes another important feature of clay pipe systems (compare laminar mangcrete, Fig. 3.19b) and its close association to the pipes is reflected in its mineralogical composition. Fine hematite impregnations strongly colour the rock and lead to the impression that hematite is the dominant phase. However, the line scan reveals that this colouration is only due to a masking effect and that hematite is a minor phase, as is goethite. Kaolinite and quartz are the two main minerals while very small peaks indicate the presence of todorokite and possibly pyrolusite. Cryptomelane cannot be detected.

Although in appearance, the Mn-laterite differs greatly from the Fe-pipe wall, the mineral assemblages are comparable. The crystallinity of kaolinite seems to have increased, the amount of quartz is similar to that in the Fe-pipe wall, and relatively small quantities of hematite and goethite are present. Manganese oxides, easily observed in hand specimen, obviously have low concentrations and they possess low crystallinities. Very weak reflections indicate small amounts of todorokite and even less pyrolusite.

Chocolate ore possesses well developed kaolinite lines and quartz is also a dominant part of the rock. Goethite, hematite, pyrolusite and todorokite are indicated by small reflections. The XRD-pattern of spherulite is dominated by quartz and kaolinite, whereas goethite and hematite show a number of relatively weak lines. Surprisingly, todorokite seems to be the only well crystallized Mn oxide in the sample. Pyrolusite and cryptomelane cannot be identified.

The ferruginous laterite exhibits quartz peaks much smaller than in the previous samples (compare Mn-laterite in the same plot). Also the kaolinite lines are prominent and goethite and hematite show small concentrations. Mn-minerals cannot be found, although a very weak and broad reflection at ~10.9 °2ϑ could indicate todorokite.

The two remaining rocks of the diagram are comparable in their mineralogical composition. Goethite predominates in the samples, hematite has slightly higher concentrations in the ferruginous pisolite, whereas massive ferricrete contains more kaolinite. The quartz levels of both rocks are fairly low and manganese phases cannot be detected. Thus, these samples seem to stand out from all other ore and rock types analyzed in that they do not contain Mn minerals. However, it must be pointed out again that in a few cases enrichments of pyrolusite were observed in both massive and pisolitic ferruginous materials.

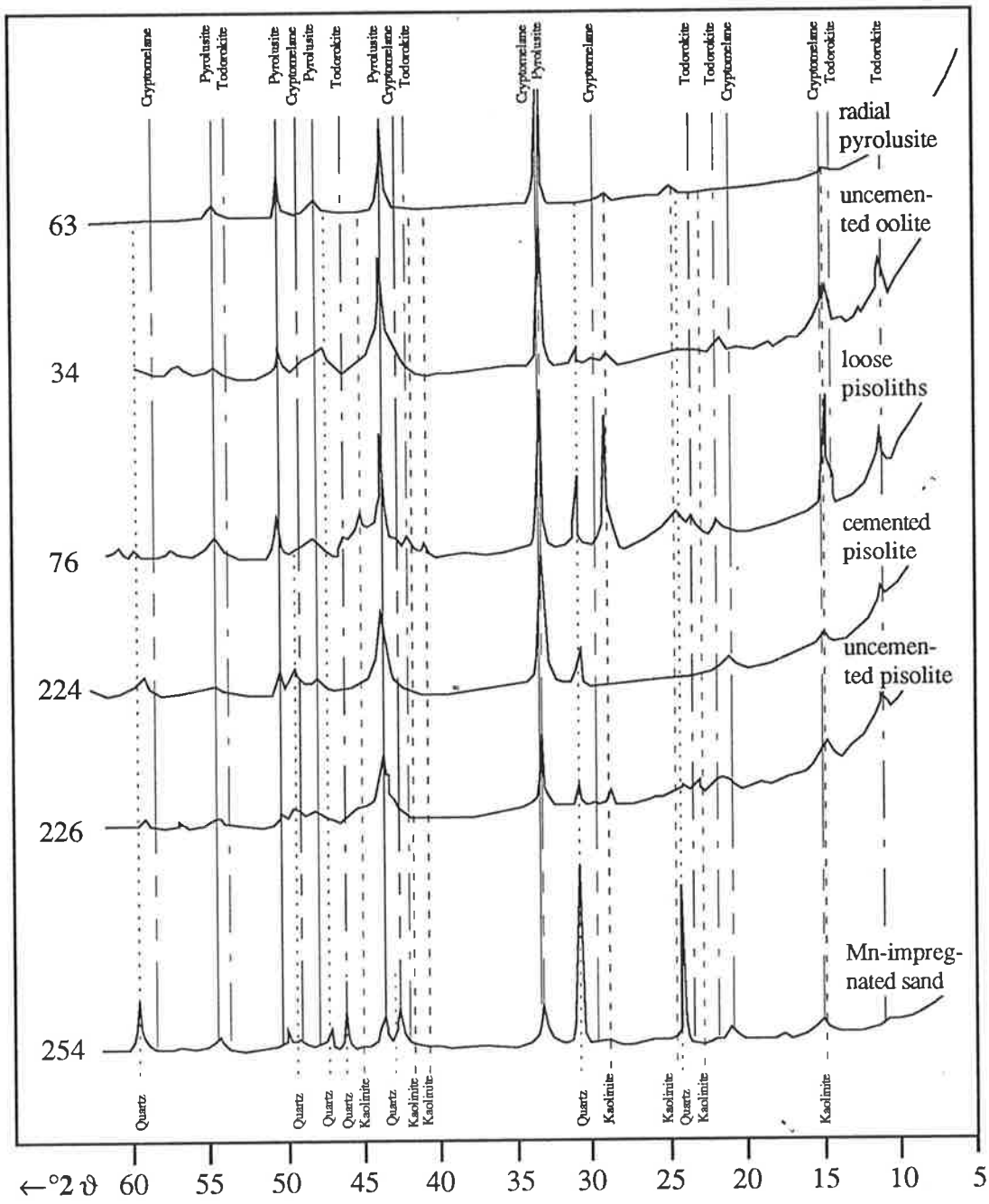


Fig. 3.19a: X-Ray Diffraction patterns of manganese oxide ores and supergene manganiferous products; sample numbers are indicated at the left of the respective spectra; all samples have the common prefix 903.

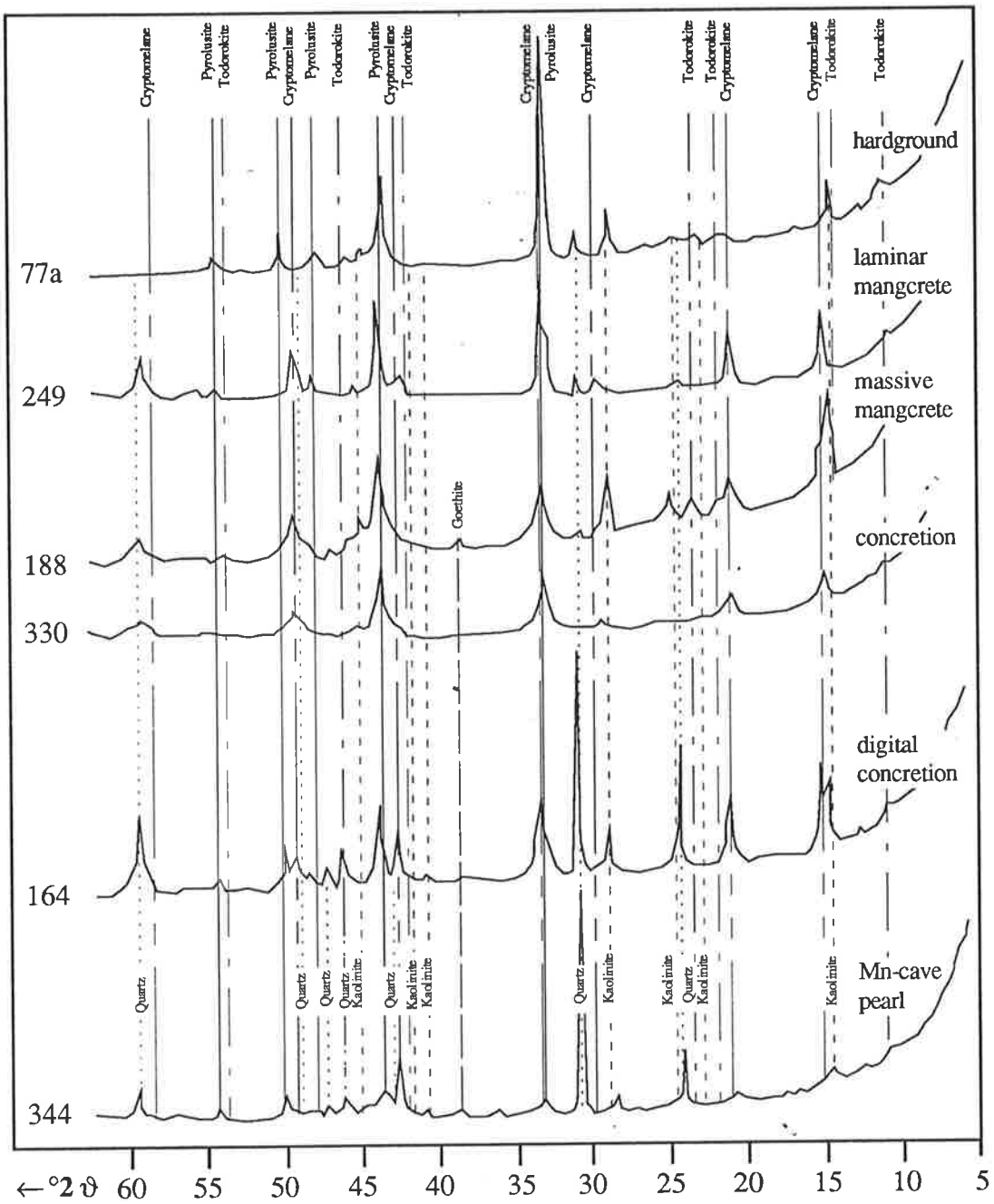


Fig. 3.19b: X-Ray Diffraction patterns of supergene manganiferous materials; sample numbers are indicated at the left of the respective spectra; all samples have the common prefix 903.

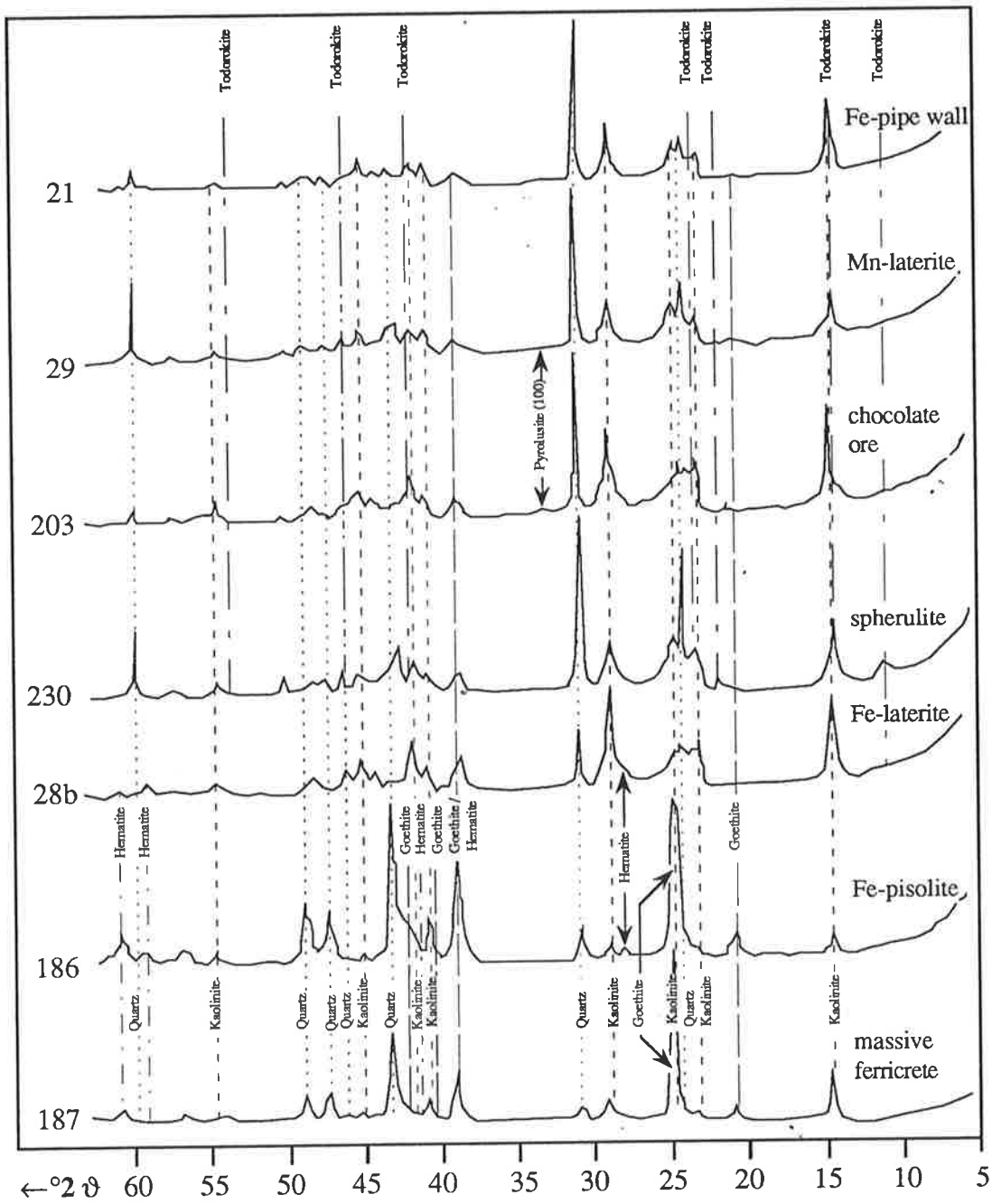


Fig. 3.19c: X-Ray Diffraction patterns of supergene and dominantly ferruginous materials; sample numbers are indicatedat the left of the respective spectra; all samples have the common prefix 903.

Table 3.2: Observed d-spacings [Å] of X-Ray diffraction (XRD) patterns from Mn-ores and associated rocks (see Figs. 3.19a-c).

Pyrolusite	Cryptomelane	Todorokite	Goethite	Hematite	Kaolinite	Quartz
		9.40				
		7.14			7.19	
	6.90					
			5.02			
	4.90					
		4.74				
					4.47	
					4.36	
		(4.3)				
						4.26
			4.22		4.19	
					3.88	
				3.71		
					3.59	
3.48	3.47					
						3.34
3.14						
	3.10					
			2.70	2.70		
			2.59		2.57	
				2.53	2.54	
		2.49			2.50	
2.41			2.45			2.46
					2.39	
					2.34	
		2.28			2.30	2.29
			2.26			2.24
2.21						
2.13	2.14		2.15		2.13	2.13
2.11						
1.98		1.97			1.99	1.98
					1.94	
					1.90	
	1.82			1.81		1.82
					1.79	
				1.72		

3.3.2 Fourier Transform Infrared Spectroscopy (FTIR)

Fourier Transform Infrared Spectroscopy was applied to a limited number of samples to examine mineralogical variations in a stratigraphic profile containing relatively homogenous ores (Fig. 3.20, Table 3.3). General data from some samples that were used for experimental investigations are also compiled in this section to assist the identification of mineral peak positions (Mn ores and kaolinite-quartz mixtures; chapter 7).

It was also attempted to determine the mineral composition of the samples from the respective spectra (Table 3.4). Such an approach involves the numerical subtraction of designated "pure" mineral spectra from the specimen to produce a relative concentration of the various minerals (Ostwald, 1984). Unfortunately, the samples contain too many different phases, and at present, these ores and rocks are thus unsuitable for a computerized analysis (CIRCOM=*C*omputerized *I*nfra*r*ed *C*haracterization *o*f *M*aterials). However, the examined spectra correlate well with the theoretical evaluation of the mineralogical composition in chapter 5, but this is discussed later (compare also Figs. 5.3a,b; all samples of this section were analyzed by FTIR, with the exception of the 2 top samples).

The sample spectra are plotted in stratigraphic order as taken from the orebody. Strong mineralogical variations are evident in the samples at the bottom of the ore (near the clay unit), when compared with higher samples. Prominent kaolinite peaks appear, together with large pyrolusite lines. Peaks typical for kaolinite can be observed at 900 - 1100 and 3600-3700 cm^{-1}, these peaks are largely unaffected by overlying lines from other minerals. Pyrolusite usually possesses a few sharp lines between 500 - 700 cm^{-1} and some smaller, but also sharp peaks at 340 - 410 cm^{-1}. Above the initial kaolinite-rich samples, the spectra smooth out and the pyrolusite content decreases gradually upwards, with the exception of sample 9. Parallel to this decrease, cryptomelane increases up the section and kaolinite also reappears in the upper parts of the orebody near the contact with the overlying laterite. The spectrum of cryptomelane is characterized by less and broader peaks, which occupy positions next to pyrolusite lines (650 - 750 cm^{-1}). Though some spectra indicate todorokite, only sample 13 in the middle of the section clearly exhibits this mineral (see peak at ~1630 cm^{-1}). However, the abundance of todorokite seems to increase in the vicinity of kaolinite-rich samples.

This vertical geological profile illustrates a broad mineralogical stratification in the deposit, although the ores examined in this sections are macroscopically relatively uniform:

- pyrolusite is obviously restricted to deeper parts of the orebody,
- cryptomelane dominates in horizons near the surface.

Another important aspect of the spectra is displayed in the shape of the individual sample scans. Generally, the overall peak intensity, and thus the crystallinity, for Mn oxides decreases

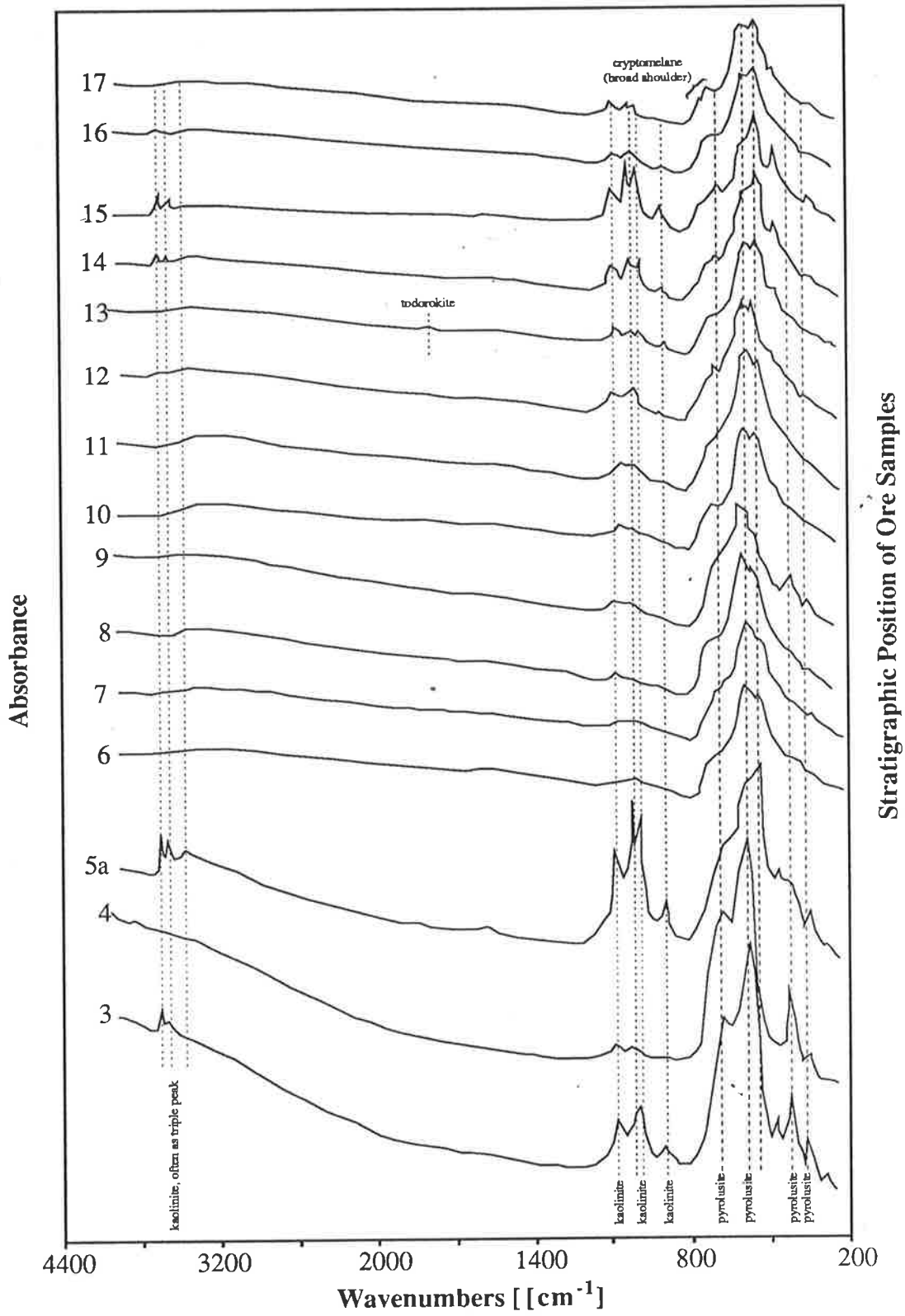


Fig. 3.20: FTIR-spectra of samples from a stratigraphic section from F3-Quarry. The ores predominantly consist of cemented pisolite, with clay enrichments at the bottom and the top of the section. All Spectra have a common scale, the sampling distance is not to scale. Sample numbers are indicatedat the left of the respective spectra; all samples have the common prefix 903.

Table 3.3: Line positions [cm^{-1}] of Fourier Transform Infrared Spectroscopy (FTIR) on samples from a vertical geological section in F3-Quarry (dominantly cemented pisolite).

Pyrolusite	Cryptomelane	Todorokite	Kaolinite
	3600*		3694 ± 1
			3620
3400*		3400-3200*	
		1633	
1100 -			1100 ± 2
- 1030			1031 ± 1
			1005 ± 2
			912 ± 2
	699 ± 5		
677 ± 2			
590.5 ± 2.5	582 ± 1		
549*	550*	550 - 560	
		516*	
470 ± 1		468	
		440*	
		430 ± 1	
407 ± 2			
390*			
340 ± 2			344
			277 ± 1

* denotes FTIR lines for Groote Eylandt Mn oxides (Ostwald, 1988) which were not detected in the spectra.

Table 3.4: Relative mineral abundances from computer spectrum analysis of FTIR diagrams (CIRCOM analysis).

No.	Pyrolusite	Cryptomelane	Todorokite	Kaolinite	Quartz
17	0	7	59	2	4
16	0	0	69	3	3
15	3	0	50	12	7
14	2	6	70	6	4
13	3	6	70	3	4
12	5	0	75	3	5
11	5	0	92	0	4
10	6	20	62	0	3
9	24	0	47	0	2
8	6	0	92	1	1
7	9	0	68	1	0
6	9	0	61	1	0
5a	41	0	0	28	0
4	97	0	0	2	0
3	94	0	0	19	0

3.4 Discussion

The petrological and mineralogical examination of ores and associated gangues demonstrates that many supergene products are stratigraphically controlled in their formation. Aspects governing the secondary overprinting of the deposit, supergene mobilization, and precipitation processes are examined later. However, when the descriptions and data of this chapter are compared, a picture emerges that reflects the dominant alteration processes in the Groote Eylandt deposit. This means in general terms that the supergene mechanisms result in the following mineralogical/geological relationships:

- depth dependency of ores and gangues,
- development of specific parageneses.

According to the stratigraphical positions of ores and gangues, two main groups are identified:

- near the surface and upper parts of ore,
- lower parts of orebody and below.

Although these groups often grade into each other and cannot be separated clearly, there are also materials that are typical for specific places.

The most restricted manganiferous products in the deposit are probably spherulites in soils and concretions slightly below soil. Todorokite shows its strongest enrichments in the spheruliths, whereas other manganese oxides are subordinate in these materials. Deeper down the section, cryptomelane is most prominent in concretionary ores, laminar mangcretes (thick near surface, disappears with depth), cave pearls, and Mn karst.

All mentioned ores commonly developed in clay-rich materials or quartz sand, and thus, the paragenesis with kaolinite, which is the main clay mineral at Groote Eylandt, and quartz, indicates a geochemical control over the formation of these ores. Additionally, the higher oxygen concentrations of groundwaters near the surface may play a role during the precipitation of manganese oxides. However, as similar parageneses exist below the ore, the availability of oxygen may be much less effective in the mineralogical control of secondary precipitates than expected.

Cemented and massive mangcretes emphasize the dominance of cryptomelane near the surface, because these ores are generally more prominent in the upper parts of the orebody, and clay minerals from the overlying laterites are easily available for interaction with local precipitation processes. Digital concretions from below the ore and siliceous ores that formed at the base of the orebody support the above findings. Again, the secondary products are dominated by cryptomelane and they are closely associated with either kaolinite or quartz, or both.

Ores in stratigraphically intermediate positions can contain larger amounts of kaolinite in their matrix (uncemented oolites/pisolites). Together with the clay impregnations of uncemented oolites/pisolites small areas of increased cementation occur, and these co-existing ore types may

indicate the initial stage of a development towards cemented mangcretes. Ores of this type are still dominated by pyrolusite.

The FTIR analyses also confirm that the abundance of pyrolusite generally increases with increasing depth, which is in contrast to the behaviour of cryptomelane. The geochemical stabilities of these two minerals are obviously linked, but the presence of one or the other phase does not explain which of the minerals is replaced. However, under the microscope it is evident that in most cases cryptomelane forms at a later stage and that it replaces pyrolusite-rich ores.

So far, the only detected exceptions to this observation are the ores of the G/G-South area. Here, pyrolusite replaces cryptomelane and other poorly crystalline manganese phases. An extreme example for this process is the radial pyrolusite which overprints oolite units near the top of the orebody. Although less evident than in the case of radial pyrolusite, but usually more common in the field, oolites and pisolites of this location possess mottled cemented patches which mainly consist of a relatively coarse pyrolusite. This contrasts strongly with findings in other areas where the cementation of primary materials is normally dominated by cryptomelane. If, through a stabilization process, such as the availability of certain trace elements, the materials of the G/G-South area altered more slowly than the ores of the surrounding locations, then they might represent an intermediate stage in the development of the orebody.

Excluding unknown initial precipitates and their early successors, formed through diagenesis and aging processes, the mineralogical history of the Groote Eylandt deposit may have proceeded in the following steps:

- poorly crystalline phases, such as those found in the G/G-South quarries, alter to pyrolusite and comparable tetravalent Mn-oxides,
- cryptomelane replaces pyrolusite, as is evident in many ores of the deposit (e.g. cemented or massive mangcretes).

The latter finding is also supported by gangue minerals, such as goethite, replacing Mn ores. Commonly, cemented mangcretes are partially destroyed by supergene processes that first act on pyrolusite-rich ooliths/pisoliths, selectively remobilizing these grains and replacing them with other phases, and excluding the cryptomelane-rich matrix.

Processes in which gangues replace manganese minerals are very common, and often, the mobilized manganese precipitates elsewhere as supergene products. These processes prevail near the surface, within laterites or closely associated in pipes, and at the interface between ore and underlying claystones. It was demonstrated that many supergene ores develop in the same position and obviously, the dissolved manganese has its highest concentration near places where the replacement reactions work. Thus, a secondary formation of Mn oxides is likely to occur nearby.

As mentioned before, goethite is the main gangue mineral to replace manganese oxides. Typically, pyrolusite is much more affected than cryptomelane, which often remains as a residual matrix mineral. Kaolinite also seems to replace manganese minerals, but polished thin sections clearly illustrate that the clay represents the latest stage in the mobilization reactions which led to the removal of both manganese and iron. This observation is particularly important, because it provides direct evidence for the remobilization of ferruginous minerals through kaolinite precipitation. It will be discussed later that this mechanism sustains the main process responsible for the reduction of manganese. Thus, the formation of supergene Mn ores indirectly depends on an earlier development of kaolinite. Hematite, although present in the deposit, mostly appears in minor quantities in higher parts of the section, where oxidation processes dominate.

This short discussion shows that a detailed petrological and mineralogical examination of ores and associated rocks provides a wealth of information on secondary alteration products and supergene processes. The following chapter on the geochemistry of the samples, analyzes the stratigraphical distribution of the various elements, and it also examines whether the broad history of the deposit described above is also reflected in the geochemical data.

4. Geochemistry

4.1 Introduction

One of the main tasks of this study was the geochemical characterization of the different ores and associated rocks at Groote Eylandt. Until recently, geochemical analyses on these materials either focused on individual minerals (Ostwald, 1988) or on larger areas of the deposit (Ellis, 1978). Thus, a close examination of the predominantly secondary alteration products is necessary to investigate supergene reduction and oxidation processes occuring in the orebody; information on the nature of trace elements in specific materials also assists mine planning operations. Additionally, some of the elements are used for comparison with ores from deposits elsewhere to identify possible genetic relationships in ore formation.

Table 4.1: Elements and methods used for geochemical characterization.

Method	No.	Elements
XRF	365	Al, Ba, Ca, Fe, K, Mg, Mn, Na, P, Si, Sr, Ti
XRF	100	As, Mo, Pb, Sc, Th, U, W
ICP	365	B, Ce, Co, Cr, Cu, Eu, Gd, La, Nd, Ni, P, Sm, Sr, Yb, Zn, Zr
INAA	8	Ba, Ce, Co, Cr, Cs, Eu, Fe, Gd, Hf, Ho, La, Lu, Mo, Na, Nd, Sb, Sc, Sm, Ta, Tb, Th, U, W, Yb, Zr
LOI	365	H_2O

All ore types and rocks identified (Pracejus et al., 1988) were the subject of detailed sampling procedure. First, five stratigraphical sections were sampled at closely spaced intervals (3 - 20 cm in ores, 40 - 50 cm in laterites; see also chapter 2). Secondly, with the exception of a few rarer ores (e.g. manganiferous hardgrounds), which did not provide sufficient material, at least 10 samples of each ore and rock type were collected to provide 10 or more "pure" samples for each individual set (up to ~40). An overview of the elements and the respective analytical techniques is given in Table 4.1.

Major, minor, and some trace elements were analyzed by X-Ray Fluorescence (XRF), Rare Earths and other trace elements were examined by Inductive Coupled Plasma Analysis (ICP) (Appendix IV., Tables 1 - 3; for methods see Appendix I.1). Initially, a small number of samples were analyzed by Instrumental Neutron Activation Analysis (INAA; Appendix IV., Table 4) to determine upper and lower concentration limits for the development of an analytical ICP program which had to cope with the unusual matrix of ores and rocks. Loss On Ignition was determined for all samples.

The Rare Earth Elements were normalized with European shales (Haskin and Haskin, 1966) to simplify comparison of multi-element patterns, the deviations of Ce and Eu from the overall trend (anomalies) were calculated from the normalized values. A statistical treatment of the raw data was attempted (correlation matrix; Appendix IV., Table 4.5), but multiple regressions for many elements made it necessary to visually compare each parameter against all other. However, average element abundances and concentration ranges of ores and rocks are provided in the respective sections.

4.2 Chemical Characterization of Ores and Rocks

The following section shows the three major components of the deposit, Mn-, Fe-, and Si/Al-phases, which occasionally incorporate specific elements; major, minor, and trace element abundances (including the Rare Earths) are depicted for individual ore and rock types. Information gained from element composition patterns of these materials is taken to determine whether it is possible at the present stage of investigation to establish a common host for each element.

4.2.1 Inter-Element Correlations

Table 4.2: Visual cross-correlation of major and trace elements; underlined elements appear in several groups; elements in brackets show weak correlations; n = 365.

main element of group	associated major and trace elements
Mn	As, B, Ba, Ca, Ce, Co, Cu, Eu, Gd, K, La, Mg, Mo, Na, Nd, Ni, P, Pb, Sc, Sm, Sr, (Ti), U, V, Yb, Zn
Fe	Al, As, Gd, Pb, Sc, Th, (U), Eu-anomaly
Al, Si	Cr, Fe, Gd, Sc, Si, Th, Ti, W (only for Si!), Zr

First, the materials dominating in the deposit are examined for their role in concentrating the various elements. Three main groups were visually identified on the basis of their major constituent (Table 4.2); these groups are the Mn oxide ores, ferruginous rocks with an iron oxyhydroxide dominance, and clay-rich materials. Since the secondary products commonly occur in close association within the samples, multiple regression trends are observed. Thus, statistical methods are often unable to fully analyze such complex aspects in large sample

sets, and examination relied on a visual cross-comparison of all samples and all elements under investigation. Below, the mentioned groups are discussed together to determine general element relationships within, and between, ores and rocks; later, ores and gangues are studied separately.

The tabulated elements illustrate the complex nature of the materials, because many elements occur in more than one particular group. Manganese and iron are good examples for the difficulties arising from such multiple element correlations. Nearly all elements identified with iron also occur in the Mn oxides. However, this finding does not surprise, because finely disseminated Fe phases are often present within the ore; the general question about the host for specific elements remains unanswered. The same applies to combinations of ferruginous/clay-rich materials and to Mn ores/clays. This means that this relatively simple and broad scheme does not provide sufficient detailed information and that small-scale differentiations, such as ore types or minerals, are necessary.

However, a few generalizations can already be made. Interestingly, many of the elements that might be expected to occur in conjunction with Mn, such as Co, Cu, or Ni (deep sea ferromanganese nodules), do not show a significant relation to manganese, although these elements appear in the manganiferous group. Thus, a strong variation within different ore types is likely to occur. Occasionally, elements with a weak correlation to one of the main groups show a much better relation to other elements, which, in turn, corrleate well with the respective major group. Such behaviour is frequently observed and was used to establish the element associations of Table 4.2.

Calcium serves as example for the observation above (Fig. 4.1a). The data in the regression plot for Ca and Mn scatter widely and the same can be said about elements such as Mg or Mo. However, these elements correlate much better to each other (U/Mo, Fig. 4.1b); they also show a negative or zero correlation to elements dominating the gangues (Mo/Al, Fig. 4.1c). In contrast, elements like U correlate well with Mn. Therefore, a combination of Ca with other elements produces recognizable patterns, which are attributed to the manganiferous group in a successive interpretation step.

Elements associated with Fe are less well correlated within the group and they also occur in the two other main groups. However, a very pronounced correlation is obtained from Fe and Eu-anomalies. This finding is later used in the interpretation of supergene processes, but is not discussed further here. The clay-rich group (alumina/silica) generally possesses relatively low trace element concentrations. Well developed regression patternss are identified for elements such as Ti or Zr (Fig. 4.1d). These good correlations are generally associated with kaolinite containing gangues. Quartz, in contrast, only correlates well with W, which obviously derived from the grinding process (tungsten carbide mill), and is not considered further.

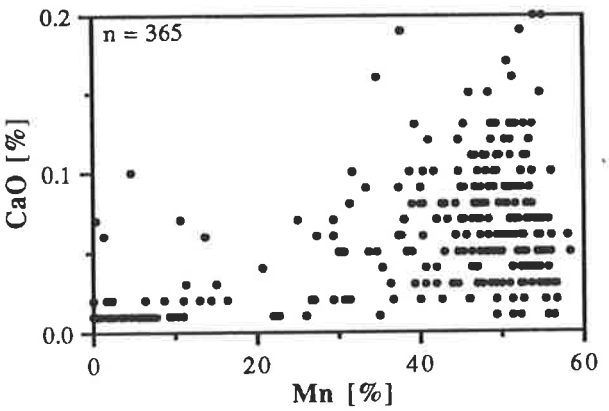


Fig. 4.1a: Correlation of Mn and CaO in ores and rocks.

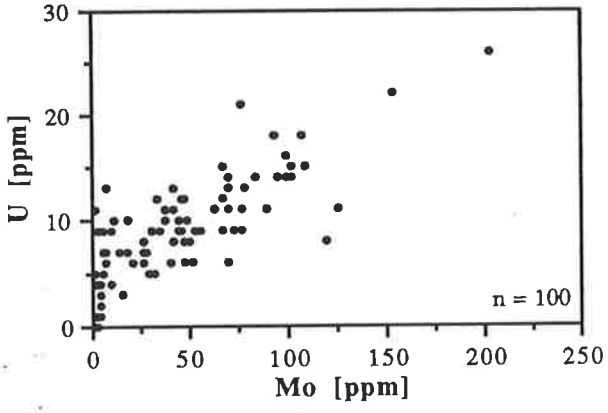


Fig. 4.1b: Correlation of Mo and U in ores and rocks.

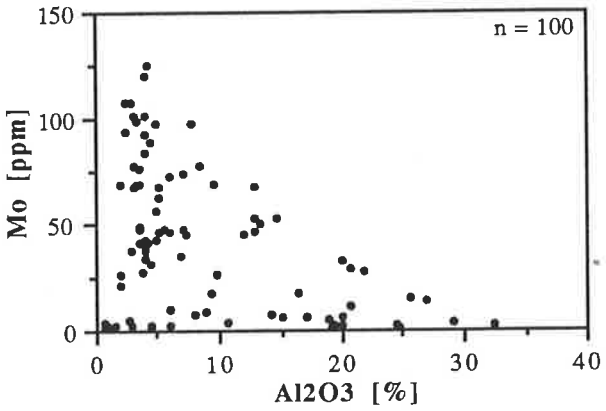


Fig. 4.1c: Correlation of Al_2O_3 and Mo in ore and rocks.

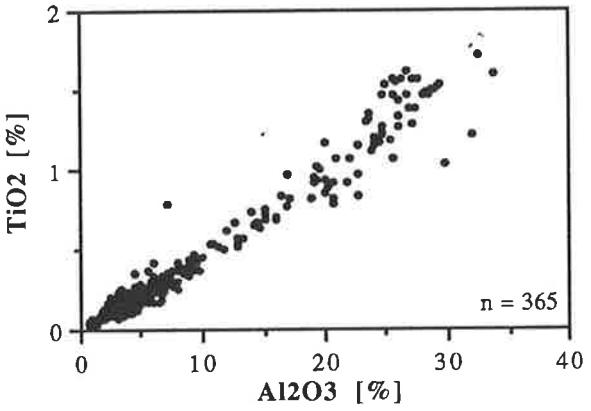


Fig. 4.1d: Correlation of Al_2O_3 and TiO_2 in ores and rocks.

4.2.2 Composition of Ores and Rocks

Below, major and trace element abundances of manganese oxide ores and associated gangues are separated into three main groups (major and trace elements, REEs); for simplicity, the groups are further sub-divided into four sets, as follows:

- cemented oolites/pisolites and soft, uncemented oolites/pisolites (often clay-rich matrix),
- concretions (surface), digital concretions (below ore), hardgrounds, aminar mangcretes, massive mangcretes, radial pyrolusites (layers), spherulites,
- sands (with Mn-impregnations), siliceous ores,
- kaolinitic clays, laterites, "chocolate" ores, Fe-pipe walls, Fe-pisolites.

For each ore and rock type the average is plotted; elements are plotted in order of the respective atomic number. Statistical data, such as average, maximum, minimum, sample number (n), and standard deviation, are provided in Tables 4.3-5 in the respective sections.

4.2.2.1 Major and Minor Elements

Table 4.3: Statistics of Major and Minor Elements; [%].

	Al	Ba	Ca	Fe	K	Mg	Mn	Na	P	Si	Sr	Ti
cemented oolites												
average	3.4	1.88	0.07	1.4	0.46	0.41	52.3	0.12	0.07	4.5	0.34	0.14
maximum	4.7	2.93	0.12	2.4	0.67	0.61	55.6	0.19	0.09	13.1	0.53	0.23
minimum	2	0.65	0.04	0.9	0.24	0.25	46.3	0.07	0.05	1.9	0.2	0.1
n	8	8	8	8	8	8	8	8	8	8	8	8
std. dev.	1	0.72	0.03	0.5	0.16	0.15	3	0.05	0.01	3.5	0.13	0.04
cemented pisolites												
average	4.7	1.62	0.07	2.7	1.59	0.33	49.2	0.23	0.08	5	0.22	0.16
maximum	8.1	5.84	0.22	23.2	2.66	0.67	56	0.57	0.42	14.2	0.4	0.29
minimum	1.8	0.01	0.03	0.6	0.71	0.01	31.8	0.12	0.03	1.2	0.03	0.07
n	31	31	31	31	31	31	31	31	31	31	31	31
std. dev.	1.7	1.6	0.04	4.8	0.49	0.22	5.2	0.08	0.09	3.1	0.12	0.07
chocolate ores												
average	24	0.21	0.02	7.5	0.36	0.04	9.8	0.04	0.02	38.8	0.02	1.41
maximum	27.3	0.34	0.08	9.2	0.76	0.09	47.9	0.17	0.06	49.2	0.03	1.62
minimum	5.5	0.05	0.01	2.6	0.22	0.03	1.9	0.01	0.01	10.1	0.01	0.36
n	10	10	10	10	10	10	10	10	10	10	10	10
std. dev.	6.6	0.09	0.02	1.9	0.17	0.02	13.7	0.05	0.02	11.5	0.01	0.37
kaolinitic clays												
average	21.5	0.02	0.01	6	0.14	0.02	0.6	0.01	0.02	57.7	0.02	0.96
maximum	33.7	0.03	0.01	16.9	0.26	0.04	3.2	0.02	0.14	78.7	0.03	1.71
minimum	6.5	0.01	0.01	0.7	0.06	0.01	0.1	0.01	0	45.5	0.01	0.3
n	8	3	5	8	8	8	8	8	8	8	3	8
std. dev.	11.9	0.01	0	6.8	0.06	0.01	1.1	0	0.05	11.4	0.01	0.55
concretions												
average	3.2	1.09	0.09	5.1	3.72	0.07	49.1	0.19	0.16	3.1	0.09	0.16
maximum	4.2	2.12	0.2	35.4	5.35	0.2	54.9	0.26	0.24	7.6	0.18	0.2
minimum	2.1	0.23	0.04	0.9	0.61	0.03	20.5	0.07	0.06	1.2	0.05	0.11
n	10	10	10	10	10	10	10	10	10	10	10	10
std. dev.	0.9	0.66	0.05	10.7	1.33	0.05	10.2	0.06	0.06	2.1	0.05	0.03
digital concretions												
average	4.2	4.65	0.04	4.8	2.28	0.03	41.8	0.08	0.19	11.4	0.08	0.23
maximum	6	8.91	0.06	10.2	4.33	0.03	52.4	0.14	0.28	35.6	0.28	0.32
minimum	3.5	0.15	0.02	1.2	0.8	0.02	31.3	0.04	0.09	1.7	0.01	0.2
n	6	6	6	6	6	6	6	6	6	6	6	6
std. dev.	0.9	4.17	0.02	3.4	1.36	0.01	7.1	0.04	0.08	15	0.1	0.05
Fe-pipe walls												
average	19.6	0.23	0.01	13.4	0.18	0.01	1.8	0.01	0.02	47.8	0.01	0.97
maximum	22.7	0.63	0.01	20.2	0.29	0.02	6.3	0.03	0.04	60.4	0.01	1.15
minimum	14.1	0.01	0.01	7.1	0.12	0.01	0.2	0.01	0.01	36.5	0.01	0.74
n	5	3	1	5	5	5	5	5	5	5	1	5
std. dev.	3.4	0.35		4.9	0.07	0	2.6	0.01	0.01	11.2		0.16
Fe-pisolites												
average	5.7	0.09	0.01	46.6	0.21	0.03	4.8	0.02	0.39	9.7	0.03	0.25
maximum	8.4	0.33	0.02	59.9	0.94	0.14	30.8	0.11	0.53	48.7	0.13	0.41
minimum	1.4	0.01	0.01	22.7	0.02	0.01	0.3	0.01	0.05	1.3	0.01	0.04
n	18	14	7	18	18	18	18	18	18	18	12	18
std. dev.	2.3	0.1	0	10.8	0.22	0.04	7.4	0.02	0.14	12.1	0.04	0.11

Table 4.3 (continued): Statistics of Major and Minor Elements; [%].

	Al	Ba	Ca	Fe	K	Mg	Mn	Na	P	Si	Sr	Ti
hardgrounds												
average	2.7	1.02	0.05	0.9	0.67	0.54	54.1	0.15	0.09	4.2	0.18	0.13
maximum	4.5	1.79	0.08	1.3	0.7	0.9	55.8	0.26	0.1	4.4	0.3	0.19
minimum	1.7	0.47	0.03	0.7	0.64	0.31	50.8	0.08	0.08	3.8	0.1	0.08
n	3	3	3	3	3	3	3	3	3	3	3	3
std. dev.	1.6	0.69	0.03	0.3	0.03	0.31	2.8	0.1	0.01	0.3	0.11	0.06
laminar mangcretes												
average	6.3	2.16	0.09	3	1.74	0.07	44.1	0.31	0.07	11.2	0.06	0.29
maximum	8.9	4.21	0.19	4.3	3.07	0.17	47.4	0.5	0.32	28.8	0.12	0.4
minimum	2.5	0.1	0.03	1.6	1.29	0.01	37.7	0.12	0.02	5.8	0.04	0.11
n	7	7	3	7	7	7	7	7	7	7	7	7
std. dev.	2	1.82	0.09	1.1	0.65	0.05	3.5	0.12	0.11	8.1	0.03	0.09
laterites												
average	23.4	0.14	0.01	12.5	0.3	0.03	5	0.02	0.02	38.8	0.02	1.2
maximum	28.3	0.46	0.06	27	0.78	0.05	16.3	0.1	0.07	66.3	0.05	1.56
minimum	16.5	0.01	0.01	0.9	0.08	0.01	0.1	0.01	0.01	26.9	0.01	0.81
n	26	24	24	26	26	26	26	26	26	26	23	26
std. dev.	3.3	0.1	0.01	5.6	0.16	0.01	4.5	0.02	0.02	9.4	0.01	0.21
massive mangcretes												
average	4.9	0.66	0.09	6.6	3.01	0.04	45.5	0.16	0.16	5.3	0.12	0.26
maximum	12.6	3.16	0.2	30.5	4.36	0.12	54.6	0.25	0.42	14.4	0.53	0.67
minimum	2	0.01	0.01	1.4	1.83	0.01	26	0.03	0.04	1.6	0.02	0.1
n	13	13	13	13	13	13	13	13	13	13	13	13
std. dev.	3.6	0.85	0.06	9.1	0.89	0.03	8.6	0.07	0.11	4.1	0.13	0.18
radial pyrolusites												
average	3	0.17	0.03	2.7	0.35	0.07	54.8	0.07	0.06	3.4	0.03	0.19
maximum	3.9	0.5	0.07	4	2.09	0.13	56.6	0.28	0.18	4.7	0.11	0.25
minimum	2.1	0.06	0.01	1.8	0.06	0.01	52.2	0.01	0.03	2.1	0.01	0.13
n	9	9	8	9	9	9	9	9	9	9	7	9
std. dev.	0.6	0.14	0.02	0.8	0.66	0.03	1.4	0.1	0.05	0.9	0.04	0.04
Mn-impregnated sands												
average	2.7	0.26	0.01	0.9	0.3	0.01	4.5	0.02	0.02	85.2	0.01	0.15
maximum	10.6	2.7	0.07	5.3	1.67	0.03	24.5	0.06	0.11	99.4	0.04	0.54
minimum	0.6	0.01	0.01	0.1	0.03	0.01	0.1	0.01	0	52.7	0.01	0.04
n	18	18	15	18	18	18	18	18	18	18	18	18
std. dev.	2.7	0.65	0.02	1.3	0.52	0.01	8.7	0.01	0.03	15.4	0.01	0.15
siliceous ores												
average	2.7	0.43	0.06	1.1	1.59	0.06	42.5	0.15	0.07	24	0.09	0.1
maximum	4.5	0.84	0.13	3.6	2.28	0.14	54.7	0.25	0.15	48.9	0.16	0.17
minimum	1.8	0.02	0.02	0.4	0.91	0.01	27.3	0.1	0.01	5.9	0.03	0.08
n	10	10	10	10	10	10	10	10	10	10	10	10
std. dev.	0.8	0.3	0.03	0.9	0.42	0.05	11.8	0.05	0.04	19	0.05	0.03
uncemented oolites												
average	4.9	1.53	0.1	2.3	0.74	0.57	46.4	0.18	0.07	9.2	0.55	0.22
maximum	14.7	2.47	0.16	10.1	1.48	0.86	55.5	0.3	0.53	30	1.07	0.64
minimum	2.4	0.41	0.01	0.7	0.28	0.09	21.9	0.03	0.04	2	0.11	0.1
n	39	39	39	39	39	39	39	39	38	39	39	39
std. dev.	3.2	0.43	0.03	1.6	0.25	0.2	8	0.07	0.08	7.4	0.24	0.13

Table 4.3 (continued): Statistics of Major and Minor Elements; [%].

	Al	Ba	Ca	Fe	K	Mg	Mn	Na	P	Si	Sr	Ti
uncemented pisolites												
average	5.4	0.81	0.04	2.1	0.45	0.1	50.1	0.07	0.06	7.7	0.04	0.24
maximum	13	4.09	0.12	5.6	1.01	0.4	61.1	0.19	0.1	19.7	0.19	0.56
minimum	0.8	0.03	0.01	0.1	0.02	0.04	36.4	0.01	0.03	0.9	0.02	0.04
n	19	19	19	19	19	19	19	19	19	19	19	19
std. dev.	3	1.34	0.03	1.2	0.31	0.08	7.1	0.07	0.02	5.8	0.05	0.13
spherulites												
average	16.6	0.46	0.04	16.7	0.28	0.07	11	0.02	0.04	31.8	0.04	0.76
maximum	23.9	1.76	0.1	37.5	0.59	0.25	46.3	0.07	0.15	55	0.2	1.17
minimum	4.7	0.06	0.01	2.4	0.1	0.02	0.7	0.01	0.01	13.1	0.01	0.23
n	15	15	9	15	15	15	15	15	15	15	12	15
std. dev.	5.2	0.51	0.03	10.8	0.15	0.06	13.9	0.02	0.03	16.3	0.06	0.26

Although markedly different in mineralogy and petrology, oolitic (G-area) and pisolitic ores (F-, A-South, and D-Quarries) exhibit remarkable similarities in their major/minor element concentration patterns (Fig. 4.2a; compare also Table 4.3). The curves of both the cemented and uncemented pisolites are almost identical to those of the oolitic ores. The largest variations are observed for Al and Si (main kaolinite components). Uncemented ores show concentrations of Al and Si which are twice as large as in cemented ores. Cemented pisolites are enriched in K; the other ores possess about half as much K.

The plot for supergene ores shows concentrations and patterns comparable to the previous group (Fig. 4.2b). The Si-, Al-, and K-concentrations of concretions (surface), hardgrounds, massive mangcretes, and radial pyrolusites (exception: K, lowest amount of all ores) approximate those of cemented oolites/pisolites. Laminar mangcretes and digital concretions from below the ore are similar to uncemented oolites/pisolites. Mn-impregnated sands and siliceous ores are dominated by silica (Fig. 4.2c). Al is of little importance and only the siliceous ores exhibit significant levels of Mn.

The remaining ores and rocks are strongly dominated by kaolinite (Fig. 4.2d). Si and Al show high concentrations and the ratio of the Si/Al peak is approximately 2 in all types. This indicates that additional silica from quartz is probably not present. With the exception of ferruginous pisolites, all other ores/rocks (laterites, chocolate ores, clays, spherulites, Fe-pipe walls) show relatively high Si and Al values. Chocolate ores are almost identical to laterites, except for the higher concentration of Mn and lower levels of Fe. The strongest variation within the group is exhibited by Fe. Rocks with the highest concentrations of Si and Al contain the least Fe, and vice versa. Generally, Mn is not very important, probably with the exception of spherulites and chocolate ores, where the concentrations of Mn are higher than those of Fe.

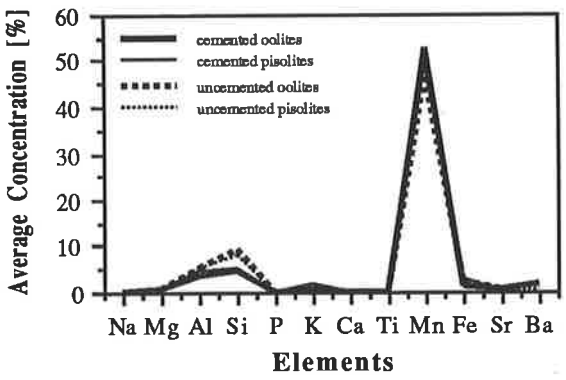


Fig. 4.2a: Major and minor element concentrations in different ore types.

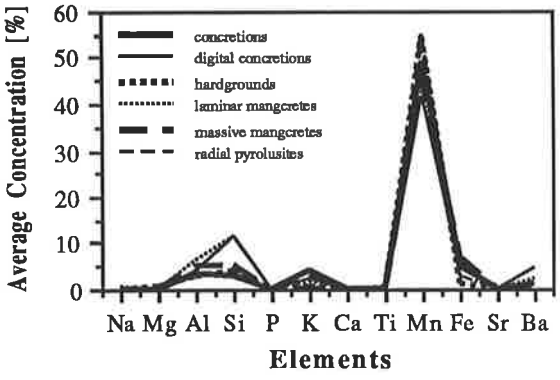


Fig. 4.2b: Major and minor element concentrations in different ore types.

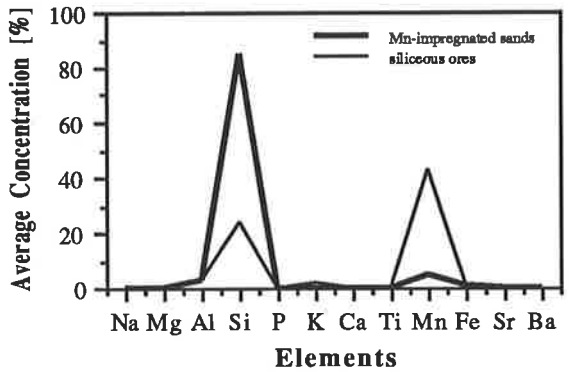


Fig. 4.2c: Major and minor element concentrations in different ore types.

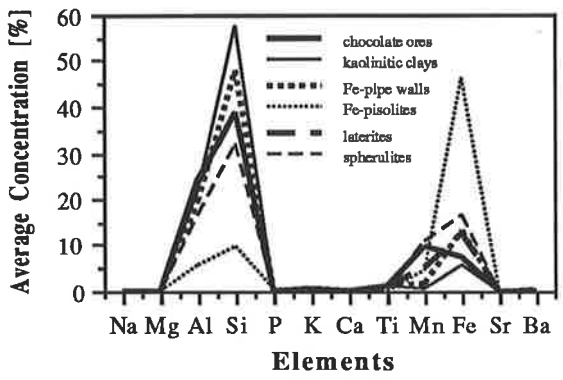


Fig. 4.2d: Major and minor element concentrations in different ore and rock types.

4.2.2.2 Trace Elements

The trace elements (TEs) allow a further separation of ore types. In general, the abundance of the TEs in oolitic ores is slightly higher than in the pisolites, and both are characterized by a sharp peak for Ni (Fig. 4.3a; see also Table 4.4). High concentrations are also observed for V in most ores and gangues (400 - 1200ppm). The highest concentration of V appears in digital concretions from beneath the main orebody (Fig. 4.3b). Here, V reaches its strongest concentration in the Mn-ores, and only oolites possess Ni concentrations that are slightly higher. Siliceous ores are generally depleted in trace elements, but depict V levels similar to those of oolitic/pisolitic ores (Fig. 4.3c). For most of the elements the curves of siliceous ores and Mn-impregnated sands are comparable, though the former materials are normally higher in their trace element concentration. The exception is Zr, which gains importance in lateritic, clay-rich products where it reaches levels similar to V (Fig. 4.3d). Ferruginous pisolites deviate from the general pattern in that they show enrichments in V, Ni, Co, Zn, As, Mo, Pb. Boron, which normally has very low concentrations, is enriched in some kaolinitic clays.

Table 4.4: Statistics of trace elements in ores and rocks.

	As	B	Co	Cr	Cu	Mo	Ni	Pb	Sc	Th	U	V	Zn	Zr
cemented oolites														
average	61	17.32	77.39	14.95	138.8	73	342	57	8	6	12	330.8	115.3	43.17
maximum	72	20.89	134.2	17.11	184.7	77	427	58	10	6	13	493	161.9	61.88
minimum	50	12.83	35.88	13.93	98.84	69	258	56	5	5	11	256.8	99.24	31.48
n	2	8	8	8	8	2	8	2	2	2	2	8	8	8
std. dev.	16	2.91	35.58	1.07	29.64	6	63	1	4	1	1	76.99	22.2	12.15
cemented pisolites														
average	39	14.13	95.06	14.5	89.5	43	132	41	9	4	10	200.5	97.53	38.27
maximum	55	31.24	171.8	18.4	191.2	56	344	72	15	8	13	516	185.7	72.75
minimum	26	0	35.78	13.4	42.9	34	28	23	4	0	6	37.33	65.29	14.79
n	14	31	31	31	31	14	31	14	14	14	14	31	31	31
std. dev.	8	7.28	28.15	1.25	36.77	6	71	15	4	2	2	101.2	28.49	15.75
chocolate ores														
average	n.d.	17.14	40.05	23.65	50.42	n.d.	22	n.d.	n.d.	n.d.	n.d.	261	49.7	257.5
maximum	n.d.	26.36	63.66	26.33	83.09	n.d.	100	n.d.	n.d.	n.d.	n.d.	396.9	81.04	274.8
minimum	n.d.	6.41	24.25	17.13	38.48	n.d.	5.3	n.d.	n.d.	n.d.	n.d.	159.7	44.95	142.3
n	n.d.	10	10	10	10	n.d.	10	n.d.	n.d.	n.d.	n.d.	10	10	10
std. dev.	n.d.	7.28	12.7	2.51	12.83	n.d.	29	n.d.	n.d.	n.d.	n.d.	72.8	11.05	40.7
kaolinitic clays														
average	2	65.02	17.87	40.16	25.26	2	2.7	10	14	14	3	136.6	42.76	193
maximum	2	511.6	22.33	76.38	40.7	3	7.7	13	15	15	4	923.7	49.48	279.5
minimum	1	0	13.5	7.09	14.92	2	0	6	13	12	1	5.58	36.23	63.34
n	2	8	8	8	8	2	8	2	2	2	2	8	8	8
std. dev.	1	180.5	2.87	24.99	9.07	0	2.9	5	1	2	2	318.8	4.81	78.15
concretions														
average	n.d.	13.83	118.7	15.16	158.7	n.d.	112	n.d.	n.d.	n.d.	n.d.	122.6	120.7	33.26
maximum	n.d.	43.57	156.3	18.82	287.8	n.d.	314	n.d.	n.d.	n.d.	n.d.	296	205.4	54.37
minimum	n.d.	1.73	89.22	13.26	53.28	n.d.	24	n.d.	n.d.	n.d.	n.d.	53.82	32.28	22.86
n	n.d.	10	10	10	10	n.d.	10	n.d.	n.d.	n.d.	n.d.	10	10	10
std. dev.	n.d.	11	22.06	1.53	70.5	n.d.	96	n.d.	n.d.	n.d.	n.d.	83.22	51.89	8.01
digital concretions														
average	n.d.	13.67	131	16.33	131.2	n.d.	59	n.d.	n.d.	n.d.	n.d.	1154	122.3	46.89
maximum	n.d.	23.67	174.1	19.98	162.4	n.d.	103	n.d.	n.d.	n.d.	n.d.	1522	141.2	74.44
minimum	n.d.	6.8	85.47	13.98	72.92	n.d.	24	n.d.	n.d.	n.d.	n.d.	344	76.02	28.97
n	n.d.	6	6	6	6	n.d.	6	n.d.	n.d.	n.d.	n.d.	6	6	6
std. dev.	n.d.	5.63	30.67	2.07	34.47	n.d.	26	n.d.	n.d.	n.d.	n.d.	423.9	25.16	20.42
Fe-pipe walls														
average	50	0.55	20.05	37.1	32.55	32	1.8	57	14	9	5	286.7	44.93	209.1
maximum	50	2.61	28.87	50.38	40.98	32	2.9	57	14	9	5	398.1	54.87	256.2
minimum	50	0	14.27	27.19	26.92	32	1.2	57	14	9	5	83.05	32.13	155.6
n	1	5	5	5	5	1	5	1	1	1	1	5	5	5
std. dev.	0	1.15	6.08	9	5.33	0	0.7	0	0	0	0	131.9	8.17	37.54
Fe-pisolites														
average	333	17.41	50.19	23.04	190.3	120	324	112	16	5	20	864.4	191.1	118.8
maximum	436	133.1	97.37	79.13	418.7	203	938	163	24	9	26	1535	281.5	180.3
minimum	228		23.86	12.85	52.13	67	90	62	13	1	15	70.89	123.5	50.75
n	5	18	18	18	18	5	18	5	5	5	5	18	18	18
std. dev.	94	34.6	22.27	16.26	113.8	57	195	47	5	3	5	426	49.21	41.32

Table 4.4 (continued): Statistics of trace elements in ores and rocks.

	As	B	Co	Cr	Cu	Mo	Ni	Pb	Sc	Th	U	V	Zn	Zr
hardgrounds														
average	n.d.	61.58	75.27	14.14	91.63	n.d.	198	n.d.	n.d.	n.d.	n.d.	171.4	86.47	58.97
maximum	n.d.	97.92	82.87	14.36	118.5	n.d.	207	n.d.	n.d.	n.d.	n.d.	185.6	89.77	85.56
minimum	n.d.	9.48	62.72	13.93	55.71	n.d.	191	n.d.	n.d.	n.d.	n.d.	159.7	82.2	37.29
n	n.d.	3	3	3	3	n.d.	3	n.d.	n.d.	n.d.	n.d.	3	3	3
std. dev.	n.d.	46.28	10.95	0.22	32.37	n.d.	8.1	n.d.	n.d.	n.d.	n.d.	13.12	3.88	24.51
laminar mangcretes														
average	n.d.	13.16	73.54	16.36	112.7	n.d.	62	n.d.	n.d.	n.d.	n.d.	509.4	79.65	62.94
maximum	n.d.	31.73	173.7	19.61	144	n.d.	186	n.d.	n.d.	n.d.	n.d.	1067	97.19	82.58
minimum	n.d.	6.8	27.23	15.59	100.4	n.d.	18	n.d.	n.d.	n.d.	n.d.	161.5	63.86	43.81
n	n.d.	7	7	7	7	n.d.	7	n.d.	n.d.	n.d.	n.d.	6	7	7
std. dev.	n.d.	8.5	46.34	1.45	14.9	n.d.	67	n.d.	n.d.	n.d.	n.d.	303.4	14.41	11.45
laterites														
average	52	4.61	41.7	40.7	43.52	5	13	51	24	17	6	301.7	50.95	243.6
maximum	94	44.97	92.26	105.7	68.58	18	32	82	33	21	9	738.4	72.83	268.6
minimum	31	0	14.67	18.79	20.43	1	0.3	25	19	13	4	9.2	39.37	180.6
n	7	26	26	26	26	7	26	7	7	7	7	26	26	26
std. dev.	23	8.77	21.71	21.62	13.55	6	10	19	6	3	2	168	8.26	19.85
massive mangcretes														
average	12	10.47	169.2	15.94	168.5	17	90	56	15	8	10	360.3	136.2	62.58
maximum	12	21.41	294.9	18.79	415.9	17	311	56	15	8	10	1189	248	166.3
minimum	12	1.52	90.98	14.33	51.39	17	19	56	15	8	10	66.2	61.22	21.67
n	1	13	13	13	13	1	13	1	1	1	1	13	13	13
std. dev.	0	4.98	69.44	1.38	119.2	0	95	0	0	0	0	385	61.12	45.93
radial pyrolusites														
average	96	31.51	23.14	16.03	51.66	28	46	122	4	6	7	397.5	77.19	35.74
maximum	96	42.72	58.88	20.65	82.69	28	88	122	4	6	7	1030	100.8	41.1
minimum	96	17.73	8.89	11.02	29.75	28	20	122	4	6	7	127.4	54.36	28.19
n	1	9	9	9	9	1	9	1	1	1	1	9	9	9
std. dev.	0	6.48	15.62	2.83	20.35	0	25	0	0	0	0	351	15.41	4.72
Mn-impregnated sands														
average	2	2.06	53.18	16.3	62.92	4	1.2	9	4	3	1	161.4	42.01	55.64
maximum	12	29.9	191.4	28.18	341.6	26	8.1	53	17	10	7	1462	86.96	121.6
minimum	0	0	8.71	14.34	11.63	1	0	2	1	0	0	1.09	32.78	32.2
n	15	18	18	18	18	15	18	15	15	15	15	18	18	18
std. dev.	3	6.99	49.72	3.35	98.16	6	2.3	13	4	2	2	392.7	15.92	22.26
siliceous ores														
average	n.d.	15.53	149.3	14.97	135.2	n.d.	84	n.d.	n.d.	n.d.	n.d.	251.4	118.1	33.41
maximum	n.d.	25.6	216.3	17.05	262.8	n.d.	187	n.d.	n.d.	n.d.	n.d.	828.5	195.8	49.92
minimum	n.d.	3.87	86.69	14.32	68.45	n.d.	24	n.d.	n.d.	n.d.	n.d.	51.39	74.38	16.6
n	n.d.	10	10	10	10	n.d.	10	n.d.	n.d.	n.d.	n.d.	10	10	10
std. dev.	n.d.	7.35	46.49	0.81	69.27	n.d.	43	n.d.	n.d.	n.d.	n.d.	230.5	34.6	10.97
uncemented oolites														
average	53	13.48	83.39	14.67	128.7	79	440	97	8	6	13	329.3	137	61.39
maximum	66	21.13	149.9	24.44	190.2	108	703	124	12	12	18	512.8	224.4	170.9
minimum	39	4.07	26.48	12.53	40.36	7	29	38	3	2	8	144.7	67.14	20.99
n	17	39	39	39	39	17	39	17	17	17	17	39	39	39
std. dev.	9	4.17	26.98	1.83	37.13	26	160	26	2	3	3	94.58	36.78	36.13

Table 4.4 (continued): Statistics of trace elements in ores and rocks.

	As	B	Co	Cr	Cu	Mo	Ni	Pb	Sc	Th	U	V	Zn	Zr
uncemented pisolites														
average	70	37.49	55.34	16.16	71.68	70	98	58	6	5	13	245.4	84.78	63.07
maximum	90	114.6	102.8	27.88	120.4	125	233	79	12	8	52	532.8	123.5	136.4
minimum	48	0	22.24	14.11	39.22	9	41	32	3	0	4	91.59	64.1	11.16
n	8	19	19	19	19	8	19	8	8	8	8	19	19	19
std. dev.	16	32.35	23.62	3.01	26.89	42	53	16	4	2	16	111.4	17.44	35.87
spherulites														
average	28	6.59	51.18	55.51	72.69	7	63	49	23	16	7	512.7	66.13	197.8
maximum	28	21.85	83.41	119.1	138.9	7	266	54	26	18	7	1471	123.3	263.9
minimum	27	0	18.17	17.11	39.3	7	5.5	44	19	13	6	172.4	42.67	61.88
n	2	14	15	15	15	2	15	2	2	2	2	15	15	15
std. dev.	1	6.85	18.07	29.33	32.2	0	90	7	5	4	1	379	28	59

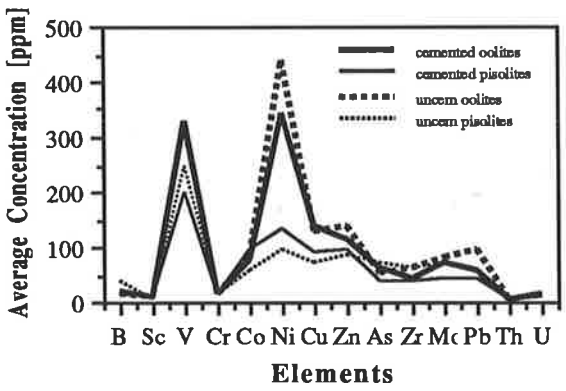


Fig. 4.3a: Trace element concentrations in different ore types.

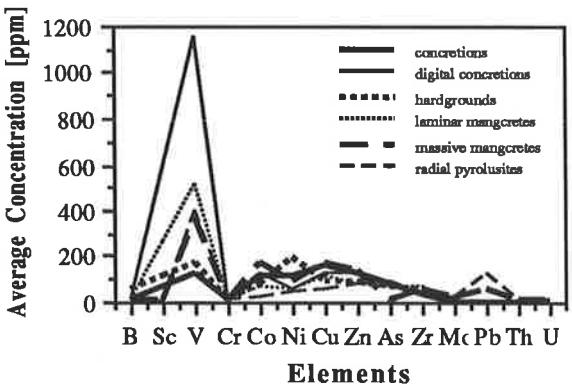


Fig. 4.3b: Trace element concentrations in different ore types.

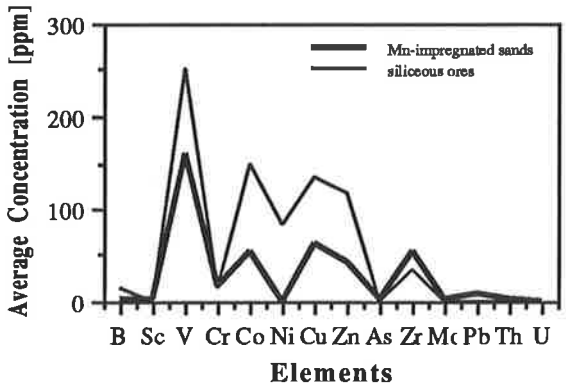


Fig. 4.3c: Trace element concentrations in different ore types.

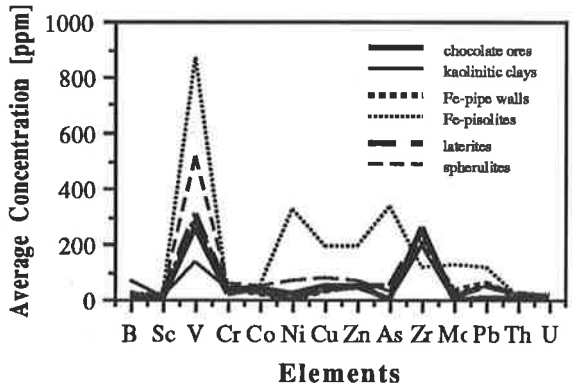


Fig. 4.3d: Trace element concentrations in different ore and rock types.

Some of the "end-members" of ores and gangues are compared in an overview, ranges of the respective materials are also provided (Figs. 4.3e,f). Although the cemented pisolitic ores from F3-Quarry possess a smaller variability in their trace element composition than the mostly uncemented oolites from the G/G-South Quarry area (Fig. 4.3e), the patterns for most elements of both areas are similar. Some of the oolitic ores show marked depletions in Cu and B, whereas others contain relatively high concentrations of these elements.

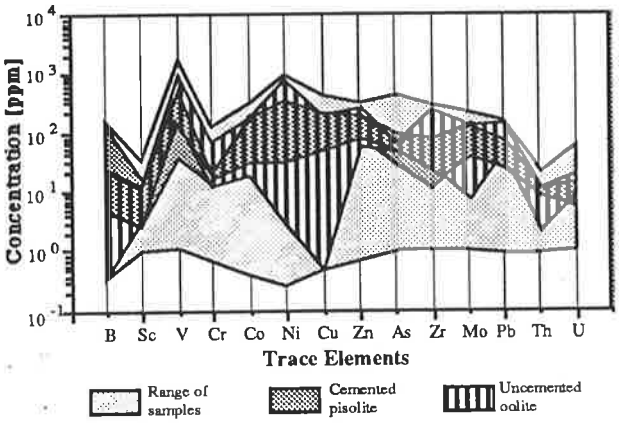


Fig. 4.3e: Trace element range of all samples, pisolitic ores (F3) and oolitic ores (G-South).

Kaolinite and goethite can also be considered as "end-members" in the sense that they are the dominant gangue minerals (in association with quartz sand). These minerals appear in almost any possible combination as gangue or within ore (Fig. 4.3f; see also chapter 3). Thus, kaolinite and goethite "dilute" bulk sample compositions of ores with lower trace element levels (e.g. As in kaolinite) or they may superimpose their signature upon ores with relatively low trace element concentrations (e.g. V in kaolinite or goethite).

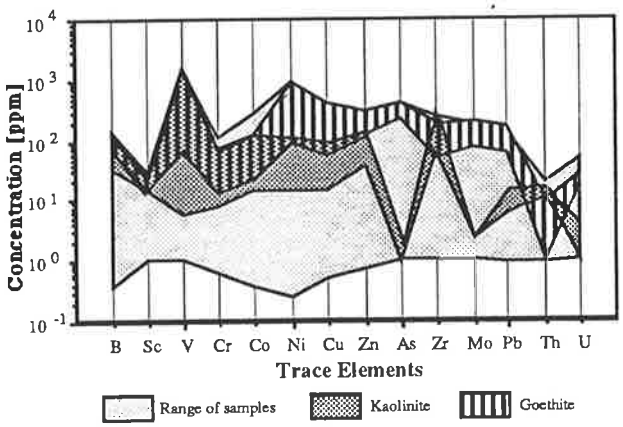


Fig. 4.3f: Trace element range of all samples, concentrations in kaolinite and goethite.

Both gangue minerals contain a number of elements in concentrations near the upper limits observed. The ranges of kaolinite and goethite overlap for the lighter elements (B to Co) and also for Zr and Th. In an intermediate group the trace elements of goethite dominate over those of kaolinite, although the trace element abundance of both gangues is above average (Ni, Cu, Zn). A third group shows insignificant levels for kaolinite (As, Mo, U) and high concentrations for goethite.

4.2.2.3 Rare Earth Elements

Although the Rare Earth Elements (REEs) belong to the trace elements in the case of the Groote Eylandt deposit, they are discussed separately because of their chemical properties. In general, the REEs occur in one oxydation stage and they are thus relatively stable over a wider range of geochemical conditions. Ce and Eu are an exception in that these elements appear in different valencies, which makes them more mobile. Therefore, a depletion or enrichment of the REEs in the various secondary materials may reflect supergene processes much better than the elements discussed before. An overview over statistical data is given in Table 4.5.

The unnormalized REE concentration patterns are used to differentiate some of the ore and rock types. Generally, the manganese oxides show a decrease from the light REEs (LREE) towards the heavy REEs (HREE), with the strongest drop in the concentration between Ce and Sm (Figs. 4.4a-d; after Pracejus et al., 1990). Most ores are depleated in Eu relative to the concentration of the neighbouring elements and are enriched in Ce. Strong differences according to the presence of the respective ore and rock types are observed. Cemented and uncemented oolites/pisolites exhibit almost identical patterns for most of the HREEs (Fig. 4.4a). A pronounced Ce enrichment occurs in the pisolitic materials and a small depletion characterizes the oolites. The latter pattern is unique, except for associated hardgrounds, and this fact can be used to chemically distinguish the oolitic/pisolitic ores of the G-Quarry area from ores of other parts of the deposit.

A variety of secondary ore types show REE patterns similar to those of cemented and unconsolidated oolites/pisolites (Fig. 4.4b). However, REE concentrations of some of these supergene ores are relatively high compared with oolitic and pisolitic materials. Radial pyrolusite, in particular, possesses an extreme enrichment of the LREEs, which is unequalled by any other ore/rock of the deposit. Laminar mangcretes and concretionary ores display patterns that are identical to each other and while massive mangcretes are also comparable, they have higher Ce concentrations. Hardgrounds and digital concretions (below main orebody) both show uncommon patterns with relatively low REE concentrations. Mn-impregnated sands and siliceous ores exhibit a positive Ce anomaly, and the concentrations are the lowest of all ores and rocks (Fig. 4.4c).

The last group of rocks analyzed is mostly dominated by Fe enrichment, with the exception of kaolinite samples and Fe-pipe walls, which are dark red and contain high amounts of clay minerals and quartz (Fig. 4.4d). All samples show high Ce concentrations and relatively high abundances of Gd. Strongly ferruginous rocks exhibit an inverse pattern with a Gd dominance over the Ce concentration (compare Fe-pisolites and laterite).

Table 4.5: Statistics of Rare Earth Elements in ores and associated rocks.

	Ce	Eu	Gd	La	Nd	Sm	Yb
cemented oolites							
average	55.3	6.5	24.8	51.5	90	22.7	6.9
maximum	126.7	7.9	29.3	60.4	114.4	27.6	10.4
minimum	31.9	3.8	21.5	37.9	51.1	15.6	4.2
n	8	8	8	8	8	8	8
std. dev.	31.4	1.4	2.8	7.6	20.7	3.6	2.3
cemented pisolites							
average	73.6	3.3	19.2	52.6	53.9	13.9	5.1
maximum	164.2	7.9	64.8	79.4	97.9	25.8	9.4
minimum	11.9	1.3	10.3	32.7	28	5.2	2.7
n	31	31	31	31	31	31	31
std. dev.	44	1.4	11.6	12.1	15.7	5.1	1.5
chocolate ores							
average	210.3	1.2	23.7	24.5	33.2	7.5	2.4
maximum	337.3	6	30	53.2	102.8	30.7	3.4
minimum	61.8	0.2	16.9	16.4	17.1	2.1	1.3
n	10	10	10	10	10	10	10
std. dev.	80.3	1.7	4	10.8	25.3	8.5	0.7
kaolinitic clays							
average	28.1	0.2	7.9	8.6	11.5	0.7	0.7
maximum	39.6	0.6	33.5	14.3	19.1	3.7	2.2
minimum	7.1	0	0	0	0	0	0
n	8	8	8	8	8	8	8
std. dev.	12.3	0.2	11.4	5	6.2	1.3	0.7
concretions							
average	115.9	2.1	20.7	37	33.4	13.7	2.6
maximum	226	3.9	75.9	55.5	55.9	20.8	6.5
minimum	11.3	0	8.7	16.1	17.8	8.7	1.1
n	10	10	10	10	10	10	10
std. dev.	67.6	1	19.9	11.3	14.2	3.4	1.8
digital concretions							
average	51.6	1.7	23.7	28.3	26.7	8.5	5.8
maximum	67.6	2.4	39	32.6	33.7	14.7	7.2
minimum	44.4	0.6	5.8	22.7	17.5	2.4	4
n	6	6	6	6	6	6	6
std. dev.	8.3	0.7	11.5	3.3	6.3	4.3	1.2
Fe-pipe walls							
average	35	0	31	11.2	11.3	1.4	1.5
maximum	66.6	0	46.4	16.5	16.3	3.1	2
minimum	11.8	0	16.8	8.4	8.7	0.2	1
n	5	5	5	5	5	5	5
std. dev.	21.3	0	11	3.1	2.9	1.4	0.5
Fe-pisolites							
average	63.8	0	93.5	16.8	20.5	12.4	6.5
maximum	94.6	0.5	112.7	35.2	36.2	17.7	11
minimum	30.6	0	48.7	6.9	0	7.6	2.1
n	18	18	18	18	18	18	18
std. dev.	15.7	0.1	17.3	7.6	9	2.3	2.1

Table 4.5 (continued): Statistics of Rare Earth Elements in ores and associated rocks.

	Ce	Eu	Gd	La	Nd	Sm	Yb
hardgrounds							
average	28.6	3.5	17.3	40.2	52.1	14.8	4.4
maximum	34.4	4.9	24.9	43.8	61	22.1	5.6
minimum	17.9	1.7	9.2	37.5	43.7	3.3	2.9
n	3	3	3	3	3	3	3
std. dev.	9.3	1.7	7.9	3.3	8.7	10	1.4
laminar mangcretes							
average	117.3	2	16.4	35.9	35.9	9.7	2.8
maximum	231	4	25.1	47.4	68.2	19.8	4.7
minimum	42.6	0.9	11.5	28.3	23.4	4.9	1.6
n	7	7	7	7	7	7	7
std. dev.	73	1.2	4.9	8.1	16.5	5.1	1.2
laterites							
average	158.5	1.1	29.6	22.2	30.3	7.3	2.8
maximum	416.8	5.4	61.5	51.6	94.5	17.6	7
minimum	28.1	0	0.5	11.4	11.8	0.4	0.4
n	26	26	26	26	26	26	26
std. dev.	105.2	1.5	12.6	11	21.7	4.6	1.5
massive mangcretes							
average	170.4	2.3	25.5	38.5	40.5	12.5	4.4
maximum	368.2	4.1	71.9	61.1	63.7	20.5	10.6
minimum	35.9	0	11.8	22.2	19.6	7	2
n	13	13	13	13	13	13	13
std. dev.	116	1.5	18.4	12.3	17.3	4.4	2.6
radial pyrolusites							
average	292.2	12.8	49.4	77	212.6	68.1	3.6
maximum	396	19.1	72.4	111.9	315.7	98.3	5.2
minimum	192.7	3.9	20.5	45.5	60.7	20.1	2.7
n	9	9	9	9	9	9	9
std. dev.	61.5	4.8	15.4	22.7	78.3	24.9	0.9
Mn-impregnated sands							
average	32.6	0.6	1.8	10.6	11.5	1.1	0.5
maximum	87.2	1.3	13.1	19.1	29.4	8.4	4.3
minimum	18.7	0.1	0	5.7	5.2	0	0
n	18	18	18	18	18	18	18
std. dev.	15.5	0.3	3.5	3.6	5.2	2.1	1.2
siliceous ores							
average	74.8	2.5	13.9	34.5	39.9	12.4	3.5
maximum	187.2	3.6	20.3	49.9	56.7	17.5	7.4
minimum	38.3	1.4	7.9	18.7	21.6	5.1	1.8
n	10	10	10	10	10	10	10
std. dev.	48	0.8	4.7	12.6	14.5	4.7	1.9
uncemented oolites							
average	50.9	3.7	20.9	43.7	58	12.1	7.1
maximum	105.6	6.5	34.8	58.4	92.5	24.7	13.4
minimum	8.5	1.4	6.9	29.3	38.6	4.1	1.6
n	39	39	39	39	39	39	39
std. dev.	23.9	1.3	7.4	6.5	14.2	5.1	2.8

Table 4.5 (continued): Statistics of Rare Earth Elements in ores and associated rocks.

	Ce	Eu	Gd	La	Nd	Sm	Yb
uncemented pisolites							
average	79.7	4.3	21.6	53.9	65.6	17.7	3.8
maximum	177.9	10.1	37.6	91.9	121.4	30.7	8.5
minimum	14.4	1.5	6.9	30.2	26.3	6	1.4
n	19	19	19	19	19	19	19
std. dev.	48.6	2.1	8.7	14.3	23.9	7.3	1.8
spherulites							
average	141.3	1.4	43.7	28.4	40.2	10.5	3.7
maximum	204.5	5.9	82.4	52.8	102.7	22	5.6
minimum	61.7	0	21.5	14.3	17.6	3	1.8
n	15	15	15	15	15	15	15
std. dev.	56.1	1.9	20.1	11.6	24.3	5.6	1.2

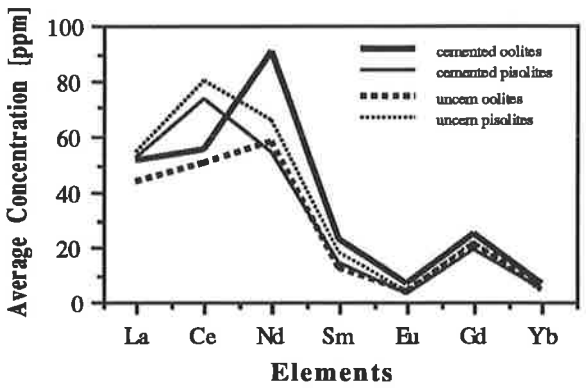


Fig. 4.4a: REEs in ores; after Pracejus et al., 1989.

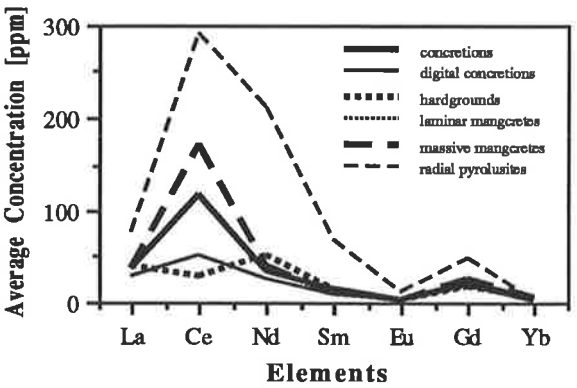


Fig. 4.4b: REEs in ores; after Pracejus et al., 1989.

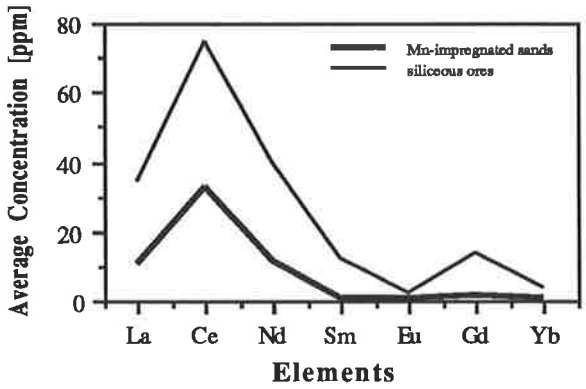


Fig. 4.4c: REEs in ores; after Pracejus et al., 1989.

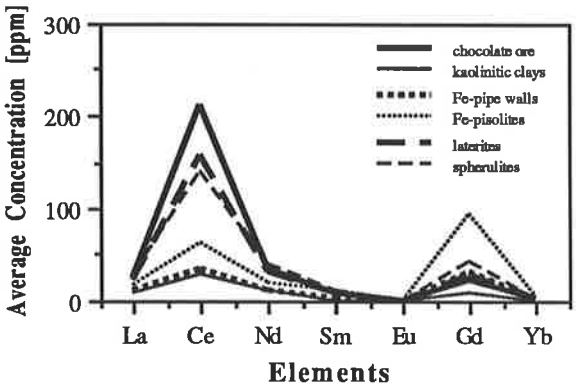


Fig. 4.4d: REEs in ores and gangues; after Pracejus et al., 1989.

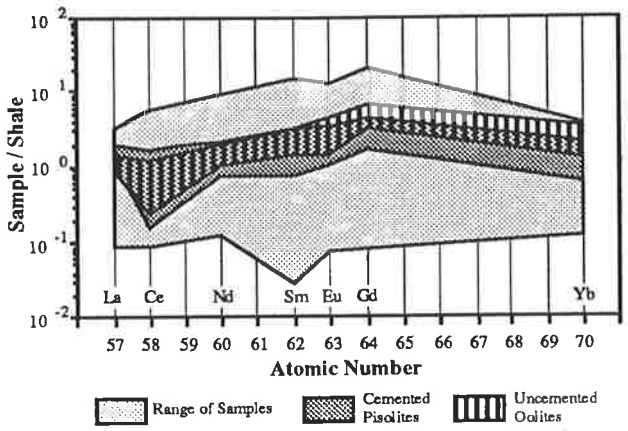


Fig. 4.4e: Range of REEs in all samples compared with cemented pisolitic materials from F3 and uncemented oolitic ores from G-South.

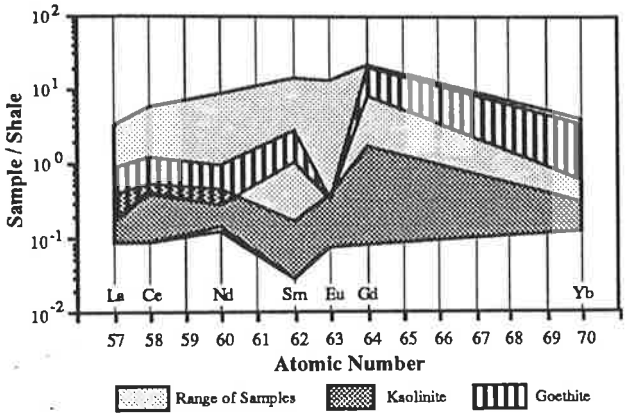


Fig. 4.4f: Range of REEs in all samples compared with kaolinite and goethite.

The shale-normalized REEs (Haskin and Haskin, 1966) of both oolitic and pisolitic ores are very similar to each other, with pisolites showing a larger variability. The IREE and HREE are slightly enriched in oolites (Fig. 4.4e). REEs of kaolinite and goethite show a comparable behaviour in the LREE, but the concentration of La, Ce, and Nd is moderately higher in the goethitic rocks (Fig. 4.4f). The heavier elements display the largest fractionation. The normalized REE concentrations of kaolinite decrease gradually from Ce to Sm and then increase slightly to Yb. In contrast, goethite possesses a reverse pattern and exhibits a strong increase from Nd to Gd, with the exception of Eu which shows a large depletion. From Gd to Yb the normalized concentrations decrease.

4.3 Elements in the Vertical Sequence

Contrary to the previous approach, which compared various ore/rock types, the distribution of elements is now examined in the stratigraphic context. Attention focuses on the ores of G/G-South Quarry (mainly unconsolidated oolites/pisolites) and F3-Quarry (cemented pisolites), because of their mineralogical differences. These locations were sampled on a small scale from vertical geological profiles (see chapter 2).

Element abundances within the vertical sequence are studied in two ways:

- as single elements, to determine zones of enrichment or depletion,
- as element group, in which variations relative to neighbouring elements are described; the role of the REEs is emphasized here, because some members of this group (Ce, Eu) behave differently in the weathering environment , when compared with the other REEs.

4.3.1 Single Element Distributions

Commonly, manganese displays a decrease with depth in one area and an increase in other locations (Fig. 4.5a). Elements such as Si, Fe or Al plot in a reverse order in the same quarries (Fig. 4.5b). It is unclear, whether such a "dilution" of Mn with gangue elements reflects a localized detrital input of sand and/or clay during sedimentation. A stratigraphy-controlled supergene mobilization of certain elements in one part of the orebody and reprecipitation elsewhere could also result in similar patterns. One of the most striking features observed with many elements is the development of one or more horizons where specific elements are concentrated. The best example for such a pronounced enrichment is Zn in samples from G-South, which reaches its highest concentrations at a depth of approximately 7m (Fig. 4.5c). Similar horizons are recognized for Sr (and many other elements) in G-Quarry (~4 m) and F3-Quarry (~12 m) (Fig. 4.5d). Data of G-South Quarry materials are plotted to generally illustrate enrichments and depletions of elements in the vertical sequence (Figs. 4.6a,b). This locality was chosen for its horizontal uniformity of ores and gangues (Gquarry, for instance, produces a similar geochemical profile); a large number of samples are also available for this particular section. Frequently, element associations occur that are comparable to those discussed above (Table 4.2).

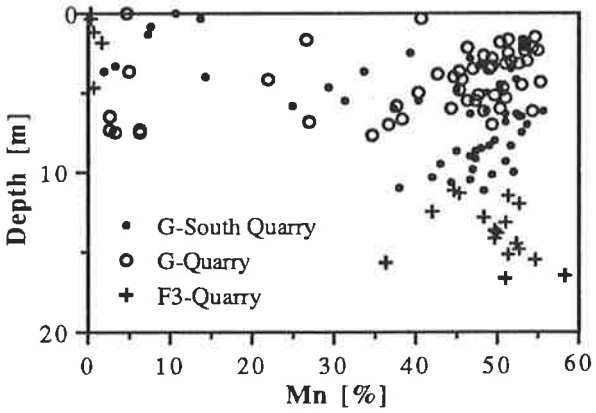


Fig. 4.5a: Mn-distribution in vertical sections of G-, G-South, and F3-Quarry.

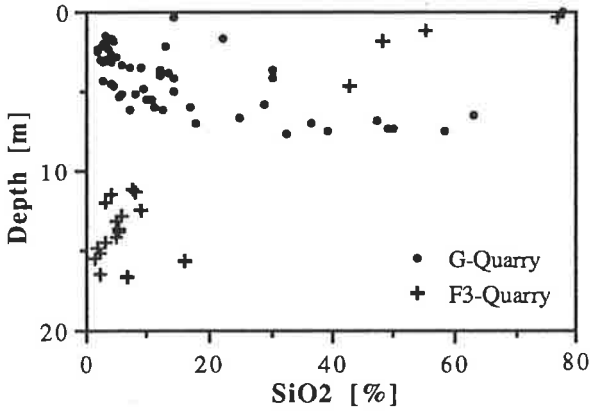


Fig. 4.5b: SiO_2-distribution in vertical sections of G- and F3-Quarry.

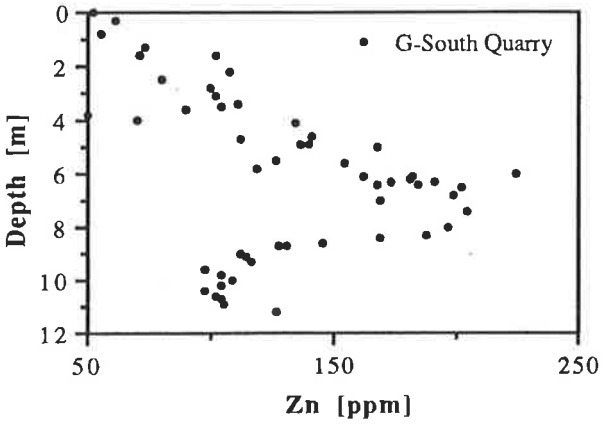


Fig. 4.5c: Zn-distribution in a vertical section of G-South Quarry.

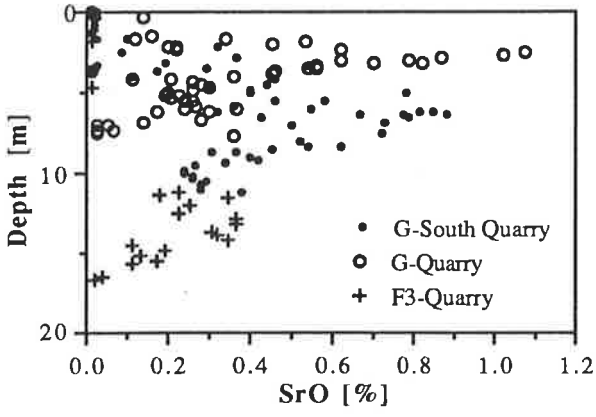


Fig. 4.5d: SrO-distribution in vertical sections of G-, G-South, and F3-Quarry.

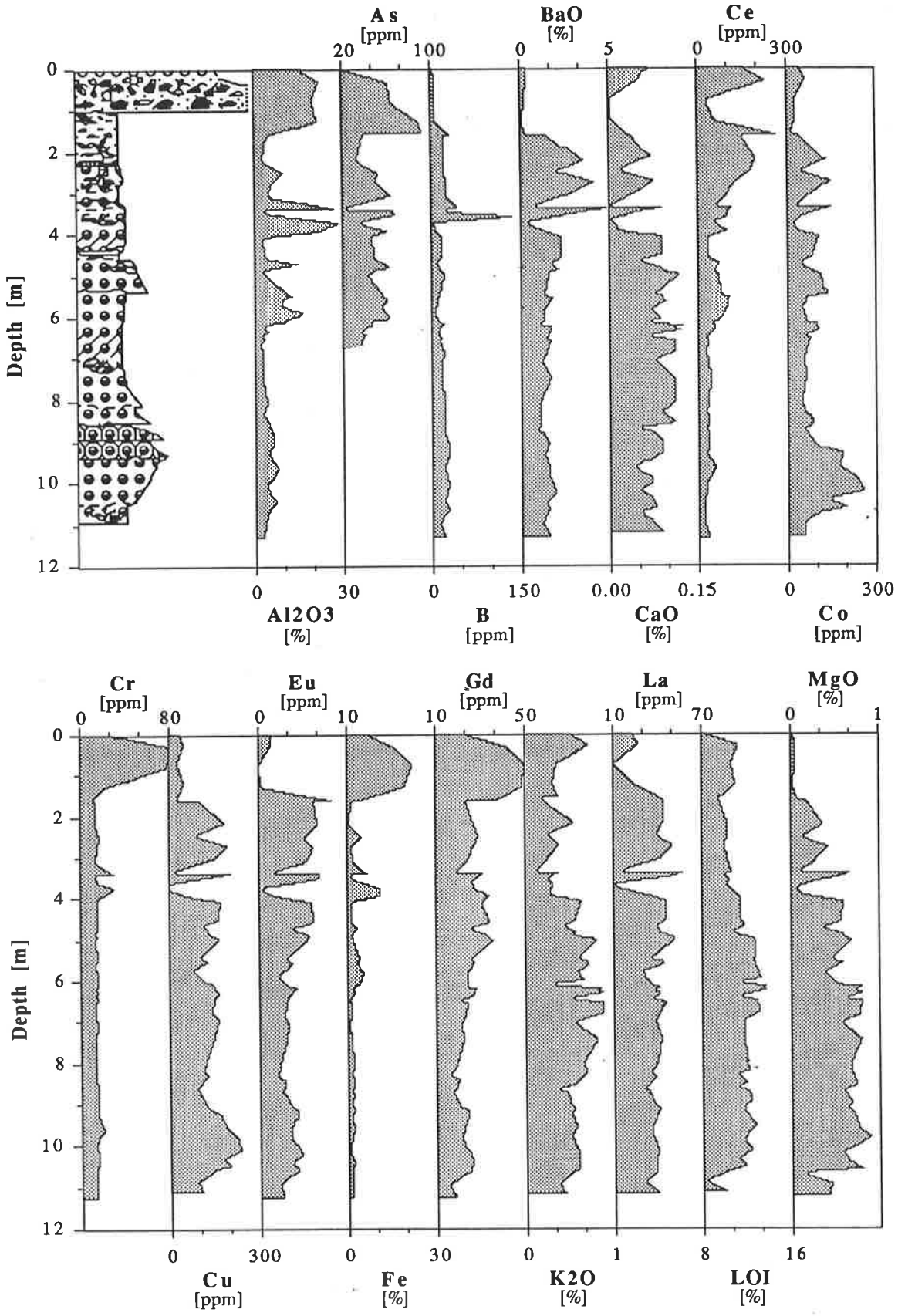


Fig. 4.6a: Element distribution in the stratigraphic section.

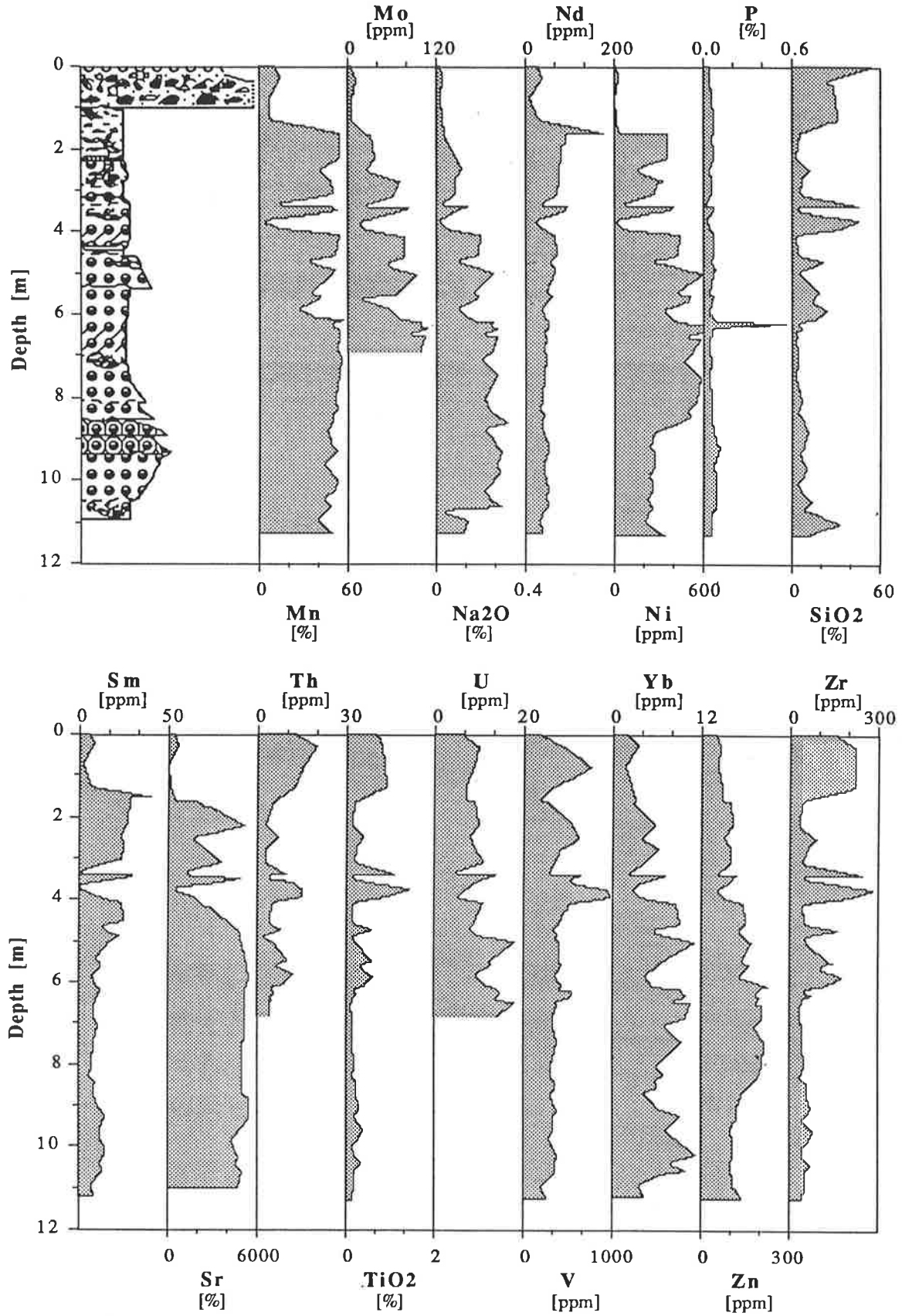


Fig. 4.6b: Element distribution in the stratigraphic section.

4.3.2 Shale-normalized REE-patterns

As with the elements discussed above, the REE concentrations of ores and rocks strongly depend on the stratigraphic level from which the samples were taken. Sampling profiles at F3 and G-South Quarry exhibit a comparable decreasing concentration of the entire group of the Rare Earths (∑REE; not plotted) downward. A similar correlation between depth and the abundance of single REEs is also observed, with the exception of Yb, which increases slightly in concentration downward.

The concentrations of Eu and Ce decrease more rapidly downward than the other REEs. This behaviour is best seen by plotting the anomalies of the shale-normalized data against depth (Fig. 4.7b). The calculated anomalies for Eu and Ce show the deviation of the respective element from the interpolated values between adjacent elements, the direction of this deflection is indicated by plus or minus signs ($Eu_{[anomaly]} = Eu^* - (^1/_2\ Sm^* + ^1/_2\ Gd^*)$; $Ce_{[anomaly]} = Ce^* - (^2/_3\ La^* + ^1/_3\ Nd^*)$; *shale-normalized element). An analysis of the normalized REE patterns from F3- and G-South Quarry demonstrates that though the ores differ in their appearance and mineralogy, the stratigraphic distribution of the Eu anomaly is comparable.

The oolitic/pisolitic ores of G-South Quarry show a decreasing Eu anomaly (~ 0 to ~ -1) from the surface to a depth of approximately 6 m, below which the anomaly increases further down to almost -0.5 at about 12 m. From about 10 m depth the cemented pisolites of F3-Quarry continue this trend until ~13 m (~ 0), from where the values again decrease to -1 at 18 m. Similar intervals of enrichment and depletion have already been detected for other trace elements and in other locations of the deposit, but at the moment it is unclear, which processes are responsible for the development of these chemical trends.

Fe-rich laterites and spherulites (Fe- and Mn-rich) near the surface from both locations display a wide range for the Eu anomalies (0 to about -4.5). The Ce anomalies (not plotted) from ores of the two areas are not as consistent in their small-scale stratigraphic variations as the Eu anomalies, but generally they have larger negative values with increasing depth. Associated Fe-rich laterites and spherulites fall into the same broad trend as the ores.

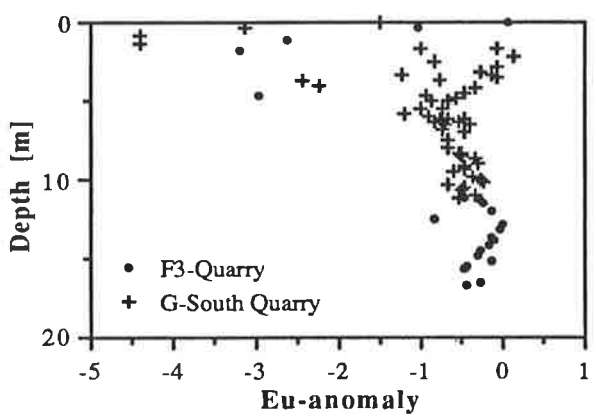


Fig. 4.7: Correlation of Eu-anomalies and depth in ores and associated rocks from F3- and G-South Quarry; after Pracejus et al., 1989.

That not only the anomalies of Ce and Eu are depth-dependent, but also the normalized concentrations of the other REEs, is demonstrated on the example of ores and rocks from F3 and G-South Quarry (Figs. 4.8a,b

and 4.8a-d). Additionally, the patterns indicate differences between the various ore and rock types. Generally, the cemented pisolitic materials from the F3 area possess a very strong negative Ce anomaly (-1.8; Fig. 4.8a). However, the most striking feature of the individual patterns is the behaviour of this anomaly, because it decreases gradually from the bottom to the top of the section. From Nd to Gd the pattern increases almost linearly, exhibiting a very small negative Eu anomaly, whereas normalized Gd is slightly higher than normalized Yb. In contrast to the cemented pisolites, Fe-rich and Mn-bearing laterite exhibits a distinctive positive Ce anomaly (up to 2.4) and a large negative Eu anomaly (until -5.5; Fig. 4.8b). In this diagram 2 samples were interpolated for Eu, which was below the detection limit.

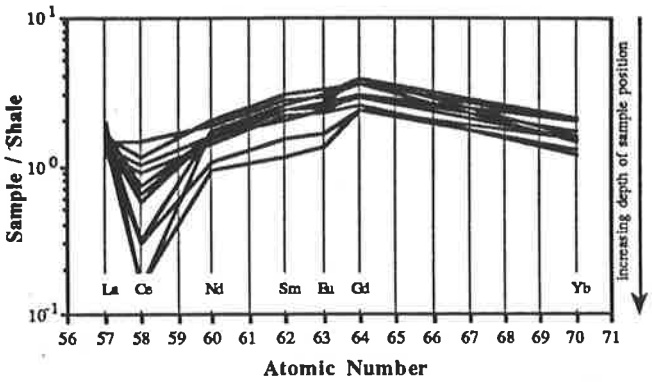


Fig. 4.8a: Shale-normalized patterns and depth (against European shales; Haskin and Haskin, 1966) of cemented pisolites from F3-Quarry; after Pracejus et al., 1989.

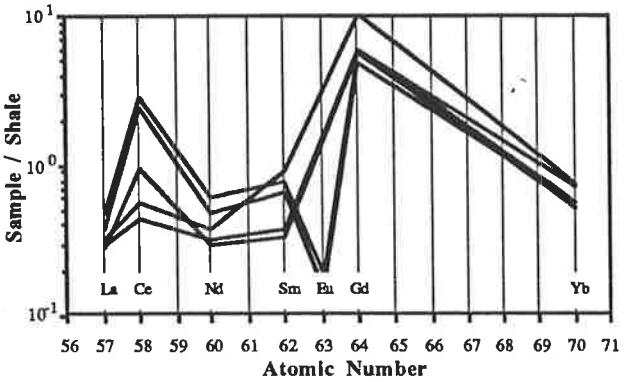


Fig. 4.8b: Shale-normalized patterns of iron-rich manganiferous laterites from F3-Quarry; after Pracejus et al., 1989.

Uncemented oolites show a surprisingly similar REE pattern to the cemented pisolites, though the former ores possess smaller negative Ce anomalies (-1.1; Fig. 5.9a). The slopes of the REE patterns of partly recrystallized manganese oxides that also contain clay minerals gradually increase from La to Gd, then decrease towards Yb (Fig. 5.9b). The Ce anomaly is absent or slightly positive and Eu exhibits small negative anomalies. One ore type which is mainly composed of radial pyrolusite, exhibits a REE pattern that does not resemble any of the other ore types. For this sample the pattern shows a marked increase of the sample-shale ratio from the LREE to the IREE, a weak negative Eu anomaly (average ~ -0.5), and a large decrease of Yb compared to Gd. Specimens of this material possess the highest ΣREE concentrations (~ 1000 ppm) encountered in the deposit.

Ce developed a small positive anomaly and the slope of the LREE curve is slight for ores and rocks containing higher amounts of kaolinite, iron hydroxides, and less recrystallized Mn-minerals (Fig. 5.9c). These REE patterns closely resemble those of Fe-rich Mn-bearing laterites (F3-area, Fig. 5.8b), although the Ce anomaly is smaller. Eu again displays a distinctive negative anomaly. Manganiferous laterites and soil spherulites (Fig. 5.9d) possess a strong positive Ce anomaly (~ -4.5), ratios that increase towards the IREEs, and a dominant negative Eu anomaly (until ~ -7.6).

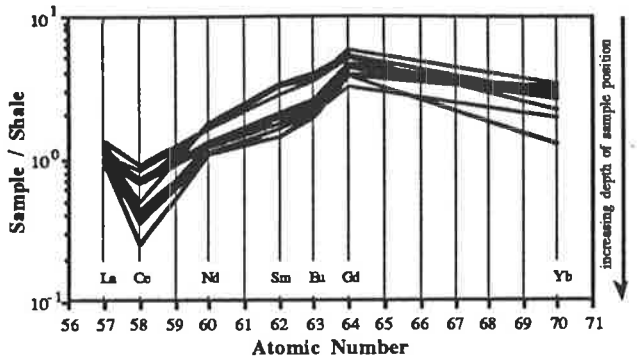


Fig. 4.9a: Shale-normalized REE-patterns of uncemented oolites from G-South Quarry, containing little or no clays; after Pracejus et al., 1989.

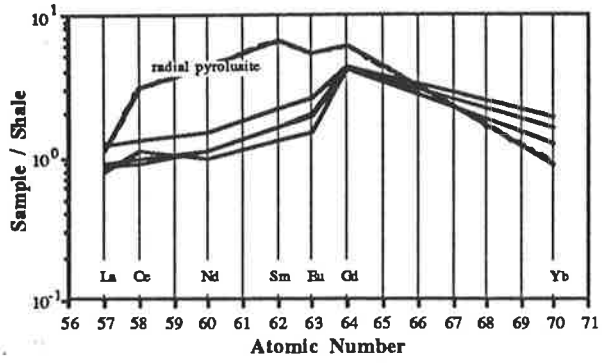


Fig. 4.9b: Shale-normalized REE-patterns of oolitic ores from G-South Quarry and radial pyrolusite, containing recrystallized Mn-minerals and clays; after Pracejus et al., 1989.

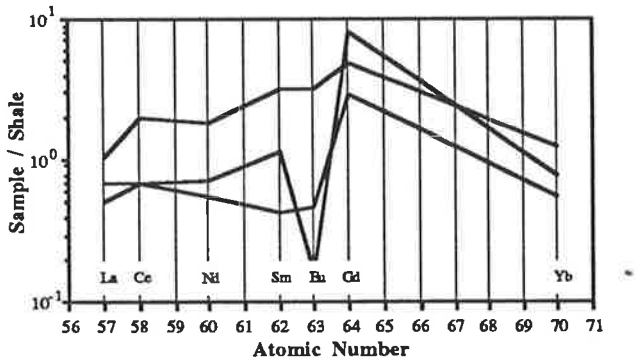


Fig. 4.9c: Shale-normalized REE-patterns of iron-rich clays from G-South Quarry; after Pracejus et al., 1989.

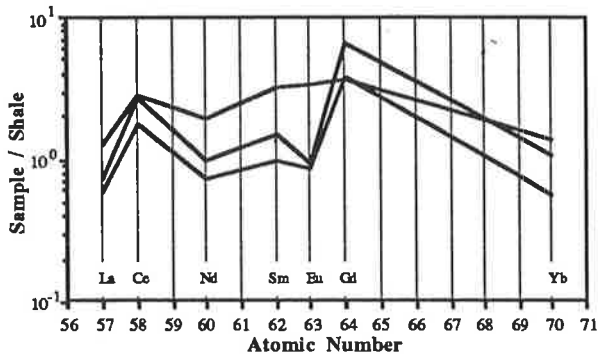


Fig. 4.9d: Shale-normalized REE-patterns of manganiferous laterites from G-South Quarry; after Pracejus et al., 1989.

4.3 Discussion

4.3.1 Relationships between Trace Elements and REEs in Different Materials

An examination of the major element concentrations in the dominant ore types of the deposit, oolites and pisolites, shows that these ores are remarkably similar. Comparable patterns are exhibited by most supergene products, and therefore, these elements cannot be used to distinguish ore and rock types from each other. Only in the very general sense of Mn/Fe-ores, laterites/clays, etc., which show a predominance of one element, it is possible to separate the materials.

In contrast, the trace elements can help to differentiate some of the ore types, mainly on the basis of strong variations in the Ni and V content. The most striking difference is noted between oolites and pisolites, the former possessing a dominant Ni-peak. With the exception of V, which often shows an elevated abundance, most of the other elements are distributed relatively evenly. Gradual elemental changes from one ore type to the next are probably due to small

variations in the mineralogy of the materials. The following chapter concentrates on this issue and with the help of normative mineralogy it is possible to elaborate in far more detail about which minerals concentrated trace elements. However, ore and rock types dominated by one particular mineral, such as ferruginous pisolites (goethite), can already be examined here in general terms.

It has also been shown that multi-element patterns of the REEs (not normalized) can readily be used to chemically distinguish some of the ore and rock types. For example, cemented pisolites from F3-Quarry and unconsolidated oolites/pisolites from the G-South area possess distinct differences in the Ce-content, although the concentrations are generally very similar for all the other Rare Earths. However, the shapes of the patterns are comparable, with the exception of strong variations for Ce, and to a smaller extent for Gd. When the samples are shale-normalized a clearer picture emerges.

The main ore types (cemented and uncemented oolites/pisolites) both possess shale-normalized REE patterns that are enriched in the LREEs, when compared with the gangues. For the IREEs, the main ore types show lower ratios than goethite, but higher ratios than kaolinite. Nevertheless, the overall patterns of the ores do not exhibit large variations. On the other hand, the normalized patterns of kaolinite and goethite are comparable in the LREEs, but the patterns diverge for the IREEs and HREEs. This behaviour, where associated minerals show a preferential uptake of LREE, IREE, or HREE, indicates fractionation by various mineral phases (Goldberg, 1965). This results from the electron charge properties of the REEs (lanthanide contraction: decreasing ionic radii with increasing atomic number).

Strong negative correlations between Eu anomalies and Fe_{total} ($\approx$ goethite) suggest that continuous redox reactions between Mn and Fe are responsible for the remobilization of manganese oxides and a subsequent removal of Eu (and other REEs). Iron-bearing kaolinite (Fe^{2+}) and iron minerals such as goethite or hematite are important reaction partners for manganese ores during supergene alteration processes in Groote Eylandt and elsewhere (Pracejus et al., 1988). The first step of this interaction is the dissolution/reduction of tetravalent Mn-oxides and their replacement by iron hydroxides. Once formed, goethitic phases can selectively remove IREEs/HREEs from the REEs available in ground waters, and these elements can be incorporated into new supergene phases. Parallel to this process, LREEs such as La and Ce, and some of the IREEs, can be taken up by other secondary minerals. During a second stage, where supergene processes result in the reduction of iron phases and a successive replacement by clay minerals (not always present), a part of the LREEs from the lattice of the iron hydroxides may be transferred to kaolinite, as the concentrations of La and Ce are seen to be very similar in both minerals. In kaolinite, IREEs and HREEs are much less abundant than in the goethite. Obviously, the lattice allows only a specific range of elements to be used for charge balances. Adsorption processes may also be very effective in the selection of a limited number of elements.

Further remobilization of secondary kaolinite, Fe-hydroxides, and manganese oxides (see chapter 8) results in the release of varying amounts of REEs. Precipitating supergene manganese oxides may reflect this changing availability of LREEs and HREEs. The fact that negative Eu and Ce anomalies of the ores increase with depth support this interpretation. Ce and Eu are the most mobile members of the REE group and a general decrease of these elements in deeper parts of the orebody can be linked to prolonged reaction times that result from an increasing availability of ground waters, which thus enable the redox reactions to take place. In contrast to the REEs, other trace elements do not show such strong fractionation between kaolinitic and goethitic materials, although supergene products such as kaolinite-rich laterites are occasionally enriched in minor or trace elements (e.g. B, Ti, Zr), when compared with other secondary ores and gangues.

Ce and Eu anomalies similar to those described from Groote Eylandt developed in supergene products from different protores, for example from manganiferous carbonates (Kalahari deposits, South Africa; N. Beukes, pers. commun., 1988) or from oxidic Mn-ores (China; P. Yang, pers. commun., 1988). This means that although the alteration materials may no longer exhibit the REE composition of their parent rock, the final product could develop characteristic features that can be recognized worldwide in supergene ores.

4.3.2 Stratigraphy-controlled Element Variations

It has been illustrated that most trace elements and Rare Earths decrease down the section and that elements such as Ce, which are geochemically more mobile than many other REEs, are relatively more depleted. Also, enrichment zones can be observed over several hundred meters. Since water movement (mobilization/precipitation processes depend on water to operate) is predominantly vertically oriented, the findings above probably reflect prolonged interaction of ores and groundwaters at greater depth within the deposit. Near the surface the water levels are subject to strong seasonal variations.

However, great care must be taken when samples are examined from different stratigraphic levels. These samples should, *sensu strictu*, not be compared directly without stratigraphical background information; materials from the top and the bottom of the section are likely to show strong variations in the element composition. Similarly, an assessment of element abundances/patterns in manganese oxide minerals and associated rocks may prove to be difficult, because a number of secondary materials occurring in the same sample possess characteristic trace element and REE concentrations. A bulk chemical analysis of such ores/gangues inevitably produces mixed patterns. Analytical work is underway to determine trace element and REE concentrations in the various materials precisely, and to prepare mineral correction factors. This will allow the development of gangue-mineral-free composition patterns for comparative work.

4.3.3 Comparison of REE Patterns from Groote Eylandt and Other Mn Oxide Deposits

The Rare Earth Elements were chosen for this comparison, because of the redox control on REE abundance and the availability of comparable data from other deposits. Most of the trace elements on the other hand are often incompatible, because different authors have determined different elements. This renders an overall comparison more difficult.

Because the ores of Groote Eylandt have a history of repeated mobilization and reprecipitation which may have been in effect since the Late Cretaceous, it is almost certain that time-dependent Eu anomalies (and similarly Ce) of initial precipitates (Fryer, 1977) have been overprinted by supergene processes, thus presenting obstacles to identifying unaltered primary manganese oxides for further comparison. At present, there seems to be no obvious way to determine whether the Rare Earths analyzed here derive from primary or secondary minerals. Mineral-specific incorporation of REEs (and also TEs) into the lattice of supergene phases and a fractionation of the various elements in the successive precipitates can produce patterns that show little or no relation to primary concentrations. It is therefore difficult to compare the Groote Eylandt ores with other deposits that are still close to their initial geochemical composition. Nevertheless, minerals that have only altered and which were not replaced totally by supergene phases, may possess signatures which could partly be comparable to the initial precipitates.

Before the Groote Eylandt ores are compared with other manganese oxide deposits, it is necessary to briefly introduce the basis for this part of the discussion. It was demonstrated that the deposit has been influenced by supergene processes (e.g. Figs. 4.8-9) and it was also possible to show that individual ore and rock types within a stratigraphic section keep a comparable shale-normalized REE signature (except for larger Ce variations), although the REE concentrations generally decrease downward. The largest REE depletions were detected in the lower parts of the orebody, where interactions with local groundwaters can persist over much longer time intervals than in the upper parts of the section.

Manganese enrichments (cementations) are observed in many positions within different sections and therefore, REE enrichment processes coupled to an additional uptake of Mn cannot be ruled out. Such processes have been noted by Fleet (1983) and Hein et al.(1989) in connection with an increasing manganese content in samples that were influenced by supergene processes. However, the present data only partly support this finding. Mn concentrations were observed to increase with depth in one locality of the deposit, elsewhere the concentrations decrease with depth, and in both cases the abundance of REEs (and other trace elements) decreases downward. It is therefore concluded that the shape of the patterns of the ores, but not the actual concentrations, remained similar to earlier precipitates. The various ores are compared on this basis.

The most important features for comparison are the pronounced negative Ce anomalies and the variations in the Eu content of the Groote Eylandt ores (Fig. 4.10). These anomalies are characteristic of the geochemical environment in which the manganese oxides developed, and the type of the anomaly (positive, negative) reflects the thermodynamic conditions during the formation of the ores (Piper, 1974; Elderfield and Greaves, 1981; Ingri and Pontér, 1987; De Carlo and McMurtry, 1989).

It is known that most marine nodules showing negative anomalies precipitated mainly under the influence of hydrothermal processes (e.g. Rankin and Glasby, 1979; De Carlo and McMurtry, 1989), although some were formed by diagenetic processes (Elderfield and Greaves, 1981; Calvert et al., 1987). It is unlikely that the Groote Eylandt ores accumulated under hydrothermal conditions, because there is no evidence of any Cretaceous volcanic activity in the region. Diagenetic formation in precisely the same way as in marine nodules is not very plausible, given the nearshore marine environments of deposition. Morphological and petrological features (e.g. cross-bedding, normal/inverse grading) also argue against a purely diagenetic origin (Bolton et al., 1988). However, the shape of the shale-normalized REE patterns and the REE concentration levels of the Groote Eylandt ores are very similar to diagenetic nodules, thus indicating that the processes influencing ore minerals and associated sediments are comparable in both types of deposits.

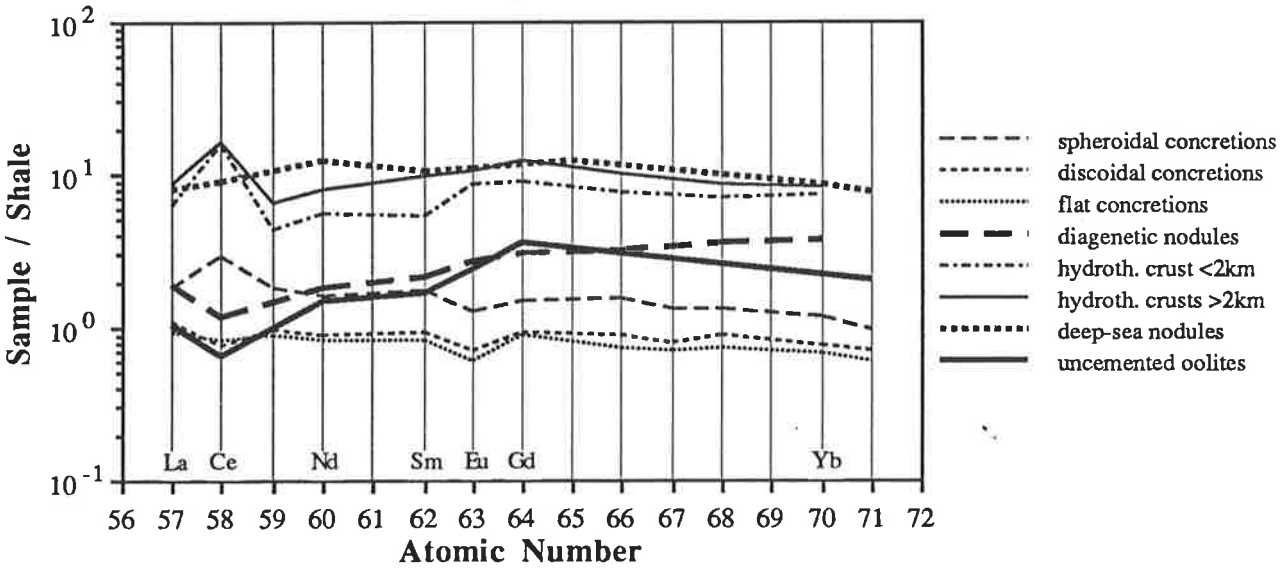


Fig. 4.10: Comparison of marine manganese oxides with oolitic ores (soft = uncemented oolites) from the G-area at Groote Eylandt. Pisolitic ores produce a similar pattern and were thus omitted. The following ore types are included above:

- deep sea marine nodules after Piper (1974),
- marine nodules formed by hydrothermal processes from depths < 2000 m, averages from De Carlo and McMurtry (1986),
- marine nodules formed by hydrothermal processes from depths > 2000 m, averages from De Carlo and McMurtry (1986),
- marine nodules associated with diagenetic processes, from Elderfield and Greaves (1981),
- shallow water marine nodules (flat, discoidal and spheroidal concretions), taken from Ingri and Pontér (1987),
- oolitic ores, averages from this study; cemented pisolites have not been plotted for simplicity reasons; their pattern is comparable to the oolitic ores, with the exception of the positive Eu anomaly.

Piper (1974a) describes marine nodules from water depths greater than 3000 m that show extraordinary similarities to a few Groote Eylandt ore samples (radial pyrolusites); though the REE concentrations differ, they possess comparable patterns. From sedimentological studies (Bolton, 1981), it is known that the ores developed in a shallow-water marine environment, so the similarities are puzzling. Nevertheless, most Groote Eylandt ores and gangue minerals do not show the pattern of radial pyrolusite.

Discoidal and flat concretions from the Gulf of Bothnia (Ingri and Pontér, 1987) collected from a water depth of 70 to 120 m possess REE concentrations similar to the Groote Eylandt ores, but the shape of the curves for the IREEs and HREEs is nearly horizontal for the concretions, whereas the Groote Eylandt ore patterns increase towards Gd. However, the concretion patterns also show negative anomalies for both Ce and Eu. On the other hand, spheroidal concretions from the same area but in water depths of about 50 to 70 m show strong positive Ce anomalies. If supergene processes are not able to completely overprint the initial pattern of the REEs, then the discoidal and/or flat concretions might represent in some aspects a modern-day analogue to the Groote Eylandt ores, which also formed under shallow-marine conditions.

Grasselly and Pantó (1988) recently examined the REE geochemistry of the Jurassic Mn-deposits at Úrkút, Hungary, and found remarkably coincident patterns for clay minerals and manganese oxide ores. Both display positive Ce anomalies, negative Eu anomalies, and are LREE enriched. At Groote Eylandt, the ores and clay minerals show different compositions, which might be due to the almost continuous activity of supergene dissolution and reprecipitation processes (Pracejus et al., 1988). Generally, the ores have negative Ce anomalies and the normalized concentration for Yb is slightly less than Gd. Depending on the sample, Eu can exhibit strong negative or positive anomalies. In ΣREE, the ores from the two deposits are nearly identical, but this is not so for the clay minerals. The levels of individual REEs in the clay minerals at Úrkút are two to thirteen times higher than in the Groote Eylandt kaolinites. This suggests significant differences in the development and subsequent alteration of the two deposits. It also indicates the possibility of a much higher mobility of REEs in a tropical to sub-tropical weathering environment. The fact that the shape of the REE patterns in the clay minerals of both deposits is comparable, could imply that the clay mineralogy in Úrkút and Groote Eylandt is similar. At present, however, the available information about supergene terrestrial deposits is too limited to allow a detailed comparison.

Some authors suggest the use of the Ce/La ratio for an assessment of the rate of Ce depletion in the sediments, which then can be taken as an indicator for the redox conditions during the formation of the ores (e.g. Dubinina and Volkov, 1986; Glasby et al., 1987). However, this technique cannot be applied to the Groote Eylandt ores, because of the strong influence of supergene processes which overprinted the ores to varying degrees. Similarly, Grasselly and Pantó (1988) came to the same conclusion in their examination of the Úrkút deposits.

The possibility that the ore minerals have only been altered during supergene processes, and that these phases may have kept most of the initial REE concentrations, leads to the conclusion that in terms of the REE geochemistry a present-day analogue to the Groote Eylandt manganese ores can probably be found in the shallow-water marine nodules of the Gulf of Bothnia (discoidal and flat concretions from depths between 70 and 120 m). These Mn-oxides bear the closest resemblance to the examined ores. Even though strong similarities to diagenetic nodules exist, sedimentological studies of the Groote Eylandt deposit suggest that the ores did not form diagenetically. However, the redox conditions within the sediments where these nodules developed may have been comparable to the geochemical environment of the supergene ores, on at least relatively small scales.

5. Application and Interpretation of Normative Mineralogy

5.1 Introduction

Until recently, researchers examining manganese oxides had to overcome a number of problems, when a quantitative mineralogical analysis of their samples was required. Many Mn-ores are extremely fine grained and their manganese minerals possess low crystallinities and are intergrown with other minerals. The crystal structures are not well defined, or hybrid structures exist. This makes quantification, and even identification very difficult, because traditional mineralogical techniques, such as ore microscopy, X-ray diffraction (XRD), and the more advanced Fourier Transform Infra Red analysis (FTIR) fail when confronted with such complex material. Therefore, a method has been developed which approaches the problem from a theoretical viewpoint (Pracejus et al, 1988a; Pracejus, 1990). Suggestions on the development of a normative method for manganese minerals can be found in a paper by Babenko et al. (1983), who quoted calculated mineral compositions (partly different to those used here) of manganese ores from Nikopol in the USSR. Unfortunately, they do not specify the method for their calculations, nor do they state whether this is only an approximation.

It is not intended here to replace sophisticated analytical techniques, such as FTIR (including Computerized Infra Red Characterization of Materials: CIRCOM) or Differential Thermal Analysis (DTA), because this would go far beyond the capability of the proposed method. However, the norm provides a tool to quickly process large sample sets, once the calculation procedure has been established in a computer program. The obtained data can then be correlated with results from other analyses.

The necessary background information for the normalization technique has been obtained from Ostwald (1980, 1988) and Pracejus et al. (1988b), who examined the mineralogy and geochemistry of supergene Mn-ores from Groote Eylandt in the Northern Territory of Australia.

The deposit shows an extensive supergene alteration of the primary sedimentary sequence, which mainly comprises oolitic and pisolitic manganese oxides. Because the secondary Mn-minerals precipitated in a number of host lithologies (e.g. Mn-ores, sands and sandstones, clays and claystones, Fe-oxides and oxihydroxides), they have created a large range of assemblages.

The deposits of Groote Eylandt contain pyrolusite, cryptomelane, romanechite and todorokite as the main ore constituents. Manganite, vernadite, birnessite, and a number of other manganese oxides can also be identified, but they appear in much smaller quantities (Ostwald, 1988) and are therefore neglected in this theoretical approach. The dominant gangue minerals are quartz, kaolinite, goethite (plus other Fe-oxihydroxides) and hematite. These minerals set the framework for the norm model and, *sensu strictu* , they can only be applied to conditions similar to those of Groote Eylandt (tropical/sub-tropical supergene alteration of manganese oxide protores), but the norm can easily be adjusted to comparable geological environments (e.g. bauxites). At the moment it is difficult to assess how well this method can be applied on manganese minerals of other origins (e.g. deep-sea nodules), but it may prove to be helpful for the understanding of other deposits.

5.2 Method of Norm Calculation

When the first mineral norm (CIPW; Cross et al., 1902) was developed, the complex structure of silicates and many other minerals was not yet known. The chemical composition of minerals was generally described in terms of molecules and the molecular weights of oxides. This idealized approach provides a relatively easy theoretical assessment of mineral quantities in very fine grained rocks or even glass, but it has serious disadvantages, when minerals occur in higher amounts in the natural sample which are not covered by the calculation.

Additional minerals such as rhodochrosite ($MnCO_3$) or alabandite (MnS) can also be incorporated into the present method without difficulty, provided that the necessary carbonate and sulfide analyses are available. However, the latter compounds can only be found in trace element quantities in Groote Eylandt and thus, they only serve as examples for possible extensions of the norm.

Often, it has not been possible to incorporate specific elements, such as K, Mg, Al, Fe, or Ba, in more than one norm mineral, because of strong element variations in a number of host minerals (see for instance Ba in cryptomelane). The minerals also rely on at least one element for their calculation, and this element is subsequently "consumed" for the formation of the respective norm mineral. K for instance, can be found in cryptomelane, romanechite, todorokite, and also kaolinite, but the normalization uses K only for cryptomelane and kaolinite, all other phases are calculated on a K-free basis. This means that relatively small errors are automatically

introduced for the remaining minerals which also accommodate K. For the same reasons, intergrowths of different manganese oxides had to be neglected (e.g. romanechite-todorokite or romanechite-hollandite; Turner and Buseck, 1979).

In the following sections, the various minerals are discussed in the same order in which they should be calculated, because a number of phases depend on preceding minerals for their respective calculations. The numbers in parenthesis next to the formulae correspond to the steps shown in Figs. 1a-d. To simplify understanding of the norm method, two example calculations are also shown (Table 5.1: Mn-ore; Table 5.2: Fe-ore). Average norm mineral concentrations and other statistical data are provided in the relevant text sections (Tables 5.3 - 6), results for all samples are given in Appendix V.1.

The norm calculation commences with the numerical division of the weight percent of the analyzed elements by their molecular weights. The result will be called mol equivalent (ME). Since the ME is represented by fairly small numbers, it is multiplied by 1000 (ME 1000). The latter step is not necessary, but it makes handling easier for separate calculations which are not done on computer. The next step distributes the ME 1000 product to the various norm minerals. The consumption of the appropriate elements must be calculated after each step. The addition of each oxide that is needed to produce one mineral, is followed by a division of the sum of all ME 1000 products of the total of the analysis, and a multiplication by 100 to produce the final mineral percentages.

As every chemical analysis contains an analytical error, the reliability on the final results may not exceed one decimal place or even less. Despite these limitations it is advisable to calculate the norm to two decimal places, this improves the quality of plots which otherwise might be distorted. Errors that could develop from the necessary simplifications for some of the minerals are in most cases negligible, especially when ores of the same type are compared, because the errors will also be comparable. The basis on which each mineral is calculated is underlined. The nomenclature of this norm has been chosen in such a way that mineral abbreviations used in already existing norms are not duplicated.

an anatase: $\underline{TiO_2}$ (1)

The mineral anatase is used instead of rutile (also TiO_2), because it is the main constituent in bauxitic and lateritic soils (Bárdossy, 1982). At present , its abundance is calculated separately. However, later development of this normalization method might lead to an incorporation of TiO_2 into kaolinite, because it has an excellent correlation with the latter mineral.

q quartz: $\underline{SiO_2}$ (2)

A decision has to be made as to whether there is excessive quartz or not. This is also the basis for the determination of kaolinite and gibbsite. In the system quartz (q) - kaolinite (ka) - gibbsite (gb) no more than two minerals can be in equilibrium at one time (Kittrick, 1969). In aqaeous systems kaolinite will form at the expense of either gb or q. This means that $q \geq 0$ when $gb = 0$ or $q = 0$ when $gb \geq 0$ in the present calculation. Under natural conditions this thermodynamic rule can be broken, because of the slow reaction kinetics of the involved mineral species. Nevertheless, the final stage leads to a two mineral configuration, which is accounted for in this calculation. The decision as to excessive quatrz depends on a preliminary calculation of kaolinite (only step 3a!). The result indicates excess quartz (remaining SiO_2) or alternatively, an overestimated consumption which leads to no quartz, but also to the calculation of gibbsite (4).

ka kaolinite: $Al_2Si_2O_5(OH)_4 \Rightarrow \underline{Al_2O_3} + 2\ SiO_2 + 2\ H_2O$ (3a)

$\Rightarrow \underline{SiO_2} + {}^1/_2\ Al_2O_3 + H_2O$ (3b)

Depending on the result of the previous decision, kaolinite is either determined from (3a) or (3b). If there is excessive quartz, then the abundance of kaolinite is calculated on the basis of the available alumina. In the case of quartz deficiency, the mineral abundance relies on the total silica content of the sample and there will be free alumina for the formation of gibbsite as an additional phase (4). Analyses of reasonably pure clay samples have shown that kaolinite from Groote Eylandt contains **~1.7% FeO** and **~0.17% K_2O**; these values are incorporated in the final result of the kaolinite calculation. The latter two steps should be checked in materials from other deposits and adjusted accordingly. Because these compounds are relatively low in their concentration, they could also be omitted from this part of the norm calculation.

gb gibbsite: $2\ Al(OH)_3 \Rightarrow \underline{Al_2O_3} + 3\ H_2O$ (4)

The conditions for the stability of gibbsite have already been discussed in context with quartz (2) and kaolinite (3). Though gibbsite has been described as an accessory in the deposits on Groote Eylandt, it must remain a theoretical phase under the present normalization program, because it is not known to what extent the excess alumina is incorporated in minerals like goethite or hematite. If excess quartz has been determined, then gibbsite does not exist in the sample.

cm cryptomelane: $K_{\leq 1}Mn_8O_{16} \Rightarrow K_2O + MnO + 15\ MnO_2$

Correlations with SrO strongly suggest that Sr is incorporated in the lattice of cryptomelane, and the size of its ionic radius (within a range of ± 15 %) implies that it can substitute for potassium. This is also in accordance with Post et al. (1982), who discuss a cryptomelane with the following formula:

$(K_{0.94}Na_{0.25}Sr_{0.13}Ba_{0.1})(Mn, Fe, Al)_8(O, OH)_{16}$.

Because cryptomelane at Groote Eylandt varies in its Ba content, and also because Ba is needed for the calculation of romanechite, this element is not used here. The same applies for Na, which is taken for the development of todorokite. The following oxide formula is used:

$$\underline{(K_2O + SrO)} + MnO + 15\ MnO_2 \qquad (5)$$

A small amount of potassium is taken for the kaolinite calculation, and it therefore may happen that manganese samples with a very low cryptomelane content give a result of cm = 0. Theoretically, such a sample could be calculated on the basis of the Sr content, if present, but the normalization procedure neglects cryptomelane if there is no K. Separate Sr-minerals such as celestite have not been detected in the deposit. MnO is calculated (!) from the total MnO_2 analysis, because it had not been determined for the Groote Eylandt samples. However, if an analysis of Mn^{2+} is available, it should preferably be used.

rm romanechite: $Ba_2[Mn_4^{3+}\ Mn_{11}^{4+}\ O_{30}] * 4\ H_2O$ fi

$$\Rightarrow \underline{BaO} + Mn_2O_3 + 5.5\ MnO_2 + 2\ H_2O \qquad (6)$$

The barium content of the sample is taken as the basis for the romanechite calculation (Giovanoli and Balmer, 1983; Burns and Burns, 1977; Burns et al., 1985). Mn_2O_3 is calculated (!) from the total MnO_2 content, as is the case for the previous mineral for MnO. The strongly varying K_2O contents of romanechite in Groote Eylandt (BaO/K_2O ratios of 1.8 to 34.7; Ostwald, 1988) have been neglected in favour of cryptomelane, because no consistent values could be obtained.

to todorokite:

This mineral seems to be fairly complicated, having different compositions in different deposits. A number of formulae have been proposed by various authors:

$(Ca, Na, K, Mn^{2+})(Mn^{4+}, Mn^{2+}, MgO)_6O_{12} * 3\ H_2O$ after Straczek, et al. (1960);

$(Ca, Na, K, Ba, Mn^{2+})Mn_5O_{12} * 3\ H_2O$ after Burns and Burns (1977);

$(Mn^{2+}, Zn, Mg, Ba, Sr, Ca, Na_2, K_2, Cu, Pb)_3Mn_{10}^{4+}\ O_{23} * 9\ H_2O$ after Larson (1962).Calculations of analytical results from Groote Eylandt ores demonstrate that a high number of rock samples show a very limited range for the ratio between calcium and sodium to magnesium $(Ca + Na_2O)/MgO \approx 0.30\text{-}0.34$. This indicates a strong structural association of these three elements, which most probably is due to a concentration in a single mineral. Though a few samples contain excess MgO, when compared with the ratio mentioned above, no correlation to any other mineral has been found for this element. Therefore calcium, sodium and magnesium are taken as the basis for the todorokite calculation. The error introduced knowingly by the incorporation of all the magnesium into todorokite is fairly small, and it saves the normalization from further complications. Frondel et al. (1960) and Straczek et al. (1960) report

significant amounts of Mg in todorokites. The present author favours the composition quoted by Larson (1962), because it contains all elements that are believed to play an important role in the todorokite under investigation. This formula is shortened and adjusted in the following way:

$(Mg, Ca, Na_2)_3Mn_{10}^{4+} O_{23} * 9\ H_2O \Rightarrow$

$$\Rightarrow \underline{(MgO, CaO, Na_2O)} + 3.33\ MnO_2 + 3\ H_2O \qquad (7)$$

pr pyrolusite: $MnO_2 \Rightarrow \underline{MnO_2} + x\ H_2O \qquad (x = 0 - 0.5)$ (8)

Pyrolusite, the last Mn-phase, is calculated from the remaining manganese which has not been consumed by the previous minerals (cm, rm, to). Correlation plots between pyrolusite and excess water also led to the additional incorporation of up to 50% water, though water does not take part in the structure of pyrolusite. However, this finding is in accordance with analytical results from Gryaznov and Danilov (1980) and Ostwald (1988). It is assumed that the pyrolusite lattice contains micro-inclusions of α-MnOOH or γ-MnOOH, which thus result in a larger LOI than expected.

As indicated by x = 0 - 0.5 for the water portion of the norm mineral, the water content of pyrolusite can be variable. Normally, the excess water of the sample will be larger than 50% of the remaining manganese (after the calculation of the previous Mn-minerals) and therefore, the "inclusion-water" can easily be accommodated, while a small rest of water is left. In a few cases however, less water is available at this stage of the calculation, and all remaining water is then added to the manganese component of the formula above.

gt goethite (a): $2\ FeOOH \Rightarrow \underline{Fe_2O_3} + H_2O$ (9)

Goethite is calculated from the remaining iron (a small amount has been used for kaolinite) and its equivalent to water. As there are many samples which have undergone oxidation, it is necessary to adjust the goethite content in a later step (11). The decision for this correction is based on step (10). If an adjustment has to be made, then it results in the production of hematite.

xw structural water: $xw \Rightarrow LOI - H_2O_{[ka,\ gb,\ gt,\ rm,\ to]}$ (10)

The loss on ignition (LOI) and most of the previously calculated phases which contain water are used for a first approximation of the remaining structural water in goethite. The only exception in this calculation is pyrolusite, because of its variable water content. If the value of the calculation becomes negative at this stage, it is an indication of the formation of hematite in iron-rich samples. Therefore this operation is essential for the adjustment of goethite in step (11) and for the establishment of hematite (12). The LOI of the Groote Eylandt ores relates entirely to water-bearing phases, because other compounds such as carbonates are absent in the deposit or exist only as traces.

gt goethite (b): $2\ FeOOH \Rightarrow \underline{\mathbf{Fe_2O_3}} + \mathbf{H_2O} - \mathbf{2\ |xw|}$ (11)

If hematite is seen to have replaced goethite, then the amount of goethite must be corrected. This is done by a correction based on negative structural water.

he hematite: $Fe_2O_3 \Rightarrow \underline{|xw|}$ (12)

In the case of oxidized goethitic rocks where hematite has formed, the amount of Fe_2O_3 is equivalent to overestimated structural water from step (10).

P_2O_5 phosphorus: $\underline{\mathbf{P_2O_5}}$ (13)

All P_2O_5 is normalized only, and it is not put into a mineral. The most appropriate phosphate mineral which has been described from Groote Eylandt is vivianite (hydrated iron phosphate), but it is very rare and is therefore not calculated as a separate phase. Further treatment relies on correlations with other minerals, where it may be incorporated. This phase is not essential for the normalization procedure and can be omitted in most cases, as long as its amount in the sample is negligible.

w excess water: $w \Rightarrow \mathbf{LOI - H_2O_{[ka,\ gb,\ gt,\ rm,\ to,\ pr]}}$ (14)

The final determination of excess (free) water is based on the Loss on Ignition (LOI) and all phases containing water.

Σ final sum: $\Sigma \Rightarrow \Sigma_{(\mathbf{norm\ minerals})}$ (15)

Normally it is not necessary to calculate the sum of the normalized minerals, because the result should be very near to 100%, if existing and normative minerals coincide. Deviations of more than ± 2% are considered to be indicative of analytical mistakes, erroneous input, or additional minerals that contain materials, which have not been accounted for in the normalization (e.g. organic remains). The latter case might be camouflaged by a larger LOI and could probably go undetected. Nevertheless, the total sum is a quick way of checking the correctness of the norm result (statistics of a large batch of samples: n = 364, Ø = 99.82, max = 102.24, min = 98.7, std.dev. = 0.529).

Additional manganese minerals which could easily be incorporated into the calculations before pyrolusite at step 8 are for instance, rhodochrosite and alabandite. These minerals are not known to occur in the Groote Eylandt deposit, but are mentioned as examples for the development of additional normative phases. Such minerals may be required for an examination of other deposits. More complex Mn-phases require an exact knowledge about the element(s) that can be taken as the calculation basis.

rh rhodochrosite: $MnCO_3 \Rightarrow \mathbf{1.6\ MnO} + \underline{\mathbf{CO_2}}$ (7B)

ad alabandite: $MnS \Rightarrow \mathbf{1.7\ Mn} + \underline{\mathbf{S}}$ (7C)

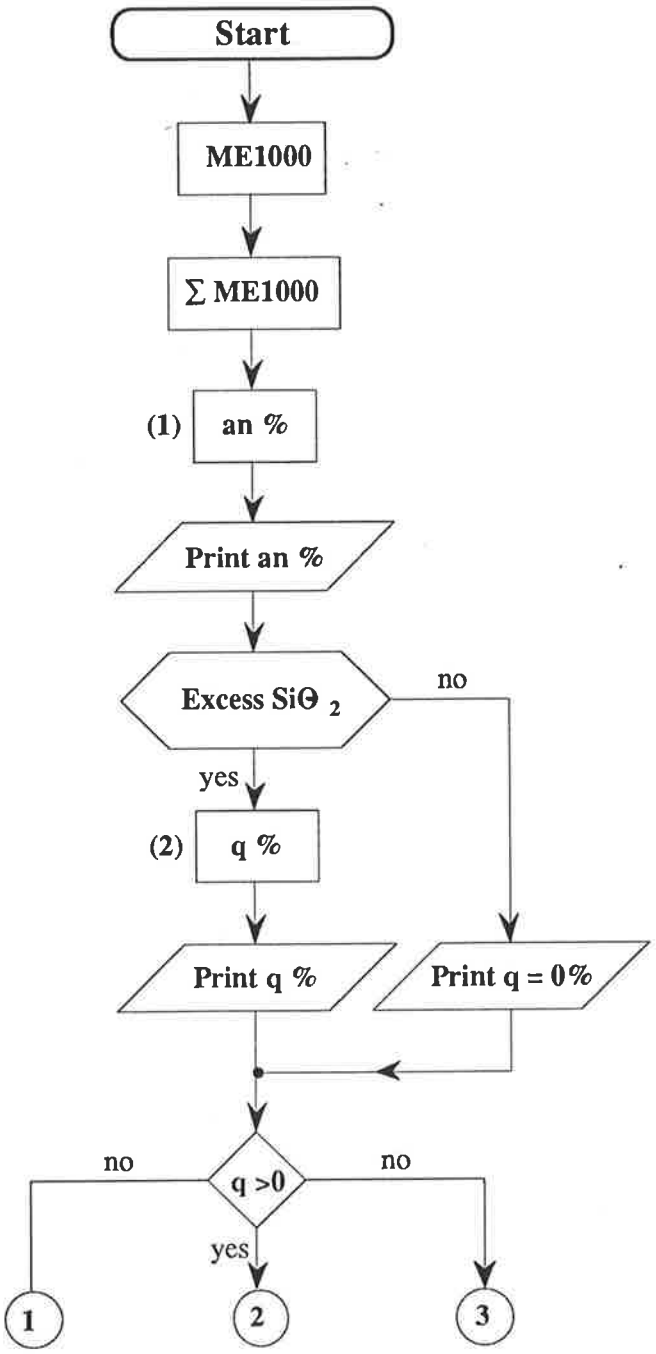


Figure 5.1a: Flow diagram of mineral normalization; for Explanation of abbreviations see text; general legend for plotting symbols in Fig. 5.1d.

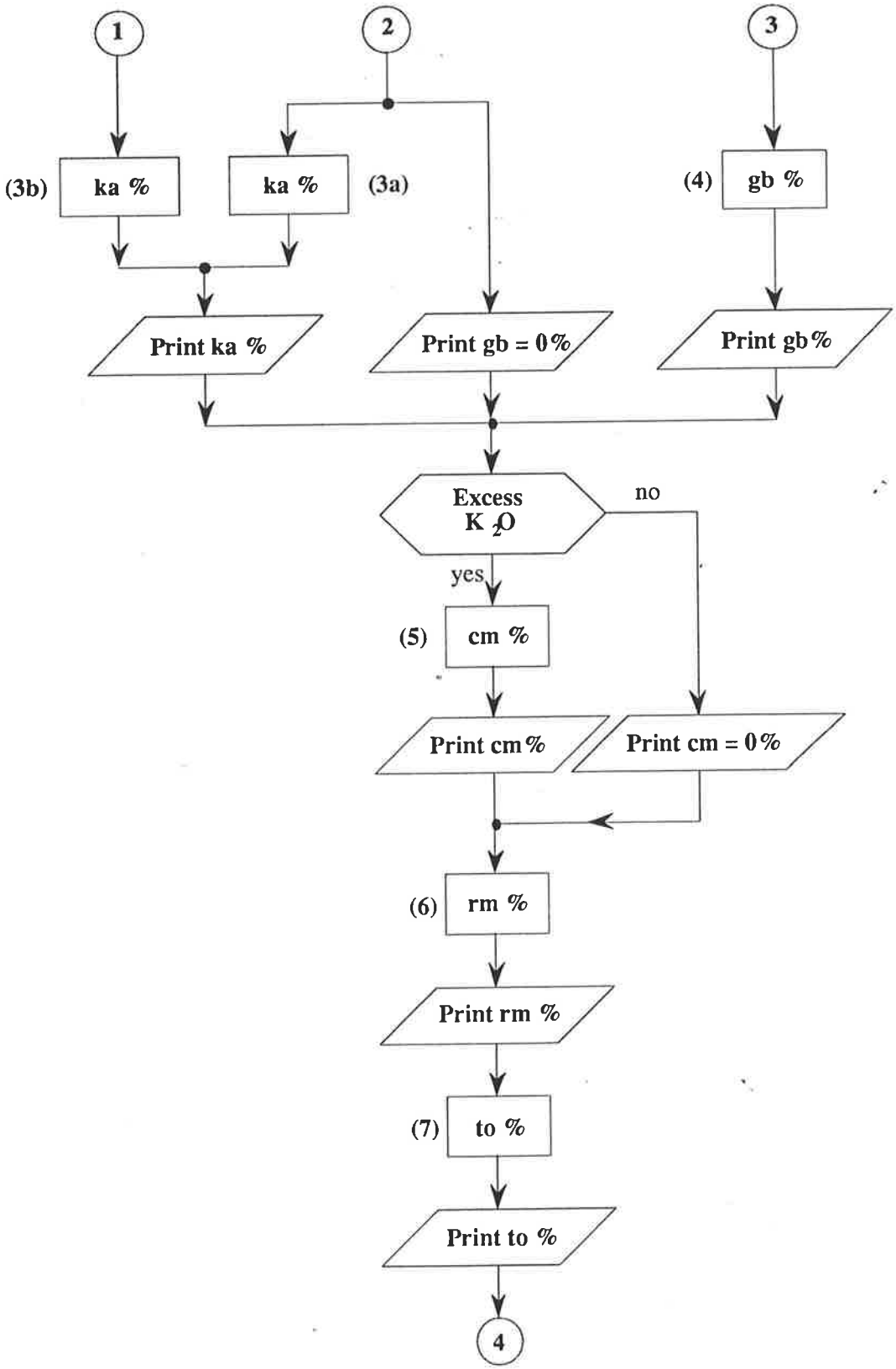


Fig. 5.1b: Flow diagram of norm calculation (continued).

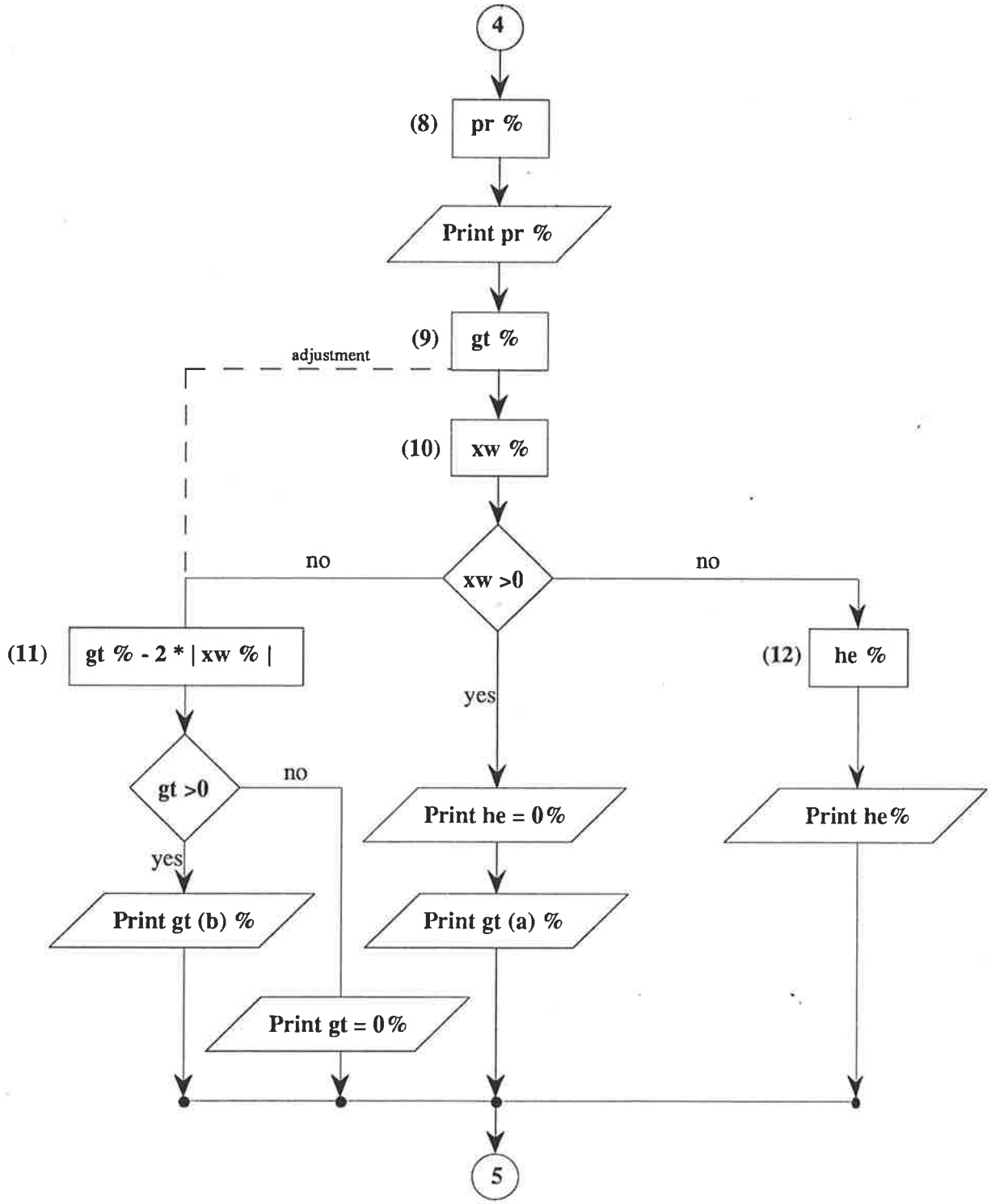


Fig. 5.1c: Flow diagram of norm calculation (continued).

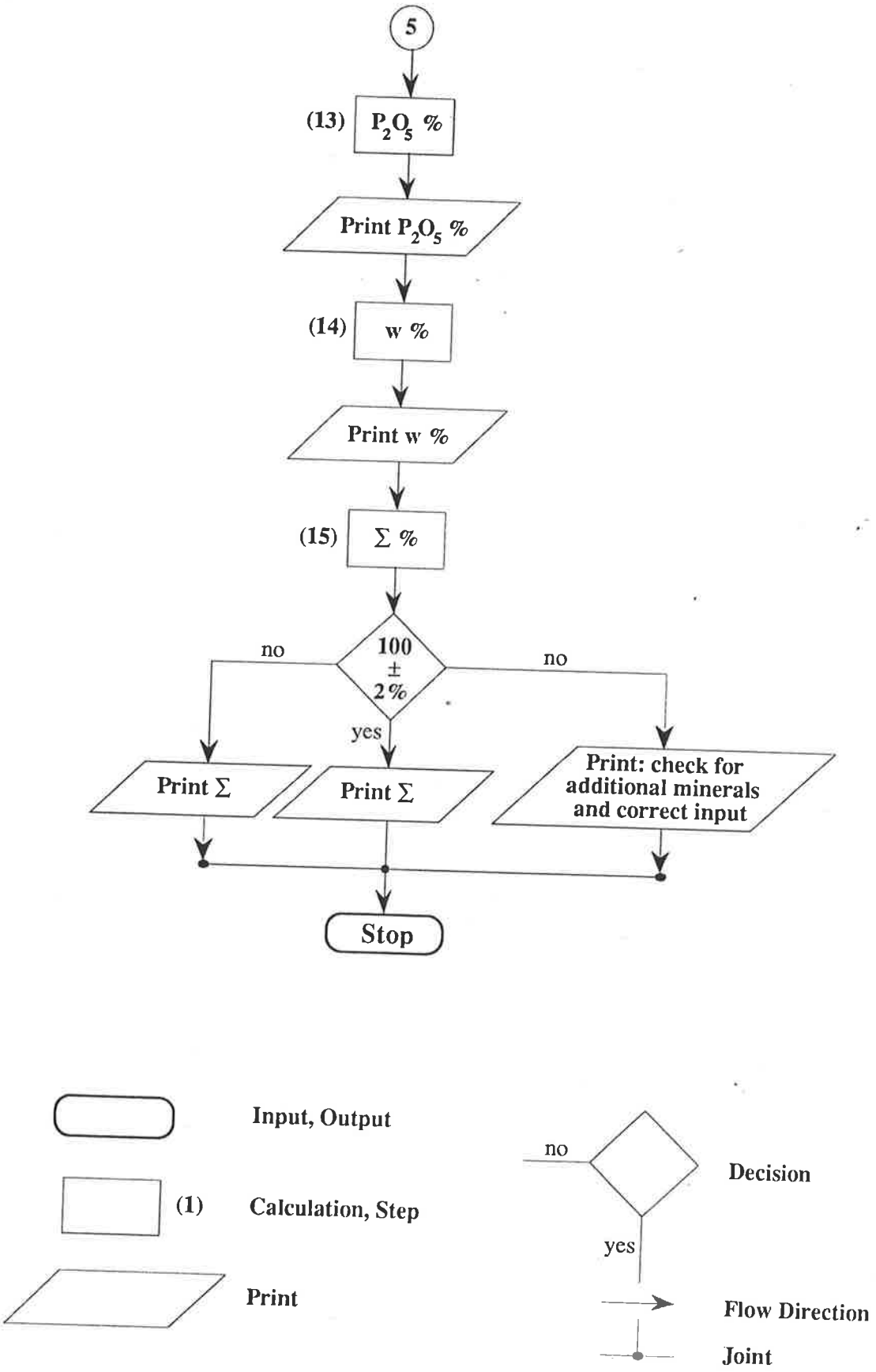


Fig. 5.1d: Flow diagram of norm calculation (continued); legend for Figs. 5.1a-d.

Table 5.1:Normalization procedure for Mn oxide ores.

Mn-Ore	Weight %	At. Weight	ME 1000	an	Δ	q	Δ	ka	Δ	gb	Δ	gt (a)	Δ	he	Δ	gt (b)	Δ
MnO2	72.3	86.936	831.6														
Fe2O3	1.5	159.692	9.4					4.2	5.2			5.2	0.0	0.0	0.0	0.0	
SiO2	5.4	60.084	89.9			0.0	89.9	89.9	0.0								
Al2O3	4.7	101.961	46.1					44.9	1.2	1.2	0.0						
P2O5	0.07	141.944	0.49														
K2O	1.29	94.203	13.7					0.4	13.3								
CaO	0.05	56.079	0.9														
SrO	0.21	103.619	2.0														
BaO	2.46	153.339	16.0														
TiO2	0.15	79.898	1.9	1.9	0.0												
Na2O	0.20	61.979	3.2														
MgO	0.5	40.304	12.4														
LOI	11.2	18.015	621.7					89.9	531.8	3.5	530.2	5.2	525.1				
Σ	100.0		1649.4	1.9		0.0		229.3		4.6		10.4					
Norm				0.1		0.0		13.9		0.3		0.6					

continued	Weight %	At. Weight	ME 1000	cm	Δ	rm	Δ	to	Δ	pr	Δ	P2O5	Δ	w	Δ	Σ
MnO2	72.3	86.936	831.6	248.3	583.3	105.6	477.7	54.9	422.8	422.8	0.0					
Fe2O3	1.5	159.692	9.4													
SiO2	5.4	60.084	89.9													
Al2O3	4.7	101.961	46.1													
P2O5	0.07	141.944	0.49									0.49	0.0			
K2O	1.29	94.203	13.7	13.3	0.0											
CaO	0.05	56.079	0.9					0.9	0.0							
SrO	0.21	103.619	2.0	2.0	0.0											
BaO	2.46	153.339	16.0			16.0	0.0									
TiO2	0.15	79.898	1.9													
Na2O	0.20	61.979	3.2					3.2	0.0							
MgO	0.5	40.304	12.4					12.4	0.0							
LOI	11.2	18.015	621.7			32.0	493.1	49.5	443.6	211.4	232.2			232.2	0.0	
Σ	100.0		1649.3	263.6		153.6		120.9		634.2		0.49		232.2		
Norm				16.0		9.3		7.3		38.5		0.03		14.1		100.1

UNIVERSITY OF ADELAIDE LIBRARY

Table 5.2: Normalization procedure for Fe oxyhydroxide ores.

Fe-Ore	Weight %	At. Weight	ME 1000	an	Δ	q	Δ	ka	Δ	gb	Δ	gt (a)	Δ	he	Δ	gt (b)	Δ
MnO2	1.4	86.936	16.1														
Fe2O3	73.7	159.692	461.5					3.5	458.0			458.0	0.0	51.8	406.2	406.2	0.0
SiO2	4.9	60.084	81.6			0.0	81.6	81.6	0.0								
Al2O3	7.7	101.961	75.5					40.8	34.7	34.7	0.0						
P2O5	1.17	141.944	8.2														
K2O	0.08	94.203	0.8					0.3	0.5								
CaO	0.01	56.079	0.2														
SrO	0.01	103.619	0.1														
BaO	0.01	153.339	0.1														
TiO2	0.36	79.898	4.5	4.5	0.0												
Na2O	0.01	61.979	0.2														
MgO	0.01	40.304	0.2														
LOI	10.7	18.015	593.9					81.6	512.4	104.2	408.2	458.0	-49.8				
W Corr.			593.9					81.6	512.4	104.2	408.2					406.2	2.0
Σ	100.0		1243.0	4.5		0.0		207.7		139.0		916.0		51.8		812.4	
Norm				0.4		0.0		16.7		11.2		-		4.2		65.4	

continued	Weight %	At. Weight	ME 1000	cm	Δ	rm	Δ	to	Δ	pr	Δ	P2O5	Δ	w	Δ	Σ
MnO2	1.4	86.936	16.1	15.3	0.8	0.4	0.3	2.0	-1.6	0.0	0.0					
Fe2O3	73.7	159.692	461.5													
Al2O3	7.7	101.961	75.5													
P2O5	1.17	141.944	8.2									8.2	0.0			
K2O	0.08	94.203	0.8	0.8	0.0											
CaO	0.01	56.079	0.2					0.2	0.0							
SrO	0.01	103.619	0.1	0.1	0.0											
BaO	0.01	153.339	0.1			0.1	0.0									
Na2O	0.01	61.979	0.2					0.2	0.0							
MgO	0.01	40.304	0.2					0.2	0.0							
LOI	10.7	18.015	593.9			0.2	-50.0	1.8	-51.8	0.0	-51.8			-51.8	-	
W Corr.			593.9			0.2	1.8	1.8	0.0	0.0	0.0			0.0	0.0	
Σ	100.0		1242.9	16.3		0.7		4.3		0.0		8.2		0.0		
Norm				1.3		0.1		0.3		0.0		0.7		0.0		100.2

5.3 Norm Minerals in the Vertical Geological Profile

Since the norm provides numerical data on the abundance of the main minerals in the deposit, it is possible to plot this information against the stratigraphic position of the respective sample. Paragenetic relationships and environmental factors, such as enrichment or depletion of minerals in specific horizons, can thus be examined easily. The five main locations with a detailed sampling, described in the petrological section (Chapter 2), are taken to illustrate the distribution and co-existence of normative ore and gangue minerals in the vertical profile. In each geological section one mineral is used as marker for defined horizons with an increased concentration of this particular phase (see horizontal lines). Commonly, kaolinite is the best indicator for supergene reactions operating in the orebody, because this mineral is important for mobilization processes affecting manganese oxide ores; also, kaolinite is often the final replacement product.

5.3.1 Costean 138

This vertical profile is covered by soils containing dense, reworked manganese oxide ores. The main part of the section consists of a sandwich-like structure, where the top and the base of a manganiferous pisolite unit is replaced by iron oxihydroxides. Manganese oxides have impregnated quartz sands underlying these ores.

Kaolinite, taken as marker mineral in this section, generally decreases downwards, but is also concentrated in two horizons at approximately one and two meters depth (Fig. 5.2a). The enrichments occur at the upper boundary of the upper goethite replacement layer (Fe-pisolite) and in the lower part of the second goethite unit, respectively. The abundance of both gibbsite and phosphorus approximately coincide with the goethitic materials that are embraced by the kaolinite, whereas hematite only appears in the top layer of the ferruginous pisolites. The presence of hematite near the top of the indicates an increasing dehydration of higher horizons. Similarly, todorokite is strongly enriched near the top of the section when compared with the materials below (Fig. 5.2b).

It also must be recalled that the dominant part of the section, a manganiferous inverse graded pisolitic layer is "sliced" by the ferruginous secondary rocks. It is most likely that the oldest material, which may still be present, can be found in the middle of this sandwich-like structure, and younger secondary manganese products should have developed further away in the upper and lower layers. This is supported by the fact that adjacent to the kaolinite peaks, cryptomelane is concentrated with two major peaks, the larger one being at the top; cryptomelane is a common supergene product. In contrast, pyrolusite has its main enrichment in the center of the sandwich structure. This means that a strong differentiation of the various Mn oxides occured, which may reflect age relationships. Romanechite shows a pattern similar to cryptomelane, but its main

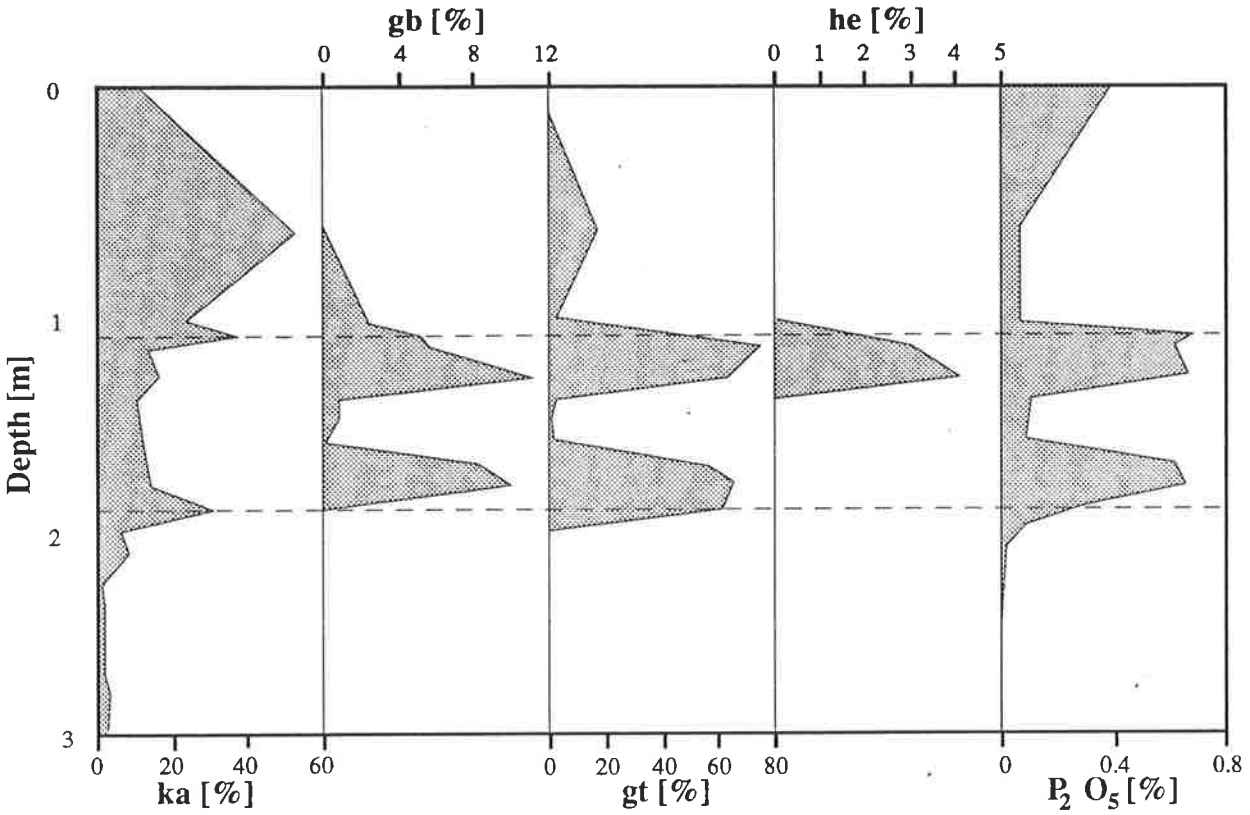


Fig. 5.2a: Vertical section of C-138 and distribution of gangue (norm-) minerals.

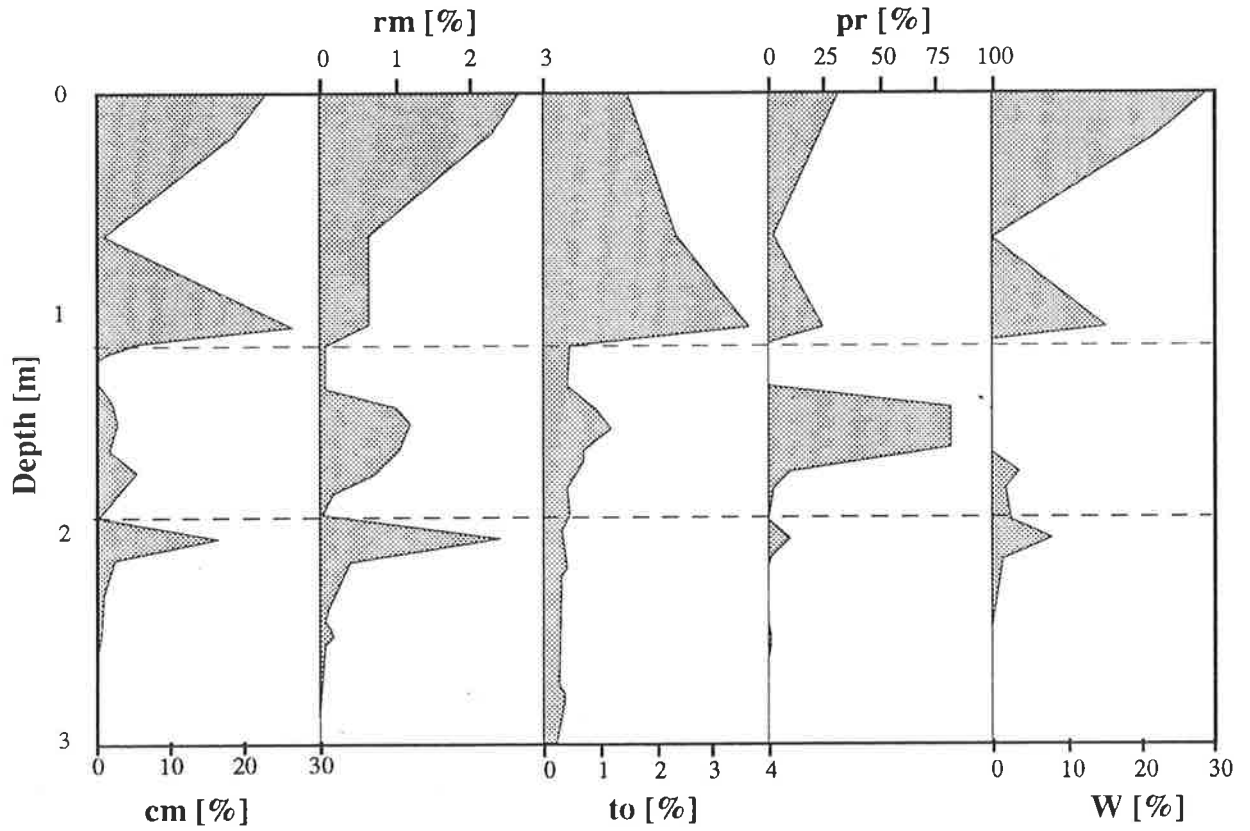


Fig. 5.2b: Vertical section of C-138 and distribution of ore (norm-) minerals.

peak coincides with the lower one of cryptomelane. The development of todorokite seems to be largely dependent on near-surface conditions, whereas pyrolusite appears as the unaltered (?) "sandwich-filling". Partly enriched within the pyrolusite layer, romanechite also seems to indicate an older age than cryptomelane. Water follows the main trends of cryptomelane and romanechite.

5.3.2 F3-Quarry

The profile shown below represents the main orebody of F3-Quarry. The ores consist predominantly of a relatively uniform cemented pisolite, which is interrupted occasionally by vertical and horizontal clay pipes. Again, kaolinite was taken as the marker mineral to identify relationships to other minerals (Fig. 5.3a). Apart from the two main kaolinite peaks in the upper and lower part of the section, the clays decrease almost linearly with depth. Gibbsite is absent at the kaolinite horizons, but it increases in the immediate vicinity of these enrichments. Generally, this mineral increases with depth. Goethite and quartz are concentrated in the kaolinite layers, whereas phosphorus seems to be enriched in some of the ferruginous phases.

The Mn ore minerals do not show a good correlation to any of the previous phases (Fig. 5.3b). Cryptomelane and todorokite generally decrease with depth, and they drop to insignificant levels below the lower kaolinite layer, where groundwaters are probably present over most of the year. An inverse pattern is observed for pyrolusite, which increases with depth. Romanechite first increases downwards, then it quickly decreases where in contact with groundwater. Surprisingly, the free water of the norm does not increase with the availability of water in the orebody down the section, but rather it decreases in parallel with cryptomelane and todorokite.

5.3.3 G- and G-South-Quarry

The first vertical section discussed below mainly consists of oolitic ores, but it also contains a distinct pisolite horizon (G-Quarry, Figs. 5.4a, c). Inverse grading is found in both the pisolites and oolites. The ores are partly covered with a thin laterite and spherulitic materials in soils. In the east the ore crops out. The profile of G-South Quarry orebody is very similar, though it is much thicker and covered by a lateritic horizon (Figs. 5.4b, d).

With the exception of three thicker horizons, kaolinite is cconcentrated in the G-Quarry section in thin subhorizontal layers (Fig. 5.4a). Kaolinite is again taken as the marker mineral. Goethite exhibits a similar pattern, but there is also one additional prominent peak at the bottom of the section. The latter coincides with the main peak of phosphorus, which displays no

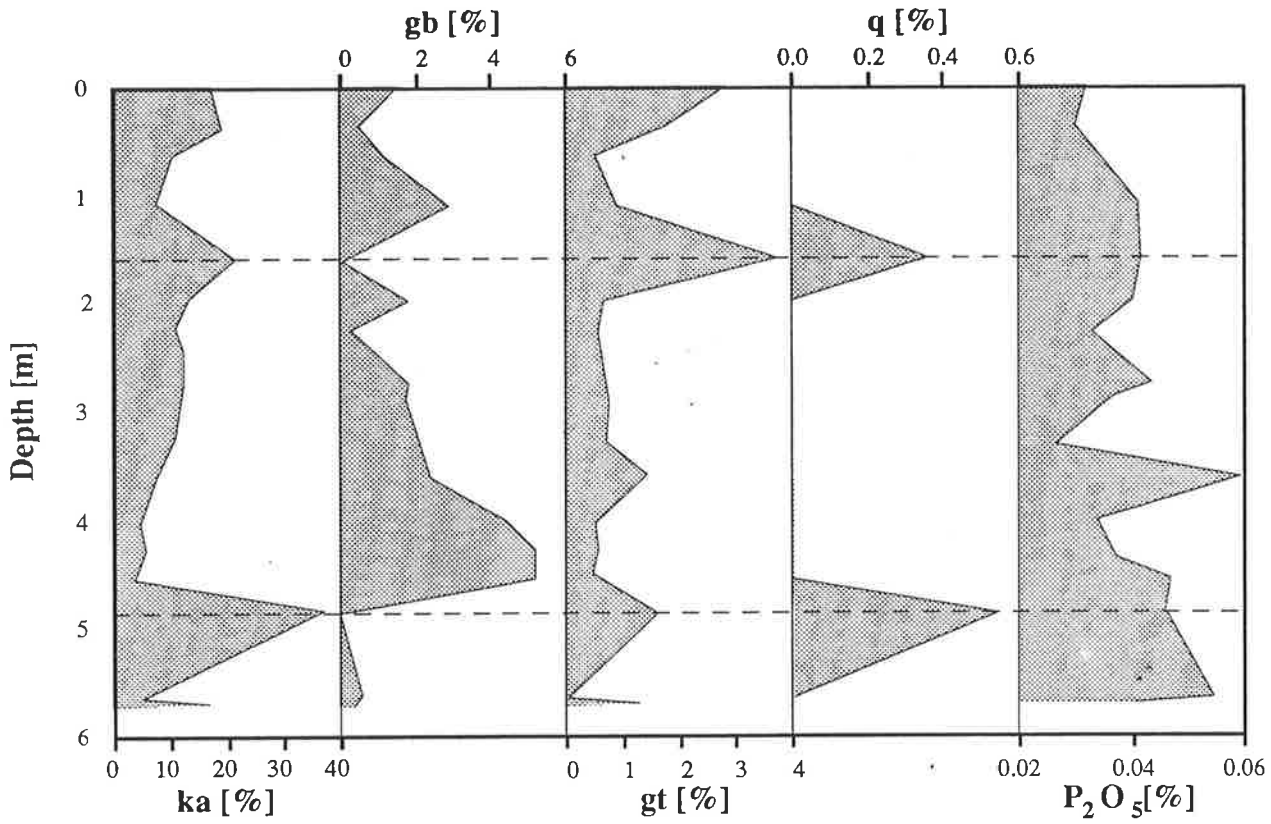


Fig. 5.3a: Vertical section of F3-Quarry orebody and distribution of gangue (norm-) minerals; the overlying laterite is not plotted.

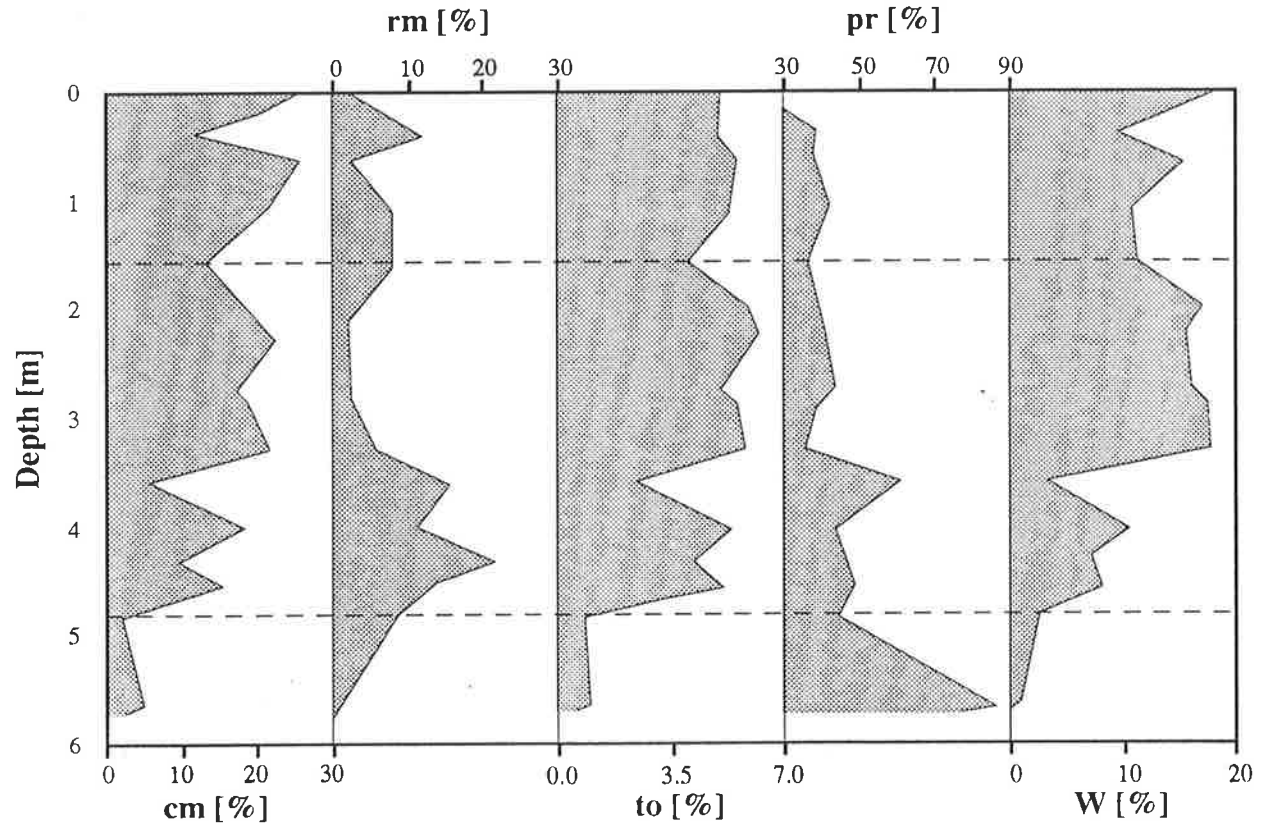


Fig. 5.3b: Vertical section of F3-Quarry orebody and distribution of ore (norm-) minerals; the overlying laterite is not plotted.

significant variation in the profile. An interesting separation between gibbsite and quartz can be observed. Gibbsite dominates the upper part of the section, from where it decreases downwards. At the top, quartz levels are insignificant. Approximately half way down the profile, gibbsite disappears and quartz gradually increases further down to relatively high concentrations. Quartz also correlates well with kaolinite.

With the exception of goethite, which is concentrated in the laterite, all other gangue minerals from G-South are comparable in their behaviour with the G-Quarry ores (Fig, 5.4b). Phosphorus does not vary much over most of the section, but shows one prominent peak in 7 - 8 m depth in the two localities. This peak only correlates positively with goethite in G-Quarry and with a strong pyrolusite peak in G-South.

When the normative stratigraphy of both G- and G-South quarry is compared, it is evident that G-South Quarry (Fig. 5.4b) exhibits more distinctive kaolinite peaks than G-Quarry. However, both locations demonstrate that the most prominent peak positions of kaolinite occur at the same depth. Thus, supergene processes clearly resulted in comparable horizons, although the initial lithologies were different.

Among the ore minerals, cryptomelane in G-Quarry initially exhibits a small increase down the section until about 3 m depth, from where it gradually decreases (Fig. 5.4c). At approximately 7 m depth the mineral shows its strongest enrichment in the examined part of the profile (digital concretions). Generally, a similar pattern is shown by todorokite, but it seems to increase gradually with depth in G-South (Figure 4d). The orebody in G-Quarry is less thick and thus it is not known whether a similar increase could have developed here. Cryptomelane and todorokite are enriched immediately below the kaolinite horizons in both locations. The free norm water depicts a pattern strongly related to those of cryptomelane and todorokite. Romanechite does not have a definite trend, but it decreases in the lower parts of the profile. Pyrolusite shows strong variations, but no definite relation to any other ore mineral. Cryptomelane and todorokite seem to suggest a negative correlation to each other.

The direct comparison between G- and G-South Quarry ores generally depicts similar patterns of the individual Mn minerals over the first seven meters. These patterns have developed on different parts of the initial sedimentary sequence (the ore in this area is dipping with approximately 10° from East to West; for the geological logs see Figs 2.10 and 2.11) Deeper down the section in G-South, the different ore components become less variable in their concentrations (Fig. 5.4d).

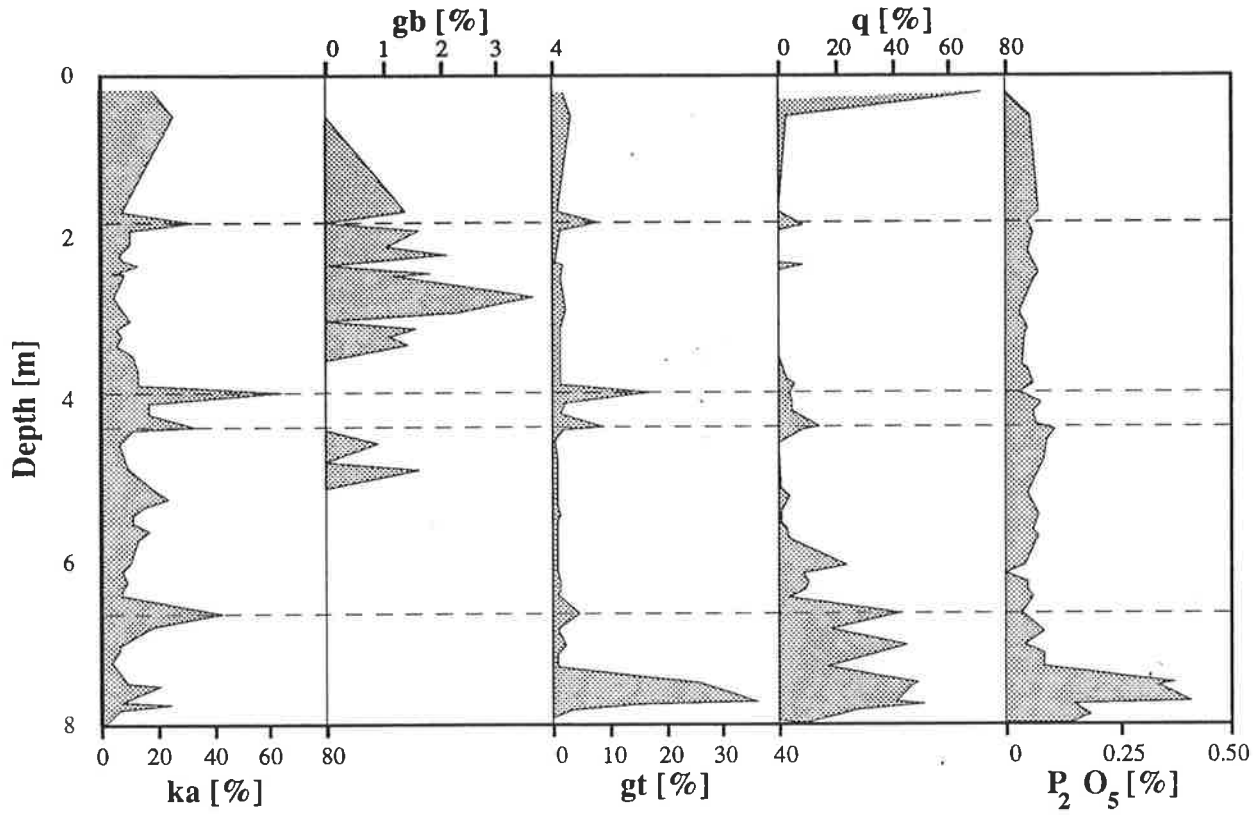


Fig. 5.4a: Vertical section of G-Quarry orebody and distribution of gangue (norm-) minerals.

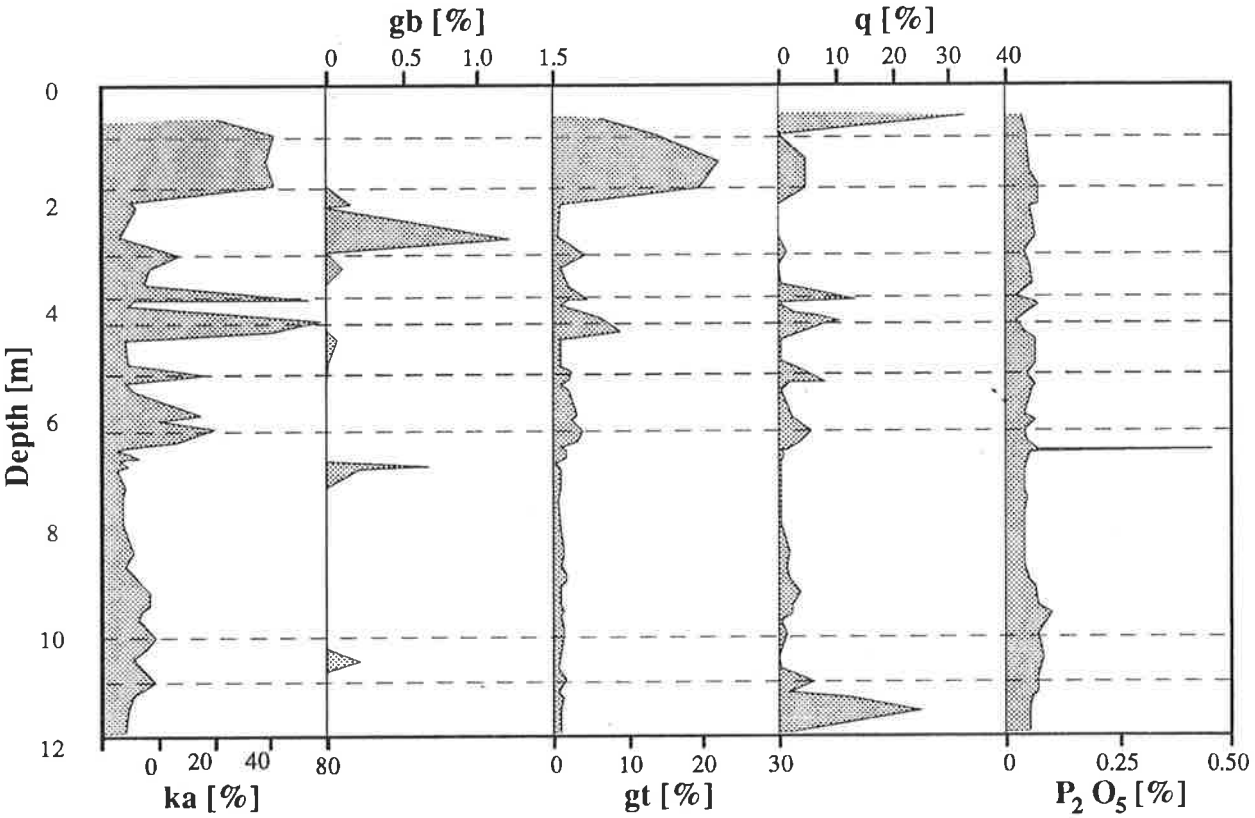


Fig. 5.4b: Vertical section of G-South-Quarry orebody and distribution of gangue (norm-) minerals.

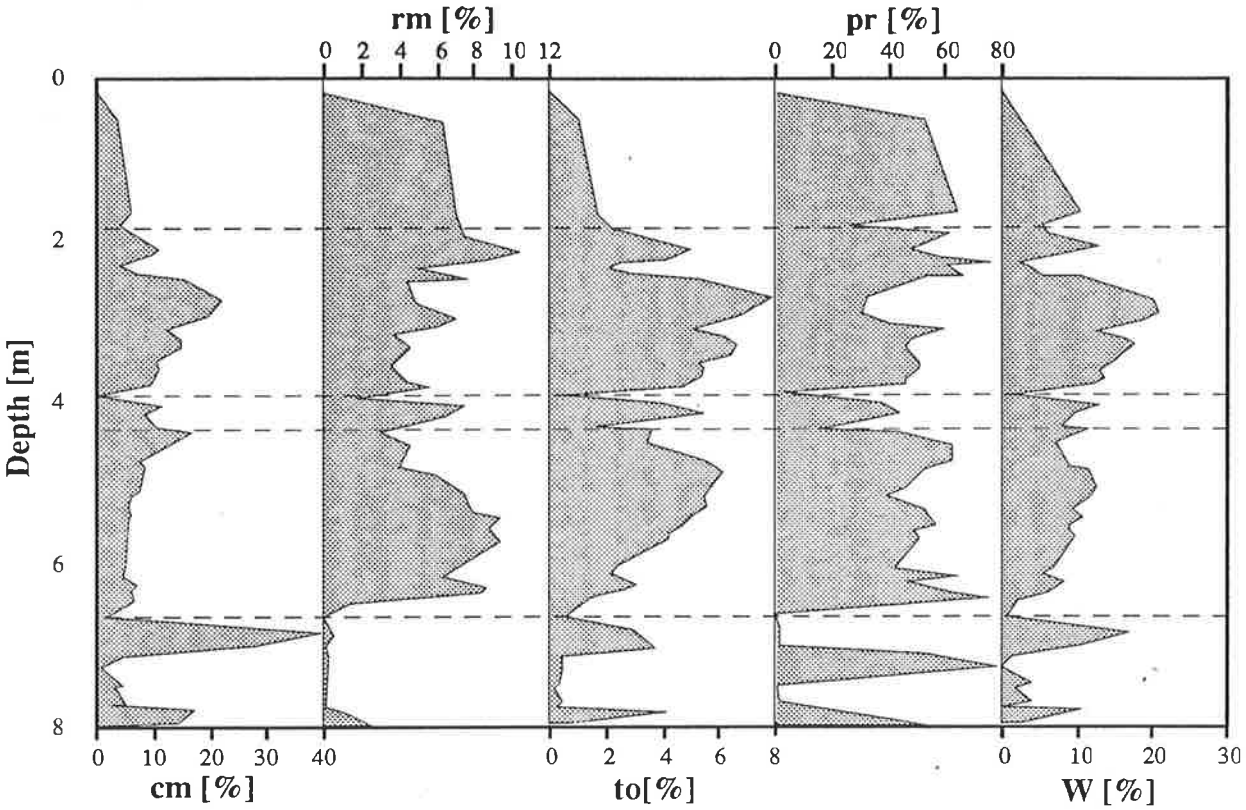


Fig. 5.4c: Vertical section of G-Quarry orebody and distribution of ore (norm-) minerals.

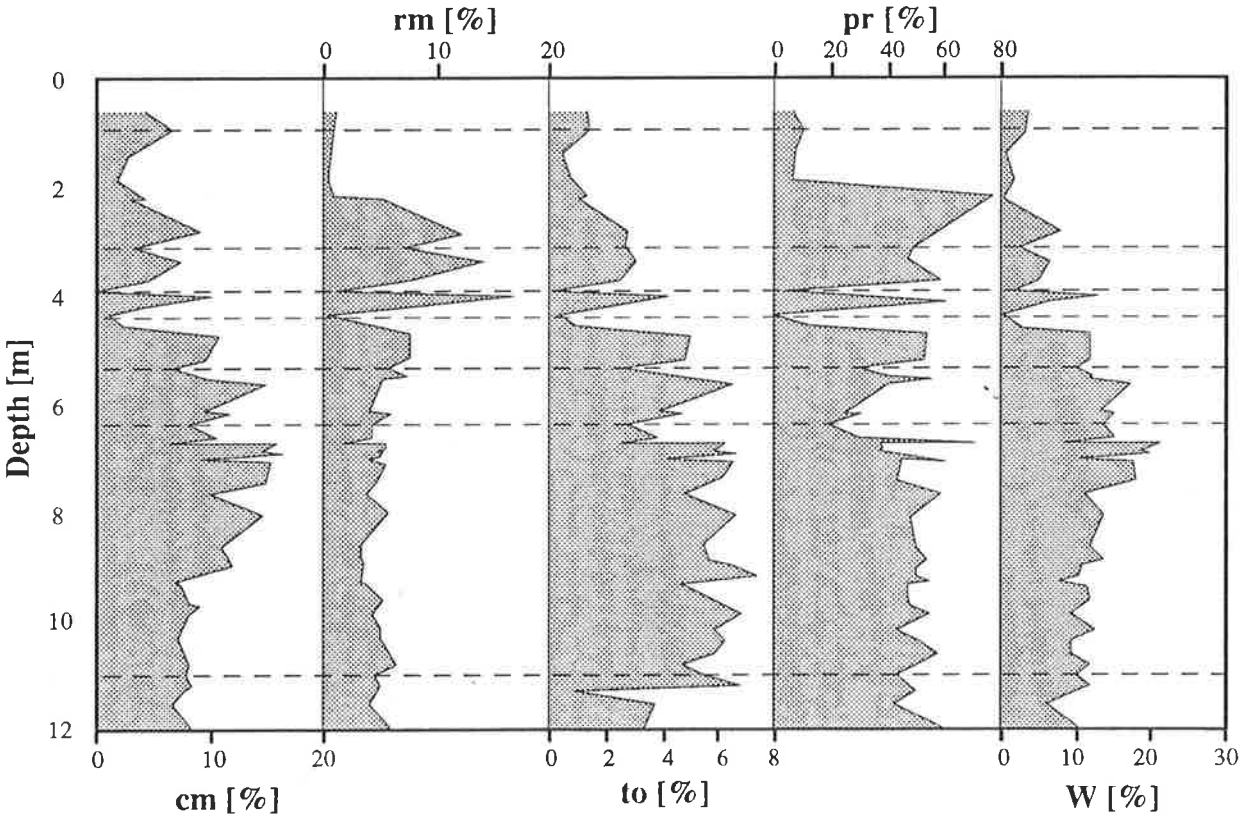


Fig. 5.4d: Vertical section of G-South-Quarry orebody and distribution of ore (norm-) minerals.

5.3.4 D-Quarry Laterite

The ores in D-Quarry are difficult to interpret, because the orebody varies greatly in some parts and a geological log may not be comparable to another which has been analyzed only a few meters away. Observations in the field demonstrate that ore horizons disappear within very short distances. Whether this lenticularity was caused by small-scale tectonics or by supergene removal of lower parts of the orebody was not examined in this study. However, the laterite overlying the ores also contains relic manganese oxides, either as loose pisoliths or as cemented fragments, and it was therefore examined in detail.

Hematite seems to play an important role in the laterite and it was used as the marker mineral for the section. The main enrichments of hematite are all found in the top five meters, depicting layers of increased oxidation (Fig. 5.5a). The same horizons also possess phosphorus peaks, which are not correlated to any other mineral. Kaolinite and goethite do not show significant variations over the entire profile, the latter mineral decreasing slightly downwards. Quartz gradually decreases with increasing depth.

The manganese oxides have higher values a short distance above the hematite horizons (≈ 50 cm) and these minerals generally increase down the section, with the exception of romanechite, which has its highest concentrations in the upper 4 m of the profile (Fig. 5.5b). The free water content of the samples increases gradually downwards.

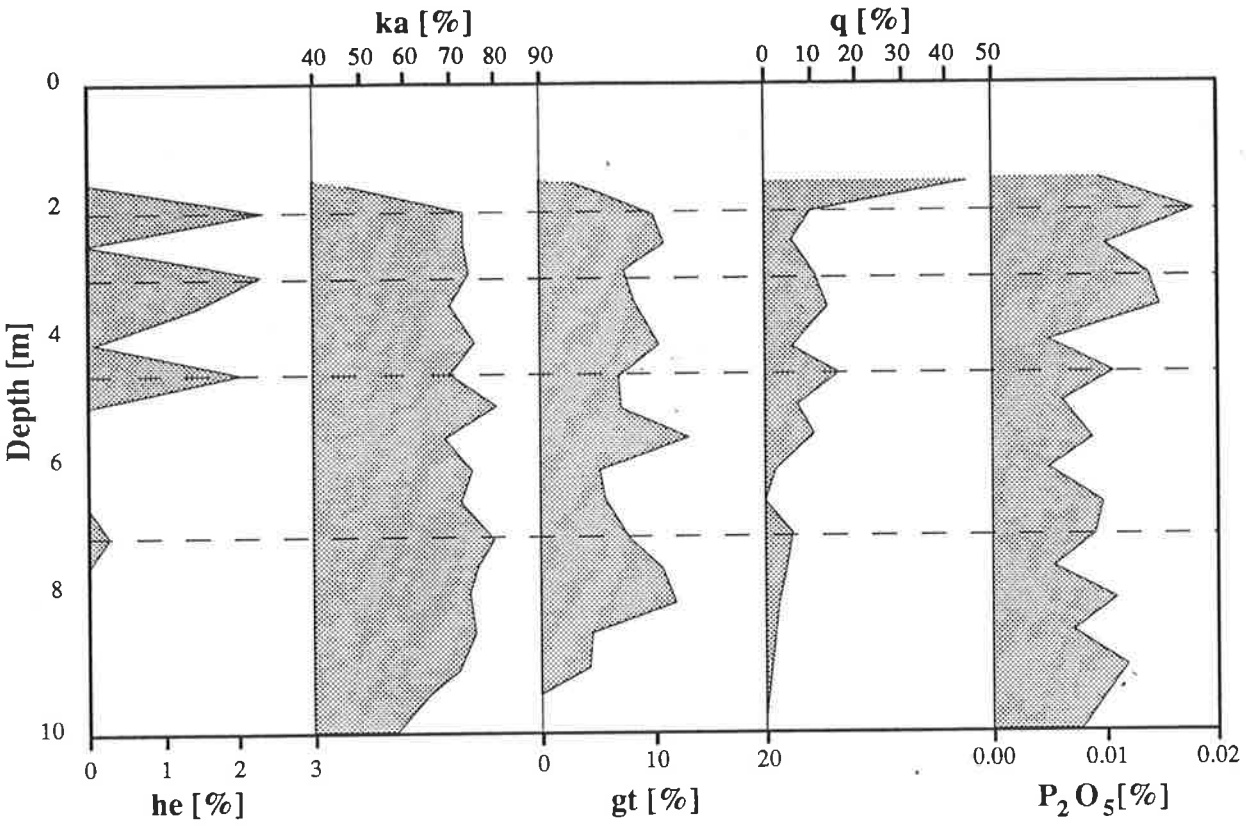


Fig. 5.5a: Vertical section of D-Quarry laterite and distribution of gangue (norm-) minerals.

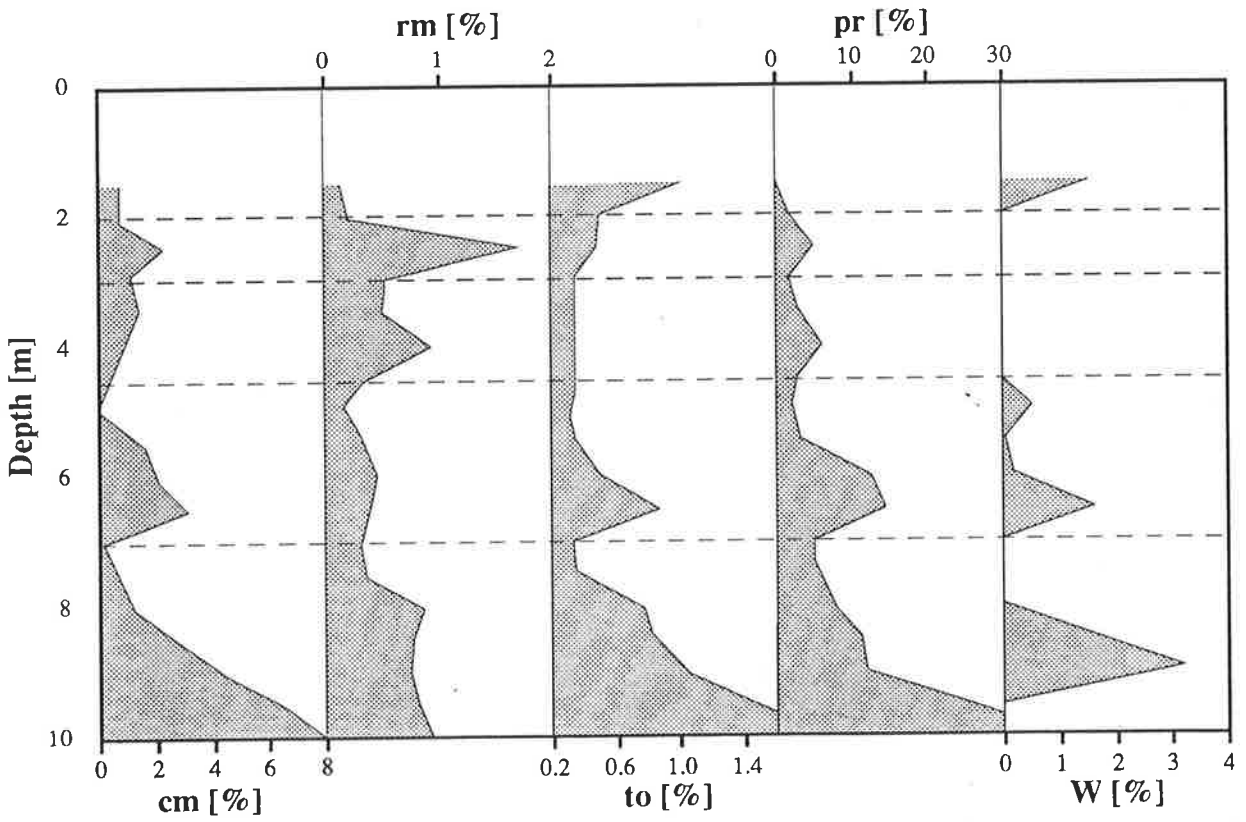


Fig. 5.5b: Vertical section of D-Quarry laterite and distribution of ore (norm-) minerals.

5.4 Characterization of Ores and Rocks

In order to compare the characteristics of the various manganese oxides and associated gangue minerals, they are displayed in two different ways. First, average concentrations are plotted to show the distribution of individual minerals in the respective ores and rocks. Second, the general relationships between the different members are illustrated in ternary diagrams as follows:

- Mn-oxide diagrams including pyrolusite (pr), romanechite (rm), cryptomelane (cm) and todorokite (to) for ores and all rocks containing Mn,
- gangue diagrams including kaolinite (ka), anatase (an), quartz (q), goethite (gt), and hematite (he) for ores, which normally contain gangue minerals in their matrix, and for all associated rocks.

The objective here is to gain an understanding of ore/rock genesis. In some cases, the results seem to support field observations, such as those bearing on parageneses. However, it must be kept in mind that points on ternary plots represent ratios rather than data that can be compared directly. Thus, a careful assessment of the data is essential and interpretations that result from this theoretical approach, while they may support the field findings, cannot overrule them.

5.4.1 Normative Composition of Ores

Below, the normative Mn oxide mineralogy of ores and rocks is examined to give an overview over phase abundances in individual materials (Table 5.3; Figs. 5.6a-f). The diagrams for ores commonly show a dominant pyrolusite peak; the gangue diagrams exhibit strong kaolinite enrichments. Although there are distinct differences between the various ore and rock types, it is difficult to distinguish some individual ores or rocks, such as cemented pisolites and cemented oolites, purely on the basis of the normative calculations.

The Mn-oxide composition patterns of uncemented and cemented mangcretes, both oolitic and pisolitic, are similar in their shape, but they possess surprising differences when mineralogically compared (Fig. 5.6a). Generally, pyrolusite dominates strongly over all other manganese minerals and reaches relatively high values, while the concentration of the other oxides remain comparatively low. However, two groups are identified according to the mineralogical composition. The first is formed by cemented oolite and uncemented pisolite, which have almost identical patterns. In both types, pyrolusite is strongly enriched (~ 70 %) over all other Mn-oxides, which are uniformly low in their concentration (~ 5-10%). The second group consists of uncemented oolite and cemented pisolite, which are also very similar to each other. In this group cryptomelane and romanechite gain importance (15-20%) and pyrolusite decreases to about 40%. These findings confirm analytical results from chapter 3 which showed that cemented pisolites increasingly contain cryptomelane, in contrast with the increasing pyrolusite

Table 5.3: Statistics of Mn oxide minerals in ores and rocks.

Ore Types	cm	rm	to	pr	W
cemented pisolite					
average	18.62	5.86	6.22	41.02	11.48
maximum	33.47	21.92	17.26	55.23	17.59
minimum	9.32	0.04	4.20	13.39	5.75
std. dev.s	6.05	5.88	2.37	9.75	3.85
cemented oolite					
average	7.71	6.74	4.11	61.55	7.55
maximum	10.93	10.23	6.05	75.33	12.42
minimum	4.37	2.25	2.36	46.95	1.95
std. dev.	2.59	2.51	1.38	9.28	3.71
chocolate ore					
average	1.90	0.80	1.20	11.10	0.40
maximum	7.80	1.20	5.40	60.60	3.00
minimum	0.30	0.20	0.40	2.10	0.00
std. dev.	2.30	0.30	1.50	17.60	0.90
clay/sandy clay					
average	0.34	0.02	0.37	0.28	0.26
maximum	2.61	0.12	0.64	1.62	1.22
minimum	0.00	0.00	0.22	0.00	0.00
std. dev.	0.92	0.04	0.14	0.55	0.42
concretion					
average	44.40	4.40	6.50	14.30	13.50
maximum	66.50	8.70	9.90	38.80	17.20
minimum	9.50	1.00	2.80	0.40	6.50
std. dev.	15.90	2.70	2.10	13.00	3.40
digital concretion					
average	26.60	19.60	2.60	13.50	10.70
maximum	50.60	38.20	3.50	19.50	17.30
minimum	9.90	0.50	1.50	2.70	4.70
std. dev.	15.40	17.80	0.70	7.00	5.70
Fe-pipe wall					
average	0.50	0.50	0.40	1.60	0.20
maximum	1.60	2.40	0.90	5.10	0.90
minimum	0.00	0.00	0.20	0.20	0.00
std. dev.	0.70	1.00	0.30	2.10	0.40
Fe-pisolite					
average	2.50	0.30	0.60	5.20	1.80
maximum	12.60	1.40	3.20	35.20	6.30
minimum	0.10	0.00	0.30	0.00	0.00
std. dev.	3.00	0.40	0.70	9.30	2.00
hardground					
average	8.40	3.60	4.10	66.10	7.70
maximum	8.80	6.10	6.80	74.60	11.40
minimum	7.90	1.70	2.40	52.80	5.10
std. dev.	0.40	2.30	2.40	11.60	3.30

Ore Types	cm	rm	to	pr	W
laminar mangcrete					
average	18.50	7.90	7.30	30.70	10.40
maximum	33.30	15.70	10.40	50.00	16.10
minimum	13.20	0.40	5.80	7.30	6.70
std. dev.	7.20	6.70	1.60	13.40	3.40
laterite					
average	1.40	0.50	0.70	4.90	0.60
maximum	6.40	1.70	2.50	14.30	5.60
minimum	0.00	0.00	0.20	0.00	0.00
std. dev.	1.60	0.40	0.50	4.60	1.30
massive mangcrete					
average	34.90	2.50	5.60	20.70	13.80
maximum	50.30	12.00	9.10	34.70	18.40
minimum	19.30	0.00	1.20	4.90	9.40
std. dev.	11.30	3,20	2.40	9.90	3.00
radial pyrolusite					
average	3.80	0.60	1.90	80.90	1.20
maximum	23.70	1.90	7.70	89.10	8.50
minimum	0.40	0.20	0.40	48.10	0.00
std. dev.	7.60	0.50	2.50	12.90	2.70
Mn-impregnated sand					
average	3.19	0.97	0.61	1.92	1.85
maximum	18.39	10.03	1.77	10.22	8.81
minimum	0.30	0.04	0.21	0.00	0.00
std. dev.	5.75	2.40	0.38	3.83	3.01
siliceous ore					
average	17.79	1.59	4.48	39.06	7.24
maximum	25.91	3.14	7.37	71.75	11.60
minimum	9.92	0.07	2.81	16.08	2.48
std. dev.	4.81	1.13	1.70	20.94	2.73
uncemented pisolite					
average	4.77	2.99	2.45	68.93	1.90
maximum	10.47	15.42	6.19	97.24	8.46
minimum	0.34	0.11	0.44	40.55	0.00
std. dev.	3.32	4.97	1.83	15.10	2.12
uncemented oolite					
average	12.09	5.28	5.66	43.78	13.45
maximum	22.36	8.77	9.24	74.47	21.34
minimum	4.97	1.50	1.71	16.15	2.00
std. dev.	3.96	1.52	1.86	12.03	4.71
spherulite					
average	1.80	1.50	0.80	9.20	1.70
maximum	4.70	6.40	2.50	52.00	6.30
minimum	0.00	0.20	0.20	0.00	0.00
std. dev.	1.80	1.70	0.70	13.10	2.00

dominance in cemented oolites. A similar separation of the ore types cannot be made on the basis of the gangue minerals. Rather, the separation which is seen between uncemented and cemented materials (Fig. 5.6b), with the latter ores having approximately half the clay content of the uncemented materials (~ 16%).

The following plot (Fig. 5.6c) shows mineral concentrations in other ore types; only radial pyrolusite and hardgrounds have larger pyrolusite concentrations than in Fig. 5.6a (70-80%). Laminar mangcretes, digital concretions, concretions, and massive mangcretes have all much less pyrolusite (~10-40%), but they contain larger amounts of cryptomelane (up to 40%) and romanechite (e.g. digital concretions: ~20%). In Fig. 5.6d the gangue mineral composition of this same group of ores is presented. Laminar and massive mangcretes are seen to contain the highest kaolinite concentrations. The remaining ore types possess 10% or less of each gangue mineral. Mn-impregnated sands have very low manganese oxide contents (generally pyrolusite; Fig. 5.6e), high quartz concentrations (~ 80%; Fig. 5.6f), and low kaolinite values (~ 10%). Siliceous ores show a reverse pattern with approximately 70% Mn-oxides and ~30% quartz and kaolinite.

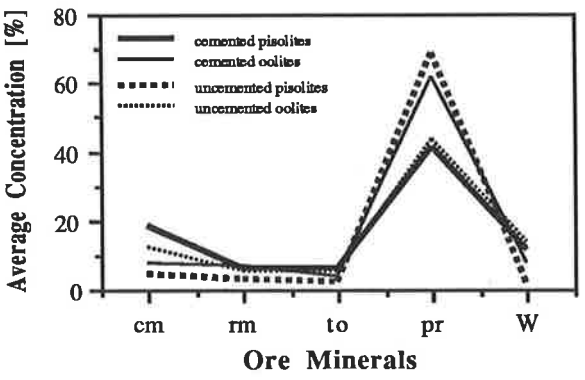


Fig. 5.6a: Mn oxide distribution in ores.

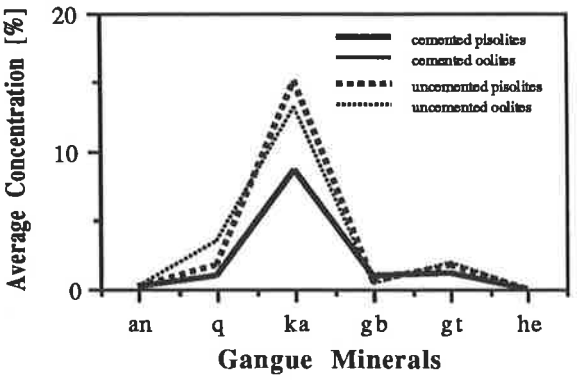


Fig. 5.6b: Gangue mineral distribution in ores.

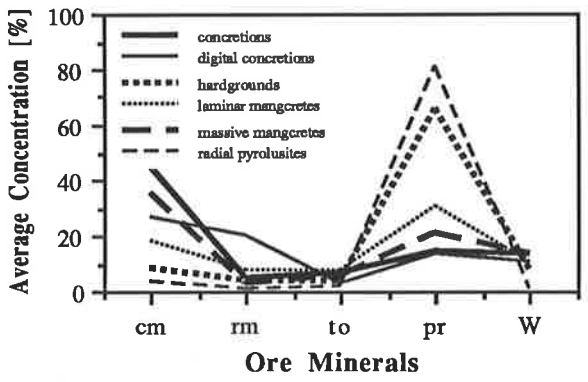


Fig. 5.6c: Mn oxide distribution in ores.

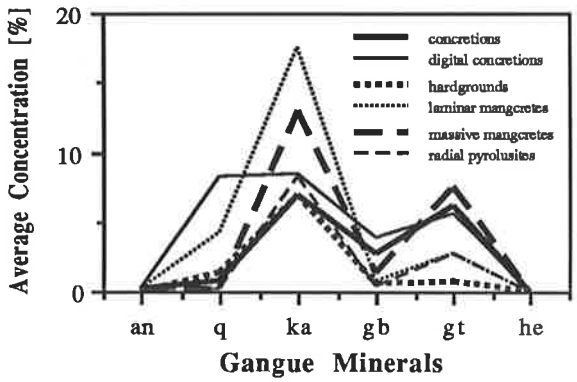


Fig. 5.6d: Gangue mineral distribution in ores.

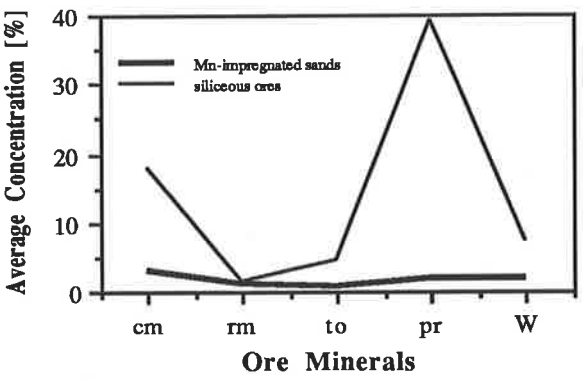


Fig. 5.6e: Mn oxide distribution in ores.

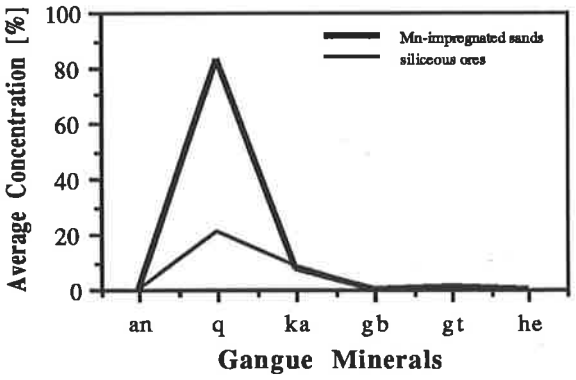


Fig. 5.6f: Gangue mineral distribution in ores.

5.4.2 Relationships between Ore Types

The distribution of the four manganese norm minerals in ores and gangues, respectively, is depicted in ternary diagrams to examine relationships between the various secondary products. The first major field is that of the pisolitic ores, which in fact covers most of the other main ore types (Fig. 5.7a). This field splits into three subgroups:

- uncemented pisolites with a relatively soft, often clay-rich matrix, and which are dominated by pyrolusite,
- cemented pisolites, which show an increasing influence of cryptomelane and romanechite, and
- siliceous ores, much of which overly the field of cemented pisolites but also cover part of that for uncemented pisolites. Siliceous ores have either quartz nuclei, quartz grains in the matrix, or both. They contain only small concentrations of romanechite and seem to concentrate considerable amounts of cryptomelane and todorokite.

The second major ore type, oolitic ores, lies entirely within the field of pisolites. Uncemented oolites occur mainly within the field of uncemented pisolites, but they extend into the cemented pisolite field and to the boundary of the siliceous ores. As is the case with the uncemented pisolites, the cemented oolites are dominated by pyrolusite and romanechite. An interesting feature is displayed by one of the rarer ore types, the hardgrounds (mainly from the G-Quarry area). This ore plots along the boundary between cemented and uncemented oolites, indicating genetic similarities.

It is now necessary to look again at the siliceous ores which are shown in a detailed section of the triangle (lower part of Fig. 5.7a). The siliceous ores are shown again, together with Mn-impregnated sands, clays, and massive mangcrete. The overlap of manganiferous clays with the siliceous ores produces a shape which is very similar to the field of the massive mangcrete. This finding suggests that the ore mineralogy of secondary Mn-precipitates strongly depends on the

chemical character of the host rock. The more clays and/or sands are available, the more it seems that the formation of cryptomelane and todorokite is favoured. This is best demonstrated by the Mn-impregnated sands, which contain virtually no pyrolusite and only small amounts of romanechite. Concretions that developed near the top of the orebody show a similar pattern with the enhanced appearance of cryptomelane and todorokite. This type of ore is always associated with clays and sands and its field overlaps partly with siliceous ores.

A more complex history of formation is suggested by spherulites. There are three major areas of spherulites in the diagram. The first field shows analyses from spherulites that formed directly on outcropping ores (G-Quarry). There are nearly no overlying materials such as laterites or soils covering the ore. Pyrolusite dominates here, cryptomelane and todorokite are of minor importance. Though the field overlaps partly with the uncemented pisolites, it is close to the cemented oolites from which the materials must have been derived. The second type of spherulites formed on an extensive laterite profile overlying pisolitic ores in F3-Quarry. As with the siliceous ores, cryptomelane and todorokite gain importance and this leads to a horizontal shift of the field, away from the pisolite field. The remaining area overlaps with the cemented pisolitic ores. This field represents spherulites from both D-Quarry (very thick laterite cover) and G-South-Quarry (thin laterite). It is uncertain whether this coincident appearance is the result of independent shifts from different initial compositions. Radially crystallized pyrolusite, not shown for reasons of simplicity, from the contact between ore and laterite from G-South, plots near the base of the siliceous ore field at the extreme left side (pyrolusite corner).

The following diagram gives an overview for the gangue minerals/rocks that are associated with the deposits (Fig. 5.7b). Since small quantities of manganese oxides are also present in these materials, it is possible to determine the field positions for the various rocks and to compare them. Mn-minerals that form within or next to goethitic rocks (either as ferruginous pisolites or massive segregations) exhibit a mineralogy that is dominated by pyrolusite, cryptomelane and todorokite. Romanechite does not seem to play any significant role in these ores. Overlying the field of goethite, a large area is shown for the laterites. They are predominantly oxidized (hematitic) and they grade from the pyrolusite-rich "chocolate ores" towards the manganiferous stains of greenish clays which are enriched with cryptomelane and todorokite. Laterites in an intermediate position seem to concentrate romanechite. Whether this is a transitional step or not, cannot be said from an analysis of these diagrams.

Close relationships are exhibited by the laminar mangcretes from pipe walls and the ferruginous coatings of the same pipes. Both rock types overlap goethitic and hematitic parts of the previously described fields, with a dominance of hematite for the laminar mangcrete. Cryptomelane and todorokite seem to be of less importance than in the clays, laterites and ferruginous rocks. Contrary to this, the dendritic concretions that formed within siltstones below the main orebody, possess only minor amounts of pyrolusite.

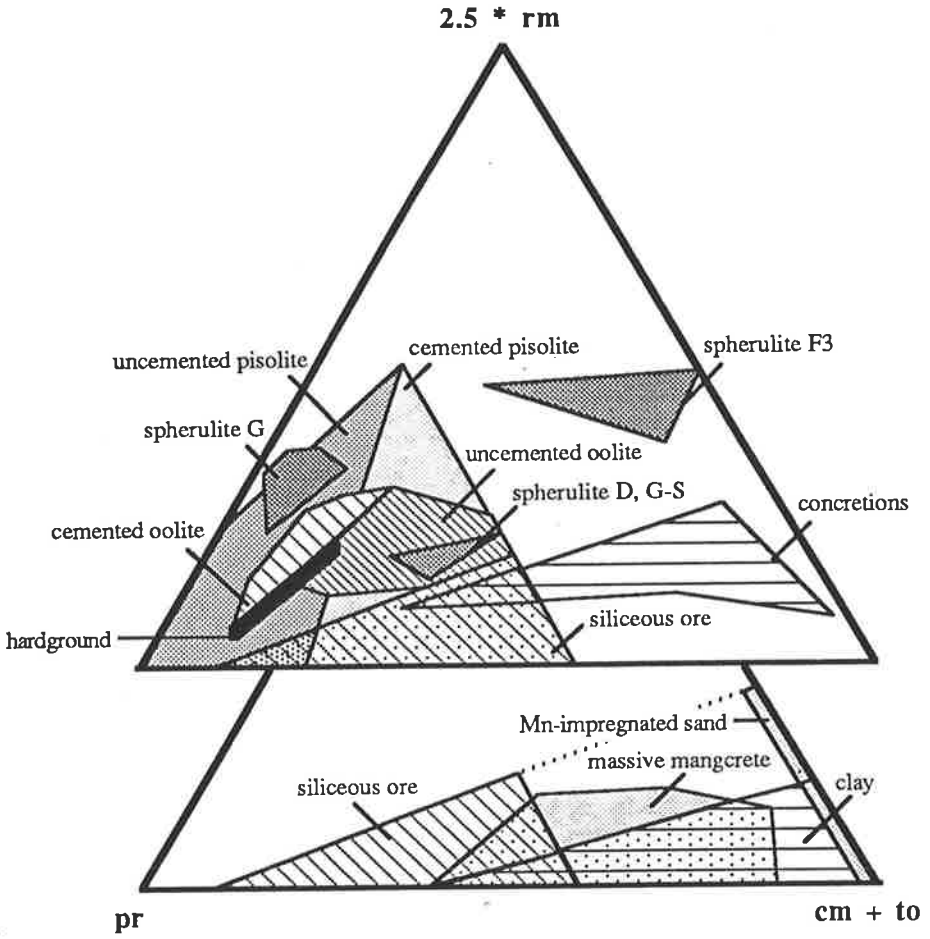


Fig. 5.7a: Ternary plot of Mn-oxide norm minerals for the main manganese ores.

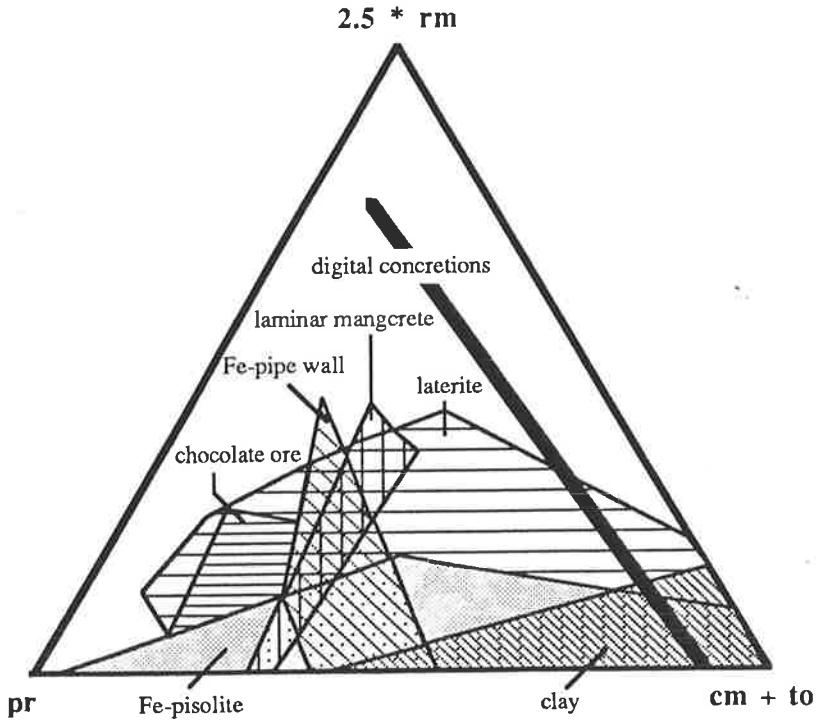


Fig. 5.7b: Ternary diagram of Mn-oxide norm minerals for some ores and the main gangues.

5.4.3 Trace Element Composition of Ore Minerals

Until recently, most of the ores and rocks of the Groote Eylandt manganese deposit had not been analyzed for their trace element contents, and it was not known which of the minerals concentrated the various trace elements. Therefore, the mineral normalization technique was applied to examine the role of individual minerals.

The previous sections have illustrated the great variety of ore and rock types and some of their inter-relationships. Variability in mineralogical composition largely results from the continuous activity of supergene processes, which produced numerous combinations of both ores and gangues. This fact is also reflected in the trace element composition of the samples. Often, the trace elements show a positive correlation to several minerals. Zn for instance, is an element that correlates to nearly all the available phases, with the exception of quartz and kaolinite. However, if the large-scale comparison is reduced to specific ores or rocks, then a clearer picture emerges.

Table 5.4: Correlation of trace elements and normative minerals; *elements show a positive correlation to uncemented oolites and a negative or no correlation to cemented pisolites.

Mineral	REEs	Radius [Å] (valency)
Pyrolusite	B	0.22 (3+)
	(Ce)	1.07 (3+), 0.94 (4+)
	Eu	1.24 (2+), 1.15 (3+)
	La	1.14 (3+)
	Nd	1.04 (3+)
	P	0.4 (3+), 0.35 (5+)
	Sm	1.00 (3+)
Cryptomelane	Co	0.72 (2+), 0.63 (3+)
	Cu	0.96 (1+), 0.72 (2+)
	Mo*	0.70 (4+), 0.62 (6+)
	U*	0.97 (4+), 0.80 (6+)
	V*	0.74 (3+), 0.59 (5+)
	Zn	0.74 (2+)
	Yb*	1.13 (2+), 0.86 (3+)
Todorokite	Mo*	0.70 (4+), 0.62 (6+)
	Ni*	0.69 (2+)
	U*	0.97 (4+), 0.80 (6+)
	V*	0.74 (3+), 0.59 (5+)
	Zn	0.74 (2+)
	Yb*	1.13 (2+), 0.86 (3+)
romanechite	---	---

The additional problem of a positive correlation of one element to a specific mineral in one location and a negative correlation to the same mineral in a different area is illustrated in the example of Mo contained in todorokite (Fig. 5.8a). Similar effects are detected for several elements. Nevertheless, it reflects the availability of the respective trace elements within the deposit, and the positive correlation to a mineral in a particular area is used below to generally determine the main host mineral for the various elements. This does not mean that other minerals do not contain small amounts of the same element, but the correlation is much weaker in these cases.

Trace elements identified in the various minerals, together with their ionic radii, are listed in Table 5.4. This tabulation shows a selective incorporation of the trace elements into the lattice of minerals, which obviously depends on

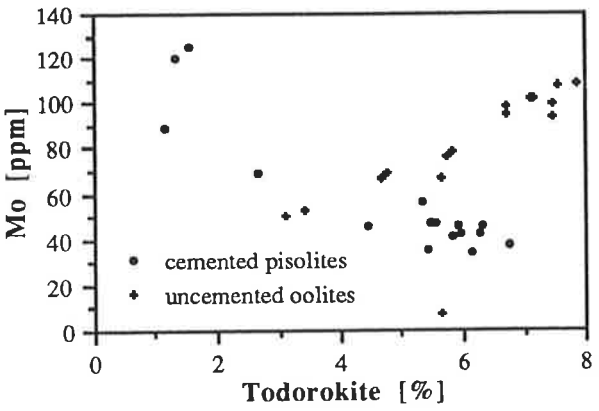


Fig. 5.8a: Correlation of todorokite and Mo in different ore types.

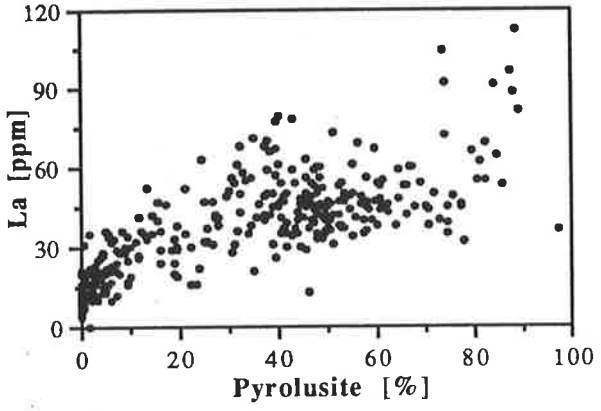


Fig. 5.8b: Correlation ofpyrolusite and La.

the ionic radius of the respective element. Pyrolusite seems to be very specific in its uptake of trace elements. It incorporates some relatively light elements with radii of less than 0.4 Å for the trivalent ions (B and P), then a large gap exists, and only from ion sizes larger than 1Å, are further trivalent elements accommodated. In the latter case pyrolusite correlates particularly well with La (Fig. 5.8b), Eu, Nd, and Sm. Ce appears to be concentrated in the pyrolusite and goethite fraction (see 5.4.6) of lateritic rocks, but it cannot be related to oolitic and pisolitic ores.

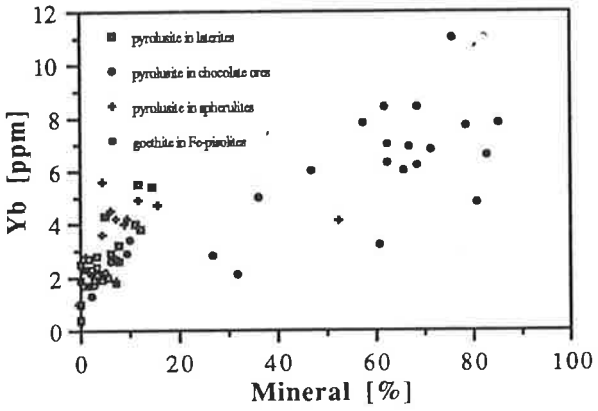


Fig. 5.8c: Correlation ofpyrolusite/goethite and Yb in different materials.

Cryptomelane and todorokite are comparable in their preference for elements with radii of approximately 0.7 Å (2+ and 3+). However, each mineral contains elements which cannot be found in the other (cryptomelane: Co, Cu; todorokite: Ni). Yb, the smallest member of the analyzed REEs when trivalent species are compared, is found in varying quantities in nearly all norm minerals (Fig. 5.8c), with the exception of kaolinite, quartz, and anatase. However, the best correlation between Yb and norm minerals is obtained for cryptomelane and todorokite in oolitic manganese oxides. No trace elements have been identified in conjunction with romanechite.

5.4.4 Normative Composition of Associated Rocks

A small group of rocks, seemingly dominated by iron oxides and oxyhydroxides when examined in the field (dark brown, red and yellow colours), demonstrates that, with the exception of ferruginous pisolites, all these rocks contain predominantly kaolinite and less quartz (Fig. 5.9a). The concentrations of kaolinite vary between 50 and 70% and those of quartz between 10 and 30%. Goethite rarely exceeds 10% in the samples and only Fe-pisolites show the expected high values of approximately 60% (Table 5.5).

Most rocks associated with the deposit also contain small amounts of manganese oxides, either in the form of primary relics or as supergene impregnations. This can be seen in the relatively high pyrolusite peak of some of the rock types (Fig. 5.9b). Chocolate ores and spherulites both show approximately 10% pyrolusite and about 2% cryptomelane. The other rocks generally differ in the pyrolusite concentration, but they are similar in other aspects of their ore mineralogy. An exception is the spherulitic ore which possesses comparable levels of both cryptomelane and todorokite. Normally, cryptomelane dominates over todorokite.

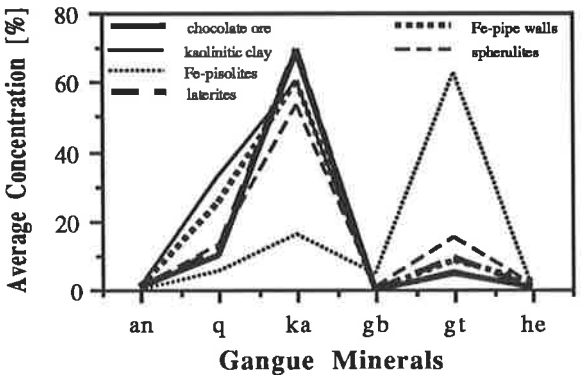


Fig. 5.9a: Gangue mineral distribution in rocks.

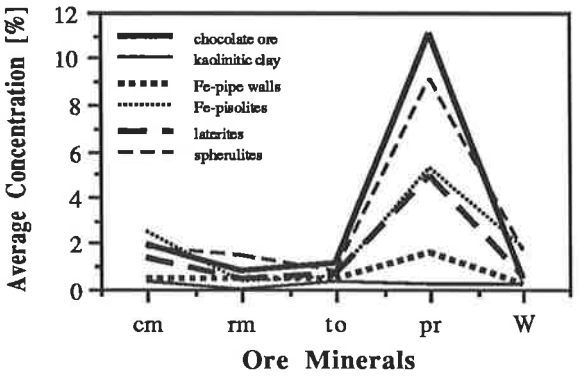


Fig. 5.9b: Ore mineral distribution in rocks.

Table 5.5: Statistics of gangue minerals in ores and rocks.

Ore Types	an	q	ka	gb	gt	Ore Types	an	q	ka	gb	gt
cemented pisolite						**laminar mangcrete**					
average	0.10	1.03	8.50	0.97	1.16	average	0.21	4.10	17.50	0.70	2.70
maximum	0.21	9.46	21.50	5.20	27.41	maximum	0.29	25.60	25.50	1.80	4.10
minimum	0.05		3.07		0.50	minimum	0.08	0.00	7.40	0.00	1.50
std. dev.	0.05	2.00	5.49	1.83	5.76	std. dev.	0.07	9.60	5.50	0.80	1.00
cemented oolite						**laterite**					
average	0.10	1.03	8.50	0.97	1.16	average	0.89	11.20	69.40	0.00	9.30
maximum	0.17	7.34	13.69	2.08	2.10	maximum	1.14	44.50	80.40		22.10
minimum	0.07		4.77		0.73	minimum	0.64	0.10	48.20	0.00	0.00
std. dev.	0.03	2.57	2.93	0.86	0.45	std. dev.	0.14	10.60	8.10	0.00	5.70
chocolate ore						**massive mangcrete**					
average	1.01	10.20	68.80	0.00	4.60	average	0.20	0.20	12.90	1.40	7.40
maximum	1.16	18.10	76.90		7.10	maximum	0.46	1.90	33.50	3.50	38.70
minimum	0.26	1.70	16.10	0.00	1.60	minimum	0.08	0.00	4.30	0.00	0.50
std. dev.	0.27	6.40	18.60	0.00	2.00	std. dev.	0.12	0.50	9.50	1.10	11.50
clay/sandy clay						**radial pyrolusite**					
average	0.67	32.75	60.12	0.00	5.13	average	0.14	0.20	8.20	0.40	2.60
maximum	1.15	68.08	90.27		18.79	maximum	0.18	0.90	11.50	2.70	3.90
minimum	0.24	7.04	20.85			minimum	0.10	0.00	5.40	0.00	1.70
std dev clay	0.35	25.57	30.44		7.83	std. dev.	0.03	0.30	2.20	0.90	0.80
concretion						**Mn-impregnated sand**					
average	0.13	0.70	6.90	2.70	6.00	average	0.12	82.92	8.09		0.66
maximum	0.17	5.90	13.10	6.60	44.00	maximum	0.40	97.15	31.11		4.66
minimum	0.10		3.10	0.00	0.90	minimum	0.03	48.24	1.76		0.00
std. dev.	0.03	1.90	3.30	2.50	13.40	std. dev.	0.11	17.34	7.89		1.18
digital concretion						**siliceous ore**					
average	0.18	8.20	8.40	3.90	5.50	average	0.08	20.61	8.12		0.97
maximum	0.24	31.40	17.70	7.00	12.50	maximum	0.13	46.56	13.36		3.68
minimum	0.16	0.00	4.60	0.00	0.70	minimum	0.06	2.77	5.35		0.15
std. dev.	0.03	13.40	5.00	3.10	4.40	std. dev.	0.02	19.03	2.23		1.00
Fe-pipe wall						**uncemented pisolite**					
average	0.75	25.10	60.20	0.00	8.40	average	0.17	1.62	15.01	0.54	1.71
maximum	0.92	44.80	72.70		11.90	maximum	0.41	10.98	37.60	2.28	5.33
minimum	0.57	10.40	43.30	0.00	5.20	minimum	0.03		2.27		
std. dev.	0.14	14.50	11.50	0.00	2.70	std. dev.	0.10	3.31	8.99	0.80	1.13
Fe-pisolite						**uncemented ooilte**					
average	0.24	5.60	15.70	4.50	62.50	average	0.16	3.47	13.17	0.36	1.89
maximum	0.39	49.60	31.60	11.10	85.20	maximum	0.44	23.91	40.09	3.65	9.74
minimum	0.04	0.00	4.50	0.00	26.50	minimum	0.07		4.63		0.53
std. dev.	0.11	13.40	7.30	3.90	17.20	std. dev.	0.09	5.14	9.17	0.77	1.50
hardground						**spherulite**					
average	0.09	1.30	6.80	0.60	0.70	average	0.62	13.00	53.00	0.80	15.60
maximum	0.13	2.20	10.30	1.70	1.00	maximum	0.90	35.70	73.20	5.70	38.70
minimum	0.06	0.00	5.00	0.00	0.60	minimum	0.26	0.00	26.70	0.00	3.30
std. dev.	0.04	1.20	3.00	1.00	0.20	std. dev.	0.17	15.30	12.10	1.80	9.90

5.4.5 Relationships between Rock Types

The concentrations of the matrix forming gangue minerals in manganese ores demonstrate that Mn-cemented materials possess compressed fields, when compared with those which contain higher amounts of gangue minerals (Fig. 5.10a). Uncemented oolitic ores exhibit strong variations in their mineralogical composition for goethite, hematite, kaolinite, and excess silica content. Cemented oolites on the other hand do not vary much and consequently their field is fairly small. Uncemented pisolites, not shown for simplicity, are comparable to cemented oolites. The shape of the field is similar, but shows an additional dominance of kaolinite.

Strongly contrasting to the previous ores, the cemented pisolites split into two groups, each with a relatively small variability of one gangue component (either q or gt+he). The first (D-Quarry ore) shows nearly no ferruginous material in its matrix, it extends approximately from the upper end of the hardground, and it overlaps with the siliceous ores. The second group (ores from F1, F3, F4, C-138) has nearly no excess quartz, but minor to high amounts of goethite and hematite. Siliceous ores show large variations in the quartz and kaolinite content and relatively small contents of iron phases. The field for the hardgrounds essentially forms at the kaolinite-quartz boundary of the cemented oolite field. Massive mangcrete and concretions (above ore) develop a comparable pattern with small quantities of quartz and large variations between the clays and the ferruginous materials. The concretionary ores are not shown, because they are similar to cemented pisolites. Dendritic concretions that formed below the main orebody also plot in this area, with a dominance of goethite and hematite and little quartz. Radial pyrolusite (not plotted) which overprinted oolitic ores, shows a field at the base of the cemented oolites with a slight increase of the iron phases.

Rocks that appear to be dominated by iron minerals when examined in the field plot far away the Fe-corner of the triangle (Fig. 5.10b). This means that these rocks contain larger amounts of other gangue mineralssuch as clays and quartz, masked by the dark color of the oxidized iron. Spherulites show marked differences in their gangue mineral content, depending on the materials on which they formed. Those spherulites that developed directly on outcropping ores or on very thin laterites plot near the base of the diagram (G- and G-South-Quarry), and they show the influence of iron phases. The others that formed on extensive laterite profiles (F3- and D-Quarry) are dominated by clays and quartz. The kaolinitic clays themselves exhibit a wide range in quartz content. Separated from all the previous rocks are the ferruginous pisolites and the dense goethitic ores (within the pisolite field). Both ores can contain up to one third clays, but quartz is negligible. Laminar mangcretes from pipe walls plot relatively near to the laterites and shows relations tospherulites. Both rock types form near or at the surface and thus they are comparable to pipes that act as conduits for fast moving meteoric waters.

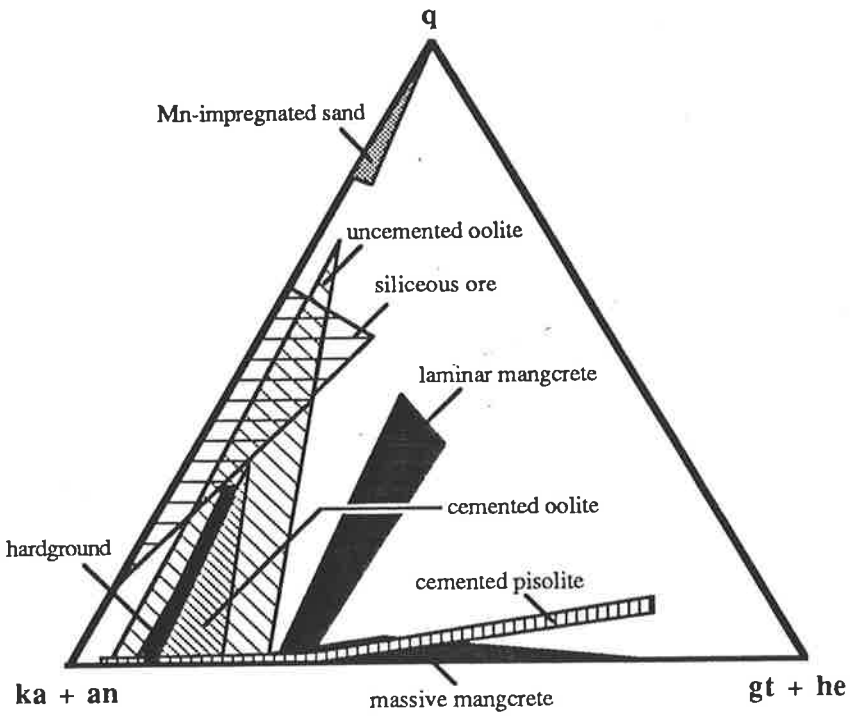


Fig. 5.10a: Ternary plot of matrix norm minerals for the main manganese ores.

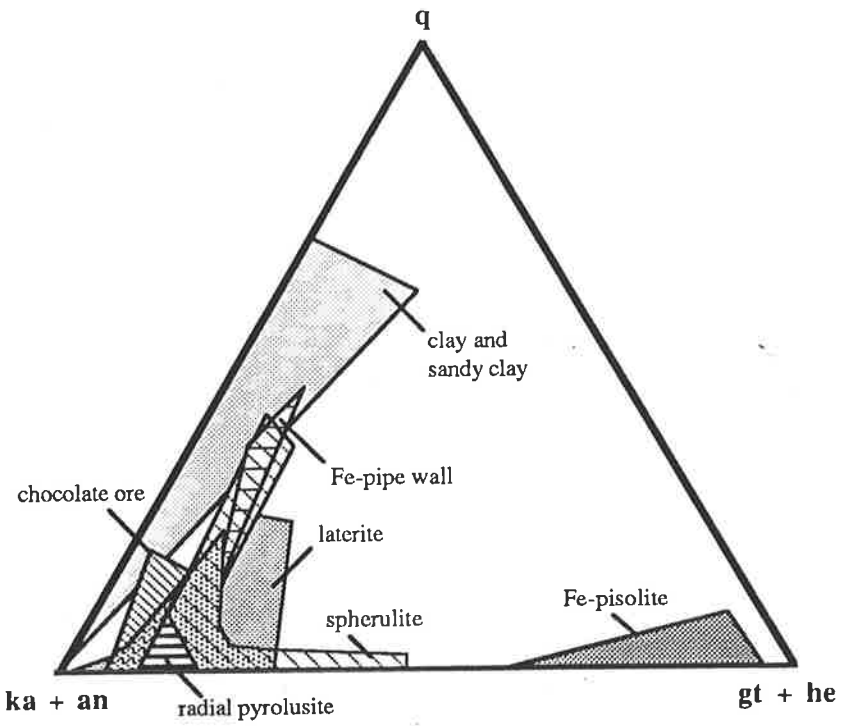


Fig. 5.10b: Ternary plot of normalized gangue minerals for the main gangue minerals and rocks.

5.4.6 Trace Element Composition of Gangue Minerals

The gangue minerals vary greatly in their ability to accommodate trace elements in their structure. Kaolinite seems to incorporate most elements that fit into regular radius intervals (~ 0.6, 0.8, and 1.0 Å; Table 5.6), regardless of the valency (2+, 3+, and 4+). This contrasts strongly with the finding that minerals such as pyrolusite obviously prefer specific valencies (3+). From the example of TiO_2 it is demonstrated that some of the trace and minor elements correlate extraordinarily well with kaolinite (Fig. 5.11a), Zr gives a comparable result. This indicates that both elements are probably incorporated directly into the lattice of kaolinite, although the Ti component of the analyses is presently calculated as a separate phase (anatase).

Table 5.6: Correlation of minor and trace elements and normative minerals.

Mineral	TEs	Radius [Å] (valency)
Kaolinite	As	0.58 (3+), 0.44 (5+)
	Cr	0.63 (3+), 0.52 (6+)
	(Gd)	0.97 (3+)
	Sc	0.81 (3+)
	Ti	0.80 (2+), 0.68 (4+)
	Zr	0.79 (4+)
	Th	1.02 (4+)
Gibbsite	Pb	1.20 (2+), 0.84 (4+)
Goethite	Gd	0.97 (3+)
	Ce	1.07 (3+), 0.94 (4+)
	P	0.40 (3+), 0.35 (5+)

Goethite concentrates fewer elements than kaolinite, leaving out the entire range of ionic sizes between ~ 0.4 and ~ 1 Å. This mineral accumulates most of the available Gd (Fig. 5.11b) and it also has a pronounced deficiency in Eu. The remaining minerals are of little or no importance. Gibbsite only seems to correlate positively to Pb, and hematite is not discussed here because it is relatively rare in the deposit (compare Fig. 5.9a) but also because it did not provide reliable correlations to any of the analyzed elements. However, the previous sections support the existence of a fractionated incorporation of the trace elements in the various minerals.

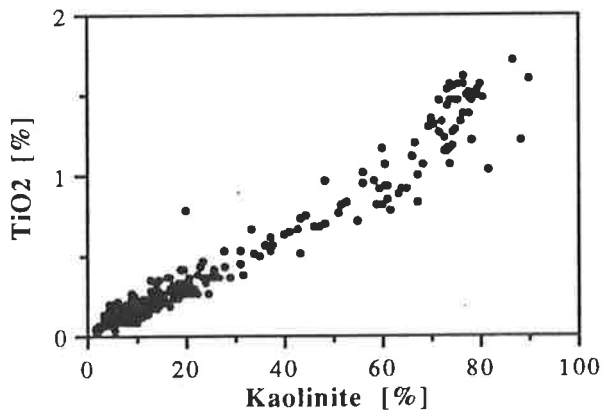


Fig. 5.11a: TiO_2 content of kaolinitic clays from ores and associated rocks (n = 364).

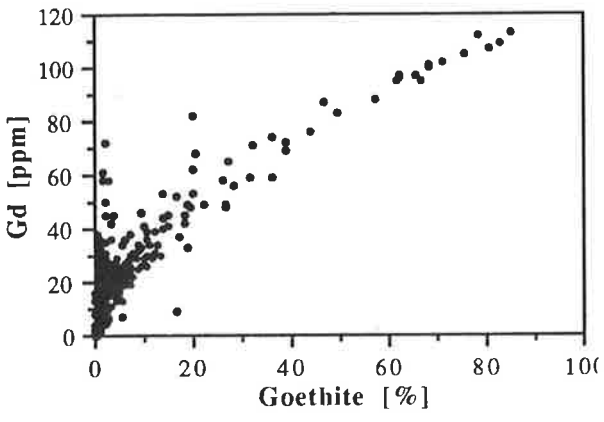


Fig. 5.11b: Correlation of Goethite and Gd in ore and rock samples (n = 364).

5.5 Normative Ore Minerals and Microbiological Leaching

Growing interest in the role of biological processes in manganese metallogenesis (Ostwald, 1981; Bolton et al., 1988) and biotechnological studies which tried to assess microbiological leaching techniques (Madgwick, 1987), led to a cooperative study which combines both fields of research. The following examination correlates norm data with results from laboratory based microbiological reduction/leaching tests.

The experiments, made by R. Varga and J. Madgwick (Dept. of Biotechnology, University of New South Wales), were conducted on cemented pisolites collected from F3-Quarry during the course of the present study, further data processing in context with norm calculations was done by the present author. Experimental setting and method are discussed in Appendix I.3.2, results from the leaching tests are compiled in Appendix V.2 (see also norm calculations in Appendix V.1).

Microbial reduction of manganese oxides can be an important mechanism for mobilizing Mn in a wide range of contemporary sediments, including anaerobic/aerobic terrestrial, freshwater and marine environments. This factor is therefore discussed together with other mobilization processes in chapter 8. It is likely that microorganisms have been active over geological time, despite the paucity of direct evidence preserved in the rock record, and it can be assumed that general conclusions drawn from laboratory studies will enhance the understanding of natural organic-inorganic systems, in both modern and ancient environments.

Throughout previous investigations, reliable methods of quantification for the various minerals were not available and thus the influence of the mineralogy on microbiological manganese reduction processes was unknown. However, the examination of norm data and experimental results illustrates that it is possible to correlate leached Mn^{2+}, pH and the calculated proportions of the manganese oxides (Figs. 5.12-13). The diagrams exhibit varying amounts of manganese in solution and associated pH-changes, both depending on the nature of the ores. Cryptomelane and todorokite give a positive correlation to the leachate (Figs. 5.12a-b), romanechite initially produces a positive trend which levels out and becomes horizontal (Fig. 5.12c), and pyrolusite correlates with a reverse curve (negative slope; Fig. 5.12d).

The theoretical background of the reduction processes is discussed in detail in chapter 8, it is however necessary to give a very brief introduction about the main factors that facilitate a microbiota-induced mobilization of Mn oxides. Thermodynamic considerations show that in a relatively simple system pyrolusite is the most stable phase within the examined group of manganese oxides (Bricker, 1965). Generally, minerals like cryptomelane are more vulnerable to changing environments, which means that any interaction of redox or other reductive processes with the ores results in a preferred selective removal of the less stable phases.

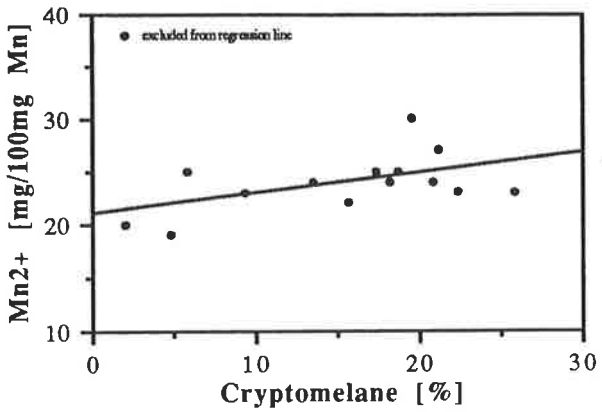


Fig. 5.12a: Levels of dissolved manganese that was reduced from ores with varying cryptomelane concentrations.

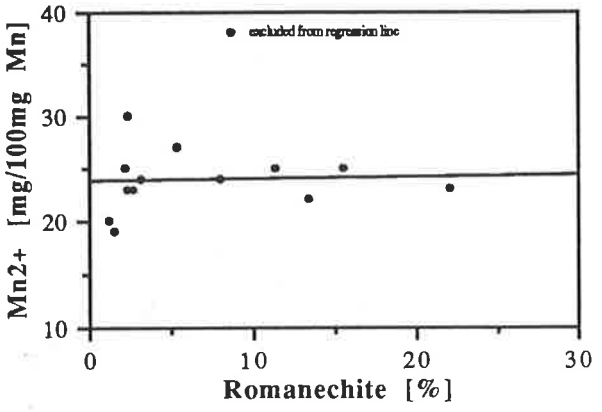


Fig. 5.12b: Levels of dissolved manganese that was reduced from ores with varying romanechite concentrations.

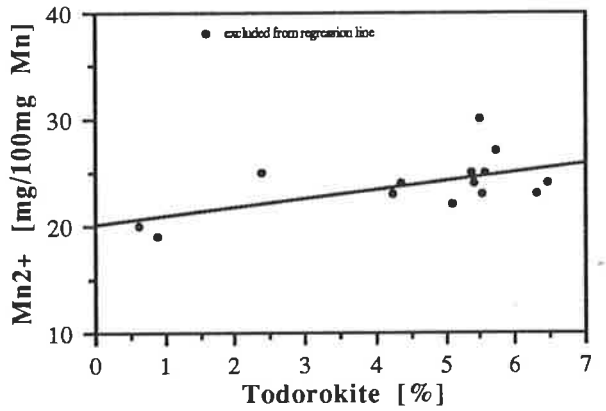


Fig. 5.12c: Levels of dissolved manganese that was reduced from ores with varying todorokite concentrations.

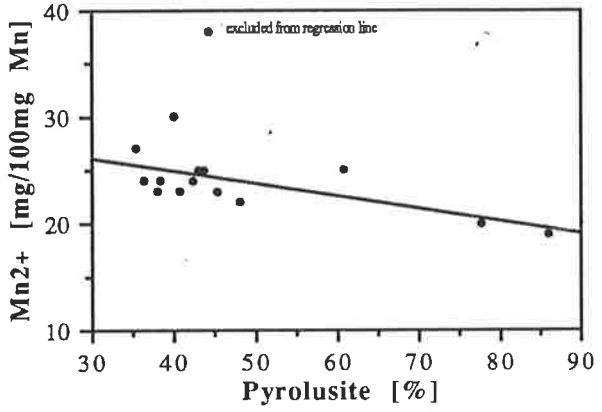


Fig. 5.12d: Levels of dissolved manganese that was reduced from ores with varying pyrolusite concentrations.

The dissolution/reduction of manganese oxides through biological mechanisms in both aqueous natural and industrial systems derives mainly from two independent processes (Madgwick, 1987):

- bacteria- or fungi-induced production of organic acids with high reducing capacities (e.g. oxalic acid),
- enzymic reduction through bacteria at the ore-water-interface.

Both types of processes operate with the help of acids, which provides a relatively easy way for monitoring the activity of microbiota through pH changes under controlled laboratory conditions.

The release of Mn^{2+} as a function of pH is plotted for two norm minerals, contained in the same samples, to demonstrate the development of prominent relationships in analyses derived from different time intervals (Fig. 5.13a). Most of the examined minerals form specific

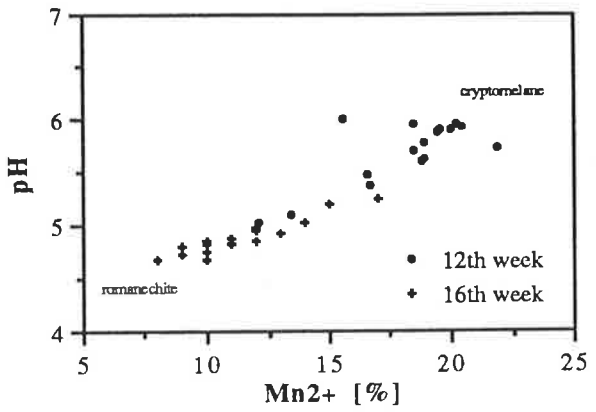


Fig. 5.13a: Breakdown of cryptomelane and romanechite monitored through pH-variations and Mn-concentrations at different time intervals.

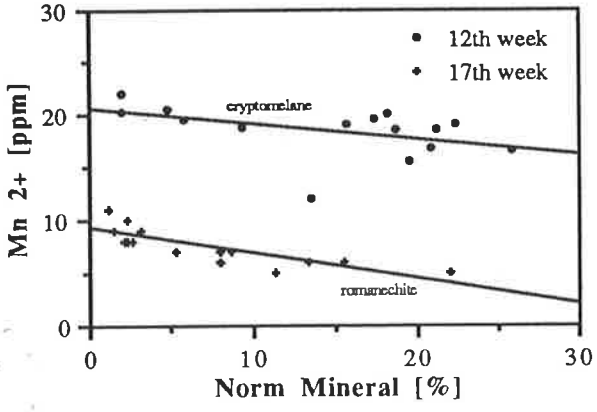


Fig. 5.13b: Negative correlation of norm oxides to reduced manganese at different time intervals.

correlation patterns only in one distinct data set, analyses outside this time interval normally scatter strongly. In the twelfth week of the test, cryptomelane (and also todorokite, which is not plotted, for simplicity) seem to be largely destroyed. Five weeks after the disappearance of cryptomelane and todorokite (sixteenth week), romanechite breaks down, and again, Mn^{2+} and pH correlate positively. The increase of manganese in the solution directly reflects the lower concentration of romanechite in the samples, and its pattern in the diagram extends from the low end of the cryptomelane pattern. That pyrolusite apparently was not removed from the samples may have resulted from the test series being too short (21 weeks), as pyrolusite is more resistant to this type of attack, and it may be inert under the conditions of the experiments. This and the preceding diagram show that the thermodynamically least stable minerals break down first, that time gaps occur before the next phase becomes unstable, and that minerals like pyrolusite resist the attack of organic acids far longer than any other of the examined manganese oxides. Therefore, the activity of microbiota leads to a selective destruction of manganese oxides, depending upon which minerals are present.

In the following diagram the calculated amounts of cryptomelane and romanechite are plotted against dissolved manganese (Fig. 5.13b). The time interval for cryptomelane is the same as in the previous diagram (week 12), whereas romanechite exhibits comparable patterns in two successive weeks (16th week, not plotted for simplicity, and the 17th week). This plot shows an unexpected feature for the two norm minerals, because the highest concentrations of Mn^{2+} in solution can be seen together with the lowest amounts of the respective minerals, thus indicating an increasing strength of the reducing capacity in low grade ores and sediments.

5.6 Normative Ore Minerals and Battery-activity Tests

The normalization technique is also applicable to data derived from battery-activity tests. Manganese oxides from some areas on Groote Eylandt are an important source for natural occurring battery grade ores. However, these materials often contain Mn-minerals which have poorly defined structures and which are problematic for an examination by XRD, DTA, or FTIR, especially when they appear in a complex sample. The normalization method may thus provide a simple predictive tool for the assessment of the battery-activity of ores, particularly because activity tests must be determined experimentally. In cases in which the norm is calculated for other purposes, the predicted battery-activity can be obtained as a by-product.

Unfortunately, the chemical analyses of Mn oxide ores from Groote Eylandt discussed by Swinkels and Williams (1982) together with activity test results are incomplete. Thus, the norm of these samples had to be interpolated for some data (e.g. LOI), while others were neglected. Nevertheless, the correlation diagrams (Figs. 5.14a-d) show positive trends for 2 of the 4

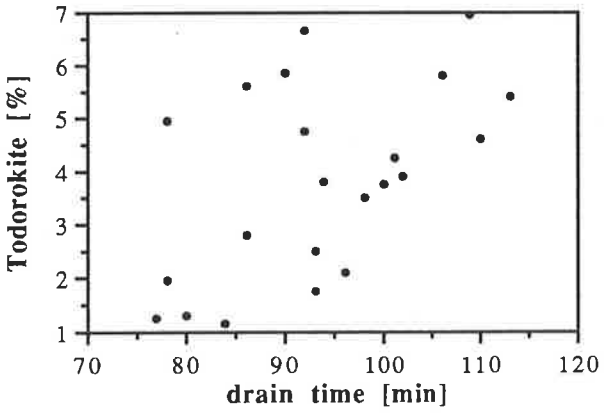


Fig. 5.14a: Drain time of battery-activity test cell versus todorokite concentration in Mn ores; after Swinkels and Williams (1982).

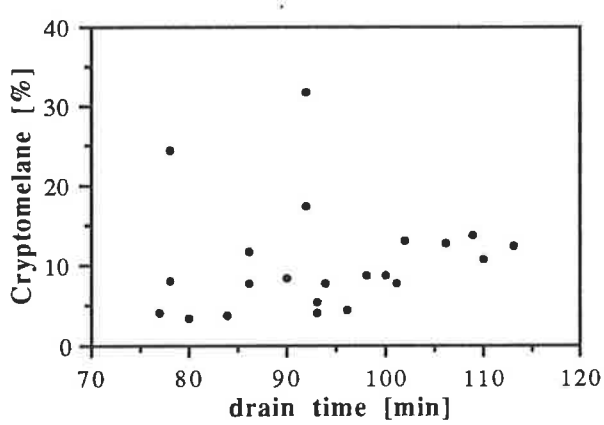


Fig. 5.14b: Drain time of battery-activity test cell versus cryptomelane concentration in Mn-ores.

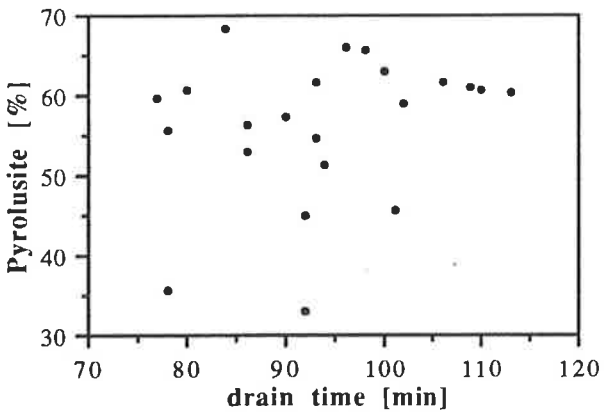


Fig. 5.14c: Drain time of battery-activity test cell versus pyrolusite concentration in Mn-ores.

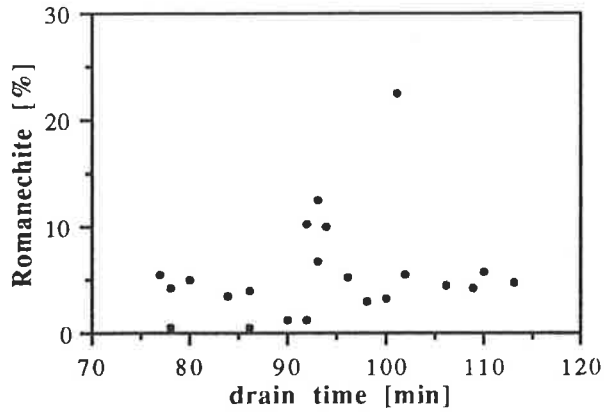


Fig. 5.14d: Drain time of battery-activity test cell versus romanechite concentration in Mn-ores.

oxides, despite the crudely reconstructed norm. Below, one of the test parameters (drain time) is plotted against the normative manganese mineral composition of the samples. The drain time represents the time interval that elapses from the initial discharge potential to a specified voltage and it is a measure for the battery-activity of the ore. Other test data, such as the charge capacity, provide similar results and are therefore not shown.

Todorokite and cryptomelane correlate positively with the drain time (Figs. 5.14a-b), whereas pyrolusite seems to show a slight negative correlation (Fig. 5.14c). The latter mineral therefore dilutes the battery-active minerals and reduces the output voltage. Romanechite does not produce any recognizable trend and probably does not take part in discharge reaction (Fig. 5.14d).

5.7 Discussion

The development of a number of normative manganese phases and associated gangue minerals has been discussed for the example of supergene Mn oxides from Groote Eylandt. The method was applied with success to over 400, partially very complex ore and rock samples (~20 different types), and the results of this normalization procedure have been encouraging. However, only further work on materials from other deposits can test the wider applicability of the technique.

The application of the normative mineralogy on vertical geological profiles demonstrates that the technique is able to detect compositional variations within ores and gangues. When the results from the different sections are compared with each other, it is seen that some of the observations can be gneralized and that genetic information on supergene ores and gangues can be derived.

The pyrolusite concentrations often increase downwards, both in the ore and laterites, whereas cryptomelane, romanechite, and todorokite have their highest concentrations near the top of the ore, usually within the first 4 m. In deeper parts of the orebody, where groundwaters are probably present over much of the year, these minerals decrease to insignificant levels. All manganese oxides exhibit enrichments shortly above hematitic layers, thus emphasizing the fact that hematite represents horizons of increased oxidation. Additionally, cryptomelane often appears enriched slightly below kaolinite horizons. The free water of the samples generally correlates positively with cryptomelane and todorokite, but in neither case can it be associated with a specific phase.

Kaolinite decreases with depth in the ores, but shows no definite trend in the laterites. However, it is found together with goethite in laterites and also in the matrix of manganese ores.

Goethite appears in various parts of the deposit, on top, within, and below the ores, and it does not show any clear preference for any specific position. Phosphorus enrichments are often related to goethite, sometimes to hematite, and in one case a strong P-peak coincides with a pyrolusite peak (G-South). Quartz increases down the section, whereas gibbsite normally decreases with depth. Sometimes, gibbsite initially increases downwards but decreases at greater depth.

This short resume of the mineral distribution in the vertical sequence shows that strong relations exist between ore and gangue minerals, and which also reflect the formation conditions for the various supergene phases (e.g. horizons of increased oxidation). The processes that lead to the development of these minerals are not discussed here, but in context with the examination and evaluation of supergene mobilization and precipitation processes in chapter 8.

Further indications for a geochemical control on the development of the manganese oxides and the associated rocks are found in the mineralogical composition of the samples. Although pyrolusite seems to predominate in the ores, a detailed analysis of the ore types reveals that pyrolusite, cryptomelane, romanechite, and also todorokite are strongly dependent on the respective gangue mineral paragenesis. The best examples to support this finding are siliceous and massive ores, Mn-impregnated sands and kaolinitic clays with manganese oxide stains. It is also demonstrated that ores such as hardgrounds and radial pyrolusite possess a mineralogy that is common with the ores from which they were derived. The latter case again reflects the mineral composition of the "host rock".

But first, silica-rich ores shall be examined. In siliceous ore, which occasionally contain quartz grains as nuclei of ooliths/pisoliths or in the matrix, pyrolusite plays a relatively strong role in samples of low quartz content. The higher the quartz concentration becomes, the lower are the pyrolusite values. In contrast, cryptomelane and todorokite gain importance with increasing amounts of quartz. This is also seen in massive mangcretes, which still contain evidence for replacement of gangue minerals (relic quartz grains, vermiform kaolinite) and in Mn-stained clays. The most extreme example is manganiferous sand, which contains nearly no pyrolusite but almost exclusively cryptomelane and todorokite. Concretions that developed near the top of the orebody, and also below the main orebody, show a similar pattern with enhanced concentrations of the latter two minerals. These ore types are always associated with clays and sands. Considering the facts presented above, the conclusion can be drawn that increased availability of kaolinitic clays and quartz sands during ore formation leads to increased development of cryptomelane and todorokite.

As with the above materials, the mineralogy of spherulites from different locations seems to be dependent on the rocks and ores on which they develop. Spherulites that formed directly above oolitic ores have compositions very similar to ores from which the manganese originated. Pyrolusite and to a lesser degree romanechite dominate here, cryptomelane and todorokite do

not play an important role (G-Quarry). Cryptomelane and todorokite gain importance in spherulites that formed on extensive laterite profiles (F3-Quarry; compare siliceous ores).

A very interesting difference between cemented and uncemented materials can be detected in the mineralogy of these ores. Generally, cemented pisolites are more enriched in cryptomelane and todorokite, when compared with uncemented pisolites, which are strongly dominated by pyrolusite. However, the reverse is observed in oolitic and pisolitic ores from the G/G-South area. Here, cemented oolites contain more pyrolusite than the uncemented oolites. This means that the development of the two ore types is distinctly different, which is also reflected in the composition of the trace elements.

In the ternary plot of the ore components, the hardground samples fall at the boundary of cemented and uncemented oolites (Fig. 5.7a). It has already been shown in the petrology chapter that many hardgrounds obviously replaced oolitic ores. Therefore, the normative mineralogy strongly supports the previous findings. Also, the geochemical environment must have been very similar to that which altered the oolitic ores; otherwise the composition of the hardgrounds could be expected to be different. A comparable material is the radial pyrolusite which occurs near the top of the oolitic ores in G-South Quarry. This ore also overprinted oolitic products (see petrology) and it plots at the base of the ternary diagram near the lower end of the hardgrounds at the pyrolusite corner. Again, close relations to the replaced protore are visible.

Close similarities are exhibited by laminar mangcretes from pipe walls and ferruginous coatings of the same pipes. Both ore/rock types compare mineralogically with goethite- and hematite-rich rocks (laterites, chocolate ores), and with an increasing hematite content the romanechite concentration seems to increase. Ores and rocks with goethite dominance possess lower romanechite values. The gangue minerals of associated rocks and gangues which form the matrix of ores, generally exhibit similarities in those cases in which the genesis of the materials is comparable, and they are therefore not discussed further.

The normalization technique is also very useful for the determination of trace element concentrations in the various minerals. Many of these elements are concentrated by manganese oxides, with the exception of romanechite, which seems to exclude "impurities" from its structure. Ba, with its large ionic radius (1.34 Å), cannot easily be replaced by the available trace elements, and therefore the other oxides are probably the preferred host minerals. Cryptomelane and todorokite both seem to take up trace elements with a relatively small range of ionic radii (~ 0.7 Å for di- and trivalent ions: Co, Cu, Ni, (U), V, Zn). Pyrolusite is also very specific in its trace element enrichment. It incorporates some relatively light elements with radii of approximately 0.4 Å (B, P) for the trivalent ions, and from ion sizes larger than 1Å, additional trivalent elements, such as Eu, La, Nd, and Sm, are accommodated in its structure. Significantly, the two elements of the analyzed group of rare earth elements (Gd and Yb) with radii of slightly less than 1Å are

not incorporated. Ce, which gives a weak positive correlation to pyrolusite, is probably more mobile than most of the other REE members. Due to its chemical nature, this element occurs in both tri- and tetravalent states according to the present geochemical conditions. Thus, it can be assumed that minerals incorporating Ce reflect the environment in which they formed.

Kaolinite and goethite, which appear as gangue minerals in almost any ore type of the deposit, occasionally show trace element concentrations above the average, and thus a control of kaolinite and goethite over a number of elements could be expected. Theoretically, this could lead to a situation where trace element patterns of gangue minerals are superimposed upon ore minerals. However, the normative mineralogy of the analyzed samples reveals that relatively few elements are specifically incorporated into these two minerals. As, Cr, Sc, Ti, Zr, and Th are associated with kaolinite (preferred radius intervals: 0.6, 0.8, (and 1.0) Å), and only P can be attributed to goethite (~ 0.40 Å). Gd, which does not fit into the pyrolusite structure, is predominantly enriched in goethite. All other minerals play a subordinate role in accumulating trace elements, although most of the ore and gangue minerals contain small amounts of many of the trace elements. However, the mineralogy of the samples generally favours a strongly fractionated incorporation of the trace elements into the various Mn and Fe minerals (Goldberg, 1965).

Another possibility to use the norm is its application on an experimental leaching of manganese oxides by microorganisms. This leads in a slightly different direction, but it provides some answers for natural and technical manganese-reducing processes. Until now, it had been very difficult or even impossible to examine mineralogical controls over microbial reduction processes, because of problems in the quantification of the Mn oxides. However, the diagrams above clearly demonstrate differences in the mobilization of these minerals. It has been shown that the thermodynamically least stable mineral breaks down first, that time gaps occur before the next phase is broken down, and that minerals like pyrolusite resist the attack of organic acids far longer than any other of the examined manganese oxides. Therefore, it can be concluded that the activity of microbiota leads to a selective destruction of manganese minerals, depending upon which Mn minerals are present.

The highest concentrations of Mn^{2+} in solution have been detected together with the lowest amounts of the respective minerals, which means that the strongest decrease of the pH and therefore the highest reduction rate is achieved, when the microbiota (which are kept constant in their concentration) can interact with relatively small amounts of the specific ore mineral. The effectiveness of this reduction process therefore seems to depend directly on the ratio of organism- and mineral-concentration. The decreasing ability to reduce the available oxide minerals probably relates to a "dilution effect" on the constant production of organic acids, through the increase of the reactive minerals. If this finding can be transposed onto natural conditions where microorganisms occur in much smaller quantities, then the most likely place for a highly effective activity of manganese reducing bacteria, algae and fungi is to be found in rocks and soils

(highest organism concentration) with relatively low Mn-levels. Preliminary results of work presently underway also suggest that the type and concentration of organisms play a significant role in the mineral breakdown. This finding is in accordance with the above interpretations and it reflects the fact that different organisms produce different types of organic acids which vary in their reducing capacities.

Oxidic ores dominated by pyrolusite are less prone to microbiological leaching than those with lower pyrolusite contents. This means that technological leaching methods are less effective when they interact with ores of high pyrolusite content. This is also true for Mn-rich ores, because of the mentioned dilution effect. On the other hand, ores with relatively unstable oxides dissolve more easily under the attack of microorganisms. Therefore, rocks with lower manganese concentrations or waste materials from mining operations are the most likely targets for the application of leaching techniques.

With the help of the normalization method a small batch of samples was examined to determine whether it is possible to predict the battery-activity of natural ore samples. At present, a common lack of battery-activity data in conjunction with chemical analyses to be used for the normalization, prevents a detailed study. Therefore, it is too early to make assumptions on the overall capability of this technique to fully quantitate the battery-activity of samples. However, the diagrams suggest a reasonably good correspondence to analytical results which correlate todorokite-rich ores to higher battery-activities in Groote Eylandt ores (e.g. Dubrawski, 1985). If the available results can be substantiated by more experimental data, then the mineral norm may provide an easy tool for a general assessment of the battery-activity of the ores.

The few examples discussed above demonstrate the practical use of the method, but it must be emphasized again that a mineral norm should only be an aid in cases where other methods of quantification have failed, are very difficult to obtain or are too expensive. Such a theoretical technique must also go hand in hand with studies of the relevant deposits and should come as close as possible to the natural conditions of the rocks/ores, otherwise the results are superficial and of no use.

6. Hydrochemistry

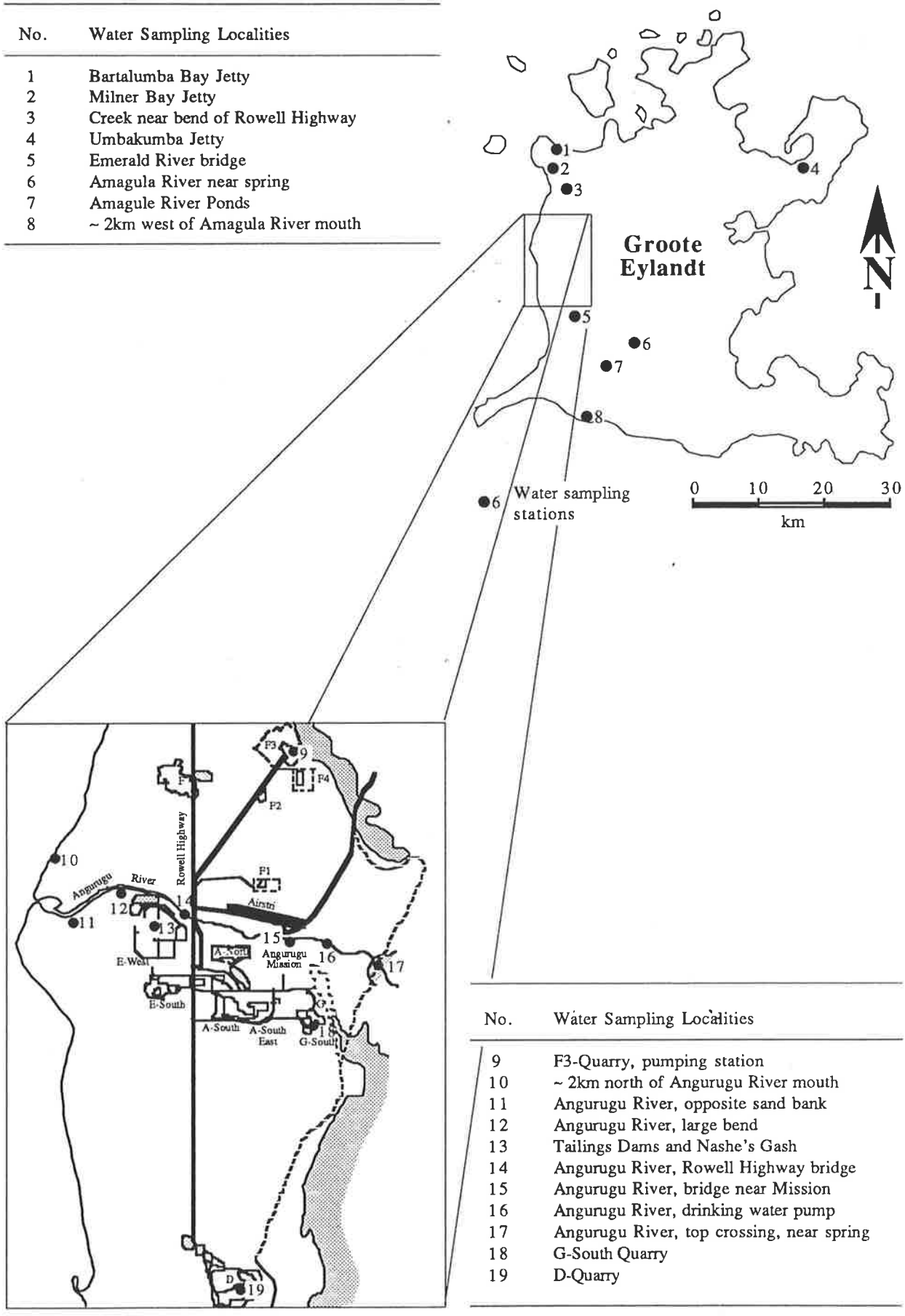
6.1 Introduction

As is demonstrated later, water is *the* essential medium for the formation of supergene manganese ores. Analyses of the various water types found in and near the deposits should therefore provide some help in understanding the nature of the ore body, its rocks and its interaction with local waters. Included in the study are also some seawaters that were collected near the shore from different localities around Groote Eylandt. The study of higher alkaline waters was undertaken to assess the importance of pH, chlorine, and electrolyte changes on dissolution and precipitation of manganese oxides. The first part of this chapter generally outlines information about environmental effects on the stability of dissolved elements. Successively, various water types are discussed to show their characteristics in context with the respective environment.

The samples were analyzed in the field for temperature, pH, oxygen content, total manganese and total iron. Untreated samples were taken for chlorine analysis ($AgNO_3$-titration), filtered, and acidified samples were later examined by Inductive Coupled Plasma Spectroscopy (ICP) for a range of 34 elements. By means of an organic carbon analyzer, total organic carbon (TOC) was determined. The flux rate of small springs and seepages was measured where possible.

The sampling stations are shown below in Fig. 6.1. Sampling methods, analytical techniques and background information are described in Appendix I.2; analytical results and rainfall data are listed in Appendix VI., Tables VI.1 - 4. Average values for individual water types are provided in the respective text sections (Tables 6.1-3). Though statistical methods were applied to the analyses, they were unsuccessful, because of multiple regressions for a number of elements (see correlation matrix in Appendix VI.5). Therefore, the interpretation of the data relied on visual evaluations of correlation diagrams.

No.	Water Sampling Localities
1	Bartalumba Bay Jetty
2	Milner Bay Jetty
3	Creek near bend of Rowell Highway
4	Umbakumba Jetty
5	Emerald River bridge
6	Amagula River near spring
7	Amagule River Ponds
8	~ 2km west of Amagula River mouth



No.	Water Sampling Localities
9	F3-Quarry, pumping station
10	~ 2km north of Angurugu River mouth
11	Angurugu River, opposite sand bank
12	Angurugu River, large bend
13	Tailings Dams and Nashe's Gash
14	Angurugu River, Rowell Highway bridge
15	Angurugu River, bridge near Mission
16	Angurugu River, drinking water pump
17	Angurugu River, top crossing, near spring
18	G-South Quarry
19	D-Quarry

Fig. 6.1: Water sampling stations on Groote Eylandt; the enlarged segment shows the mining area; numbers of individual localities correspond to tabulated locations.

6.2 General Environmental Influences on Dissolved Ionic Species

6.2.1 Rainfall, Tides, Chlorine and pH

To be able to estimate the influence of the water input, rainfall data and all analyses were correlated. A plot of the rainfall between 1980 and 1987, measured at the meteorological station, Angurugu Mission, and the mean rainfall for 1921 to 1985 shows a distinct separation of dry and rainy season (Fig. 6.2). The highest water input occurs between December and March, while the time between June to September is the driest period.

Correlation with the dissolved ionic species (inclusive of particulates, which are partly analyzed by additional field tests (see Fe^* and Mn^*)) demonstrates that most of the elements decrease in abundance with a higher water input. This is due to a simple dilution effect. Nevertheless, there is no straightforward trend, because the samples exhibit very diffuse patterns. An exception to this behavior can be found with P, Ba, and Ga, which seem to increase together with the availability of more water.

Higher phosphorus contents may be related to increasing biological activity in the rainy season (December-March); barium and gallium are probably flushed out and collected from areas that normally are out of the reach of groundwaters. Because there is no other information available on groundwater chemistry, the subject is not considered any further.

Since the deposits are situated near the western coast and the island is fairly flat, tides can easily force seawater upstream into rivers and creeks for several kilometers. This estuarine water may interact with local groundwaters and thus have an effect on dissolution and precipitation processes. Indications for alkaline groundwaters were found in Nashe's Gash near the tailing dams, where water is being pumped for industrial purposes (J. Alcott, pers. commun., 1985). Water samples taken from rivers suspected of having tidal influence should therefore be tested for their chlorine content, because this allows an easy assessment of the water type.

The following plot shows minimum and maximum tide levels for the Milner Bay Jetty on Groote Eylandt, together with a water level curve taken approximately 2 km upstream from the mouth of the Angurugu River during water tests (Fig. 6.3; after data from the Horace Lamb Institute of Oceanography). Although these samples are discussed later (6.3.2), the diagram already demonstrates strong vertical fluctuations of the river level several kilometers inland.

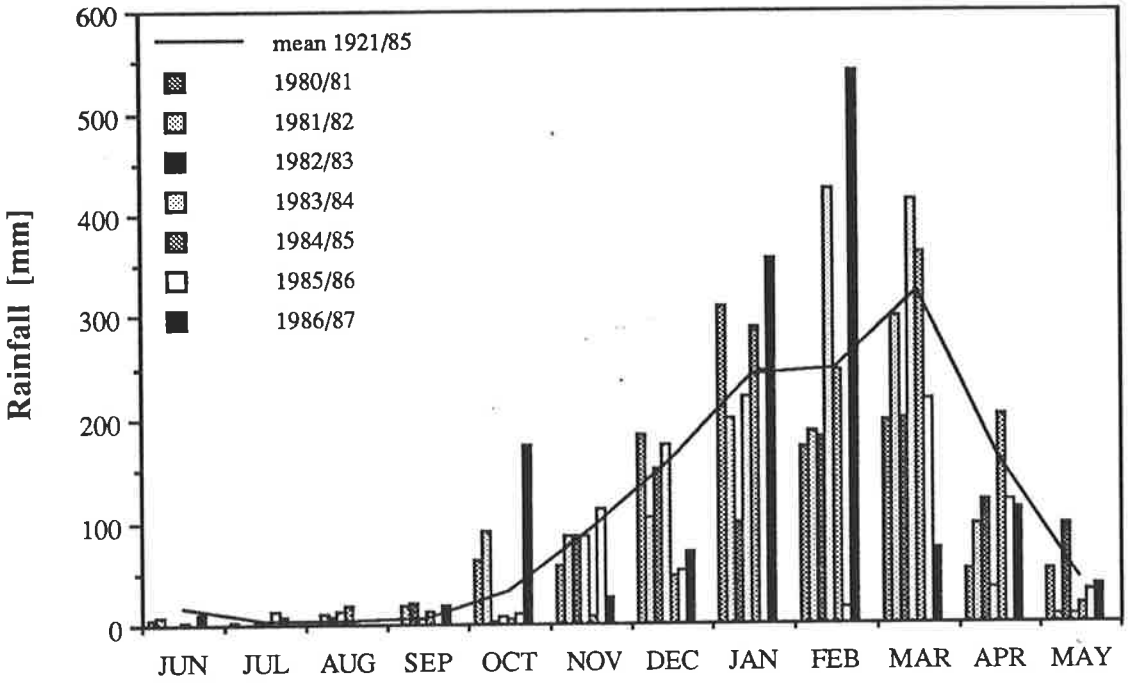


Fig. 6.2: Rainfall on Groote Eylandt for the time between 1980 and 1987, measured at Angurugu Mission. The line indicates the mean values for the time interval 1921/1985.

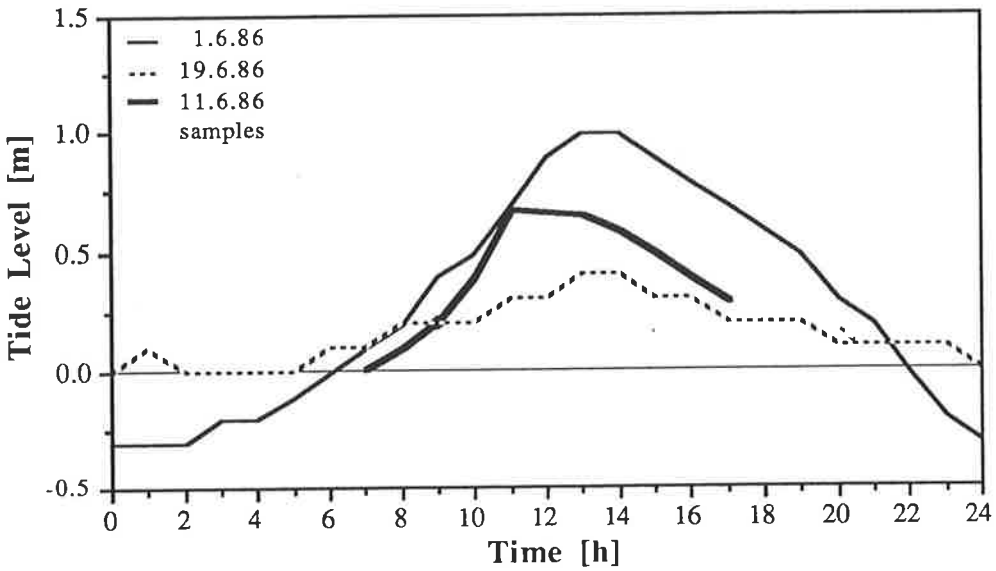


Fig. 6.3: Tide levels for Milner Bay, Groote Eylandt, and the tide dependent level of the Angurugu River near its mouth (~ 2km upstream).

When the effect of chlorine on the water system is analyzed, it can be seen that many elements that appear in "fresh water" samples, are in fact imported from the sea (e.g. Ca, K, Na, Mg, Sr). These elements correlate almost perfectly with Cl (e.g. Ca in Fig. 6.4). An excellent correlation coefficient can be produced for Cl and pH, incorporating two groups of samples (Fig. 6.5). The first part represents fresh waters with very little or no relation between chlorine and pH; only for pH values > 6 is the regression almost linear. Similar developments are found in a number of analyses and this demonstrates that an examination of the statistics of a large sample set, which includes various types, must be accompanied by a visual confirmation.

Finally, the statistics fail in the example of cerium and chlorine which exhibit a negative trend in the regression curve, but they possess a positive correlation coefficient and a positive regression line (Fig. 6.6). At or near the detection limit a large cluster of coinciding values almost certainly produces the statistically erroneous values. Nevertheless, the behaviour of Ce is very interesting, because it reveals that although the highest concentrations of this Rare Earth Element (REE) were recorded from seawater, it was most probably imported by fresh waters.The REEs are discussed in detail in section 6.3.3.

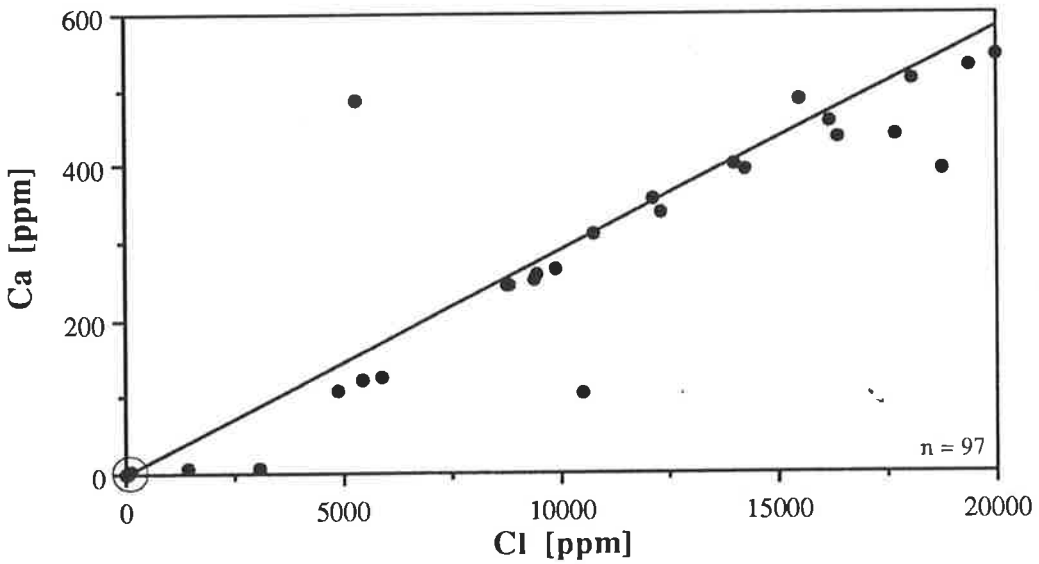


Fig. 6.4: Regression pattern of 97 water samples for chlorine and calcium, with a large cluster of analyses at the detection limit for both elements (indicated by circle).

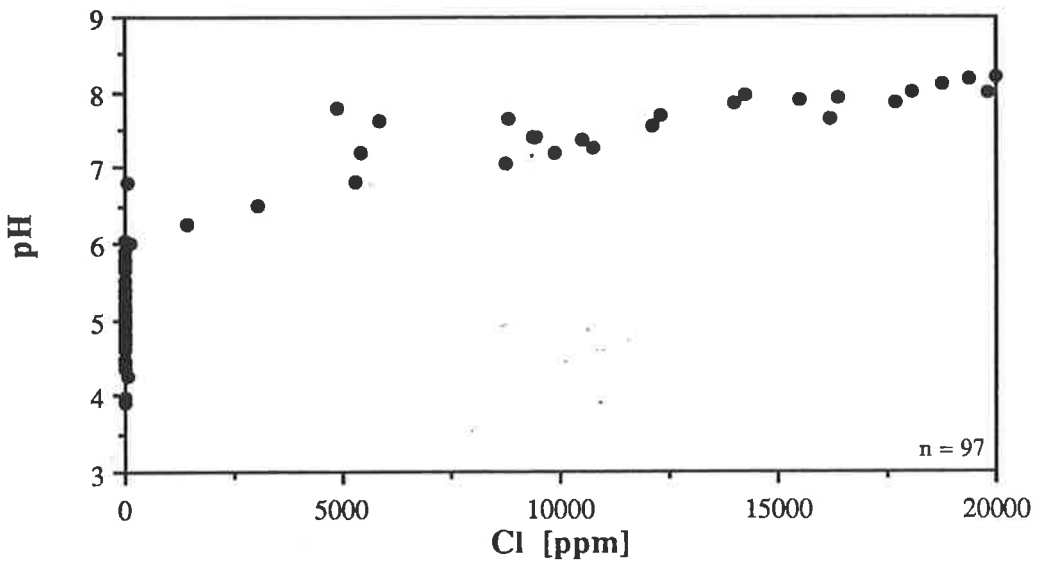


Fig. 6.5: Regression pattern of 97 water samples for chlorine and pH, exhibiting a chlorine independent pH (<6) and a linear dependent pH for values >6.

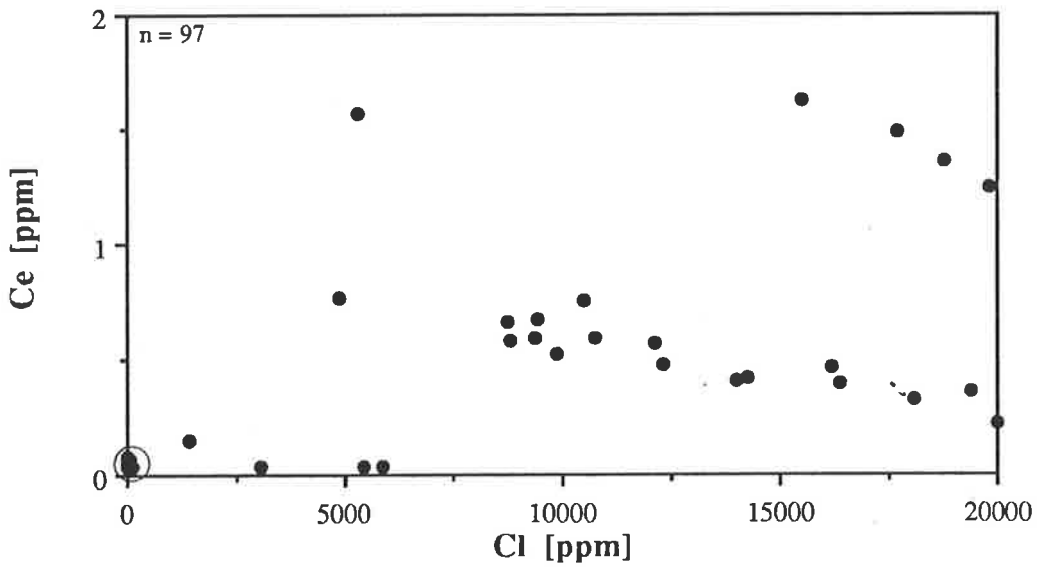


Fig. 6.6: Regression pattern of 97 water samples for chlorine and cerium, showing clustering near the detection limits of both elements (circle) and a negative correlation for the remaining samples.

6.2.2 Temperature, Oxygen Saturation

The correlation of all elements to the temperature of the water samples does not provide many recognizable patterns, but as the oxygen saturation partly depends on the temperature (also on mixing conditions), there is an indirect effect on the concentration of some elements. The best positive correlation is shown by silver (Fig. 6.7). It is difficult to determine in the present study in which form the Ag species are present, but their correlation to the oxygen content could be an indication for the presence of oxo-complexes. Similar trends, but not as well developed as for silver, are exhibited by Cr, Zn and Zr. Negative correlations are obtained from boron (Fig. 6.8), lithium and strontium. All other patterns are diffuse and difficult to interpret.

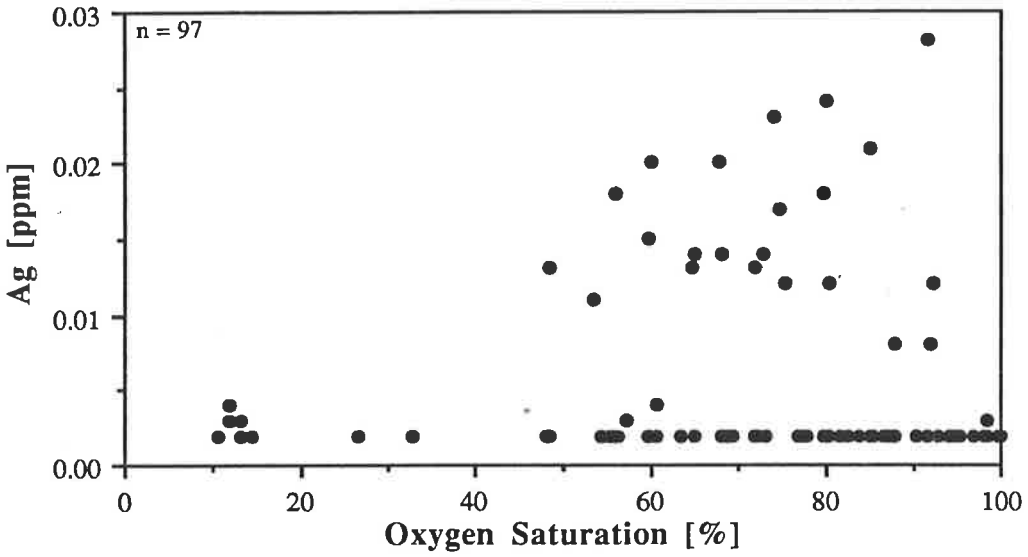


Fig. 6.7: Regression pattern of 97 water samples for oxygen saturation and silver, with positive correlation for some samples.

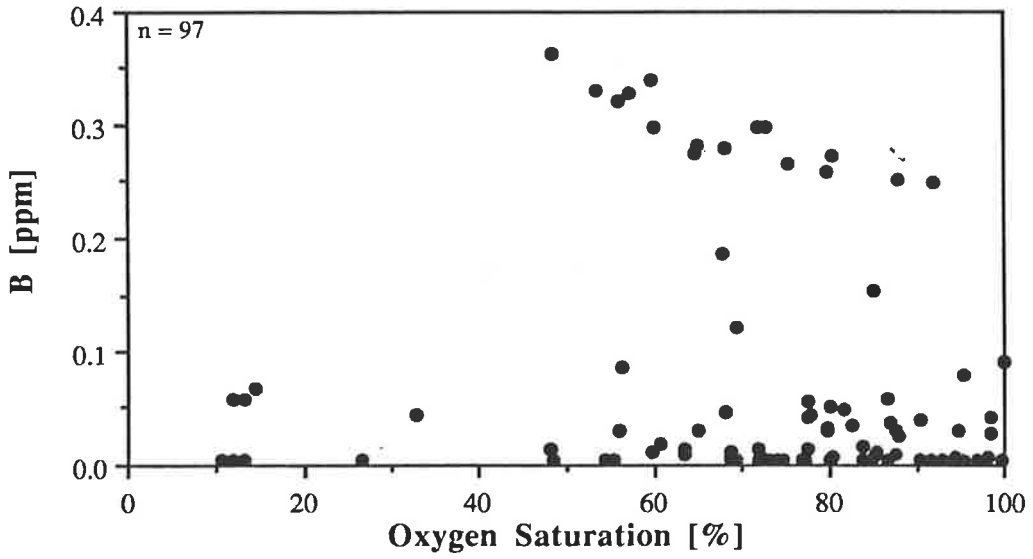


Fig. 6.8: Regression pattern of 97 water samples for oxygen saturation and boron, with negative correlation for some samples.

6.2.3 Organic Compounds, Phosphorus

Organic carbon does not relate well to most of the analyzed elements, but there are a few positive and even fewer negative associations. The best correlation is given by Ce with a positive regression for some samples (Fig. 6.9). This might be an indication for an adsorption or bondage of cerium to organic macromolecules. B, Ba, Ca, K, Li, Na and Sm belong to the same group with positive correlation and some of these elements may also be fixed to organic compounds. Ag, Be and Gd show a reverse development when compared with the carbon content. Phosphorus exhibits only some very weak positive correlations and it is not plotted.

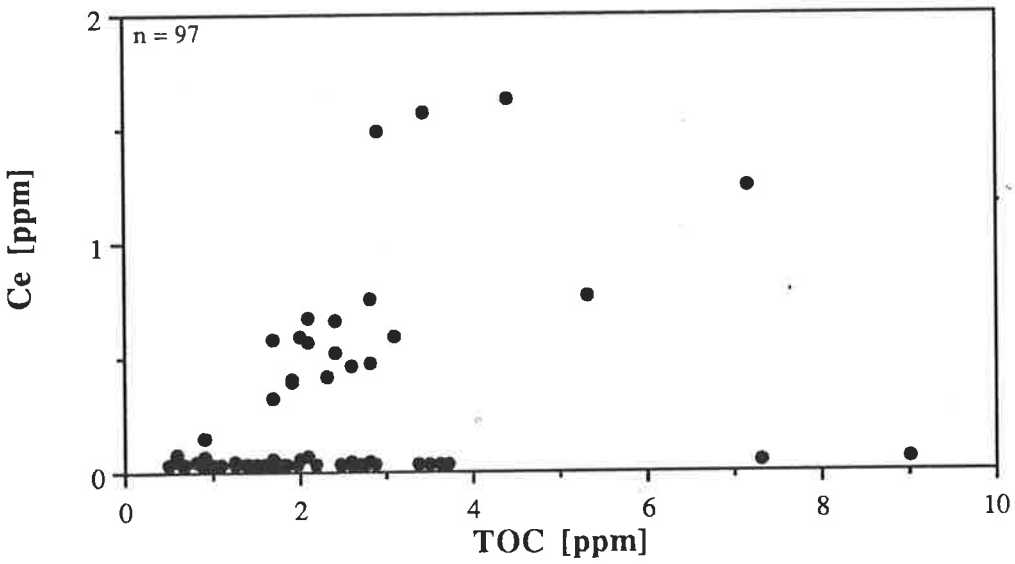


Fig. 6.9: Regression pattern of 97 water samples for cerium and total organic carbon (TOC), with the development of a positive trend for some samples.

6.3 Characterization of Water Types

6.3.1 Mine Water

Waters sampled from the mine site, came from various host materials such as laterites and ores and therefore it was difficult to obtain reasonably good information. Nevertheless, some diffuse trends could be recognized which might help in further interpretations (see also average values in Table 6.1). Generally, elements like K, Mg, and Na which would normally be typical for a marine environment are associated positively with the very low chlorine content (~10 - 40 ppm). This could be an indication of preferred dissolution of specific minerals in the deposit. Silica can be found increasingly together with ΔFe (total Fe minus dissolved Fe), which may be due to a bondage of iron to silica polymers. The most interesting information for this study comes from ΔMn (total Mn minus dissolved Mn) and organic carbon. This sample set yielded the best

correlation observed.There is a negative regression for the two parameters, which means that at least the additional particulate manganese transported together with the dissolved manganese in the mine waters, is not complexed by organic compounds. For the groundwaters of the mining area, the existence of various manganese species in solution can therefore be reduced to inorganic complexes and/or ionic forms (mainly Mn^{2+}).

Table 6.1: Statistics of water analyses from the deposit; n = sample no., average to std.dev. = ppm.

laterite	Ag	Al	B	Ba	Be	org. C	Ca	Cd	Ce
n	10	10	10	10	10	9	10	10	10
average	0.002	0.136	0.025	0.015	0.000	3.112	0.074	0.005	0.050
minimum	0.002	0.017	0.004	0.000	0.000	0.600	0.003	0.001	0.030
maximum	0.004	0.276	0.067	0.028	0.002	9.000	0.254	0.017	0.082
std. dev.	0.001	0.103	0.026	0.009	0.001	3.052	0.074	0.005	0.019
	Cl	Co	Cr	Cu	Eu	Fe	Ga	Gd	K
n	8	10	10	10	10	10	10	10	10
average	13.688	0.004	0.006	0.002	0.001	0.011	0.076	0.027	0.143
minimum	9.200	0.003	0.002	0.002	0.001	0.001	0.060	0.010	0.080
maximum	15.000	0.012	0.028	0.002	0.003	0.078	0.122	0.060	0.473
std. dev.	2.222	0.003	0.008	0.000	0.001	0.025	0.026	0.021	0.122
	La	Li	Mg	Mn	Mo	Na	Nb	Ni	O-sat
n	10	10	10	10	10	10	10	10	10
average	0.007	0.017	0.540	0.045	0.100	8.846	0.399	0.017	32.688
minimum	0.003	0.017	0.413	0.007	0.030	7.261	0.110	0.004	10.470
maximum	0.013	0.017	0.790	0.089	0.227	14.319	0.874	0.033	79.700
std. dev.	0.004	0.000	0.125	0.026	0.082	2.152	0.296	0.011	27.356
	P	Pb	Si	Sm	Sr	Ti	V	Yb	Zn
n	10	10	10	10	10	10	10	10	10
average	0.274	0.054	3.895	0.028	0.005	0.007	0.007	0.002	0.026
minimum	0.040	0.030	3.396	0.020	0.000	0.004	0.003	0.001	0.001
maximum	1.767	0.250	5.064	0.050	0.008	0.013	0.027	0.004	0.056
std. dev.	0.549	0.069	0.547	0.013	0.003	0.004	0.008	0.001	0.016
	Zr	°C	pH	O2	Fe*	Mn*			
n	10	10	9	10	10	9			
average	0.005	29.560	4.493	2.460	0.010	0.142			
minimum	0.003	29.000	4.350	0.800	0.000	0.000			
maximum	0.009	31.000	4.620	6.000	0.040	0.600			
std. dev.	0.002	0.800	0.109	2.043	0.012	0.182			

Table 6.1 (continued): Statistics of water analyses from the deposit.

ore	Ag	Al	B	Ba	Be	org. C	Ca	Cd	Ce
n	18	18	18	18	18	9	18	18	18
average	0.002	0.083	0.014	0.005	0.000	1.531	0.353	0.001	0.031
minimum	0.002	0.017	0.004	0.000	0.000	0.890	0.003	0.001	0.030
maximum	0.002	0.251	0.046	0.018	0.003	2.810	1.251	0.004	0.047
std. dev.	0.000	0.083	0.014	0.005	0.001	0.769	0.438	0.001	0.004
	Cl	Co	Cr	Cu	Eu	Fe	Ga	Gd	K
n	16	18	18	18	18	18	18	18	18
average	14.488	0.003	0.004	0.002	0.001	0.002	0.060	0.011	0.407
minimum	7.800	0.003	0.001	0.002	0.001	0.001	0.060	0.010	0.080
maximum	30.000	0.003	0.019	0.002	0.001	0.009	0.060	0.022	1.390
std. dev.	5.883	0.000	0.005	0.000	0.000	0.002	0.000	0.003	0.407
	La	Li	Mg	Mn	Mo	Na	Nb	Ni	O-sat
n	18	18	18	18	18	18	18	18	18
average	0.003	0.017	0.694	0.200	0.032	9.744	0.144	0.010	66.112
minimum	0.003	0.017	0.296	0.024	0.030	5.749	0.110	0.004	26.600
maximum	0.007	0.017	1.936	0.672	0.057	20.020	0.520	0.039	98.200
std. dev.	0.001	0.000	0.364	0.188	0.006	3.685	0.105	0.011	17.932
	P	Pb	Si	Sm	Sr	Ti	V	Yb	Zn
n	18	18	18	18	18	18	18	18	18
average	0.205	0.039	5.494	0.020	0.006	0.004	0.005	0.001	0.147
minimum	0.040	0.030	2.409	0.020	0.000	0.004	0.003	0.001	0.001
maximum	1.850	0.195	9.990	0.023	0.029	0.006	0.023	0.005	0.905
std. dev.	0.429	0.039	2.015	0.001	0.008	0.000	0.006	0.001	0.224
	Zr	°C	pH	O2	Fe*	Mn*			
n	18	18	16	18	18	18			
average	0.003	29.344	4.616	5.033	0.068	0.296			
minimum	0.003	26.000	3.900	2.000	0.000	0.030			
maximum	0.008	30.500	5.370	7.500	0.250	0.800			
std. dev.	0.001	0.976	0.372	1.400	0.082	0.272			

sump	Ag	Al	B	Ba	Be	org. C	Ca	Cd	Ce
n	10	10	10	10	10	7	10	10	10
average	0.002	0.076	0.007	0.007	0.001	1.503	0.163	0.001	0.032
minimum	0.002	0.017	0.004	0.001	0.000	0.660	0.003	0.001	0.030
maximum	0.002	0.211	0.016	0.023	0.003	2.890	0.650	0.001	0.039
std. dev.	0.000	0.076	0.005	0.007	0.001	0.695	0.210	0.000	0.003
	Cl	Co	Cr	Cu	Eu	Fe	Ga	Gd	K
n	7	10	10	10	10	10	10	10	10
average	12.157	0.005	0.010	0.002	0.001	0.019	0.060	0.011	0.160
minimum	7.800	0.003	0.002	0.002	0.001	0.001	0.060	0.010	0.080
maximum	21.000	0.013	0.031	0.002	0.001	0.083	0.060	0.015	0.367
std. dev.	4.593	0.003	0.013	0.000	0.000	0.028	0.000	0.002	0.112
	La	Li	Mg	Mn	Mo	Na	Nb	Ni	O-sat
n	10	10	10	10	10	10	10	10	10
average	0.003	0.014	0.596	0.228	0.033	6.417	0.136	0.013	86.691
minimum	0.003	0.000	0.187	0.032	0.030	1.844	0.110	0.004	72.300
maximum	0.005	0.017	0.964	0.621	0.041	8.052	0.228	0.048	96.770
std. dev.	0.001	0.007	0.220	0.204	0.005	1.856	0.048	0.015	8.648
	P	Pb	Si	Sm	Sr	Ti	V	Yb	Zn
n	10	10	10	10	10	10	10	10	10
average	0.600	0.116	3.419	0.020	0.002	0.004	0.008	0.001	0.047
minimum	0.040	0.030	0.893	0.020	0.000	0.004	0.003	0.001	0.001
maximum	2.545	0.325	5.913	0.020	0.007	0.004	0.024	0.002	0.101
std. dev.	0.804	0.139	1.563	0.000	0.003	0.000	0.008	0.000	0.037
	Zr	°C	pH	O2	Fe*	Mn*			
n	10	10	10	10	10	10			
average	0.021	29.500	4.937	6.570	0.008	0.281			
minimum	0.003	27.000	3.910	5.600	0.000	0.000			
maximum	0.060	33.000	5.520	7.500	0.030	1.200			
std. dev.	0.027	2.014	0.425	0.595	0.010	0.361			

6.3.2 River Water (Angurugu River)

The diagrams presented in this section concern the chemistry of the Angurugu River as it varies due to seasonal or diurnal variations (averaged data in Table 6.2). This river crosses the main ore body from east to west and is probably fed by ore fluids, but it may also contribute to local groundwater compositions. The plots are oriented on the geographical position of the sampling stations, thus covering the deposit (0 km = sea = W; 10 km = upstream = E; see Fig.6.1).

Table 6.2: Statistics of water analyses from the Angurugu/Emerald Rivers; n = sample no., average to std.dev. = ppm.

river	Ag	Al	B	Ba	Be	org. C	Ca	Cd	Ce
n	48	48	47	48	48	42	48	48	48
average	0.006	0.065	0.111	0.026	0.000	2.199	118.081	0.006	0.258
minimum	0.002	0.017	0.004	0.002	0.000	0.500	0.003	0.001	0.030
maximum	0.028	0.287	0.339	0.073	0.002	5.300	512.900	0.018	1.575
std. dev.	0.007	0.072	0.124	0.018	0.000	0.903	165.557	0.005	0.341
	Cl	**Co**	**Cr**	**Cu**	**Eu**	**Fe**	**Ga**	**Gd**	**K**
n	42	48	48	48	48	48	48	48	48
average	4697.767	0.008	0.012	0.009	0.010	0.005	0.074	0.042	96.858
minimum	9.900	0.003	0.002	0.002	0.001	0.001	0.060	0.010	0.080
maximum	18080.00	0.047	0.070	0.143	0.040	0.060	0.379	0.138	419.000
std. dev.	5862.308	0.008	0.014	0.024	0.012	0.012	0.048	0.041	132.409
	La	**Li**	**Mg**	**Mn**	**Mo**	**Na**	**Nb**	**Ni**	**O-sat**
n	48	48	48	48	48	40	48	48	48
average	0.037	0.025	327.687	0.170	0.185	1697.141	0.438	0.037	78.978
minimum	0.003	0.017	0.368	0.013	0.030	3.720	0.110	0.004	53.420
maximum	0.143	0.229	1613.500	0.540	0.648	14126.50	1.226	0.106	100.000
std. dev.	0.046	0.033	470.707	0.137	0.198	3057.993	0.322	0.034	13.658
	P	**Pb**	**Si**	**Sm**	**Sr**	**Ti**	**V**	**Yb**	**Zn**
n	48	48	48	48	48	48	48	48	48
average	0.307	0.054	3.974	0.049	1.991	0.011	0.028	0.001	0.082
minimum	0.040	0.002	1.014	0.020	0.000	0.004	0.003	0.001	0.001
maximum	3.699	0.458	6.373	0.165	9.041	0.030	0.106	0.004	0.585
std. dev.	0.643	0.072	1.210	0.042	2.867	0.008	0.034	0.001	0.116
	Zr	**°C**	**pH**	**O2**	**Fe***	**Mn***			
n	48	48	48	48	46	46			
average	0.010	26.929	6.311	6.031	0.300	0.175			
minimum	0.003	3.000	5.030	0.100	0.000	0.000			
maximum	0.040	35.000	7.980	8.200	0.800	0.500			
std. dev.	0.011	4.283	1.066	1.316	0.180	0.113			

6.3.2.1 pH, Cl, Oxygen Saturation, P, C

Chlorine analysis is essential for estimating the effect of salt water intrusions into the river system, which affect the stability of many inorganic and organic compounds being transported in the fresh waters of the river. The plots for Cl in the various seasons are similar, though often it is not possible to sample river waters with comparable chlorinities from the same locality, due to tidal changes and the complex nature of mixing of fresh and sea waters (Fig. 6.10). The diagram shows that saline solutions pushed into the river system by high tides can travel upstream

for about 4.5 kilometers, though they are strongly diluted on their way. The plots for pH are almost linear and they exhibit small changes which probably are due to varying tidal influences (Fig. 6.11). The values for January, which represents the peak of the rainy season, increase only slightly. Both chlorine content and pH therefore seem to be far more dependent on short-term changes than on seasonal intervals.

Oxygen exhibits a recognizable trend in the river (Fig. 6.12). However, this does not seem to be related to any season. From the spring the water gradually saturates with O_2 on its way downstream, until the tides enter the river. Their influence leads to a sharp decrease in the oxygen content, because under a higher salinity many dissolved elements precipitate as oxides or oxyhydroxides.

Organic carbon begins with high values near the spring, decreasing on its way and again taking up organics further down the stream, coincident with peaks for oxygen and Mn, until the tides cause a second decrease (Fig. 6.13). The curves for carbon and the ratios of Fe^* and Mn^* are comparable in their shape (see also Fig. 6.18). In areas of the river where iron is more abundant, the carbon content is significantly higher than in parts with manganese dominance. The analysis of the data did not produce any easily recognizable relations between the dissolved species, particulates and the organics; the nature of interaction is probably very complex. Perhaps there are few direct links among these compounds. Therefore, inorganic species seem to become more important in this river system. Phosphorus, which would be expected to form stable complexes, is difficult to interpret, because it changes drastically within short distances and from one sampling run to the other.

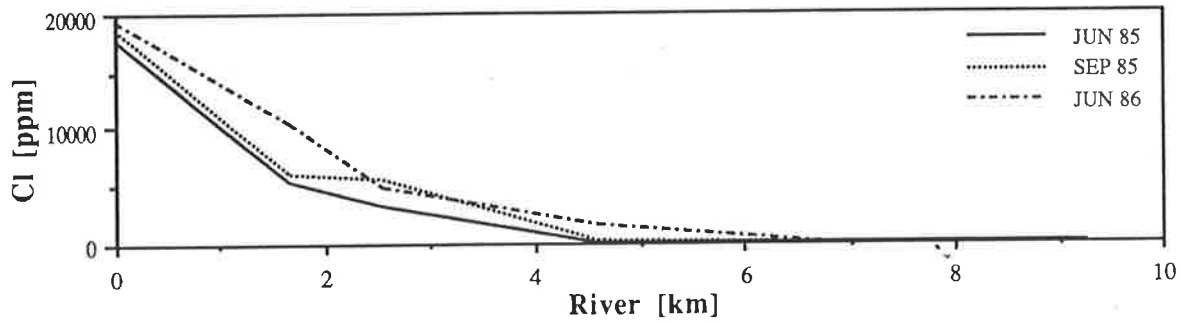


Fig. 6.10: Cl concentration in the Angurugu River on Groote Eylandt (distances are measured from the sea).

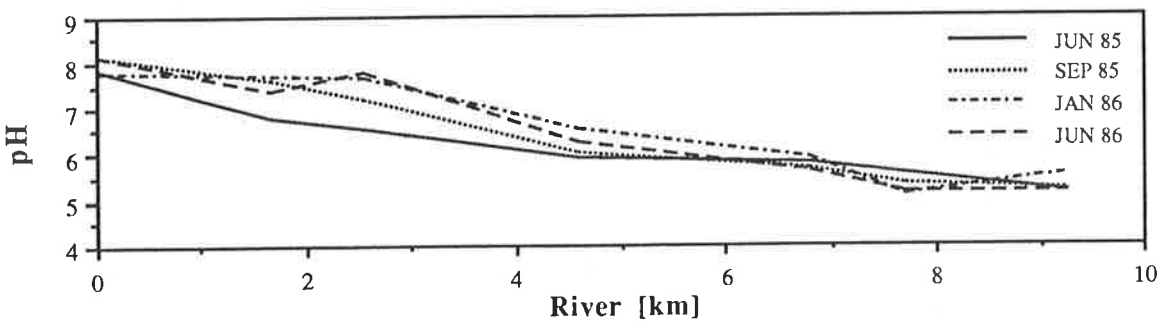


Fig. 6.11: pH values in the Angurugu River.

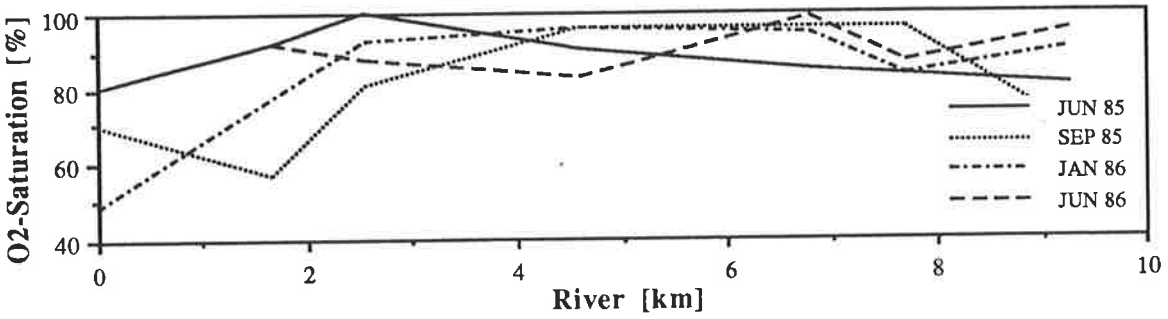


Fig. 6.12: Oxygen saturation in the Angurugu River.

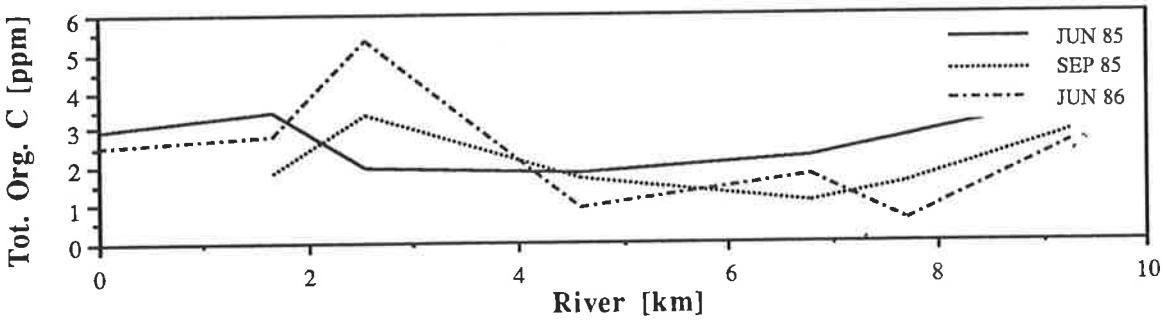


Fig. 6.13: Organic carbon in the Angurugu River.

6.3.2.2 Mn, Fe, Si and Al

It has already been mentioned that the Angurugu River crosses the deposit. This means that if there is any interaction with the ores, this should be reflected in one way or the other in the river waters. First, manganese and iron are examined to determine whether any elemental changes occur that are independent from tidal input. Indeed, dissolved and total manganese both appear increasingly to form an anomaly when the river passes over the deposit. Under the influence of incoming tides, Mn is no longer in equilibrium with the fresh water and decreases (Figs. 6.14 - 15; Sholkovitz, 1976; Laxen et al., 1984). Iron on the other hand, does not seem to get enriched when in contact with the local groundwaters. Fe values generally decrease with the higher pH towards the sea (Figs. 6.16 - 17).

That nonetheless both elements are in a very stable relationship to each other, is shown by the ratio of total iron and manganese. The curves for all four sample sets from different seasons are nearly identical (Fig. 6.18). Going downstream, with manganese in dominance over the deposit, the plots reach a minimum which is broken by the influence of alkaline seawaters. Obviously, the processes are linked which are responsible for the appearance of both elements in the river. Possible factors for the dissolution of the two elements are discussed later.

Dissolved silica varies during the different seasons in the following manner: June > September > January (Fig. 6.19). This clearly indicates a strict dependence on the most significant environmental change, the rain. June is one of the driest months, in January the annual rainfall peak is reached. This means that the highest amount of Si is set free in the dry season, which generally produces more acidic conditions in the groundwaters. The behavior of silica and clay minerals is discussed in detail in chapter 8. However, it is necessary to examine this element here, together with alumina, to improve the knowledge about physico-chemical conditions that govern the supergene processes. Further information may derive for the understanding of the replacement of Mn- and Fe-phases by clays and quartz, and also for the development of new supergene manganese and iron minerals under varying concentrations of Si and Al. When silica-rich solutions come in contact with more alkaline conditions (tides), then the amount of dissolved Si decreases. Alumina shows strong variations upstream, but it does not follow the general trend of Si. It seems to decrease in its concentration on its way down the river. Only under tidal influence does it exhibit the same sharp drop in concentration (Fig. 6.20). The interpretation of the ratio of Si and Al is somewhat difficult, because of an inconsistency in January. For June and September the ratio shows reverse curves, with silica dominance during the dry season (Fig. 6.21).

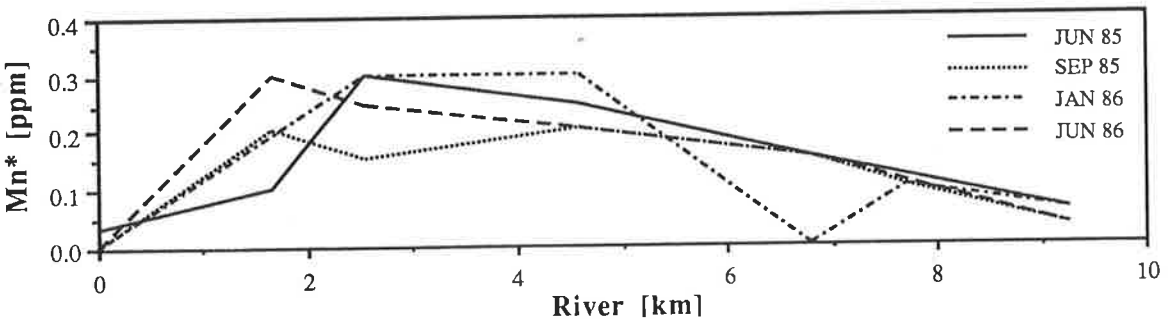


Fig. 6.14: Total manganese concentration in the Angurugu River, measured with field test.

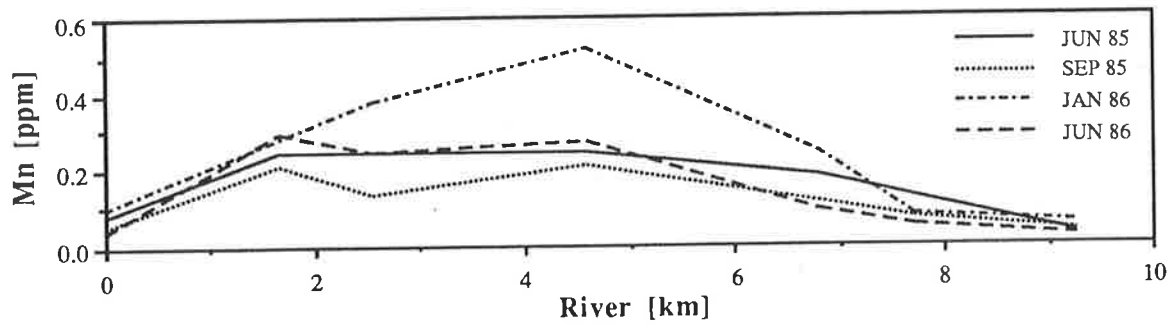


Fig. 6.15: Dissolved manganese in the Angurugu River; compare Laxen et al, 1984.

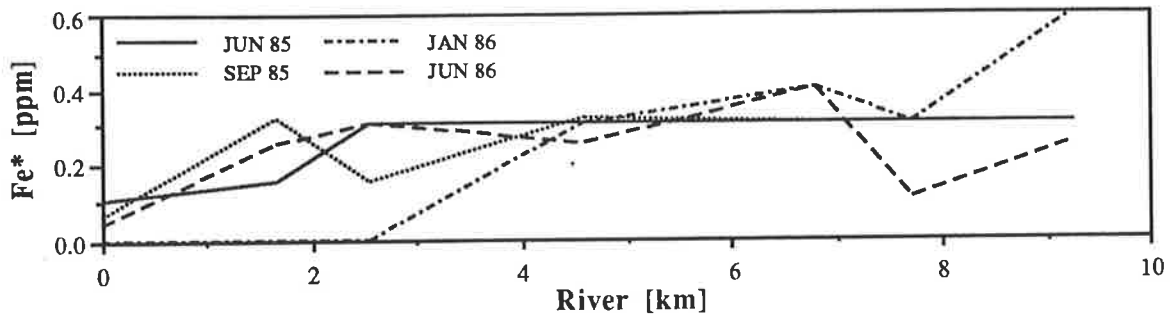


Fig. 6.16: Total iron concentrations in the Angurugu River, measured with field tests.

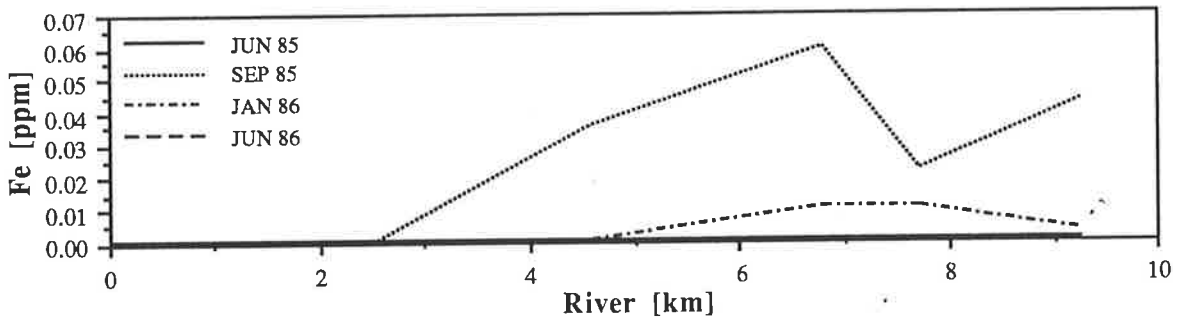


Fig. 6.17: Dissolved iron in the Angurugu River.

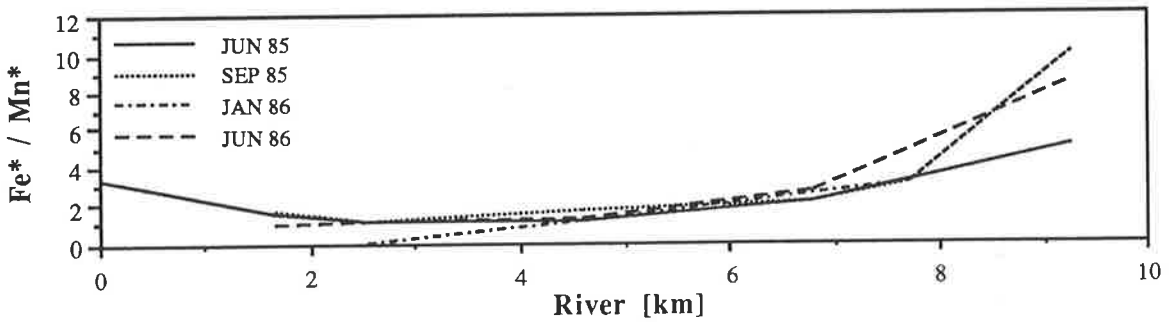


Fig. 6.18: Ratio of total iron and manganese in the Angurugu River, exhibiting strong relationships.

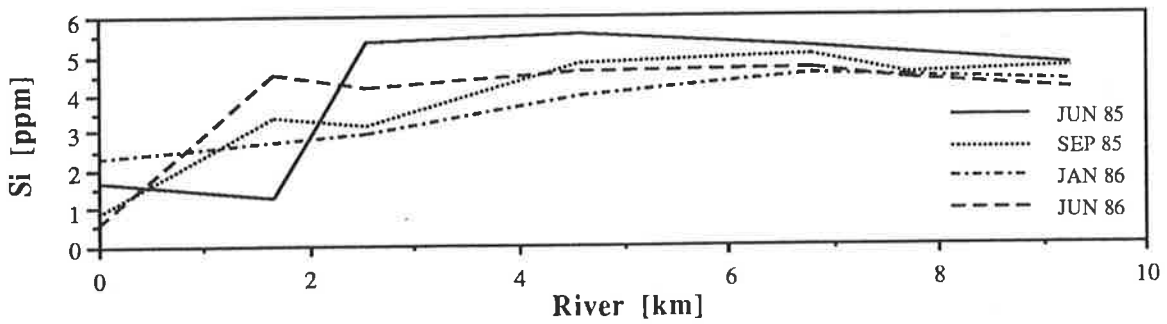


Fig. 6.19: Silica concentrations in the Angurugu River.

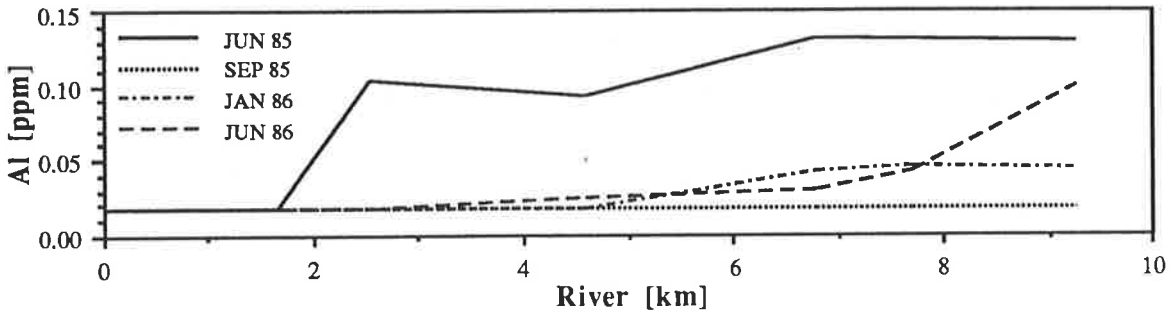


Fig. 6.20: Alumina in the Angurugu River.

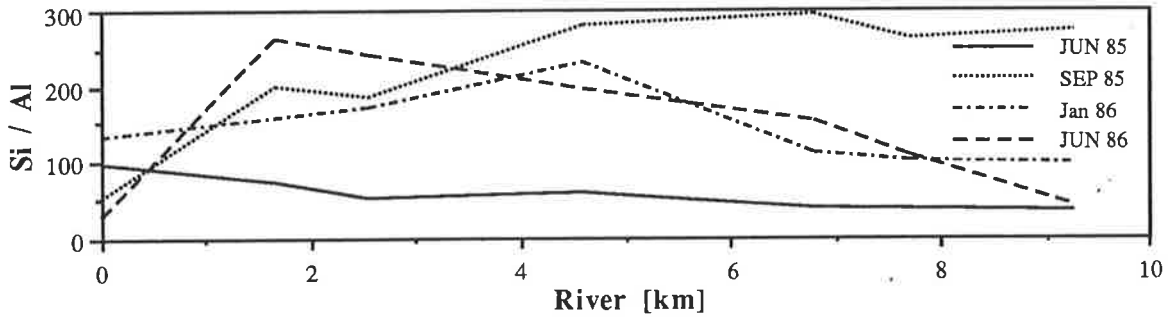


Fig. 6.21: Silica/alumina ratio in the Angurugu River.

6.3.2.3 Rare Earth Elements

Cerium is the most interesting element in the group of the Rare Earths (analyzed: La, Ce, Sm, Eu, Gd, Yb), because the concentrations of about 1.5 ppm reached in the waters near the deposit are extraordinarily high (Great Whale River estuary ≈ 0.3ppm Ce; Goldstein and Jacobsen, 1988). As similar results are obtained from different samples and seasons, these data are considered to be true from the aspect of incidental contamination. The island lacks rock types other than the manganese ores that could provide sufficient amounts of REE. Therefore, the dominant member of this group, cerium, is used as example for the enrichment of these elements in the

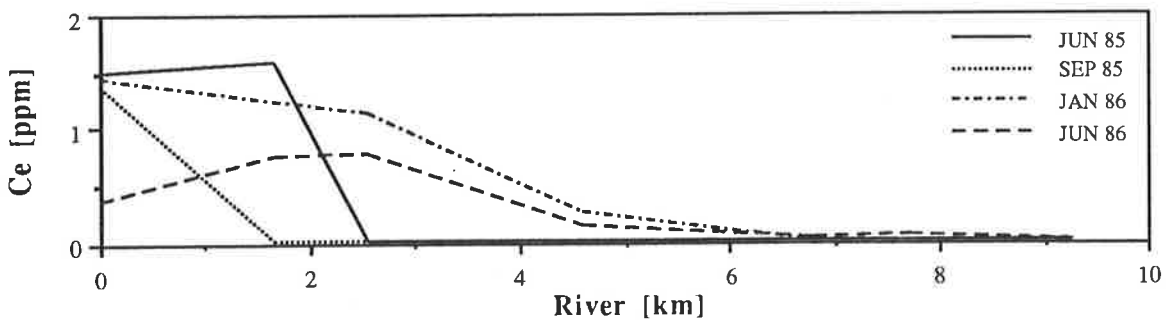


Fig. 6.22: Cerium concentrations in the Angurugu River, as example for the Rare Earth Elements.

river (Fig. 6.22). Its level is at the detection limit upstream near the spring, but it increases gradually over the deposit and drops slightly when the sea is reached. All other analyzed Rare Earths have similar patterns, but are lower in their actual concentrations. The appearance of REEs in the waters can also serve as a reasonably good indicator for the existence of dissolution/ mobilization processes that operate within the orebody.

6.3.2.4 Further Stream Load and Tidal Interaction

The remaining elements can be separated into two groups:

- Elements predominantly transported by the stream and those carried upstream by tides, where they mix to some extent with the stream load. Barium is the best example for elements that derive from the local groundwaters (Fig. 6.23). Its concentration increases almost linearly downstream, with the highest input during the rain season. An addition to seawater values at the river mouth is not detectable. B, Cr, Mo and Zn show comparable patterns.
- All other analyzed elements show the typical high input from the sea at the river mouth and then decrease rapidly: Ag, Ca, Cd, Co, Cu, Ga, K, Li, Mg, Na, Nb, Ni, Pb, Sr, V and Zr. Some of these also indicate an enrichment from groundwaters, thus demonstrating mobilizations from local rocks (Fig. 6.24; K, Na, Sr).

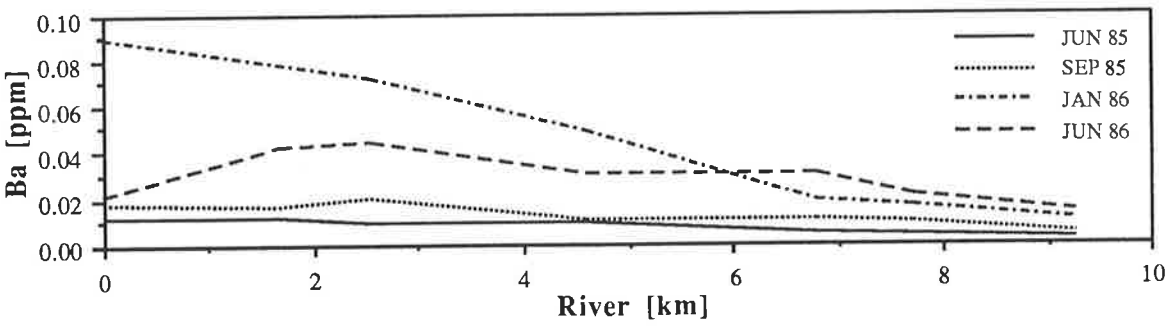


Fig. 6.23: Barium load of the Angurugu River.

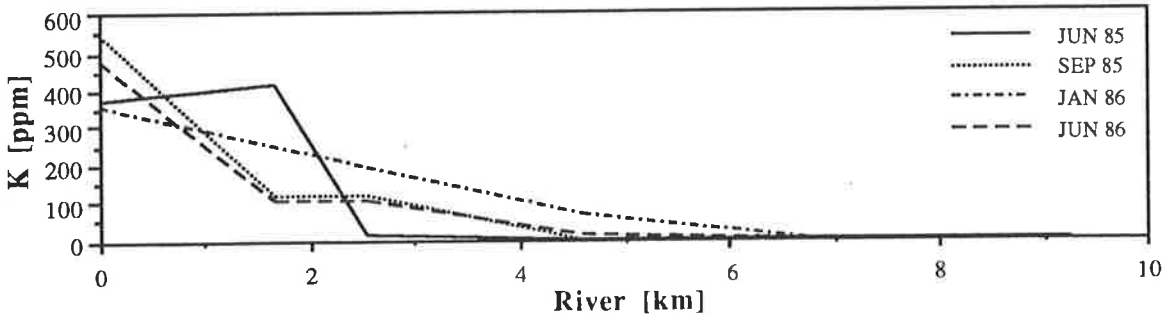


Fig. 6.24: Potassium concentration near the mouth of the Angurugu River and enrichment on the way downstream.

The influence of tides on the river system was studied in detail on a day with high tides at a sampling station approximately 2.5 km upstream of the river mouth (Appendix VI., Table VI.3, sample nos. W55 - W65). Many elements illustrate the existence of the two groups mentioned above. As expected, B, Ba, Ce, Mn, Si and a number of other elements decrease with higher salinity (Fig. 6.25), and the typical seawater elements, Ca, K, Mg, Na, increase.

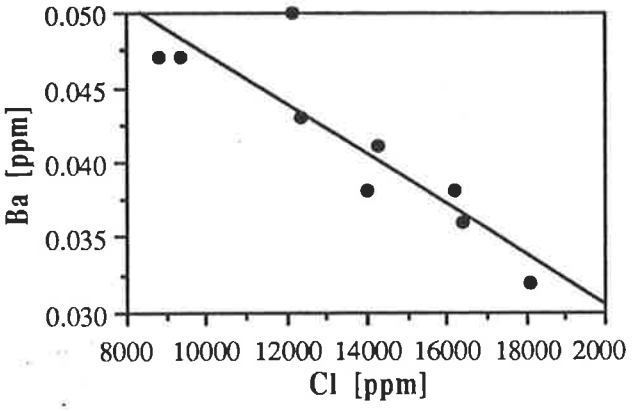


Fig. 6.25: Barium concentrations in the Angurugu River, depending on the tidal input of chlorine (compare Fig. 6.2).

6.3.2.5 Diurnal Fluctuations

A fascinating aspect was found in a part of the Angurugu River which is beyond the reach of tidal influences. Waters sampled from a small dam at the fresh water pumping station near Angurugu Mission exhibit time dependent concentrations, which in some aspects are reverse to results that Harbison (1986) reported about elemental release from mangrove muds of tidal swamps. Harbison showed that in the examined area, oxygen saturation, pH, and Eh reached the highest values in the early afternoon (~15.00h) and related this to biological activities, which includes bacterial sulphate reduction at night (H_2S-production). This system leads to an increasing reduction (solubilization) of compounds like manganese and iron during the night.

On Groote Eylandt however, the pH exhibits the lowest values in the afternoon and increases towards the night. The tests in the River were started at 15.00h and repeated every hour until 19.00h (one hour after sunset). Corresponding to an increasing pH, organic carbon decreases in its concentration, indicating a lower availability of organic compounds at night.

The oxygen saturation possesses a very similar shape of the curve over the time, which demonstrates the strong relation between organics, oxygen and time. Most probably, the acidification of the water is caused by the production of organic acids that are released during photosynthesis, which reaches its peak around midday. Even though organic carbon does not correlate very well with most of the analyzed elements, it can interact indirectly with various elements via pH-changes.

Organo-metallic complexations, which could influence the solubilities of the present species, do not seem to play a significant role, otherwise the analyses would provide much better correlation coefficients and regression patterns. Whether organics have played an active role in the dissolution of manganese or in short-terme stabilization processes, cannot be established, but if

pH-variations were the main driving forces for the development of the compositional pattern, then three major groups could be expected in the water:

- elements with increasing solubility under acidic conditions,
- elements with increasing solubility under alkaline conditions, and
- elements that are independent of pH-variations.

Indeed, these groups can be identified in the following diagrams. Al and Mn* are shown as examples for decreasing concentrations towards the night, together with an increasing pH, (Fig. 6.26; same trend: B, Ba, Ca, Cd, Co, Eu, Fe*, Mg, Na, Pb, Zn). If manganese and iron are considered to be the dominating elements in this group, they could be responsible for the behavior of most of the other members. Adsorption of the latter to particulates of Mn and Fe would result in a coupled co-existence. During the development of more alkaline conditions, the second group increases in its concentration (Fig. 6.27; Ga, Gd, Mo, Nb, Ni, oxygen saturation, P, and Sm). All other elements are relatively stable in their quantities.

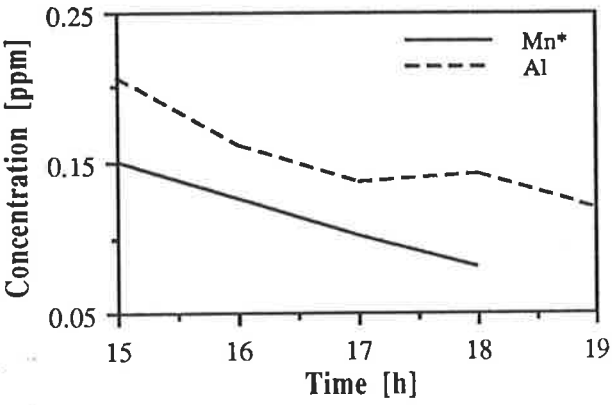


Fig. 6.26: Examples for time dependent decrease of elements in the Angurugu River, out of the reach of tidal influences.

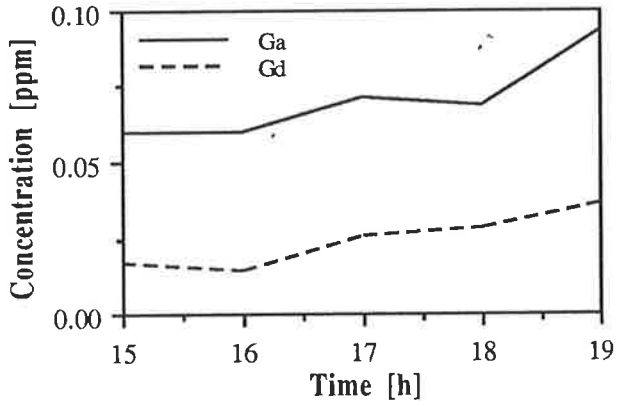


Fig. 6.27: Examples for time dependent increase of elements in the Angurugu River, out of the reach of tidal influences.

Unfortunately, the sample number is too limited to allow a quantitative examination of the results and a relation to environmental factors (C, Cl, pH, oxygen saturation, P, temperature). Later work should focus on these findings, because knowledge of processes responsible for elemental changes in fresh waters could improve the general understanding of the manganese related hydrochemistry.

6.3.3 Coastal Seawater

6.3.3.1 General Composition Pattern

The diagram that summarizes the analyses of seawater samples from around Groote Eylandt clearly illustrates that the sample set contains three major groups (Fig. 6.28). The first one shows elements that are nearly identical to values that were given by Krauskopf (1979) for average seawater (atomic numbers ≤ 20). This includes all major seawater species like Na, Mg, Cl, K and Ca. The second group exhibits slight to intermediate enrichments of the elements with atomic numbers between 21 and 56; included are, for instance, Mn, Fe, and Ba. Heavier elements, mainly members of the lanthanide group, but also lead, are strongly enriched, when compared with average seawater. The group of the REEs is discussed separately below (6.3.3.2), because it is significant for the identification of redox conditions in the waters and it is also believed to be a strong indicator for manganese deposits that undergo supergene alteration processes. Table 6.3 presents statistical information on the seawater samples. Data from other parts of the Gulf of Carpentaria are not available for comparison.

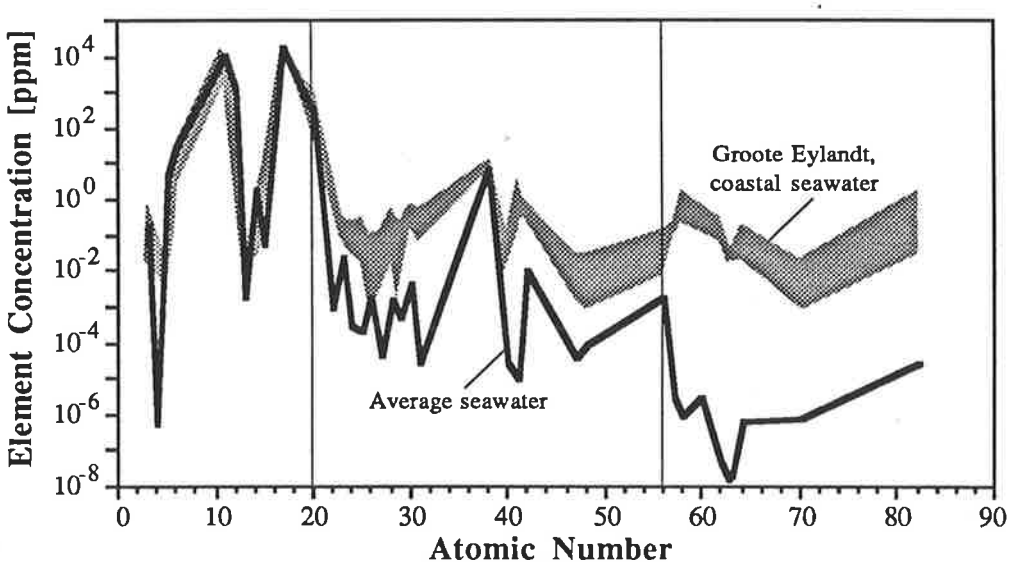


Fig. 6.28: Pattern of elements from seawaters around Groote Eylandt, average seawater after Krauskopf (1979).

Table 6.3: Statistics of seawaters; n = sample no., average to std.dev. = ppm.

sea	Ag	Al	B	Ba	Be	C*	Ca	Cd	Ce
n	9	9	9	9	9	6	9	9	9
average	0.016	0.019	0.213	0.035	0.000	15.865	525.454	0.013	1.082
minimum	0.002	0.017	0.004	0.007	0.000	2.920	377.390	0.001	0.221
maximum	0.024	0.034	0.784	0.105	0.001	28.700	1002.984	0.023	1.632
std. dev.	0.008	0.006	0.248	0.036	0.001	12.236	190.211	0.008	0.584
sea	Cl*	Co	Cr	Cu	Eu	Fe	Ga	Gd	K
n	6	9	9	9	9	9	9	9	9
average	19280.00	0.033	0.062	0.060	0.032	0.001	0.154	0.086	450.609
minimum	17700.00	0.003	0.028	0.002	0.017	0.001	0.060	0.025	351.769
maximum	20070.00	0.125	0.218	0.239	0.043	0.002	0.514	0.148	545.300
std. dev.	916.144	0.038	0.059	0.087	0.010	0.000	0.162	0.047	70.817

Table 6.3 (continued): Statistics of seawaters.

sea	La	Li	Mg	Mn	Mo	Na	Nb	Ni	O-sat
n	9	9	9	9	9	6	9	9	8
average	0.147	0.182	1514.527	0.051	0.509	11577.18	1.137	0.123	71.524
minimum	0.110	0.020	970.064	0.019	0.212	1754.000	0.110	0.024	48.500
maximum	0.220	0.572	1749.900	0.099	0.976	16748.0	2.974	0.344	84.920
std. dev.	0.036	0.191	299.479	0.030	0.259	5408.472	1.249	0.096	11.908

sea	P	Pb	Si	Sm	Sr	Ti	V	Yb	Zn
n	9	9	9	9	9	9	9	9	9
average	1.171	0.378	1.129	0.171	8.969	0.031	0.153	0.005	0.331
minimum	0.040	0.030	0.500	0.070	7.207	0.004	0.089	0.001	0.150
maximum	7.491	1.692	2.281	0.282	10.688	0.105	0.312	0.022	0.575
std. dev.	2.454	0.550	0.603	0.067	1.388	0.031	0.071	0.007	0.167

sea	Zr	[°C]	pH	O2*	Fe*	Mn*
n	9	9	9	8	8	8
average	0.038	27.967	7.933	5.550	0.050	0.035
minimum	0.009	24.000	7.190	3.500	0.000	0.000
maximum	0.127	33.000	8.200	6.700	0.100	0.250
std. dev.	0.037	2.740	0.317	1.007	0.044	0.088

That strong enrichments of many elements in waters from the coast of Groote Eylandt are not due to artificial sample contamination or erroneous analysis is demonstrated in the example of Ce data, although the points below also apply to other analytical results:

- the sample bottles were soaked in concentrated HCl for over 1 week,
- the amount of analysis-grade HNO_3 is far too small to cause final Ce concentrations of ~2ppm; the acid must have contained Ce concentrations of between 100 and 200 ppm to result in such large values,
- fresh- and saltwaters were treated in the same way; however, some freshwater samples are near the detection limit for Ce,
- there should not be any positive anomaly over the deposit, if the samples contained a random contamination,
- artificial seawater (sea salt for aquarium) sampled in the same way as the natural samples generally possessed trace element concentrations below detection limit (# BW5a, Table VI.2),
- seawater samples re-analyzed after approximately four months showed a decrease of most trace elements due to adsorption to the bottle walls,
- saltwater analyses are consistent for specific localities; different locations possess different element patterns when compared with each other.

Thus, it is most unlikely that the data are false, except for small analytical errors, although the unusually high values of some samples might be interpreted to be erroneous.

6.3.3.2 Rare Earth Elements

It was already mentioned that unusually high concentrations of Rare Earth Elements were found in coastal seawaters from around Groote Eylandt, but the extent of their deviations from "normal" or average quantities only becomes obvious in the following diagram, which is derived from the data discussed in the previous section (Fig. 6.29). The elements are normalized to european shales after Haskin and Haskin (1966). To my knowledge these are the highest values ever reported. The samples were taken from near the mouth of the Angurugu River on western Groote Eylandt (W13, W29, J8, J9, J22) , and from localities on the eastern side of the island, further away from the assumed input area (W43 from Umbakumba and W68 ~2km west of the mouth of the Amagula River; for localities see also Fig. 6.1). The levels of the Rare Earths vary according to the sample location. Average sea water, far below the concentrations of the Gulf of Carpentaria near the island, is plotted as a line after data from Goldberg (1965). Even if these data have been adjusted by other authors in recent years, dramatic differences still exist.

Near the area of input from streams, a small positive Ce anomaly is shown. From Sm to Yb the values decrease (Fig. 6.29). When the pattern that exists farther away from the deposit, for instance on the other side of the island, is compared with the initial input area, it can be seen that

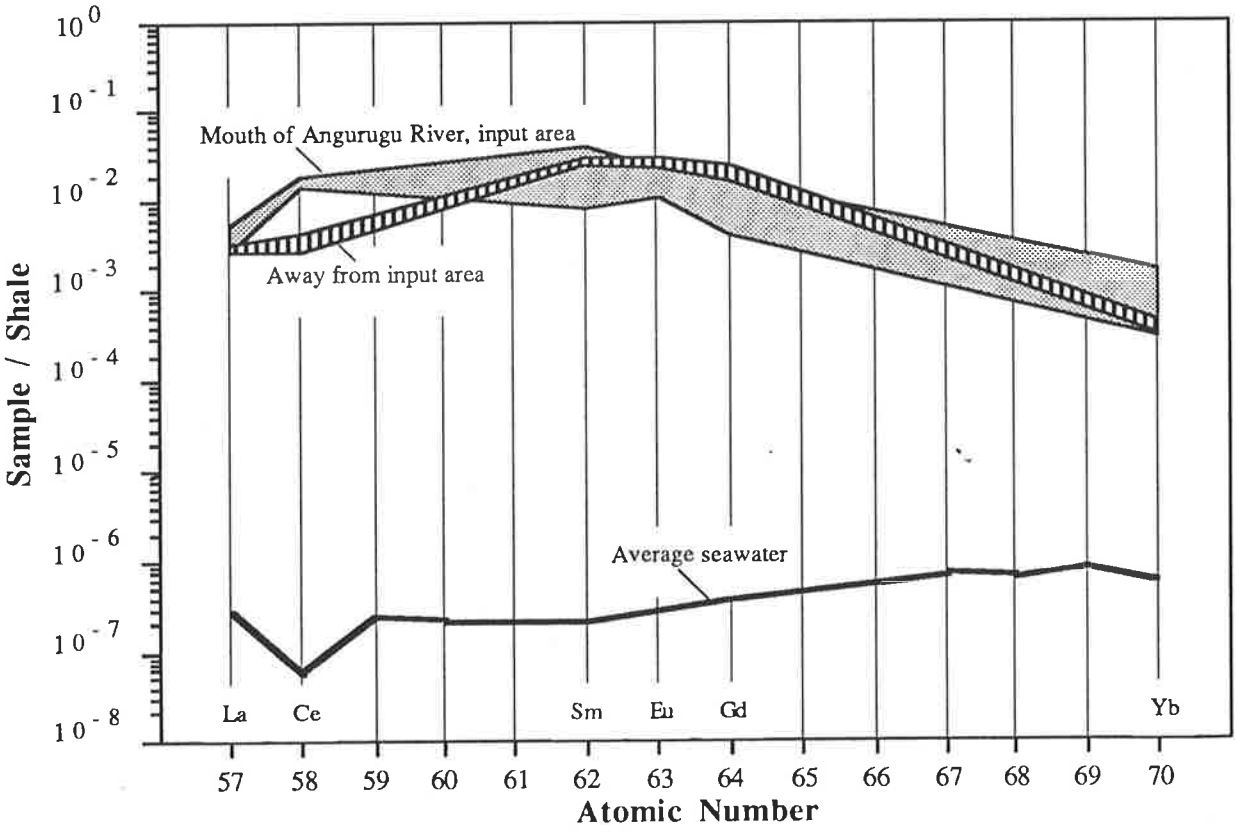


Fig. 6.29: Shale normalized patterns (Haskin and Haskin, 1966) of seawater analyses from different localities around Groote Eylandt and average seawater (Goldberg, 1965); samples W43 and W68 represent striped field; samples W13, W29, J8, J9, J22 are plotted in the shaded area.

although the concentrations are remarkably high, the lighter Rare Earths change their behaviour. Cerium no longer possesses a positive anomaly, but develops a slightly negative tendency. Generally, the curve pattern of these waters begins to resemble average seawater in its shape.

6.4 Discussion

Below, some of the most important elements are discussed to see whether chemical or physical indications can be found to prove that these elements derived from the island itself. Though manganese is the main target for this study, it is also necessarry to look at its co-existence with other elements, because of their role in dissolution, stabilization, and precipitation processes. Cornell and Giovanoli (1987) showed that for instance higher Mn concentrations in solutions can trigger or suppress the formation of specific iron minerals. Effects similar to this interaction, but on the side of Mn oxide development, can also be expected. This matter is not discussed further here, but it is vital for the understanding of supergene manganese ore formation that the type and abundance of dissolved elements appearing together with manganese are known.

It was demonstrated that most of the fresh waters carry manganese, more or less independently of seasonal variations of the water supply. A manganese anomaly develops over the orebody through the input of local groundwaters and a continuous mobilization seems to take place in the deposit. The process that is thought to be mainly responsible for this liberation is examined separately. At the moment the dissolution of manganese is considered to be a fact, though it may seem to be difficult to reduce and release tetravalent Mn into the water.

Till now, the state in which Mn is being transported in the river-, ground- and minewaters has not been discussed in detail. All studies indicate that inorganic complexes and/or ionic forms (e.g. Mn^{2+}) are the dominant species. Correlation plots between dissolved manganese and organic carbon do not provide recognizable patterns, and negative regressions were obtained from particulate manganese (total Mn minus dissolved Mn) and organic carbon. This means that it is almost certain that neither dissolved nor particulate Mn is associated with organic complexes. Nevertheless, an indirect influence of organics on dissolution rates via pH changes cannot be excluded.

It is also possible that short-term interactions (complexations) with several elements may increase solubilities, but none of these effects has been detected during this study. Contrary to manganese, a number of elements show positive correlations with organic carbon (e.g. B, Ba, Ca, K, Li, Na and Sm). This might be indicative of adsorption on organic macromolecules or the presence of organo-metallic compounds. Phosphorus, another complex-forming element, does not provide better correlations, and in our case it may not be important as a stabilizing reagent for any of the analyzed elements.

The Rare Earths are of particular interest for further discussion, because this group of elements indirectly confirms the dissolution of manganese ores. Though it could be argued that the REEs are brought into the river system by tides which press saline waters upstream, where they could influence local groundwaters, it is demonstrated on the example of cerium that these elements have been mobilized under freshwater conditions. When the chlorine value of a specific sampling station is examined (e.g. 2.5 km; Fig. 6.10) and it is assumed that Cl is equivalent to the amount of saltwater that mixed with the riverwater, then the Cl concentration would lead to approximately one quarter of the seawater concentration of Ce, considering a simple mixing model. Cerium nevertheless shows values near those of the sea. This means that Ce and most other trace elements are being transported to the sea by the river. This fact is supported by the negative correlation between cerium and chlorine (Fig. 6.6).

It was also illustrated that the Angurugu River gradually becomes enriched in the Rare Earths downstream (Fig. 6.22), and that apart from the manganese ores there are no other possible rocks from which REE could be mobilized in sufficient quantities. Although the other REEs do not follow Ce with the same regression patterns (indistinct), there is no reason to believe that they derive from different materials before they are enriched in the sea to comparable levels. It is known that their chemical characteristics are different to that of cerium, which is far more susceptible to environmental changes such as Eh or pH. This means that the redox behavior of Ce and the knowledge of the geochemistry of the ores not only provide the confirmation for Groote Eylandt being the source area, but they also identify the manganese ores as source rocks. This information and probably an enhanced study of the REE in seawater may provide an ideal tool for the selection of target areas for manganese exploration at river mouths along the coasts, where specific curve shapes should develop near input areas.

When the remaining elements are examined, a large number of elements is found that also move with the freshwaters. Occasionally, mobilizations can be linked to seasonal variations of water input or dehydration processes, but very often there is no clear picture that could indicate one or the other. One of the few elements that clearly reflect changing conditions is silica. Kittrick (1969) showed that kaolinite ($Al_2Si_2O_5(OH)_4$) breaks down when it dehydrates, releasing silica sheets from its structure into solution and leaving gibbsite ($Al(OH)_3$) as the remaining mineral.

As this reaction is reversible, it is difficult to prove in the Groote Eylandt deposits, because gibbsite is a fairly rare phase, it also becomes unstable under the increasingly acid regime of the dry-season. That probably most of the dissolved Si originates from kaolinite destabilization, seems to be supported by the increase of Si concentration in waters during the dry-season. In some instances, sandstones and recent quartz sands, which are both common in this area, are also subject to mobilization of silica, butthis is probably much less important, because of the higher stability of quartz.

Until now, seawaters were only mentioned as the final place, where elements derived from Groote Eylandt can become enriched. The interaction of various compounds with the saltwater in the course of the Angurugu River is another interesting aspect and it provides an ideal model for mixing and inter-elemental dependencies. Manganese and iron are coupled strongly to each other, even when their total amount decreases drastically under the influence of incoming tides (Figs. 6.14 - 18). Increasing salinity is probably the cause for the cracking of organic compounds such as humic and fulvic acids or inorganic complexes. Elements bound to these compounds would be released and might be subject to oxidation, which would show up immediately in decreasing oxygen saturation (compare Fig. 6.12). Oxidized species could flocculate and precipitate. Elements like iron and manganese in fact are found in much smaller concentrations in areas with increasing tidal influence. Most likely, these and other elements are found in river sediments (clay fraction) in quantities that depend directly on the nature of the waters above. Unfortunately, the above interpretation for the organics is only partly supported by the analysis of organic carbon. Relatively high concentrations of organic carbon have been analyzed from the jetty at Milner Bay, which could theoretically contradict the statements made above. Though many of the analyzed elements decrease when in contact with seawater, a comparison with average seawater shows that an overall enrichment exists.

In contrast to the elements that precipitate in contact with saltwater, the Rare Earths seem to retain reasonably constant concentrations (compare final values from the river). That their residence times in the sea are probably much longer than a few hours could be indicated by the extraordinarily high amounts of Ce (and the other REEs) which can even be found on the other side of the island. If these elements had only a very short residence in the seawater, they would not concentrate to quantities of up to 1.6 ppm (Ce), which is equivalent to an enrichment factor of about 4000, when compared with average seawater. Goldstein and Jacobsen (1988) studied the removal of REE in estuaries and although these authors discuss concentrations in the pmol/kg-range, they were able to show for the Great Whale River that the Rare Earths already start to disappear from the water column at a reasonably low salinity (<2%) and that the concentrations drop to about one quarter of the initial values at seawater salinities. This seems to contradict the findings of the present study, but if the input from Groote Eylandt (rivers, but also submarine freshwater springs that have been in contact with orebody fluids) was large enough, it could well compensate for the loss that occurred during the mixing.

7. Experimental Work

7.1 Introduction

During the first field trip of this research work a geochemical redox reaction between manganese oxides and kaolinitic clays was detected which soon became very important for the description of supergene mobilization processes in the Groote Eylandt deposits (Pracejus, 1985). Earlier studies had noted a number of manganiferous precipitates that were believed to be of supergene origin, but no process seemed to be appropriate for large scale dissolution, from where successive precipitation of Mn-oxides could derive (Bolton, 1982; Ostwald, 1988). Sulfuric acid for instance, which is being produced during the weathering of sulfides in other types of deposits, can account for extensive remobilization reactions (Thornber, 1983). The manganese ores, associated sedimentary and lateritic rocks on Groote Eylandt however, contain extremely small amounts of sulfides and are therefore not able to use this type of liberation process.

Initial investigations demonstrated that the natural conditions of the redox reaction could be simulated and examined in the laboratory. The basic necessities for this study were Mn-oxide ores, kaolinitic clays, water, and the possibility to observe the occurring variations and to store the obtained geochemical data. Since the reaction involves an electron transfer between different minerals, the varying charges between the two separated materials can be monitored for instance with a continuous chart recorder, together with pH-changes. Below, the experimental setup and results are presented.

Major and trace elements of all samples were analyzed as well, as XRD and FTIR spectra were determined.Sampled solutions were examined by ICP for their contents of dissolved elements, and the electro-chemical variations were recorded continuously (Appendix VII., Tables 1-3). The theoretical background for the redox reactions and their wider context for the formation of the various supergene rocks will be given in chapters 8 and 9.

7.2 Design of Experiments

One of the outstanding features in the field are the vertical and horizontal pipe systems which cross-cut the orebody in many places. These clay pipes must play a dominant role in reducing the ore, because they cross-cut primary and secondary ore units. Thus, a detailed study was undertaken which led to the development of a battery-cell by modelling one side of such a pipe. To see the relations between field findings and experiments, it is necessary to look briefly at a pipe and a generalized model, before the laboratory setup and the design of the cell are being discussed (Fig. 7.1, after pipes in F3-Quarry, and Plate 7.1, Figs. 7.2a-c).

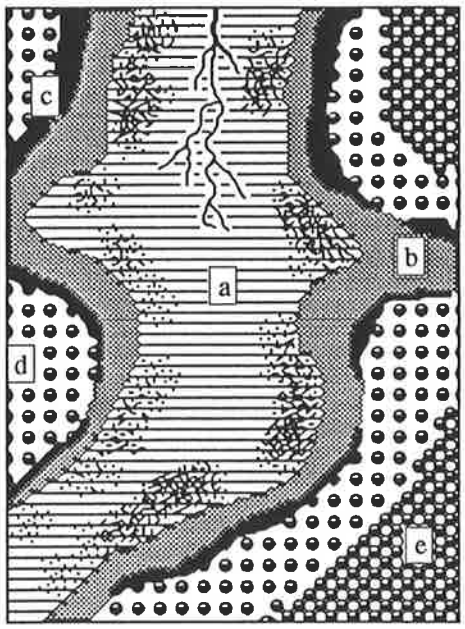


Fig. 7.1: Model of a clay pipe from F3-Quarry (see also Plate 7.1). The size of such pipes varies between a few centimeters and some 60 cm in diameter; a = kaolinitic clays with roots and Fe-oxyhydroxide impregnation; b = Fe-oxides/hydroxides on pipe walls; c = Mn-cementation (laminar mangcrete); d = altered pisolite with diffuse clay impregnation in Mn matrix; d = Mn cemented pisolite.

As already mentioned, the center of the pipe is filled with kaolinitic clays and varying amounts of quartz sands (a). Occasionally, tree roots are observed some fifteen meters in the ground. Whether these roots opened cracks in the orebody or if they followed existing pipes (water conduits), is unknown. Goethitic stains occur in irregular patches within the clays. Lining the kaolinite, iron oxides have cemented existing materials (b; kaolinite, sand grains or Mn pisoliths). Laminar Mn cementations occur further outward in contact with manganese ores (c). The next zone is comprised of pisolitic ores with a relatively soft, clay-rich matrix (d). Gradually, this type of ore changes towards a very hard cemented pisolite with little or no gangue minerals (e).

Considering this succession of rock types, it is possible to identify two materials that are the endmembers of the electro-chemical reaction:

- kaolinitic clay (carrier of divalent Fe), the innermost part of the pipe, and
- pisolite ores (tetravalent Mn), farther away from the pipe.

In the field a portable mV-meter can measure a potential difference between these two rocks. Therefore, a reaction vessel was constructed to duplicate this process. To come as close as possible to the natural conditions in the experimental setup, ores, clays, and waters were taken from the area where the mentioned pipes had been examined in detail (F3-Quarry).

Plate 7.1

Fig. 7.2a: Pipe in F3-Quarry; scale shows centimeters.

Fig. 7.2b: Part of pipe from F3-Quarry; thin laminar mangcrete in contact with clay; scale shows 2cm.

Fig. 7.2c: Relics of vertical pipe systems in F3-Quarry laterite; the hammer is ~ 30cm long.

Plate 7.1


1a


1b


1c

The cell closely resembles a car battery. It contains compartments for both solids and water (Fig. 7.3; for cell parameters see Appendix I.3). To increase the reactive surface area of the materials, the rocks were ground to a fine powder. The materials are in direct contact with carbon electrodes connected to a multi-channel chart recorder. The various water types used in the experiments (distilled, mine-, and seawater) can permeate through sintered glass plates into the rock powders to facilitate the redox reaction. Since the field conditions generally vary between 26 and 32°C, the closed system was kept at a constant temperature of 30°C in a sand bath. Additionally, a small magnetic stirrer produced a permanent convection in the inner water-containing chamber. A recorder monitored pH-changes and voltage variations between the solids. After the finish of the respective experiments, the cell was topped with controlled amounts of distilled water to replace water that had been used for mineral reactions and to reach the initial volume, which was necessary to avoid dilution errors in the final analysis.

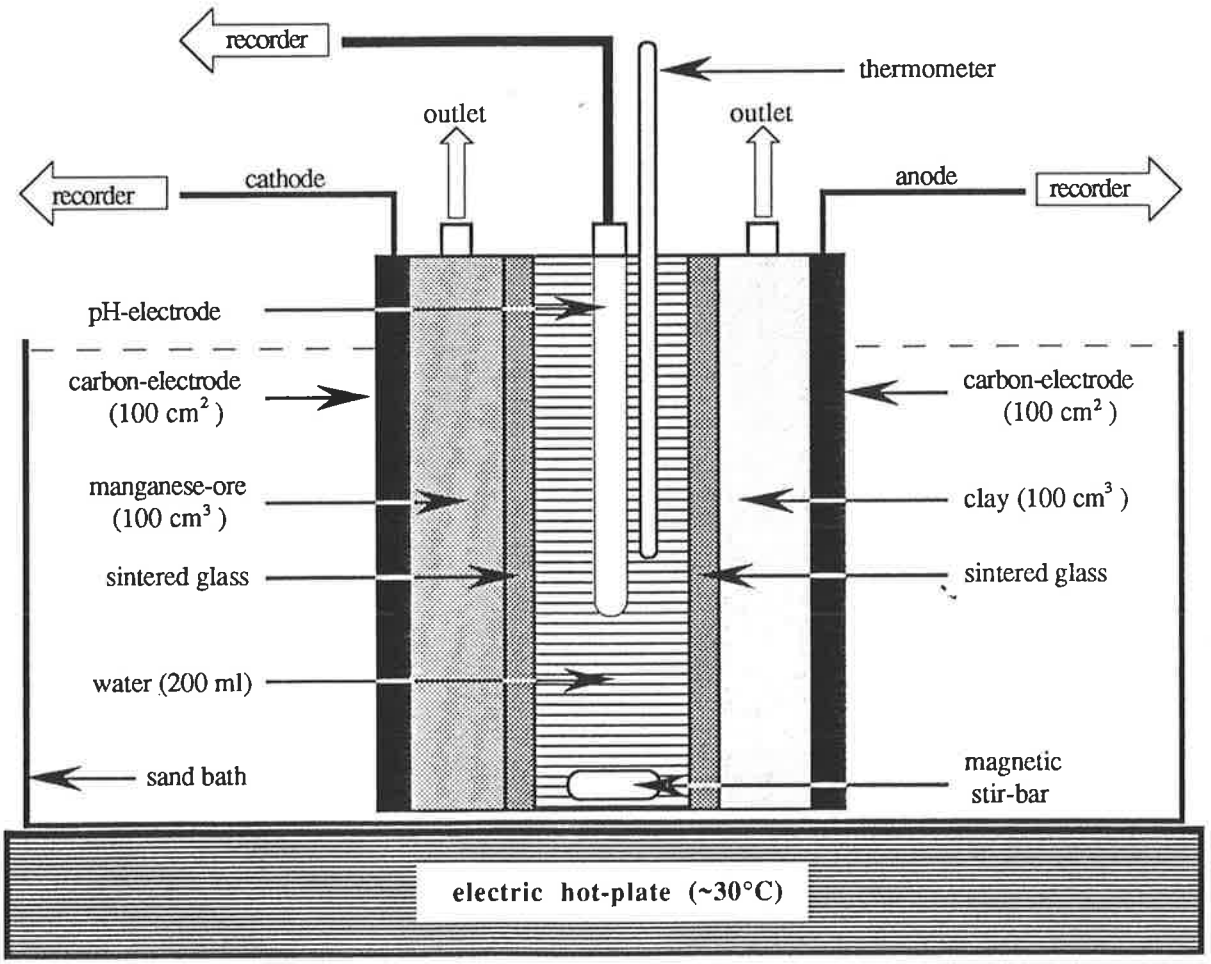


Fig. 7.3: Experimental setup for manganese-clay battery; for further information see Appendix I.3.

7.3 Results

A number of short initial tests with distilled and natural fresh water were conducted in order to overcome problems in the filling operations, such as air bubbles trapped in rock powders or the temperature control, to ensure undisturbed battery runs. The solids used in all tests are the same, only water types and the setup of the experiments vary.

7.3.1 Fresh Water Experiments

In this section, results of three different tests are presented:

- 15 days (BW 1); connected to recorder, rocks and water were analyzed,
- 89 days (BW 2); connected to recorder, rocks and water were analyzed,
- 7, 14, 21, and 28 days (BW 3 parallel tests); separate test vessel, not connected to recorder, rocks and water were analyzed.

Because these experiments and the obtained data are strongly related to each other, they are discussed together.

7.3.1.1 Electro-Chemical Data

The first two tests provided almost identical results for the recorded mV and pH values of the same time interval (15 days; Table 7.1; see also Appendix VII., Table 1). Therefore, the second test is used to illustrate the geochemical reactions of the cell (89 days; Figs. 7.4). The changes of the electrical potential can be separated into three major intervals:

- generally increasing values for ~35 days,
- overall decreasing values between 35-55 days, and
- very small oscillations after 55 days.

The shape of the curve is not linear, but a saw-tooth pattern develops, where the first part of the individual peak increases relatively slowly. Then it drops abruptly until the next peak rises, without leveling out in the intermediate positions. The shape of the pH-curve shows much less variations. The values quickly reach an equilibrated level of pH ≈ 4.2 (after 20 days), from where only small-scale oscillations occur. That despite these seemingly so different curves strong relations between both exist, is demonstrated in the enlarged segment of the diagram (day 15-20; lower part of Fig. 7.4). This intermediate stage, replotted on an expanded time scale for clarity, shows small short-term changes superimposed on the two main curves. The pH depicts depressions and highs that generally do not deviate from the original curve for more than ±0.05, and with the beginning of most pH depressions the mV-readings also decrease.

Table 7.1: Electro-chemical variations in battery tests.

No.	Water type	Test length [days]	pH_{start}	pH_{end}	mV_{start}	mV_{end}	mV_{max}
BW 1	mine water	15	5.00	4.35	364	85	470
BW 2	distilled water	89	4.87	4.13	306	394	605

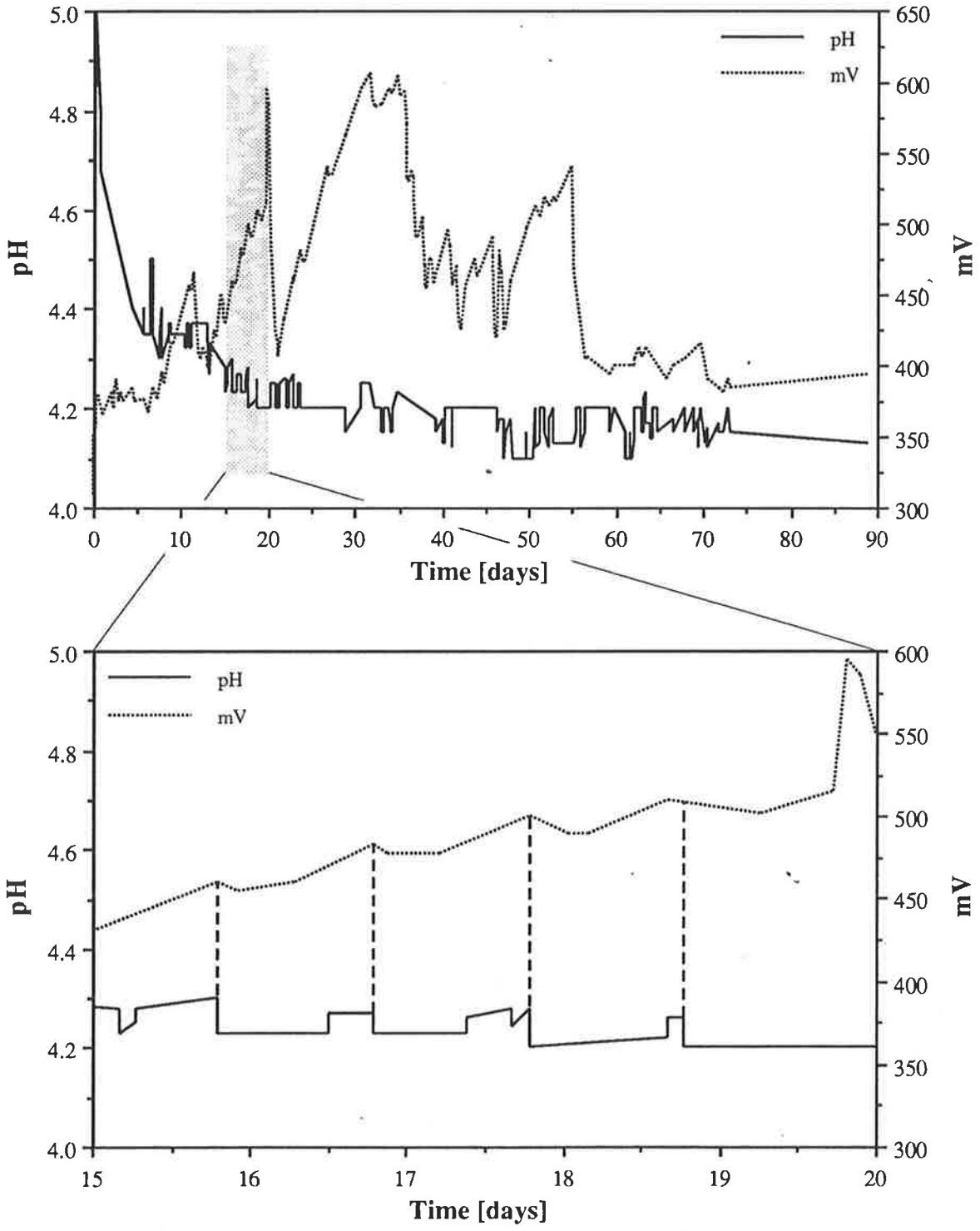


Figure 7.4: Electric potential and pH versus time during battery test; below enlarged segment of upper diagram.

7.3.1.2 Hydrochemistry

The chemical analyses of the waters confirm that the redox reaction is able to reduce/dissolve manganese oxide ores in the battery cell (Appendix VII., Table 2). Potassium shows the most impressive increase in solution of all elements (enrichment factor after 15 days: $3*10^3$). Manganese is also strongly enriched ($2*10^2$); less prominent are Sr, Ba, Ca, and B (all 1 to $2*10^2$). However, almost all dissolved elements increase after a short time, except for some trace elements and Fe, which generally remain below the detection limit. Together with the elements deriving from manganese ores, the main clay components Si and Al also appear in solution, with silica being far more enriched than alumina.

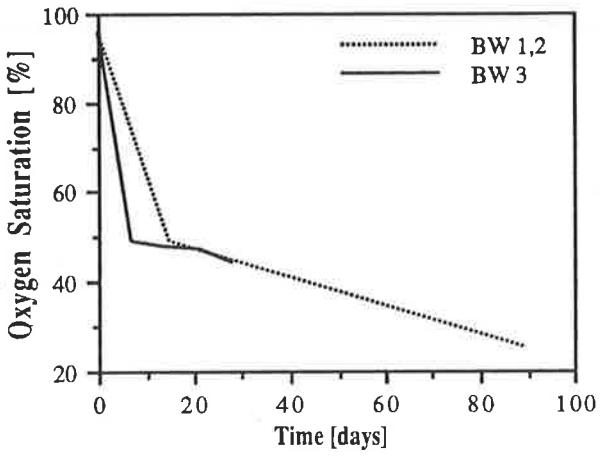


Fig. 7.5: Oxygen saturation of test solutions versus experiment time BW1 and 2 and BW3 (adjusted to first set).

The concentration of most elements commonly decreases after a period of two or three weeks, independently to the experimental setup; only Zn increases steadily. This general decrease indicates the presence of a mechanism responsible for element removal, such as adsorption of dissolved species onto existing solids or oxidation/precipitation reactions. The continually decreasing oxygen saturation of the water shows that parallel to the reduction and dissolution of manganese minerals oxygen consumption occurs (oxidation; Fig. 7.5). Additionally, the volume of the cell water reduces approximately 10% in the 89-day test. This fact clearly illustrates that in this closed system hydroxyl groups are being used for the formation of precipitating materials. An analysis of the test conditions reveals that the essential factor for O_2 depletion is not the variation of amounts/volumes of the test materials, but rather the ratio of the weights of Mn ore and kaolinite. The first set of tests had ore/clay-ratios of ~2:1 (BW 1 and 2), the second showed a ~1:1 ratio (BW 3). When the oxygen saturation of this latter test was adjusted to the first test group, then almost identical curves were derived.

7.3.1.3 Mineralogical Investigations

Another aim of the experimental work was to see whether the redox reaction also resulted in mineralogical changes of the two reaction partners, ore and clay, apart from the dissolution of the manganese ores. To determine this, the materials were analyzed by infrared and X-ray techniques. The examination of the infrared spectrum provided information about more subtle

changes within the material, whereas X-ray diffraction was used to back up results obtained by this method, where possible.

It was also hoped to gain information about chemical changes in the rock samples, but most data obtained lay within the analytical error margins of the original materials. An exception to this general observation was observed in a short-term enrichment of boron in kaolinite (~110ppm; normally less than 10ppm; see Appendix VII., Table 3). The time interval of this concentration increase co-incided with intermittent mineralogical changes that occurred in both the clay and the Mn oxide fractions (see following section). Fleet (1965) and Palmer et al. (1987) demonstrated a B adsorption onto kaolinite and other clay minerals. Although they point out that the highest concentration occurs in alkaline media such as seawater, this does not contradict the experimental findings at low pHs, because the adsorption strongly depends on the mineralogy of the respective sample. Prominent B variations thus reflect a variation of the present phases. The examination of all other elements provided no valuable information about geochemical changes and therefore, this technique is not discussed further.

7.3.1.3.1 FTIR-Characterization

FTIR spectra of ore and kaolinite were examined to determine whether the mineralogy of the materials varied according to the length of the experiments (Fig. 7.6a,b). The patterns of the ore do not change very much, when all samples are compared, but it must be remembered that the manganese oxide minerals are mainly reduced and dissolved during the interaction with the clays. The largest variations are observed between the initial material and the ore specimen of the longest test run (89 days; B II.c). The Mn oxide peaks for wave numbers from 200 to 800 become stronger and indicate an increasing crystallinity through aging and maturation of existing phases. However, much more interesting is the appearance of peaks at wave numbers greater than 3200 and between 800-1200, together with the overall vertical shift of the left part of the pattern. These additional lines are kaolinite peaks, and they derive from increasing amounts of clays in the ore (see Fig. 7.6b).

This observation is evidence for a direct replacement of manganese oxides by kaolinite. Iron hydroxides, which are commonly the first replacing phases, in this case only stained the carbon electrode that was in contact with the manganese oxides. A small sulfur contamination of the electrode may in fact support precipitation in this place, rather than within the manganiferous material. However, a diffuse Fe distribution and essentially cryptocrystalline Fe phases could also contribute to a masking effect. This would explain why the low concentration levels were not detected by the analytical techniques. The structural variations in the examined kaolinites are more obvious than in the ores (Fig. 7.6b). Strong oscillations of the left shoulder of the patterns (high wave numbers), together with increasing or decreasing peak heights, can be correlated to

the duration of the experiments. The spectra plotted are representative examples, all FTIR analyses demonstrate similar behaviour. Sample B I.a is the initial test clay, B I.b shows the same material after 14 days. The height of all kaolinite peaks and the shoulder part of the spectrum increases for a few weeks and then declines. For comparison a clay sample from below the orebody is shown (no. 20), which most probably has been in permanent contact with groundwater. In this case the shoulder of the pattern flattened out significantly, although the positions of the peaks have not changed.

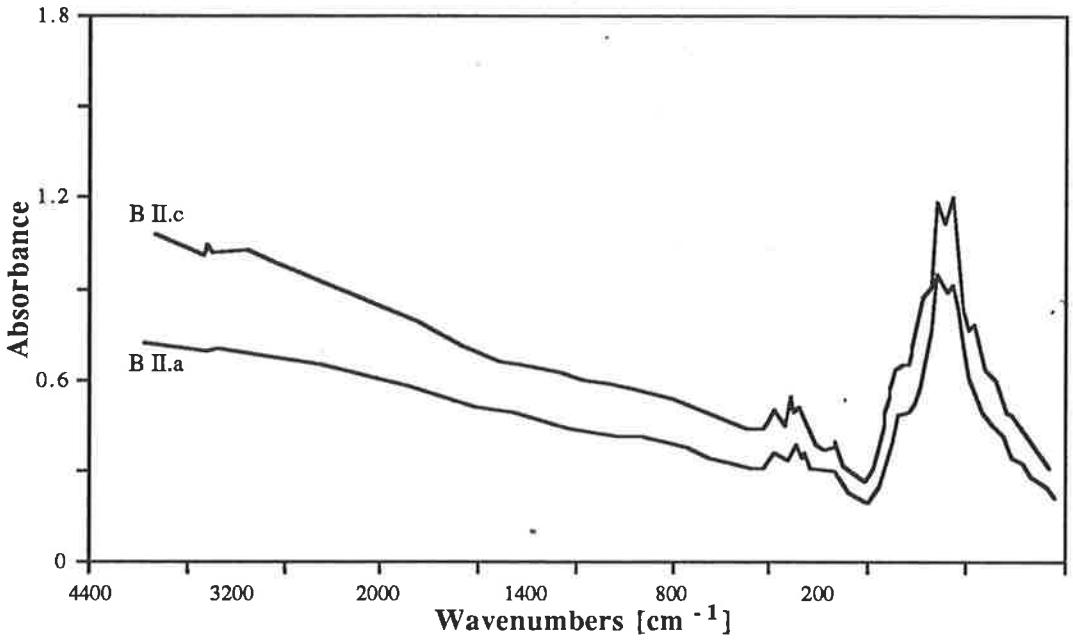


Fig. 7.6a: FTIR patterns of Mn ores; B II.a = starting material, B II.c = after 89 days; prefix for samples: 903.

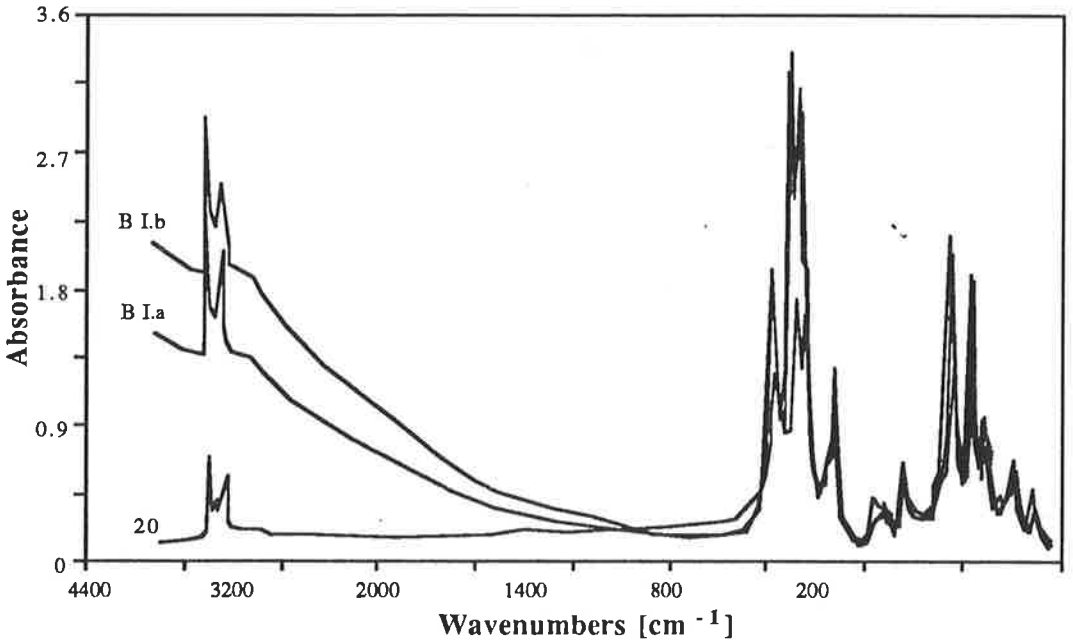


Fig. 7.6b: FTIR patterns of kaolinite: B I.a = starting material, B I.b = after 15 days, 20 = below ore (F3-Quarry); prefix for samples: 903.

7.3.1.3.2 XRD-Characterization

The X-ray diffraction patterns of ores and clays exhibit only small variations, when compared with the initial materials (Fig. 7.7a). Nevertheless, some of the kaolinite peaks demonstrate a reorganization of the lattice through an increase of peak intensity. On the other hand, the d-spacings do not shift which means that no new clay phases are formed. The manganese mineralogy contrasts with this last observation (Fig. 7.7b). The two main peaks of the ore initially resemble the pattern of cryptomelane depicting comparable peak heights at 33.1 °2ϑ and 43.6 °2ϑ. After the experiments the peak at 33.1 °2ϑ increases and suggests an increasing amount of pyrolusite in the sample.

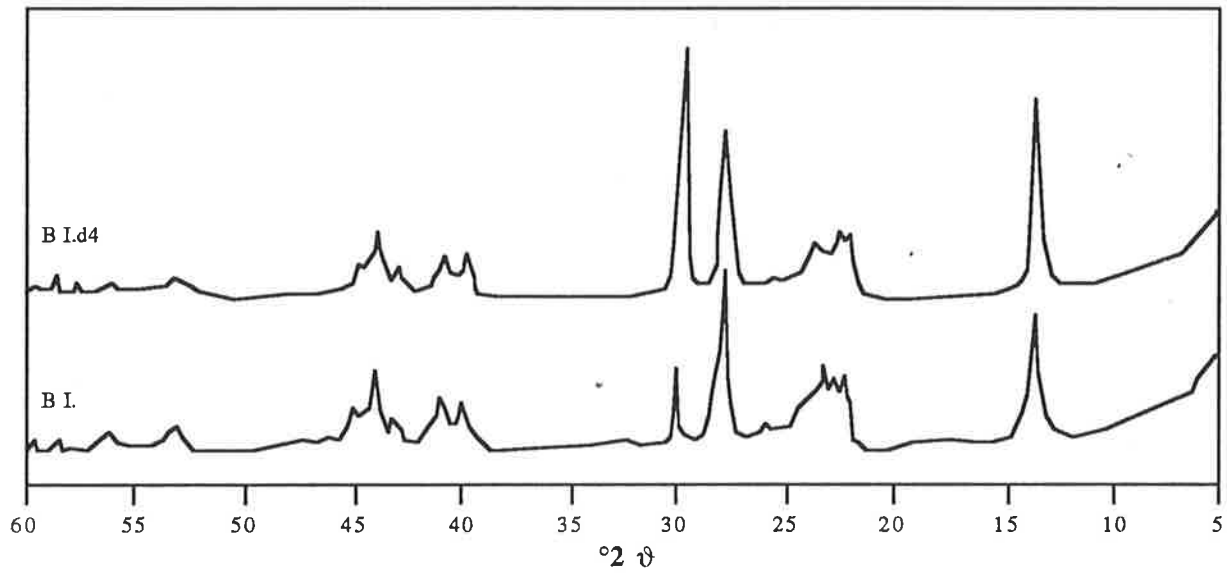


Fig. 7.7a: X-ray diffraction pattern of kaolinite; B I. = initial sample, B I.d4 = after 4 weeks; sample prefix: 903.

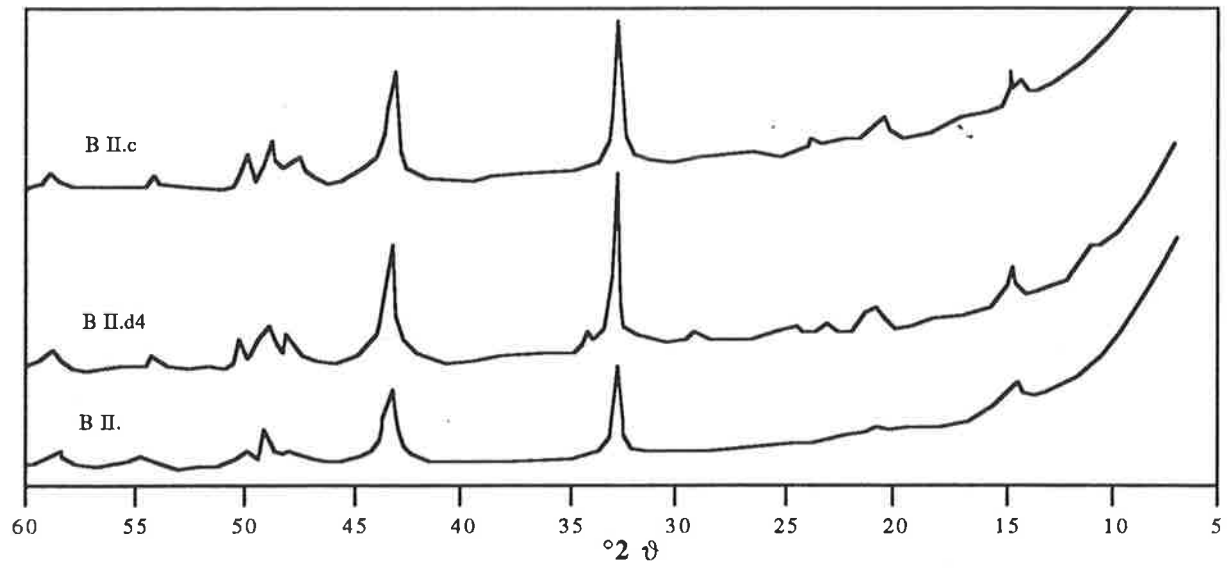


Fig. 7.7b: X-ray diffraction pattern of Mn oxides; B II. = initial sample, B II.d4 = after 4 weeks, B II.c = after 89 days; sample prefix: 903.

Unfortunately, the strongest lines of both minerals appear approximately at the same position, and it is therefore difficult to make precise statements about mineralogical changes. It is unclear, why the intensity of this particular peak decreases slightly after 89 days.

7.3.2 Salt Water, General Observations

For technical reasons the experiment which used artificial seawater was only partially successful. Nevertheless, some of the general observations assist in understanding the redox process examined in the following chapter. Almost certainly, the test vessel material (clear plastic) took part in the interaction between the solids and the alkaline water by adsorbing some of the major seawater constituents (e.g. Cl^-, SO_4^{2-}, and other ionic species). Thus, it is difficult to correlate specific findings to natural conditions. Later work could focus on this aspect of the experiments. Though for a short time the electron transfer seemed to work in a comparable manner as with the fresh water, it soon reversed its flow direction, indicating that manganese ores were no longer being reduced/dissolved, but stabilized instead through oxidation processes. This occurred despite the behaviour of the pH, which quickly became very low (3.77 in test cell, 3.45 in filtered sample).

After the test the solids were washed to remove sea salt, dried and then analyzed by chemical and physical methods. The chemical analyses provide no evidence for any significant mineralogical changes in the rock samples, but some very faint peaks in XRD-patterns of the ore indicate early stages of the formation of manjiroite, the sodium analogue to the potassium-carrying cryptomelane, and also an increase in manganese oxide crystallinity (Fig. 7.8a). A maturation of the kaolinite is also observable in some of the main peaks (Fig. 7.8b). The fact that both clay and ore minerals develop well defined lattices, instead of being dissolved, is supported by a strong increase of the infrared absorbance patterns of the two reaction products. There is no significant change in the position of the FTIR-peaks, which would indicate the existence of new minerals.

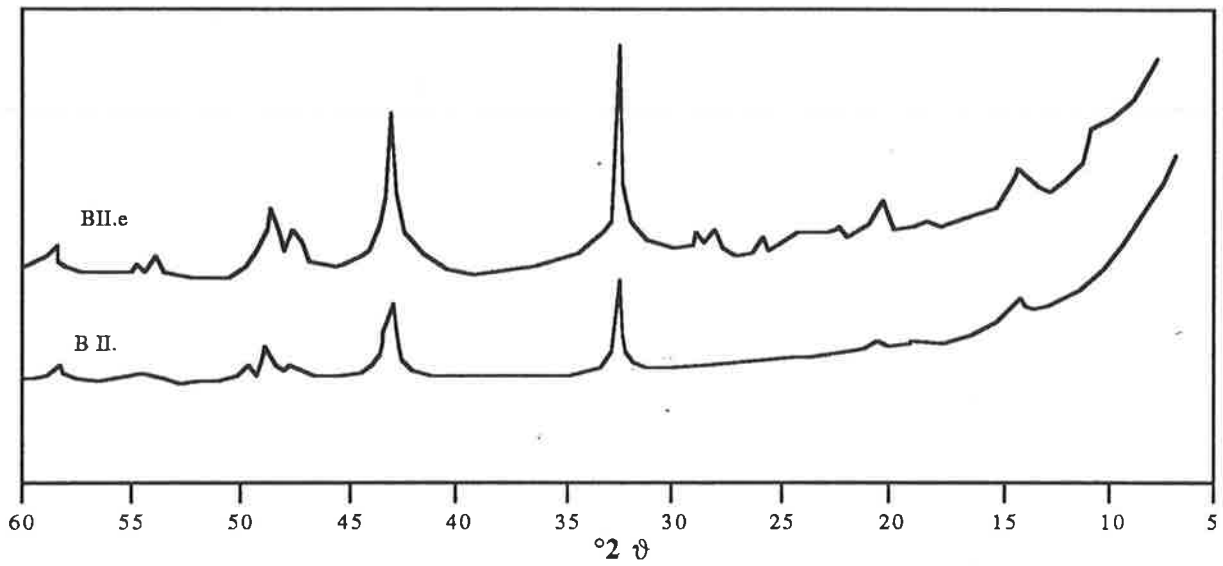


Fig. 7.8a: X-ray diffraction pattern of Mn oxides; B II. = initial sample, B II.e = after 7 weeks; sample prefix: 903.

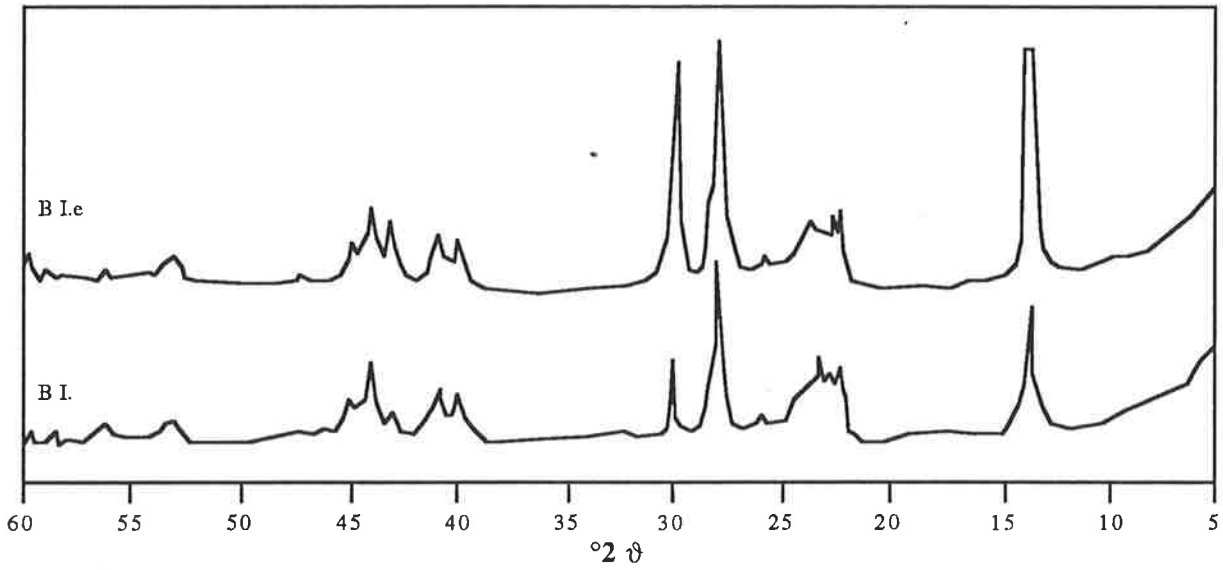


Fig. 7.8b: X-ray diffraction pattern of kaolinite; B I. = initial sample, B I.e = after 7 weeks; sample prefix: 903.

7.4 Discussion

This chapter illustrates that it is possible to duplicate the redox reaction between kaolinitic clays and manganese dioxides under controlled conditions in the laboratory. Though the experimental setup was based on a relatively simple closed system, in contrast to the open system in the field, it can be expected that similar conditions prevail on a small scale in the orebody and in the adjacent laterites. Future investigations should examine different materials and changing conditions. Additions to the cell that allow a continuous water exchange or the variation of the oxygen content of the water, could be used to study the development of laminar mangcretes in pipes.

The initial large increase of dissolved elements that specifically derive from manganese oxides demonstrates that the redox reaction is a driving force for reduction of the ores. This mobilization occurs in cycles which probably depend on the thermodynamic stability of the different Mn minerals that are present, and which break down successively (see mV/time curve, Fig. 7.4). Iron, being oxidized during the reaction, remains constantly below the detection limit in the cell water. This finding is supported by the detection of brown iron oxihydroxide precipitates near the Mn chamber of the cell and on the electrode itself. Iron continually consumes oxygen and when its availability ceases, divalent manganese is increasingly oxidized. This is indicated by a strong overall loss of oxygen from solution (see Fig. 7.5). The concentration levels of most elements in the water also decrease after a while, thus indirectly confirming precipitation processes. Zinc, however, increases until the end of the experiments, probably because of conditions that exclude this element from incorporation into the lattice of existing or newly forming minerals.

Parallel to the reduction of the Mn oxides a smaller amount of kaolinite ($Al_2Si_2O_5(OH)_4$) initially also dissolves, with Si being far more dominant in solution than Al. Under an acidic regime, kaolinite alters to gibbsite ($Al(OH)_3$) by loosing a silicon sheet from its lattice (Birkeland, P.W., 1974). The hydrochemistry of the cell seems to back up this fact, but the mineralogical analyses do not confirm it. Obviously, the time of the experiments was not sufficient for a total mineralogical change, and some of the alterations may have reversed when the conditions changed in the later stages of the tests. Successively, kaolinite precipitates within the ore compartment. This appearance in place of the ore can often be found in the field, where manganese oxides are being replaced by goethite and kaolinite.

The general impression gained from the mineralogical analyses of the remaining materials after the tests is that the manganese oxides mature, as shown by an increase of crystallinity. Recrystallization processes also seem to favour pyrolusite at the expense of less stable oxide phases, despite the availability of sufficient cations. On the other hand, the kaolinite samples do not exhibit indications for new minerals, though small variations in XRD and FTIR patterns occur. Similarly, kaolinite is preferentially formed under the natural conditions at Groote Eylandt, as demonstrated by its strong dominance over other clay phases.

An improved maturation of the minerals was observed in the salt water experiment, which probably is due to the growing thermodynamic stability of the ores and clays in the alkaline medium. It is not known, how far kaolinite was involved in the drastic drop of pH in these tests. However, Zachara et al. (1988) showed that the tendency of kaolinite to adsorb anions, such as SO_4^{2-} or Cl^-, increases with decreasing pH values. An auto-catalytic effect, where adsorption of initially small amounts of the mentioned anions leads to a lower pH, could indeed trigger an increasing removal of these compounds from the solution. Whether this is the case or not, was not the objective of this study and has not been determined.

However, another mechanism discussed by Balzer (1982) may provide an answer to this question. He reported experimental studies of Mn and Fe solubilities at the water/sediment interface of the western Baltic Sea. His data are in many aspects similar to the present seawater experiment. The redox potential measured *in situ* dropped from initially +600 mV to -300 mV, oxygen became dedepleted, and the pH also decreased towards more acidic values (from 8.3 to 7.5). Balzer explains these geochemical changes with sulfate reduction processes exerting control over anoxic conditions; redox couples are in this case either SO_4^{2-}/HS^- or SO_4^{2-}/S^0. Sulfate was not determined in the test solutions and it is therefore unknown whether this reaction also occurred in the battery-cell.

Nevertheless, whatever process finally dominated the saltwater system, kaolinite with its small Fe^{2+} content acted as an electron donator for a short time until other reactions proved to be stronger. Therefore, it can be assumed that even in a nearshore marine environment the redox reaction may contribute to a short-term mobilization of manganese and other elements, if kaolinite is available through riverine sediment input.

8. Origin of Supergene Manganese Deposits

8.1 Introduction

A number of aspects of the development of supergene manganese deposits were examined in previous sections, but processes that mobilize or precipitate Mn oxides were not fully analyzed, and the driving forces were not discussed. In view of the fact that runoff from the Groote Eylandt deposit causes an accumulation of many elements in the sea surrounding the island (atomic numbers > 20), it appears that all major ore and rock types contribute to this enrichment, and therefore, supergene mechanisms need a careful assesment as to their ability to alter primary ores. The dominant type of alteration also determines the strength of overprint and if it is possible to discern some of the main mobilization processes, it is much easier in geochemical exploration to identify the best target area.

In this chapter a detailed discussion is given on dissolution, transport, and precipitation processes, including their "supergene alteration potential". The main gangues associated with the deposit are examined first, because some liberation and fixation processes of these rocks have direct implications for the formation or destruction of manganese ores, and a discussion of these initial conditions is vital for the understanding of more complex geochemical, mineralogical, and biological reactions.

Thermodynamic data for the theoretical calculations are taken from Bricker (1965), Robie and Waldbaum (1968), Robie et al. (1978), Hem and Lind (1983), and from the Handbook of Chemistry and Physics (1976). Theoretical stability conditions were calculated on the basis of the maximum concentration of the respective element in water samples to determine the type of naturally occurring ionic species, to examine the oversaturation of ions relative to minerals, and to analyze phase stabilities. Generally, the thermodynamic determination of the stability of minerals and dissolved ionic species focuses on the main phases expected for the given natural

conditions. The more "exotic" compounds are not discussed here, although many were examined for possible interactions. In cases of polymorphy, such as for MnO_2 (α = cryptomelane, β = pyrolusite, γ = nsutite, δ = birnessite), the most stable mineral is used to represent the entire group. The less stable phases usually appear within the stability fields of the respective dominant mineral.

8.2 Evidence of Supergene Activity

The formation of many materials in the deposit has been interpreted to be related to supergene processes on the basis of cross-cutting relationships between ore and rock units, replacement features, and the distribution of trace elements. Other direct evidence for secondary mobilization and precipitation comes from K/Ar dating of glauconite, found immediately below the orebody and from paleontologic data. These data show that the ores are probably of Cenomanian age (~95 Ma; Smith et al., 1965; Taylor, 1979, 1980; Amdel, 1981). Ages younger than Cenomanian therefore suggest supergene alteration.

Cryptomelane (K-rich) is the main supergene product at Groote Eylandt and it is present in most samples. Five samples consisting predominantly of cryptomelane were selected for K/Ar dating. The initial examination was of an experimental nature (Amdel, 1986), because this mineral had not been dated previously. In addition to these and further age determinations (Amdel, 1987), four manganese oxide samples from Groote Eylandt were examined by Varentsov and Golovin (1987), who used the same technique (all samples are represented in Fig. 8.1 and Table 8.1).

The data demonstrate that the cryptomelane of the examined samples is much younger than the deposit itself, despite the primary structures that prevail in pisolite samples or hardgrounds. No cryptomelane-age in excess of 41.5 Ma was identified, which is approximately half of the age of the primary ore. One pyrolusite-rich sample from Varentsov and Golovin that contained detrital material, was dated at 168 Ma. In this case, the obtained age is not directly related to the supergene material. However, it is demonstrated below that even this "deviating" result has implications for the analysis of some of the other data.

The fact that all cryptomelane analyses point to the relatively short time interval from about 21 to 41 Ma (early Miocene to late Eocene) indicates that a strong alteration of the deposit occurred at this time. Obviously, the climatic conditions of this period significantly enhanced alteration processes operating on the early manganese precipitates. Although no ages younger than 21 Ma were detected, it is shown later in different context that supergene alteration processes continue to be active at Groote Eylandt, and that secondary ores and rocks form in the present geochemical environment.

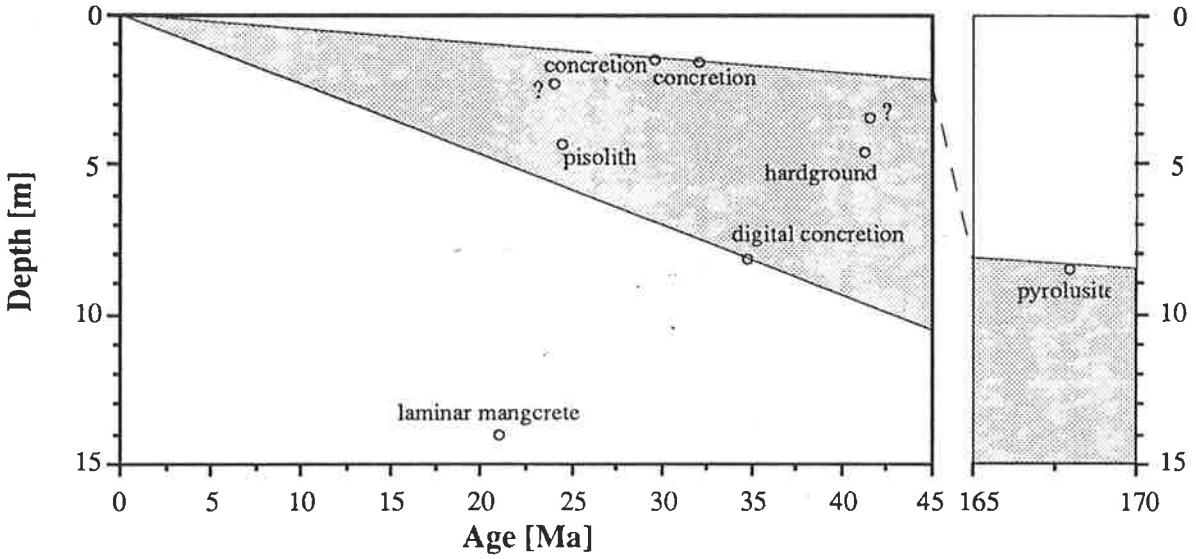


Fig. 8.1: K/Ar age distribution of manganese oxides versus stratigraphical position of samples; own data and data from Varentsov and Golovin (1987); upper limit: y = -0.049405x; lower limit: y = -0.23362x.

Table 8.1: Results of K/Ar-Age determinations on cryptomelane-rich samples; except for sample 13 (pyrolusite) which is shown for comparison.

No.	Ore Type	Location	Depth [m]	Age [Ma]
903-78b	hardground	G	4.6	41.3 ± 0.8
903-85	large pisolith	G	4.3	24.5 ± 0.5
903-164	digital concretion	G	8.1	34.8 ± 0.0
BB66150	concretion	A-S	~1.5	29.6 ± 0.2
24*	concretion	A-S	~1.5	32.0 ± 0.4
21*	?	A-S	~3.5	41.5 ± 0.5
13*	pyrolusite	A-S	~8.2	168.0 ± 20.0
903-252	laminar mangcrete	F3	~14.0	21.0 ± 0.2
27*	?	E-NW	~2.3	24.0 ± 1.0

Prefix 903 and BB = own data; prefix BB = sample from B.R. Bolton; *afterVarentsov and Golovin (1987).

Generally, the data scatter widely when plotted against the sample depth, although an overall age increase with increasing depth can be observed (Fig. 8.1). Since the sample set is very limited, it is difficult to state how representative the analyses are. Nevertheless, the data depict two major trends and one sample with a large discrepancy:

- "pure" samples with little or no contamination by detrital minerals such as clays; the materials possess a larger depth gradient than the other samples and they plot at the lower boundary of the shaded field (isolated pisoliths, digital concretions);
- samples that contain detrital products are strongly affected by ages deriving from these inclusions, with sample 13 of Varentsov and Golovin as the best example which should not contain potassium, because it is predominantly composed of pyrolusite; the age of this sample group increases together with increasing contamination and thus, the depth gradient is smaller than before and the ores plot near the upper boundary of the shaded area (interpolated until sample 13);
- laminar mangcrete seemingly appears far below all other samples; it must, however, be recalled that this ore type develops at the wall of drainage pipes, and therefore, the oxygen availability is comparable to conditions near or at the surface; thus, the age is independent of the sample depth of such materials.

If the interpretation above is correct, and the findings reflect the natural conditions of the samples with variable contaminant concentrations, then samples with no admixed detrital materials (near lower limit) can be used to re-calculate other ages (Table 8.2). Sample 903-164 was examined under the microscope and with the exception of occasional quartz grains the sample consists of dense cryptomelane. Therefore, it is probably the most suitable supergene product of the ores under investigation to use as calibration standard.

Table 8.2: Re-calculated K/Ar ages of Table 8.1.

No.	Age [Ma]	$Age_{corr.}$ [Ma]
903-78b	41.3	19.6
903-85	24.5	18.5
903-164	34.8	34.8
BB66150	29.6	~6.4
24*	32.0	~6.4
21*	41.5	~15.0
13*	168.0	~(35.1)†
903-252	21.0	(21.0)††
27*	24.0	9.8

*samples from Varentsov and Golovin (1987); †pyrolusite-rich sample; ††laminar mangcrete not corrected.

The corrected data illustrate variations from recent geological times (~6 Ma) to ages of approximately 35 Ma. This is consistent with the present knowledge that a lateritic alteration of the Groote Eylandt deposit is currently active, and that the supergene overprint must have worked over a considerable length of time to produce the large secondary ore units. The uncorrected data on the other hand possess an age gap of some 20 million years. Younger supergene products have not been identified, despite an ongoing alteration of the ores. The re-calculated data thus account for a crucial part of the geological history of the deposit,

whereas the initial analyses of both sample sets imply that during the past 20 million years no further supergene ores have formed. Laminar mangcrete has not been corrected, as this ore type has almost unique formation conditions. Its direct contact to aerated meteoric water classifies it as a surface material which may be very young, an incorporation of kaolinite (K-carrier) additionally complicates a correct K/Ar age determination.

In a general sense, both the raw data and the corrected values show a broad tendency of increasing sample ages with increasing depth, with the youngest ores at the top of the deposit. Since mobilization and reprecipitation processes occur most commonly in higher parts of the stratigraphic profile, due to water abundance, temperature, and organic activity, the supergene products here are recycled continuously and must, therefore, reflect the lowest values.

The close agreement between the two data sets demonstrates that K/Ar dating of cryptomelane provides reproducable results. Further studies should evaluate differences between various secondary ore types to identify materials most suitable for age analysis, the role of different detrital minerals such as kaolinite or other Mn oxides in producing erroneous data should also be investigated. Nevertheless, all analyses demonstrate that the deposit underwent a strong alteration which probably overprinted most, if not all ores. Therefore, it is necessary to look in detail at mobilization and precipitation processes. An understanding of these supergene mechanisms should reveal the nature of processes that dominate at Groote Eylandt.

8.3 Mobilization Processes

8.3.1 Dissolution of Quartz, Kaolinite, and Gibbsite

Quartz, gibbsite ($Al(OH)_3$), and their hydrated forms are closely associated with soils, laterites, and bauxites. Numerous combinations of ionic compounds result in various clay minerals, depending on the geochemical environment. Under the present tropical/subtropical conditions at Groote Eylandt, kaolinite is obviously the most stable phase and it strongly dominates over all other clay minerals in the laterite profile. Montmorillonite and nontronite were found recently (pers. commun. B.R. Bolton, 1986; H. Berents, 1989), but are of subordinate importance. The latter clays are not incorporated into the calculations and plots because of their scarcity. Although gibbsite has been described at Groote Eylandt, this mineral is also rare in the deposit and is considered here as an intermittent unstable phase. However, gibbsite stabilities are examined to determine the major dissolved Al-species.

Many previous studies indicate that kaolinite and quartz interact in many ways with associated minerals, although they are often regarded as relatively immobile phases. It has, for instance, been illustrated that both quartz and kaolinite invade the manganese orebody through

pipe systems, that kaolinite replaces ores and rocks, and that quartz is replaced by manganese. This, and the fact that solutions sampled from various localities of Groote Eylandt carry dissolved Si and Al, clearly implies that these two minerals are mobilized in the present geochemical environment.

8.3.1.1 Thermodynamics of Si-Al-H_2O Systems

Fresh- and seawater samples are plotted in the SiO_2-H_2O system, which is described by Eqs. (8.1-3) (Fig. 8.2a). All results plot in the H_4SiO_4 field and they are slightly undersaturated with respect to quartz. Towards higher pH values (seawater) the concentrations decrease and trend parallel to the $H_4SiO_4/H_3SiO_4^-$ boundary. The samples thus indicate an increasing removal of dissolved silica from solution in contact seawater. If this were not the case, silica would continue its trend parallel to the SiO_2/H_4SiO_4 interface. The only hydrated silica compound detected in this diagram is H_4SiO_4.

$$SiO_2 + 2\,H_2O \Rightarrow H_4SiO_4 \quad (8.1)$$

$$SiO_2 + 2\,H_2O \Rightarrow H_3SiO_4^- + H^+ \quad (8.2)$$

$$H_4SiO_4 \Rightarrow H_3SiO_4^- + H^+ \quad (8.3)$$

The stability fields of gibbsite and dissolved species are determined by Eqs. (8.4-6b). Although the Al concentrations of many samples are below the detection limit, the remaining analyses demonstrate that the speciation of alumina is more versatile than that of silica (Fig. 8.2b). Al^{3+} and $Al(OH)_2^+$ dominate in waters associated with the deposit (ore, laterite, river), whereas $Al(OH)_4^-$ seems to gain importance with increasing alkalinity at the river mouth and in the sea. Although $Al(OH)_4^-$ cannot be represented properly because only one sample is above the detection limit, the pH of these waters indicates that $Al(OH)_4^-$ is present, if these samples contain any alumina.

$$Al(OH)_3 + 3\,H^+ \Rightarrow Al^{3+} + 3\,H_2O \quad (8.4)$$

$$Al(OH)_3 + H^+ \Rightarrow Al(OH)_2^+ + H_2O \quad (8.5)$$

$$Al(OH)_3 + H_2O \Rightarrow Al(OH)_4^- + H^+ \quad (8.6a)$$

$$Al(OH)_3 \Rightarrow AlO_2^- + H_2O + H^+ \quad (8.6b)$$

(not plotted, parallel to (8.6a) and slightly below)

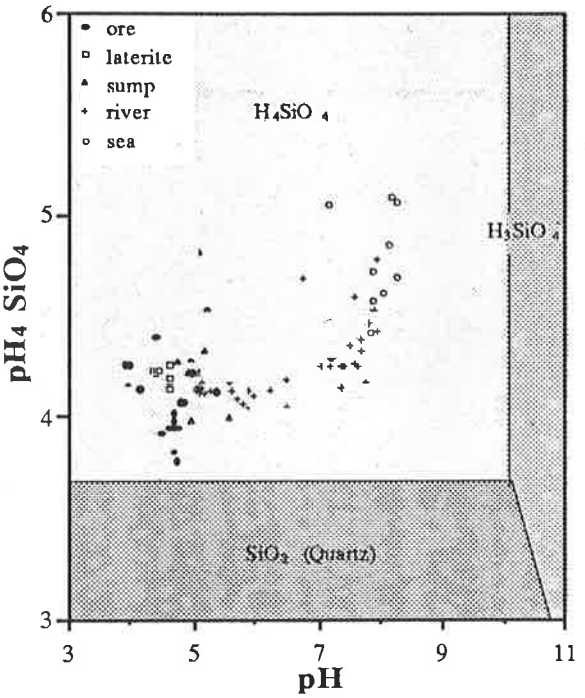


Fig. 2a: Thermodynamic stability of silica compounds in aqueous systems.

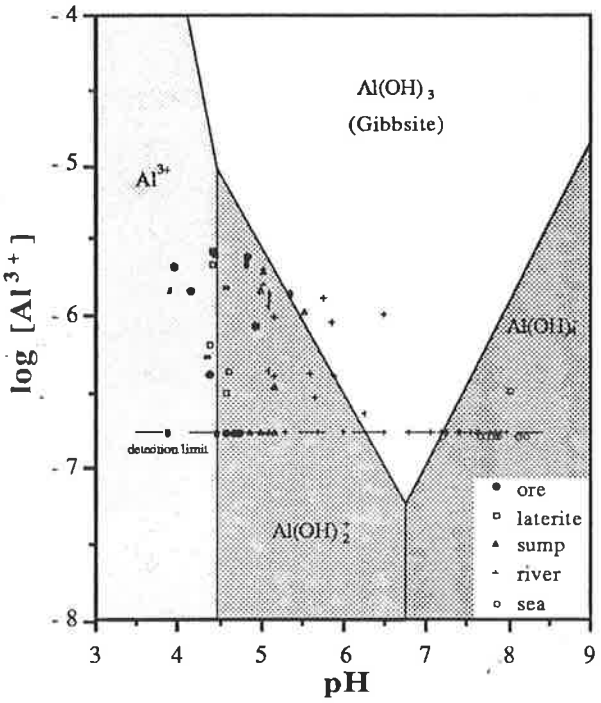


Fig. 2b: Thermodynamic stability of alumina compounds in aqueous systems.

In addition, some analyses fall within the gibbsite stability field. This means that in a pure Al-H_2O system this mineral precipitates. In mixed chemical systems however, which for instance contain dissolved silica, other phases form. For the composition of the waters in this study, kaolinite or montmorillonite (Mg-carrying seawater) are the most likely clay minerals to develop. To approximate a diagram with general applicability that includes quartz, gibbsite, and kaolinite, it is assumed here that all dissolved alumina species are represented by Al^{3+}. All hydrated silica is considered to be equivalent to H_4SiO_4 (Eq. 8.7a).

$$Al_2Si_2O_5(OH)_4 + 6\,H^+ \Rightarrow 2\,Al^{3+} + 2\,H_4SiO_4 + H_2O \quad (8.7a)$$

$$Al_2Si_2O_5(OH)_4 + 5\,H_2O \Rightarrow 2\,Al(OH)_3 + 2\,H_4SiO_4 \quad (8.7b)$$

According to the phase relationships, mineral couples form which explicitly exclude the coexistence of three or more minerals (Kittrick, 1969). Thus, the following mineral pairs are possible in the system Si-Al-H_2O: quartz/kaolinite and kaolinite/gibbsite (Fig. 8.2c). Amorphous silica and montmorillonite are not considered, because their stability boundaries are above the observed H_4SiO_4 concentrations. Analyses that plot above or to the left of the mineral stability lines are supersaturated relative to the respective phase, whereas samples below or to the right are undersaturated.

The samples cover a wide range above the kaolinite boundary and only very few data from seawater plot above the gibbsite stability line. This suggests that in the Si/Al group of minerals, kaolinite is the main phase to take part in remobilization processes. Nevertheless, small quantities of hydrated silica compounds deriving from dissolved quartz may be masked by the higher abundance of silica originating from kaolinite. Waters from the orebody indicate an increasing influence of dissolved quartz, because some of these samples plot near the stability line for quartz. Those waters that show a supersaturation in respect to gibbsite are alkaline seawaters that probably precipitated aluminosilicates, thus causing a shift towards gibbsite.

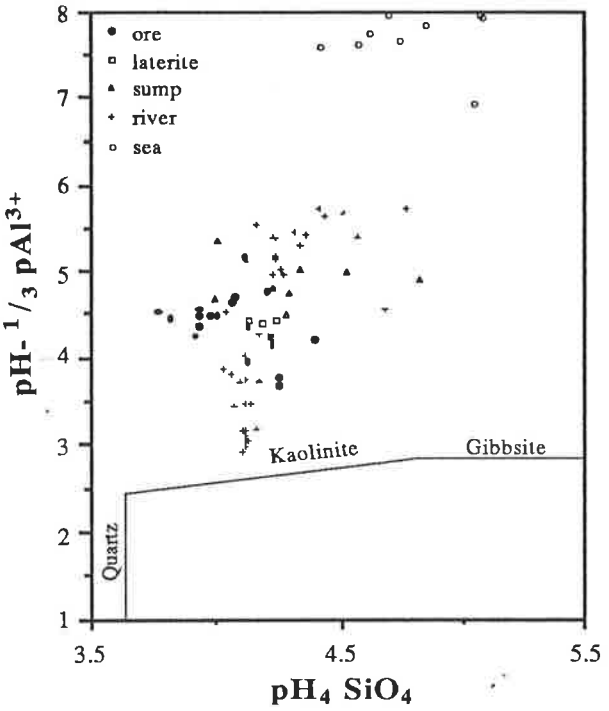


Fig. 2c: Thermodynamic stability of quartz, kaolinite, and gibbsite in aqueous systems.

The mobilization products from quartz and kaolinite and the pH provide the basic tools for an understanding of the weathering processes (Figs. 8.2a-c). It was demonstrated that natural pH variations do not change the dissolved silica species (H_4SiO_4), that mobilized alumina is dominated by one compound ($Al(OH)_2^+$), and that almost all water samples indicate a mobilization from kaolinite (Fig. 8.2c). It was also shown that the pH is predominantly acidic, with the exception of seawater and some river waters that are influenced by a tidal input of saltwater. Therefore, the discussion focuses on dissolution processes associated with relatively low pH values.

The mobility of quartz is constantly very low over a large pH range (Kittrick, 1969) and thus, variations in pH most probably do not play a direct role in the dissolution of this mineral. Also, quartz does not contain structural water, which makes dehydration and destabilization processes ineffective. Mechanisms that form unstable inorganic or organic complexes are much more likely to mobilize quartz under lateritic conditions (see 8.3.1.2 and 8.3.1.3). Alumina on the other hand, strongly reflects the geochemical environment in which it occurs through the formation of pH dependent ionic species. Since the groundwaters of the deposit are acidic, gibbsite is highly unstable in most places (Eqs. 8.4-5). This finding is also supported by the scarcity of this mineral at Groote Eylandt.

Similarly, a pH control over the dissolution of kaolinite also seems to be insignificant; the water samples depict only small variations within a large pH range. Probably, much more

effective in the remobilization of kaolinite is the dehydration of this mineral. The breakdown of kaolinite involves the initial removal of a silica sheet from its structure (Birkeland, 1974) and successive dissolution of the remaining gibbsite under the acid regime (Eq. 8.7b). That both steps occur is demonstrated by most samples, in that they concentrate above the kaolinite stability field (Fig. 8.2c). If, for instance, the second step in kaolinite dissolution did not take place, then the samples would plot above the gibbsite stability field (low H_4SiO_4 activity), and gibbsite would appear more frequently in the deposit.

8.3.1.2 Complexation of Quartz by Fe and Mn

Iron (or manganese) phases and quartz seem to be so different in their chemical and mineralogical characteristics that reactions affecting the two would appear to be irrelevant. However, Morris and Fletcher (1987) were able to demonstrate that ferrous iron may form an ephemeral microlayer of ferrous silicate on the grain surface of quartz. Surface or near-surface seasonal variations that result in more oxidizing conditions break down the complex, mobilizing silica in quantities far in excess of normal silica solubility, and replacing it with goethite.

How far comparable reactions apply for kaolinite is not known, but this mineral may also be sensitive to such replacement processes, because its structure contains silica layers that might develop similar complexes. An indication of the possible formation of these compounds might be seen in the small Fe^{2+}-concentrations of most kaolinite samples. If this is the case, then it could mean that kaolinite also disintegrates faster than simple thermodynamic considerations would allow.

Another possibility for the destabilization of quartz and kaolinite is seen in some of the supergene manganese ores. A regular feature of siliceous ores and Mn-impregnated sands is the replacement of quartz grains by manganese oxides (see Plate 3.5, Fig. 3.13d; also Ostwald, 1988). Vermiform kaolinite can also be observed to be replaced by Mn phases (Plate 3.2, Fig. 3.4c). These findings strongly point in the same direction as the iron replacement reactions above, particularly since the chemical properties of Fe and Mn are very similar in many aspects.

8.3.1.3 Organically Induced Kaolinite Dissolution

It is uncertain how far microorganisms, such as bacteria, take part in the destabilization of kaolinite in the Groote Eylandt laterite. Bacteria undoubtedly are resident in the deposit, because the rocks and ores are not isolated and sterile, but the availability of microorganisms may vary considerably laterally and vertically within the stratigraphic section. Thus, it is difficult to determine the overall efficiency of an organically induced breakdown of kaolinite.

It has been demonstrated that bacteria are able to reduce octahedral Fe^{3+} to Fe^{2+} in clay minerals (Stucki et al., 1987; Wu et al., 1988). This process is accompanied by a partial or total collapse of the kaolinite structure. This leads to a general increase of the pH and in turn, the precipitation of other minerals is favoured. Near the surface, other organogenic processes may include:

- the degradation of kaolinite through interaction with the metabolic products of microorganisms (McFarlane and Heydeman, 1985; Heinen, 1979; Silverman, 1979),
- the change of soil properties by filamentous algae and fungi (Bond and Harris, 1964), or
- the formation of organo-clay complexes cementing sand grains (Tazaki et al., 1989).

This incomplete list of microbially induced destruction of minerals includes some processes which involve a direct interaction with the environment via the production of organic acids, which lowers the pH. Also, siliceous or aluminous organic complexes can develop under special conditions. Once the physico-chemical parameters of the accompanying solutions change, the compounds break down and dissolve. Such a destabilization of inorganic/organic complexes most likely releases much higher element quantities into the water system, than "normal" pH variations could induce. Therefore, the formation of complexes is probably more effective in the remobilization of clays and quartz. The successive breakdown of these complexes results in the development of more alkaline conditions.

8.3.2 Dissolution of Iron Oxyhydroxides

The laterites at Groote Eylandt indicate that iron is mobilized within the rock and transported to other locations, where it either precipitates directly or takes part in redox reactions (see following section). The remobilization often occurs on a small scale, resulting in mottled materials with dark brown ferruginous patches and light parts dominated by kaolinite. Dissolved Fe also occurs in water samples from various localities, thus supporting the observation that iron is mobile under certain conditions. It was mentioned earlier that the deposit is practically devoid of minerals such as sulfides that could strongly influence Eh/pH conditions during their own breakdown. Therefore, less potent processes must be present that are still able to liberate iron. Such mechanisms may include small-scale Eh/pH variations or a biologically controlled reduction.

8.3.2.1 Thermodynamics of the Fe-H_2O System

Goethite dominates in the deposit, but from thermodynamic considerations it is certain that the mineral is an alteration product of initially amorphous or poorly crystalline precipitates, such as

iron hydroxide or ferrihydrite. Hematite plays a subordinate role, although frequent stains in many rocks seem to suggest a larger importance. The remaining Fe minerals reported from Groote Eylandt, such as siderite, vivianite, and pyrite, only occur as traces in one particular area (G-Quarry; Ostwald, 1988), and they are not discussed further here. For the majority of ferruginous rocks in the deposit, carbonate, phosphate, and sulfide activities are negligible and they are thus not considered in the following phase stability diagrams.

Iron occurs both in divalent and trivalent ionic forms, from which Fe^{2+} is stable over a much larger Eh and pH range than Fe^{3+}. The extended stability of divalent Fe and the strong dominance of the goethite precursor ($Fe(OH)_3$), are thus the main factors to be examined in the following section. The highest detected Fe concentration from all water samples (0.083 ppm) was used for the calculation of the stability diagrams. Therefore, the stability of iron minerals is minimal in the diagrams, whereas dissolved iron is at its maximum. The equilibria of all examined iron redox couples and the stability boundaries for water are given below (Eqs. 8.8-14 and 8.15-16, respectively).

Data from water samples cannot be plotted in Eh/pH diagrams, because there is no information on the natural Eh conditions of the deposit. However, this type of diagram can be examined on a theoretical basis to determine the general stability of the two major phases (Fig. 8.3a). The stability fields of Fe^{2+} and $Fe(OH)_3$ are approximately equal in size, although the boundaries were calculated for the maximum amount of dissolved iron. Since most samples are less

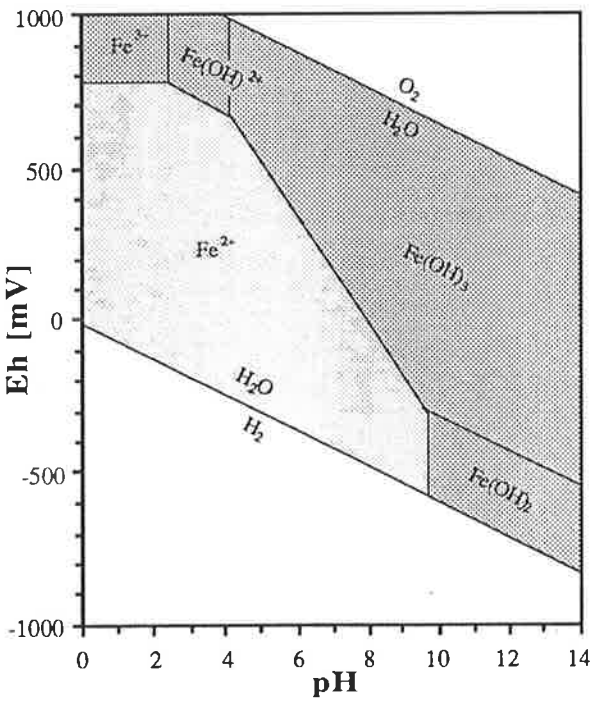


Fig. 3a: Thermodynamic stability of Fe compounds in aqueous systems.

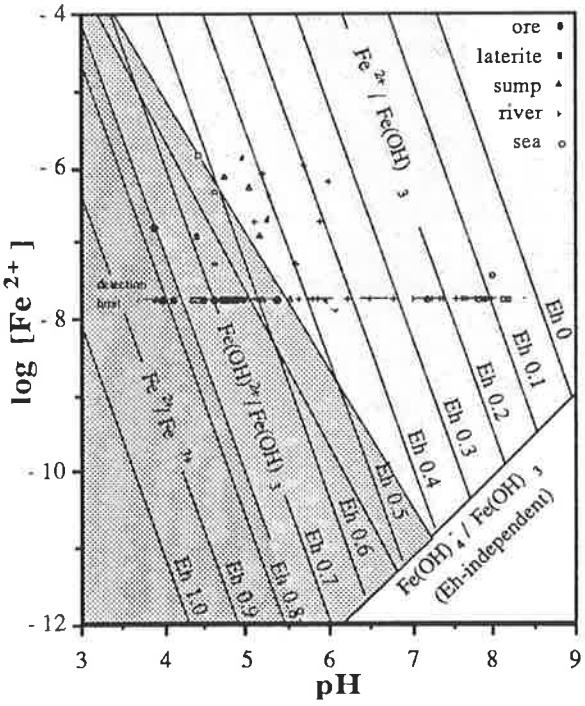


Fig. 3b: pH-controlled ionic species of Fe in aqueous systems.

concentrated, many fall below detection limit; the stability of $Fe(OH)_3$ is generally larger and it dominates over all other iron phases. This means that under natural conditions iron mobility is restricted to a relatively acid geochemical environment.

$$Fe^{3+} + e^- \Rightarrow Fe^{2+} \quad (8.8)$$

$$Fe(OH)_2 + 2\,H^+ \Rightarrow Fe^{2+} + 2\,H_2O \quad (8.9)$$

$$Fe(OH)_3 + 3\,H^+ + e^- \Rightarrow Fe^{2+} + 3\,H_2O \quad (8.10)$$

$$Fe(OH)^{2+} + H^+ + e^- \Rightarrow Fe^{2+} + H_2O \quad (8.11)$$

$$Fe(OH)^{2+} + H^+ \Rightarrow Fe^{3+} + H_2O \quad (8.12)$$

$$Fe(OH)_3 + 2\,H^+ \Rightarrow Fe(OH)^{2+} + 2\,H_2O \quad (8.13)$$

$$Fe(OH)_3 + H^+ + e^- \Rightarrow Fe(OH)_2 + H_2O \quad (8.14)$$

$$2\,H_2O \Leftrightarrow O_2 + 4\,H^+ + 4\,e^- \quad (8.15)$$

$$H_2 \Leftrightarrow 2\,H^+ + 2\,e^- \quad (8.16)$$

When plotted in a pH/concentration diagram, the samples fall near the boundary, indicating a strong association with the field of Fe^{2+} mobilized from $Fe(OH)_3$ (Fig. 8.3b). However, some water samples appear in the $Fe(OH)^{2+}/Fe(OH)_3$ field or even in the area of Fe^{2+}/Fe^{3+}. This can be explained by precipitation processes resulting in an overall decrease of the Fe concentration, which, at a constant pH, leads to a change of the ionic species. Since goethite dominates in the deposit over other iron minerals, and its stability field is comparable to that of $Fe(OH)_3$, it can be expected that it is the main iron phase to release Fe^{2+} into solution.

8.3.2.2 Dependency of Fe Minerals upon Kaolinite Stability

The most common mineral of the laterite is kaolinite and the data suggest that within the Al-Si-H_2O system this mineral is the most mobile (compare Fig. 8.2c). Therefore, its equilibrium reaction is again examined in context with the relevant reaction for iron (Eqs. 8.7a and 8.10).

$$Al_2Si_2O_5(OH)_4 + 6\,H^+ \Leftarrow 2\,Al^{3+} + 2\,H_4SiO_4 + H_2O \quad (8.7a;\ rep.)$$

$$Fe(OH)_3 + 3\,H^+ + e^- \Rightarrow Fe^{2+} + 3\,H_2O \quad (8.10;\ rep.)$$

The equations demonstrate that during the formation of kaolinite the conditions in the vicinity of the precipitate become more acidic, the equilibrium shifts from the right side of the reaction towards the left. This means in general terms that the geochemical environment supports the remobilization of ferruginous minerals, and that parallel to this process kaolinite can replace the

dislocated iron. This Fe mobilization is evident in most parts of the deposit where kaolinite and goethite are associated, and the physical appearance of the reaction products obviously supports the theory (Plate 3.6, Fig. 3.16b,c). Although such replacements are discussed later, it must be mentioned here that this mechanism of kaolinite precipitation and Fe reduction is vital for the existence of supergene manganese dissolution.

8.3.2.3 Biological Reduction of Fe Phases

Among biogenic reactions in which organisms gain part of their energy needs from interacting with iron minerals, most processes result in the oxidation of ferrous compounds to ferric phases (MacDonald and Clark, 1970). However, Woolfolk and Whiteley (1962) demonstrated that enzymic reduction of Fe^{3+} by bacteria can occur under natural conditions and that the enzymes involved in these reactions are widely distributed in soils. Therefore, it is likely that bacteria and other microorganisms take part in the solubilization of Fe in the deposit. Unfortunately, few studies focus on this subject and it is difficult to assess the overall importance of the biota.

Mercz and Madgwick (1982) showed that Mn reducing capabilities of microorganisms are enhanced by the addition of organic nutrients (e.g. decomposing leaf litter). Thus, humic compounds may be more important as substances sustaining biological processes than as direct Eh/pH regulators. How far this mechanism can be transposed onto the Fe reduction process is unclear, but comparable reactions could be expected (Shafia and Wilkinson, 1969), because iron and manganese have similar chemical characteristics. Release of divalent iron from pyrite in the presence of bacteria has also been described by Hiltunen et al. (1981), but as sulfide minerals are extremely rare at Groote Eylandt, this process is not discussed further.

8.3.3 Dissolution of Manganese Oxides

A number of chemical reactions can reduce/dissolve tetra- and trivalent manganese oxides under natural conditions. These minerals have long been considered to be very stable in oxygenated waters, and only to become unstable under anoxic conditions in the presence of reducing agents. The presence of extensive secondary ore units examined in previous chapters clearly illustrates that large quantities of manganesewere available for alteration to supergene materials. As the ores of the Groote Eylandt manganese deposit are highly oxidized, the following discussion focuses on the tetravalent oxides. Lower valency Mn minerals are only mentioned where appropriate although they may have played an important role in the early history of the deposit.

8.3.3.1 Thermodynamics of the Mn-H_2O System

As mentioned above, manganese oxides are generally highly insoluble in aqueous solutions. However, under certain conditions the solubility of these minerals can increase considerably. Hem (1978) demonstrated that the only significant dissolved Mn species in natural systems are divalent ionic forms. As carbonates are practically absent in the deposit, the $MnHCO_3^+$ complex and rhodochrosite ($MnCO_3$) stabilities are not examined in the following diagrams. The stability fields of major ore minerals are determined only in context with Mn^{2+}. Where applicable, the highest detected concentration of dissolved manganese (0.672 ppm) was used to calculate boundaries. This produces a minimal size for the mineral stability fields and a maximum area for dissolved Mn.

Unfortunately, no Eh-values for the water samples from Groote Eylandt are available. Thus, the data cannot be plotted in Eh/pH-diagrams and it is not possible to determine whether Eh/pH variations are important for the reduction of ore minerals. Nevertheless, minerals such as sulfides that could strongly influence these parameters through their own breakdown (e.g. formation of sulfuric acid) are generally absent, and this seems to largely exclude a mineralogy driven control over the pH ((Eq. 8.17); Burdige and Nealson, 1986).

Generally, the thermodynamic stability fields for manganese oxides and hydroxides become relatively small when the maximum Mn concentration of Groote Eylandt waters is used for the calculation ((Eqs. 8.17-23); Fig. 8.4a; Morgan and Stumm, 1965, Dubinina, 1973; Crerar and Barnes, 1974). This means that at almost all pH values of the samples the minerals are unstable for a wide range of Eh conditions. However, many samples possess concentrations far less than those used in the diagram, and this leads to a considerable increase of the overall stability.

$$MnO_2 + 4\,H^+ + 2\,e^- \Rightarrow Mn^{2+} + 2\,H_2O \quad (8.17)$$

$$MnOOH + 3\,H^+ + e^- \Rightarrow Mn^{2+} + 2\,H_2O \quad (8.18)$$

$$Mn_3O_4 + 8\,H^+ + 2\,e^- \Rightarrow 3\,Mn^{2+} + 4\,H_2O \quad (8.19)$$

$$Mn(OH)_2 + 2\,H^+ \Rightarrow Mn^{2+} + 2\,H_2O \quad (8.20)$$

$$Mn_3O_4 + 2\,H_2O + 2\,H^+ + 2\,e^- \Rightarrow 3\,Mn(OH)_2 \quad (8.21)$$

$$3\,MnOOH + H^+ + e^- \Rightarrow Mn_3O_4 + 2\,H_2O \quad (8.22)$$

$$MnO_2 + H^+ + e^- \Rightarrow MnOOH \quad (8.23)$$

Although the Eh is not known, the data of manganese concentration and pH can be compared with the theoretical Eh-dependent mineral stability areas (Fig. 8.4b; Crerar et al., 1981). Such plots should indicate the range of Eh-values to be expeceted under natural conditions, if Eh and pH were the main driving forces.

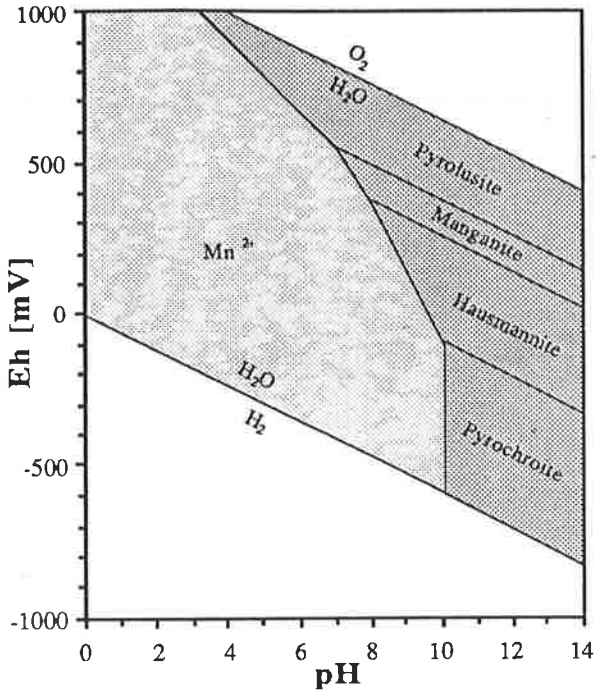


Fig. 4a: Thermodynamic stability of Mn compounds in aqueous systems.

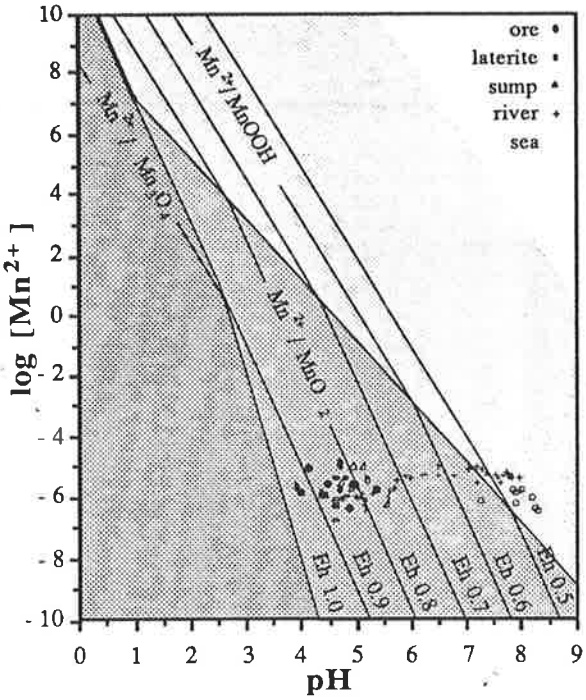


Fig. 4b: pH-controlled ionic species of Mn in aqueous systems.

The majority of the waters plot in a narrow range within the field of divalent manganese which derives from the dissolution of tetravalent oxides (pyrolusite was used for this calculation, cryptomelane and comparable minerals possess a slightly smaller stability area). The diagram clearly demonstrates that much higher Mn enrichments in the solutions are possible, when lower valence minerals are broken down at the encountered pH values. Therefore, the main minerals to dissolve under natural conditions at Groote Eylandt are found in the normally most stable group, the tetravalent manganese oxides, including pyrolusite, cryptomelane, birnessite, nsutite. This does not surprise, because oxides with lower valencies are rare in the deposit.

On the other hand, some samples from the mouth of the Angurugu River and nearly all seawater samples appear in the field of Mn^{2+} mobilized from manganite. This suggests that different types of equilibria develop which lead to successive precipitation of manganite and associated hydroxide minerals. A recalculated version of this diagram is used later to distinguish between different reduction processes.

8.3.3.2 Redox Reactions Between Iron Phases and Manganese Oxides

During the course of study it became obvious that redox reactions between Fe^{2+} and Mn^{4+} are probably the most powerful mobilization processes at Groote Eylandt (Pracejus, 1985). Although these processes are very common in the deposit, they were not recognized and described until recently (Pracejus et al., 1986, 1988). Experimental work examined this type of reaction in detail (chapter 7) and the results are discussed and put into a theoretical framework below. That the process under examination is not confined to tropical/subtropical environments, such as those on Groote Eylandt, was demonstrated by Pracejus (1989), who described supergene replacement products from the Wafangze ferromanganese deposit in northeastern China. Elsewhere, reactions between Co^{2+} and Mn^{4+} may also be important (Hem et al., 1985), but as cobalt is a trace element in Groote Eylandt, it is not considered further.

Aqueous chemical systems that contain either manganese or iron proceed from dissolved ionic species towards more or less ordered solids which precipitate (amorphous, crystalline). Below, the main independent half-cell reactions of Mn and Fe illustrate the processes and compounds (Eqs. 8.17, 8.20, 8.10). Mn^{2+} and $Mn(OH)_2$ oxidize to Mn^{4+} (MnO_2), Fe^{2+} reacts to Fe^{3+} ($Fe(OH)_3$), and all reactions produce free electrons.

$$Mn^{2+} + 2\,H_2O \Rightarrow MnO_2 + 4\,H^+ + 2\,e^- \qquad (8.17;\ \text{rep.})$$

$$Mn(OH)_2 \Rightarrow MnO_2 + 2\,H^+ + 2\,e^- \qquad (8.20;\ \text{rep.})$$

$$Fe^{2+} + 3\,H_2O \Rightarrow Fe(OH)_3 + 3\,H^+ + e^- \qquad (8.10;\ \text{rep.})$$

Thus far, stability considerations for manganese and iron were separated, but it will be demonstrated that as soon as Mn and Fe appear in an aqueous system, they will interact immediately. Then, the "normal" Eh/pH conditions for the stability of tetravalent manganese oxides are no longer valid. Electrons are exchanged with dissolved iron and the reaction of manganese reverses from Mn^{4+} to Mn^{2+} (or $Mn(OH)_2$) to reach an overall equilibrium (Eqs. 8.24-25). Iron on the other hand retains its previous reaction path and precipitates. This is examined in more detail for its role in replacement processes in the section on precipitation. Here, emphasis is directed towards manganese dissolution. However, it must be recalled that although many water samples possess Fe concentrations below the detection limit, this does not mean that iron has not been frequently remobilized on a small scale. Also, Fe^{2+} can physically be transported adsorbed on kaolinite. This almost continuous supply of divalent iron guarantees the basis for further redox reactions. It is important to note that only tetravalent manganese oxides are affected by these redox reactions. Though Mn-minerals with lower valencies are considered to be less stable, they are passive under these conditions, thus being concentrated when the higher valence oxides are leached away.

$$MnO_2 + 2\,Fe^{2+} + 4\,H_2O \Rightarrow Mn^{2+} + 2\,Fe(OH)_3 + 2\,H^+ \quad (8.24)$$

$$MnO_2 + 2\,Fe^{2+}+ + 6\,H_2O \Rightarrow Mn(OH)_2 + 2\,Fe(OH)_3+ 4\,H^+ \quad (8.25)$$

The calculation of $E_{o(net)}$ and $K_{(net)}$ demonstrates that both reactions will go from left to right (Eqs. 8.26-27). Since the half-cell reactions of Mn involves twice the electrons as does the Fe reaction, only half (!) the potential of manganese is required for this calculation (Campbell, 1970), in which pyrolusite as the most stable tetravalent oxide was used as basis. The other members of the MnO_2-group produce similar results, but slightly smaller values.

$$E_{o\,(net,\,(8.24))} = 443\ [mV] \qquad K_{(net,\,(8.24))} = 3.04 * 10^7 \quad (8.26)$$

$$E_{o\,(net,\,(8.25))} = 665\ [mV] \qquad K_{(net,\,(8.25))} = 1.72 * 10^{11} \quad (8.27)$$

As already mentioned in chapter 7, the highest voltage recorded in experimental work with the battery-cell was 605 [mV], which lies between the theoretical values of Eq. (8.26) and Eq. (8.27). Though pyrochroite ($Mn(OH)_2$) normally precipitates under alkaline conditions, it is assumed here that it also forms in an acidic environment as a meta-stable or transitional phase which breaks down quickly. If this mineral additionally takes part in the redox reaction, then the recorded potential of the battery and the even higher values of the field can be explained.

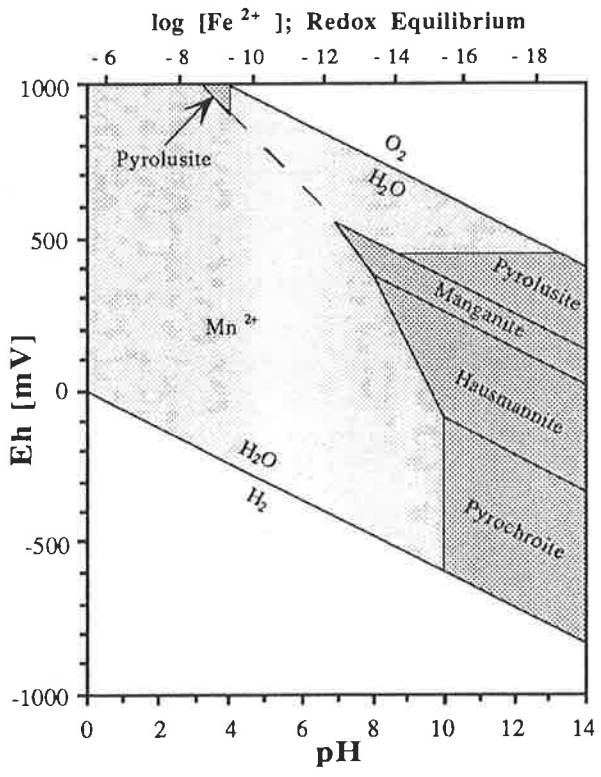


Fig. 8.5: Fe-dependent stability gap of tetravalent Mn oxides (pyrolusite represents all Mn^{4+} minerals).

The theoretical $E_{o(net)}$ of 443 mV (Mn^{2+}/ MnO_2) and the remarkably low pH of 3.9 detected in the field are used to modify the manganese stability diagram (Fig. 8.5; see also Fig. 8.4a), consequences for iron stability are later discussed in detail. Above the redox potential of 443 mV (horizontal boundary) and at higher pHs, Mn^{4+} is reduced to Mn^{2+}, and Fe^{2+} precipitates as Fe^{3+} (Eqs. 8.24-25). Such fixed parameters for Mn and Fe result in an equilibrium and therefore, the concentrations of both elements in solution are directly linked. Since the process consumes all free electrons, the border between the two sides of the reaction formulae must be Eh-independent (vertical). At a pH <3.9 and at relatively high natural Eh values, tetravalent manganese oxides are stable; similarly, Mn^{4+} can exist at potentials < 443 mV and higher pHs. These remaining stability

fields lie in extreme Eh/pH regions and are probably rarely met in the deposit. Thus, outside the set limits the redox reactions examined here do not apply and the electro-chemical conditions return to independent half-cell reactions. All tetravalent Mn oxides possess such a stability gap, where individual stabilities of mineral are interrupted by a region of instability. In deposits with an iron mobility higher than at Groote Eylandt, the vertical pH boundary shifts further to the left towards lower pH values and thus, the stability gap widens. In contrast, the stability of the oxidized iron phases generallly increases.

The diagram also demonstrates that the Fe concentrations required to produce the recorded manganese enrichments are very low (approximately 10^{-9} - 10^{-12} mol/l for the pH range of 4-6). However, these values cover the range described by Kopeykin and Lebedev (1985) in their examination of iron mobilities during leaching processes in bauxites of Central Timan (10^{-10} - 10^{-11} mol/l). Most water samples showed Fe concentration below the detection limit (~10^{-8} mol/l). Whether this reflects redox reactions that precipitated iron, or whether the solutions had low amounts of Fe initially, is unclear. Some waters contain additional dissolved iron, when compared with the required minimum. In this case, organic complexes might inhibit or slow down the interaction with manganese.

One fact that needs attention is the dominance of cryptomelane over pyrolusite in many of the supergene ores. Thermodynamic considerations reveal that pyrolusite is the most stable phase of all tetravalent manganese oxides, but often, cryptomelane is the latest phase to replace all precursors, including pyrolusite. On the other hand, experimental data indicate that cryptomelane takes part in the redox driven dissolution of manganese minerals. These statements seemingly contradict each other and an explanation is needed that can accommodate these apparant contradictions. To preferentially remobilize pyrolusite in the presence of cryptomelane, stabilization processes must occur which increase the stability of cryptomelane relative to pyrolusite. Such protective mechanisms might be found in small quantities of Fe^{3+} occupying Mn^{3+} sites of the cryptomelane lattice (Post et al., 1981). Trivalent iron incorporated in a mineral might slightly shift the redox equilibrium towards the left side of the reaction, where MnO_2 and Fe^{2+} can coexist. Additionally, other trace elements such as Co or V apparent in cryptomelane might cause similar effects.

The above process leads to an initial removal of pyrolusite and a successive breakdown of cryptomelane, once new redox equilibria form. That the latter reduction processes are less dominant in the deposit follows from the relative enrichment of cryptomelane during the development of the supergene ore units. Eventually however, large parts of former orebodies (5-6 m) are leached out and replaced by secondary lateritic materials. This vast amount of dislocated manganese is available for the formation of supergene ores at other locations in the deposit.

8.3.3.3 Dependency of Mn Minerals upon Kaolinite Stability

That the formation of kaolinite can directly influence the activity of iron was illustrated above (8.3.2.3). Through a similar process, kaolinite can also affect the stability of manganese oxides. When kaolinite precipitates, the solutions become more acid, and Mn phases dissolve in this increasingly acid environment (Eqs. 8.7a and 8.17). In thermodynamic terms, the least stable of the tetravalent Mn oxides is reduced first, whereas pyrolusite as the most stable mineral of this group breaks down last. However, it is difficult to estimate the relative strength of this process, because of the presence of other reduction reactions, which are probably much stronger, and which mask the effect of a purely pH-dependent dissolution.

$$Al_2Si_2O_5(OH)_4 + 6\,H^+ \Leftarrow 2\,Al^{3+} + 2\,H_4SiO_4 + H_2O \qquad (8.7a;\ rep.)$$

$$MnO_2 + 4\,H^+ + 2\,e^- \Rightarrow Mn^{2+} + 2\,H_2O \qquad (8.17;\ rep.)$$

8.3.3.4 Pedogenic Conditions

To understand conditions that could lead to the mobilization of manganese in soils, a brief characterization of Groote Eylandt soils is necessary. Langkamp and Dalling (1979) examined the Red Acid Earth (Stace et al., 1968; Northcote, 1974) of Groote Eylandt and showed that the O-horizon is absent and the top of the A_1-horizon is hardsetting with an earthy fabric. A_1 is about 30 cm thick, structureless and it grades evenly into the B-horizon (~50cm thick), which contains increased amounts of clays. Manganiferous spheruliths (5-20 mm) are concentrated in this horizon. The materials below are characterized as hardpan, but probably they belong to the top of the underlying laterites.

The data provided by Langkamp and Dalling (1979) demonstrate that elements such as C, P, or N, which theoretically could influence the solubility of manganese oxides through the formation of complexes or through the increase of surface reactivity, are present only in low concentrations (Fig. 8.6; Wadsley and Walkley, 1951). Elements like K and S that could change the pH towards more alkaline or acidic conditions are also very low. The pH itself, buffered by atmospheric carbon dioxide, does not seem to be influenced strongly by other processes. It decreases only slightly over the first 150 cm of the profile.

As oxygen generally concentrates in surface waters, the environment is also highly oxidizing. This fact, and the findings above point to a very low mobility of manganese in soils. This is supported by the manganese analysis which shows only small variations over about 130 cm depth. Though Langkamp and Dalling state that spheruliths are concentrated in the relatively thin B-horizon (depth ~30-80 cm), the diagram (Fig. 8.6) indicates that manganese is present in

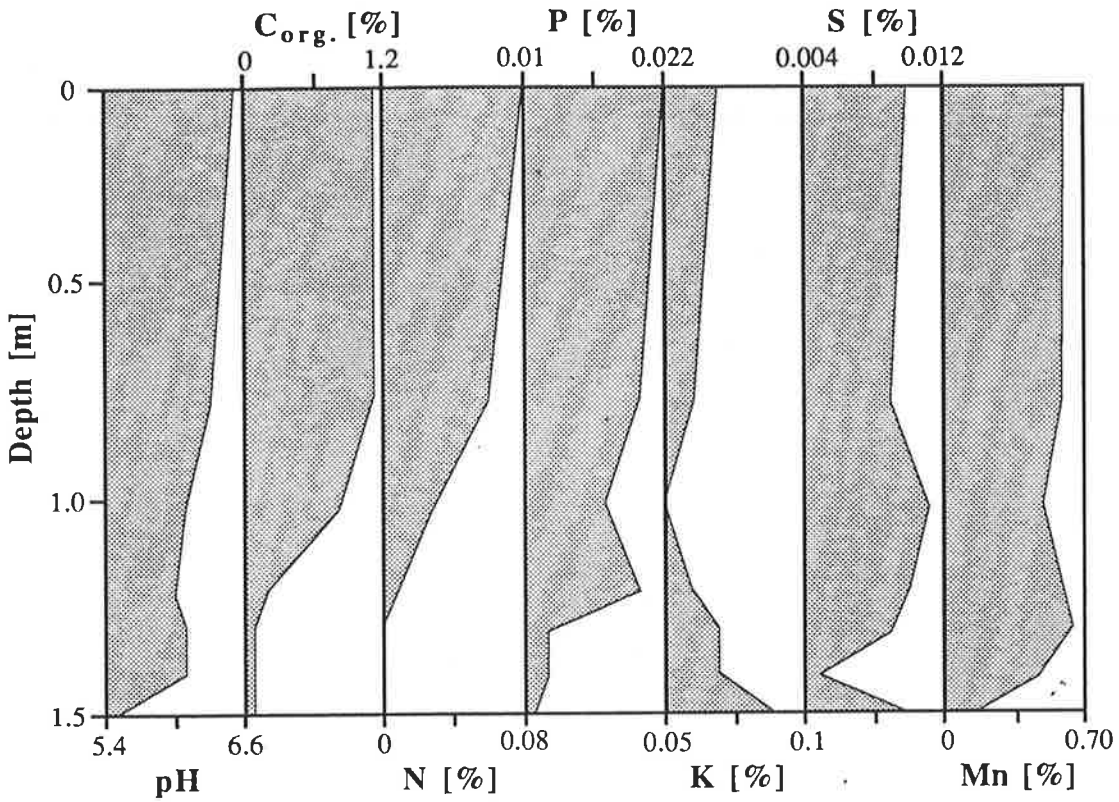


Fig. 6: Vertical soil profile, showing elements and pH-conditions in the top 150 cm of the Groote Eylandt Acid Red Earth which could influence manganese solubility; data from Langkamp and Dalling (1979).

similar concentrations above and below this horizon, macroscopically certainly less evident than the solid spheruliths. Evaporative precipitation processes therefore are probably far more important in the soils than the remobilization of manganese oxides. However, solubilization may be induced by organic substances, such as amino-, carboxyl-, or phosphorus-containing compounds (decomposition of leaf litter), which have been identified to reduce manganese oxides (Putilina and Varentsov, 1980). These dissolution processes may act for short time intervals and over relatively small distances.

8.3.3.5 Biological Activities

Microbial reduction of manganese oxides can be an important mechanism for mobilizing Mn in a wide range of contemporary sediments, including anaerobic/aerobic terrestrial freshwater and marine environments (Hariya and Kikuchi, 1964; Stone, 1987; Adams and Ghiorse, 1988). It is likely that microorganisms have been active over geological time, despite the paucity or lack of direct evidence preserved in the rock record. However, some studies indicate that microbiota have taken part in the metallogenesis of the Groote Eylandt deposit (Ostwald, 1981; Bolton et al., 1988) and it has been demonstrated that microorganisms are able to remobilize the ores under laboratory conditions (Madgwick, 1987).

More than thirty organisms have been recorded, including bacteria, fungi, and algae, which are capable of catalysing the reduction of manganese dioxides. These microorganisms produce extracellular organic acids such as formic, citric, or oxalic acid during their carbohydrate metabolism, and these acids attack the ore (Perkins and Novielli, 1962; Troshanov, 1968; Agate and Deshpande, 1977; Marsalek, 1977; Marshall, 1979; Ehrlich, 1980). The acids reduce Mn^{4+} to Mn^{2+}, being oxidized themselves to CO_2 and water (Eq. 8.28) (Hart and Madgwick, 1986).

$$MnO_2 + H_2(CO_2)_n + 2\,H^+ + 2\,e^- \Rightarrow Mn^{2+} + n\,CO_2 + 2\,H_2O \qquad (8.28)$$

Investigations indicate that the reducing capacities of bacteria generally seem to be stronger than those of algae. However, the co-existence of bacteria and algae improves the overall strength of the dissolution process (Mercz and Madgwick, 1982). Such an improvement results from the addition of algae or other organic energy sources for the bacteria (e.g. yeasts, molasses). Similar nutrients may also be found in natural surface waters that carry humic acids or phenolic compounds (J. Madgwick; pers. commun., 1985), which accumulate in decomposing organic litter. In a number of cases an electron transfer process between organics and Mn oxides is coupled to an intermediate formation of organo-metallic complexes (Marshall, 1979; Kung and McBride, 1988). Although this can take place in a highly aerated system, demonstrating that an organogenic reduction process can actively inhibit oxidation reactions, it has also been shown that some bacteria are only able to reduce Mn oxides under anaerobic conditions (Myers and Nealson, 1988). Organisms which are naturally resident on Groote Eylandt manganese ores (*Pseudomonads*, *Enterobacter cloacae*, *Chlostridia*, *Aspergilli*; Kozub and Madgwick, 1983) show improved reducing capabilities under microaerobic to anaerobic conditions and at a pH of approximately 5, which is comparable to the natural geochemical environment of the deposit (see chapter 6).

It was demonstrated that microbiological processes preferentially mobilize the thermodynamically least stable manganese oxides first (chapter 5). Thus, the introduction of organic acids into the aqueous system leads to a pH-dependent manganese reduction that parallels inorganic dissolution processes. Such biologically controlled processes might be indicated by the oxides of one particular area (G/G-South Quarry). Although in most other parts of the deposit an increasing alteration and cementation of the ore results in cryptomelane dominance, the ores of this location show that pyrolusite replaces the thermodynamically less stable cryptomelane. This means that the latter mineral must be remobilized by processes that are in contrast to the reduction processes of other areas. A biota-controlled dissolution of the ores could explain this observed succession of the major manganese oxides, since inorganic compounds such as sulfates or phosphates, with high reducing or complexing capacities, are either absent or negligible in their concentration. The input of organic nutrients that would enhance microbiological activities is also favoured in this location, because the orebody is close to the surface (in places it crops out). Additional findings to support this interpretation are discussed in the section on precipitation.

8.3.3.6 Electrolytic Weathering

Investigations demonstrated that rocks in connection with waters of both high and low electrolyte content can form a voltaic cell (Kurdyukov, 1967; Taylor and Fischer, 1973; Winkler, 1973; Taylor and Bond, 1979). The small potential which always develops at the electrolyte-mineral interface accelerates weathering processes and it leads to the destruction and dissolution, or re-ordering of the mineral structure.

At its western margin the Groote Eylandt deposit extends to the sea. Intruding seawater, a strong electrolyte, therefore can come in contact with some parts of the orebody. Generally, the groundwaters of the island contain only small trace element concentrations, and most parts of the deposits are out of the reach of seawaters. Therefore, interactions with seawater are probably of subordinate importance. However, at "Nashe's Gash" near the tailing dams, where pumping operations move large water volumes, occasionally a relatively high salinity can be observed, probably due to a subsurface saltwater wedge. Although dissolution effects related to electrolyte variations are regionally restricted to coastal parts of the deposit, such processes can be expected to take place on a small scale.

The experimental section showed that in a closed chemical system, alkaline seawater quickly becomes acid when in contact with manganese oxides and clay (chapter 7). Unfortunately, the mineralogical and chemical reactions leading to the dramatic drop of pH are not fully understood. Partial adsorption of some of the major seawater ions, such as Na, K, or Mg, to the surface of manganese or clay minerals, or an incorporation into new manganese phases (detection of traces of manjiroite = Na-analogue to cryptomelane) may have led to the increasing acidity. Elements like Mg possess a strong buffering capacity and if such elements are removed from the chemical system, then the pH can be expected to change towards lower pH values (Corliss et al., 1979). Parallel to the increasing acidity the dissolution rate of the present mineral species will increase. How far these experimental results can be transposed onto the open chemical system of the orebody is not known, but small-scale geochemical environments may develop that are comparable to the closed system of the laboratory cell.

8.3.3.7 Pressure Solution

The basic concept for this process is that at point contacts between grains pressures can develop that result in the preferential dissolution of the material at this point of stress. Immediately adjacent precipitation occurs in open pores or at places with less pressure. Additionally, the presence of thin clay films can speed up the transfer of dissolved material to open pore spaces via the provision of diffusion paths (Pettijohn et al., 1987).

The consideration of pressure solution may seem to lead off the main track, because evidence indicating this type of mobilization process is very scarce in the Groote Eylandt orebody. However, some specimens exhibit features which strongly suggest that pressure solution has been responsible for dissolution on a small scale (Plate 3.1, Fig. 3.2a). Unfortunately, the complex nature of manganese oxides together with the additional complication of pressure-, volume-, temperature-, and redox-dependencies, obviously inhibits detailed scientific discussions about this subject.

Nordstrom and Munoz (1985) demonstrated that it is possible to obtain reasonably good results from simplified calculations using their theoretical results on the pressure solution of quartz and data from Walther and Helgeson (1977). They showed that the assumption that the molecular volumes are not functions of pressure and temperature is relatively good for lower pressures. They also state that at higher temperatures changes in the actual mol volume become more apparent. This suggests that for the ambient conditions of the manganese orebody the temperature control is negligible, that molecular volumes are approximately constant, and that the main factor for pressure solution is the overall pressure. However, the complex manganese mineralogy with its tunnel structures, structural inhomogeneties, mineral intergrowths, etc., suggests a totally different situation and therefore, the simplified theoretical approach cannot be applied to the ores.

The above mechanism of intergranular pressure solution, which is often believed to be the dominant process of pressure solution, is nonetheless 7 to 9 orders of magnitude smaller than a different type of mobilization described by Tada et al. (1987). They propose a "plastic deformation plus free-face pressure solution", which is especially effective when the grain contact area is very small (beginning of compaction of sediment). Intergranular pressure solution only gains importance at the final stages of compaction. As the overburden of the deposit possesses a relatively low density (porous laterites), it can be expected that pressures large enough to induce any type of pressure solution are rarely reached. However, diffuse clay impregnations in the matrix of the oolitic/pisolitic ores occur frequently and they may have resulted from this mechanism. Nevertheless, textural evidence for pressure solution reactions is rare and it can be concluded that this process is very limited in the deposit.

8.3.3.8 Disproportionation and Protonation Reactions

Various manganese oxides undergo aging processes in an aqaeous system after their formation. Early stages of the ore development were probably dominated by diagenetic and aging processes that included disproportionation (Eqs. 8.29-30) and protonation reactions (Eq. 8.31). Two of these alteration paths are discussed to demonstrate the type of reactions that occur (Hem and Lind, 1983). A disproportionation reaction is illustrated by the examples of feitknechtite

(β-MnOOH) altering to pyrolusite and related minerals (MnO_2), and by hausmannite (Mn_3O_4) altering to pyrolusite, respectively. During a protonation reaction, initial divalent and trivalent oxidation stages of the manganese phases are preserved in the newly formed minerals and/or ionic species, in contrast to the previous two reactions.

$$2\beta\text{-MnOOH} + 2\,H^+ \Leftrightarrow MnO_2 + Mn^{2+} + 2\,H_2O \quad (8.29)$$

$$Mn_3O_4 + 4\,H^+ \Leftrightarrow MnO_2 + 2\,Mn^{2+} + 2\,H_2O \quad (8.30)$$

$$Mn_3O_4 + 2\,H^+ \Leftrightarrow \gamma\text{-MnOOH} + 2\,Mn^{2+} \quad (8.31)$$

An examination of these equilibrium conditions reveals that through the reactions, approximately half to two thirds of the original precipitate are remobilized. Most probably this release of Mn^{2+} happened during early diagenesis of the sediments, because feitknechtite and hausmannite have been recognized among the initial precipitates from alkaline solutions (Bricker, 1965; Morgan, 1967; Hem et al., 1985). After the deposit of Groote Eylandt was uplifted above sea level, the environment could have provided the more acidic conditions which are necessary for both the disproportionation and the protonation reactions. However, supergene alteration produces manganese oxides of higher valencies (pyrolusite, cryptomelane, etc.). This means that in the present geochemical environment, phases such as feitknechtite are not available for disproportionation, or if they are, then only in quantities which are negligible for the overall mobilization processes.

Generally, protonation reactions are still likely to occur in deeper parts of the deposit, especially in sections of the orebody which are under the influence of strongly fluctuating groundwaters, or in areas with seawater input. Such waters are subject to drastic changes in their physico-chemical parameters, and a continuous oscillation between reducing and oxidizing environments could favour the formation of minerals that take up protons during subsequent aging/alteration reactions.

8.4 Transport of Dissolved Manganese

Examination of transport mechanisms focuses only on manganese, since the dissolution of gangue minerals is mainly of interest for the reduction/re-mobilization of Mn oxides. For this reason, transport conditions for ionic species of gangues are not discussed here. However, these minerals are again examined for their role in replacement processes. Several geochemical and biochemical processes were described that are able to reduce manganese ores and associated rocks. It was also demonstrated that all dissolution processes depend directly on the availability of groundwaters. Therefore, a good drainage system within the deposit is a prerequisite. Without water, any mechanism that could lead to the redistribution of manganese is unlikely.

Dissolved manganese can be transported either in divalent ionic form, in complexes or as particulates. Laxen et al. (1984) demonstrated that for a pH <7.5 in river waters, essentially all Mn in the fraction <0.015 µm is present as reduced Mn^{2+} -species, which seems to indicate that particulates do not play a significant role in oxic freshwaters and that they are not in equilibrium with dissolved manganese.

In places with a high input of organic matter, manganese is complexed by various biogenic compounds, such as amino-, carboxyl-, sulphur-, or phosphorus-containing groups with high molecular weights. Putilina and Varentsov (1980) state that in the presence of these compounds Mn can increase dramatically in concentration, whereas Mn^{2+} is oxidized much faster without the protective mechanisms of the phases mentioned (Hallberg et al. 1979). The formation of chelate complexes thus enable freshwaters to carry high amounts of manganese in a relatively stable condition over large distances.

Contrary to freshwaters, manganiferous oxyhydroxide particulates seem to dominate in the marine environment, where they may be associated with organic molecules or bacteria (Van Der Sloot, et al., 1988). Although particulates generally tend to flocculate in strong electrolytes, manganese seems to have a surprisingly long residence time in the sea (~20 years; Bishop and Fleisher, 1987). This finding is supported by the strong enrichment of manganese along the coast of Groote Eylandt. Despite this, large quantities of the river load are removed from solution through precipitation processes (see chapter 6).

The two dominant mechanisms of manganese liberation at Groote Eylandt are pH controlled dissolution processes (e.g. kaolinite precipitation, biological acidification of water) and redox reactions between Mn and Fe; they are distinctly different in their physico-chemical parameters. For instance, redox reactions produce their own electrochemical environments (electron transfer, pH, etc.), largely suppressing other co-existing reduction processes. An acidification of the water on the other hand, be it biologically or mineralogically mediated, is generally more passive. Such pH variations frequently occur as a result of environmental changes and then the pH alone may affect the solubility of present minerals.

Thus, the mobilized reaction products and physico-chemical parameters should reflect their origin. To identify the predominant mode of reduction, a diagram was developed that superimposes both the theoretical Eh values and the "equilibrium Fe concentration" (EFC) onto a pH/log $[Mn^{2+}]$ plot. The EFC is here defined as the amount of iron needed to balance Mn-Fe redox reactions at preset pH and Mn concentration values. Occasionally, the amounts of Fe in solution can be much higher than the EFC, but if this surplus iron is complexed by organics, then it probably does not take part in redox reactions.

Sample data shown in this type of diagram indeed illustrate some important features (Fig. 8.7). Although water samples from ores, laterites, and mine sumps do not develop a definite trend, they plot exactly in the EFC range that was described by Kopeykin and Lebedev (1985) for iron mobilized from bauxites (10^{-10} - 10^{-11} mol/l). Nevertheless, these samples are probably not in equilibrium with surrounding materials, and therefore the data are relatively diffuse. Once local groundwaters reach river systems, reduction processes are interrupted, and the waters equilibrate with the new environment, forming element patterns that reflect the respective mobilization (or precipitation) reaction.

The manganese concentration of river samples generally increases with increasing pH, parallel to an EFC value of approximately -11.5. Obviously, Mn reaches an equilibrium and stabilizes in solution. Such a stabilization of Mn compounds may be the result of chelate-complexes that can develop through the activity of bacteria (e.g. formation of 2-ketogluconic acid; Duff et al., 1963). This interpretation is not supported by TOC analyses (total organic carbon), which do not demonstrate a significant correlation to any element, but more complex organic/inorganic interactions with other dissolved elements could mask the presence of manganiferous chelates. At a pH of about 5.8 the pattern suddenly becomes horizontal under the influence of tidal seawater mixing with the riverwater. Here, the geochemical conditions seem to inhibit Mn concentrations above 10^{-5} mol/l, and the variation of the Mn load is generally small. On the other hand, the pH interval of this transitional brackish zone is large (5.8 - 8.0).

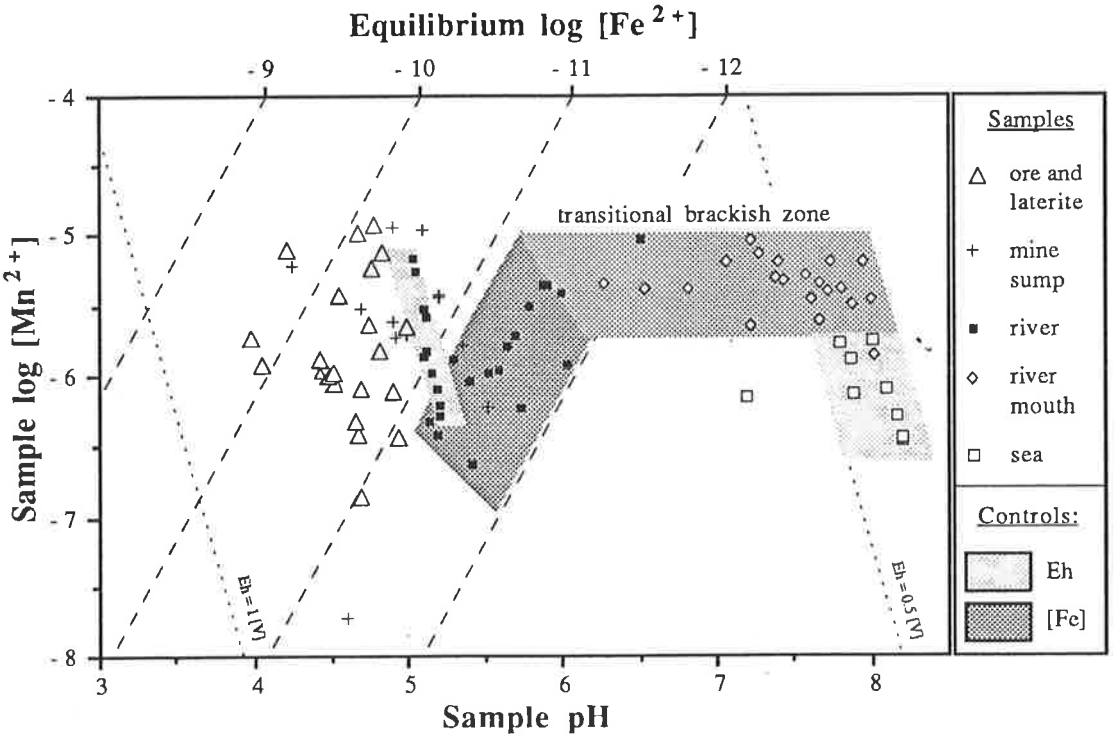


Fig. 8.7: pH versus Mn concentration of various water types; boundaries are shown for theoretical Fe2+ concentrations necessary to mobilize the found Mn quantities; the calculated Eh boundaries are also given.

In the sea, the samples again change their orientation and they finally align parallel to Eh boundaries (0.5 - 0.45 V). The manganese concentration now decreases with increasing pH. This means that Eh/pH controlled processes result in the destruction of the previously stable complexes and manganese is removed from solution. The type of precipitate (MnOOH) is determined by the electrochemical parameters that dominate this environment; this is discussed in the following section.

A particularly interesting sample group (freshwaters) collected from a sampling station at the eastern edge of the deposit, where the aquifer has little or no contact with the main orebody, clearly illustrates an Eh/pH control over Mn reduction. The manganese enrichments probably originate from outcrops in swampy areas where biological processes dominate the geochemical environment (see 6.3.2.5). The Mn concentration in the samples increases with decreasing pH, parallel to an Eh of about 0.8 V.

The descriptions above illustrate that manganese reduction processes can be distinguished easily. Thus, the waters are grouped into two major sets:

- samples not in equilibrium with their surrounding and with diffuse trends; from ores, laterites, and mine sumps, and
- samples at equilibrium, depicting Eh/pH or redox control mechanisms (shown with [Fe] pattern on Fig. 8.7); from rivers and the sea.

When the second group is examined, it is possible to determine the type of process that dominates the mobilization of manganese. This has serious implications for the detection of supergene ores, because deposits similar to Groote Eylandt do not possess a strong Eh control. If, for example, samples from rivers indicate an Eh dominance, then the waters are likely to have collected their Mn near the surface of a deposit, under the control of biological mechanisms. In such a case, redox processes in deeper parts of the orebody may be of minor importance for the formation of secondary ore units, and therefore, the ore is less well upgraded. If, on the other hand, a redox control appears to dominate, then supergene overprinting and upgrading was probably active for significant time intervals.

8.5 Fixation Processes

Although water samples collected in the deposit itself do not show much evidence for precipitation processes, the presence of many supergene ores and rocks illustrates active deposition of secondary minerals. Many of these newly formed phases change their geochemical environment, for instance by influencing the pH, and thus, the formation of one particular mineral has direct implications for the stability or instability of other co-existing phases (Merino and Ransom, 1982; Jones and Weir, 1983). The various replacement products observed in the

Groote Eylandt deposit support this view and it is demonstrated below that most of the precipitation and replacement processes can be explained in relatively simple terms. Since most of the chemical equations were discussed earlier, only with a reverse reaction direction, the formulae are only mentioned by their respective numbers.

8.5.1 Precipitation of Si-Al Minerals

The stabilities of minerals and ions in the Si-Al-H_2O system are not redox-dependent, because all species retain their valency state during dissolution or precipitation processes. Thus, redox reactions with other elements need not be considered (Eqs. 8.1-7a). Although this seems to simplify the discussion, silica and alumina are known to form numerous polymers (Hemingway, 1982), which can result in rather complex interactions. Such mechanisms that could retard or increase the development of equilibrium with stable phases are not discussed, because of a general lack of data. Instead, attention is focused on element interaction during precipitation.

Since Al and Si co-exist in most water samples, these elements are discussed together. The fact that silica always dominates in the waters (Si/Al ratios vary between $5x10^1$ and $3x10^2$) leads to the conclusion that pure Al minerals, such as gibbsite or boehmite, are generally less mobile than silicates under present-day conditions. It is also deduced that the Al deficiency reflects a much lower availability of these phases. Additionally, a high silica input further decreases the Al potential through the formation of kaolinite (May et al., 1986).

Thus, the development of kaolinite in the presence of surplus dissolved silica results in the suppression of stable alumina phases, which explains the scarcity of minerals like gibbsite in the deposit (compare also Figs. 8.2b,c). Because of its implication for the reduction of iron oxyhydroxides, the formation of kaolinite was already examined earlier. During kaolinite precipitation, OH^--ions are consumed and the H^+ concentration in the solution increases, which means that the pH becomes more acidic (Eq.8.7a). This happens under the generally more alkaline regime of the wet season, when water is more abundant, because this clay mineral strongly depends on the presence of water for its development (Eq. 8.7b) and because dehydration destroys the kaolinite structure.

To a certain degree, kaolinite formation (and dissolution) counters the seasonal variations normally imposed on laterite profiles with a different mineralogy (e.g. in bauxites). Small pH changes in the Angurugu River over the year support this view (Fig. 6.11). The probability for kaolinite to precipitate is also larger than for gibbsite, because both Si and Al in most waters of the deposit are oversaturated with respect to kaolinite (Fig. 8.2c). Only a few alkaline seawater samples indicate the possibility of gibbsite formation (Figs. 8.2b,c).

8.5.2 Precipitation of Fe Minerals

8.5.2.1 Precipitation of Fe During Redox Reaction with Mn

That redox reactions with manganese oxides result in the dissolution of Mn was demonstrated above. However, the basic principle of such a redox reaction is that parallel to the reduction of one reaction partner the other must precipitate (Eqs. 8.24-25, rep.). This leads to a situation where the newly forming iron mineral takes the place of the dissolving Mn oxide (Plate 3.2, Fig. 3.3c). Thus, manganese and iron dominate their geochemical environment during their interaction and other less powerful reduction processes normally affecting either element are interrupted.

$$MnO_2 + 2\,Fe^{2+} + 4\,H_2O \Leftrightarrow Mn^{2+} + 2\,Fe(OH)_3 + 2\,H^+ \qquad (8.24\ rep.)$$

$$MnO_2 + 2\,Fe^{2+} + 6\,H_2O \Leftrightarrow Mn(OH)_2 + 2\,Fe(OH)_3 + 4\,H^+ \qquad (8.25\ rep.)$$

During the redox reaction the generally large $Fe(OH)_3$ stability field extends further towards the boundaries dictated by the available Fe^{2+} concentration and the developing pH, contrary to the stability gap that forms for pyrolusite and other tetravalent manganese oxides (Fig. 8.8a). When the stability diagrams of both the manganese and the iron systems are superimposed, it can be seen that the thermodynamic theory supports the field and laboratory observations (Fig. 8.8b). The entire area in which pyrolusite is unstable is covered by $Fe(OH)_3$, although the

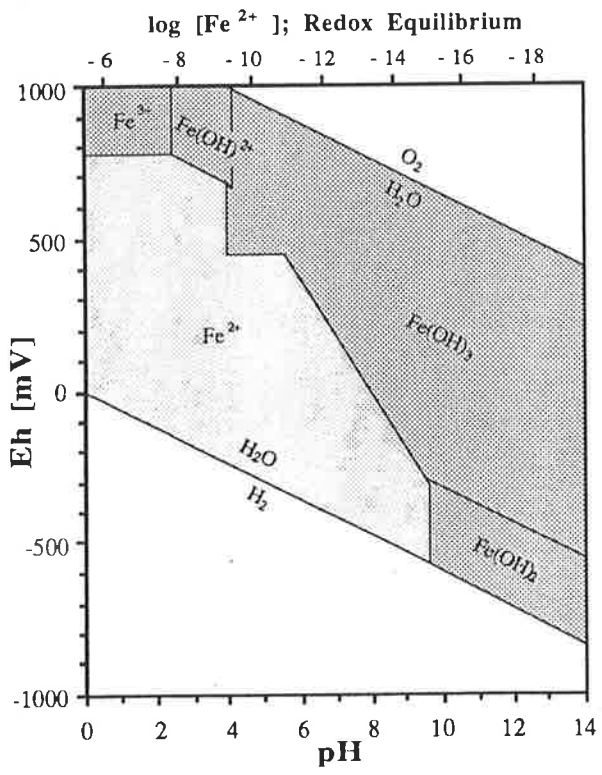


Fig. 8.8a: Increasing thermodynamic stability of Fe precipitates during redox reaction with Mn.

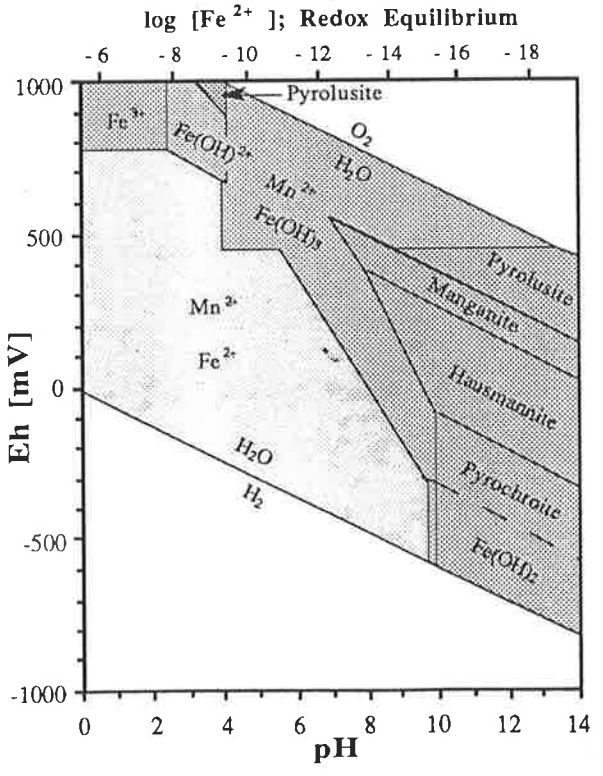


Fig. 8.8b: Replacement conditions for Mn and Fe phases.

boundaries for the latter compound were calculated for a minimal size (maximum Fe^{2+}). Therefore, a redox reaction between Fe and Mn under the natural conditions at Groote Eylandt always results in a total replacement of pyrolusite, etc., by iron phases, as long as divalent iron is available. The type of ferruginous precipitates is discussed in the following section, because the initial iron minerals strongly depend on other co-existing elements.

8.5.2.2 Influence of Foreign Ions on Initial Fe Precipitates

Transformation reactions of the initial unstable Fe precipitate (ferrihydrite) display strong dependencies on the presence of foreign ions (Cornell et al., 1987; Cornell and Giovanoli, 1987, 1989) and on the availability of various minerals (Krishnamurti and Huang, 1988). Although most of these processes were examined in alkaline media and at elevated temperatures, it can be expected that the results of these studies can be applied to field conditions with lower temperatures and more acid pHs (Fischer and Schwertmann, 1975; Cornell and Schwertmann, 1979; Schwertmann and Murad, 1983). However, for kinetic reasons, the transformations are then likely to be much slower.

The implications for mechanisms influencing the mineralogy of the deposit are far reaching. If, for instance, iron phases form that are relatively stable in the present geochemical environment (e.g. hematite or magnetite), then redox related reduction processes of manganese oxides cease to operate and the alteration of the orebody slows down significantly. On the other hand, preferential formation of less stable minerals, such as goethite, support the continuation of supergene enrichment processes.

The transformation of ferrihydrite to more crystalline phases (goethite, hematite) is strongly retarded in the presence of high concentrations of silica, alumina, cobalt and copper, which seem to stabilize the structure of ferrihydrite (Cornell et al., 1987; Cornell and Giovanoli, 1987, 1989; Krishnamurti and Huang, 1988). When the concentrations of Si, Al or Cu are low enough to allow transformations to proceed, the development of hematite is promoted and the formation of goethite is hindered. Manganese shows the opposite effect by supporting the transformation of ferrihydrite to goethite and by suppressing hematite development.

Both of the above observations are indeed valid for the Groote Eylandt manganese deposit and the associated laterites. Near the surface in soils and ferruginous laterites, where quartz and kaolinite dissolution products are abundant, hematite can be observed occasionally. However, in manganiferous laterites and within the orebody itself, goethite dominates strongly. A fascinating relationship is thus developed, in which the two main metalliferous components of the deposit, Fe and Mn, obviously are interdependent in their formation and destruction:

- dissolved manganese favours goethite, which is less stable than hematite or magnetite, and which can be reduced more quickly;
- dissolving goethite in turn facilitates redox reactions that reduce tetravalent manganese oxides.

8.5.2.3 Further Oxidation of Goethite

Above, it was demonstrated that under the present geochemical conditions $Fe(OH)_3$ predominantly transforms into goethite after dehydration (Eq. 8.32). Further dehydration may occur and hematite is formed (Eq. 8.33), which can be found in pipes and laterites. However, when compared with the overall amount of goethite in the deposit, hematite is far less abundant than goethite, and it also concentrates in horizons near the surface, where higher oxygen concentrations are available. Changing Eh/pH conditions and precipitation of new minerals (e.g. kaolinite) can trigger a re-dissolution of the iron phases. Fe^{2+} is again mobilized to take part in Mn-Fe redox reactions and the entire process of replacement and dissolution starts again.

$$Fe(OH)_3 \Leftrightarrow FeOOH + H_2O \quad (8.32)$$

$$2\,FeOOH \Leftrightarrow Fe_2O_3 + H_2O \quad (8.33)$$

8.5.2.4 Microbial Influences on Fe Precipitation

Near the surface, filamentous iron-oxidizing bacteria, such as *Thiobacillus Ferrooxidans*, are known to utilize available organic matter for their carbohydrate metabolism. These bacteria comprise a group of acidophilic and chemolithotrophic organisms, which are also able to use Fe^{2+} as an energy source (Lundgren et al., 1974). Generally, precipitates of poorly ordered Fe-oxides and ferrihydrite are described together with iron bacteria and it can be assumed that such organic-inorganic interactions are widely distributed (Chukrov et al., 1973; Carlson and Schwertmann, 1980).

However, Fe commonly forms chelate complexes with humic and fulvic acids, and in this condition iron is relatively stable. Once the organic ligands are oxidized, Fe can be oxidized by biological or inorganic mechanisms (Schwertmann et al., 1974). Although it is generally accepted that organic processes concentrate near the surface, it is not known how far this biologically active horizon extends downwards. Therefore, it is impossible at present to estimate the strength of a microbially induced Fe precipitation in the Groote Eylandt deposit.

8.5.2.5 Precipitation of Iron Phases in Seawater

Together with most other elements with atomic weight greater than 20, dissolved iron was observed to decrease strongly at the mouth of the Angurugu River, where fresh- and seawaters mix. Therefore, the geochemical parameters of this particular environment, such as salinity, Eh, or pH, cause Fe^{2+} to oxidize and precipitate. It was demonstrated in the example of manganese that a narrow Eh/pH range develops at the river mouth and in the sea (Fig. 8.7; Eh ≈ 0.45 - 0.5V, pH ≈ 8.0 - 8.5). Since the data reflect general conditions in these specific water types, the parameters are also applicable to other elements. An examination of the Eh/pH stability diagram reveals that these set conditions lead to the precipitation of $Fe(OH)_3$.

It is difficult to deduce generally reliable precipitation rates, because Fe^{2+}, forming complexes with the different ligands present in solution, can be expected to vary considerably (Millero, 1985). However, experimental results discussed by Millero et al. (1986) indicate that salinity and pH possess pseudo-first-order oxidation rates in the range of pH 6-9, although it is also stated that this is only applicable to waters with low amounts of organic ligands.

8.5.3 Precipitation of Mn Minerals

At several places in the deposit it can be seen that a thickness of five or six meters of ore has been leached out and replaced by secondary materials. The following section examines the precipitation conditions for this vast amount of dislocated manganese. Manganiferous cementation occurs in many parts of the orebody, and thus, low grade ores are enriched by these supergene products.

8.5.3.1 Pedogenic Oxidation of Mn

Enrichments of manganese near the surface in the form of spherulites, concretions, or manganiferous laterites indicate the presence of evaporation processes with upwards moving solutions. Although dissolved manganese is generally transported down the section (see chapter 4), precipitation is obviously far more important in the upper horizons than is remobilization. This mechanism is particularly visible in the spherulites, which show a normal grading. Evaporating waters carry dissolved Mn from deeper parts of te orebody and precipitate most of their load in soils above the deposit. A coalescence of the grain coatings is prevented by gradual soil movement ("creep") in a manner somewhat similar to that described for calcretes (Read, 1974). The most intense movement occurs near the surface and thus, the spheruliths in this position are abundant but relatively small. Grains deeper down are moved less and they form larger accretions that occasionally resemble concretions.

That manganese (and iron) is fixed at or near the surface, no doubt depends strongly on the availability of oxygen (O_2 saturations: river water ≈ 85%, water from laterite ≈ 68%, water from the orebody ≈ 55%; Pracejus, 1986). Therefore, ore minerals from near the surface are mostly cryptocrystalline, caused by rapid precipitation of the oxides. Atmospheric CO_2 also contributes to precipitation processes in upper parts of the deposit through a buffering of the groundwaters. This effect stabilizes the pH at about 5.5 - 6.5, thus preventing stronger acidification reactions which could enhance the dissolution of manganese oxides. The appearance of laminar mangcretes in vertical pipe systems supports this view. These ore types can be several centimeters thick near the surface, but they often disappear in deeper parts of the section.

Tyuryukanova and Konova (1987) state that supergene Mn accumulation in soils is generally of biogenic origin, but nonetheless, it is difficult to assess the role of organics in the deposit, because of very limited data. Initially, biological degradation products may form stable organometallic complexes that break down successively during further oxidation. The manganese oxides then take part in the cementation of the surrounding material. Ionic Mn compounds could also be adsorbed on large organic molecules and would, thus, be retained *in situ*.

8.5.3.2 Microbial Mn Oxidation

The influence of bacteria or algae on precipitation reactions has attracted some interest in recent years, because microorganisms seem to enhance the oxidation of Mn^{2+} (Chapnik et al., 1982; Burdige and Kepkay, 1983). Diem and Stumm (1984) reported that even in the presence of relatively high oxygen levels Mn did not precipitate from sterile solutions, implying the need for catalysis. Such catalytic reactions have, for instance, been observed on the surfaces of dormant bacterial spores (Nealson and Tebo, 1980; Rosson and Nealson, 1982) or in association with exopolymers (extracellular oxidation; Ghiorse, 1986).

Studies of Morgan (1964) also indicate that the oxidation of manganese is strongly influenced by particulates acting as surface catalysts. In natural systems, organisms of the *leptothrix* family often catalyze the manganese oxidation (Adams and Ghiorse, 1988). Other publications refer to these bacteria as *metallogenium* and Ostwald (1981) indicates that this bacterium was identified in samples from the Groote Eylandt deposit. It can thus be assumed that organisms of the *metallogenium* type are active.

At present, the concentration and distribution of microorganisms in the Groote Eylandt orebody is unknown, although many biota were identified (pers. commun., J. Madgwick, 1989). Therefore, extensive research is needed, before a qualified assessment of the biological influence on precipitation processes can be made.

8.5.3.3 Mn Precipitation During Disproportionation Reactions

As mentioned above (8.3.3.8), precipitation and aging processes of manganese oxides can involve disproportionation of the manganese phases, where a new solid is formed, but also where Mn^{2+} is liberated into solution from the pre-existing mineral (Eqs. 8.29-30). Minerals coupled to disproportionation during their formation reduce the amount of manganese in the rock, thus leading to degradation of the deposit.

8.5.3.4 Precipitate Dependency upon Mineralogy of Substrate Rocks

It was noted in numerous instances above (chapters 3 and 5) that depending upon the type of substrate, different manganiferous parageneses develop. For instance, cryptomelane and todorokite form increasingly in the presence of kaolinite and quartz (e.g. in spherulites and concretions), whereas pyrolusite overprints Mn ores in cases where little or no silicates are associated. This clearly illustrates that supergene precipitation processes are at least partly controlled by the materials in which the precipitation occurs.

It has been demonstrated in the example of ferruginous precipitates that the type of mineral formed strongly depends on the presence of various other dissolved elements. From the chemical similarities between Mn and Fe it would appear that comparable dependencies are possible in the case of manganese precipitation. This seems to support the findings above, but so far, research work on this aspect is very limited (Ebinger and Schulze, 1989) and thus, the observations above remain tentative.

The replacement of quartz and kaolinite by manganese oxides also results from chemical/mineralogical interactions between Mn-carrying solutions and specific substrate rocks, and it probably relates directly to observations made earlier (see 8.3.1.2). Manganiferous silicate complexes, if they do exist under natural conditions, are likely to form in more acid environments containing abundant dissolved manganese. Once these complexes dehydrate, silica is mobilized and Mn oxides develop. However, the dissolution of silica produces an increase in alkalinity, which in turn forces more manganese to precipitate. Similar reactions may apply to the replacement of kaolinite by Mn minerals. Except for general microscopic observations, there is no direct evidence at present for the existence of such Mn-Si complexes in the deposit. Therefore, this mechanism only provides a speculative answer to the fact that quartz and kaolinite are being replaced by Mn oxides.

8.5.3.5 Grainsize Variation of Substrate

Above, various possibilities were discussed that lead to the formation of manganese oxide minerals. This section examines the enhancement of precipitation processes through grainsize variations of the substrate, regardless of the type of process that is active. In the field it was observed that cementation frequently concentrates at grainsize boundaries (Fig. 8.9; see also Pracejus et al., 1988). To determine the parameters responsible for this preferred precipitation, a number of assumptions about initial conditions are necessary:

- the sediment is largely unconsolidated,
- pores are open and interconnected,
- a vertical grainsize gradient or a grainsize boundary exists,
- the hydrostatic pressure is constant,
- the solution moves vertically,
- the Mn input is constant, and
- the precipitation rate is constant.

Following these basic settings, the resulting model is relatively simple. In ores with large grainsize, the open-pore volume is large and the internal surface area of the material is small. In contrast to this, ores consisting of small grains have small pore volumes and large internal surface areas. Under constant hydrostatic pressure the water passes relatively quickly through fine grained materials, whereas in coarse grained ores the velocity of the solution generally decreases, caused by the increase in open-pore space. Therefore, the velocity of a solution changes abruptly at grainsize boundaries.

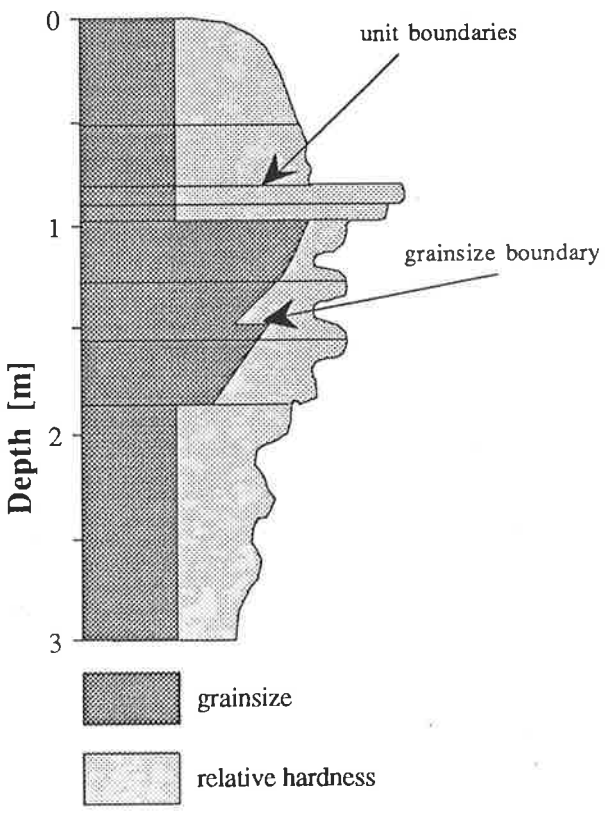


Fig. 8.9: Correlation of ore grainsize and increased Mn cementation; for futher information on log see Fig. 2.8.

Precipitation processes are more effective when more time is available and thus, the pores in coarse materials promote more rapid precipitation and are filled much faster than those of fine grained ores/rocks. This mechanism works until an equilibrium between both coarse and fine ores is reached, but the degree of cementation is finally much larger in coarse materials. This is especially evident in the field, where boundaries between sedimentation units can often be identified by their resistance to weathering in quarry faces.

8.5.3.6 Mn Precipitation in Seawater

Hydrochemical data show that the load of dissolved Mn in the Angurugu River decreases by a factor of about 6, where the freshwaters mix with seawater (Figs. 6.14-15; Laxen et al. 1984). Although this interaction of highly saline water with manganese carrying solutions does not affect most areas within the deposit, marginal parts of the subsurface orebody may be under the influence of invading seawater. As the physico-chemical parameters are likely to change in the same way as they do at the river mouth, precipitation reactions therefore dominate in this type of environment. It can be expected that the resulting cementation of ore causes the build-up of a barrier with which the orebody effectively "plugs" itself against further seawater intrusions. Such barriers probably contain high grade ores, because most of the Mn load of the groundwater is forced out of solution.

An examination of the thermodynamics allowing the precipitation of manganese oxides under such specific geochemical conditions reveals that the most likely minerals to form are those of the MnOOH group (α = groutite, β = feitknechtite, γ = manganite). These minerals are stable at the narrow Eh/pH intervals that prevail (Eh $\approx$ 0.45 - 0.5, pH $\approx$ 8.0 - 8.5; see Figs. 8.4a, 8.5, and 8.7).

8.6 Discussion

During the course of this chapter a great diversity of mechanisms leading to the mobilization or precipitation of manganese oxide ores and associated rocks was examined. It is almost certain that all of these processes have altered the orebody at Groote Eylandt at one or the other stage of the geological history of the deposit. At present however, the majority of these processes are of minor importance to the supergene overprinting of the deposit, or they can even be neglected, if considered individually. The only exception is the redox reaction between Mn and Fe, which seems to be much more prevalent than all other mechanisms. A combination of several reduction or precipitation processes can nevertheless enhance the overall effectivity, and it is the coexistence of such reactions that probably drives the continuous alteration of the ore.

The following example illustrates that a combination of different processes may also result in a decreasing effectivity of the overall system. If, for instance, redox reactions and microorganisms are working parallel to reduce the ore, then organo-metallic complexes of both Mn and Fe are likely to form. These compounds, however, lead to a general decrease of the dissolved ionic species of both elements. It is shown above that the pH of the examined redox process is a function of the Fe^{2+} activity and that with increasing iron concentration the geochemical environment becomes more acid. A complex development reducing the concentration of dissolved iron thus results in an increasing alkalinity, because less Fe is available for redox reactions. This

also means that less manganese is mobilized through the co-operation of both mechanisms. Although an addition of individual reaction effectivities could be expected, the general efficiency decreases when these particular processes act together.

Age analysis of supergene manganese oxides illustrates that the secondary materials at Groote Eylandt are less than half the age of the deposit. This supports previous petrological and mineralogical findings showing a large variety of supergene features within ores and rocks. The age data generally demonstrate that the youngest cryptomelane occurs at the top of the stratigraphic section and that the age increases downwards, where the ores are less overprinted. Since supergene minerals such as cryptomelane or todorokite appear increasingly near the top of the section (see chapters 3 and 5), they contribute most to the stratification of the deposit. Similarly, the trace element geochemistry is also stratigraphically controlled. Thus, it is possible to state that the youngest ores and rocks accumulated the highest trace element concentrations.

It is evident that many supergene processes depend on each other to operate, including the availability of water which can stabilize or destabilize certain reactions. Therefore, a generalized alteration path for the dominant minerals (kaolinite, goethite, tetravalent Mn oxides) is outlined to demonstrate the interdependence of the phases. Kaolinite was shown to precipitate from solution mainly during the wet season when abundant water is available (compare January and June in Figs. 6.19-20). This clay formation results in an acidification of the respective microenvironment, which in turn leads to the reduction of goethite on a small scale and its successive replacement by kaolinite. The oxidation of Fe^{2+} to ferrihydrite by Mn^{4+} is the main factor for the reduction and dissolution of manganese, because this dominating redox reaction imposes specific geochemical conditions on the environment. It must be repeated that only tetravalent manganese oxides participate in the described redox reactions, lower valence minerals are passive under these conditions. The generally balanced nature of these processes is illustrated by the lateritic products that overprint former orebodies. Here, mottles of oxidized and bleached Fe-free parts often co-exist in a ratio of approximately 1:1, which is remarkable considering the fact that the overall system is dynamically changing with the seasons.

Once Mn enters solution, the alteration of ferrihydrite to goethite predominates. Because α-MnOOH (groutite) is isostructural with goethite, up to 15 mol% of the Fe in this mineral can also be substituted by manganese. The formation of more stable ferruginous phases, such as hematite, is suppressed by the presence of Mn. It must be noted here, that some observations also point to a comparable dependency of various Mn minerals upon foreign ions (Si, Al $\rightarrow$ cryptomelane or todorokite, but much less pyrolusite). During dissolution, manganese is responsible for its own replacement by a mineral that is reduced easier than hematite or magnetite. The preferential formation of goethite ultimately closes the described cycle of iron mobilization/ reprecipitation and manganese reduction, because any process liberating Fe^{2+} from goethite results in the continuation of redox reactions with Mn^{4+}.

It is unclear whether the formation of kaolinite, as described initially, is the only mechanism to reduce goethite, which is suggested because of a lack of direct evidence for other processes. However, it can be assumed that for instance microorganisms participate in the dissolution of goethite in at least some places near the surface, where additional organic nutrients are available. Such an organically active zone may extend further down into the orebody through drainage pipes. It is also possible that organisms or ferruginous/manganiferous silica complexes contribute to the mobilization of silica and alumina compounds from quartz and kaolinite. These ionic species then precipitate elsewhere and again, their geochemical environment changes.

Although Fe mainly precipitates during the redox reaction with Mn, microbial influences on the formation of iron oxyhydroxides cannot be excluded (e.g. *Thiobacillus Ferrooxidans*). Similarly, bacteria such as *Metallogenium* may support the successive formation of manganese minerals under conditions that favour Mn oxidation. Other processes leading to the development of manganese minerals at Groote Eylandt include rapid precipitation through oxygen-rich surface waters or the mixing of groundwater with highly saline seawater. Field observations indicate that whatever precipitation process is active, it is strongly supported by grainsize variations of the substrate. The larger the size difference between different units, the higher is the precipitation rate in the larger grained material.

An examination of dissolved manganese during transport in river waters revealed that only in one situation, where Mn is reduced in freshwater, do Eh controlled processes dominate. Elsewhere in the deposit and associated rivers, manganese is dissolved by interactive redox processes with iron. Thus, this mobilization mechanism appears to be the most effective process to liberate Mn at Groote Eylandt. As the solutions reach equilibrium with the river water, the geochemical parameters of these waters should favour the precipitation of tetravalent Mn oxides, once the concentrations are high enough. However, the development of chelate complexes protects manganese from rapid oxidation and the concentration limits of Mn^{2+} are exceeded, thus enabling manganese to travel larger distances in the river load. In seawater the geochemistry changes dramatically and much of the reduced Mn is forced out of solution. Under these circumstances, manganese precipitates in the form of Mn oxyhydroxides, such as manganite or groutite.

This chapter presented individual supergene mobilization and precipitation processes and discussed arguments for or against the existence of these mechanisms. In the final section an overview over the dominating processes is given in context with geochemical and geological models.

9. The Mangcrete Model

9.1 Introduction

Above, detailed investigations focused on various aspects of the Mn oxide orebody to determine the type and geological history of residual ores and associated rocks at Groote Eylandt. Some of the supergene mobilization and precipitation processes are now combined to produce a genetic model for the dominant alteration mechanisms operating in the deposit. A supergene reaction cycle is examined and the following discussion puts secondary products into context with their respective geological position within an idealized stratigraphic section (modified after Pracejus et al., 1988b). A comparison of the Groote Eylandt manganese orebody with other deposits assists in the identification of general concepts and their applicability to deposits with similar mineralogy and alteration systems.

9.2 Cyclic Mobility of Supergene Ores and Rocks

The tropical to subtropical conditions at Groote Eylandt create a strongly changing geochemical environment affecting both ores and rocks through the seasonal input of water. It is certain that supergene processes are influenced by such variations, because all examined alteration mechanisms directly depend on water to operate. Thus, it can be expected that supergene cycles generally follow climatic patterns. However, as the dehydration of the deposit proceeds much slower than the weather changes, the geochemical reactions are likely to continue into the dry season. Deeper parts of the orebody may rarely dry out and here continuous mobilization and precipitation processes are supported.

The following model illustrates interactions between the main ore and gangue minerals of the deposit (Fig. 9.1). Processes relevant for the formation of each specific phase are summarized by a keyword such as oxidation, and mechanisms such as biogenic influences, are not described separately; further information is provided in the previous section. The model does not distinguish between different tetravalent Mn oxides, because these minerals behave similarly during alteration or mobilization processes. Contrasting with this necessary simplification for manganese, goethite is taken to represent the FeOOH minerals (α = goethite, β = åkaganeite, γ = lepidocrocite, δ = feroxyhyte) for an examination of aging processes of the initial iron precipitate. Although gibbsite ($Al(OH)_3$) is rare in the deposit, it is incorporated in the model as an analogue for quartz during the alteration of kaolinite.

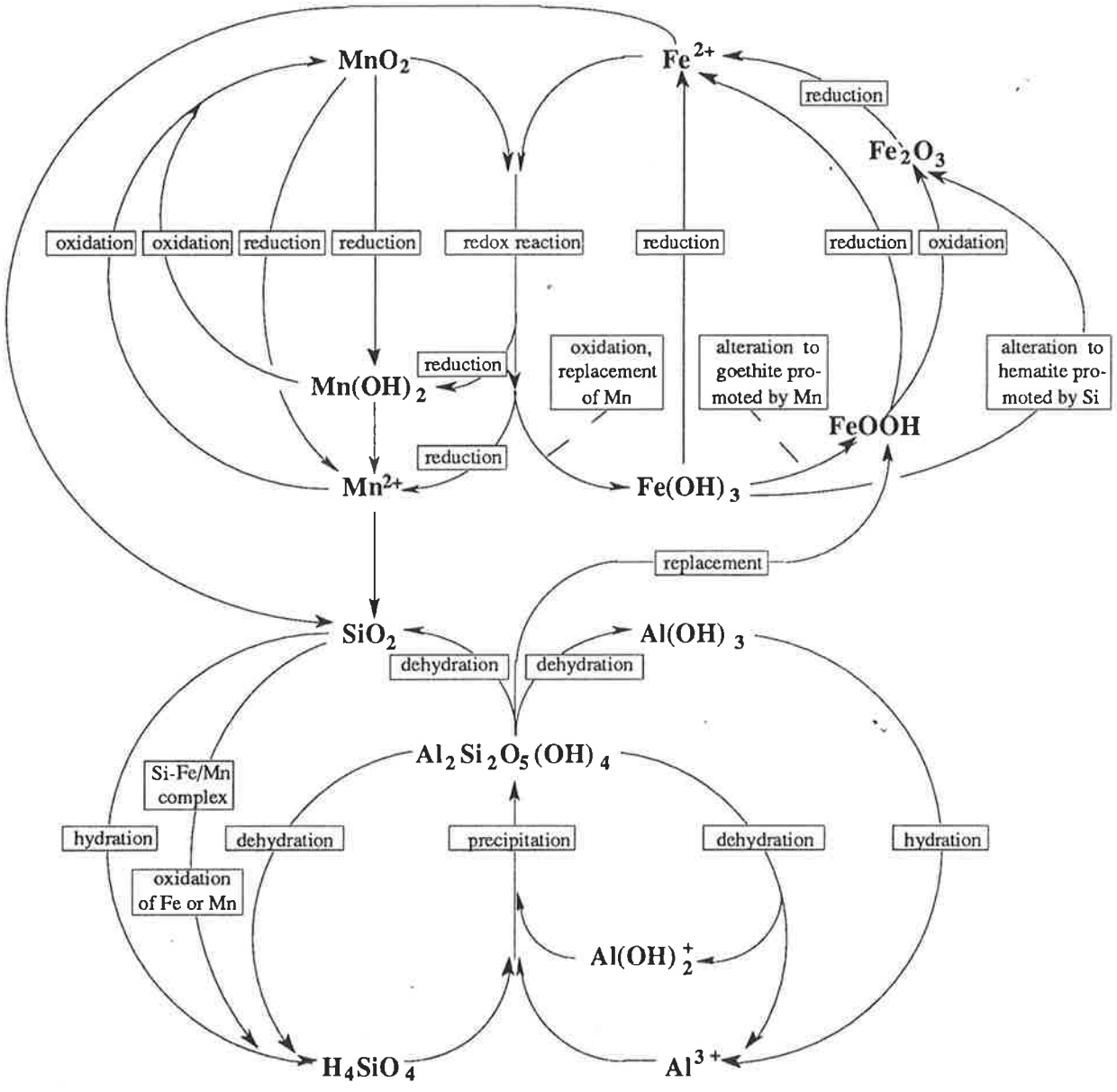


Fig. 9.1: Model of mobilization and precipitation paths for dominant supergene ore and gangue minerals in the lateritic weathering environment of Groote Eylandt.

To start the model mechanisms operating in the deposit, abundant water is needed. Therefore, the beginning of the wet season sets the parameters for all further geochemical reactions. Silica and alumina previously liberated from unstable phases co-precipitate as kaolinite under the influence of abundant water. This clay formation results in an increased acidification of the aqueous system in the vicinity of the newly formed mineral. Locally, the pH becomes low enough to reduce goethite to Fe^{2+}. This mobilized iron can either form semi-stable ferrous silica complexes, it can be oxidized through contact with oxygen, or it can take part in redox reactions with Mn oxides. If goethite is mobilized through the formation of kaolinite, and many findings suggest that this is the main reduction process for this phase, then successive kaolinite development leads to the replacement of goethite by clay (see Plate 3.6, Figs. 3.16c and 3.17).

The availability of divalent iron is the major factor for the reduction of tetravalent manganese at Groote Eylandt, although other processes such as microbial interactions with the ore may be involved. Nevertheless, redox reactions with iron seem to outlast other mechanisms, because ferruginous replacements of manganese oxides are commonly found in the deposit. During the reaction manganese predominantly dissolves as Mn^{2+}, although experimental data also point to an intermittent formation of the relatively unstable $Mn(OH)_2$. Parallel to the reduction of Mn^{4+}, Fe^{2+} is oxidized and it precipitates at the reaction site, replacing manganese with ferrihydrite. This phase is also unstable and it alters to the generally more crystalline minerals of the FeOOH-group. The presence of manganese in solution promotes a further alteration to goethite. Although goethite is the most abundant ferruginous mineral in the deposit, it can be remobilized faster than, for instance, hematite. This strong dominance of goethite over all other Fe phases is a clear indication of the continuous interaction of the minerals examined so far; otherwise different parageneses would have developed at Groote Eylandt.

Similar to iron, dissolved manganese can participate in the formation of semi-stable Mn-Si complexes, ultimately replacing quartz and kaolinite, or it can be transported by pore waters to precipitate elsewhere. Thus, new materials such as siliceous ores develop elsewhere or low-grade Mn ores are upgraded to economically significant concentrations. The precipitation of manganese oxides is particularly supported during the dry season, when environments in the deposit become more oxidizing. However, kaolinite is destabilized by dehydration and the mineral breaks down, liberating hydrated silica polymers and Al ions into solution. This process is reversed once sufficient water is available in the wet season. Thus, the cycle closes and the reduction of iron and manganese minerals again proceeds in successive steps.

Although this model seemingly represents a closed geochemical system, field observations clearly demonstrate that the various processes belong to a dynamic open system with a strong vertical component. Ores are predominantly replaced by goethite and kaolinite near the top of the deposit and manganese precipitates deeper down the section. Successively, goethite is also removed from higher parts of the stratigraphic section and the remaining materials are strongly

bleached white clays. Chemical systems that are almost closed form wherever porewater movement is restricted to a micro-environment. Here, a balance between reduction and oxidation processes develops, which is similar to the final equilibrium of the kaolinite-ore-battery examined in the experimental section (compare Fig. 7.4).

9.3 The Mangcrete Profile

Contrary to detailed stratigraphic profiles analyzed earlier, the following cross section is strongly generalized to provide the geological context for the supergene manganese orebody at Groote Eylandt (Fig. 9.2a). Enlargements of the section are used to point out secondary features of ores and associated rocks. Additionally, the dominant direction of water movement is indicated by arrows (Fig. 9.2b; Figs. 9.2 modified after Pracejus et al., 1988b).

The ore occurs as a stratiform body within an essentially undeformed sedimentary sequence (Fig. 9.2a). The close contact of the ore with underlying siltstones and overlying laterites illustrates that many parts of the deposit are exposed to geochemical reactions associated with these clay-rich rocks. Additionally, the siltstones below the ore form an impermeable horizon and local groundwaters must move through the overlying ores. At Groote Eylandt, a high annual water input through rainfall provides extremely favourable conditions for the continuous activity of supergene alteration and enrichment processes.

Below, small sections of this profile are examined individually, starting at the top and going down successively (Fig. 9.2b). However, it should be noted that the natural mangcrete profile does not necessarily contain all discussed features in one locality. This model combines supergene rock types and superficially influenced rocks found in different areas of the deposit. "Multiple profiles" occur commonly in the form of repeated cycles of mangcretes probably caused by erosion, removal of manganese from higher horizons, and a coupled invasion of lateritic materials. Incomplete mangcrete sections form where local factors, such as outcropping ores or deep burial under extensive laterites, inhibited development.

Where basement sandstones/quartzites and the orebody occur together at the surface, a manganese karst is developed with massive, coarsely layered and concretionary oxidic ores (Fig. 9.2b/G; east of G-Quarry and on K-deposit). Additionally, manganese cave pearls similar to carbonate cave pearls, can be found at the bottom of solution channels in the karst. Mn stalactites have not been observed at Groote Eylandt but have been reported from pisolitic manganese oxide deposits in Western Australia (B.R. Bolton, pers. commun., 1986).

In other areas, the uppermost, unconsolidated earthy zone mainly consists of a yellow to brown sand or a conglomerate, composed of clasts of manganese and iron oxides/hydroxides

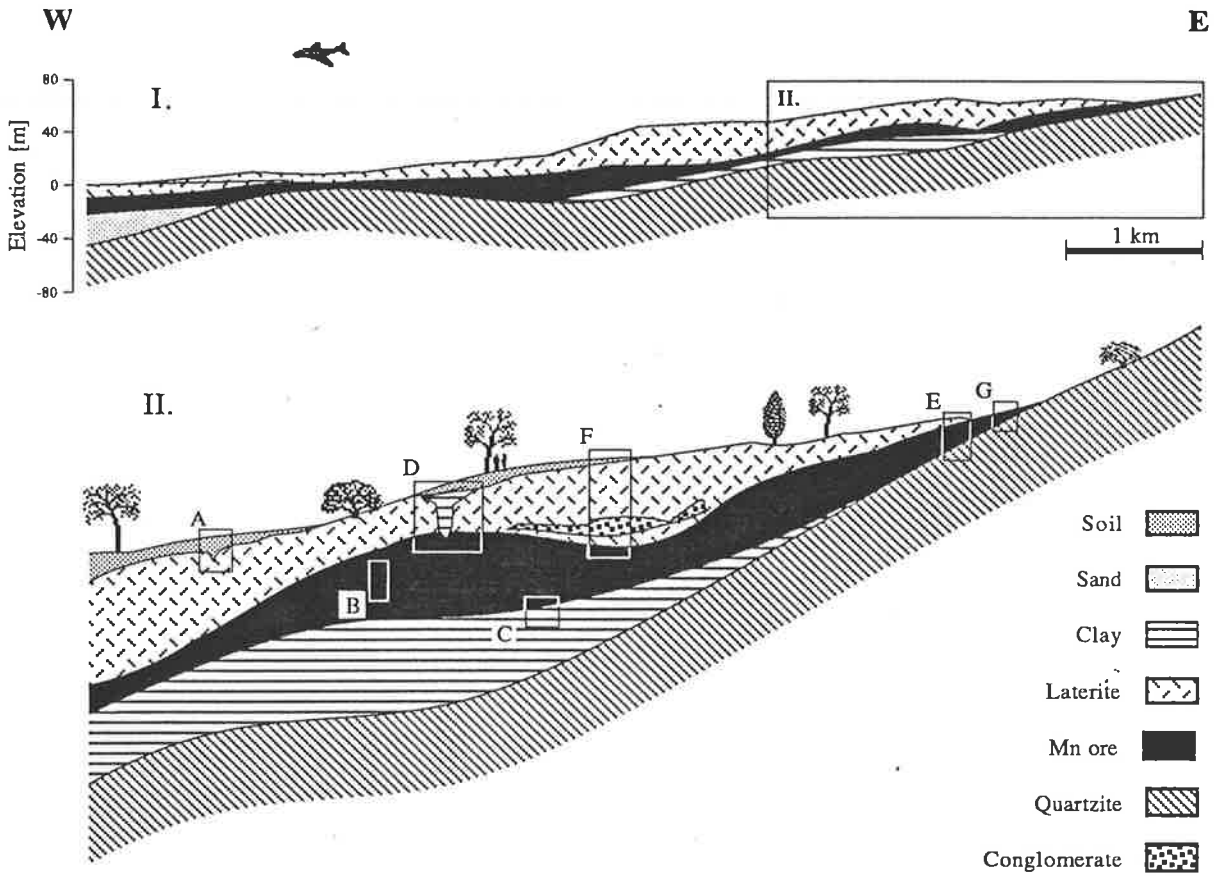


Fig. 9.2a: Idealized section through the Mn oxide deposit of Groote Eylandt; I. overview; II. enlarged segment; details of II. in Fig. 2b.

and sandstones (and quartzites) with sizes ranging from pebbles to cobbles. Above the deposit, sands generally contain manganiferous spherulites and occasionally Mn concretions. Both are mainly horizontally distributed, but they also occur as fillings of sinkholes and vertical pipes (Figs. 9.2b/A,D). Spherulitic and concretionary ores from near the surface are related to pedogenic processes, where evaporation and oxidation are the main controlling factors. Generally normally graded, spherulites indicate rapid precipitation through the occurrence of many small grains in higher parts of the profile. A slower, but probably more continuous growth in deeper areas is depicted by fewer large grains. The same process is applicable to concretions, which sometimes form below the spherulites. Concretions mostly show an upward oriented digital growth.

Farther down the spherulitic zone grades into manganiferous laterites that display dense cementation of predominantly Mn and smaller amounts of Fe. This type of laterite often consists of vugular material, through which water can drain reasonably quickly. The ferruginous laterite that follows, contains little or no manganese phases. Horizontal or vertical pipe structures occur throughout both types of laterite. Often, the vertical pipe systems of laterites form subparallel columns of strongly oxidized and altered manganese ores (referred to as chocolate

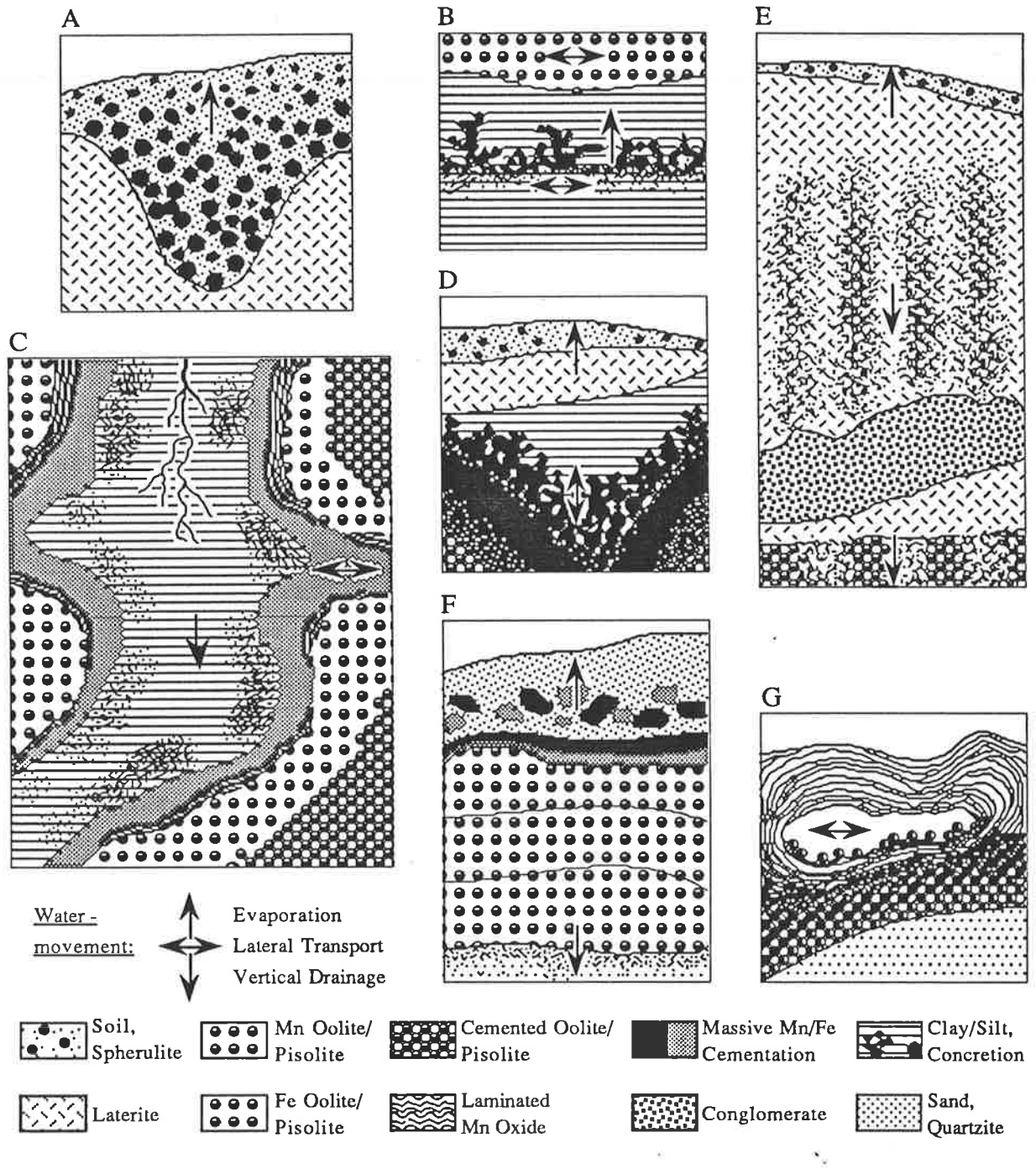


Fig. 2b: Detail sections of Fig. 2a; the capital letters correspond to the outlined geological positions of the previous figure; for explanation see text; modified after Pracejus et al., 1988b.

ore), which are separated by bleached white clays (Fig. 9.2b/F). Seen from a distance the columns clearly outline the shape of former ore bodies (5-6 m thick). Occasionally, erosion of these bodies is indicated by strongly undulating upper contacts. The columns were produced by mostly vertical clay pipes that developed along fractures in the ore. Infilled Fe^{2+}-bearing kaolinite reacted with the surrounding manganese phases (see redox process) and dissolved and replaced them with trivalent iron minerals and clays (Fig. 9.2b/B; particularly F3- and D-Quarry; compare also Figs. 7.1 and 7.2a-c). Similar pipes appear beneath the laterites in the present

orebody. Development of laminar mangcretes in these pipes strongly depends on the availability of oxygen. This secondary ore generally decreases in thickness with increasing depth. The same reaction products, which can be recognized throughout the deposit, are found in connection with diffuse clay impregnations or horizontally continuous clay layers and siltstones. Within the ground water zone and at lower levels of the orebody, the dominant electro-chemical reaction that produced the pipes, also created a boxwork of patchy relict ores and clays. Here the extent of the process is much more visible, because these horizons permanently contain water and replacement reactions are continuously active.

Elsewhere, massive mangcrete develops when primary manganese ores are replaced by dense secondary Mn-phases, which overprint initial structures and textures (lower parts of Fig. 9.2b/D). Cemented mangcretes can grade into massive mangcretes without distinct boundaries. As mentioned earlier, cemented horizons and/or massive mangcretes are often found at sedimentation unit boundaries, where the cementation is usually associated with coarser grains. Siliceous ores commonly underlie primary orebodies (Fig. 9.2b/E; D-, F2-Quarry, C-138). The latter ores mainly derive from supergene processes mobilizing manganese from other parts of the section and reprecipitating the material within quartz sands.

At the contact between the manganese ore and underlying siltstones, hydrated iron phases often replaced primary Mn-ores, thus creating "Fe-oolites/pisolites" (upper part of Fig. 9.2b/C; F1-, F2-, F4-, G-Quarries). Again the first step of the redox reaction can be recognized. The liberated manganese then migrated and precipitated within siltstones as digital concretions or "dendrites" (lower part of Fig. 9.2b/C). Reaction products, such as iron oxides, may also be replaced by clays, thus camouflaging the existence of former orebodies. In other places, where only iron was available and no clays precipitated from ground waters, the replacement features are clearly visible in pisolite grains that have been cross cut by their alteration products (Fig. 9.2b/E; Costean 138; see also Plate 3.2, Figs. 3.3c,d).

9.4 Review of Supergene Influenced Mn-Deposits

An idealized section through the orebody of Groote Eylandt was developed above to demonstrate that specific localities within the profile consistently produce distinct ore and rock types. Below, a few other manganese deposits of the "Non-Volcanogenic-Sedimentary-Type" (Roy, 1981), which include the Groote Eylandt ores, are discussed to examine whether the same supergene rock types and secondary features appear elsewhere under similar alteration conditions (Pracejus et al., 1988b), and whether formation conditions can be generalized.

In only a relatively small number of deposits supergene ores developed directly from oxidic minerals; in most cases residual ores are superimposed on carbonate or metamorphic rocks.

Recent descriptions of manganese occurrences from Western Australia (B.R. Bolton, pers. commun., 1986) and China (Pracejus, 1989) indicate that similar alteration patterns resulted in parageneses and mangcrete profiles identical or comparable to those at Groote Eylandt. It is worth noting that the assemblage oxidic manganese ores-goethite-kaolinite-gibbsite is very often described in context with strong supergene/lateritic processes (Holtrop, 1965; Weber, 1970; Anderson et al., 1974; Nahon et al., 1984). This suggests that chemical redox reactions like those discussed in Pracejus et al. (1986, 1988b) are probably very abundant and that the proposed model section may be useful for other deposits.

The sequence of supergene manganese ores has many equivalents in other weathering profiles (e.g. calcretes, silcretes, ferricretes, bauxites and laterites) and the developing secondary products show parallels in their physical appearance (e.g. laminar mangcrete laminar calcrete; manganese spherulites lateritic spherulites; manganese cave pearls carbonate cave pearls; manganese karst carbonate karst). The terminology for the description of the residual manganese ores therefore was kept close to that used for other rock types. Though supergene processes occasionally overprint the initial rock so extensively that it becomes difficult to identify primary structures, the final minerals will be, whatever their protores, pyrolusite, cryptomelane, todorokite, nsutite, and lithiophorite, plus a few rarer phases. Thus, low concentration ores are upgraded and develop into economically interesting deposits.

9.4.1 Moanda, Gabon

According to Leclerc and Weber (1980) the superficial manganese ores of Moanda developed from a Mn-carbonate-bearing carbonaceous black shale containing 10-20% manganese. They conclude that the main enrichment derives from drastic changes of the ground water levels and a coupled oxidation of the shales. The richest parts of the deposit are said to have formed *in situ* during the decarbonation of the shale, producing mainly manganese oxides and hydroxides in association with minor amounts of Fe-Al-hydroxides, kaolinite and illite. In opposition to this more "passive" formation of supergene ore, the Groote Eylandt deposit shows evidence of vertical and horizontal transport of leached manganese, which leads to an upgraded ore in other areas. In Moanda remobilization produces topographically controlled concretionary cementation of cryptomelane in lower parts of the deposit. Here the dissolution of manganese-bearing rocks seems to degrade supergene rocks, which is in contrast to Groote Eylandt. Nevertheless, in both deposits the topography is important for the control of dissolution and precipitation. Features favoured by specific conditions themselves take part in shaping the landscape and the internal structure of the deposit.

Moanda also exhibits rock types similar to some ores at Groote Eylandt. These are pisoliths (or spheruliths?) embedded in ochreous materials. Though the pisoliths from Gabon basically

differ in their mineralogy (alternate concentric layers of lithiophorite, gibbsite and goethite), it is known from the present study that a selective replacement of specific minerals occurs in many cases. Another similarity is a clay-sand/manganese unit: "This superficial horizon is leached of manganese, but still contains some pisolites" (Leclerc and Weber, 1980, p.105). In Groote Eylandt it was demonstrated that clays are important iron carriers, although the overall Fe^{2+} concentration of the examined kaolinite is low (~1.7%). The redox reaction between Mn and Fe may have worked in Moanda as well, replacing manganese oxides with clay phases.

9.4.2 Janggun Mine, South Korea

The manganese deposits at the Janggun Mine, South Korea, initially consisted of Mn carbonate ores (rhodochrosite, manganiferous dolomitic limestone). Metamorphism, hydrothermal solutions, and supergene alterations later overprinted the ores. The latter process resulted in a number of superficial rocks comparable in many aspects with the mangcrete profile observed in Groote Eylandt. Kim (1980) listed the following secondary materials:

- Earthy zone: wad, dolomite and quartz particles, rock fragments, small manganese grains. The last could be similar to Mn-Spherulites (?).
- Network zone: Mn-oxides that fill fissures and replace the host rock (mostly carbonates). Though this sort of pseudomorphism is fairly rare in Groote Eylandt, it can be observed in small amounts in several areas with the replacement of quartz grains, clays and iron phases. These replacements are not stratigraphy controlled in the Groote Eylandt deposit.
- Concretionary zone: large concretions, often with hollow centers, which sometimes are filled with different minerals. Similar concretions, but much smaller in most cases, can be found near the surface and below the main orebody at several places on Groote Eylandt.
- Cementation zone: Mn-oxides plus intermixed supergene carbonates. In many quarries of Groote Eylandt parts of the orebody are also strongly cemented, but by oxides. Occasionally, this cementation grades into massive ore types (see the following zone), in other cases it is affected again by supergene dissolution processes.
- Compact zone: in the Janggun mining area this compact, massive material is developed at the contact with rhodochrosite ore and replaces it. In contrast to this, the massive ores of Groote Eylandt are not restricted to deeper levels and a specific protore, but finally they also replace and overprint existing manganese-rich rocks.
- Dendritic ores and karstic features: these materials and structures indicate extensive migration of manganese. They also occur in some areas of Groote Eylandt (e.g. in and west of G-Quarry; K-deposit).

There are many similarities between the two deposits in terms of rock types, but because the initial mineralogical composition of the rocks is different and the climatic conditions are also not the same, the reaction tracks for the formation of supergene phases differ as well. Thus, the

following manganese minerals reported from the Janggun deposits are absent or very rare on Groote Eylandt: manganite, nsutite, rhodochrosite, manganocalcite, janggunite, birnessite, braunite, hausmannite. Minerals common to both deposits are cryptomelane, pyrolusite and todorokite.

9.4.3 Nikopol / Chiatura, USSR

The sedimentological characteristics and the development of the giant manganese deposits at Nikopol and Chiatura are described by Varentsov and Rakhmanov (1980). The formation of the two deposits is said to be very similar. The ores contain primary oxides and and carbonates, both as oolites/pisolites, and a massive matrix. Gryaznov and Danilov (1980) suggested a transformation of the primary manganese hydroxides to Mn- carbonates under reducing conditions.

From these initial rocks, supergene hydrated Mn oxides and Fe oxyhydroxides formed secondary ores, all of which can be seen in the Groote Eylandt deposit, with the exception of laminated ores which inherited their structure from carbonates. Manganese impregnation and cementation occur as colloform, concentric and partly very fine grained masses in sandstones and underlying rocks. Additionally, massive or earthy ores, sintered films, and concretions can be observed. Similar to some of the Groote Eylandt ores, the colloform (laminar) material consists mainly of romanechite (psilomelane). Some authors (Stanaway et al., 1978) attribute the greater abundance of romanechite over pyrolusite in supergene mineralizations to the availability of barium. Whenever manganese hydroxides precipitate in the presence of Ba, the colloidal Mn-phases strongly adsorb Ba to build a crystal structure with increased stability.

The coincident appearance of green silts and clays (Fe^{2+}-bearing), manganese oxides and an intermediate reaction horizon containing iron oxides/hydroxides (brown, Fe^{3+}) indicates the existence of the same redox reactions described earlier from Groote Eylandt. Also the replacement of oxidic manganese ores by clays is very typical for this sort of reaction (Varentsov and Rakhmanov, 1980).

9.4.4 Úrkút Basin, Hungary

Similar to many other manganese deposits, the ores in the Urkút basin initially consisted mainly of rhodochrosite and manganocalcite with possibly smaller amounts of additional primary oxides in the northern part of the basin (Szabó and Grasselly, 1980; Grasselly and Pantó, 1988). Since the deposit contains many sulfides, such as pyrite, the development of secondary oxide ores is certainly much different to those previously discussed. The weathering of pyrite

releases SO_4^{2-}-ions into solution, which, in addition to HCO_3^- from carbonates, strongly influence geochemical conditions and mineral solubilities through Eh/pH variations.

However, the final products show some of the characteristics recognized in Groote Eylandt. Szabó and Grasselly (1980) describe nodular (concretionary?) and blocky (massive?) oxidic ores in lower parts of the deposit. These developed from carbonates that dissolved in higher horizons. Manganese dendrites in underlying rocks were also observed. All these features are direct indicators for the mobilization of Mn, but the assemblage of manganite, pyrolusite, cryptomelane and nsutite in the secondary ores clearly points to different conditions during precipitation (Zwicker et al., 1962). Layered (laminar) manganese oxides in the Úrkút deposits resulted from *in situ* oxidation of primary carbonates and they are most probably not comparable to the laminar mangcrete in pipe systems at Groote Eylandt.

Whether dissolution factors other than strongly acidic sulfurous waters are relevant for the production of supergene ores cannot be decided here. Nevertheless, the existence of green clays (Fe^{2+}-bearing?) and goethitic materials could indicate the presence of redox-reactions between iron and manganese. A remobilization of manganese due to such processes might occur at least on a small scale. Again, the secondary manganese profile here and in Groote Eylandt is similar in some aspects of the geology, but not in the mineralogy of the residual manganese ores.

9.4.5 General Comparison of Supergene Products in Different Areas

When all the information about supergene ores and rocks from the discussed localities are considered, the following comparison emerges (Table 9.1). Supergene reaction products and redox partners described from Groote Eylandt can be detected in most other deposits. Concretionary ores, laminar and massive mangcrete, and manganiferous dendrites are commonly found in many places. Spherulites seem to be restricted to tropical and sub-tropical deposits, and only the cemented mangcrete is restricted to Groote Eylandt and the Janggun deposits, although the materials are not directly comparable. It is very interesting to see that kaolinitic clays and iron oxides/oxyhydroxides are nearly always associated with supergene ores. Obviously, they play a role in the formation of superficial manganese ores and minerals which is far more important than was assumed before.

Table 9.1: Comparison of supergene manganese products from different localities* (after Pracejus et al., 1988b).

Supergene ores/rocks	Localities				
	Groote Eylandt Australia	Moanda Gabon	Nikopol/Chiatura USSR	Úrkút Basin Hungary	Janggun, S-Korea
Spherulites	x	x?	n.d.**	n.d.	x?
Concretions	x	x	x	(x)	x
Massive mangcretes	x	(x)	x	(x)	x
Laminar mangcretes	x	n.d.	x	(x)	n.d.
Digital concretions	x	n.d.	n.d.	x	x
Cemented mangcretes	x	n.d.	n.d.	n.d.	x
Clays	x	x	x	x	n.d.
Fe-oxides/oxyhydroxides	x	x	x	x	n.d.

*Clays and Fe-oxides/oxyhydroxides are mentioned, for their relevance in supergene processes at Groote Eylandt;
**n.d. = not described.

9.5 Discussion

The genetic model above illustrates that many of the supergene processes are interdependent and that the resulting secondary materials effectively control the destruction or formation of associated phases. The best example for this dependence is the promotion of goethite development by the presence of dissolved Mn. If for instance the precipitation of minerals such as hematite were supported instead, redox reactions between Fe and Mn would certainly be less prevailing in the deposit, because less iron would be available from a reduction of the more stable hematite. With sufficient time, this process might cease or only work at insignificant levels. Thus, a deposit similar to Groote Eylandt but which lacks one of the main reaction partners (e.g. kaolinite), thus inhibiting any of the necessary processes, is unlikely to develop prominent supergene units.

As most of these residual ores and rocks are bound to specific geological positions, it is possible to generalize the description of various superficial features and materials. In some aspects, the supergene mangcrete profile recognized in this study also seems to be applicable to other deposits. Though elsewhere protores and dissolution processes can be totally different, for instance Mn carbonates being leached with sulfuric acid, the final products are partly similar to the secondary ores described from Groote Eylandt. The mangcrete model should, therefore, be applicable to a wide variety of other manganese deposits with necessary adaptations to additional mobilization processes.

10. Résumé and Conclusions

- The stratigraphy of the Groote Eyladt manganese oxide deposit exhibits both clearly defined and gradational supergene ore and rock units. Generally, these materials occur as sub-horizontal layers extending over tens to hundreds of meters. When in contact with clay-rich horizons, Mn ores tend to be replaced by ferruginous phases and/or clay minerals. This replacement is particularly prominent at the top and at the base of the orebody. A cementation of ores by secondary manganese oxides of the main orebody commonly develops at grain-size or unit boundaries.

- Petrological and mineralogical examinations indicate a relatively small number of minerals representing the bulk of ores and associated rocks. Pyrolusite and cryptomelane are by far the most common manganese oxides, followed by small amounts of todorokite and romanechite. Similarly, kaolinite and goethite dominate the gangue minerals. Quartz and additional clay phases are generally less important within the deposit, although quartzite forms the basement. The dominance of specific minerals in defined stratigraphic positions (e.g. todorokite or cryptomelane near the surface) points to a selective geochemical environment that supports the development of these minerals in dependence on the concentration of oxygen or organic compounds. Additionally, many of the typical parageneses directly depend on the presence of particular precursors. Goethite, for instance, predominantly replaces manganese oxides, and goethite itself is replaced by kaolinite. Thus, the paragenesis of Mn minerals, goethite, and kaolinite is common in the deposit.

- Major, minor, and trace element analyses of ore and rock samples show a strong differentiation of most elements within the stratigraphic section. Generally, the elements decrease with increasing depth, although some initially increase downwards before the trends reverses. The Rare Earth Elements possess particularly marked variations reflecting enrichment

processes in higher horizons.

- A normative method has been developed to assist in the mineralogical quantification of very complex supergene ore and rock samples. The technique demonstrates that secondary units can be traced over at least hundreds of meters and that similar units develop on different lithologies. Individual norm minerals also possess a good correlation with specific trace elements. Additionally, the abundance of various minerals can be used to determine genetic aspects of the respective materials. A prominent example is the development of cryptomelane in association with kaolinite. The application of the norm on microbial reduction/leaching processes showed that the thermodynamically most stable Mn oxides are broken down later than less stable minerals, which is in contrast to some other reduction processes (see redox reaction). Initial correlations of normative mineralogy and battery-activity of ore samples also indicate that it is possible to determine the electric potential of such materials. Thus, the technique seems to be useful for a wide range of geological and mineralogical applications.

- The analysis of water samples demonstrates a mobilization of many elements from the deposit. The fact that manganese occurs in all examined water types during all seasons is evidence for a continuous Mn reduction in the orebody. Thus, supergene ores are forming at present. Since the climatic conditions were comparable over relatively long geological times, it is certain that the supergene overprint of the deposit was active for prolonged time spans. This is supported by determination of cryptomelane-ages that are less than half the age of the deposit (≤41 Ma compared with ~95 Ma).

- Experimental work on a redox process between Mn and Fe operating in the Groote Eylandt manganese deposit duplicated the reaction under controlled laboratory conditions. The mechanism causes the reduction of tetravalent manganese oxides and the replacement of manganese by trivalent iron phases. Because such replacements are common in the field, it is possible to state that the destruction of manganese minerals and the formation of iron phases is strongly interdependent.

- The above mentioned reaction was determined to be the main process for the reduction of manganese oxides in the deposit. Other mechanisms leading to the mobilization of Mn are of subordinate nature, although processes such as microbial leaching or inorganic Eh/pH variations are not discounted entirely. However, without a continuous supply of divalent iron, the redox reactions does not work uninterrupted. Therefore, other reactions must be coupled to provide sufficient Fe. Such mechanisms are for instance found in the formation of kaolinite, which causes a partial reduction and mobilization of goethite. The development or destruction of kaolinite on the other hand are both strongly dependent on the seasonal availability of water. Other inorganic and organic reactions are also impossible in the absence of water and thus, the climatic variations are finally responsible for all supergene process.

- It was demonstrated that manganese deposits elsewhere show supergene products comparable to those at Groote Eylandt, although the geological history of these deposits is different to the geochemical environment examined in this study. Therefore, the "Mangcrete Model" is suggested as an initial idea for more elaborate future models that incorporate mobilization and precipitation mechanisms adjusted to local or global conditions.

References

Adams, L.F. and Ghiorse, W., 1988. Oxidation State of Mn in the Mn Produced by *Leptothrix discophora SS-1*. Geochim. Cosmochim. Acta, 52: 2073-2076.

Agate, A.D. and Deshpande, H.A., 1977. Leaching of Manganese Ores Using Arthrobacter Species. In: Conference Bacterial Leaching Braunschweig-Stöckheim (ed. W. Schwarz). Verlag Chemie: Weinheim, New York. 243-250.

Alexandri, R.Jr., Force, E.R., Cannon, W.F., Spiker, E.C., and Zantop, H.,1985. The Sedimentary Manganese Carbonate Deposits of the Molango District, Mexico. Geol.Soc. America. Abstracts with Programs, 17/7: 511 pp.

Amdel, 1981. Geochronology Report and Data. Report to L.A. Frakes, 2 pp.

Amdel, 1986. Geochronology Report and Data. Report to B.R. Bolton, 3 pp.

Amdel, 1987. Geochronology Report and Data. Report to B. Pracejus, 3 pp.

Anderson, W.L., Dyer, R.C., and Torres, D.D., 1974. Manganese Occurrences in the Itacaiunas River Basin, Southern Amazon Region, Brazil. Problems of Ore Deposition, 4th IAGOD-Symposium, Varna, 3: 114-121.

Anthony, K.E., Fredericks, P.M., and Ostwald, J., 1983. Mineralogical Investigations on G-Quarrry Drill Hole Battery Activity Samples, pp. 26.

Babenko, Yu. S., Dolgikh, L.M., and Serebryanaya, M.Z., 1984. Characteristics of the Bacterial Breakdown of Primarily Oxidized Manganese Ores from the Nikopol Deposit. Plenum Publishing Corporation, 674-679.

Balzer, W., 1982. On the Distribution of Iron and Manganese at the Sediment/Water Interface: Thermodynamic Versus Kinetic Control. Geochimica et Cosmochimica Acta, 46: 1153-1161.

Bárdossy, G., 1982. Karst Bauxites: Bauxite Deposits on Carbonate Rocks. Akadémiai Kiadó, Budapest., pp. 441.

Birkeland, P.W., 1974. Pedology, Weathering and Geomorphological Research. Oxford University Press, London, pp. 285.

Bishop, J.K.B. and Fleisher, M.Q., 1987. Particulate Manganese Dynamics in Gulf Stream Warm-core Rings and Surrounding Waters of the N.W. Atlantic. Geochimica et Cosmochimica Acta, 51: 2807-2825.

Bolton, B.R., 1981 (unpublished). An Investigation of Groote Eylandt Manganese Deposits. Report to B.H.P. Co. Ltd., 52 pp.

Bolton, B.R., 1982 (unpublished). An investigation of Groote Eylandt Manganese Deposits. Final report to B.H.P.Co.Ltd., pp. 141.

Bolton, B.R., 1986 (unpublished). Preliminary Comments on Field Investigations of Manganese Occurrences in Proterozoic Sediments of the Hamersley, Nabberu and Bangemall Basins, Western Australia. Report to B.H.P.Co.Ltd, pp. 23.

Bolton, B.R., Frakes, L.A., and Cook, J.N., 1988. Petrography and Origin of Inversely Graded Manganese Pisolite from Groote Eylandt, Australia. Ore Geology Reviews, 4: 47-69.

Bond, R.D. and Harris, J.R., 1964. The Influence of the Microflora on the Physical Properties of Soils. I. Effects Associated with Filamentous Algae and Fungi. Aust. Soil Res., 2: 111-122.

Bricker, O., 1965. Some Stability Relations in the System $Mn\text{-}O_2\text{-}H_2O$ at 25° and One Atmosphere Total Pressure. American Mineralogist, 50: 1296-1354.

Brown, H.Y.L., 1908. Geological Reconnaissance from Van Diemens Gulf to McArthur River by the Government Geologist, 1907. S. Aust. Parl. Pap., pp. 25.

Burdige, D.J. and Kepkay, P.E., 1983. Determination of Bacterial Mn Oxidation Rates in Sediments Using an in-situ Dialysis Technique. I. Laboratory Studies. Geochim. Cosmochim Acta, 47: 1907-1916.

Burdige, D.J. and Nealson, K.H., 1986. Chemical and Microbiological Studies of Sulfide-mediated Manganese Reduction. Geomicrobiology J., 4: 361-387.

Burns, R.G. and Burns, V.M., 1977. Mineralogy of Manganese Nodules. In: G.P. Glasby (Editor), Marine Manganese Deposits. Elsevier, 185-248.

Burns, R.G., Burns, V.M., and Stockman, H.W., 1985. The Todorokite—Buserite Problem: Further Considerations.American Mineralogist, 70: 205-208.

Butler, L.R.P. and Kokot, M.L., 1971. Atomic Absorption. In: R.E. Wainerdi and E.A. Uken (eds), Modern Methods of Geochemical Analysis. Plenum Press, New York, 245-270.

Calvert, S.E., Piper, D.Z., and Baedecker, P.A., 1987. Geochemistry of the Rare Earth Elements in Ferromanganese Nodules from DOMES Site A, Northern Equatorial Pacific. Geochimica et Cosmochimica Acta, 51: 2331-2338.

Campbell, J.A., 1970. Solubility and Redox Equilibria. In: Chemical Systems, W.H. Freeman and Company, 479-491.

Carlson, L. and Schwertmann, U., 1980. A Natural Occurrence of Feroxhyite (∂-FeOOH). Clays and Clay Minerals, 28/4: 272-280.

Chapnik, S.D., Moore, W.S., and Nealson, K.H., 1982. Microbiologically Mediated Manganese Oxidation in a Fresh Water Lake. Limnol. Oceanogr., 27: 1004-1014.

Chukrov, F.V., Zvyagin, B.B., Ermilova, L.P., and Gorshkov, A.I., 1973. New Data on Iron Oxides in the Weathering Zone. Proc. 6th Clay Conf. 1972 (Madrid), 1: 333-341.

Corliss, J.B., Dymond, J., and Gordon, L.I., 1979. Submarine Thermal Springs on the Galapagos Rift. Science, 203/4385: 1073-1083.

Cornell, R.M. and Giovanoli, R., 1987. Effect of Manganese on the Transformation of Ferrihydrite into Goethite and Jacobsite in Alkaline Media. Clay and Clay Minerals, 35/1: 1-20.

Cornell, R.M. and Giovanoli, R., 1989. Effect of Cobalt on the Formation of Crystalline Iron Oxides from Ferrihydrite in Alakline Media. Clay and Clay Minerals, 37/1: 65-70.

Cornell, R.M. and Schwertmann, U., 1979. Influence of Organic Anions on the Crystallization of Ferrihydrite. Clays and Clay Minerals, 27: 402-410.

Cornell, R.M., Giovanoli, R., and Schindler, P.W., 1987. Effect of Silicate Species on the Transformation of Ferrihydrite into Goethite and Hematite in Alkaline Media. Clay and Clay Minerals, 35/1: 21-28.

Crerar, D.A. and Barnes, H.L., 1974. Deposition of Deep-sea Manganese Nodules. Geochim. Cosmochim. Acta, 38: 279-300.

Crerar, D.A., Cormick, R.K., and Barnes, H.L., 1981. The Geochemistry of Manganese: An overview. In: I.M. Varentsov and G. Grasselly (eds.), Geology and Geochemistry of Manganese. E. Schweizerbartsche Verlagsbuchhandlung (Nägele und Obermiller), Stuttgart, 1: 293-334.

Cross, W., Iddings, P.J., Pirsson, L.V., and Washington, H.S., 1902. Quantitative Classification of Igneous Rocks. Chicago University Press, pp. 286.

De Carlo, E.H. and McMurtry, G.M., 1989 (in press). Rare Earth Element Geochemistry of Seamount Ferromanganese Deposits from the Hawaiian Archipelago. Geochimica et Cosmochimica Acta.

Diem, D. and Stumm, W., 1984. Is dissolved Mn^{2+} being Oxidized by O_2 in Absence of Mn-bacteria or Surface Catalysts? Geochim. et Cosmochim. Acta, 48: 1571-1573.

Dorr, J.V.N., Coelho, I.S., and Horen, A., 1956. 20th Internat. Geol. congr., Sympos. Sobre Yacimentos de Manganeso, 3: 279-364.

Dubinin, A.V. and Volkov, I.I., 1986. Rare Earth Elements in Metalliferous Sediments of the East Pacific Rise. Geokhimija, 5: 645-662.

Dubinina, G.A., 1973. The Significance of Microbiological Processes in Lacustrine Manganese Ore Formation. Int. Ver. Theor. angew. Limnol. Verh., 18: 1261-1276.

Dubrawski, J.V., 1985. Characterization of Battery Active Manganese Oxides by X-Ray Diffraction and Thermal Analysis. Internal Report to B.H.P. Co. Ltd., CRL/R/2/8, pp. 27.

Duff, R.B., Webley, D.M., and Scott, R.O., 1963. Solubilization of Minerals and Related Materials by 2- Ketogluconic Acid-producing Bacteria. Soil Sci., 95: 105-114.

Dunn, P.R., 1962. Explanatory Notes on the Roper River and Cape Beatrice 1:250,000 Geological Sheets, Northern Territory. Bur. Min. Resour. Aust. Rec., 94.

Ebinger, M.H. and Schulze, D.G., 1989. Mn-Substituted Goethite and Fe-Substituted Groutite Synthesized at Acid pH. Clays and Clay Minerals, 37/2: 151-156.

Ehrlich, H.L., 1980. Bacterial Leaching of Manganese Ores. In: Biogeochemistry of Ancient and Modern Environments (eds. P.W. Trudinger, M.R. Walter and B.J. Ralph). Australian Academy of Science: Canberra, 609-614.

Elderfield, H. and Greaves, M.J., 1981. Negative Cerium Anomalies in the Rare Earth Element Patterns of Oceanic Ferromanganese Nodules. Earth and Planetary Science Letters, 35: 163-170.

Ellis, A.H., 1978 (unpublished). Textural, Mineralogical and Geochemical Variations in the Manganese Oxide Mineralization on Groote Eylandt, Northern Territory, Australia. Thesis, University of Sydney, 210 pp.

Fermor, L.L., 1909. The Manganese Ore Deposits of India. Geol. Surv. India, Mem., 37.

Fischer, W.R. and Schwertmann, U., 1975. The Formation of Hematite from Amorphous Iron(III) Hydroxide. Clays and Clay Minerals, 23: 33-37.

Flanagan, F.J. and Gottfried, D., 1980. USGS Rock Standards, III: Manganese-Nodule Reference Samples USGS-Nod-A-1 and USGS-Nod-P-1. Geological Survey Professional Paper, 1155: 1-39.

Fleet, M.E.L., 1965. Preliminary Investigations into the Sorption of Boron by Clay Minerals. Clay Minerals, 6: 3-16.

Fleet, A.J., 1983. Hydrothermal and Hydrogenous Ferro-manganese Deposits: Do They Form a Continuum? The Rare Earth Evidence. In: Rona, P.A., Boström, K., Loubier, L., and Smith, K.L. (eds.), Hydrothermal Processes at Seafloor Spreading Centers, Plenum Press, New York, 535-555.

Flinders, M., 1814. A Voyage to Terra Australia. Nicol, G. & W. (eds.), London.

Frakes, L.A., 1979 (unpublished). Modern and Ancient Analogues for Groote Eylandt Ores. Report to B. H. P. Co. Ltd., 119 pp.

Frakes, L.A. and Bolton, B.R., 1984. Origin of Manganese Giants: Sea-level Change and Anoxic-Oxic History. Geology, 12: 83-86.

Frazer, F.W., 1969 (unpublished). Characterization of the Groote Eylandt Manganese Ores Part II-X-Ray Diffraction Methods for the Quantitative Analysis of Pyrolusite and Cryptomelane in Groote Eylandt Manganese Ores. CRL/TC 22, pp. 21.

Fredericks, P.M., Osborne, P.R., and Swinkels, D.A.J., 1983. Materials Characterization by Fourier Transform Infrared Spectroscopy. BHP Tech. Bull., 27/1:26-32.

Fredericks, P.M., Osborn, P.R., and Swinkels, D.A.J., 1984 (unpublished). Grade Control in Manganese Mining by FTIR Spectroscopy. B.H.P. Report, pp. 10.

Freeman, D.S., Pelter, P.F., Tye, F.L., and Wood, L.L., 1971. Screening of Manganese Dioxide for Battery Activity with Thermogravimetric Analysis. J. Appl. Electrochem., 1: 127-136.

Frondel, C., Marvin, U.B., and Ito, J., 1960. New Occurrences of Todorokite. American Mineralogist, 45: 1167-1173.

Fryer, B.J., 1977. Rare Earth evidence in Iron Formations for Changing Precambrian Oxidation States. Geochimica et Cosmochimica Acta, 41: 361-367.

Fysh, A.S. and Fredericks, P.M., 1983. Fourier Transform Infrared Studies of Aluminous Goethites and Hematites. Clays and Clay Minerals, 31/5: 377-382.

GEMCO, 1984 (unpublished). Bead Preparation for XRF. In: Chemical Methods for Manganese Ore, pp. 29.

Ghiorse, W.C., 1986. Applicability of Ferromanganese-depositing Microorganisms to Industrial Metal Recovery Processes. Biotechnol. Bioeng. Symp., 16: 141-148.

Giovanoli, R. and Balmer, B., 1983. Darstellung und Reaktionen von Psilomelan (Romanéchit). Chimia, 37/11: 424-42.

Glasby, G.P., Gwozdz, R., Kunzendorf, H., Friedrich, G., and Thijssen, T., 1987. The Distribution of Rare Earth and Minor Elements in Manganese Nodules and Sediments from the Equatorial and S.W. Pacific. Lithos, 20: 97-113.

Goethe, J.W. von, 1830. Musenalmanach (ed. A. Wendt), Leipzig.

Goldberg, E.D., 1965. Minor Elements in Sea Water. In: Riley, J.P. and Skirrow, G. (eds.). Chemical Oceanography, 1: 163-196.

Goldstein, S.J. and Jacobsen, S.B., 1988. REE in the Great Whale River Estuary, Northwest Quebec. Earth and Planetary Science Letters, 88: 253-262.

Grasselly, Gy. and Pantó, Gy., 1988. Rare Earth Elements in the Manganese Deposit of Úrkút (Bakony Mts., Hungary). Ore Geology Reviews, 4: 115-124.

Gryaznov, V.I. and Danilov, I.S., 1980. Oxidized Ores of Nikopol Deposit. In: Varentsov I.M. and Grasselly, Gy. (eds.), Geology and Geochemistry of Manganese. E. Schweizerbartsche Verlagsbuchhandlung (Nägele und Obermiller) Stuttgart, 2: 403-416.

Hallberg, R.O., Bubela, B., and Ferguson, J., 1979. Metal Chelation in Sedimentari Systems. Geomicrobiology Journal, 2/2: 99-113.

Handbook of Chemistry and Physics, 1976. CRC Press, Inc., Cleveland, Ohio.

Harbison, P. 1986. Mangrove Muds-A Sink and a Source for Trace Metals. Marine Pollution Bulletin, 17/6:246-250.

Hariya, Y. and Kikuchi, T., 1964. Precipitation of Manganese by Bacteria in Mineral Springs. Nature, 202/4930: 416-417.

Hart, M.J. and Madgwick, J.C., 1986 (manuscript). Biodegradation of Manganese Dioxide Tailings, pp.22.

Haskin, M.A. and Haskin, L.A., 1966. Rare Earths in European Shales: A Redetermination. Science, 154: 507-509.

Hein, J.R., Schulz, M.S., and Kang, J.-K., 1989 (in press). Insular and Submarine Ferromanganese Mineralization of the Tonga-Lau Region. In: Ballance, P.F., Herzer, R.H. and Vallier, T.L. (eds.), Geology of the Tonga-Lau Regions of the Southwest Pacific, Circum-Pacific Council for Energy and Mineral Resources, Earth Science Series, Houston, Texas.

Heinen, W., 1979. Evolutionary Aspects of Biological Involvement in the Cycling of Silica. In: P.A. Trudinger and D.J. Swaine (eds.), Biogeochemical Cycling of Mineral-Forming Elements. Elsevier, Amsterdam, 431-443.

Hem, J.D., Redox Processes at Surfaces of Manganese Oxide and Their Effects on Aqueous Metal Ions. Chem. Geol., 21: 199-218.

Hem, J.D. and Lind, C.J., 1983. Nonequilibrium Models for Predicting Forms of Precipitated Manganese Oxides. Geochimica et Cosmochimica Acta, 47: 2037-2046.

Hem, J.D., Roberson, C.E., and Lind, C.J., 1985. Thermodynamic Stability of CoOOH and its Coprecipitation with Manganese. Geochimica et Cosmochimica Acta, 49: 801-810.

Hemingway, B.S., 1982. Gibbs Free Energies of Formation for Bayerite, Nordstrandite, $Al(OH)^{2+}$, Aluminium Mobility, and the Formation of Bauxites and Laterites. In: Advances in Physical Geochemistry, S.K. Saxena (ed.), Springer Verlag, New York, 2: 285-315.

Hiltunen, P., Vuorinen, A., Rehtijärvi, P., and Tuovinen, O.H., 1981. Bacterial Pyrite Oxidation: Release of Iron and Scanning Electron Microscopic Observations. Hydrometallurgy, 7: 147-157.

Hofmann, K.A. and Erhardt, U., 1913. Berichte, 46: 1457-1466.

Holtrop, J.F., 1965. The Manganese Deposits of the Guiana Shield. Economic Geology, 60: 1185-1212.

Ingri, J. and Pontér, C., 1987. Rare Earth Abundance Patterns in Ferromanganese Concretions from the Gulf of Bothnia and the Barents Sea. Geochimica et Cosmochimica Acta, 51: 155-161.

Jones, B.F. and Weir, A.H., 1983. Clay Minerals of Lake Abert, an Alkaline, Saline Lake. Clays and Clay Minerals, 31: 161-172.

Kim, S.J., 1980. Genesis of Manganese Carbonate and Oxide Deposits at the Janggun Mine, South Korea. In: Varentsov I.M. and Grasselly, Gy. (eds.), Geology and Geochemistry of Manganese. E. Schweizerbartsche Verlagsbuchhandlung (Nägele und Obermiller) Stuttgart, 2: 297-318.

Kittrick, J.A., 1969. Soil Minerals in the Al_2O_3-SiO_2-H_2O System and a Theory of their Formation. Clay and Clay Minerals, 17: 157-167.

Kopeykin, V.A. and Lebedev, V.A., 1985. Iron Accumulation and Loss During Weathering. Scripta Technica, Inc., 23/3: 90-99.

Kozub, J. and Madgwick, J.C., 1983. Microaerobic Microbial Manganese Dioxide Leaching. Proc. Australas. Inst. Met., 288: 51-54.

Krauskopf, K.B., 1979.Introduction to Geochemistry. Mc Graw-Hill Intern. Series in the Earth and Planetary Sciences, 2nd Edition, pp. 617.

Krishnamurti, G.S.R. and Huang, P.M., 1988. Influence of Manganese Oxide Minerals on the Formation of Iron Oxides. Clay and Clay Minerals, 36/5: 467-475.

Kung, H.-H. and McBride, M.B., 1988. Electron Transfer Processes between Hydroquinone and Hausmannite (Mn_3O_4). Clays and Clay Minerals, 36/4: 297-302.

Kurdyukov, A.A., 1967. Galvanic Effect of Minerals and Rocks. Dokl. Akad. Nauk SSSR, 176/3: 668-671.

Langkamp, P.J. and Dalling, M.J., 1979. Studies on the Rehabilitation of Mined Areas on Groote Eylandt, Northern Territory. II. Soil Characterization and Rehabilitation with Pasture. Reclamation Review, 2: 157-166.

Larson, L.T., 1962. Zinc-bearing Todorokite from Philipsburg, Montana. American Mineralogist, 47: 59-66.

Laxen, D.P.H., Davis, W., and Woof, C., 1984. Manganese Chemistry in Rivers and Streams. Geochimica et Cosmochimica Acta, 48: 2107-2111.

Leclerc, J. and Weber, F., 1980. Geology and Genesis of the Moanda Manganese Deposits, Republic of Gabon. In: Varentsov I.M. and Grasselly, Gy. (eds.), Geology and Geochemistry of Manganese. E. Schweizerbartsche Verlagsbuchhandlung (Nägele und Obermiller) Stuttgart, 2: 89-109.

Liebhafsky, H.A. and Pfeiffer, H.G., 1971. X-Ray Techniques. In: R.E. Wainerdi and E.A. Uken (eds), Modern Methods of Geochemical Analysis. Plenum Press, New York, 245-270.

Lundgren, D.G., Vestal, J.R., and Tabita, F.R., 1974. The Iron-oxidizing Bacteria. In: J.B. Neilands (ed.), Microbial Iron Metabolism. Academic Press, NY, 457-473.

MacDonald, D.G. and Clark, R.H., 1970. The Oxidation of Aqueous Ferrous Sulfate by Thiobacillus Ferrooxidans. Can. J. Chem. Eng., 48: 669-676.

Madgwick, J.C., 1987. Microbial Processing of Manganese. Australian Journal of Biotechnology, 1/2: 41-43.

Marsalek, J., 1977. Microbiological Leaching of Manganese. Rudy, 25/9: 254-257.

Marshall, K.C., 1979. Biogeochemistry of Manganese Minerals. In: Biogeochemical Cycling of Mineral Forming Elements (Eds. P.A. Trudinger and D.J. Swaine), Elsevier, Amsterdam. 253-292.

May, H.M., Kinniburgh, D.J., Helmke, P.A., and Jackson, M.L., 1986. Aqueous Dissolution, Solubilities and Thermodynamic Stabilities of Common Aluminosilicate Clay Minerals: Kaolinite and Smectites. Geochim. Cosmochim. Acta, 50: 1667-1677.

McFarlane, M.J. and Heydeman, M.T., 1985. Some Aspects of Kaolinite Dissolution by a Laterite-Indigenous Micro-Organism. Geogr. Ecol. Trop., 8: 73-91.

McHugh, L., 1983 (unpublished). Geology of Secondary Manganese Deposits on Groote Eylandt, Northern Territory. Thesis, La Trobe University, Melbourne, 86 pp.

Merck. Manganese. Information leaflets, Aquaquant®14406. E. Merck, Darmstadt, FRG.

Merck. Oxygen. Information leaflets, Aquamerck®11107. E. Merck, Darmstadt, FRG.

Merck. Reaction of Iron(II) with Ferrospectral in a Thioglycolate Buffer to form a violet color complex. Information leaflets, Aquaquant®14403. E. Merck, Darmstadt, FRG.

Mercz, T.I. and Madgwick, J.C., 1982. Enhancement of Bacterial Manganese Leaching by Microalgal Growth Products. Proc. Australas. Inst. Min. Metall., 283: 43-46.

Merino, E. and Ransom, B., 1982. Free Energies of Formation of Illite Solid Solutions and their Compositional Dependence. Clays and Clay Minerals, 30: 29-39.

Millero, F.J., 1985. The Effect of Ionic Interactions on the Oxidation of Metals in Natural Waters. Geochimica et Cosmochimica Acta, 49: 547-553.

Millero, F.J., Sotolongo, S., and Izaguirre, M., 1986. The Oxidation Kinetics of Fe(II) in Seawater. Geochimica et Cosmochimica Acta, 51: 793-801.

Morgan, J.J., 1964 (unpublished). Chemistry of Aqueous Manganese II and IV. PhD. dissertation, Harvard University, Cambridge, MA, pp. 224.

Morgan, J.J., 1967. Chemical Equilibria and Kinetic Properties of Manganese in Natural Waters. In: Principles and Applications of Water Chemistry (eds. S.D.Faust and J.V. Hunter), John Wiley & Sons. 561-624.

Morgan, J.J. and Stumm, W., 1965. Colloid-chemical Properties of Manganese Dioxide. J. Colloid Sci., 19: 347-359.

Morris, R.C. and Fletcher, A.B., 1987. Increased Solubility of Quartz Following Ferrous-Ferric Iron Reactions. Nature, 330:558-561.

Myers, C.M. and Nealson, K., 1988. Bacterial Manganese Reduction and Growth with Manganese Oxide as the Sole Electron Acceptor. Science, 20:1319-1321.

Nahon, D., Beauvais, A., Nziengui-Mapangou, P., and Ducloux, J., 1984. Chemical Weathering of Mn-Garnets under Lateritic Conditions in Northwest Ivory Coast (W-Africa). Chemical Geology, 45: 53-71.

Näser, K.-H., 1974. Physikalische Chemie. VEB Deutscher Verlag für Grundstoffindustrie, Leipzig. pp. 489.

Nealson, K.H. and Tebo, B., 1980. Structural Features of Manganese Precipitating Bacteria. Origins of Life, 10: 117-126.

Netterberg, F., 1976. Comments on a Paper by G.D. Aitchinson and K.Grant. In: 4th Regional Conference for Africa on Soil Mechanics and Foundation Engineering Proc., 2: 34.

Nordstrom, D.K. and Munoz, J.L., 1985. Geochemical Thermodynamics. The Benjamin/Cummings Publishing Co., Inc. pp. 477.

Northcote, K.H., 1974. A Factual Key for the Recognition of Australian Soils. Rellim Technical Publications, Adelaide.

Ostwald, J., 1976. Aspects of the Mineralogy, Petrology and Genesis of the Groote Eylandt Manganese Ores. 25th Internat. Geol. Congr. Sydney, I.A.G.O.D. Symposium, Geology Geochemistry Manganese Abstracts, 3: 788 pp.

Ostwald, J., 1980. Aspects of the Mineralogy, Petrology and Genesis of the Groote Eylandt Manganese Ores. In: I.M. Varentsov and Gy. Grassely (Editors), Geology and Geochemistry of Manganese. E. Schweizerbartsche Verlagsbuchhandlung (Nägele und Obermiller), Stuttgart, 2: 149-18.

Ostwald, J.,1981. Evidence for a Biological Origin of the Groote Eylandt Manganese Ores. Econ. Geology, 76: 556-567.

Ostwald, J., 1984. Some Observations on the 7 Å X-Ray Reflection in Marine Manganese Nodules. N. Jb. Miner. Mh., 1: 1-8.

Ostwald, J., 1988. Mineralogy of the Groote Eylandt Manganese Oxides: A Review. Ore Geology Reviews, Elsevier, 4: 3-45.

Palmer, M.R., Spivack, A.J., and Edmond, J.M., 1987. Temperature and pH Controls over Isotopic Fractionation During Adsorption of Boron on Marine Clay. Geochimica et Cosmochimica Acta, 51: 2319-2323.

Perkins, E.C. and Novielli, F., 1962. Bacterial Leaching of Manganese Ores. United States Department of the Interior Bureau of Mines. Report 6102.

Perseil, E.A. and Grandin, G., 1978. Evolution Mineralogique du Manganèse Gisement d'Afrique de l'Ouest : Mokta, Tambao, Nsuta. Miner. Deposita, 13: 295-311.

Pettijohn, F.J., Potter, P.E., and Siever, R., 1987. Sand and Sandstone (2nd edition). Springer Verlag Berlin, pp. 553.

Piper, D.Z., 1974. Rare Earth Elements in the Sedimentary Cycle: A Summary. Chem. Geol., 14: 285-304.

Plumb, K.A., Derrick, G.M., and Wilson, I.H., 1980. Precambrian Geology of the Mc Arthur River - Mount Isa Region, Northern Australia. In: Henderson, R.A. and Stephenson, P.J. (eds.). The Geology and Geophysics of Northeastern Australia. Geol. Soc. Austr. (Qld. Division), 71-88.

Post, J.E., Von Dreele, R.B. and Buseck, P.R. 1982. Symmetry and Cation Displacements in Hollandites: Structure Refinements of Hollandite, Cryptomelane and Priderite. Acta Cryst., 38, 1056-1065.

Potter, R.M. and Rossman, G.R., 1979. The tetravalent Manganese Oxides: Identification, Hydration, Structural Relationships by IR Spectroscopy. American Mineralogist, 64: 1199-1218.

Pracejus, B., 1985 (unpublished). Geological Investigations on Secondary Manganese Ores. Initial Field Report to B.H.P. Co. Ltd., 33 pp.

Pracejus, B., 1986 (unpublished). Experimental and Analytical Investigations on the Geochemistry and Mineralogy of Secondary Mn-Phases from Groote Eylandt, N.T., Australia. Report to B.H.P. Co. Ltd., 57 pp.

Pracejus, B., 1989. The Wafangzi Ferromanganese Deposit, China-An Overview. The Australian Geologist, 70: 24-25.

Pracejus, B., 1990 (in press). Groote Eylandt Manganese Norm-New Application of Mineral Normalization Techniques on Supergene Alteration Products. IAS Special Publication.

Pracejus, B., Bolton, B.R., and Frakes, L.A., 1986. Electrochemical Process in Mn-Ores from Groote Eylandt (N.T., Australia): Significance for the Generation of Supergene Mn-Deposits. Abstract for the 12th Int. Sed. Congr., Canberra, 247-248.

Pracejus, B., Bolton, B.R., and Frakes, L.A., 1988a. Mineral Normalization for Supergene Mn-Oxides and Associated Rocks on Ores from Groote Eylandt, N.T., Australia. Abstract for the IAS Symposium on Sedimentology Related to Mineral Deposits 1988, Beijing, China, p. 202.

Pracejus, B., Bolton, B.R., and Frakes, L.A., 1988b. Nature and Development of Supergene Manganese Deposits, Groote Eylandt, Northern Territory, Australia. Ore Geology Reviews, Elsevier, 4: 71-98.

Pracejus, B., Bolton, B.R., Frakes, L.A., and Abbot, M., 1989 (in press). Rare Earth Element Geochemistry of Supergene Manganese Deposits from Groote Eylandt, Northern Territory, Australia. Ore Geology Reviews, Elsevier.

Putilina, V.S. and Varentsov, I.M., 1980. Interaction Between Organic Matter and Heavy Metals in the Waters of Recent Basins - A Review of the Current State of the Problem. Chem. Erde, 39: 298-310.

Rankin, P.C. and Glasby, G.P., 1979. Regional Distribution of Rare Earth and Minor Elements in Manganese Nodules and Associated Sediments in the Southwest Pacific and other Localities. In: Marine Geology and Oceanography of the Pacific Manganese Province. Bischoff, J.L. and Piper, D.Z. (eds.), Plenum Publishing Corporation; 681-697.

Read, J., 1974. Carbonate Bank and Wave-built Platform Sedimentation, Edel Province, Western Australia. Am. Assoc. Petrol. Geol., Mem., 22: 1-60.

Robie, R.A., Hemingway, B.S., and Fisher, J.R., 1978. Thermodynamic Properties of Minerals and Related Substances at 298.15 °K and 1 bar (10^5 pascals) Pressure and at Higher Temperatures. U.S. Geol. Survey Bull., 1452, pp. 456.

Rosson, R.A. and Nealson, K.H., 1982. Manganese Binding and Oxydation by Spores of a Marine Bacillus. J. Bacteriol., 151: 1027-1034.

Roy, S.J., 1981. Manganese Deposits. Acad Press. London, 458 pp.

Schwertmann, U. and Murad, E., 1983. The Effect of pH on the Formation of Goethite and Hematite from Ferrihydrite. Clays and Clay Minerals, 31: 277-284.

Schwertmann, U., Fischer, W.R., and Taylor, R.M., 1974. New Aspects of Iron Oxide Formation in Soils. Trans. 10th Int. Congr. Soil Sci. (Moscow), 6: 237-249.

Shafia, F. and Wilkinson, R.F., 1969. Growth of *Ferrobacillus Ferrooxidans* on Organic Matter. J. Bacteriol., 97: 256-260.

Sholkovitz, E.R., 1976. Flocculation of Dissoved Organic and Inorganic Matter During the Mixing of River Water and Seawater. Geochimica et Cosmochimica Acta, 40: 831-845.

Silverio, C.M. and Madgwick, J.C., 1985 (manuscript). Biodegradation of Manganese Dioxide By Purified Leaching Microorganisms, pp. 20.

Silverman, M.P., 1979. Biological and Organic Chemical Decomposition of Silicates. In: P.A. Trudinger and D.J. Swaine (eds.), Biogeochemical Cycling of Mineral-Forming Elements. Elsevier, Amsterdam, 445-465.

Slee, K.J., 1976 (unpublished). The Setting, Geology and Origin of the Groote Eylandt Manganese Deposits, Australia. Corrected Version. Report to B.H.P. Co. Ltd., Nr. 191.

Slee, K.J., 1980. Geology and Origin of the Groote Eylandt Manganese Oxide Deposits, Australia. In: Varentsov I.M. and Grasselly, Gy. (eds.), Geology and Geochemistry of Manganese. E. Schweizerbartsche Verlagsbuchhandlung (Nägele und Obermiller) Stuttgart, 2: 125-148.

Smith, W.C. and Gebert, H.W., 1969. Manganese at Groote Eylandt, Australia. In: 9th Commonwealth Mining and Metallurgical Congress, 1969, Mining and Petroleum Geology Section, 2: 585-604.

Smith, W.C., Crohn, P.W., and O'Brien, R.T., 1965. The Manganese Deposits of Groote Eylandt, Northern Territory. Paper presented at ANZAAS Section C, Hobart, pp. 18.

Stace, H.C.T., Hubble, G.D., Brewer, R., Northcote, K.H., Sleeman, J.R., Mulcahy, M.J., and Hallsworth, E.G., 1968. A Handbook of Australian Soils. Rellim Technical Publications, Adelaide.

Stanaway, K.J., Kobe, H.W., and Sekula, J., 1978. Manganese Deposits and the Associated Rocks of Northland and Auckland, New Zealand. N. Z. Journal of Geology and Geophysics, 21/1: 21-32.

Stone, A.T., 1987. Microbial Metabolites and the Reductive Dissolution of Manganese Oxides: Oxalate and Pyruvate. Geochimica et Cosmochimica Acta, 51: 919-925.

Straczek, J.A., Horen, A., Ross, M., and Warsaw, C.M., 1960. Studies of the Manganese Oxides—IV, Todorokite. American Mineralogist, 45: 1174-1184.

Stucki, J.W., Komadel, P., and Wilkinson, H.T., 1987. Microbial Reduction of Structural Iron (III) in Smectites. Soil Sci. Soc. Amer. J., 51: 1663-1665.

Swinkels, D.A.J. and Williams, J.P., 1982. Evaluation of Battery Activity of Groote Eylandt Ore. Tech. Bull., 26/1, pp. 56.

Sybron, Barnstead. Instruction Manual for the PHOTOchem™ Organic Carbon Analyzer. Sybron/Barnstead, Boston, Massachusetts.

Szabó, Z. and Grasselly, GY., 1980. Genesis of Manganese Oxide Ores in the Urkút Basin, Hungary. In: Varentsov I.M. and Grasselly, Gy. (eds.), Geology and Geochemistry of Manganese. E. Schweizerbartsche Verlagsbuchhandlung (Nägele und Obermiller) Stuttgart, 2: 223-236.

Tada, R., Maliva, R., and Siever, R., 1987. A New Mechanism for Pressure Solution in Porous Quartzose Sandstone. Geochimica et Cosmochimica Acta, 51: 2295-2301.

Taylor, D.G., 1979. Age and Paleobiology of the Groote Eylandt Manganiferous Sediments. Report from Paltech. to B.H.P. Co. Ltd., 65 pp.

Taylor, D., 1980. Paleontological Examination of Samples from G-Quarry - Groote Eylandt. Report from Paltech to BHP, 19: 1-2.

Taylor, D.G., 1981. Probable Early Cenomanian Planktonic Foraminifera in Groote Eylandt 1981 Drill Hole Samples. Report from Paltech. to B.R. Bolton, 3 pp.

Taylor, R.M. and Bond,R.D., 1979. Electrolytic Weathering Effects in Minerals. Geoderma, 22: 85-97.

Taylor, R.M. and Fischer, W.R., 1973. Electric Potentials Between Different Rocks. Naturwissenschaften, 6: 298.

Thornber, M.R., 1983 (unpublished). Weathering of Sulfide Bodies. In: Geochemical Exploration in Deeply Weathered Terrain. CSIRO Report, 67-72.

Troshanov, E.P., 1968. Iron and Manganese Leaching Microorganism in Ore Containing Lakes of the Karelian Isthmus. Mikrobiologya, 37/5: 934-940.

Truesdale, G.A., Downing, A.L., and Lowden, G.F., 1955. Determination of Oxygen Saturation as a Function of the Temperature Under a Total Pressure of the Water Vapor-saturated Atmosphere of 760 mm Hg. J. Appl. Chem., 5: 53-62.

Turner, S. and Buseck, P.R. 1979. Manganese Oxide Tunnel Structures and their Intergrowths. Science, 203, 256-458.

Tyuryukanova, E.B. and Konova, N.I., 1987. Behaviour of Mn and Fe in Young Supergene Deposits. Geochemistry International, 24: 105-112.

Van Der Sloot, H.A., Hoede, D., Hamburg, G., De Lange, G.J., Middelburg, J.J., and Sophiah, S., 1988. Suspended Manganese-Rich Particles in Kau Bay, Halmahera (Eastern Indonesia). Marine Geology, 82: 251-259.

Varentsov, I.M., 1982. Groote Eylandt Manganese Oxide Deposits, Australia. Chem. Erde, 41: 157- 173.

Varentsov, I.M. and Golovin, D.I., 1987. The Manganese Ore Deposit of Groote Eylandt, Northern Australia: K-Ar Age of Cryptomelane Ores and Aspects of their Genesis. Doklady Akademii Nauk SSSR, 294/1:203-207.

Varentsov, I.M. and Rakhmanov, V.P., 1980. Manganese Deposits of the USSR (A Review). In: Varentsov I.M. and Grasselly, Gy. (eds.), Geology and Geochemistry of Manganese. E. Schweizerbartsche Verlagsbuchhandlung (Nägele und Obermiller) Stuttgart, 2: 320-3.

Wadsley, A.D. and Walkley, B.A., 1951. The Structure and Reactivity of the Oxides of Manganese. Rev. Pure Appl. Chem., 1: 203-213.

Walther, J.V. and Helgeson, H.C., 1977. Calculation of the Thermodynamic Properties of Aqueous Silica and the Solubility of Quartz and its Polymorphs at high Pressures and Temperatures. Am. J. Sci., 277: 1315-1351.

Weber, F., 1970. Genesis and Supergene Evolution of the Precambrian Sedimentary Manganese Deposit at Moanda (Gabon). Earth Sciences, 9: 307-322.

Winkler, E.M., 1973. Stone: Properties, Durability in Man's Environment. Springer Verlag, Wien.

Woolfolk, C.A. and Whiteley, H.R., 1962. Reduction in Inorganic Compounds with Molecular Hydrogen by *Micrococcus Lactulyticus*. J. Bacteriol., 84: 647-658.

Wu, J., Roth, C.B., and Low, P.F., 1988. Biologicaal Reduction of structural iron in Na-nontronite. Soil Sci. Soc. Amer. J., 52: 295-296.

Zachara, J.M., Cowan, C.E., Schmidt, R.L., and Ainsworth, C.C., 1988. Chromate Adsorption by Kaolinite. Clays and Clay Minerals, 36/4: 317-326.

Zwicker, W.K., Groeneveld Meijer, W.O.I., and Jaffe, H.W., 1962. Nsutite - A Wide-Spread Manganese Oxide Mineral. American Mineralogist, 47: 246-266.

Appendix I.

1 Rock Samples

1.1 Sampling Technique

Selected Locations of the Groote Eylandt manganese deposit were stratigraphically logged (see chapter 2) and sampled, beginning at the base of the section to avoid contamination from overlying materials. Sampling intervals of uniform ores were approximately 20 - 40cm, more complex parts of the orebody were sampled at 3 - 20cm apart. Sub-samples were taken, where necessary, to show local mineralogical and petrological variations.

1.2 Equipment and Sample Preparation

Massive and hard materials were broken into chips of a few cm^3 with a hand-operated jaw breaker. The instrument was thoroughly cleaned after each sample to prevent contamination from previous material. Soft ores and rocks and crushed chips were ground to a fine powder in a tungsten carbide mill (inner Ø ~ 15cm). Depending on the sample type, the mill was cleaned 5 - 10 times with quartz sand ground to powder and washed with ethanol. Larger samples were then quartered in a sample divider until the remaining sample was reduced to 100 - 200g, small samples were totally retained.

1.3 Rock Analyses

1.3.1 X-Ray Fluorescence (XRF)

1.3.1.1 Analytical Background

Fused samples or pressed mineral powders are irradiated with X-rays. Elements present in the sample are excited to emit a radiation with an element-specific wavelength. This wavelength together with the respective intensity of the line allow the measurement of a large number of elements.

1.3.1.2 Equipment

A Siemens SRS-1 X-ray Fluorescence instrument at the Department of Geology and Geophysics, Adelaide University, was used to analyse 100 ore and rock samples for trace elements (As, Mo, Pb, Sc, Th, U, W). All major and minor elements were determined in the quality control laboratory of GEMCO, Groote Eylandt (Philips, PW 1410).

1.3.1.3 Sample Preparation for Pressed Powder Buttons

5 drops of PVA-solution were added to 2.5 g of the powdered sample and mixed for some minutes. The sample was then filled into a plastic cylinder and pressed by hand into a preliminary tablet. This tablet was transferred to a steel cylinder with a slightly larger diameter. The empty space between sample and cylinder wall was filled with boric acid (H_3BO_3). The button is finally pressed for some minutes under a pressure of about 50,OOO kPa (≈7000 lb/inch^2).

1.3.1.4 Sample Preparation for Fusion Beads (GEMCO, 1984)

Dried lithium tetraborate ($Li_2B_4O_7$; 6g) is mixed thoroughly with 0.6000±0.0005 g of powdered sample, transferred to a Pt crucible, and fused at 1200°C for 12 minutes in a muffle furnace. The sample is stirred intermittently at about 4 and 8 minutes. Successively, the melt is poured into a pre-heated mould and removed from the oven. After the glass bead has cooled, the sample can be analyzed.

1.3.2 X-Ray Diffraction (XRD)

1.3.2.1 Analytical Background

Randomly oriented mineral grains (powder) are irradiated with X-rays, which are reflected at the lattice of the examined phases. The reflection angle and the peak intensity are mineral-specific and through the Bragg equation ($n*\lambda = 2d*\sin\vartheta$) the d-spacings of the mineral is obtained. Tabulated phase data (e.g. ASTM) allow the comparison and identification of the sample spectrum (Liebhafsky and Pfeiffer, 1971).

1.3.2.2 Equipment and Sample Preparation

Most samples were analyzed with a Philips diffractometer (PW 1370) at the Department of Geology, La Trobe University, Melbourne, using both CuK_α and CoK_α tubes. Additional patterns were recorded with a Philips diffractometer (PW1050) at the Department of Geology and Geophysics, Adelaide University, where CoK_α radiation was used.

The sample is ground by hand in a agate mortar until it is finely powdered. A small amount is then mixed with methanol, mixed, and poured onto a glass sample holder, to produce a fine coating of the holder. This procedure was applied to all samples to allow direct spectra comparison of small sub-samples with larger samples.

1.3.3 Fourier Transform Infrared Spectroscopy (FTIR)

1.3.3.1 Analytical Background

For about twenty years Infrared (IR) Spectroscopy has been used for the characterization of both organic and inorganic compounds. Though this method was mainly applied to organic materials (Fredericks et al., 1983), minerals have been analyzed increasingly over the last few years. Fourier Transform Spectroscopy is a time dependent technique which analyzes the whole spectrum together. It has improved the initial method dramatically in its resolution and in contrast to X-ray diffraction (XRD), it provides a good tool for poorly crystalline or amorphous phases (e.g. complex manganese oxides; Potter and Rossman, 1979), because it does not depend on the presence of reasonably well ordered structures. Instead, the IR absorption of the sample produces spectra which contain information about oscillations of chemical bonds and about atoms that are present in the sample. Thus, additional information about hydroxyl groups, structural water, etc. can be obtained.

1.3.3.2 Equipment and Method (Fysh and Fredericks, 1983)

FTIR analyses were made at the Central Research Laboratories (CRL) of B.H.P.Co.Ltd. in Newcastle. The spectra were produced with a Nicolet MX-1E FTIR spectrometer equipped with a Nicolet 1200S data processing terminal. The instrument is continually purged with dry nitrogen and is internally referenced to a He-Ne laser (632.8 nm), thus requiring no external calibration.

The applied method of transmitting the sample with laser light obeys Lambert-Beer's Law, which states that the absorption is proportional to the sample concentration ($E = \varepsilon cd$; Näser, 1974). It must be noted that this law is only valid for strongly diluted samples. The diluting medium, caesium iodide, is transparent for IR over the whole analyzed range of wavelengths ($\lambda \approx$ 50-4000). Nevertheless, it produces a spectrum which is subtracted automatically to give a true sample spectrum.

1.3.3.3 Sample Preparation

Exactly 2 mg of the sample are finely ground (< 70µ) in an agate mill, added to 450 mg of high purity caesium iodide (CsI from Merck, 99.5%) and placed in the agate vessel of a small vibratory mill. After 2 minutes two pellets each weighing 200 ± 1 mg are pressed in a die (Ø 13 mm) with a load of approximately 9 tons for 1 minute. To minimize the analytical error which can develop from the small sample size and possible inhomogeneties of the mixture, normally two pellets are prepared and analyzed.

1.3.3.4 Further Computerized Handling

The digital form and the high accuracy of the data make it suitable for further computerized manipulations, like subtraction and addition of mineral spectra (evaluation of quantities) or curve differentiation. Also, CRL has developed a method which presently is used for the quality control of processed ores and other materials (CIRCOM = Computerized Infrared Characterization of Materials). Here, the FTIR analysis in connection with CIRCOM provides chemical analyses as well. Unfortunately, this technique cannot be applied at the moment to most of the samples that were examined in this thesis, because they contained a number of different minerals (Mn-, Fe-ores, clays) that obscure the sample spectrum.

1.3.4 Inductive Coupled Plasma Spectrometry (ICP)

1.3.4.1 Analytical Background

The technique is based on the excitation of atoms from the dissolved sample in a plasma. The resulting light spectrum is analyzed at wavelengths which show little or no interferences from neighboring peaks. Inductive Coupled Plasma Analysis offers a range of advantages over other methods. It is normally considered to have less matrix effects than other emission techniques (e.g. X-Ray Fluorescence or Atomic Absorption Spectrometry) and it is highly sensitive for the detection of trace elements, especially for those with low atomic numbers. This leads to improved accuracy, speed of analysis, easier sample preparation and decreases dilution problems. Computer manipulation further helps in the interpretation, because it is possible to view the spectrum of a specific sample and to identify overlapping lines for various elements.

1.3.4.2 Equipment and Method

365 rock samples were analyzed by a sequential ICP (ARL 3520) at the School of Earth Sciences at Flinders University (Adelaide). An inert Ar atmosphere is used to prevent sample oxidation and ionization effects. The argon itself is ionized in the induction coil of a high frequency generator and ignited by Tesla sparks. The sample solution is nebulized and introduced into the center of the flame. The high temperatures of the plasma (≥8000°C) result in the excitation of sample atoms, which emit element specific spectra. The intensities depend on the concentrations of the various elements.

Since most of the manganese oxides were expected to contain relatively high Trace Element (TE) and Rare Earth Element (REE) concentrations (previous neutron activation analyses for instance showed Ce levels of up to 250 ppm), it was possible to analyze the ores directly by Inductive Coupled Plasma Spectroscopy (ICP), after a simple dissolution technique and without pre-concentration in ion exchange columns. TEs and REEs were not separated from the major matrix elements (Mn, Fe, Al).

The instrument was calibrated with USGS standards (Nod-A-1 and Nod-P-1; Flanagan and Gottfried, 1980), single element standards, and mixed standards, which were prepared to simulate the matrix of the various ore types and gangue minerals. Another standard contained a combination of both manganese and iron concentrations equivalent to 60 % of the respective element, alumina equivalent to 30 %, and the TEs/REEs with the highest expected concentrations. Results of an Instrumental Neutron Activation Analysis of 8 samples (INAA; Australian National University, Canberra) were also used in the development of the the final calibration curves. Because of strong spectral interference from manganese and iron, all element peaks were scanned to identify possible interferences from neighbouring peaks. Different analytical

channels were selected in cases where associated lines seemed to dominate, matrix corrections were applied for peaks with less interference. Subsequently, REE concentrations were normalized against European shales (Haskin and Haskin, 1966) to allow direct comparison with published data.

1.3.4.3 Calibration Standards

Table I.1: Artificial standards prepared to simulate various natural samples ([ppm]; a-d: Mn ores; e: clay; f: Fe ore; Himix: mixture containing maximum element concentrations; Lomix (not shown): distilled water); all concentrations equal to samples with a dilution factor of 100.

Element	a	b	c	d	e	f	Himix
Al	0	500	1000	1500	3000	500	3000
B	7	6	5	5	1	17	17
Ba	500	200	50	5	0.5	50	
Ca	20	10	5	1	0.1	0.1	
Ce	2	1	0.5	0.1	0.2	1	2
Co	3	2	1	0.5	0.1	0.5	3
Cr	2	1	0.5	0.1	0.5	1	2
Cu	4	3	2	1	0.1	1	4
Eu	0.1	0.08	0.06	0.04	0.02	0.06	0.1
Fe	0	100	500	1000	0	6000	6000
Gd	0.05	0.2	0.4	0.6	0.6	1.5	1.5
K	350	150	50	5	0.1	0.5	
La	1.5	1	0.5	0.1	0.25	0.25	1.5
Li	0	0.05	0.1	0.15	0.3	0.15	
Mg	80	40	10	1	0.1	0.1	
Mn	6000	5000	4000	3000	0	0	6000
Na	30	20	10	5	10	10	
Nd	1	0.5	0.1	0.05	0.1	0.5	1
Ni	2.5	2	1.5	1	0.3	4	4
P	0	5	10	20	0	60	60
Sm	0.5	0.4	0.3	0.2	0.05	0.3	0.5
Sr	100	50	10	1	0.1	0.1	100
Ti	1	10	50	100	200	50	
V	15	10	5	2.5	1	10	15
Yb	0.1	0.08	0.06	0.04	0.02	0.1	0.1
Zn	6	4	2	1	0.1	3	6
Zr	0.5	1	1	1.5	2.5	1	2.5

1.3.4.4 Calibration Curves

Table I.2: Equations for ICP calibration curves.

Element	Calibration Curve
B	IF(Intensity<3.81,0,(4.8349-4.1877*Intensity+0.786*Intensity^2-0.0051*Intensity^3)/Weight)
Ce (Mn)	IF(Intensity<150.9,0,(-303.3776+2.2821*Intensity-0.0018*Intensity^2)/Weight)
Ce (Fe)	IF(Intensity<157.48,0,(-138+0.8763*Intensity)/Weight)
Ce	IF(Fe<15,Ce (Mn),Ce (Fe))
Co	IF(Intensity<2.39,0,(-19.347+8.0932*Intensity)/Weight)
Cr	(1.4092+3.9281*Intensity+0.7137*Intensity^2)/Weight
Cu	(0.5279+0.0531*Intensity)/Weight
Eu	IF(Intensity<123,0,(-12.1887+0.1058*Intensity-0.00005436*Intensity^2)/Weight)
Gd	IF(Intensity<127.25,0,(-27.8057+0.2278*Intensity-0.00007285*Intensity^2)/Weight)
La	IF(Intensity<192.1,0,(-12.382+0.0518*Intensity+0.00006586*Intensity^2)/Weight)
Nd	IF(Intensity<191.65,0,(-48.9626+0.2417*Int.+0.00007191*Intensity^2)/Weight)
Ni	IF(Intensity<=24.43,0.7309-1.3279*Int.+0.1996*Intensity^2+0.0066*Intensity^3,-104.8052+11.5594 *Intensity-0.0009502*Intensity^2)
P	IF(Intensity<3.5974,0,(8.8151-32.1877*Int.+8.6595*Intensity^2-0.1092*Intensity^3)/Weight)
Sm	IF(Intensity<103.07,0,(-46.3545+0.4497*Intensity)/Weight)
Sr	IF(Intensity<231.48,0,(-141.6986+0.6158*Intensity-0.00001579*Intensity^2)/Weight)
V	IF(Intensity<8.82,0,(-1.5619+0.0185*Intensity+0.0182*Intensity^2-0.0000241*Intensity^3)/Weight)
Yb	IF(Intensity<189.5,0,(-3.0135+0.0159*Intensity)/Weight)
Zn	(27.8839+1.0524*Intensity-0.0002018*Intensity^2)/Weight
Zr	IF(Intensity<6.42,0,(-4.3923+0.6395*Intensity+0.0072*Intensity^2-0.00002096*Intensity^3)/Weight)

1.3.4.5 Instrument Setting

Table I.3: Analytical Instrument Settings of ICP.

Channel	Number	Brfval	Wavelength	Sp. Ord.	H. Voltage	Bgrd Corr., l.	Bgrd Corr., r.
B 1	112	0.00000	182.589	3	127		
Ce 4	257	160.738	413.380	1	127	0.0320	-0.0390
Co 1	133	2.64000	228.616	3	127	0.0110	-0.0110
Cr 1	135	2.20000	205.552	3	127	-0.0083	0.0077
Cu 2	139	0.00000	324.754	2	110		
Eu 1	144	135.600	381.965	2	127	0.0190	-0.0190
Gd 2	154	108.600	342.247	2	127	-0.0230	0.0000
La 2	171	0.00000	398.852	1	127		
Nd 1	188	0.00000	430.357	1	127		
Ni 3	191	0.00000	231.604	2	127		
P 1	193	2.61490	178.287	3	127	0.0202	-0.0194
Sm 1	220	104.584	359.260	2	127	0.0240	-0.0380
Sr 2	224	0.00000	407.771	1	80		
V 1	244	0.00000	290.881	2	110		
Yb 1	250	0.00000	328.937	2	127		
Zn 1	251	2.65104	202.551	3	127	0.0118	-0.0277
Zn 3	253	0.00000	213.856	3	127		
Zr 2	255	14.9001	343.823	2	110	0.0444	-0.0556

1.3.4.6 Sample Preparation

Powdered ore samples (1g) were digested in a teflon beaker with 5 drops of $HClO_4$ and 10 ml HF and dried on a hot plate to break down clay minerals and to drive off all silica. Five additional drops of $HClO_4$ were added and the samples were dried again. Residues were dissolved 10 ml HCl, heated, diluted with ~20 ml distilled water, and kept hot until they were transferred to a 100 ml flask for the final dilution (1:100). This procedure prevented the formation of colourless precipitates occasionally produced by Fe-rich samples when the solutions came in contact with the cold flasks.

1.3.5 Atomic Absorption

1.3.5.1 Analytical Background

This technique uses the spectral interference of light of a specified wavelength from a lamp with light emitted from vapourized and heated atoms. Sample atoms act as a filter by absorbing the light from the lamp.

1.3.5.2 Equipment and Method

365 ore and rock samples were analyzed by AA (Perkin Elmer, model 5000) in the quality control laboratory of GEMCO, Groote Eylandt. The dissolved sample is nebulized and passed through a flame where the ionic species are reduced to their atomic states (Butler and Kokot, 1971). The temperature of the flame is kept sufficiently low to prevent the formation of ionic states; too high temperatures significantly decrease the detection limit of the respective elements. Light with a wavelength characteristic for the element to analyze illuminates the atomic vapour and the light is partially absorbed by the excited element. The overall decrease in intensity of the analytical wavelength is measured by a photo-spectrometer.

1.3.5.3 Sample Preparation (GEMCO, 1984)

Powdered and dried ore samples (0.1000±0.0005g) are dissolved in 5ml of concentrated HCl. The sample is boiled until the ore is dissolved. After cooling the solution is transferred to a volumetric flask, 20ml of KCl (2 weight %) are added as ionization buffer, and this mixture is diluted with distilled water (1:1000). This procedure prepares the sample for Na_2O and MgO analysis.

1.3.6 K/Ar-Age Determinations

1.3.6.1 Analytical Background

The analyses that were carried out were part of an investigation to identify primary manganese oxides in the deposit and to see, whether it was possible to determine the age with a K/Ar method. Normally, minerals like glauconite which contains potassium, can easily be analyzed by this technique, but the behavior of K-carrying manganese phases (preferably cryptomelane) was not known. Though this work was of experimental nature, it will be assumed that the samples behaved similar to other minerals which are used conventionally. The samples also were analyzed by X-Ray Diffraction to identify the cryptomelane and to exclude detrital K-bearing minerals.

1.3.6.2 Equipment, Sample Preparation and Method

The samples were analyzed by AMDEL (Service Reports, 1985 and 1986). First they were crushed and a -36+72 B.S. mesh (-0.42+0.21 mm) fraction was screened out for analysis. Argon was extracted by fusion under vacuum following a degassing bake-out at 180°C. This removes most of the adsorbed atmospheric argon from the sample without interfering with radiogenic Ar. The reports state that significant amounts of radiogenic Ar^{40} were detected which can be distinguished from atmospheric contamination.

2 Water Samples

2.1 Sampling

2.1.1 Equipment

The waters were collected with a syringe (50 ml) and filtered through a micro filter, contained in a Micro-Syringe 25 mm Filter Holder with Luer Inlet (Millipore Pty. LTD.). The filter material had a pore size of 0.22µ. Samples for ICP- and Cl-analysis were stored in polyethylene bottles, samples for organic carbon determinations were kept in glass bottles and covered with Al-lined caps. The polyethylene bottles were soaked in concentrated HCl for approximately 2 weeks to eliminate the possibility of sample contamination from the bottle walls.

For the collection of borehole waters a sampler was built in the Department of Geology and Geophysics, Adelaide University, in close resemblance to that one developed by Dr. A. Giblin, Division of Mineralogy, Institute of Energy and Earth Resources, CSIRO Sydney. It basically consists of a plastic cylinder (~50 cm long, Ø 4 cm) with with a screw top and a one way valve on each end, where the water can only pass when the sampler is lowered.

2.1.2 Sampling Procedures

The various waters were taken from a number of localities on Groote Eylandt under different sampling conditions (e.g. availability of organic macro molecules, amount of particulates). Thus, it was necessary to obtain a basis for comparison. This was done by applying a standard procedure for each sample. The procedure includes collection, preservation and field tests. The sampling was done with a syringe that was rinsed three times with the water from the location, where it was taken. Then the sample was passed through the filter to prevent polution by particulates or coarser solids. The samples for the ICP were acidified with approximately 1 ml concentrated HNO_3, samples collected for organic carbon determinations were acidified with 10 drops of concentrated HCl. Additionally, untreated waters were collected for chlorine analysis.

Waters were also taken from a number of new boreholes, where it was attempted to sample approximately from the middle of the orebody. Thus, the samples were expected to resemble those springs deriving from ores. Once obtained, further treatment was the same as above.

2.2 Field Tests

2.2.1 Temperature

For pH-measurements and oxygen determinations it was necessary to know the exact temperatures of the sampled waters. Therefore a laboratory thermometer (-10 to 40°C) was used.

2.2.2 pH

The pH was measured with a portable pH-meter (Watson Victor 5003) and a glass electrode was used. The meter was standardized against two buffer solutions (pH 4 and 7) in the laboratory and recalibrated in the field for temperature and against one buffer (pH 7).

2.2.3 Flux Rate of Springs and Seepages

The flux rate was determined, where possible, by collecting the water in a 500 ml beaker and measuring the time to fill the vessel. This was repeated 5 times to obtain an average value. The result is expressed in l/min.

2.2.4 Total Manganese

2.2.4.1 Analytical Background

The colorimetric determination of manganese is based on the formation of a red-brown complex of Mn with formaldoxime (Hofmann and Erhardt, 1913), after an initial addition of an alkaline masking solution. Complexes of accompanying metals such as Co or Ni, formed despite masking are selectively destroyed afterwards by a reducing Titriplex® solution. This method offers an increased reproducibility and higher sensitivity, when compared with the well-established colorimetric determination of manganese as permanganate. The only limitation seems to be the use of the test for sea waters which together with the color complex produce colorless precipitates. These could theoretically be filtered out, but it is not known whether the reaction is also affected.

2.2.4.2 Method and Equipment (Merck information leaflets, manganese)

To determine the total amount of manganese transported in the waters (Mn^*; including dissolved Mn^{2+}, compounds adsorbed on organic macro molecules, and particulates), a field test kit was used (Merck; Aquaquant® 14406 Manganese). The two test vessels were rinsed three times with the test solution, the chemicals were added to one of the tubes and after a final reaction time of five minutes the colour of the solution was compared against a colour chart and the solution without chemicals to compensate for its own colour.

Since these samples could not be filtered, it was always attempted to get waters as clean as possible. In some cases small particles changed the result to higher values, but normally this could be detected, because they settled down fast and a reaction halo built up around them. Those waters were tested again. The detection limit for this test kit is approximately 0.03 ppm Mn. Occasionally, the measured concentrations were higher than the upper limit of the test kit. In such cases the test solutions were diluted to 50% with distilled water. When necessary, the dilution was repeated. The sensitivity of the test kit was tested in the laboratory against ICP analysis, with a setting similar to field conditions, and it showed only an error of approximately 10% after an 80fold dilution of the initial solution. This includes the dilution error, which is most probably much larger than the analytical error.

2.2.5 Total Iron

2.2.5.1 Analytical Background

A similar colorimetric method was used for the determination of iron. The red to blue-violet color of the solution is produced by the reaction of iron with an aromatic compound. In this region of the spectrum the human eye is most sensitive. A reagent, which contains ammonium thioglycolate, is added to the water sample. This mineralizes weak iron complexes, reduces trivalent iron, while at the same time, acting as a buffer. This procedure is essential, because the main reagent Ferrospectral® reacts only with divalent iron. Sea waters, when in contact with the chemicals, also produce colorless precipitates (see manganese) and it is not known, if there is any interference with the iron.

2.2.5.2 Method and Equipment (Merck information leaflets, iron)

As already mentioned for manganese, iron can be transported in aquatic systems in a number of conditions, therefore total iron (Fe^* in tables and plots) must be determined additionally. A field test kit was used (Merck; Aquaquant® 14403 Iron). The same technical procedure as for

manganese is applied.

2.2.6 Oxygen-saturation

2.2.6.1 Analytical Background

The method used in this field test is based on the Winkler titration. Divalent manganese reacts in an alkaline medium with the dissolved oxygen and it is oxidized to Mn hydroxides with higher valencies. After acidification trivalent Mn ions are formed which are able to oxidize iodide ions to elementary iodine. During this reaction, an amount of iodine equivalent to the dissolved oxygen is liberated and this is titrated against sodium thiosulfate ($Na_2S_2O_3$). Most oxidizing and reducing substances (like organics, higher valent Mn, Fe, sulfide and sulfite ions) can interfere with the reaction, but as the sampled waters in most cases are very pure, the resulting error is expected to be relatively small.

2.2.6.2 Method and Equipment (Merck information leaflets, oxygen)

A test kit (Merck, Aquamerck® 11107) was used. The test vessel is rinsed three times with the water to be measured, then the solution is conditioned for the titration with four different reagents. The developing blue complex is titrated until it disappears. It is essential to know the temperature of the water to calculate the oxygen saturation on which all samples can be compared, because oxygen concentrations depend strongly on the temperature (Truesdale et al., 1955). The detection limit is approximately 0.2 ppm O_2. Every three months field tests are made by GEMCO and samples were taken for further analysis. Sample sets were taken in May/June 1985, September 1985, January 1986, September 1986.

2.3 Laboratory Analyses

2.3.1 Chlorine

Chlorine was first determined with a chloride sensitive electrode (June 1985) and an Orion Eh/pH meter was used. The read out was in mV. The Cl-concentration was taken from a calibration curve. Since September 1985 samples are analyzed in the chemical laboratory of GEMCO with an $AgNO_3$-titration.

2.3.2 Total Organic Carbon (TOC)

2.3.2.1 Application of TOC

Very little is known about the interaction between organic matter and major elements like iron and manganese in the waters from the deposits of Groote Eylandt. A number of publications indicate that in contrast to iron manganese does not seem to undergo a strong bonding with organics. It was part of the study to investigate the conditions in the examined area.

2.3.2.2 Equipment and Method (Sybron/Barnstead, Instruction Manual for the PHOTOchem™ Organic Carbon Analyzer)

The water samples were examined at Chisholm College in Melbourne with a Barnstead PHOTOchem™ Organic Carbon Analyzer. After introducing the sample 1 ml of UVDR solution (0.05N H_3PO_4 with 4% dissolved $(NH_4)_2S_2O_8$) is injected into the analyzer at the beginning of each analysis cycle to stabilize the pH in the irradiation chamber. Inorganic carbon, in the form of dissolved CO_2 is first stripped out of the sample by a continuous stream of carrier air. The air carries the inorganic carbon dioxide to a measuring chamber containing 18 megohm-cm, zero-organic water. The CO_2 dissolved in the pure water , and the resultant change in resistivity of the pure water is measured, converted to ppm as carbon, and stored in memory. At the end of this first cycle, the analyzer automatically subtracts the stored inorganic carbon value and the background value, which is determined by running a cycle with 1 ml UVDR solution alone. Then the ultra-violet lamp in the irradiation chamber is energized , and in the following 6.5 minutes all dissolved organic compounds, both volatile and non-volatile are oxidized. The resulting carbon dioxide is carried by the air stream to the measuring chamber where it dissolves in the water. The analyzer again measures the resistivity of the water to determine the total organic carbon of the sample, which is displayed on the digital readout.

2.3.2.3 Procedure

The preparation of the sample is fairly simple. Samples that are known to be free of alkalinity do not need a special pre-treatment. All other samples need an adjustment of the pH to slightly less than 4 with with a dilute solution of 0.1 or 1.0 N of ACS grade H_3PO_4 before analysis. The few sea waters that were collected were not analyzed. As all samples were filtered when they were taken, it was not necessary to homogenize them with an acid treatment prior to analysis.

After the calibration, which will not be described here, the samples can be analyzed in intervals of roughly 15 minutes. This time is required for the analysis and the rinsing cycle. The syringe that is used for injecting the sample must be rinsed three times with the sample liquid.

After 10 ml of the sample have been entered, 1 ml of UVDR solution must be added within 30 seconds. The result is displayed in ppm after 10 minutes.

2.3.3 Bulk Chemical Analysis by ICP

The water samples were examined with a ARL ICP machine (ARL 34000) at the Department of Earth Sciences, Melbourne University. For pre-treatment of samples and further information see 1.3.4 and 2.1-2.1.2.

3 Experimental work

3.1 Investigations on Redox Reaction

3.1.1 Equipment

A Multi-Pen Recorder (R-OX Series; Rikadenki Kogyo Co., Ltd.) and two portable pH-V-meters (Watson Victor 5003; glass electrode) were used to record parameter changes of an experimental battery cell. The vessel was kept at a constant temperature with a hot plate (including a magnetic stirrer) that had been modified to allow a small-scale temperature adjustment.

3.1.2 Test Vessel Specifications

The battery cell was built at the Department of Geology, La Trobe University, Melbourne, from clear perspex for visual examination during experiments (inner size: 100 x 100 x 10mm; see also Fig. 7.2). It has a rectangular design comparable to a car battery and it contains three compartments separated by permeable plates of sintered glass beads. Each sample compartment for the solid materials has a volume of 100 cm^3. The water compartment in the center of the cell has a volume of 200 cm^3 and it is also equipped with the stir bar of a magnetic stirrer. The solids compartments are in direct contact with rectangular carbon electrodes (100 x 100 x 5mm). Although the electrodes were relatively pure (see listing of analyses below), they were additionally boiled in concentrated HCl for several days.

Carbon electrode specifications:
grade ATJ; NITECH, Adelaide
Total ash average: 0.158%, containing 0.042% Fe, 0.004% V, 0.043% S, 0.0111% Ca.

3.2 Biological Leaching of Mn-oxides

A laboratory scale process has been developed by Madgwick and Varga, University of New South Wales, which can dissolve/reduce manganese oxides from slurry tailings residues, where a bacterium under microaerobic conditions has been demonstrated to be an efficient, low-cost system. Each ore sample (1.89 g) was heat sterilized three times for 2 hour intervals at 100°C, mixed with 8 ml of 1% (w/v) molasses, inoculated with leaching bacteria, *Enterobacter species* (Silverio and Madgwick, 1985) and incubated at 32 °C. After one week each culture was treated with concentrated H_2SO_4 (0.02 ml), centrifuged and Mn^{2+} concentrations determined in the supernatant. Soluble manganese (Mn^{2+}) was determined by Atomic absorption spectroscopy (Varian, AA-1475). Fresh molasses and leaching bacteria were then added to the solids and incubated for a further week. This process was repeated for 21 weeks.

3.3 Battery-activity Tests

The method described here is the Pulse Galvanostatic Analysis which was adopted by the Central Research Laboratories of BHP in Newcastle (Freeman et al., 1971; Swinkels and Williams, 1982). A battery-cell is filled with the ores to be tested and discharged under controlled conditions. The discharge current is interrupted frequently and the potential of the test material is measured against a reference electrode. The drain time between the initial voltage and a specified voltage is used as an indicator for the battery-activity of the sample.

Appendix II.

Table II.1. Sample Localities, Sampling Position in Vertical Section [m], Grainsize [mm].

Table II.1: Sampling Localities, Positions, and Grainsizes.

No.	Location	Depth [m]	Grainsize [mm]	No.	Location	Depth [m]	Grainsize [mm]
903 - 3	F3	16.60	3-4	903 - 62	G-South	1.62	1
903 - 4	F3	16.55	3-4	903 - 63	G-South	1.60	
903 - 5a	F3	15.75	3-4	903 - 64	G-South	1.30	
903 - 5b	F3	15.75		903 - 65a	G-South	0.80	
903 - 6	F3	15.45	3-4	903 - 65b	G-South	i.s.	
903 - 7	F3	15.20	3	903 - 66	G-South	0.30	
903 - 8	F3	14.90	3-4	903 - 67	G-South	0.00	
903 - 9	F3	14.50	3-4	903 - 68a	G-quarry	i.s.	
903 - 10	F3	14.20	3-5	903 - 68b	G-quarry	i.s.	
903 - 11	F3	13.80	5	903 - 69	G-quarry	5.53	2
903 - 12	F3	13.65	5	903 - 70	G-quarry	5.43	2-3
903 - 13	F3	13.15	4	903 - 71	G-quarry	5.33	2-3
903 - 14	F3	12.90	3-4	903 - 72	G-quarry	5.23	3
903 - 15	F3	12.50	3	903 - 73	G-quarry	5.13	5
903 - 16	F3	12.00	2-3	903 - 74	G-quarry	4.98	
903 - 17	F3	11.55	3-5	903 - 75	G-quarry	4.88	
903 - 18	F3	11.30	4-6	903 - 76	G-quarry	i.s.	
903 - 19	F3	11.10	4-5	903 - 77a	G-quarry	4.68	
903 - 20	F3	i.s.		903 - 77b	G-quarry	i.s.	
903 - 21	F3	i.s.		903 - 78	G-quarry	4.58	2-3 + 15
903 - 22	F3	i.s.	4	903 - 79	G-quarry	6.43	
903 - 23	F3	i.s.	4	903 - 80	G-quarry	6.23	1-2
903 - 24	F3	i.s.	5	903 - 81	G-quarry	6.13	1-2
903 - 25	F3	i.s.	10	903 - 82	G-quarry	6.03	1-2
903 - 26	F3	i.s.		903 - 83	G-quarry	5.93	1-2
903 - 27	F3	i.s.		903 - 84	G-quarry	5.83	1-2
903 - 28a	F3	4.60		903 - 85	G-quarry	4.33	2-5 + 20
903 - 28b	F3	i.s.		903 - 86	G-quarry	4.18	1-5
903 - 29	F3	1.90		903 - 87	G-quarry	4.13	5
903 - 30	F3	1.10	5-20	903 - 88	G-quarry	3.98	2-5
903 - 31a	F3	0.40	10	903 - 89	G-quarry	3.83	1
903 - 31b	F3	i.s.		903 - 90	G-quarry	3.73	
903 - 32	F3	0.00		903 - 91	G-quarry	3.63	1
903 - 33	G-South	6.82	1	903 - 92	G-quarry	3.53	1
903 - 34	G-South	6.47	2	903 - 93	G-quarry	3.43	1-2
903 - 35	G-South	6.42	1-2	903 - 94	G-quarry	3.33	1-2
903 - 36	G-South	6.37	1-2	903 - 95	G-quarry	3.23	2
903 - 37	G-South	6.31	1-2	903 - 96	G-quarry	3.13	2-3
903 - 38	G-South	6.27	<<1	903 - 97	G-quarry	3.03	2-3
903 - 39	G-South	6.23	<<1-1	903 - 98	G-quarry	2.93	2-3
903 - 40	G-South	6.13	<<1	903 - 99	G-quarry	2.83	2-3
903 - 41	G-South	6.10	1	903 - 100	G-quarry	2.73	1-2
903 - 42	G-South	6.03	<<1	903 - 101	G-quarry	2.53	<1 + -5
903 - 43	G-South	5.78	<<1	903 - 102	G-quarry	2.28	
903 - 44	G-South	5.58	<<1	903 - 103	G-quarry	2.25	1
903 - 45	G-South	5.53	<<1	903 - 104	G-quarry	2.15	<1
903 - 46	G-South	5.03	<1	903 - 105	G-quarry	2.10	1-2
903 - 47	G-South	4.93	<<1	903 - 106	G-quarry	2.00	1-2
903 - 48	G-South	4.87	<1	903 - 107	G-quarry	1.90	2
903 - 49	G-South	4.72	<<1	903 - 108	G-quarry	i.s.	
903 - 50	G-South	4.57	<1	903 - 109	G-quarry	1.70	2-3
903 - 51	G-South	4.10	1-2	903 - 110	G-quarry	1.60	<1
903 - 52	G-South	3.95	<<1	903 - 111	G-quarry	1.50	1
903 - 53	G-South	3.75	<1	903 - 112	G-quarry	0.30	
903 - 54	G-South	3.60	<<1	903 - 113	G-quarry	i.s.	
903 - 55	G-South	3.50	<1	903 - 114	G-quarry	0.00	
903 - 56	G-South	3.40	<1	903 - 115a	D, a	12.90	
903 - 57	G-South	3.37		903 - 115b	D, a	i.s.	
903 - 58	G-South	3.12	<1	903 - 116a	D, a	12.10	
903 - 59	G-South	2.77	1	903 - 116b	D, a	i.s.	
903 - 60	G-South	2.52		903 - 117b	D, a	11.80	<1
903 - 61	G-South	2.22	1	903 - 118a	D, a	11.40	
903 - 118b	D	i.s.		903 - 180	C-138	1.75	4
903 - 119	D	10.50	3-6	903 - 181	C-138	1.65	4-6
903 - 120	D	10.20	2	903 - 182	C-138	1.55	5-7
903 - 121	D	9.80	<5	903 - 183	C-138	1.45	3-5
903 - 122	D	9.50	5	903 - 184	C-138	1.35	5-7
903 - 123	D	9.20	2-3	903 - 185	C-138	1.25	7
903 - 124	D	8.50	2-3	903 - 186	C-138	1.10	8-10

i.s. = individual sample belonging to no particular stratigraphic set; m† = mixture of materials.

No.	Location	Depth [m]	Grainsize [mm]	No.	Location	Depth [m]	Grainsize [mm]
903 - 125	D	8.00	2-3	903 - 187	C-138	1.05	
903 - 126	D	7.50	2-3	903 - 188	C-138	0.98	
903 - 127	D	7.00	3-5	903 - 189	C-138	0.58	
903 - 128	D	6.50	5	903 - 191B	C-138	i.s.	
903 - 129	D	6.00		903 - 190	C-138	0.10	
903 - 130	D	5.50	5-10	903 - 200	D	i.s.	
903 - 131	D	5.00	5-6	903 - 201	D	i.s.	
903 - 132	D	4.50	5	903 - 202	D	i.s.	
903 - 133	D	4.00	4-5	903 - 203	D	i.s.	
903 - 134	D	3.50	3-5	903 - 204	D	i.s.	
903 - 135	D	3.00	3-5	903 - 205	D	i.s.	
903 - 136	D	2.50	5	903 - 206	D	i.s.	
903 - 137	D	2.00	1	903 - 207	D	i.s.	
903 - 138	D	1.50	10	903 - 208	D	i.s.	
903 - 139	D	1.00		903 - 209	D	i.s.	
903 - 140	D	0.50		903 - 210	D	i.s.	
903 - 141a	D	i.s.		903 - 211	D	i.s.	
903 - 141b	D	i.s.		903 - 212	D	i.s.	
903 - 141c	D	i.s.		903 - 213	D	i.s.	
903 - 141B	D	i.s.		903 - 215	D	i.s.	
903 - 142	D	13.80	2-3	903 - 216	D	i.s.	
903 - 143	D	13.30	3	903 - 217	D	i.s.	
903 - 144	D	12.80	2-3	903 - 218	D	i.s.	
903 - 145	D	12.30	2-3	903 - 219	D	i.s.	
903 - 146	D	11.80	2-3	903 - 220	D	i.s.	
903 - 147	D	11.30	1-2	903 - 221	F3	i.s.	
903 - 148	D	10.80	2-3	903 - 222	F3	i.s.	
903 - 149	D	10.30	2-4	903 - 223	F3	i.s.	
903 - 150	D	i.s.	2-4	903 - 224	F3	i.s.	
903 - 151	D	10.00	1-2	903 - 225	F3	i.s.	
903 - 152a	D	9.60	1-2	903 - 226	F3	i.s.	
903 - 152b	D	i.s.	1-2	903 - 227	F3	i.s.	
903 - 153	D	9.30		903 - 228	F3	i.s.	
903 - 154	D	9.00		903 - 229	F3	i.s.	
903 - 155	G-quarry	8.93		903 - 230	F3	i.s.	
903 - 156	G-quarry	8.86		903 - 232	C-138	i.s.	
903 - 157	G-quarry	8.81		903 - 233	C-138	i.s.	
903 - 158	G-quarry	8.63		903 - 234	C-138	i.s.	
903 - 159	G-quarry	8.58	1	903 - 235	C-138	i.s.	
903 - 160	G-quarry	8.38	1	903 - 237	C-138	i.s.	
903 - 161	G-quarry	8.23	1	903 - 239	F2	i.s.	
903 - 162	G-quarry	8.13	2-3	903 - 241	F3	i.s.	
903 - 164	G-quarry	7.93		903 - 245	F3	i.s.	
903 - 170a	C-138	2.80		903 - 246	F3	i.s.	
903 - 170b	C-138	i.s.		903 - 249	F3	i.s.	
903 - 171a	C-138	2.70		903 - 250	F3	i.s.	
903 - 171b	C-138	i.s.		903 - 251	F3	i.s.	
903 - 172	C-138	2.60		903 - 252	F3	i.s.	
903 - 173	C-138	2.50		903 - 253	F3	i.s.	
903 - 174	C-138	2.40		903 - 254	F3	i.s.	
903 - 175	C-138	2.30		903 - 255	F4	i.s.	
903 - 176	C-138	2.20		903 - 256	F4	i.s.	
903 - 177	C-138	2.05		903 - 259	A-South	i.s.	
903 - 178	C-138	1.95		903 - 260	A-South	i.s.	
903 - 179	C-138	1.85	2-3	903 - 261	F4	i.s.	
903 - 262	F4	i.s.		903 - 318	G-South	8.72	2
903 - 263	F4	i.s.		903 - 319	G-South	8.62	1-2
903 - 264	F4	i.s.		903 - 320	G-South	8.37	1-2
903 - 265	F4	i.s.		903 - 322	G-South	7.77	1-2
903 - 266	F4	i.s.		903 - 323	G-South	7.37	1-2
903 - 268	F4	i.s.		903 - 324	G-South	i.s.	
903 - 269	F4	i.s.		903 - 325	G-South	i.s.	
903 - 270	F1	i.s.		903 - 326a	G-quarry	i.s.	
903 - 271	F1	i.s.		903 - 326b	G-quarry	i.s.	
903 - 272	F1	i.s.		903 - 326c	G-quarry	i.s.	
903 - 273	F1	i.s.		903 - 327	G-quarry	i.s.	
903 - 274	F1	i.s.		903 - 328	G-quarry	i.s.	
903 - 275	F1	i.s.		903 - 329	G-quarry	i.s.	
903 - 276	F1	i.s.		903 - 330	A-South	i.s.	

i.s. = individual sample belonging to no particular stratigraphic set; m† = mixture of materials.

No.	Location	Depth [m]	Grainsize [mm]	No.	Location	Depth [m]	Grainsize [mm]
903 - 277	F1	i.s.		903 - 331	A-South	i.s.	
903 - 278	F1	i.s.		903 - 332	A-South	i.s.	
903 - 279	F1	i.s.		903 - 333	A-South	i.s.	
903 - 280	F1	i.s.		903 - 334	A-South	i.s.	
903 - 281	F1	i.s.		903 - 335	A-South	i.s.	
903 - 282	F1	i.s.		903 - 336	F4	i.s.	
903 - 283a	F1	i.s.		903 - 337	F3	i.s.	
903 - 283b	F1	i.s.		903 - 338	F3	i.s.	
903 - 283c	F1	i.s.		903 - 339	A-South	i.s.	
903 - 283d	F1	i.s.		903 - 340a	A-South	i.s.	
903 - 283e	F1	i.s.		903 - 340b	A-South	i.s.	
903 - 284	G-quarry	i.s.		903 - 341a	A-South	i.s.	
903 - 285	G-quarry	i.s.		903 - 342a	A-South	i.s.	
903 - 286	G-quarry	i.s.		903 - 343	K	i.s.	
903 - 287	G-quarry	i.s.		903 - 344	K	i.s.	
903 - 290	G-South	i.s.		903 - A	F	i.s.	
903 - 291	G-South	i.s.		903 - B	F	i.s.	
903 - 292	G-South	i.s.		903 - B I.a	F3	i.s.	
903 - 293	G-South	i.s.		903 - B I.b	F3	i.s.	
903 - 294	G-South	i.s.		903 - B I.c	F3	i.s.	
903 - 295	G-quarry	i.s.		903 - B I.d1	F3	i.s.	
903 - 296	G-quarry	i.s.		903 - B I.d2	F3	i.s.	
903 - 297	G-quarry	i.s.		903 - B I.d3	F3	i.s.	
903 - 298	G-quarry	i.s.		903 - B I.d4	F3	i.s.	
903 - 299	G-quarry	i.s.		903 - B I.e	F3	i.s.	
903 - 300	G-South	i.s.		903 - B II.a	F3	i.s.	
903 - 301	G-South	i.s.		903 - B II.b	F3	i.s.	
903 - 302	G-South	i.s.		903 - B II.c	F3	i.s.	
903 - 303	G-South	11.57	1-2	903 - B II.d1	F3	i.s.	
903 - 304	G-South	11.27	1-2	903 - B II.d2	F3	i.s.	
903 - 305	G-South	11.02	1-2	903 - B II.d3	F3	i.s.	
903 - 306	G-South	10.72	3	903 - B II.d4	F3	i.s.	
903 - 307	G-South	10.52	4	903 - B II.e	F3	i.s.	
903 - 308	G-South	10.32	4	Mn 2			
903 - 309	G-South	10.12	5				
903 - 310	G-South	9.92	5-11				
903 - 311	G-South	10.92	2				
903 - 312a	G-South	9.62	2-10				
903 - 312b1	G-South	i.s.					
903 - 312b2	G-South	i.s.					
903 - 312b3	G-South	i.s.					
903 - 312b4	G-South	i.s.					
903 - 315b5	G-South	i.s.					
903 - 313	G-South	9.44	5				
903 - 314	G-South	9.34	4				
903 - 315	G-South	9.07	4				
903 - 316	G-South	9.02	4				
903 - 317	G-South	8.92	3				

i.s. = individual sample belonging to no particular stratigraphic set; m† = mixture of materials.

Appendix III.

Table III.1: Ore and Rock Types.

Table III.1: Ore and rock types.

No.	Rock Type	No.	Rock Type
903 - 3	uncemented pisolite	903 - 61	mixed materials
903 - 4	uncemented pisolite	903 - 62	mixed materials
903 - 5a	uncemented pisolite	903 - 63	radial pyrolusite
903 - 5b	clay	903 - 64	laterite
903 - 6	cemented pisolite	903 - 65a	laterite
903 - 7	cemented pisolite	903 - 65b	mixed materials
903 - 8	cemented pisolite	903 - 66	mixed materials
903 - 9	uncemented pisolite	903 - 67	spherulite
903 - 10	cemented pisolite	903 - 68a	mixed materials
903 - 11	cemented pisolite	903 - 68b	mixed materials
903 - 12	cemented pisolite	903 - 69	mixed materials
903 - 13	cemented pisolite	903 - 70	mixed materials
903 - 14	cemented pisolite	903 - 71	mixed materials
903 - 15	cemented pisolite	903 - 72	mixed materials
903 - 16	cemented pisolite	903 - 73	mixed materials
903 - 17	cemented pisolite	903 - 74	mixed materials
903 - 18	cemented pisolite	903 - 75	mixed materials
903 - 19	cemented pisolite	903 - 76	mixed materials
903 - 20	clay	903 - 77a	hardground
903 - 21	Fe-pipe wall	903 - 77b	mixed materials
903 - 22	uncemented pisolite	903 - 78	mixed materials
903 - 23	cemented pisolite	903 - 79	mixed materials
903 - 24	mixed materials	903 - 80	uncemented oolite
903 - 25	mixed materials	903 - 81	uncemented oolite
903 - 26	sand	903 - 82	uncemented oolite
903 - 27	laterite	903 - 83	uncemented oolite
903 - 28a	laterite	903 - 84	uncemented oolite
903 - 28b	laterite	903 - 85	uncemented oolite
903 - 29	laterite	903 - 86	uncemented oolite
903 - 30	spherulite	903 - 87	uncemented oolite
903 - 31a	sand	903 - 88	uncemented oolite
903 - 31b	sand	903 - 89	uncemented oolite
903 - 32	sand	903 - 90	mixed materials
903 - 33	uncemented oolite	903 - 91	uncemented oolite
903 - 34	uncemented oolite	903 - 92	uncemented oolite
903 - 35	uncemented oolite	903 - 93	uncemented oolite
903 - 36	uncemented oolite	903 - 94	uncemented oolite
903 - 37	uncemented oolite	903 - 95	uncemented oolite
903 - 38	uncemented oolite	903 - 96	uncemented oolite
903 - 39	uncemented oolite	903 - 97	uncemented oolite
903 - 40	uncemented oolite	903 - 98	uncemented oolite
903 - 41	cemented oolite	903 - 99	uncemented oolite
903 - 42	uncemented oolite	903 - 100	uncemented oolite
903 - 43	uncemented oolite	903 - 101	uncemented oolite
903 - 44	uncemented oolite	903 - 102	uncemented oolite
903 - 45	uncemented oolite	903 - 103	uncemented oolite
903 - 46	uncemented oolite	903 - 104	uncemented oolite
903 - 47	uncemented oolite	903 - 105	cemented oolite
903 - 48	uncemented oolite	903 - 106	cemented oolite
903 - 49	uncemented oolite	903 - 107	cemented oolite
903 - 50	uncemented oolite	903 - 108	mixed materials
903 - 51	cemented oolite	903 - 109	cemented oolite
903 - 52	mixed materials	903 - 110	mixed materials
903 - 53	mixed materials	903 - 111	mixed materials
903 - 54	mixed materials	903 - 112	spherulite
903 - 55	mixed materials	903 - 113	spherulite
903 - 56	mixed materials	903 - 114	sand
903 - 57	mixed materials	903 - 115a	clay
903 - 58	mixed materials	903 - 115b	clay
903 - 59	mixed materials	903 - 116a	mixed materials
903 - 60	mixed materials	903 - 116b	mixed materials
903 - 117b	mixed materials	903 - 176	Mn-impregnated sand
903 - 118a	mixed materials	903 - 177	Mn-impregnated sand
903 - 118b	mixed materials	903 - 178	Mn-impregnated sand
903 - 119	cemented pisolite	903 - 179	ferruginous pisolite
903 - 120	uncemented pisolite	903 - 180	ferruginous pisolite
903 - 121	uncemented pisolite	903 - 181	ferruginous pisolite
903 - 122	uncemented pisolite	903 - 182	uncemented pisolite
903 - 123	cemented pisolite	903 - 183	uncemented pisolite

No.	Rock Type	No.	Rock Type
903 - 124	laterite	903 - 184	uncemented pisolite
903 - 125	laterite	903 - 185	ferruginous pisolite
903 - 126	laterite	903 - 186	ferruginous pisolite
903 - 127	laterite	903 - 187	massive ferricrete
903 - 128	laterite	903 - 188	massive mangcrete
903 - 129	laterite	903 - 189	laterite
903 - 130	laterite	903 - 190	mixed materials
903 - 131	laterite	903 - 191B	uncemented oolite (battery)
903 - 132	laterite	903 - 200	chocolate ore
903 - 133	laterite	903 - 201	chocolate ore
903 - 134	laterite	903 - 202	chocolate ore
903 - 135	laterite	903 - 203	chocolate ore
903 - 136	laterite	903 - 204	chocolate ore
903 - 137	laterite	903 - 205	chocolate ore
903 - 138	laterite	903 - 206	chocolate ore
903 - 139	laterite	903 - 207	chocolate ore
903 - 140	laterite	903 - 208	chocolate ore
903 - 141a	clay	903 - 209	chocolate ore
903 - 141b	clay	903 - 210	spherulite
903 - 141c	clay	903 - 211	spherulite
903 - 141 B	clay (battery)	903 - 212	laminar mangcrete
903 - 142	cemented pisolite	903 - 213	cemented pisolite
903 - 143	mixed materials	903 - 215	Fe-pipe wall
903 - 144	cemented pisolite	903 - 216	uncemented pisolite
903 - 145	mixed materials	903 - 217	Fe-pipe wall
903 - 146	mixed materials	903 - 218	laminar mangcrete
903 - 147	mixed materials	903 - 219	uncemented pisolite
903 - 148	mixed materials	903 - 220	cemented pisolite
903 - 149	mixed materials	903 - 221	Fe-pipe wall
903 - 150	uncemented pisolite	903 - 222	Fe-pipe wall
903 - 151	cemented pisolite	903 - 223	cemented pisolite
903 - 152a	mixed materials	903 - 224	cemented pisolite
903 - 152b	mixed materials	903 - 225	cemented pisolite
903 - 153	mixed materials	903 - 226	cemented pisolite
903 - 154	mixed materials	903 - 227	laminar mangcrete
903 - 155	mixed materials	903 - 228	laminar mangcrete
903 - 156	clay	903 - 229	spherulite
903 - 157	mixed materials	903 - 230	spherulite
903 - 158	mixed materials	903 - 232	massive mangcrete
903 - 159	ferruginous pisolite	903 - 233	massive mangcrete
903 - 160	mixed materials	903 - 234	ferruginous pisolite
903 - 161	mixed materials	903 - 235	ferruginous pisolite
903 - 162	mixed materials	903 - 237	Mn-impregnated sand
903 - 164	digital concretions	903 - 239	digital concretions
903 - 168 B	cemented pisolite (battery)	903 - 241	mixed materials
903 - 169 B	uncemented pisolite (battery)	903 - 245	ferruginous pisolite
903 - 170a	Mn-impregnated sand	903 - 246	ferruginous pisolite
903 - 170b	Mn-impregnated sand	903 - 249	laminar mangcrete
903 - 171a	Mn-impregnated sand	903 - 250	ferruginous pisolite
903 - 171b	Mn-impregnated sand	903 - 251	concretions
903 - 172	Mn-impregnated sand	903 - 252	laminar mangcrete
903 - 173	Mn-impregnated sand	903 - 253	siliceous ore
903 - 174	Mn-impregnated sand	903 - 254	siliceous ore
903 - 175	Mn-impregnated sand	903 - 255	cemented pisolite
903 - 256	cemented pisolite	903 - 314	mixed materials
903 - 259	siliceous ore	903 - 315	mixed materials
903 - 260	siliceous ore	903 - 316	mixed materials
903 - 261	ferruginous pisolite	903 - 317	mixed materials
903 - 262	ferruginous pisolite	903 - 318	mixed materials
903 - 263	cemented pisolite	903 - 319	mixed materials
903 - 264	cemented pisolite	903 - 320	mixed materials
903 - 265	uncemented pisolite	903 - 322	mixed materials
903 - 266	uncemented pisolite	903 - 323	mixed materials
903 - 268	massive mangcrete	903 - 324	spherulite
903 - 269	massive mangcrete	903 - 325	spherulite
903 - 270	massive mangcrete	903 - 326a	spherulite
903 - 271	massive mangcrete	903 - 326b	spherulite
903 - 272	cemented pisolite	903 - 326c	spherulite
903 - 273	cemented pisolite	903 - 327	spherulite

No.	Rock Type	No.	Rock Type
903 - 274	uncemented pisolite	903 - 328	hardground
903 - 275	uncemented pisolite	903 - 329	hardground
903 - 276	ferruginous pisolite	903 - 330	concretions
903 - 277	ferruginous pisolite	903 - 331	concretions
903 - 278	Mn-impregnated sand	903 - 332	massive mangcrete
903 - 279	siliceous ore	903 - 333	massive mangcrete
903 - 280	massive mangcrete	903 - 334	siliceous ore
903 - 281	concretions	903 - 335	siliceous ore
903 - 282	concretions	903 - 336	ferruginous pisolite
903 - 283a	concretions	903 - 337	laterite
903 - 283b	concretions	903 - 338	laterite
903 - 283c	concretions	903 - 339	siliceous ore
903 - 283d	concretions	903 - 340a	siliceous ore
903 - 283e	concretions	903 - 340b	siliceous ore
903 - 284	digital concretions	903 - 341a	mixed materials
903 - 285	digital concretions	903 - 342a	massive mangcrete
903 - 286	digital concretions	903 - 343	laminar mangcrete
903 - 287	digital concretions	903 - 344	Mn cave pearl
903 - 290	radial pyrolusite	903 - B I.a	clay (battery)
903 - 291	radial pyrolusite	903 - B I.b	clay (battery)
903 - 292	radial pyrolusite	903 - B I.c	clay (battery)
903 - 293	radial pyrolusite	903 - B I.d1	clay (battery)
903 - 294	radial pyrolusite	903 - B I.d2	clay (battery)
903 - 295	ferruginous pisolite	903 - B I.d3	clay (battery)
903 - 296	ferruginous pisolite	903 - B I.d4	clay (battery)
903 - 297	uncemented pisolite	903 - B I.e	clay (battery)
903 - 298	massive mangcrete	903 - B II.a	cemented pisolite (battery)
903 - 299	massive mangcrete	903 - B II.b	cemented pisolite (battery)
903 - 300	radial pyrolusite	903 - B II.c	cemented pisolite (battery)
903 - 301	radial pyrolusite	903 - B II.d1	cemented pisolite (battery)
903 - 302	radial pyrolusite	903 - B II.d2	cemented pisolite (battery)
903 - 303	mixed materials	903 - B II.d3	cemented pisolite (battery)
903 - 304	mixed materials	903 - B II.d4	cemented pisolite (battery)
903 - 305	mixed materials	903 - B II.e	cemented pisolite (battery)
903 - 306	mixed materials	903 - Mn 2	Mn standard (GEMCO)
903 - 307	mixed materials		
903 - 308	mixed materials		
903 - 309	mixed materials		
903 - 310	mixed materials		
903 - 311	mixed materials		
903 - 312a	mixed materials		
903 - 312b1	envelope grains		
903 - 312b2	envelope grains		
903 - 312b3	envelope grains		
903 - 312b4	envelope grains		"mixed materials" contain numerous
903 - 315b5	envelope grains		ores and gangues and were not further
903 - 313	mixed materials		specified to avoid misinterpretation

Appendix IV.

Table IV.1: XRF/AA Major and Minor Element Analyses; [%].

Table IV.2: ICP Trace Element Analyses of Ores and Rocks; [ppm].

Table IV.3: XRF Trace Element Analyses of Ores and Rocks; [ppm].

Table IV.4: INAA Analyses of Selected Ore Samples; [ppm].

Table IV.5: Element Correlation Matrix for Ore and Rock Samples.

Table IV.1: XRF/AA major and minor element analyses.

No.	Al2O3	BaO	CaO	Fe	K2O	MgO	Mn	Na2O	P
903 - 3	5.9	0.30	0.03	1.7	0.22	0.05	51.0	0.01	0.043
903 - 4	2.0	0.40	0.05	0.1	0.42	0.05	58.3	0.01	0.056
903 - 5a	13.0	2.41	0.03	2.7	0.20	0.15	36.4	0.02	0.049
903 - 5b	32.5	0.01	0.01	1.2	0.13	0.01	0.1	0.01	0.008
903 - 6	3.5	3.67	0.05	0.6	1.32	0.35	54.6	0.21	0.049
903 - 7	4.1	5.84	0.04	0.7	0.75	0.30	51.3	0.17	0.038
903 - 8	3.5	3.04	0.05	0.6	1.57	0.38	52.7	0.22	0.035
903 - 9	3.5	4.09	0.03	1.6	0.45	0.16	52.4	0.09	0.061
903 - 10	4.9	1.56	0.06	1.0	1.82	0.52	49.6	0.25	0.030
903 - 11	5.2	0.71	0.05	1.1	1.73	0.55	50.0	0.25	0.042
903 - 12	5.5	0.65	0.05	1.1	1.51	0.56	49.6	0.23	0.050
903 - 13	4.1	0.65	0.06	0.9	1.87	0.61	51.1	0.27	0.036
903 - 14	5.9	0.93	0.06	1.1	1.55	0.65	48.3	0.26	0.045
903 - 15	7.4	2.20	0.04	4.2	1.13	0.41	42.1	0.17	0.045
903 - 16	4.0	2.20	0.06	1.1	1.77	0.45	52.7	0.22	0.043
903 - 17	4.0	0.72	0.07	0.8	2.17	0.50	51.3	0.22	0.037
903 - 18	7.1	3.41	0.05	2.2	1.04	0.32	45.2	0.21	0.032
903 - 19	6.8	1.75	0.05	2.8	1.82	0.31	44.6	0.21	0.033
903 - 20	19.4	0.01	0.01	0.9	0.11	0.01	0.1	0.02	0.002
903 - 21	20.0	0.63	0.01	12.6	0.29	0.01	6.3	0.03	0.042
903 - 22	7.0	3.79	0.04	5.6	0.44	0.40	40.5	0.07	0.054
903 - 23	5.0	2.63	0.05	1.1	1.38	0.50	48.9	0.21	0.035
903 - 24	21.8	0.60	0.01	10.5	0.28	0.01	5.9	0.02	0.044
903 - 25	15.0	0.40	0.01	17.5	0.40	0.03	7.6	0.01	0.034
903 - 26	1.5	0.01	0.01	0.3	0.03	0.01	0.1	0.01	0.001
903 - 27	19.2	0.01	0.01	27.0	0.08	0.03	0.1	0.01	0.036
903 - 28a	24.4	0.04	0.01	14.9	0.17	0.01	0.7	0.01	0.014
903 - 28b	24.6	0.01	0.01	15.5	0.14	0.02	0.1	0.01	0.014
903 - 29	20.0	0.16	0.01	13.3	0.23	0.02	1.8	0.01	0.016
903 - 30	17.1	0.06	0.01	11.3	0.17	0.03	0.8	0.01	0.016
903 - 31a	10.6	0.02	0.01	5.3	0.11	0.02	0.2	0.01	0.005
903 - 31b	6.0	0.01	0.02	1.3	0.07	0.01	0.1	0.01	0.001
903 - 32	4.4	0.01	0.07	1.6	0.06	0.01	0.2	0.01	0.004
903 - 33	3.2	1.46	0.11	1.4	0.91	0.79	51.1	0.25	0.048
903 - 34	2.4	1.67	0.11	1.3	0.90	0.82	52.8	0.27	0.048
903 - 35	3.6	1.17	0.07	0.8	0.57	0.50	52.9	0.16	0.050
903 - 36	2.5	1.55	0.10	1.2	0.78	0.70	52.3	0.23	0.050
903 - 37	2.8	1.67	0.13	1.9	0.93	0.82	51.1	0.27	0.055
903 - 38	5.0	1.52	0.11	2.7	0.85	0.70	46.5	0.23	0.056
903 - 39	3.9	1.64	0.12	2.2	0.88	0.72	48.5	0.24	0.059
903 - 40	3.4	1.64	0.13	2.2	0.91	0.80	48.5	0.25	0.530
903 - 41	2.0	0.65	0.07	1.2	0.38	0.36	55.6	0.09	0.093
903 - 42	9.6	1.30	0.09	4.1	0.68	0.50	37.3	0.15	0.050
903 - 43	14.7	1.26	0.07	5.8	0.62	0.39	25.1	0.10	0.045
903 - 44	7.9	1.83	0.10	3.3	0.77	0.60	40.3	0.18	0.072
903 - 45	13.0	1.27	0.08	4.3	0.64	0.46	31.3	0.15	0.049
903 - 46	4.0	1.59	0.12	2.1	0.86	0.69	48.7	0.25	0.067
903 - 47	3.0	1.59	0.09	1.4	0.58	0.59	50.7	0.19	0.080
903 - 48	3.2	2.15	0.09	2.4	0.63	0.60	44.9	0.18	0.073
903 - 49	13.4	1.62	0.06	3.7	0.48	0.34	29.4	0.09	0.060
903 - 50	3.5	2.21	0.09	1.2	0.59	0.58	50.4	0.18	0.074
903 - 51	3.0	2.24	0.09	1.2	0.67	0.60	52.2	0.19	0.075
903 - 52	20.7	1.27	0.02	10.4	0.33	0.16	14.3	0.04	0.048
903 - 53	26.8	0.11	0.01	11.0	0.35	0.04	2.0	0.01	0.025
903 - 54	12.8	1.93	0.05	4.0	0.31	0.27	33.6	0.06	0.059
903 - 55	3.3	3.14	0.08	1.2	0.36	0.49	51.8	0.10	0.077
903 - 56	3.9	4.65	0.11	2.1	0.52	0.66	47.8	0.14	0.074
903 - 57	25.5	0.35	0.01	6.9	0.19	0.04	3.3	0.01	0.011
903 - 58	5.1	2.27	0.05	2.4	0.30	0.28	47.9	0.09	0.063
903 - 59	5.9	3.90	0.08	1.5	0.43	0.44	46.7	0.09	0.058
903 - 60	9.7	1.91	0.03	4.8	0.31	0.11	39.2	0.11	0.043
903 - 61	2.9	3.33	0.07	0.9	0.59	0.35	53.4	0.09	0.071
903 - 62	4.4	1.47	0.04	1.5	0.25	0.16	53.1	0.03	0.059
903 - 63	3.8	0.25	0.04	3.7	0.44	0.06	53.3	0.04	0.076
903 - 64	20.0	0.13	0.01	19.3	0.35	0.03	7.2	0.03	0.071
903 - 65a	18.8	0.18	0.01	21.2	0.41	0.05	7.7	0.02	0.050
903 - 65b	4.5	0.74	0.19	1.5	3.56	0.01	52.4	0.16	0.186
903 - 66	20.6	0.34	0.06	14.7	0.75	0.05	13.6	0.03	0.045
903 - 67	14.2	0.33	0.07	7.5	0.53	0.03	10.5	0.02	0.039

No.	Al2O3	BaO	CaO	Fe	K2O	MgO	Mn	Na2O	P
903 - 68a	3.6	1.89	0.05	1.7	0.28	0.32	39.0	0.07	0.052
903 - 68b	4.4	2.67	0.08	1.3	0.40	0.66	46.9	0.17	0.077
903 - 69	5.0	2.73	0.08	1.2	0.39	0.63	47.5	0.16	0.078
903 - 70	6.1	2.66	0.07	1.3	0.40	0.63	46.3	0.17	0.066
903 - 71	4.0	2.49	0.07	1.1	0.40	0.68	50.9	0.19	0.072
903 - 72	4.0	2.65	0.08	1.6	0.44	0.79	49.6	0.20	0.077
903 - 73	5.4	2.25	0.08	1.3	0.42	0.77	47.7	0.23	0.069
903 - 74	8.8	2.24	0.06	1.8	0.53	0.80	40.4	0.24	0.057
903 - 75	6.8	2.24	0.07	1.4	0.62	0.86	45.5	0.25	0.065
903 - 76	7.6	1.92	0.07	1.4	0.63	0.75	43.5	0.23	0.055
903 - 77a	4.5	1.79	0.08	1.3	0.64	0.90	50.8	0.26	0.078
903 - 77b	3.1	2.12	0.06	0.9	0.70	0.63	52.7	0.17	0.079
903 - 78	3.2	1.14	0.07	1.2	0.53	0.74	53.1	0.24	0.096
903 - 79	15.2	n.d.	0.01	6.5	0.36	0.0	2.8	0.02	0.037
903 - 80	2.8	0.41	0.05	1.3	0.52	0.09	54.2	0.03	0.061
903 - 81	2.6	2.30	0.07	1.4	0.33	0.36	48.3	0.07	0.052
903 - 82	3.8	2.47	0.08	1.6	0.40	0.42	44.2	0.10	0.053
903 - 83	2.7	1.73	0.06	1.3	0.28	0.33	50.3	0.07	...056
903 - 84	3.5	1.98	0.06	1.4	0.31	0.35	37.7	0.08	0.046
903 - 85	2.7	1.27	0.05	0.7	1.04	0.40	55.5	0.13	0.098
903 - 86	4.1	0.94	0.06	2.2	1.48	0.29	45.8	0.14	0.124
903 - 87	11.4	0.77	0.01	10.1	0.98	0.12	21.9	0.07	0.069
903 - 88	6.3	1.83	0.10	1.9	0.58	0.55	44.7	0.21	0.069
903 - 89	5.8	2.08	0.08	2.7	0.83	0.48	42.6	0.15	0.086
903 - 90	22.7	0.49	n.d.	19.0	0.24	0.02	5.1	0.03	0.024
903 - 91	5.0	1.62	0.09	1.9	0.57	0.56	45.4	0.18	0.061
903 - 92	5.1	1.34	0.10	2.0	0.64	0.64	47.0	0.21	0.054
903 - 93	4.5	1.19	0.10	2.0	0.63	0.63	49.1	0.22	0.053
903 - 94	4.3	1.06	0.10	1.8	0.62	0.67	49.5	0.21	0.050
903 - 95	3.8	1.26	0.12	1.7	0.74	0.77	51.0	0.25	0.046
903 - 96	2.8	1.39	0.13	1.6	0.82	0.85	52.6	0.26	0.047
903 - 97	3.2	1.27	0.13	1.7	0.81	0.74	51.8	0.24	0.049
903 - 98	2.6	1.06	0.10	1.4	0.67	0.65	53.7	0.19	0.052
903 - 99	3.9	1.73	0.13	2.2	0.87	0.70	49.5	0.22	0.044
903 - 100	4.4	2.13	0.15	2.7	1.11	0.77	48.3	0.26	0.035
903 - 101	3.4	1.44	0.16	1.9	1.31	0.86	51.3	0.30	0.045
903 - 102	3.5	1.23	0.12	1.5	0.90	0.48	53.3	0.18	0.073
903 - 103	2.4	2.04	0.05	1.3	0.57	0.30	54.9	0.12	0.074
903 - 104	4.7	1.36	0.04	2.4	0.27	0.25	46.3	0.07	0.068
903 - 105	3.1	1.36	0.06	0.9	0.24	0.25	54.4	0.07	0.064
903 - 106	3.3	2.39	0.09	0.9	0.52	0.49	53.3	0.15	0.054
903 - 107	4.2	2.93	0.12	1.3	0.62	0.61	50.4	0.17	0.057
903 - 108	5.0	3.34	0.11	2.1	0.77	0.58	46.4	0.18	0.045
903 - 109	4.3	2.10	0.07	1.7	0.37	0.39	51.5	0.10	0.063
903 - 110	11.8	2.00	0.02	9.7	0.39	0.15	26.5	0.09	0.046
903 - 111	3.2	2.10	0.06	1.3	0.45	0.20	54.8	0.05	0.083
903 - 112	9.1	1.76	0.03	3.9	0.29	0.17	40.5	0.03	0.055
903 - 113	12.9	0.32	n.d.	33.4	0.16	0.05	6.9	0.01	0.149
903 - 114	6.1	0.24	n.d.	2.8	0.14	0.03	4.7	0.01	0.009
903 - 115a	10.1	n.d.	n.d.	0.7	0.08	0.01	0.3	0.01	0.006
903 - 115b	6.5	n.d.	n.d.	16.9	0.06	0.01	0.3	0.01	0.016
903 - 116a	3.7	0.54	n.d.	2.4	1.97	0.01	30.6	0.10	0.092
903 - 116b	3.2	0.41	0.01	4.9	1.63	0.01	35.0	0.19	0.083
903 - 117b	3.1	0.15	n.d.	2.2	2.81	0.02	51.6	0.60	0.050
903 - 118a	3.0	0.06	0.05	24.3	1.68	0.07	30.1	0.12	0.134
903 - 118b	16.1	0.01	0.01	3.1	0.23	0.02	4.5	0.02	0.014
903 - 119	3.9	0.02	0.15	1.6	2.66	0.02	46.0	0.30	0.153
903 - 120	7.5	0.03	0.12	2.4	0.75	0.07	41.1	0.17	0.075
903 - 121	5.0	0.06	0.09	2.8	1.01	0.05	49.0	0.19	0.095
903 - 122	7.0	0.10	0.08	2.9	0.78	0.07	40.4	0.16	0.068
903 - 123	4.2	0.05	0.11	1.2	1.26	0.09	49.2	0.27	0.089
903 - 124	23.7	0.24	0.02	6.5	0.78	0.03	16.3	0.06	0.011
903 - 125	26.0	0.22	0.02	6.6	0.62	0.04	13.0	0.04	0.013
903 - 126	27.0	0.22	0.02	6.8	0.47	0.04	11.0	0.03	0.008
903 - 127	25.4	0.23	0.01	13.2	0.31	0.03	7.0	0.03	0.012
903 - 128	26.0	0.10	0.01	12.4	0.26	0.03	4.6	0.01	0.005
903 - 129	27.5	0.08	0.01	10.5	0.22	0.04	3.4	0.01	0.010
903 - 130	26.0	0.12	0.02	7.9	0.48	0.04	13.0	0.03	0.011
903 - 131	26.7	0.13	0.01	7.4	0.39	0.04	10.4	0.02	0.005

No.	Al2O3	BaO	CaO	Fe	K2O	MgO	Mn	Na2O	P
903 - 132	23.3	0.10	0.01	14.4	0.32	0.03	3.9	0.01	0.009
903 - 133	28.3	0.05	0.01	9.5	0.22	0.05	1.7	0.01	0.007
903 - 134	23.5	0.10	0.01	12.4	0.22	0.03	2.4	0.01	0.011
903 - 135	25.5	0.25	0.01	12.4	0.27	0.04	5.4	0.01	0.005
903 - 136	23.5	0.13	0.01	12.5	0.31	0.04	3.7	0.01	0.016
903 - 137	24.6	0.14	0.01	13.0	0.28	0.03	2.5	0.01	0.014
903 - 138	24.7	0.46	0.02	12.6	0.38	0.04	6.4	0.01	0.010
903 - 139	24.1	0.06	0.02	15.2	0.25	0.04	2.3	0.01	0.018
903 - 140	16.8	0.04	0.06	4.0	0.19	0.04	1.3	0.01	0.011
903 - 141a	33.7	n.d.	0.01	1.0	0.17	0.04	0.2	0.01	0.005
903 - 141b	32.1	n.d.	0.01	5.3	0.17	0.04	0.2	0.01	0.012
903 - 141c	29.8	n.d.	0.01	5.7	0.16	0.04	0.2	0.01	0.008
903 - 141 B	35.0	0.00	0.02	1.4	0.18	0.01	0.1	0.01	0.006
903 - 142	6.7	0.04	0.05	2.4	1.55	0.11	48.2	0.26	0.043
903 - 143	6.7	0.04	0.08	1.7	1.63	0.12	49.7	0.38	0.036
903 - 144	4.7	0.12	0.08	1.3	1.51	0.18	53.0	0.31	0.047
903 - 145	3.7	0.10	0.03	1.1	1.16	0.07	55.2	0.21	0.051
903 - 146	6.5	0.10	0.03	1.5	1.92	0.05	50.1	0.31	0.068
903 - 147	4.8	0.07	0.01	1.5	1.49	0.06	51.4	0.26	0.078
903 - 148	3.7	0.43	0.10	13.2	1.04	0.14	41.8	0.23	0.128
903 - 149	7.9	0.08	0.08	9.1	1.56	0.04	38.9	0.26	0.072
903 - 150	3.1	0.08	0.03	1.0	0.93	0.07	56.6	0.17	0.040
903 - 151	7.4	0.08	0.03	3.0	1.30	0.07	47.0	0.24	0.064
903 - 152a	9.4	0.04	0.09	7.5	1.33	0.04	40.0	0.25	0.071
903 - 152b	5.8	0.04	0.09	15.3	1.30	0.10	37.4	0.23	0.130
903 - 153	7.1	0.68	0.05	3.9	2.31	0.02	46.4	0.23	0.106
903 - 154	8.2	0.14	0.07	3.6	1.60	0.03	45.2	0.24	0.081
903 - 155	2.4	0.32	0.16	4.0	1.36	0.17	34.7	0.09	0.179
903 - 156	8.0	0.03	n.d.	15.9	0.26	0.02	3.2	0.01	0.137
903 - 157	2.2	0.02	n.d.	29.3	0.47	0.02	6.4	0.02	0.367
903 - 158	6.4	0.04	n.d.	23.0	0.25	0.02	2.7	0.01	0.309
903 - 159	3.0	0.04	0.01	22.7	0.37	0.09	6.3	0.01	0.350
903 - 160	1.2	0.07	0.02	0.8	0.07	0.06	49.3	0.01	0.085
903 - 161	2.4	0.06	0.02	1.3	0.44	0.02	36.5	0.01	0.087
903 - 162	2.3	0.05	0.02	2.6	2.41	0.03	27.1	0.16	0.041
903 - 164	6.0	0.15	0.05	1.2	3.48	0.03	38.4	0.11	0.091
903 - 168 B	7.4	0.10	0.05	1.8	1.81	0.05	47.2	0.33	0.040
903 - 169 B	6.0	0.09	0.07	2.1	1.34	0.05	50.2	0.22	0.042
903 - 170a	0.9	0.01	0.01	0.2	0.03	0.01	0.1	0.01	0.001
903 - 170b	2.8	0.02	0.01	0.3	0.08	0.01	0.3	0.01	0.005
903 - 171a	1.0	0.01	0.01	0.3	0.04	0.01	0.1	0.01	0.001
903 - 171b	0.9	0.01	0.01	0.2	0.04	0.01	0.1	0.01	0.001
903 - 172	0.8	0.01	0.01	0.2	0.04	0.01	0.1	0.01	0.001
903 - 173	0.8	0.01	0.01	0.2	0.06	0.01	0.2	0.01	0.002
903 - 174	0.8	0.04	0.01	0.3	0.11	0.01	1.0	0.01	0.005
903 - 175	0.6	0.03	0.01	0.2	0.09	0.01	0.7	0.01	0.003
903 - 176	0.6	0.06	0.01	0.3	0.14	0.01	1.6	0.01	0.006
903 - 177	2.7	0.10	0.01	0.5	0.19	0.01	2.0	0.01	0.013
903 - 178	2.1	0.67	0.01	0.4	1.53	0.01	22.5	0.01	0.072
903 - 179	8.4	0.01	0.01	46.9	0.10	0.01	0.3	0.01	0.209
903 - 180	7.1	0.05	0.01	48.5	0.29	0.01	3.6	0.01	0.528
903 - 181	6.6	0.16	0.01	44.0	0.46	0.01	9.5	0.02	0.522
903 - 182	4.4	0.28	0.04	2.0	0.21	0.09	52.9	0.01	0.080
903 - 183	4.3	0.33	0.04	1.7	0.31	0.10	54.7	0.03	0.095
903 - 184	4.0	0.28	0.04	2.6	0.24	0.08	54.0	0.02	0.101
903 - 185	7.7	0.01	0.01	51.8	0.08	0.01	0.9	0.01	0.515
903 - 186	5.1	0.01	0.01	54.6	0.06	0.01	0.4	0.01	0.448
903 - 187	12.1	0.02	0.01	41.0	0.53	0.01	3.2	0.01	0.583
903 - 188	9.4	0.18	0.08	2.7	2.56	0.01	43.0	0.13	0.074
903 - 189	16.5	0.15	0.01	16.5	0.21	0.01	3.5	0.10	0.056
903 - 190	8.8	0.71	0.13	3.4	1.84	0.02	39.5	0.01	0.333
903 - 191 B	2.3	1.69	0.11	1.2	0.91	0.78	53.0	0.25	0.047
903 - 200	25.8	0.05	0.01	6.9	0.22	0.03	1.9	0.01	0.015
903 - 201	26.3	0.09	0.01	6.9	0.24	0.03	2.4	0.01	0.015
903 - 202	24.6	0.19	0.01	8.6	0.27	0.03	3.8	0.02	0.012
903 - 203	25.0	0.17	0.01	8.1	0.24	0.03	3.7	0.03	0.013
903 - 204	25.5	0.26	0.01	8.0	0.25	0.03	4.7	0.02	0.011
903 - 205	26.7	0.24	0.01	8.6	0.30	0.04	5.8	0.03	0.009
903 - 206	27.1	0.31	0.01	8.1	0.31	0.03	6.7	0.03	0.012

Table IV.1: XRF/AA major and minor element analyses.

No.	Al2O3	BaO	CaO	Fe	K2O	MgO	Mn	Na2O	P
903 - 207	26.0	0.28	0.01	9.2	0.50	0.03	10.9	0.05	0.006
903 - 208	27.3	0.21	0.01	7.8	0.46	0.04	9.7	0.04	0.010
903 - 209	5.5	0.34	0.08	2.6	0.76	0.09	47.9	0.17	0.059
903 - 210	23.9	0.07	0.02	16.0	0.26	0.03	1.8	0.01	0.025
903 - 211	20.9	0.15	0.10	8.3	0.23	0.05	4.8	0.01	0.011
903 - 212	8.9	0.23	0.03	3.7	1.38	0.07	42.0	0.26	0.027
903 - 213	3.0	0.01	0.22	0.6	1.96	0.13	55.4	0.57	0.104
903 - 215	14.1	n.d.	n.d.	11.4	0.12	0.01	0.5	0.01	0.005
903 - 216	3.5	0.05	0.03	0.9	0.86	0.08	55.8	0.16	0.041
903 - 217	19.1	0.04	n.d.	7.1	0.21	0.02	1.9	0.01	0.009
903 - 218	7.6	0.10	0.05	2.3	1.30	0.07	47.3	0.27	0.049
903 - 219	5.2	0.11	0.02	1.8	0.85	0.08	51.4	0.11	0.048
903 - 220	8.1	0.06	0.03	1.9	1.44	0.07	47.8	0.32	0.046
903 - 221	22.7	n.d.	n.d.	20.2	0.13	0.01	0.2	0.01	0.018
903 - 222	21.9	0.01	n.d.	15.5	0.15	0.01	0.3	0.01	0.026
903 - 223	3.4	3.07	0.04	0.7	1.80	0.45	53.6	0.24	0.035
903 - 224	3.6	3.72	0.04	0.6	1.27	0.38	53.7	0.18	0.037
903 - 225	3.9	1.40	0.05	0.8	1.02	0.56	52.9	0.16	0.053
903 - 226	6.6	1.25	0.04	1.4	1.39	0.61	47.1	0.25	0.039
903 - 227	5.3	3.62	n.d.	2.5	1.32	0.17	47.4	0.50	0.020
903 - 228	6.3	4.21	n.d.	4.3	1.29	0.01	44.2	0.38	0.022
903 - 229	15.9	0.11	n.d.	13.2	0.16	0.04	1.1	0.01	0.019
903 - 230	16.8	0.08	n.d.	12.4	0.18	0.04	0.7	0.01	0.018
903 - 232	10.8	0.21	0.08	3.9	1.83	0.03	40.0	0.10	0.106
903 - 233	12.6	0.45	0.10	1.5	2.40	0.03	38.8	0.13	0.044
903 - 234	7.3	n.d.	n.d.	50.9	0.06	0.01	0.3	0.01	0.527
903 - 235	8.1	n.d.	n.d.	52.0	0.10	0.01	0.8	0.01	0.505
903 - 237	2.0	0.73	n.d.	0.1	1.67	0.01	24.5	0.06	0.085
903 - 239	3.5	0.45	0.02	4.0	2.24	0.02	31.3	0.14	0.095
903 - 241	3.2	0.71	0.03	0.9	0.79	0.08	56.4	0.17	0.031
903 - 245	3.7	0.04	n.d.	56.1	0.20	0.03	3.0	0.01	0.445
903 - 246	2.7	0.06	n.d.	59.9	0.09	0.02	2.0	0.01	0.527
903 - 249	6.6	3.27	n.d.	2.5	1.99	0.09	46.5	0.34	0.016
903 - 250	3.6	0.33	0.02	26.3	0.94	0.01	30.8	0.11	0.054
903 - 251	2.1	0.23	0.04	35.4	0.61	0.20	20.5	0.07	0.109
903 - 252	7.0	3.32	n.d.	4.3	1.81	0.09	43.9	0.28	0.025
903 - 253	4.5	0.11	0.09	0.6	2.26	0.03	50.8	0.25	0.017
903 - 254	2.0	0.25	0.06	1.1	1.50	0.01	27.3	0.12	0.020
903 - 255	2.8	0.43	0.06	17.4	2.63	0.04	37.3	0.14	0.277
903 - 256	1.8	0.50	0.10	23.2	1.97	0.04	31.8	0.12	0.425
903 - 259	2.8	0.67	0.03	0.6	1.48	0.10	53.8	0.14	0.091
903 - 260	2.4	0.84	0.04	0.7	1.67	0.14	54.5	0.18	0.085
903 - 261	6.1	0.13	n.d.	49.1	0.27	0.01	5.7	0.02	0.390
903 - 262	8.4	0.07	n.d.	49.3	0.19	0.01	3.2	0.01	0.312
903 - 263	4.4	4.23	0.06	2.5	0.97	0.52	49.5	0.17	0.040
903 - 264	6.3	4.41	0.07	1.7	0.71	0.67	47.2	0.13	0.046
903 - 265	0.8	0.11	0.05	0.5	0.02	0.09	61.1	0.01	0.032
903 - 266	1.7	2.66	0.06	0.6	0.24	0.05	57.9	0.04	0.045
903 - 268	3.0	0.82	0.08	6.5	4.06	0.04	47.3	0.23	0.226
903 - 269	3.0	1.17	0.17	4.1	3.16	0.05	50.5	0.17	0.095
903 - 270	3.7	0.01	0.01	30.5	2.36	0.03	26.0	0.11	0.231
903 - 271	3.7	0.24	0.10	5.5	4.04	0.04	48.1	0.19	0.274
903 - 272	2.1	0.69	0.10	1.4	2.18	0.01	56.0	0.13	0.183
903 - 273	2.4	0.18	0.10	1.4	2.30	0.01	55.9	0.15	0.190
903 - 274	9.6	0.05	0.02	2.8	0.11	0.07	42.8	0.01	0.056
903 - 275	8.3	0.07	0.02	2.6	0.16	0.08	45.9	0.02	0.052
903 - 276	7.5	0.05	n.d.	48.0	0.19	0.01	3.8	0.01	0.503
903 - 277	5.7	0.27	n.d.	29.0	0.16	0.01	2.7	0.01	0.302
903 - 278	3.7	2.70	n.d.	1.3	1.03	0.01	22.5	0.05	0.113
903 - 279	3.1	0.02	0.07	0.4	1.45	0.01	29.3	0.22	0.014
903 - 280	2.6	0.27	0.05	22.5	1.96	0.03	34.5	0.10	0.420
903 - 281	4.2	0.51	0.05	2.3	4.58	0.06	50.0	0.17	0.093
903 - 282	2.9	0.80	0.13	3.4	3.77	0.06	51.4	0.26	0.195
903 - 283a	2.5	0.44	0.07	0.9	5.35	0.07	54.2	0.12	0.130
903 - 283b	3.9	1.75	0.08	1.4	4.16	0.06	50.2	0.20	0.238
903 - 283c	4.0	1.76	0.07	1.3	4.35	0.05	51.8	0.21	0.226
903 - 283d	3.8	1.54	0.06	1.8	4.30	0.08	51.7	0.18	0.183
903 - 283e	4.0	2.12	0.06	1.4	4.36	0.05	52.4	0.21	0.226
903 - 284	3.9	7.67	0.03	6.6	1.49	0.02	44.0	0.07	0.224

No.	Al2O3	BaO	CaO	Fe	K2O	MgO	Mn	Na2O	P
903 - 285	3.7	2.12	0.06	1.4	4.33	0.03	52.4	0.04	0.233
903 - 286	3.8	8.59	0.03	5.6	1.36	0.03	44.7	0.07	0.213
903 - 287	4.1	8.91	0.02	10.2	0.80	0.02	39.9	0.04	0.284
903 - 290	2.9	0.50	0.07	2.1	2.09	0.01	54.1	0.28	0.182
903 - 291	2.7	0.20	0.01	1.9	0.08	0.08	56.3	0.01	0.025
903 - 292	3.9	0.09	0.01	4.0	0.08	0.09	52.2	0.02	0.051
903 - 293	2.9	0.06	0.01	2.2	0.06	0.08	55.7	0.01	0.050
903 - 294	3.3	0.08	n.d.	2.7	0.16	0.07	54.5	0.03	0.027
903 - 295	2.5	n.d.	n.d.	55.5	0.03	0.07	0.3	0.03	0.241
903 - 296	6.9	0.06	n.d.	37.5	0.12	0.14	13.0	0.01	0.410
903 - 297	6.3	0.18	0.01	2.6	0.35	0.04	49.3	0.01	0.076
903 - 298	2.7	0.15	0.02	1.6	4.36	0.12	52.5	0.03	0.127
903 - 299	2.4	0.08	0.04	1.9	4.22	0.04	53.6	0.25	0.200
903 - 300	2.1	0.22	0.03	3.2	0.06	0.05	55.2	0.18	0.027
903 - 301	2.4	0.09	0.02	1.8	0.09	0.13	56.6	0.01	0.034
903 - 302	2.7	0.08	0.02	2.5	0.09	0.09	55.5	0.01	0.031
903 - 303	3.2	1.58	0.09	1.4	0.47	0.44	48.4	0.12	0.061
903 - 304	3.4	1.25	0.07	1.2	0.42	0.46	37.9	0.14	0.057
903 - 305	4.1	1.42	0.06	1.6	0.54	0.08	44.2	0.01	0.064
903 - 306	6.8	1.26	0.07	2.3	0.61	0.64	42.1	0.23	0.079
903 - 307	5.1	1.95	0.06	1.0	0.63	0.57	49.5	0.20	0.091
903 - 308	4.0	1.76	0.07	1.0	0.57	0.77	52.1	0.25	0.092
903 - 309	6.4	1.57	0.07	1.5	0.55	0.90	47.0	0.28	0.086
903 - 310	7.6	1.60	0.05	2.1	0.60	0.77	43.1	0.27	0.075
903 - 311	5.1	1.52	0.08	1.3	0.62	0.82	46.7	0.29	0.079
903 - 312a	4.7	1.32	0.09	1.3	0.55	0.71	50.9	0.29	0.102
903 - 312b1	1.7	0.79	0.05	0.9	0.41	0.72	56.1	0.26	0.084
903 - 312b2	1.9	0.67	0.07	0.7	0.61	0.90	55.1	0.43	0.096
903 - 312b3	2.1	0.59	0.06	1.1	0.47	0.68	54.3	0.28	0.113
903 - 312b4	1.9	0.73	0.07	1.0	0.57	0.72	55.0	0.31	0.106
903 - 315b5	2.1	0.56	0.05	1.0	0.48	0.70	54.8	0.28	0.099
903 - 313	5.2	1.48	0.09	1.9	0.57	0.65	47.3	0.26	0.112
903 - 314	6.2	1.58	0.09	1.7	0.52	0.70	46.6	0.25	0.088
903 - 315	6.4	1.21	0.07	1.8	0.49	0.59	44.9	0.20	0.074
903 - 316	5.4	0.94	0.06	1.7	0.44	0.63	47.2	0.24	0.073
903 - 317	5.1	1.03	0.11	2.2	0.56	0.74	47.9	0.31	0.058
903 - 318	4.2	1.09	0.10	2.0	0.67	0.72	49.1	0.26	0.051
903 - 319	3.0	1.07	0.09	1.3	0.71	0.70	51.7	0.23	0.050
903 - 320	4.1	1.08	0.11	1.8	0.68	0.70	49.8	0.21	0.050
903 - 322	2.6	1.70	0.11	1.3	0.85	0.81	53.1	0.27	0.044
903 - 323	2.9	1.20	0.08	1.0	0.60	0.58	53.8	0.19	0.057
903 - 324	20.7	0.36	0.03	16.4	0.59	0.06	11.5	0.03	0.046
903 - 325	20.3	0.23	0.02	18.5	0.49	0.05	8.5	0.02	0.037
903 - 326a	19.5	0.23	n.d.	29.1	0.14	0.02	3.0	0.01	0.042
903 - 326b	14.4	0.69	n.d.	29.0	0.24	0.06	9.8	0.01	0.067
903 - 326c	15.2	0.22	n.d.	37.5	0.10	0.02	3.4	0.01	0.041
903 - 327	22.6	0.95	0.03	11.8	0.40	0.11	15.0	0.02	0.033
903 - 328	1.8	0.81	0.04	0.8	0.70	0.42	55.6	0.11	0.095
903 - 329	1.7	0.47	0.03	0.7	0.67	0.31	55.8	0.08	0.097
903 - 330	2.1	1.02	0.20	1.1	2.99	0.04	54.9	0.23	0.171
903 - 331	2.5	0.73	0.13	2.0	2.72	0.03	53.7	0.22	0.064
903 - 332	2.0	0.63	0.15	2.2	3.06	0.04	54.6	0.24	0.106
903 - 333	2.3	1.24	0.20	1.7	2.94	0.05	54.0	0.18	0.144
903 - 334	3.2	0.21	0.03	1.2	1.26	0.09	49.4	0.10	0.058
903 - 335	1.8	0.23	0.03	1.0	0.91	0.11	54.7	0.11	0.062
903 - 336	1.4	n.d.	n.d.	56.0	0.02	0.03	0.3	0.01	0.269
903 - 337	23.9	n.d.	n.d.	0.9	0.14	0.02	0.2	0.01	0.006
903 - 338	19.4	n.d.	n.d.	18.5	0.10	0.02	0.2	0.01	0.026
903 - 339	2.4	0.48	0.13	3.6	2.28	0.04	45.3	0.17	0.148
903 - 340a	2.5	0.65	0.05	1.0	1.64	0.01	30.7	0.11	0.090
903 - 340b	2.6	0.84	0.02	1.1	1.50	0.02	29.5	0.11	0.071
903 - 341a	1.7	0.33	0.06	1.2	4.03	0.02	55.9	0.13	0.071
903 - 342a	5.8	3.16	0.03	1.4	2.21	0.03	48.5	0.24	0.055
903 - 343	2.5	0.40	0.19	1.6	3.07	0.01	37.7	0.12	0.316
903 - 344	5.5	0.49	0.04	6.7	0.82	0.03	35.3	0.04	0.545
903 - A	1.8	0.60	0.12	12.9	3.04	0.04	44.5	0.12	0.197
903 - B	7.2	0.01	0.09	2.8	2.03	0.18	33.4	0.63	0.015
903 - B I.a	29.1	0.01	0.01	1.0	0.12	0.01	0.1	0.01	0.003
903 - B I.b	28.6	0.01	0.01	1.0	0.15	0.01	0.1	0.01	0.005

No.	Al2O3	BaO	CaO	Fe	K2O	MgO	Mn	Na2O	P
903 - B I.c	28.6	n.d.	n.d.	0.8	0.14	0.01	0.2	0.01	0.006
903 - B I.d1	28.5	n.d.	n.d.	0.8	0.12	0.01	0.2	0.01	0.006
903 - B I.d2	28.5	n.d.	n.d.	0.8	0.12	0.01	0.2	0.01	0.003
903 - B I.d3	29.3	n.d.	n.d.	0.8	0.12	0.01	0.1	0.01	0.009
903 - B I.d4	29.0	n.d.	n.d.	0.8	0.12	0.02	0.2	0.01	0.008
903 - B I.e	27.9	n.d.	0.01	0.8	0.13	0.01	0.1	0.03	0.006
903 - B II.a	4.2	5.10	0.05	0.6	0.93	0.34	52.0	0.19	0.036
903 - B II.b	4.2	5.20	0.05	0.6	0.97	0.34	52.7	0.19	0.039
903 - B II.c	4.0	5.06	0.04	0.6	0.94	0.33	52.4	0.27	0.039
903 - B II.d1	4.1	5.08	0.03	0.6	0.91	0.36	52.3	0.20	0.039
903 - B II.d2	4.2	5.10	0.03	0.6	0.92	0.36	52.5	0.20	0.037
903 - B II.d3	3.9	5.11	0.03	0.6	0.92	0.35	52.7	0.20	0.040
903 - B II.d4	4.0	5.06	0.03	0.6	0.92	0.35	52.4	0.20	0.032
903 - B II.e	3.9	5.05	0.05	0.6	0.94	0.33	52.9	0.27	0.041
903 - B III.	4.0	2.18	0.06	1.0	0.70	0.65	49.4	0.17	0.067
903 - B V.	5.2	4.54	0.05	1.1	0.25	0.39	49.7	0.05	0.064
903 - Mn 2	3.5	2.13	0.06	2.8	0.99	0.32	51.4	0.16	0.059

No.	SiO2	SrO	TiO2	LOI 105-800°	LOI 800-1000°	LOI 1000-1200°
903 - 3	6.8	0.02	0.26	10.3	n.d.	n.d.
903 - 4	2.1	0.04	0.10	9.9	2.70	n.d.
903 - 5a	15.9	0.11	0.56	11.1	n.d.	n.d.
903 - 5b	51.3	0.01	1.71	11.9	n.d.	n.d.
903 - 6	1.5	0.17	0.09	10.5	n.d.	n.d.
903 - 7	2.3	0.13	0.12	10.3	n.d.	n.d.
903 - 8	1.9	0.19	0.10	10.6	n.d.	n.d.
903 - 9	3.0	0.11	0.12	9.9	n.d.	n.d.
903 - 10	4.7	0.35	0.15	12.7	n.d.	n.d.
903 - 11	5.2	0.32	0.16	13.2	n.d.	n.d.
903 - 12	5.5	0.31	0.17	13.2	n.d.	n.d.
903 - 13	4.7	0.37	0.12	11.8	n.d.	n.d.
903 - 14	5.9	0.37	0.17	13.3	n.d.	n.d.
903 - 15	9.1	0.23	0.28	11.6	n.d.	n.d.
903 - 16	3.2	0.25	0.15	10.7	n.d.	n.d.
903 - 17	4.2	0.35	0.11	11.1	n.d.	n.d.
903 - 18	8.1	0.18	0.28	11.2	n.d.	n.d.
903 - 19	7.5	0.23	0.24	11.8	n.d.	n.d.
903 - 20	67.2	0.01	1.02	7.1	n.d.	n.d.
903 - 21	38.8	0.01	0.93	10.0	n.d.	n.d.
903 - 22	9.8	0.19	0.30	11.2	n.d.	n.d.
903 - 23	5.8	0.22	0.16	12.0	n.d.	n.d.
903 - 24	42.1	0.01	0.91	10.2	n.d.	n.d.
903 - 25	37.6	0.03	0.68	8.9	n.d.	n.d.
903 - 26	95.4	0.01	0.09	0.5	n.d.	n.d.
903 - 27	29.6	0.01	0.92	9.6	n.d.	n.d.
903 - 28a	42.7	0.01	1.16	9.7	0.30	n.d.
903 - 28b	40.0	0.01	1.22	9.1	n.d.	n.d.
903 - 29	47.9	0.01	1.17	8.9	n.d.	n.d.
903 - 30	55.0	0.01	0.81	7.8	n.d.	n.d.
903 - 31a	76.7	0.01	0.54	4.7	0.30	n.d.
903 - 31b	82.6	0.01	0.41	2.5	n.d.	n.d.
903 - 32	90.6	0.01	0.35	3.2	n.d.	n.d.
903 - 33	3.9	0.73	0.13	13.5	1.80	n.d.
903 - 34	2.7	0.79	0.11	13.3	n.d.	n.d.
903 - 35	3.9	0.43	0.15	12.0	n.d.	n.d.
903 - 36	2.7	0.67	0.12	13.0	n.d.	n.d.
903 - 37	3.6	0.88	0.15	14.0	n.d.	n.d.
903 - 38	6.9	0.77	0.23	13.9	n.d.	n.d.
903 - 39	5.2	0.81	0.19	14.1	n.d.	n.d.
903 - 40	4.5	0.85	0.17	14.3	n.d.	n.d.
903 - 41	3.3	0.32	0.10	12.0	1.20	n.d.
903 - 42	14.6	0.55	0.42	13.8	n.d.	n.d.
903 - 43	23.7	0.36	0.64	13.4	n.d.	n.d.
903 - 44	12.5	0.58	0.30	13.0	n.d.	n.d.
903 - 45	17.9	0.46	0.56	13.2	n.d.	n.d.
903 - 46	5.4	0.78	0.17	13.2	n.d.	n.d.
903 - 47	5.3	0.40	0.13	12.0	n.d.	n.d.
903 - 48	12.7	0.40	0.14	11.3	n.d.	n.d.
903 - 49	21.8	0.30	0.57	12.2	n.d.	n.d.
903 - 50	4.8	0.44	0.16	11.8	n.d.	n.d.
903 - 51	3.5	0.46	0.14	11.9	n.d.	n.d.
903 - 52	29.5	0.11	0.81	11.7	n.d.	n.d.
903 - 53	42.3	0.01	1.39	10.7	n.d.	n.d.
903 - 54	17.4	0.17	0.53	11.1	n.d.	n.d.
903 - 55	4.0	0.29	0.15	10.4	n.d.	n.d.
903 - 56	4.9	0.54	0.19	11.7	n.d.	n.d.
903 - 57	43.3	0.03	1.06	11.0	n.d.	n.d.
903 - 58	6.3	0.19	0.20	10.7	n.d.	n.d.
903 - 59	6.9	0.37	0.25	10.4	n.d.	n.d.
903 - 60	12.7	0.09	0.37	10.7	n.d.	n.d.
903 - 61	2.8	0.32	0.13	10.7	n.d.	n.d.
903 - 62	5.2	0.10	0.18	10.0	n.d.	n.d.
903 - 63	4.4	0.03	0.23	10.2	n.d.	n.d.
903 - 64	28.3	0.01	0.85	11.5	n.d.	n.d.
903 - 65a	26.9	0.02	0.81	11.0	0.70	n.d.
903 - 65b	3.4	0.13	0.26	9.6	n.d.	n.d.
903 - 66	24.6	0.03	0.78	11.9	n.d.	n.d.
903 - 67	50.9	0.03	0.65	8.3	n.d.	n.d.

No.	SiO2	SrO	TiO2	LOI 105-800°	LOI 800-1000°	LOI 1000-1200°
903 - 68a	26.2	0.24	0.18	8.9	n.d.	n.d.
903 - 68b	11.1	0.27	0.18	11.5	n.d.	n.d.
903 - 69	9.7	0.26	0.21	11.8	n.d.	n.d.
903 - 70	10.8	0.24	0.23	11.8	n.d.	n.d.
903 - 71	5.4	0.21	0.16	11.8	n.d.	n.d.
903 - 72	5.9	0.23	0.19	12.2	n.d.	n.d.
903 - 73	8.2	0.19	0.21	12.1	n.d.	n.d.
903 - 74	14.4	0.20	0.34	12.8	n.d.	n.d.
903 - 75	9.3	0.26	0.29	12.9	n.d.	n.d.
903 - 76	9.7	0.26	0.30	13.0	n.d.	n.d.
903 - 77a	4.4	0.30	0.19	12.7	n.d.	n.d.
903 - 77b	4.6	0.25	0.10	11.4	n.d.	n.d.
903 - 78	3.8	0.28	0.15	11.9	n.d.	n.d.
903 - 79	63.0	n.d.	0.75	6.8	n.d.	n.d.
903 - 80	7.0	0.17	0.14	9.7	n.d.	n.d.
903 - 81	12.6	0.30	0.15	9.9	n.d.	n.d.
903 - 82	16.9	0.37	0.19	10.2	n.d.	n.d.
903 - 83	10.9	0.24	0.15	10.2	n.d.	n.d.
903 - 84	29.1	0.27	0.17	8.8	n.d.	n.d.
903 - 85	2.7	0.26	0.10	10.5	n.d.	n.d.
903 - 86	14.1	0.21	0.21	10.4	n.d.	n.d.
903 - 87	30.0	0.11	0.52	10.0	n.d.	n.d.
903 - 88	12.2	0.36	0.24	11.6	n.d.	n.d.
903 - 89	13.3	0.45	0.30	11.5	n.d.	n.d.
903 - 90	30.2	0.01	0.83	12.3	n.d.	n.d.
903 - 91	11.9	0.46	0.23	11.9	n.d.	n.d.
903 - 92	8.8	0.54	0.23	12.9	n.d.	n.d.
903 - 93	6.9	0.56	0.23	12.5	n.d.	n.d.
903 - 94	5.7	0.56	0.21	13.2	n.d.	n.d.
903 - 95	4.1	0.70	0.19	13.4	n.d.	n.d.
903 - 96	2.5	0.82	0.16	13.6	14.80	15.8
903 - 97	3.2	0.79	0.17	13.1	n.d.	n.d.
903 - 98	2.2	0.62	0.13	12.3	13.60	14.9
903 - 99	4.7	0.87	0.20	13.3	n.d.	n.d.
903 - 100	3.9	1.02	0.19	14.1	n.d.	n.d.
903 - 101	2.0	1.07	0.13	13.5	n.d.	n.d.
903 - 102	3.5	0.62	0.12	11.5	n.d.	n.d.
903 - 103	1.9	0.22	0.10	10.6	n.d.	n.d.
903 - 104	13.1	0.20	0.23	10.1	n.d.	n.d.
903 - 105	3.1	0.22	0.12	10.1	n.d.	n.d.
903 - 106	2.8	0.45	0.12	11.5	n.d.	n.d.
903 - 107	4.4	0.53	0.16	12.2	n.d.	n.d.
903 - 108	6.8	0.68	0.18	12.0	n.d.	n.d.
903 - 109	4.2	0.34	0.16	11.2	n.d.	n.d.
903 - 110	22.4	0.12	0.50	10.7	n.d.	n.d.
903 - 111	3.0	0.16	0.11	12.8	n.d.	n.d.
903 - 112	14.0	0.14	0.36	10.5	n.d.	n.d.
903 - 113	17.2	0.02	0.52	11.6	n.d.	n.d.
903 - 114	77.7	0.01	0.33	3.4	n.d.	n.d.
903 - 115a	78.7	n.d.	0.45	3.7	n.d.	n.d.
903 - 115b	63.3	n.d.	0.30	5.0	n.d.	n.d.
903 - 116a	39.4	0.03	0.24	6.5	n.d.	n.d.
903 - 116b	28.5	0.04	0.17	7.9	n.d.	n.d.
903 - 117b	6.3	0.03	0.23	9.1	n.d.	n.d.
903 - 118a	6.9	0.04	0.13	10.7	n.d.	n.d.
903 - 118b	65.2	n.d.	0.68	6.8	n.d.	n.d.
903 - 119	14.2	0.05	0.23	9.4	n.d.	n.d.
903 - 120	19.7	0.02	0.29	9.8	11.60	13.3
903 - 121	9.3	0.02	0.28	10.1	n.d.	n.d.
903 - 122	19.6	0.03	0.34	9.8	n.d.	n.d.
903 - 123	10.7	0.03	0.13	10.3	n.d.	n.d.
903 - 124	28.3	0.05	1.12	12.8	n.d.	n.d.
903 - 125	32.2	0.03	1.26	12.6	n.d.	n.d.
903 - 126	33.9	0.03	1.29	12.4	n.d.	n.d.
903 - 127	32.4	0.01	1.19	11.6	n.d.	n.d.
903 - 128	35.8	0.01	1.33	11.4	n.d.	n.d.
903 - 129	38.8	0.01	1.56	11.2	n.d.	n.d.
903 - 130	30.7	0.03	1.34	12.5	n.d.	n.d.
903 - 131	34.3	0.03	1.47	11.9	n.d.	n.d.

No.	SiO2	SrO	TiO2	LOI 105-800°	LOI 800-1000°	LOI 1000-1200°
903 - 132	38.3	0.01	1.30	10.7	n.d.	n.d.
903 - 133	41.2	n.d.	1.49	11.8	12.70	13.1
903 - 134	44.1	0.01	1.35	9.6	n.d.	n.d.
903 - 135	35.8	0.02	1.47	10.9	n.d.	n.d.
903 - 136	41.6	0.01	1.32	9.8	n.d.	n.d.
903 - 137	40.5	0.02	1.27	10.0	n.d.	n.d.
903 - 138	35.4	0.02	1.23	10.9	n.d.	n.d.
903 - 139	38.2	0.01	1.15	10.2	n.d.	n.d.
903 - 140	66.3	0.01	0.96	7.1	n.d.	n.d.
903 - 141a	49.3	n.d.	1.60	12.2	12.20	12.5
903 - 141b	45.5	n.d.	1.21	12.1	n.d.	n.d.
903 - 141c	48.3	n.d.	1.04	11.7	n.d.	n.d.
903 - 141 B	52.6	0.01	1.79	11.7	n.d.	n.d.
903 - 142	5.9	0.04	0.29	11.7	n.d.	n.d.
903 - 143	5.9	0.03	0.18	11.6	n.d.	n.d.
903 - 144	3.3	0.04	0.11	11.0	n.d.	n.d.
903 - 145	5.5	0.02	0.13	10.4	n.d.	n.d.
903 - 146	5.0	0.03	0.16	11.3	n.d.	n.d.
903 - 147	5.0	0.02	0.16	10.7	n.d.	n.d.
903 - 148	3.9	0.09	0.14	11.3	n.d.	n.d.
903 - 149	10.6	0.03	0.36	11.0	n.d.	n.d.
903 - 150	2.6	0.02	0.11	10.1	n.d.	n.d.
903 - 151	8.3	0.04	0.29	11.0	n.d.	n.d.
903 - 152a	9.8	0.05	0.37	11.1	n.d.	n.d.
903 - 152b	5.3	0.03	0.21	11.5	n.d.	n.d.
903 - 153	6.8	0.05	0.30	11.2	n.d.	n.d.
903 - 154	9.0	0.03	0.38	11.2	n.d.	n.d.
903 - 155	32.5	0.36	0.10	8.0	n.d.	n.d.
903 - 156	58.3	0.03	0.37	5.2	n.d.	n.d.
903 - 157	39.0	0.03	0.08	6.9	7.20	7.7
903 - 158	49.8	0.03	0.27	6.4	n.d.	n.d.
903 - 159	48.7	0.07	0.13	6.2	n.d.	n.d.
903 - 160	18.0	0.03	0.06	8.3	n.d.	n.d.
903 - 161	36.5	0.05	0.13	6.8	8.00	10.2
903 - 162	47.3	0.14	0.14	5.3	n.d.	n.d.
903 - 164	25.0	0.28	0.32	8.3	n.d.	n.d.
903 - 168 B	7.5	0.04	0.23	10.2	n.d.	n.d.
903 - 169 B	5.8	0.03	0.23	10.4	n.d.	n.d.
903 - 170a	98.3	0.01	0.05	0.3	n.d.	n.d.
903 - 170b	85.6	0.01	0.14	1.2	n.d.	n.d.
903 - 171a	89.6	0.01	0.06	0.4	n.d.	n.d.
903 - 171b	99.4	0.01	0.06	0.4	n.d.	n.d.
903 - 172	96.5	0.01	0.05	0.4	n.d.	n.d.
903 - 173	98.5	0.01	0.05	0.3	n.d.	n.d.
903 - 174	94.7	0.01	0.06	0.6	n.d.	n.d.
903 - 175	96.5	0.01	0.04	0.5	0.05	n.d.
903 - 176	97.9	0.01	0.05	0.5	n.d.	n.d.
903 - 177	87.4	0.01	0.14	1.4	n.d.	n.d.
903 - 178	59.4	0.04	0.11	4.5	n.d.	n.d.
903 - 179	11.5	0.01	0.39	11.1	n.d.	n.d.
903 - 180	4.4	0.01	0.35	11.5	1.00	n.d.
903 - 181	4.5	0.03	0.33	11.6	n.d.	n.d.
903 - 182	5.1	0.03	0.20	10.1	n.d.	n.d.
903 - 183	4.6	0.03	0.20	10.2	n.d.	n.d.
903 - 184	4.3	0.02	0.19	10.0	n.d.	n.d.
903 - 185	4.9	0.01	0.36	10.8	n.d.	n.d.
903 - 186	3.9	0.01	0.23	10.3	n.d.	n.d.
903 - 187	12.1	0.01	0.62	10.8	n.d.	n.d.
903 - 188	9.8	0.11	0.46	11.9	n.d.	n.d.
903 - 189	40.6	0.01	0.84	8.8	n.d.	n.d.
903 - 190	14.4	0.26	0.43	14.7	n.d.	n.d.
903 - 191 B	2.3	0.77	0.11	12.2	n.d.	n.d.
903 - 200	49.2	0.01	1.55	9.6	n.d.	n.d.
903 - 201	48.3	0.01	1.57	9.9	n.d.	n.d.
903 - 202	46.0	0.01	1.47	9.6	n.d.	n.d.
903 - 203	45.3	0.01	1.54	9.8	n.d.	n.d.
903 - 204	43.0	0.01	1.57	10.3	n.d.	n.d.
903 - 205	40.5	0.02	1.62	10.8	n.d.	n.d.
903 - 206	38.5	0.01	1.57	11.4	n.d.	n.d.

No.	SiO2	SrO	TiO2	LOI 105-800°	LOI 800-1000°	LOI 1000-1200°
903 - 207	33.1	0.03	1.44	11.9	n.d.	n.d.
903 - 208	34.0	0.02	1.39	12.1	n.d.	n.d.
903 - 209	10.1	0.02	0.36	10.2	n.d.	n.d.
903 - 210	38.1	n.d.	1.17	10.2	n.d.	n.d.
903 - 211	48.5	0.01	1.06	9.4	n.d.	n.d.
903 - 212	13.3	0.04	0.40	10.9	n.d.	n.d.
903 - 213	1.7	0.04	0.07	10.1	n.d.	n.d.
903 - 215	60.4	n.d.	0.74	6.5	n.d.	n.d.
903 - 216	3.0	0.02	0.10	10.3	n.d.	n.d.
903 - 217	58.8	n.d.	0.95	7.7	n.d.	n.d.
903 - 218	8.0	0.04	0.29	11.4	n.d.	n.d.
903 - 219	6.4	0.03	0.26	10.4	n.d.	n.d.
903 - 220	7.7	0.04	0.25	11.3	n.d.	n.d.
903 - 221	36.5	n.d.	1.15	9.5	n.d.	n.d.
903 - 222	44.5	n.d.	1.07	8.8	n.d.	n.d.
903 - 223	1.4	0.21	0.09	10.3	n.d.	n.d.
903 - 224	1.8	0.17	0.09	10.4	n.d.	n.d.
903 - 225	3.1	0.32	0.11	12.2	n.d.	n.d.
903 - 226	7.1	0.33	0.21	13.8	n.d.	n.d.
903 - 227	5.8	0.12	0.24	11.0	n.d.	n.d.
903 - 228	7.5	0.04	0.32	10.5	n.d.	n.d.
903 - 229	53.8	n.d.	0.70	7.8	n.d.	n.d.
903 - 230	53.4	0.01	0.77	8.2	n.d.	n.d.
903 - 232	11.6	0.14	0.53	11.9	n.d.	n.d.
903 - 233	14.4	0.09	0.67	12.5	n.d.	n.d.
903 - 234	6.1	n.d.	0.34	11.2	n.d.	n.d.
903 - 235	6.1	n.d.	0.41	11.5	n.d.	n.d.
903 - 237	54.4	0.04	0.10	4.7	n.d.	n.d.
903 - 239	35.6	0.10	0.22	7.2	n.d.	n.d.
903 - 241	2.1	0.06	0.12	10.1	n.d.	n.d.
903 - 245	1.9	n.d.	0.18	10.2	n.d.	n.d.
903 - 246	1.3	0.01	0.13	10.7	11.20	11.5
903 - 249	6.9	0.07	0.31	10.6	n.d.	n.d.
903 - 250	3.7	0.13	0.13	10.2	n.d.	n.d.
903 - 251	7.6	0.18	0.11	10.4	n.d.	n.d.
903 - 252	7.9	0.07	0.34	11.4	n.d.	n.d.
903 - 253	8.1	0.14	0.17	9.7	n.d.	n.d.
903 - 254	48.9	0.14	0.09	5.4	n.d.	n.d.
903 - 255	5.0	0.26	0.17	9.8	n.d.	n.d.
903 - 256	4.8	0.23	0.10	10.5	n.d.	n.d.
903 - 259	6.9	0.04	0.08	9.5	n.d.	n.d.
903 - 260	5.9	0.07	0.08	9.1	n.d.	n.d.
903 - 261	4.2	0.01	0.28	10.7	n.d.	n.d.
903 - 262	7.4	0.01	0.35	10.8	n.d.	n.d.
903 - 263	3.0	0.24	0.17	11.5	13.70	14.5
903 - 264	5.2	0.26	0.28	12.0	n.d.	n.d.
903 - 265	0.9	0.02	0.04	9.7	n.d.	n.d.
903 - 266	1.6	0.05	0.07	9.4	n.d.	n.d.
903 - 268	4.1	0.16	0.19	8.3	n.d.	n.d.
903 - 269	2.9	0.53	0.19	9.6	n.d.	n.d.
903 - 270	2.9	0.03	0.19	9.7	n.d.	n.d.
903 - 271	3.4	0.18	0.23	9.3	n.d.	n.d.
903 - 272	1.2	0.37	0.09	9.3	n.d.	n.d.
903 - 273	1.2	0.40	0.12	9.8	n.d.	n.d.
903 - 274	12.7	0.02	0.43	11.1	n.d.	n.d.
903 - 275	11.0	0.02	0.37	11.1	12.30	14.6
903 - 276	7.3	0.01	0.27	12.1	n.d.	n.d.
903 - 277	34.1	n.d.	0.26	8.5	n.d.	n.d.
903 - 278	52.7	0.03	0.15	5.4	6.20	6.8
903 - 279	46.9	0.16	0.09	6.1	n.d.	n.d.
903 - 280	2.1	0.09	0.11	10.9	n.d.	n.d.
903 - 281	4.8	0.05	0.20	7.9	n.d.	n.d.
903 - 282	1.9	0.17	0.14	8.8	n.d.	n.d.
903 - 283a	1.8	0.08	0.13	6.3	n.d.	n.d.
903 - 283b	5.2	0.06	0.19	8.0	11.80	12.2
903 - 283c	1.9	0.06	0.19	7.7	n.d.	n.d.
903 - 283d	2.3	0.08	0.19	7.6	n.d.	n.d.
903 - 283e	1.7	0.06	0.20	7.3	n.d.	n.d.
903 - 284	2.2	0.02	0.21	8.2	n.d.	n.d.

No.	SiO2	SrO	TiO2	LOI 105-800°	LOI 800-1000°	LOI 1000-1200°
903 - 285	1.7	0.06	0.20	8.3	n.d.	n.d.
903 - 286	2.1	0.01	0.20	8.3	n.d.	n.d.
903 - 287	1.8	0.01	0.20	8.7	n.d.	n.d.
903 - 290	2.1	0.11	0.16	9.9	n.d.	n.d.
903 - 291	2.6	0.02	0.19	10.4	n.d.	n.d.
903 - 292	4.7	0.01	0.22	10.5	n.d.	n.d.
903 - 293	3.5	n.d.	0.19	10.5	n.d.	n.d.
903 - 294	4.1	0.02	0.25	10.6	n.d.	n.d.
903 - 295	8.0	n.d.	0.09	10.1	n.d.	n.d.
903 - 296	9.1	0.01	0.27	11.0	n.d.	n.d.
903 - 297	8.6	0.02	0.26	10.3	12.00	13.6
903 - 298	5.0	0.02	0.16	7.7	n.d.	.
903 - 299	3.0	0.02	0.20	7.6	n.d.	n.d.
903 - 300	3.4	0.01	0.13	10.2	n.d.	n.d.
903 - 301	2.9	n.d.	0.17	10.3	n.d.	n.d.
903 - 302	3.2	0.01	0.20	10.5	n.d.	n.d.
903 - 303	11.8	0.38	0.16	11.0	n.d.	n.d.
903 - 304	29.9	0.28	0.17	8.7	n.d.	n.d.
903 - 305	17.0	0.28	0.18	11.0	n.d.	n.d.
903 - 306	14.7	0.26	0.34	11.6	n.d.	n.d.
903 - 307	6.6	0.26	0.18	12.7	n.d.	n.d.
903 - 308	4.6	0.24	0.15	12.2	n.d.	n.d.
903 - 309	8.5	0.24	0.27	12.3	n.d.	n.d.
903 - 310	10.7	0.27	0.36	13.1	n.d.	n.d.
903 - 311	7.6	0.29	0.20	12.4	n.d.	n.d.
903 - 312a	5.6	0.34	0.17	12.1	n.d.	n.d.
903 - 312b1	2.1	0.17	0.08	12.2	n.d.	n.d.
903 - 312b2	2.2	0.28	0.07	12.8	n.d.	n.d.
903 - 312b3	3.8	0.22	0.11	12.3	n.d.	n.d.
903 - 312b4	2.1	0.26	0.08	12.4	14.70	15.1
903 - 315b5	2.7	0.19	0.10	12.4	n.d.	n.d.
903 - 313	8.4	0.42	0.27	12.2	n.d.	n.d.
903 - 314	9.2	0.40	0.28	12.8	n.d.	n.d.
903 - 315	11.8	0.37	0.24	12.6	n.d.	n.d.
903 - 316	10.1	0.31	0.24	11.6	n.d.	n.d.
903 - 317	8.5	0.45	0.24	12.3	n.d.	n.d.
903 - 318	6.7	0.62	0.22	11.7	n.d.	n.d.
903 - 319	4.9	0.54	0.15	12.6	n.d.	n.d.
903 - 320	7.0	0.52	0.18	12.3	n.d.	n.d.
903 - 322	3.2	0.72	0.12	12.2	14.20	14.9
903 - 323	3.6	0.50	0.13	12.1	n.d.	n.d.
903 - 324	26.2	0.03	0.92	13.0	n.d.	n.d.
903 - 325	27.1	0.02	0.89	11.0	n.d.	n.d.
903 - 326a	23.2	0.01	1.00	9.8	n.d.	n.d.
903 - 326b	15.7	0.01	0.66	12.4	13.10	13.6
903 - 326c	16.7	n.d.	0.72	8.0	n.d.	n.d.
903 - 327	23.7	0.03	0.97	12.7	n.d.	n.d.
903 - 328	3.8	0.13	0.11	10.7	n.d.	n.d.
903 - 329	4.3	0.10	0.08	10.3	n.d.	n.d.
903 - 330	1.2	0.07	0.13	9.3	n.d.	n.d.
903 - 331	2.4	0.05	0.16	8.9	n.d.	n.d.
903 - 332	1.6	0.06	0.10	8.6	n.d.	n.d.
903 - 333	1.8	0.10	0.16	9.3	n.d.	n.d.
903 - 334	13.6	0.03	0.13	8.8	n.d.	n.d.
903 - 335	7.7	0.03	0.09	9.2	n.d.	n.d.
903 - 336	7.7	n.d.	0.04	10.0	n.d.	n.d.
903 - 337	63.5	n.d.	1.20	8.5	n.d.	n.d.
903 - 338	42.6	n.d.	0.93	9.0	n.d.	n.d.
903 - 339	14.7	0.13	0.10	8.9	n.d.	n.d.
903 - 340a	42.9	0.08	0.09	6.4	n.d.	n.d.
903 - 340b	44.7	0.05	0.09	5.9	n.d.	n.d.
903 - 341a	1.1	0.02	0.09	7.1	n.d.	n.d.
903 - 342a	6.5	0.03	0.18	9.4	n.d.	n.d.
903 - 343	28.8	0.05	0.11	7.7	n.d.	n.d.
903 - 344	19.7	0.03	0.26	12.3	13.00	14.8
903 - A	2.0	0.03	0.10	9.0	n.d.	n.d.
903 - B	27.2	0.07	0.78	10.3	n.d.	n.d.
903 - B I.a	56.1	0.01	1.52	11.0	n.d.	n.d.
903 - B I.b	54.8	0.01	1.49	10.7	n.d.	n.d.

No.	SiO2	SrO	TiO2	LOI 105-800°	LOI 800-1000°	LOI 1000-1200°
903 - B I.c	55.7	n.d.	1.50	10.9	11.00	11.0
903 - B I.d1	56.9	n.d.	1.49	10.3	n.d.	n.d.
903 - B I.d2	55.8	n.d.	1.47	10.4	n.d.	n.d.
903 - B I.d3	55.8	n.d.	1.53	10.8	n.d.	n.d.
903 - B I.d4	55.5	n.d.	1.50	10.6	10.70	10.8
903 - B I.e	57.1	0.01	1.46	11.5	n.d.	n.d.
903 - B II.a	2.3	0.14	0.10	11.0	n.d.	n.d.
903 - B II.b	2.2	0.14	0.10	11.0	n.d.	n.d.
903 - B II.c	2.2	0.14	0.10	10.7	n.d.	n.d.
903 - B II.d1	2.2	0.14	0.10	10.5	n.d.	n.d.
903 - B II.d2	2.2	0.14	0.10	10.5	n.d.	n.d.
903 - B II.d3	2.2	0.14	0.10	10.5	n.d.	n.d.
903 - B II.d4	2.1	0.14	0.10	10.4	n.d.	n.d.
903 - B II.e	2.0	0.13	0.10	10.9	n.d.	n.d.
903 - B III.	6.4	0.25	0.16	12.3	n.d.	n.d.
903 - B V.	4.8	0.15	0.18	10.8	n.d.	n.d.
903 - Mn 2	3.3	0.2	0.13	11.3	n.d.	n.d.

Table IV.2: ICP trace element analyses of ores and rocks.

No.	B	Ce	Co	Cr	Cu	Eu	Gd	La
903 - 3	46.67	35.96	36.91	15.40	45.55	2.21	13.46	45.14
903 - 4	55.34	40.88	64.85	14.72	49.87	3.29	15.72	52.60
903 - 5a	17.99	58.58	26.49	16.83	43.19	1.96	12.46	30.19
903 - 5b	1.41	38.29	19.14	23.50	20.35	0.44	0.48	14.29
903 - 6	20.41	12.84	76.62	13.90	60.06	2.00	14.08	60.31
903 - 7	18.77	111.72	69.23	14.48	75.42	2.87	12.94	47.25
903 - 8	18.81	24.17	70.06	14.31	69.51	2.49	14.29	53.97
903 - 9	19.20	131.96	33.26	14.91	54.46	3.51	16.07	46.84
903 - 10	18.42	59.57	91.66	13.51	88.13	3.65	18.71	70.73
903 - 11	18.80	46.28	68.26	13.73	62.70	3.90	17.95	61.39
903 - 12	16.96	51.18	65.80	13.76	62.31	3.81	17.66	58.86
903 - 13	18.99	11.93	35.78	13.48	75.11	4.09	18.89	79.41
903 - 14	15.81	94.18	82.80	13.42	76.87	4.99	21.25	65.89
903 - 15	14.15	123.37	77.59	18.06	67.16	3.03	21.71	45.74
903 - 16	17.71	73.32	109.89	13.66	141.97	3.46	15.98	50.28
903 - 17	18.12	25.03	150.21	13.41	108.69	4.53	23.41	69.68
903 - 18	15.96	117.36	91.30	15.77	125.32	4.46	21.37	58.62
903 - 19	15.52	82.48	103.44	16.87	117.91	4.07	23.40	55.72
903 - 20	6.97	34.27	13.50	56.83	18.24	0.00	0.00	8.57
903 - 21	2.61	66.57	17.72	32.16	29.72	0.00	29.88	16.48
903 - 22	9.21	114.00	61.00	27.88	39.22	1.77	6.87	40.66
903 - 23	10.33	56.40	84.75	13.40	49.71	2.65	10.30	56.70
903 - 24	2.24	64.01	17.43	29.82	29.71	0.00	24.81	15.33
903 - 25	1.70	56.77	28.80	47.20	43.50	0.00	44.80	17.19
903 - 26	0.00	18.71	191.36	14.41	11.63	0.13	0.00	5.73
903 - 27	1.26	45.35	18.77	105.67	33.37	0.00	61.51	13.01
903 - 28a	6.93	79.04	14.67	63.23	26.00	0.00	33.84	11.41
903 - 28b	6.34	34.94	15.36	65.51	27.01	0.00	36.15	11.91
903 - 29	2.28	238.68	38.86	39.71	37.29	0.29	35.99	19.28
903 - 30	2.13	203.88	45.12	44.45	47.44	0.23	29.53	15.52
903 - 31a	1.84	87.17	25.67	28.18	25.11	0.36	13.10	12.06
903 - 31b	0.98	27.53	18.34	17.82	16.23	0.39	0.82	9.28
903 - 32	0.84	33.35	8.71	18.74	23.75	0.36	1.59	8.81
903 - 33	20.02	28.38	64.00	13.54	155.38	2.87	22.94	42.96
903 - 34	14.62	33.32	80.46	13.09	163.49	3.06	24.15	47.94
903 - 35	17.24	20.27	46.24	14.32	169.75	3.10	19.88	38.06
903 - 36	14.89	34.77	80.35	14.51	181.68	3.39	23.18	40.79
903 - 37	12.47	53.19	105.19	13.93	173.86	3.65	26.84	44.64
903 - 38	11.73	54.68	82.37	15.60	163.93	3.45	26.44	40.41
903 - 39	12.61	56.42	97.35	14.46	161.03	3.90	27.46	42.21
903 - 40	11.60	60.18	102.98	13.90	158.91	3.99	28.50	42.28
903 - 41	20.89	31.91	35.88	14.63	157.35	3.78	22.57	37.91
903 - 42	9.22	72.76	62.52	15.47	134.14	2.95	24.42	35.56
903 - 43	8.00	90.34	49.11	15.81	93.25	2.23	24.29	32.94
903 - 44	11.47	105.61	72.90	13.95	151.71	3.92	26.92	49.86
903 - 45	13.77	79.19	128.00	15.53	124.59	3.02	26.17	37.37
903 - 46	21.13	74.61	116.40	13.56	187.00	5.22	34.79	53.93
903 - 47	19.58	54.65	84.29	14.33	153.97	5.49	32.33	49.78
903 - 48	15.16	67.60	73.30	13.74	140.56	5.20	30.88	43.18
903 - 49	9.39	72.95	41.39	15.49	127.52	3.37	25.55	41.11
903 - 50	17.12	38.90	83.80	14.56	181.99	5.95	32.59	46.60
903 - 51	19.30	38.71	108.21	14.87	184.73	5.64	29.31	46.57
903 - 52	8.47	99.87	29.84	19.44	62.71	1.89	32.42	35.38
903 - 53	2.42	47.56	18.04	31.25	0.86	0.00	27.40	14.47
903 - 54	128.67	102.23	46.62	14.60	129.63	4.43	26.08	45.21
903 - 55	29.99	91.47	90.33	14.12	210.27	6.57	28.20	53.93
903 - 56	22.59	112.05	140.26	13.75	243.35	6.61	30.17	67.40
903 - 57	41.16	55.94	18.19	31.37	37.02	0.70	17.70	20.51
903 - 58	26.17	99.56	70.25	13.97	166.36	5.21	24.53	44.17
903 - 59	25.71	129.94	140.61	14.94	217.79	6.04	27.39	52.70

Table IV.2: ICP trace element analyses of ores and rocks. A IV.2 - 2

No.	B	Ce	Co	Cr	Cu	Eu	Gd	La
903 - 60	20.86	161.68	43.34	17.25	108.43	4.81	28.78	42.14
903 - 61	20.90	175.08	129.28	14.28	209.87	6.43	27.02	45.43
903 - 62	21.76	132.13	34.68	14.28	108.54	5.92	23.69	45.21
903 - 63	32.49	250.41	13.87	11.02	41.26	8.08	36.08	46.17
903 - 64	5.37	54.27	25.34	22.61	67.60	0.24	48.23	28.19
903 - 65a	5.95	28.14	29.36	76.35	44.54	0.00	49.20	12.40
903 - 65b	15.27	234.25	111.24	15.60	87.80	5.11	22.19	51.87
903 - 66	5.93	217.31	63.13	79.24	63.56	1.43	40.06	30.08
903 - 67	3.38	141.26	40.25	27.83	47.38	1.32	22.77	23.75
903 - 68a	9.58	39.69	63.13	14.58	71.07	1.56	7.47	29.07
903 - 68b	16.45	27.13	76.90	13.29	58.60	1.35	8.39	35.48
903 - 69	16.58	30.19	87.68	15.02	55.18	1.37	8.34	35.59
903 - 70	15.09	25.61	67.16	14.15	50.31	1.11	7.26	33.36
903 - 71	14.95	28.31	61.82	14.73	51.53	1.15	7.18	36.09
903 - 72	15.35	30.27	52.77	13.79	53.26	1.04	8.87	37.27
903 - 73	11.27	33.02	56.10	14.65	50.33	1.21	8.06	37.82
903 - 74	7.33	37.80	59.51	14.73	43.49	0.83	7.75	31.15
903 - 75	9.75	37.19	73.74	15.02	53.84	1.36	8.34	34.99
903 - 76	11.25	35.55	77.64	n.d.	50.26	1.72	8.14	33.51
903 - 77a	9.48	34.41	80.23	14.36	55.71	1.66	9.17	37.52
903 - 77b	11.16	47.87	125.85	15.39	144.28	6.26	17.56	47.03
903 - 78	17.36	28.44	55.21	14.44	61.43	3.30	11.52	43.48
903 - 79	0.37	37.55	18.06	28.93	16.84	0.37	12.72	12.24
903 - 80	13.15	8.49	26.48	13.29	40.36	1.99	8.31	35.40
903 - 81	12.90	29.97	72.00	14.36	89.72	1.76	8.75	35.22
903 - 82	10.08	43.56	75.01	13.72	85.01	1.41	7.79	40.00
903 - 83	14.36	29.82	68.98	14.65	76.96	1.58	7.17	37.51
903 - 84	8.42	36.28	56.99	14.29	70.82	1.64	6.85	29.81
903 - 85	16.93	26.96	85.29	15.09	106.24	5.26	14.35	45.52
903 - 86	15.96	55.77	81.60	14.73	89.06	5.70	20.25	48.88
903 - 87	4.07	81.88	55.29	24.44	56.33	2.01	29.11	29.26
903 - 88	12.84	37.07	82.62	14.44	110.27	4.12	14.86	40.99
903 - 89	15.42	71.07	59.32	15.54	101.20	4.56	19.11	49.10
903 - 90	1.68	34.98	24.19	71.31	0.53	0.01	42.15	19.99
903 - 91	20.84	42.22	67.27	14.58	97.21	3.96	17.10	50.14
903 - 92	18.00	20.22	83.70	13.15	109.08	3.44	16.03	48.24
903 - 93	20.92	34.18	68.48	13.43	117.42	3.32	16.10	46.06
903 - 94	16.79	29.96	86.81	14.65	124.22	3.41	15.77	45.62
903 - 95	14.04	30.73	93.48	13.93	133.27	3.12	16.62	44.50
903 - 96	11.80	31.23	93.26	12.53	133.62	3.02	16.48	45.46
903 - 97	10.75	30.62	113.10	14.08	130.45	3.32	16.77	46.43
903 - 98	9.69	33.28	76.32	14.29	139.98	4.15	16.58	46.40
903 - 99	8.02	56.56	124.37	14.95	147.91	3.99	17.27	45.61
903 - 100	6.86	80.04	142.03	16.91	111.13	5.28	22.55	50.68
903 - 101	9.05	78.53	149.93	15.17	136.38	6.46	25.04	58.44
903 - 102	14.92	97.79	119.20	13.97	190.19	6.31	23.80	54.05
903 - 103	19.16	126.66	71.20	13.93	115.70	7.87	27.61	60.40
903 - 104	16.29	71.32	44.96	17.11	98.84	5.60	21.52	47.96
903 - 105	17.34	36.11	39.74	14.53	104.86	6.59	21.82	49.11
903 - 106	13.50	40.09	92.39	14.19	148.28	7.35	24.64	56.22
903 - 107	12.83	53.56	134.20	14.38	155.60	7.92	26.54	59.38
903 - 108	28.35	73.04	108.42	8.82	127.59	8.88	13.40	40.70
903 - 109	19.21	44.04	92.56	15.98	145.30	7.34	24.60	54.56
903 - 110	6.59	135.13	62.89	104.33	95.10	4.19	33.49	42.19
903 - 111	22.76	94.63	64.78	15.34	117.40	8.48	23.16	59.45
903 - 112	11.94	172.29	59.67	19.86	117.82	5.91	22.80	52.81
903 - 113	overrange	61.74	52.09	111.61	115.37	0.00	69.46	34.30
903 - 114	0.00	53.64	18.26	19.21	22.90	0.89	4.46	13.11
903 - 115a	0.18	19.66	14.42	20.40	17.08	0.23	0.00	8.44
903 - 115b	0.00	15.70	18.73	69.90	40.70	0.00	33.45	8.05

Table IV.2: ICP trace element analyses of ores and rocks.

No.	B	Ce	Co	Cr	Cu	Eu	Gd	La
903 - 116a	8.59	79.05	92.55	14.63	134.96	1.50	7.43	35.51
903 - 116b	1136.90	107.03	109.89	15.49	104.45	1.95	15.88	37.80
903 - 117b	12.18	166.01	171.12	13.95	86.49	1.85	9.61	43.19
903 - 118a	10.87	56.29	168.94	12.70	67.90	0.00	55.80	30.45
903 - 118b	4.08	37.85	24.80	106.91	23.81	0.70	4.98	14.42
903 - 119	21.86	89.35	171.82	14.89	80.23	2.72	10.27	46.56
903 - 120	19.93	35.17	67.56	17.37	60.83	2.84	12.82	44.65
903 - 121	23.52	26.92	66.04	17.03	57.17	5.53	21.74	66.90
903 - 122	12.07	83.64	65.04	16.21	51.94	3.96	15.93	52.33
903 - 123	21.07	61.19	125.07	14.54	89.79	3.12	10.35	48.82
903 - 124	5.16	270.07	82.85	18.79	65.54	5.37	23.10	51.58
903 - 125	7.42	223.29	68.40	20.58	56.06	4.15	21.89	40.73
903 - 126	1.19	231.40	51.31	20.44	46.85	2.97	20.17	31.82
903 - 127	3.96	183.38	41.76	30.10	41.82	0.97	29.11	20.24
903 - 128	0.00	143.92	31.48	27.68	37.27	0.20	26.08	15.60
903 - 129	44.97	123.80	32.53	22.67	34.23	0.36	21.86	15.42
903 - 130	1.84	261.93	70.16	21.12	56.40	3.92	23.64	41.74
903 - 131	5.26	244.10	55.19	21.46	52.58	3.00	20.86	35.79
903 - 132	0.00	138.91	34.31	38.89	43.13	0.42	30.29	17.95
903 - 133	0.00	98.54	29.05	26.18	33.74	0.48	18.59	16.20
903 - 134	0.00	115.26	27.43	34.58	33.48	0.00	26.32	15.60
903 - 135	0.00	243.99	39.57	42.62	39.83	0.78	29.71	22.80
903 - 136	0.00	236.30	47.26	50.80	40.13	0.74	29.04	24.91
903 - 137	0.00	348.54	49.93	39.78	37.92	0.53	30.50	21.55
903 - 138	7.52	416.80	92.26	32.31	64.48	2.08	33.54	36.47
903 - 139	0.00	135.15	76.23	70.29	57.13	0.00	32.97	15.21
903 - 140	0.00	81.47	35.77	25.71	32.32	0.90	7.11	14.52
903 - 141a	0.00	38.46	22.33	28.54	27.88	0.58	0.00	14.13
903 - 141b	0.00	39.63	17.07	76.38	29.65	0.21	9.80	11.91
903 - 141c	0.00	31.53	19.82	38.67	33.28	0.11	10.55	3.59
903 - 142	0.00	48.45	88.21	13.93	90.47	5.01	20.13	59.71
903 - 143	0.00	63.95	87.97	14.44	138.46	3.93	15.03	54.50
903 - 144	0.00	62.36	128.03	14.00	186.72	4.93	16.17	60.61
903 - 145	0.00	44.39	58.43	13.58	95.14	4.39	13.88	53.06
903 - 146	0.00	56.81	103.35	14.29	138.60	5.06	19.41	62.67
903 - 147	0.00	89.22	84.00	15.69	121.57	6.91	22.90	68.78
903 - 148	0.00	155.13	81.25	15.92	171.05	4.73	53.36	55.56
903 - 149	0.00	165.44	79.88	17.30	102.83	4.76	33.63	56.47
903 - 150	0.00	55.90	69.44	15.02	102.20	10.09	33.13	91.87
903 - 151	0.00	156.75	115.08	18.40	118.37	7.87	26.26	72.87
903 - 152a	0.00	179.78	134.34	15.69	193.23	7.86	37.86	77.20
903 - 152b	5.26	86.24	123.42	15.47	220.01	6.82	52.46	68.48
903 - 153	6.53	235.50	165.42	17.22	117.52	6.59	24.22	68.30
903 - 154	8.84	212.15	101.24	16.29	104.20	7.15	25.30	77.77
903 - 155	896.88	50.60	108.36	14.65	84.07	2.11	14.79	32.06
903 - 156	511.62	7.05	17.96	7.09	14.92	0.00	9.09	0.00
903 - 157	3.78	34.06	43.46	13.79	40.39	0.00	58.62	11.69
903 - 158	13.02	36.88	47.58	14.58	50.04	0.00	47.60	16.04
903 - 159	11.04	48.53	43.21	13.58	61.70	0.49	48.68	25.80
903 - 160	92.75	14.64	49.45	14.00	60.04	3.98	16.07	32.38
903 - 161	31.80	44.80	52.28	14.00	69.80	3.00	12.31	30.85
903 - 162	12.10	33.87	67.01	14.44	39.31	0.55	5.85	17.79
903 - 164	13.08	44.39	85.47	14.86	161.83	0.59	5.80	22.73
903 - 170a	0.00	24.43	38.84	15.33	15.20	0.58	0.00	7.81
903 - 170b	0.00	35.12	13.69	16.37	19.72	0.68	0.00	12.48
903 - 171a	0.00	26.62	24.16	14.64	15.48	0.52	0.00	8.88
903 - 171b	0.00	27.41	16.22	14.91	16.26	0.50	0.00	8.76
903 - 172	0.00	24.99	42.79	14.59	16.25	0.47	0.00	8.46
903 - 173	0.00	28.27	48.15	14.43	18.08	0.51	0.00	8.36
903 - 174	0.00	30.06	39.52	14.63	25.78	0.66	0.00	9.35

Table IV.2: ICP trace element analyses of ores and rocks. A IV.2 - 4

No.	B	Ce	Co	Cr	Cu	Eu	Gd	La
903 - 175	0.00	26.32	49.16	14.47	23.50	0.57	0.00	8.12
903 - 176	0.00	22.03	67.76	14.35	32.89	0.57	0.00	7.96
903 - 177	0.00	29.59	30.45	15.21	38.75	0.55	0.00	9.41
903 - 178	0.98	27.20	83.50	14.91	251.61	0.93	2.40	17.45
903 - 179	44.81	72.78	36.52	45.38	257.66	0.00	95.66	20.54
903 - 180	13.17	94.62	39.92	16.54	418.72	0.00	94.89	35.18
903 - 181	133.07	89.87	60.22	15.23	201.53	0.00	87.69	29.21
903 - 182	100.95	177.92	68.77	14.67	99.44	4.35	24.23	62.11
903 - 183	114.64	146.54	102.84	15.43	118.13	4.58	24.76	55.12
903 - 184	84.10	150.93	85.67	15.30	109.70	4.84	28.15	55.18
903 - 185	7.22	60.22	35.84	19.41	306.58	0.00	96.79	13.48
903 - 186	8.87	77.98	76.05	15.88	127.99	0.00	104.90	19.97
903 - 187	11.80	49.88	40.19	37.55	101.69	0.00	83.12	10.97
903 - 188	7.75	164.69	205.37	17.56	415.92	4.10	16.67	46.87
903 - 189	9.90	59.96	45.81	54.65	68.58	0.00	36.98	14.49
903 - 190	28.26	246.08	192.72	18.28	144.17	6.59	34.78	63.02
903 - 200	10.37	118.37	24.25	23.36	38.48	0.22	16.93	16.39
903 - 201	6.41	165.03	30.54	23.53	40.87	0.33	18.04	18.92
903 - 202	7.80	207.55	33.11	23.94	43.34	0.35	23.97	21.00
903 - 203	17.82	201.47	34.16	24.39	43.20	0.41	22.48	18.32
903 - 204	14.93	243.06	35.64	24.95	45.29	0.51	23.70	19.54
903 - 205	23.65	236.41	40.04	25.56	49.74	0.51	24.77	21.04
903 - 206	21.68	239.00	41.07	22.99	50.16	0.75	23.68	21.42
903 - 207	25.83	337.31	63.66	24.30	57.20	1.41	30.03	30.14
903 - 208	26.36	292.45	61.06	26.33	52.85	1.29	25.11	24.85
903 - 209	16.58	61.80	36.96	17.13	83.09	5.98	28.64	53.20
903 - 210	0.00	183.22	83.41	61.32	55.80	0.08	41.18	17.25
903 - 211	0.00	204.52	67.93	48.05	64.49	1.68	26.79	28.40
903 - 212	11.09	113.83	68.67	19.61	110.63	4.03	25.13	47.35
903 - 213	7.27	22.36	144.83	14.70	191.17	2.39	15.22	42.34
903 - 215	0.00	45.12	28.87	27.19	40.98	0.00	26.28	8.41
903 - 216	16.34	62.90	63.89	14.41	120.38	6.94	36.60	71.90
903 - 217	0.00	11.75	23.61	34.43	33.79	0.01	16.84	10.63
903 - 218	10.83	42.55	67.15	16.00	105.65	2.98	20.36	47.22
903 - 219	6.52	78.74	45.71	15.96	89.84	5.82	26.77	59.89
903 - 220	3.84	67.70	97.57	14.86	130.71	3.52	24.53	55.53
903 - 221	0.00	27.82	15.76	50.38	31.36	0.00	46.43	9.69
903 - 222	0.14	23.56	14.27	41.33	26.92	0.00	35.69	10.66
903 - 223	31.24	19.68	79.95	14.18	58.23	1.54	10.93	46.79
903 - 224	20.74	41.83	83.76	14.06	80.70	2.45	13.71	49.81
903 - 225	17.17	146.71	83.62	13.68	72.94	3.49	15.06	49.49
903 - 226	11.00	159.49	107.65	13.88	70.35	3.21	16.49	50.10
903 - 227	8.91	92.36	54.60	15.64	100.38	1.40	12.38	35.39
903 - 228	6.80	76.00	27.23	16.20	100.83	0.88	15.58	28.32
903 - 229	0.00	185.10	50.32	63.61	47.15	0.37	34.36	16.25
903 - 230	0.09	203.15	47.69	50.74	55.34	0.21	31.16	14.31
903 - 232	11.78	248.66	277.04	17.73	413.52	3.98	27.33	54.26
903 - 233	10.35	368.21	294.93	18.79	205.83	3.72	17.19	38.13
903 - 234	1.73	64.89	26.82	19.17	355.36	0.00	102.19	16.39
903 - 235	3.74	64.56	23.86	20.19	300.52	0.00	100.77	16.46
903 - 237	29.90	27.67	157.69	14.34	341.56	0.83	3.71	19.07
903 - 239	23.67	67.62	174.09	13.98	72.92	1.26	18.18	26.96
903 - 241	63.89	122.16	44.88	15.40	91.34	7.64	32.84	104.31
903 - 245	1.78	83.70	34.70	13.82	109.65	0.00	111.58	20.15
903 - 246	2.55	64.06	44.95	15.67	86.94	0.00	112.69	10.48
903 - 249	31.73	205.65	61.28	15.80	114.26	1.20	11.53	31.11
903 - 250	5.88	30.57	96.77	13.53	52.13	0.00	59.32	20.52
903 - 251	1.73	47.71	121.21	13.26	53.28	0.00	75.89	16.05
903 - 252	13.98	59.92	62.15	15.70	113.04	1.19	16.63	32.28
903 - 253	15.00	187.15	115.41	14.93	153.42	2.96	13.20	36.80

Table IV.2: ICP trace element analyses of ores and rocks.

No.	B	Ce	Co	Cr	Cu	Eu	Gd	La
903 - 254	3.87	90.54	183.91	14.32	177.63	1.90	9.44	23.52
903 - 255	7.02	164.19	74.49	13.95	75.52	2.49	52.60	32.72
903 - 256	5.18	107.00	63.67	13.79	56.08	2.11	64.75	34.77
903 - 259	24.06	96.49	140.29	14.47	73.64	3.19	14.60	47.30
903 - 260	20.46	111.95	156.44	14.82	96.07	3.26	15.26	49.30
903 - 261	0.00	58.74	97.37	16.71	196.69	0.00	99.97	9.91
903 - 262	0.00	59.10	74.02	21.94	172.57	0.00	97.13	9.93
903 - 263	18.23	56.04	100.00	14.39	42.90	1.79	11.82	39.29
903 - 264	12.39	61.68	93.50	14.34	45.05	1.80	12.54	35.44
903 - 265	59.92	18.93	28.89	14.11	49.02	1.49	12.55	36.02
903 - 266	23.29	14.41	32.08	14.16	51.65	5.66	37.63	66.05
903 - 268	7.36	168.14	234.31	14.33	157.47	2.01	25.12	35.79
903 - 269	8.54	328.32	182.78	15.18	122.90	4.08	25.96	46.14
903 - 270	1.52	83.08	156.39	16.10	73.46	0.00	71.91	22.21
903 - 271	8.98	75.79	122.48	15.96	51.39	1.05	18.84	27.98
903 - 272	11.54	52.15	106.27	14.91	108.90	1.29	10.38	32.97
903 - 273	10.60	74.96	105.83	15.25	95.48	1.88	13.10	36.88
903 - 274	37.10	111.89	22.24	16.99	68.01	4.14	24.47	53.19
903 - 275	37.99	105.40	25.04	15.69	73.12	3.39	20.76	54.08
903 - 276	0.00	59.03	46.27	79.13	96.89	0.00	95.28	12.54
903 - 277	0.00	64.55	42.99	30.55	343.65	0.00	73.68	10.91
903 - 278	2.58	37.39	82.93	16.89	217.83	1.31	7.07	15.62
903 - 279	4.29	40.47	89.10	15.20	80.58	1.93	7.91	24.30
903 - 280	6.64	35.92	105.85	15.84	81.42	0.57	57.73	22.24
903 - 281	13.10	100.08	110.31	18.82	200.56	2.16	14.85	35.47
903 - 282	12.15	11.27	156.27	15.08	161.35	3.87	25.44	46.82
903 - 283a	12.30	60.53	147.35	14.38	287.82	1.60	8.73	30.85
903 - 283b	10.01	154.15	134.53	16.57	116.29	2.03	12.56	33.45
903 - 283c	10.85	132.95	110.95	14.40	127.89	1.87	11.33	31.94
903 - 283d	9.78	93.22	96.19	14.63	231.01	2.11	13.10	35.69
903 - 283e	10.27	129.94	99.23	14.46	147.88	1.90	11.72	34.16
903 - 284	6.80	49.45	135.39	16.43	141.91	2.43	30.59	28.85
903 - 285	14.86	46.10	111.09	15.96	162.41	1.59	20.28	30.34
903 - 286	12.92	50.83	149.92	16.77	138.35	2.34	28.10	32.57
903 - 287	10.67	51.03	129.95	19.98	109.64	1.82	39.03	28.56
903 - 290	17.73	192.66	58.88	14.75	82.69	3.94	20.47	45.53
903 - 291	33.45	290.25	13.73	14.85	78.96	16.20	58.34	111.91
903 - 292	32.30	256.20	15.42	20.65	29.75	11.11	45.39	68.82
903 - 293	33.87	320.59	8.89	16.13	33.07	14.50	50.49	88.40
903 - 294	32.14	280.10	35.61	19.45	47.95	15.41	58.09	91.44
903 - 295	0.93	54.35	39.35	14.34	82.54	0.00	106.96	8.78
903 - 296	3.88	47.80	55.23	30.83	154.58	0.00	86.61	16.00
903 - 297	27.50	62.81	85.76	15.00	78.28	4.64	26.04	40.01
903 - 298	17.48	58.34	93.77	15.45	203.73	1.51	13.36	29.13
903 - 299	21.41	38.86	90.98	16.35	152.49	1.42	13.52	30.36
903 - 300	42.72	278.10	24.31	14.63	30.30	10.12	42.32	63.92
903 - 301	29.85	365.49	23.31	15.79	55.81	16.38	61.27	80.94
903 - 302	29.00	395.98	14.22	17.04	65.17	19.10	72.39	95.80
903 - 303	22.44	33.95	56.03	14.04	122.72	2.63	18.58	44.30
903 - 304	15.03	24.87	55.78	13.81	108.19	2.39	14.70	34.92
903 - 305	20.90	18.05	116.84	14.06	159.05	3.23	21.09	39.86
903 - 306	22.60	22.98	126.04	14.48	191.11	3.81	25.87	39.56
903 - 307	26.75	29.54	250.03	14.61	250.30	4.52	24.88	41.76
903 - 308	28.15	27.72	236.48	14.08	244.31	4.12	22.72	40.10
903 - 309	23.61	42.67	211.36	14.86	232.51	3.54	21.22	37.02
903 - 310	20.88	56.34	169.95	20.16	196.93	3.48	22.82	37.29
903 - 311	26.79	22.23	191.40	13.98	217.60	4.14	25.51	40.51
903 - 312a	27.94	29.77	181.25	14.71	177.26	4.09	24.33	40.78
903 - 312b1	32.33	24.00	140.50	13.88	143.07	5.29	28.94	45.30
903 - 312b2	29.04	19.65	81.08	13.75	88.47	3.91	26.28	45.81

Table IV.2: ICP trace element analyses of ores and rocks.

No.	B	Ce	Co	Cr	Cu	Eu	Gd	La
903 - 312b3	33.74	21.66	105.20	14.15	129.82	4.47	25.88	42.08
903 - 312b4	30.56	36.60	78.74	14.09	93.74	4.72	21.88	47.66
903 - 315b5	30.69	28.92	110.46	14.03	140.52	5.09	27.73	45.06
903 - 313	28.99	33.71	94.25	14.77	134.16	3.96	24.12	44.51
903 - 314	27.31	36.13	89.12	14.41	128.04	3.51	20.39	38.66
903 - 315	22.76	34.31	58.52	14.84	108.02	2.79	17.15	35.39
903 - 316	22.21	25.04	63.71	14.55	105.43	2.72	16.83	33.70
903 - 317	20.70	38.11	88.73	14.83	121.46	2.79	19.19	35.71
903 - 318	21.20	38.17	76.11	13.98	139.74	2.96	20.05	40.04
903 - 319	20.04	28.98	59.87	13.55	125.39	2.15	16.99	36.75
903 - 320	21.43	34.95	47.99	13.77	133.67	2.44	19.16	41.71
903 - 321	17.41	34.98	55.06	14.06	140.10	2.34	19.70	42.43
903 - 322	17.82	39.64	66.07	14.05	163.85	3.02	22.75	44.04
903 - 323	19.53	36.45	57.16	14.35	175.29	3.34	21.28	40.17
903 - 324	4.64	138.55	56.64	65.88	62.23	1.11	45.22	30.48
903 - 325	4.56	126.23	39.45	63.54	60.74	1.14	49.35	28.97
903 - 326a	7.18	65.99	20.93	57.29	39.30	0.00	67.57	27.21
903 - 326b	7.13	90.82	75.72	56.35	138.93	0.54	71.29	25.92
903 - 326c	13.12	72.65	18.17	119.05	41.34	0.00	82.42	21.73
903 - 327	21.85	198.10	65.28	25.97	98.23	2.37	39.37	40.39
903 - 328	97.92	17.91	82.87	14.13	118.53	4.93	24.89	43.80
903 - 329	77.33	33.51	62.72	13.93	100.66	3.97	17.93	39.19
903 - 330	43.57	226.00	121.39	14.84	182.97	3.25	16.73	55.47
903 - 331	14.55	203.42	89.22	15.16	78.03	2.59	16.30	50.24
903 - 332	11.20	118.28	96.97	14.78	108.58	1.38	12.04	37.75
903 - 333	9.68	321.21	143.73	14.41	128.87	3.67	20.55	61.11
903 - 334	16.13	45.07	125.41	14.55	71.17	3.37	18.72	44.38
903 - 335	18.79	42.76	86.69	14.57	68.45	3.64	20.31	49.91
903 - 336	74.78	53.12	29.32	12.85	99.81	0.00	108.81	6.87
903 - 337	2.61	50.47	14.75	30.09	20.43	0.41	0.45	15.16
903 - 338	1.98	32.13	15.71	56.44	33.66	0.00	43.55	12.89
903 - 339	25.60	56.38	213.08	14.42	144.69	1.90	19.92	30.93
903 - 340a	15.40	38.30	166.77	15.38	262.83	1.86	11.38	20.04
903 - 340b	11.69	39.31	216.30	17.05	223.63	1.42	8.38	18.69
903 - 341a	20.64	122.71	114.33	17.26	63.98	2.08	12.13	40.93
903 - 342a	13.38	205.90	195.01	14.71	74.91	2.02	11.75	48.93
903 - 343	8.77	230.95	173.72	15.59	144.04	2.15	13.36	29.36
903 - 344	6.66	115.77	148.14	15.44	52.15	0.87	21.00	26.07
903 - A	11.09	145.85	97.98	13.92	148.90	2.00	40.83	34.61
903 - B	8.41	376.75	130.05	14.12	133.71	11.45	45.20	134.84
903 - B I.a	6.97	41.14	14.58	29.39	19.31	0.44	0.00	12.98
903 - B I.c	1.09	32.94	13.39	28.84	21.76	0.44	0.00	13.62
903 - B I.d1	1.62	39.35	14.03	29.40	21.67	0.48	0.00	14.15
903 - B I.d2	5.50	39.81	13.65	28.68	21.63	0.50	0.56	14.09
903 - B I.d3	109.59	41.31	13.81	43.25	22.44	0.53	0.52	14.75
903 - B I.d4	9.09	34.83	13.74	29.28	21.00	0.38	0.01	14.27
903 - B I.e	1.54	35.77	12.59	28.66	22.19	0.39	0.00	12.80
903 - B II.a	39.53	73.08	70.16	14.11	74.40	2.52	11.87	46.50
903 - B II.c	44.00	80.83	72.43	14.40	78.99	2.53	12.82	48.19
903 - B II.d1	48.79	84.86	71.85	13.40	78.32	2.48	12.72	13.43
903 - B II.d2	20.62	77.55	73.06	13.46	79.50	2.23	11.72	46.74
903 - B II.d3	21.91	83.66	73.39	14.49	79.30	2.51	12.91	48.40
903 - B II.d4	19.00	81.49	74.95	13.72	79.91	2.57	13.05	48.52
903 - B II.e	24.59	82.18	73.72	16.15	79.61	2.63	13.15	48.02
903 - Mn 2	16.79	95.80	76.77	27.38	91.31	3.01	20.26	49.98
903 - Mn 3	15.15	120.56	74.53	35.00	96.98	3.52	24.99	52.55

Table IV.2: ICP trace element analyses of ores and rocks. A IV.2 - 7

No.	Nd	Ni	P	Sm	Sr	V	Yb	Zn	Zr
903 - 3	39.16	62.81	161.75	10.97	255.89	159.39	1.38	109.80	67.09
903 - 4	54.63	87.43	222.73	16.20	730.77	278.48	1.46	115.57	23.01
903 - 5a	38.68	40.77	120.56	10.27	2047.61	367.20	1.48	68.18	136.43
903 - 5b	13.62	0.00	0.00	0.00	0.00	14.92	0.88	39.85	254.03
903 - 6	37.69	92.29	177.30	8.27	3073.56	183.91	5.03	95.82	19.33
903 - 7	48.95	71.55	146.71	13.84	2435.62	194.60	2.74	67.07	22.49
903 - 8	41.31	102.07	146.41	11.06	3395.73	184.28	4.22	96.05	22.00
903 - 9	60.68	71.55	201.65	18.25	2114.25	532.80	2.30	78.52	26.99
903 - 10	62.63	143.57	125.68	14.84	4990.18	153.77	5.80	97.89	33.52
903 - 11	62.32	135.02	156.77	17.05	4639.67	161.94	5.52	85.75	35.82
903 - 12	61.14	145.32	181.78	17.23	4677.72	178.39	4.99	84.67	37.18
903 - 13	69.33	171.16	141.91	17.01	5159.55	143.25	6.69	126.09	28.64
903 - 14	79.30	130.20	159.43	22.41	5158.26	186.52	6.53	82.60	38.69
903 - 15	53.43	70.64	135.96	14.80	3918.14	286.27	3.90	65.69	61.51
903 - 16	55.68	108.42	166.70	15.72	4111.00	209.09	3.98	77.78	33.02
903 - 17	69.46	179.44	158.59	18.72	5008.27	136.53	6.86	129.53	26.50
903 - 18	75.50	66.38	114.36	21.10	3098.84	391.79	4.73	65.29	60.04
903 - 19	65.24	78.77	126.00	17.73	3967.79	273.24	5.13	91.50	53.31
903 - 20	5.81	0.00	0.00	0.00	0.00	5.58	0.00	37.21	223.09
903 - 21	16.26	1.86	31.21	3.07	149.11	398.05	1.83	46.61	205.34
903 - 22	35.14	72.18	104.21	6.54	1549.93	91.59	3.09	64.10	95.59
903 - 23	49.81	108.27	156.32	9.81	2324.90	134.60	4.63	89.47	31.84
903 - 24	14.07	1.71	30.87	2.40	94.68	293.01	1.44	43.84	199.90
903 - 25	19.06	4.87	33.66	6.22	594.51	471.39	2.12	55.81	188.38
903 - 26	5.16	0.00	0.00	0.00	0.00	1.09	0.00	32.78	32.20
903 - 27	14.64	3.83	12.86	6.62	0.00	644.31	2.50	61.42	246.61
903 - 28a	11.99	1.94	0.00	2.39	0.00	285.47	1.67	46.32	256.07
903 - 28b	12.45	1.61	0.00	2.79	0.00	358.97	1.87	47.08	268.62
903 - 29	24.83	4.22	0.00	5.76	3.22	278.56	2.32	44.33	243.40
903 - 30	18.88	5.47	0.00	4.80	0.00	246.16	1.84	42.67	200.93
903 - 31a	16.53	1.54	0.00	2.47	0.00	52.28	0.58	37.77	121.63
903 - 31b	11.19	0.00	0.00	0.75	0.00	8.73	0.00	34.96	78.49
903 - 32	9.88	0.00	0.00	0.46	0.00	10.47	0.00	36.31	64.64
903 - 33	41.43	504.83	174.29	10.32	overrange	321.67	9.97	199.07	38.96
903 - 34	45.59	551.68	165.93	10.44	overrange	388.16	10.69	201.82	36.29
903 - 35	42.62	395.89	190.00	11.71	overrange	313.70	6.25	167.81	40.82
903 - 36	45.20	505.98	181.43	12.09	overrange	415.56	9.13	184.22	39.61
903 - 37	50.87	598.04	173.26	13.27	overrange	502.85	10.06	190.78	48.38
903 - 38	48.28	522.59	171.62	13.23	overrange	502.17	8.52	173.54	82.00
903 - 39	52.66	568.05	179.35	14.07	overrange	512.83	9.39	181.41	56.57
903 - 40	53.43	590.14	169.29	14.87	overrange	494.11	9.15	182.67	50.29
903 - 41	51.05	348.70	314.66	15.60	4804.26	345.16	4.17	161.90	31.48
903 - 42	44.49	391.75	127.02	11.86	overrange	437.76	5.24	224.37	106.21
903 - 43	39.05	299.30	81.89	9.46	5139.09	364.16	4.18	118.35	170.85
903 - 44	59.84	492.45	177.84	16.03	overrange	427.23	6.37	154.52	90.34
903 - 45	45.65	376.49	111.65	11.83	overrange	395.41	6.32	126.76	142.98
903 - 46	66.75	566.34	201.89	20.65	overrange	414.56	11.13	167.55	57.59
903 - 47	68.42	426.64	245.62	23.05	overrange	367.20	8.84	140.18	46.86
903 - 48	65.20	419.64	213.25	20.94	overrange	370.87	7.18	137.13	57.09
903 - 49	50.80	239.28	128.50	15.06	4417.32	333.90	4.75	112.77	158.09
903 - 50	70.21	395.08	235.75	24.68	overrange	403.38	9.16	140.56	52.26
903 - 51	68.64	410.58	241.56	23.75	overrange	492.97	8.60	134.93	41.79
903 - 52	44.52	49.75	56.81	11.57	1784.13	955.91	3.61	70.35	198.42
903 - 53	18.01	5.01	5.81	2.31	135.84	907.44	2.69	50.34	278.71
903 - 54	67.95	199.13	145.10	22.09	3049.50	499.34	3.69	89.55	144.65
903 - 55	87.44	324.35	268.26	30.13	4522.68	486.93	5.70	104.54	42.93
903 - 56	90.42	364.78	208.64	28.76	overrange	615.19	7.23	111.41	56.26
903 - 57	22.16	4.06	0.00	3.12	536.27	273.87	1.80	45.75	243.95
903 - 58	70.82	274.36	226.48	24.12	3290.19	368.95	4.20	101.75	45.30
903 - 59	77.58	305.85	185.91	25.54	overrange	417.00	6.33	100.35	65.68

No.	Nd	Ni	P	Sm	Sr	V	Yb	Zn	Zr
903 - 60	74.32	147.96	130.49	23.52	1637.61	584.96	4.05	80.13	95.18
903 - 61	78.75	329.75	242.58	27.21	4925.25	524.81	5.67	107.35	35.03
903 - 62	87.98	323.32	212.18	29.00	1845.17	268.14	2.56	102.38	40.12
903 - 63	171.30	27.14	238.64	48.59	474.45	161.12	3.04	70.72	36.78
903 - 64	28.65	11.92	82.92	8.17	197.67	322.62	2.57	72.83	215.75
903 - 65a	11.80	6.97	49.31	4.56	11.14	738.41	1.84	55.94	212.42
903 - 65b	75.18	42.03	606.04	24.00	2384.56	53.66	4.48	105.79	45.13
903 - 66	38.44	22.91	49.22	10.79	646.06	446.99	3.50	61.47	211.48
903 - 67	29.15	10.47	32.91	7.21	478.35	197.67	1.87	52.62	146.99
903 - 68a	38.26	214.78	158.85	4.30	2464.00	197.14	2.23	103.71	54.71
903 - 68b	40.23	200.51	268.69	3.49	2679.32	264.49	4.51	101.80	40.68
903 - 69	41.06	186.58	290.16	3.13	2693.78	273.82	4.71	99.86	43.88
903 - 70	36.77	176.84	241.97	2.50	2535.91	241.62	4.37	95.56	45.75
903 - 71	38.36	210.17	291.98	1.90	2179.15	235.93	4.99	101.04	33.81
903 - 72	38.80	209.25	288.35	2.41	2274.54	253.47	5.21	98.08	35.86
903 - 73	41.98	181.05	256.48	3.27	1955.86	231.87	5.44	100.11	38.70
903 - 74	33.87	174.48	176.98	1.60	1981.70	166.84	5.07	89.73	70.49
903 - 75	38.62	223.75	217.23	2.43	2703.55	178.26	6.43	92.75	50.14
903 - 76	25.25	216.96	229.08	4.54	3385.17	154.85	5.68	76.96	95.53
903 - 77a	43.67	190.72	257.35	3.32	2744.23	185.59	5.59	89.77	37.29
903 - 77b	83.23	193.83	301.15	16.57	2196.84	195.43	8.51	84.50	24.20
903 - 78	59.86	245.95	443.69	8.72	2667.51	216.13	4.12	85.74	32.91
903 - 79	25.48	6.94	29.37	1.97	0.00	155.83	1.46	53.89	193.29
903 - 80	42.11	204.19	282.03	5.43	1304.47	144.73	1.55	107.31	31.30
903 - 81	41.44	331.82	320.79	4.93	2712.66	202.36	2.65	117.65	38.51
903 - 82	45.27	342.96	215.62	4.06	3295.93	203.30	2.75	118.15	46.15
903 - 83	41.52	328.14	221.28	5.02	2267.99	185.39	2.15	120.91	38.21
903 - 84	38.64	252.28	174.76	4.10	2523.92	175.94	2.39	105.29	49.11
903 - 85	78.68	197.51	501.41	14.74	2517.46	215.89	5.23	84.23	20.99
903 - 86	87.51	149.21	527.85	15.50	2098.12	206.29	5.55	86.86	62.01
903 - 87	54.51	29.23	207.64	10.21	1116.57	370.32	3.64	67.14	153.32
903 - 88	67.05	308.95	252.18	11.33	3313.98	285.98	5.05	88.31	52.88
903 - 89	58.38	282.75	282.03	12.61	3709.96	362.59	5.29	96.27	70.72
903 - 90	33.29	2.80	7.91	7.35	3.60	816.28	3.65	50.91	202.68
903 - 91	69.43	412.41	201.35	9.87	3811.61	311.36	6.86	114.01	52.55
903 - 92	63.72	533.13	221.28	8.35	4407.20	289.13	7.06	136.48	51.21
903 - 93	60.16	598.96	403.34	8.25	4612.24	278.28	6.51	145.48	52.93
903 - 94	60.16	588.20	293.81	8.18	4639.80	267.56	6.65	146.44	46.02
903 - 95	58.23	661.06	293.81	7.37	5161.37	279.61	8.54	151.97	44.56
903 - 96	57.49	702.90	189.01	7.69	0.00	288.45	9.56	147.42	39.88
903 - 97	57.84	652.26	116.72	7.89	0.00	282.17	9.17	146.95	41.28
903 - 98	68.04	594.04	126.28	11.17	4797.18	255.72	7.29	128.43	36.68
903 - 99	66.21	560.27	117.98	10.21	0.00	334.69	8.35	115.22	53.74
903 - 100	75.98	584.99	129.53	13.28	0.00	335.30	10.84	108.92	45.30
903 - 101	87.61	615.43	122.42	15.81	0.00	289.47	13.41	104.87	43.64
903 - 102	92.48	401.74	328.81	21.56	overrange	312.94	9.28	99.93	47.90
903 - 103	114.37	290.33	394.31	27.59	3019.70	384.13	7.06	101.93	31.48
903 - 104	87.57	257.91	307.67	19.77	2925.30	305.52	4.61	100.38	61.88
903 - 105	94.14	284.01	364.59	22.39	3123.40	256.83	4.81	113.91	31.69
903 - 106	99.69	396.12	316.21	23.98	5034.40	279.60	8.74	107.72	39.73
903 - 107	103.69	426.52	295.04	24.67	overrange	302.15	10.41	99.24	48.93
903 - 108	49.40	117.46	29.30	14.05	overrange	173.46	7.43	78.13	40.07
903 - 109	101.15	325.50	349.19	23.59	4277.60	279.87	7.10	102.04	58.36
903 - 110	81.26	88.20	153.66	17.72	1670.70	454.22	4.67	67.35	140.92
903 - 111	120.67	252.62	441.24	29.89	2249.40	277.74	4.90	95.30	29.68
903 - 112	102.69	266.42	236.23	22.01	2041.00	260.93	4.12	85.40	87.74
903 - 113	44.35	73.87	540.40	11.41	327.98	479.74	4.18	123.31	263.93
903 - 114	29.39	3.33	1.14	3.13	118.52	41.50	0.30	40.24	81.44
903 - 115a	17.97	0.00	0.00	0.00	0.00	12.04	0.00	36.23	135.05
903 - 115b	19.12	0.89	5.74	3.70	0.00	923.67	2.16	49.48	113.21

Table IV.2: ICP trace element analyses of ores and rocks. A IV.2 - 9

No.	Nd	Ni	P	Sm	Sr	V	Yb	Zn	Zr
903 - 116a	44.05	9.60	419.97	5.90	232.88	176.19	1.56	70.59	73.22
903 - 116b	50.45	24.69	361.88	8.03	398.49	127.53	3.73	83.67	68.73
903 - 117b	46.70	56.61	249.11	6.87	366.54	78.70	2.29	115.53	49.26
903 - 118a	44.57	52.49	666.77	12.49	547.25	160.43	4.05	125.94	80.90
903 - 118b	26.23	3.19	11.27	1.33	0.00	33.43	0.75	44.24	189.33
903 - 119	53.78	41.35	891.34	8.32	670.87	256.78	3.69	150.05	56.70
903 - 120	57.58	60.70	354.47	9.28	209.28	117.95	3.75	66.04	78.67
903 - 121	94.85	60.28	466.66	16.48	285.76	211.70	5.49	69.30	109.97
903 - 122	76.96	62.17	290.52	12.24	270.51	169.91	4.85	69.04	94.01
903 - 123	57.94	156.08	453.65	8.65	411.64	76.23	5.03	105.42	36.42
903 - 124	94.52	29.23	16.09	17.63	563.45	237.58	7.00	64.92	241.76
903 - 125	79.29	25.96	10.85	14.00	382.61	234.32	5.55	62.16	255.90
903 - 126	44.61	25.77	1.92	11.42	310.14	207.67	4.03	55.62	255.58
903 - 127	28.42	15.54	0.33	7.31	138.30	495.83	3.23	48.60	239.34
903 - 128	20.80	13.14	0.00	4.61	48.16	308.23	2.05	46.88	235.59
903 - 129	18.84	14.96	0.00	3.87	3.52	252.69	1.86	45.08	251.42
903 - 130	65.53	31.77	7.31	16.86	442.25	219.09	5.35	48.10	257.93
903 - 131	53.37	22.37	1.12	12.90	251.91	201.27	3.77	44.32	243.22
903 - 132	22.87	9.04	0.00	6.53	87.89	290.92	2.45	47.52	235.29
903 - 133	18.33	10.11	0.00	4.07	0.00	146.08	1.68	45.36	259.47
903 - 134	18.11	8.78	0.00	4.30	0.00	244.97	1.90	47.44	244.02
903 - 135	29.72	13.46	3.01	8.30	161.28	294.43	2.93	47.93	262.45
903 - 136	30.26	7.71	0.00	8.59	153.08	238.64	2.76	50.57	252.39
903 - 137	27.14	7.88	2.19	7.34	4.42	227.55	2.73	52.08	259.22
903 - 138	49.99	24.25	4.41	14.12	185.18	263.74	4.27	48.90	254.30
903 - 139	17.98	29.79	7.31	5.64	0.00	265.89	2.31	47.96	256.63
903 - 140	19.12	3.98	0.00	2.68	0.00	34.87	0.97	39.37	180.56
903 - 141a	12.88	4.24	0.00	0.80	0.00	11.52	0.88	41.99	279.48
903 - 141b	12.15	4.56	0.00	1.07	0.00	73.17	0.96	44.86	233.15
903 - 141c	10.58	4.54	0.00	0.20	0.00	31.13	0.84	44.57	242.97
903 - 142	64.87	182.20	226.18	15.47	450.54	199.73	5.49	91.13	72.75
903 - 143	49.59	238.94	198.23	10.85	413.65	168.99	5.54	114.82	37.14
903 - 144	59.79	344.34	244.51	13.82	506.91	123.15	6.74	108.59	22.40
903 - 145	57.62	195.33	221.28	15.13	211.39	175.76	4.46	110.95	4.78
903 - 146	56.90	244.34	332.24	12.52	338.87	100.48	8.88	131.84	39.20
903 - 147	84.36	229.27	405.42	20.74	276.64	112.39	6.80	117.17	36.56
903 - 148	72.34	204.30	625.23	22.34	291.40	459.25	9.81	127.04	55.09
903 - 149	69.59	90.96	276.66	18.97	343.65	363.07	7.08	103.30	79.87
903 - 150	121.39	212.36	250.47	30.70	220.21	195.11	8.48	99.18	27.85
903 - 151	97.86	157.55	307.64	25.78	350.24	149.94	7.88	102.54	61.71
903 - 152a	101.11	160.14	306.71	26.07	468.65	542.54	12.71	116.92	84.39
903 - 152b	94.26	480.07	617.80	27.53	374.06	929.67	13.05	157.41	64.09
903 - 153	84.55	67.38	512.84	22.24	696.74	154.04	7.72	130.60	61.17
903 - 154	93.81	56.11	419.08	24.28	369.46	193.11	8.29	96.99	81.35
903 - 155	29.25	110.20	947.06	6.49	4005.37	52.85	3.96	145.62	54.25
903 - 156	0.00	7.71	0.00	0.00	66.70	20.42	0.00	47.91	63.34
903 - 157	12.50	187.15	2424.61	7.92	458.92	122.81	4.31	145.59	72.28
903 - 158	18.18	104.64	1849.76	7.58	421.08	177.63	3.09	150.20	135.38
903 - 159	34.24	133.01	2441.87	11.43	892.48	264.21	2.82	186.94	88.11
903 - 160	27.88	199.59	432.92	9.33	286.38	90.73	1.95	96.29	29.19
903 - 161	31.67	97.45	389.90	8.17	642.54	75.56	1.39	88.79	52.06
903 - 162	10.80	34.66	171.09	1.81	1731.80	238.23	1.02	100.84	69.27
903 - 164	17.46	61.30	227.37	2.39	4522.92	1115.69	3.96	140.41	71.24
903 - 170a	7.80	0.00	0.00	0.00	0.00	5.46	0.00	33.74	40.98
903 - 170b	12.19	0.00	0.00	0.00	0.00	31.55	0.25	35.55	79.50
903 - 171a	9.70	0.00	0.00	0.00	0.00	6.54	0.00	33.63	43.45
903 - 171b	9.46	0.00	0.00	0.00	0.00	6.99	0.00	33.69	45.14
903 - 172	8.89	0.00	0.00	0.00	0.00	6.16	0.00	33.70	44.70
903 - 173	8.77	0.00	0.00	0.00	0.00	5.39	0.00	34.04	41.64
903 - 174	9.82	0.00	0.00	0.00	0.00	11.08	0.00	36.51	42.36

No.	Nd	Nl	P	Sm	Sr	V	Yb	Zn	Zr
903 - 175	8.48	0.00	0.00	0.00	0.00	8.97	0.00	35.29	38.81
903 - 176	8.77	0.00	0.00	0.00	0.00	20.43	0.00	38.02	39.14
903 - 177	9.12	0.00	0.00	0.00	10.90	50.73	0.00	39.80	57.06
903 - 178	14.66	3.43	125.36	1.67	689.90	943.18	2.90	80.96	44.90
903 - 179	23.49	344.80	417.53	12.08	29.58	1534.63	6.29	144.59	180.31
903 - 180	36.20	156.81	1773.66	13.68	243.60	1219.75	6.86	153.26	166.71
903 - 181	31.23	90.04	1742.12	13.40	436.19	1203.85	7.81	124.01	148.91
903 - 182	65.77	104.78	247.82	19.68	416.34	219.76	4.04	81.44	67.31
903 - 183	64.38	81.72	294.87	20.27	458.87	269.71	4.38	83.69	55.89
903 - 184	67.80	72.36	299.84	21.70	330.95	268.48	4.54	80.83	49.72
903 - 185	17.74	349.27	1686.88	11.82	0.00	830.58	5.97	203.94	138.35
903 - 186	25.91	937.98	1399.30	14.39	0.00	1521.35	11.00	281.47	98.10
903 - 187	11.58	188.65	2141.00	8.83	48.93	332.80	6.18	181.84	208.27
903 - 188	52.32	113.64	285.82	12.92	1096.68	520.92	8.42	197.79	110.90
903 - 189	15.38	24.50	41.68	3.57	22.16	634.03	2.20	65.44	221.26
903 - 190	102.58	93.90	1123.21	27.94	3944.16	160.31	6.53	242.57	87.85
903 - 200	17.10	5.30	0.00	2.07	74.88	160.43	1.31	45.81	266.15
903 - 201	19.78	5.99	0.00	2.93	117.04	159.67	1.72	46.71	268.70
903 - 202	21.74	7.05	0.00	3.34	144.20	254.68	2.15	47.22	274.80
903 - 203	21.05	7.25	0.00	4.01	154.06	224.85	2.06	45.31	267.31
903 - 204	23.82	9.75	0.00	3.98	179.59	249.98	2.25	45.20	269.82
903 - 205	26.23	12.62	0.00	4.43	280.52	279.53	2.63	45.71	274.05
903 - 206	27.26	14.99	0.00	4.97	282.40	269.71	2.70	47.45	274.43
903 - 207	38.51	22.84	0.33	10.04	506.54	343.91	3.40	47.60	274.51
903 - 208	33.57	33.97	0.00	8.86	424.11	270.40	2.94	44.95	263.01
903 - 209	102.82	100.04	167.37	30.65	307.69	396.87	3.23	81.04	142.27
903 - 210	22.11	19.97	0.00	4.45	0.00	355.20	2.80	48.37	256.20
903 - 211	39.88	22.12	0.00	9.91	124.13	172.44	3.56	43.90	224.34
903 - 212	68.20	129.32	101.41	19.76	776.57	471.46	4.30	89.32	82.58
903 - 213	34.76	270.85	378.97	8.71	881.46	47.35	7.30	185.65	14.79
903 - 215	8.68	1.50	0.00	0.45	0.00	227.05	0.97	44.76	155.55
903 - 216	98.84	232.86	184.11	29.41	493.56	135.60	6.54	123.52	21.88
903 - 217	11.34	2.88	0.00	0.61	0.00	83.05	0.96	32.13	198.59
903 - 218	48.67	185.51	174.08	12.98	680.55		4.65	96.96	61.82
903 - 219	93.27	148.02	190.91	28.04	571.48	225.11	4.07	83.79	60.16
903 - 220	52.49	249.59	148.88	13.88	734.88	128.25	9.36	136.04	60.67
903 - 221	10.12	1.34	0.00	2.88	0.00	344.12	1.99	54.87	256.20
903 - 222	10.32	1.21	0.00	0.21	0.00	380.96	1.54	46.28	229.75
903 - 223	29.35	116.49	137.72	5.17	3832.94	233.32	4.11	102.81	21.81
903 - 224	40.67	100.41	150.97	9.04	3088.55	174.49	3.66	90.96	18.18
903 - 225	57.61	141.62	197.70	15.69	4891.81	258.03	4.02	74.32	25.43
903 - 226	52.68	133.70	136.98	14.26	5007.36	242.81	4.39	71.48	48.40
903 - 227	29.61	38.99	96.99	6.43	2397.38	547.13	2.44	66.32	43.81
903 - 228	23.41	19.80	79.75	4.94	748.25	1067.22	2.17	63.86	65.51
903 - 229	21.27	6.57	0.00	3.00	0.00	326.07	2.32	44.56	180.93
903 - 230	17.58	6.51	0.00	3.23	0.00	292.85	1.94	44.50	192.09
903 - 232	61.59	144.81	327.65	16.62	2696.30	1188.63	10.59	220.16	166.27
903 - 233	57.88	107.20	117.29	15.75	1824.46	152.43	5.40	247.98	138.26
903 - 234	20.64	204.17	2021.52	11.95	0.00	883.76	6.76	167.46	146.38
903 - 235	19.84	161.20	1905.20	11.38	0.00	811.64	6.25	155.71	158.59
903 - 237	13.62	4.61	163.55	2.21	958.09	1462.35	4.26	86.96	49.25
903 - 239	21.22	23.90	216.04	5.54	1862.83	343.97	4.88	76.02	74.44
903 - 241	115.58	43.63	160.29	36.74	1141.01	183.10	5.20	56.40	20.39
903 - 245	26.68	388.72	1588.61	17.65	0.00	708.39	7.70	172.05	92.23
903 - 246	14.25	416.47	2049.01	13.88	0.00	494.00	7.83	182.40	76.42
903 - 249	25.06	18.85	87.39	7.55	1322.51	364.89	1.62	71.67	58.09
903 - 250	19.58	112.79	105.87	7.63	2405.65	70.89	2.12	199.19	50.75
903 - 251	17.79	151.39	191.64	8.66	3065.18	237.33	2.93	205.37	54.37
903 - 252	28.49	17.86	86.13	7.35	1240.93	444.14	1.94	72.25	64.38
903 - 253	46.90	62.40	98.37	16.05	2668.30	88.13	3.41	112.25	30.77

Table IV.2: ICP trace element analyses of ores and rocks. A IV.2 - 11

No.	Nd	Ni	P	Sm	Sr	V	Yb	Zn	Zr
903 - 254	32.88	61.44	50.55	8.71	2641.44	192.47	1.99	154.20	49.92
903 - 255	52.56	28.44	926.03	19.67	4292.48	51.53	4.49	65.75	50.71
903 - 256	52.10	28.13	1809.60	20.11	3898.00	37.33	4.30	93.92	38.03
903 - 259	54.19	85.40	299.45	16.78	897.55	154.95	2.04	97.90	17.01
903 - 260	56.15	86.34	311.19	16.66	1038.24	175.47	2.25	98.58	16.60
903 - 261	12.22	299.73	1307.21	10.43	91.27	727.77	8.37	281.27	125.31
903 - 262	12.07	293.46	878.23	9.26	13.71	584.86	6.96	242.90	140.56
903 - 263	35.92	191.09	150.59	7.76	4410.48	290.93	5.02	66.08	33.53
903 - 264	34.75	202.29	154.40	8.57	4392.43	315.58	4.22	66.80	57.72
903 - 265	26.29	64.89	168.45	6.00	326.57	471.19	3.31	71.55	11.16
903 - 266	66.18	55.19	200.55	23.30	854.30	273.72	4.81	75.46	15.10
903 - 268	36.36	43.10	854.68	12.52	2834.07	101.99	2.66	114.16	40.10
903 - 269	63.71	21.05	312.87	20.52	overrange	66.20	3.57	61.22	33.64
903 - 270	27.41	253.61	667.37	12.10	560.24	1170.60	4.95	115.61	65.06
903 - 271	24.30	47.46	1090.16	6.98	3151.07	363.05	2.70	205.08	53.19
903 - 272	28.03	70.71	670.39	7.37	overrange	296.05	2.99	135.70	28.00
903 - 273	33.79	86.94	772.57	9.60	overrange	515.95	4.67	120.90	35.16
903 - 274	71.23	108.68	165.28	20.68	277.23	228.48	3.46	82.10	101.61
903 - 275	60.08	129.24	171.72	16.89	402.52	204.03	2.99	86.25	89.89
903 - 276	24.25	444.75	2056.01	11.80	15.25	1528.78	8.43	123.53	115.60
903 - 277	15.46	495.31	934.13	16.51	0.00	1225.95	4.98	159.99	179.01
903 - 278	13.01	8.12	239.16	8.40	631.31	232.37	0.49	52.17	56.16
903 - 279	23.45	24.31	32.46	10.40	3106.71	51.39	1.76	74.38	41.62
903 - 280	19.55	310.51	1737.82	13.16	2000.12	207.47	3.22	136.63	41.24
903 - 281	28.68	314.49	305.61	13.75	1049.18	93.08	1.40	188.49	34.31
903 - 282	55.85	71.25	660.94	20.81	3026.28	70.94	6.47	32.28	30.99
903 - 283a	19.84	216.56	472.53	11.09	1458.98	125.60	1.06	168.11	22.86
903 - 283b	27.77	55.52	840.27	12.93	1159.61	53.82	1.30	97.81	31.67
903 - 283c	24.57	45.30	869.15	11.89	1160.01	57.69	1.28	96.70	31.91
903 - 283d	28.81	153.40	642.69	13.32	1778.89	75.43	1.75	113.29	30.58
903 - 283e	26.33	51.09	848.76	12.27	1216.36	63.51	1.39	103.28	32.82
903 - 284	29.00	60.73	769.42	14.65	316.52	1450.47	6.23	129.74	36.25
903 - 285	26.93	44.97	713.34	7.52	319.13	1265.06	5.88	111.30	28.97
903 - 286	33.73	59.66	733.05	10.61	398.10	1226.90	6.35	135.00	31.53
903 - 287	32.06	103.07	957.60	10.45	223.87	1521.63	7.19	141.24	38.92
903 - 290	60.66	20.16	636.79	20.08	2088.59	127.39	3.65	99.97	38.29
903 - 291	284.00	37.77	141.26	90.24	262.13	139.52	3.54	72.05	37.98
903 - 292	175.30	32.28	178.82	58.84	105.81	220.57	2.90	64.73	40.34
903 - 293	249.02	27.38	188.06	81.49	95.66	146.51	2.66	71.61	34.46
903 - 294	254.99	64.79	123.81	82.49	144.09	282.67	3.68	84.04	41.10
903 - 295	0.00	402.67	546.98	11.78	0.00	634.95	4.78	172.82	67.77
903 - 296	24.37	322.26	1491.95	12.28	10.58	664.94	6.02	251.52	109.73
903 - 297	53.76	126.63	232.49	19.55	392.51	242.35	2.22	102.40	66.01
903 - 298	21.83	24.98	413.35	6.96	460.44	132.37	2.93	99.48	31.91
903 - 299	23.12	27.31	731.23	7.18	433.20	138.25	2.04	114.13	41.75
903 - 300	157.96	79.85	133.90	51.97	178.21	568.89	2.92	76.41	28.22
903 - 301	244.33	87.78	164.72	80.71	99.47	900.62	4.67	100.78	28.19
903 - 302	315.72	34.45	162.86	98.26	110.53	1030.23	5.20	54.36	36.33
903 - 303	38.38	319.94	198.56	10.81	overrange	271.66	4.17	127.03	42.56
903 - 304	34.41	215.41	142.98	9.86	4396.58	193.38	3.51	105.54	47.31
903 - 305	43.08	233.43	198.06	12.71	4504.19	319.85	6.31	104.86	48.05
903 - 306	48.66	226.34	219.15	14.78	4333.08	347.51	7.40	97.24	74.63
903 - 307	53.84	255.85	265.23	16.48	4367.69	389.51	11.47	104.74	41.64
903 - 308	49.98	259.64	270.45	16.14	4141.53	327.99	10.12	109.32	40.09
903 - 309	44.63	248.95	215.43	13.81	4007.76	295.80	8.44	104.92	62.78
903 - 310	45.17	276.59	215.21	14.35	4442.90	334.53	7.21	98.18	81.05
903 - 311	50.35	254.72	244.94	15.74	4717.22	352.62	10.04	102.57	53.37
903 - 312a	51.67	266.36	320.44	16.39	5081.39	336.39	9.01	116.69	36.29
903 - 312b1	67.39	253.56	300.87	22.06	2927.25	263.33	7.37	103.70	33.54
903 - 312b2	51.96	255.17	309.48	14.15	4412.87	271.48	12.51	116.53	25.73

Table IV.2: ICP trace element analyses of ores and rocks.

No.	Nd	Ni	P	Sm	Sr	V	Yb	Zn	Zr
903 - 312b3	56.97	253.62	377.91	18.76	3681.32	247.85	7.22	122.18	37.56
903 - 312b4	62.11	233.35	354.15	19.24	4178.17	307.92	8.77	93.36	28.66
903 - 315b5	62.49	244.41	331.25	20.83	3470.30	253.31	7.92	119.44	28.35
903 - 313	52.68	236.97	348.05	15.54	overrange	387.18	6.56	114.25	62.07
903 - 314	47.82	263.13	258.66	13.61	overrange	367.82	5.74	112.49	68.21
903 - 315	38.62	276.05	218.28	10.79	5126.04	320.33	4.35	127.84	55.34
903 - 316	38.23	294.17	219.98	10.56	4715.03	300.55	4.63	131.03	56.96
903 - 317	39.22	372.16	177.88	10.96	overrange	350.76	6.09	145.65	59.98
903 - 318	42.64	482.86	179.67	11.54	overrange	345.79	5.82	168.46	56.09
903 - 319	33.83	476.45	178.93	8.15	overrange	308.87	6.75	188.19	39.00
903 - 320	38.57	522.90	176.70	9.77	overrange	317.53	5.84	197.04	48.26
903 - 321	37.26	561.37	166.58	8.84	overrange	316.76	6.97	213.32	50.12
903 - 322	42.87	554.58	172.95	10.99	overrange	389.37	9.36	204.28	40.30
903 - 323	45.71	442.94	212.20	12.83	overrange	332.48	6.93	169.40	41.57
903 - 324	37.34	17.12	43.87	10.86	690.53	528.75	4.03	61.54	229.63
903 - 325	37.09	10.72	25.83	11.70	505.15	699.63	4.18	57.98	231.18
903 - 326a	32.28	6.51	16.21	8.95	193.14	1470.64	5.57	55.87	248.79
903 - 326b	36.34	145.80	83.57	13.41	186.43	674.43	4.87	123.15	183.61
903 - 326c	27.35	8.33	24.74	11.41	92.06	1235.53	4.51	57.55	220.75
903 - 327	49.52	93.78	28.09	15.42	462.23	445.56	4.66	50.16	237.25
903 - 328	60.97	206.86	330.95	22.06	2522.78	159.73	4.76	82.20	85.56
903 - 329	51.71	197.89	333.43	18.86	1854.24	168.82	2.85	87.45	54.05
903 - 330	53.65	33.02	628.95	17.13	1346.58	295.96	4.85	109.60	31.27
903 - 331	50.18	24.06	207.54	14.95	1013.07	152.57	3.34	91.99	31.79
903 - 332	30.77	29.26	353.13	8.32	1144.12	160.07	2.97	101.14	21.67
903 - 333	62.63	32.15	476.95	17.95	1846.55	342.05	5.67	95.87	37.74
903 - 334	51.60	93.43	193.17	15.94	515.16	185.79	2.91	104.87	38.54
903 - 335	56.65	106.73	218.67	17.49	502.52	192.92	2.64	98.45	25.60
903 - 336	10.46	283.13	625.29	11.98	0.00	649.14	6.64	236.73	55.79
903 - 337	13.98	0.27	0.00	0.44	0.00	9.20	0.40	39.37	262.78
903 - 338	13.95	1.03	0.00	4.37	0.00	408.15	1.93	49.05	220.29
903 - 339	30.85	187.16	462.79	10.34	2328.23	177.60	5.88	195.77	42.44
903 - 340a	25.17	65.69	198.70	6.91	1573.43	467.03	7.41	129.51	34.55
903 - 340b	21.55	68.37	162.31	5.09	951.28	828.53	4.55	114.81	37.08
903 - 341a	39.28	28.48	256.76	10.80	610.92	130.68	2.35	83.45	15.38
903 - 342a	45.55	18.98	179.71	11.42	544.55	140.27	2.02	61.84	31.84
903 - 343	27.95	24.53	1226.13	8.54	1053.01	161.50	2.61	97.19	64.38
903 - 344	23.20	14.31	2581.53	6.83	544.93	165.43	1.42	63.36	80.99
903 - A	37.99	57.45	630.76	13.74	601.75	99.64	4.52	119.63	42.09
903 - B	194.02	8.80	67.11	57.55	1641.71	38.65	7.93	61.86	143.06
903 - B I.a	9.88	0.00	0.00	0.00	0.00	11.95	0.45	39.82	279.51
903 - B I.c	10.85	216.61	0.00	0.00	0.00	13.71	0.44	39.07	276.86
903 - B I.d1	13.08	0.00	0.00	0.00	0.00	12.93	0.64	39.53	279.23
903 - B I.d2	13.64	0.00	0.00	0.00	0.00	12.51	0.63	39.46	280.02
903 - B I.d3	14.86	6.41	0.00	0.00	0.00	13.09	0.71	40.38	280.00
903 - B I.d4	12.42	0.00	0.00	0.00	0.00	12.80	0.80	38.99	274.36
903 - B I.e	11.29	0.16	0.00	0.00	0.00	11.64	0.41	39.18	278.92
903 - B II.a	41.31	62.60	129.89	10.41	2587.69	170.95	3.10	74.55	18.17
903 - B II.c	44.06	74.65	140.53	11.10	2728.30	183.76	3.23	73.94	18.69
903 - B II.d1	46.76	69.90	142.53	11.08	2676.26	181.46	3.23	74.28	18.78
903 - B II.d2	42.28	71.42	141.69	9.91	2658.12	182.72	3.08	74.39	18.10
903 - B II.d3	43.42	68.85	135.29	11.17	2707.60	184.74	3.28	73.40	19.51
903 - B II.d4	44.00	73.03	136.10	11.18	2685.99	184.99	2.53	73.45	19.51
903 - B II.e	43.10	82.85	134.21	11.11	2680.86	181.19	3.23	74.23	18.48
903 - Mn 2	52.35	178.36	189.69	14.40	3531.25	295.95	4.05	95.21	32.18
903 - Mn 3	60.69	117.00	155.31	16.86	3068.98	321.20	4.48	89.42	48.97

ble IV.3: XRF trace element analyses of ores and rocks.

No.	As	Mo	Pb	Sc	Th	U	W
903 - 3	48	9.4	32	4.7	5	4	<5.0
903 - 4	54	21.0	41	2.5	6	6	25
903 - 5a	55	52.0	52	10.5	8	6	5
903 - 5b	1	2.5	6	15.0	15	4	30
903 - 6	34	47.0	30	4.0	1	8	85
903 - 7	32	40.0	23	10.5	0	6	60
903 - 8	31	41.0	26	4.8	3	8	60
903 - 9	86	69.0	63	10.5	0	6	55
903 - 10	32	42.0	37	8.1	2	8	50
903 - 11	43	46.0	44	7.6	6	12	25
903 - 12	48	47.0	37	7.7	8	12	45
903 - 13	32	37.0	24	4.8	6	11	55
903 - 14	44	46.0	46	9.9	4	12	30
903 - 15	48	45.0	57	15.2	3	10	35
903 - 16	36	42.0	48	13.1	5	13	75
903 - 17	26	34.0	25	6.3	2	12	125
903 - 18	55	47.0	72	14.3	2	6	40
903 - 19	41	35.0	59	13.7	5	9	50
903 - 20	2	2.3	13	13.1	12	1	15
903 - 21	50	32.0	57	13.5	9	5	25
903 - 22	73	74.0	72	12.3	6	52	15
903 - 23	37	56.0	42	8.0	5	9	40
903 - 24	39	27.0	50	13.1	5	6	20
903 - 25	48	5.8	33	28.0	11	5	20
903 - 26	1	2.7	2	1.7	2	0	1675
903 - 27	53	1.4	44	33.0	21	5	15
903 - 28a	32	2.3	31	21.0	17	4	10
903 - 28b	31	1.7	25	19.0	17	4	10
903 - 29	32	2.9	54	30.0	20	9	15
903 - 30	27	6.6	54	26.0	18	7	45
903 - 31a	12	3.7	16	16.6	10	4	100
903 - 31b	3	2.2	5	7.3	5	1	110
903 - 32	2	1.9	7	6.0	5	0	<5.0
903 - 33	39	101.0	63	3.3	4	14	<5.0
903 - 34	42	107.0	82	4.2	4	18	5
903 - 35	47	69.0	38	4.2	5	14	10
903 - 36	41	94.0	74	7.0	4	14	10
903 - 37	45	108.0	123	9.8	6	15	<5.0
903 - 38	51	98.0	107	9.1	5	14	10
903 - 39	51	101.0	112	10.4	6	15	5
903 - 40	51	99.0	120	11.8	4	14	10
903 - 41	72	69.0	56	4.8	6	13	<5.0
903 - 42	66	69.0	111	9.1	9	11	10
903 - 43	60	53.0	122	9.0	12	9	10
903 - 44	65	7.2	124	7.6	5	13	5
903 - 45	60	67.0	108	7.9	10	12	45
903 - 46	46	93.0	122	6.9	5	18	10
903 - 47	52	78.0	76	7.3	2	13	5
903 - 48	66	67.0	90	7.2	3	9	45
903 - 49	64	50.0	107	7.7	8	8	5
903 - 50	52	76.0	70	7.4	4	9	10
903 - 51	50	77.0	58	10.1	5	11	10
903 - 52	68	29.0	136	13.7	15	5	15
903 - 53	41	13.2	42	15.9	15	7	15
903 - 54	72	46.0	98	11.8	12	9	15
903 - 55	69	69.0	54	9.8	2	11	15
903 - 56	67	84.0	107	10.7	5	14	10
903 - 57	28	15.3	27	14.0	10	3	15
903 - 58	70	62.0	51	6.0	3	11	20
903 - 59	55	72.0	79	8.9	3	9	10
903 - 60	57	26.0	91	8.7	7	8	15
903 - 61	38	37.0	56	5.9	3	10	15
903 - 62	42	31.0	40	4.2	6	9	10
903 - 63	96	28.0	122	4.2	6	7	55
903 - 64	94	5.9	56	19.4	13	7	15
903 - 65a	68	4.9	82	19.3	16	9	20
903 - 65b	26	1.7	21	14.2	8	11	20
903 - 66	66	11.3	74	25.0	20	10	15
903 - 67	28	7.1	44	19.2	13	6	40
903 - 170a	1	2.8	4	2.3	1	0	405
903 - 170b	2	2.3	6	3.0	2	1	75
903 - 171a	1	1.1	5	2.2	3	1	270
903 - 171b	0	2.2	5	1.9	3	0	120
903 - 172	0	1.6	4	2.4	2	1	490
903 - 173	1	2.0	4	2.5	2	0	480
903 - 174	3	2.4	6	4.0	1	1	350
903 - 175	2	1.8	4	2.2	0	0	525
903 - 176	1	4.1	7	1.0	2	1	600
903 - 177	4	4.5	12	4.1	2	2	220
903 - 178	3	26.0	53	4.3	3	7	205
903 - 179	240	77.0	73	24.0	4	21	40
903 - 180	392	153.0	158	15.1	9	22	35
903 - 181	436	203.0	163	13.6	5	26	45
903 - 182	69	89.0	79	3.0	4	11	15
903 - 183	85	125.0	66	3.3	4	11	50
903 - 184	90	120.0	58	2.9	6	8	15
903 - 185	371	98.0	62	13.0	1	16	15
903 - 186	228	67.0	103	13.4	5	15	20
903 - 187	85	45.0	94	12.4	8	9	10
903 - 188	12	17.4	56	15.2	8	10	10
903 - 189	52	17.7	63	24.0	17	7	30
903 - 190	22	9.3	129	33.0	4	9	75
903 - B I.a	2	4.1	12	14.2	15	3	10
903 - B II.a	31	41.0	25	7.4	4	11	75
903 - B III.	45	62.0	30	9.5	4	8	10
903 - B IV.	48	58.0	34	9.1	4	10	<5.0
903 - B 141	4	3.9	10	22.0	20	2	10
903 - B 168	38	17.5	34	13.4	5	6	80
903 - B 169	55	27.0	55	8.1	11	3	80
903 - B 191	39	106.0	74	5.0	3	13	<5.0
Mn 2	52	49.0	52	9.9	6	10	5

Table IV.4: INAA trace element analyses of selected ore samples.

No.	Ba	Ce	Co	Cr	Cs	Eu	FeO %	Gd	Hf	Ho	La	Lu	Mo
903 - 20	45	18.5	2	54	0.5	0.25	0.96	1.0	6.0	0.6	18.0	0.30	2
903 - 22	0.022	99.0	90	33	1.1	2.00	7.20	5.8	1.2	1.1	29.0	0.33	54
903 - 23	0.015	63.0	102	4	2.7	2.60	1.37	9.5	0.5	1.9	53.0	0.73	41
903 - 63	1650	250.0	36	27	0.1	10.40	4.60	29.0	1.0	2.8	67.0	0.48	22
903 - 76	0.011	46.0	99	7	2.6	1.56	1.70	7.2	1.2	2.4	27.0	1.10	65
903 - 108	0.02	75.0	230	14	1.4	6.80	2.60	26.0	1.0	4.9	64.0	1.55	52
903 - 164	1150	44.0	104	3	0.4	1.07	0.68	3.7	0.4	1.1	12.8	0.57	5
903 - 188	1200	178.0	360	22	1.1	3.30	2.90	11.0	1.8	3.1	42.0	1.25	16

No.	Na2O %	Nd	Sb	Sc	Sm	Ta	Tb	Th	U	W	Yb	Zr	
903 - 20	0.03	8.0	0.8	8	1.4	0.8	0.16	11.5	1.2	12	1.7	240	
903 - 22	0.07	34.0	2.1	13	8.2	<0.1	0.99	4.7	1.4	14	2.5	102	
903 - 23	0.17	45.0	1.3	7	10.3	<0.1	1.60	1.9	1.5	25	4.8	65	
903 - 63	0.05	159.0	1.1	6	46.0	0.2	4.70	3.4	0.7	48	3.8	137	
903 - 76	0.20	23.0	1.8	8	5.6	0.2	1.20	3.3	1.4	10	6.3	96	
903 - 108	0.16	80.0	2.8	9	24.0	<0.1	4.30	3.8	1.4	15	11.0	125	
903 - 164	0.15	17.6	<0.1	19	4.6	0.2	0.69	5.4	1.7	1	3.5	70	
903 - 188	0.12	47.0	0.2	11	12.7	0.3	2.10	6.4	1.9	11	7.8	137	

	Al2O3	As	B	BaO	CaO	Ce	Co	Cr	Cu	Eu	Fe	Gd
Al2O3	1.000	-0.014	-0.136	-0.286	-0.356	0.113	-0.409	0.642	-0.279	-0.433	0.283	0.176
As		1.000	0.390	-0.065	-0.118	0.130	-0.056	-0.005	0.539	-0.095	0.807	0.827
B			1.000	0.098	0.079	0.261	0.142	-0.192	0.219	0.327	0.079	0.221
BaO				1.000	0.416	0.137	0.356	-0.319	0.232	0.535	-0.317	-0.131
CaO					1.000	0.228	0.603	-0.356	0.428	0.714	-0.363	-0.047
Ce						1.000	0.260	0.053	0.174	0.411	0.052	0.209
Co							1.000	-0.354	0.509	0.573	-0.232	-0.015
Cr								1.000	-0.261	-0.477	0.396	0.293
Cu									1.000	0.405	0.294	0.492
Eu										1.000	-0.454	-0.082
Fe											1.000	0.909
Gd												1.000
K2O												
La												
LOI												
MgO												
Mn												
Mo												
Na2O												
Nd												
Ni												
P												
Pb												
Sc												
SiO2												
Sm												
SrO												
Th												
TiO2												
U												
V												
Yb												
Zn												
Zr												

Table IV.5: Element correlation matrix for ore and rock samples (n=365).

	K2O	La	LOI	MgO	Mn	Mo	Na2O	Nd	Ni	P	Pb	Sc
Al2O3	-0.229	-0.367	0.226	-0.370	-0.486	-0.328	-0.371	-0.328	-0.331	-0.084	0.023	0.660
As	-0.130	0.048	0.302	-0.083	-0.069	0.644	-0.120	0.076	0.268	0.751	0.555	0.182
B	-0.006	0.401	0.271	0.026	0.358	0.526	-0.018	0.371	0.065	0.236	0.320	-0.128
BaO	0.258	0.577	0.385	0.560	0.644	0.311	0.543	0.469	0.285	-0.105	0.196	-0.151
CaO	0.592	0.641	0.541	0.735	0.706	0.383	0.702	0.598	0.621	0.071	0.408	-0.116
Ce	0.197	0.298	0.275	-0.145	0.218	0.047	-0.105	0.538	-0.064	0.145	0.373	0.391
Co	0.574	0.558	0.292	0.428	0.530	0.294	0.470	0.464	0.366	0.128	0.268	-0.083
Cr	-0.248	-0.437	0.000	-0.381	-0.484	-0.338	-0.369	-0.399	-0.315	-0.060	-0.086	0.709
Cu	0.281	0.385	0.453	0.352	0.369	0.641	0.303	0.374	0.572	0.503	0.571	0.010
Eu	0.455	0.828	0.491	0.610	0.861	0.358	0.567	0.940	0.439	-0.034	0.358	-0.268
Fe	-0.245	-0.314	0.136	-0.352	-0.454	0.257	-0.353	-0.270	0.124	0.714	0.358	0.485
Gd	-0.076	0.016	0.429	-0.063	-0.116	0.461	-0.094	0.088	0.375	0.751	0.597	0.475
K2O	1.000	0.651	0.424	0.411	0.568	0.082	0.664	0.446	0.111	0.050	0.087	0.019
La		1.000	0.660	0.666	0.907	0.457	0.720	0.827	0.369	0.033	0.359	-0.181
LOI			1.000	0.587	0.604	0.533	0.566	0.555	0.524	0.280	0.652	0.297
MgO				1.000	0.719	0.522	0.902	0.495	0.705	-0.054	0.368	-0.270
Mn					1.000	0.475	0.733	0.800	0.453	-0.046	0.294	-0.339
Mo						1.000	0.404	0.362	0.606	0.510	0.648	-0.179
Na2O							1.000	0.487	0.541	-0.072	0.239	-0.219
Nd								1.000	0.354	0.071	0.459	-0.128
Ni									1.000	0.343	0.559	-0.173
P										1.000	0.530	0.189
Pb											1.000	0.211
Sc												1.000
SiO2												
Sm												
SrO												
Th												
TiO2												
U												
V												
Yb												
Zn												
Zr												

Table IV.5: Element correlation matrix for ore and rock samples (n=365).

	SiO2	Sm	SrO	Th	TiO2	U	V	Yb	Zn	Zr
Al2O3	0.096	-0.324	-0.329	0.837	0.983	-0.147	0.133	-0.276	-0.284	0.940
As	-0.389	0.235	-0.074	-0.022	-0.027	0.515	0.720	0.365	0.400	0.160
B	-0.412	0.426	-0.016	-0.114	-0.156	0.266	0.204	0.210	0.143	-0.120
BaO	-0.526	0.450	0.425	-0.355	-0.345	0.318	0.021	0.324	0.158	-0.418
CaO	-0.542	0.557	0.818	-0.222	-0.367	0.358	-0.032	0.692	0.615	-0.439
Ce	-0.312	0.539	-0.099	0.219	0.104	0.191	0.096	0.103	0.061	0.082
Co	-0.382	0.449	0.465	-0.350	-0.423	0.270	0.041	0.550	0.463	-0.460
Cr	0.148	-0.337	-0.351	0.745	0.635	-0.101	0.175	-0.273	-0.281	0.716
Cu	-0.543	0.474	0.419	-0.228	-0.284	0.504	0.587	0.711	0.692	-0.181
Eu	-0.632	0.908	0.560	-0.360	-0.464	0.258	-0.063	0.546	0.402	-0.567
Fe	-0.135	-0.088	-0.306	0.278	0.282	0.296	0.720	0.171	0.271	0.498
Gd	-0.456	0.277	-0.018	0.224	0.156	0.431	0.796	0.480	0.508	0.356
K2O	-0.477	0.362	0.371	-0.169	-0.273	0.240	-0.082	0.439	0.336	-0.362
La	-0.798	0.772	0.542	-0.311	-0.435	0.418	0.013	0.612	0.436	-0.523
LOI	-0.898	0.570	0.569	0.213	0.157	0.571	0.393	0.719	0.621	0.118
MgO	-0.576	0.446	0.937	-0.293	-0.413	0.448	0.014	0.737	0.527	-0.468
Mn	-0.782	0.750	0.624	-0.399	-0.536	0.393	-0.057	0.584	0.461	-0.644
Mo	-0.631	0.445	0.521	-0.292	-0.342	0.665	0.489	0.728	0.598	-0.252
Na2O	-0.590	0.413	0.815	-0.304	-0.423	0.361	-0.048	0.689	0.459	-0.504
Nd	-0.695	0.966	0.433	-0.251	-0.367	0.308	0.049	0.516	0.381	-0.451
Ni	-0.540	0.433	0.782	-0.253	-0.338	0.475	0.428	0.843	0.838	-0.290
P	-0.343	0.219	0.030	-0.097	-0.070	0.407	0.547	0.436	0.565	0.085
Pb	-0.588	0.517	0.474	0.111	-0.018	0.559	0.627	0.668	0.628	0.103
Sc	-0.097	-0.075	-0.204	0.702	0.652	0.104	0.344	-0.007	-0.010	0.704
SiO2	1.000	-0.743	-0.502	0.054	0.164	-0.618	-0.408	-0.742	-0.641	0.178
Sm		1.000	0.389	-0.238	-0.361	0.354	0.204	0.572	0.451	-0.397
SrO			1.000	-0.240	-0.351	0.418	0.072	0.774	0.643	-0.386
Th				1.000	0.836	-0.065	0.164	-0.197	-0.213	0.838
TiO2					1.000	-0.173	0.108	-0.305	-0.294	0.945
U						1.000	0.417	0.610	0.513	-0.091
V							1.000	0.480	0.469	0.282
Yb								1.000	0.859	-0.258
Zn									1.000	-0.227
Zr										1.000

Table IV.5: Element correlation matrix for ore and rock samples (n=365).

Appendix V.

Table V.1: Mineral Normalization Results from Ores and Rocks; [%].

Table V.2: Microbiological Leaching of Mn Ores from Groote Eylandt.

Table V.3: Battery-activity Data and Mineral Norm of Samples.

Table V.1: Mineral normalization results from ores and rocks.

No.	Anatase	Quartz	Kaolinite	Gibbsite	Goethite	Hematite	Cryptomelane
903 - 3	0.192	0.000	16.979	0.301	1.292	0.000	2.050
903 - 4	0.075	0.000	5.303	0.510	0.000	0.000	4.758
903 - 5a	0.406	0.558	37.601	0.000	1.688	0.000	2.066
903 - 5b	1.145	11.571	86.809	0.000	0.000	0.000	0.000
903 - 6	0.066	0.000	3.747	5.152	0.523	0.000	15.585
903 - 7	0.091	0.000	5.903	5.106	0.585	0.000	9.324
903 - 8	0.075	0.000	4.811	4.427	0.500	0.000	18.661
903 - 9	0.091	0.000	7.736	2.279	1.515	0.000	5.821
903 - 10	0.105	0.000	11.085	1.992	0.669	0.000	21.166
903 - 11	0.109	0.000	11.989	1.682	0.717	0.000	19.506
903 - 12	0.116	0.000	12.694	1.781	0.697	0.000	17.255
903 - 13	0.085	0.000	11.301	0.250	0.580	0.000	22.276
903 - 14	0.116	0.000	13.631	1.913	0.671	0.000	18.177
903 - 15	0.204	0.367	21.503	0.000	3.740	0.000	13.452
903 - 16	0.110	0.000	7.931	2.949	0.917	0.000	20.859
903 - 17	0.080	0.000	10.366	0.997	0.528	0.000	25.864
903 - 18	0.204	0.000	19.953	0.518	1.700	0.000	12.062
903 - 19	0.173	0.000	18.347	0.988	2.352	0.000	20.621
903 - 20	0.739	42.713	56.070	0.000	0.000	0.000	0.000
903 - 21	0.708	15.408	60.706	0.000	11.918	0.000	1.553
903 - 22	0.222	1.528	20.701	0.000	5.326	0.000	5.960
903 - 23	0.113	0.000	13.923	0.175	0.704	0.000	15.760
903 - 24	0.669	16.045	63.957	0.000	9.154	0.000	1.245
903 - 25	0.539	20.995	47.425	0.000	18.438	0.000	3.533
903 - 26	0.069	95.198	4.575	0.000	0.000	0.426	0.301
903 - 27	0.782	7.885	65.146	0.000	19.874	5.525	0.000
903 - 28a	0.879	14.047	73.745	0.000	5.755	4.106	0.000
903 - 28b	0.972	11.663	78.200	0.000	1.353	7.001	0.000
903 - 29	0.883	24.413	60.210	0.000	10.786	0.895	0.888
903 - 30	0.616	35.244	51.886	0.000	10.648	0.056	0.487
903 - 31a	0.397	62.802	31.105	0.000	4.657	0.000	0.378
903 - 31b	0.322	78.929	18.811	0.000	0.905	0.000	0.361
903 - 32	0.250	81.069	12.529	0.000	1.263	0.000	0.354
903 - 33	0.088	0.116	8.672	0.000	1.104	0.000	15.166
903 - 34	0.075	0.000	6.229	0.233	1.083	0.000	15.725
903 - 35	0.106	0.000	9.318	0.644	0.532	0.000	9.515
903 - 36	0.083	0.000	6.341	0.455	1.004	0.000	13.717
903 - 37	0.100	0.267	7.473	0.000	1.597	0.000	16.476
903 - 38	0.155	0.902	13.428	0.000	2.203	0.000	14.663
903 - 39	0.128	0.539	10.441	0.000	1.803	0.000	15.343
903 - 40	0.114	0.439	9.078	0.000	1.838	0.000	15.981
903 - 41	0.070	0.877	5.581	0.000	1.036	0.000	6.608
903 - 42	0.282	2.936	25.739	0.000	3.180	0.000	10.702
903 - 43	0.438	5.795	40.091	0.000	4.486	0.000	8.196
903 - 44	0.206	2.916	21.668	0.000	2.605	0.000	12.243
903 - 45	0.387	2.372	35.883	0.000	3.194	0.000	9.535
903 - 46	0.117	0.627	10.970	0.000	1.741	0.000	15.241
903 - 47	0.092	1.667	8.502	0.000	1.171	0.000	9.424
903 - 48	0.100	8.464	9.101	0.000	2.178	0.000	9.954
903 - 49	0.401	5.625	37.644	0.000	2.613	0.000	6.571
903 - 50	0.115	0.644	10.018	0.000	0.935	0.000	9.957
903 - 51	0.100	0.000	8.435	0.068	0.973	0.000	10.932
903 - 52	0.588	4.922	59.896	0.000	9.019	0.000	2.792
903 - 53	1.012	10.371	77.828	0.000	6.305	1.423	1.554
903 - 54	0.387	2.249	37.324	0.000	3.078	0.000	3.833
903 - 55	0.112	0.110	9.835	0.000	0.991	0.000	6.438
903 - 56	0.138	0.293	11.299	0.000	1.847	0.000	10.264
903 - 57	0.770	12.799	73.915	0.000	4.985	0.000	0.000
903 - 58	0.149	0.287	15.204	0.000	2.116	0.000	4.661
903 - 59	0.188	0.000	17.558	0.107	1.094	0.000	7.807
903 - 60	0.275	1.253	28.762	0.000	4.253	0.000	3.380
903 - 61	0.096	0.000	7.001	1.214	0.744	0.000	9.184
903 - 62	0.134	0.014	13.028	0.000	1.207	0.000	3.277
903 - 63	0.170	0.000	11.007	0.154	3.586	0.000	4.666
903 - 64	0.654	4.836	61.369	0.000	19.421	0.000	2.236
903 - 65a	0.637	4.961	58.998	0.000	22.112	0.000	3.177
903 - 65b	0.196	0.000	8.692	3.824	1.363	0.000	39.807
903 - 66	0.583	0.319	61.410	0.000	13.897	0.000	6.627
903 - 67	0.472	32.971	41.113	0.000	6.570	0.000	4.661

No.	Anatase	Quartz	Kaolinite	Gibbsite	Goethite	Hematite	Cryptomelane
903 - 68a	0.131	21.232	10.444	0.000	1.459	0.000	4.926
903 - 68b	0.127	5.530	12.343	0.000	0.942	0.000	6.193
903 - 69	0.147	3.542	13.956	0.000	0.788	0.000	5.922
903 - 70	0.160	3.345	16.954	0.000	0.794	0.000	5.727
903 - 71	0.113	0.646	11.301	0.000	0.780	0.000	5.712
903 - 72	0.133	1.106	11.196	0.000	1.275	0.000	6.248
903 - 73	0.147	1.707	15.063	0.000	0.855	0.000	5.547
903 - 74	0.231	3.644	23.879	0.000	1.045	0.000	6.301
903 - 75	0.198	1.167	18.520	0.000	0.819	0.000	7.903
903 - 76	0.207	0.682	20.944	0.000	0.764	0.000	8.033
903 - 77a	0.131	0.000	10.290	1.660	0.980	0.000	8.799
903 - 77b	0.071	0.899	8.831	0.000	0.658	0.000	9.296
903 - 78	0.106	0.027	9.001	0.000	0.944	0.000	7.720
903 - 79	0.553	44.171	44.676	0.000	5.529	0.000	2.553
903 - 80	0.103	3.629	8.239	0.000	1.128	0.000	6.940
903 - 81	0.110	9.271	7.583	0.000	1.240	0.000	6.138
903 - 82	0.136	11.853	10.878	0.000	1.321	0.000	7.309
903 - 83	0.108	7.420	7.788	0.000	1.114	0.000	4.972
903 - 84	0.122	23.908	10.052	0.000	1.144	0.000	5.479
903 - 85	0.073	0.000	6.696	0.939	0.536	0.000	13.292
903 - 86	0.151	8.842	11.735	0.000	1.911	0.000	16.950
903 - 87	0.387	16.374	33.808	0.000	9.741	0.000	10.614
903 - 88	0.168	4.455	17.633	0.000	1.385	0.000	8.676
903 - 89	0.213	6.100	16.419	0.000	2.255	0.000	12.210
903 - 90	0.615	3.397	67.124	0.000	18.161	0.000	0.752
903 - 91	0.160	5.572	13.913	0.000	1.484	0.000	9.542
903 - 92	0.157	2.535	13.904	0.000	1.544	0.000	10.747
903 - 93	0.159	1.469	12.420	0.000	1.612	0.000	11.010
903 - 94	0.144	0.575	11.726	0.000	1.413	0.000	10.795
903 - 95	0.129	0.000	9.419	0.683	1.372	0.000	13.201
903 - 96	0.108	0.000	5.719	1.438	1.378	0.000	15.093
903 - 97	0.117	0.000	7.441	1.044	1.451	0.000	14.925
903 - 98	0.091	0.000	5.241	1.618	1.255	0.000	12.370
903 - 99	0.137	0.094	10.636	0.000	1.837	0.000	16.069
903 - 100	0.128	0.000	8.890	2.303	2.338	0.000	19.529
903 - 101	0.089	0.000	4.626	3.647	1.720	0.000	22.357
903 - 102	0.085	0.000	8.436	1.184	1.278	0.000	14.787
903 - 103	0.074	0.000	4.767	1.830	1.237	0.000	8.093
903 - 104	0.168	7.339	13.686	0.000	2.101	0.000	4.366
903 - 105	0.090	0.000	7.886	1.106	0.734	0.000	4.543
903 - 106	0.086	0.000	6.819	2.084	0.725	0.000	9.444
903 - 107	0.113	0.000	10.505	1.032	1.001	0.000	10.907
903 - 108	0.129	0.863	14.262	0.000	1.726	0.000	13.906
903 - 109	0.116	0.000	10.328	1.677	1.461	0.000	6.819
903 - 110	0.372	8.401	35.017	0.000	9.286	0.000	4.356
903 - 111	0.075	0.000	6.943	1.403	1.066	0.000	5.673
903 - 112	0.264	3.199	26.669	0.000	3.309	0.000	3.661
903 - 113	0.435	2.222	43.066	0.000	38.713	0.000	0.924
903 - 114	0.249	70.665	18.340	0.000	2.476	0.000	1.098
903 - 115a	0.345	68.079	30.882	0.000	0.000	0.000	0.005
903 - 115b	0.241	59.488	20.849	0.000	18.794	0.015	0.102
903 - 116a	0.181	35.080	11.113	0.000	2.256	0.000	21.365
903 - 116b	0.129	24.905	9.669	0.000	5.023	0.000	17.922
903 - 117b	0.175	2.679	9.414	0.000	2.117	0.000	30.871
903 - 118a	0.106	3.658	9.786	0.000	28.138	0.000	19.957
903 - 118b	0.488	44.154	46.136	0.000	1.820	0.000	1.069
903 - 119	0.170	9.457	11.521	0.000	1.354	0.000	28.558
903 - 120	0.209	10.419	21.586	0.000	1.838	0.000	7.376
903 - 121	0.206	3.328	14.654	0.000	2.509	0.000	10.474
903 - 122	0.247	10.979	20.315	0.000	2.417	0.000	7.889
903 - 123	0.094	5.554	12.172	0.000	0.887	0.000	13.137
903 - 124	0.781	0.341	65.909	0.000	4.532	0.000	6.421
903 - 125	0.870	1.430	71.631	0.000	4.401	0.000	4.406
903 - 126	0.895	1.919	74.761	0.000	4.539	0.000	2.849
903 - 127	0.877	2.414	74.636	0.000	11.700	0.000	1.264
903 - 128	0.979	5.050	76.378	0.000	10.802	0.000	0.683
903 - 129	1.137	6.193	79.969	0.000	7.964	0.310	0.132
903 - 130	0.936	0.053	72.439	0.000	5.749	0.000	3.046
903 - 131	1.037	2.657	75.145	0.000	5.245	0.000	2.106

No.	Anatase	Quartz	Kaolinite	Gibbsite	Goethite	Hematite	Cryptomelane
903 - 132	0.968	10.729	69.189	0.000	13.287	0.000	1.563
903 - 133	1.061	7.432	80.411	0.000	7.300	0.000	0.000
903 - 134	1.010	16.316	70.124	0.000	7.074	2.060	0.475
903 - 135	1.092	5.677	75.572	0.000	10.618	0.162	0.936
903 - 136	0.990	13.869	70.327	0.000	8.378	1.478	1.450
903 - 137	0.961	11.582	74.280	0.000	7.123	2.377	1.140
903 - 138	0.911	6.194	72.973	0.000	11.190	0.000	2.175
903 - 139	0.880	9.968	73.570	0.000	9.711	2.376	0.765
903 - 140	0.691	44.514	48.248	0.000	2.692	0.000	0.693
903 - 141a	1.074	8.555	90.268	0.000	0.000	0.000	0.000
903 - 141b	0.835	7.038	88.389	0.000	2.617	0.000	0.000
903 - 141c	0.717	12.075	81.915	0.000	3.194	0.000	0.000
903 - 141 B	1.141	9.622	89.012	0.000	0.000	0.000	0.000
903 - 142	0.208	0.000	14.353	3.816	2.043	0.000	16.031
903 - 143	0.128	0.000	14.211	3.778	1.310	0.000	16.599
903 - 144	0.080	0.000	8.137	4.338	1.114	0.000	16.010
903 - 145	0.093	1.089	10.611	0.000	0.817	0.000	11.910
903 - 146	0.116	0.000	12.239	5.117	1.190	0.000	19.955
903 - 147	0.118	0.000	12.469	1.288	1.212	0.000	15.666
903 - 148	0.107	0.000	10.106	0.938	14.157	0.000	12.094
903 - 149	0.268	1.274	23.428	0.000	8.984	0.000	16.346
903 - 150	0.081	0.000	6.513	2.074	0.866	0.000	9.933
903 - 151	0.210	0.000	20.335	0.811	2.505	0.000	13.368
903 - 152a	0.273	0.000	24.510	2.512	7.202	0.000	13.955
903 - 152b	0.161	0.000	13.792	3.140	16.419	0.000	14.319
903 - 153	0.218	0.000	16.710	3.027	3.556	0.000	24.180
903 - 154	0.274	0.000	21.951	1.273	3.061	0.000	16.281
903 - 155	0.073	28.902	7.013	0.000	3.984	0.000	17.621
903 - 156	0.299	52.518	25.791	0.000	16.404	0.608	2.613
903 - 157	0.069	41.914	7.598	0.000	36.066	0.000	5.991
903 - 158	0.223	46.448	21.105	0.000	26.574	0.000	2.704
903 - 159	0.107	49.559	9.876	0.000	26.507	0.000	4.878
903 - 160	0.045	16.409	3.562	0.000	0.746	0.000	0.942
903 - 161	0.096	33.080	7.074	0.000	1.165	0.000	4.970
903 - 162	0.106	44.871	6.944	0.000	2.609	0.000	27.487
903 - 164	0.236	17.606	17.676	0.000	0.745	0.000	39.260
903 - 168 B	0.172	0.000	19.025	2.434	1.367	0.000	19.409
903 - 169 B	0.170	0.000	14.540	2.504	1.795	0.000	14.187
903 - 170a	0.038	97.093	2.696	0.000	0.000	0.338	0.346
903 - 170b	0.114	89.503	9.135	0.000	0.081	0.000	0.791
903 - 171a	0.049	96.204	3.264	0.000	0.000	0.190	0.486
903 - 171b	0.044	96.793	2.658	0.000	0.123	0.005	0.448
903 - 172	0.038	96.883	2.433	0.000	0.146	0.000	0.470
903 - 173	0.037	97.148	2.390	0.000	0.000	0.222	0.678
903 - 174	0.046	95.084	2.434	0.000	0.255	0.000	1.240
903 - 175	0.030	96.238	1.808	0.000	0.163	0.000	1.028
903 - 176	0.037	95.259	1.764	0.000	0.264	0.000	1.534
903 - 177	0.109	87.330	8.399	0.000	0.309	0.000	1.999
903 - 178	0.081	55.854	6.182	0.000	0.239	0.000	16.488
903 - 179	0.368	2.009	31.646	0.000	62.427	0.000	0.585
903 - 180	0.337	0.000	14.362	10.176	66.483	0.000	3.750
903 - 181	0.301	0.000	13.917	7.966	57.100	0.000	6.023
903 - 182	0.149	0.000	12.855	0.170	1.750	0.000	2.182
903 - 183	0.146	0.000	11.402	0.911	1.443	0.000	3.236
903 - 184	0.141	0.000	10.820	0.819	2.445	0.000	2.459
903 - 185	0.360	0.000	16.592	11.108	65.388	4.128	0.813
903 - 186	0.241	0.000	13.835	5.883	75.321	3.066	0.650
903 - 187	0.567	0.000	37.459	5.256	49.280	1.629	6.043
903 - 188	0.327	0.000	23.552	2.414	2.045	0.000	26.560
903 - 189	0.676	22.652	53.008	0.000	17.440	0.000	1.035
903 - 191B	0.078	0.000	5.508	0.773	1.052	0.000	16.267
903 - 190	0.279	3.471	22.745	0.000	2.478	0.000	18.749
903 - 200	1.125	18.136	74.695	0.000	1.612	1.671	0.271
903 - 201	1.129	16.541	75.426	0.000	2.302	1.281	0.435
903 - 202	1.076	16.553	71.832	0.000	4.046	1.417	0.901
903 - 203	1.129	15.434	73.099	0.000	4.276	1.027	0.552
903 - 204	1.142	12.526	74.017	0.000	6.137	0.000	0.611
903 - 205	1.162	8.615	76.398	0.000	6.551	0.006	1.116
903 - 206	1.116	6.202	76.860	0.000	5.963	0.000	1.083

No.	Anatase	Quartz	Kaolinite	Gibbsite	Goethite	Hematite	Cryptomelane
903 - 207	1.016	2.305	73.159	0.000	7.118	0.000	3.280
903 - 208	0.979	1.709	76.687	0.000	5.588	0.000	2.672
903 - 209	0.264	3.530	16.100	0.000	2.253	0.000	7.775
903 - 210	0.898	10.140	73.200	0.000	10.217	2.595	0.795
903 - 211	0.773	23.152	60.820	0.000	6.862	0.000	0.784
903 - 212	0.288	2.689	25.543	0.000	3.052	0.000	13.965
903 - 213	0.052	0.000	4.307	3.654	0.515	0.000	21.421
903 - 215	0.569	44.799	43.283	0.000	9.560	0.854	0.099
903 - 216	0.074	0.000	7.492	2.207	0.728	0.000	9.129
903 - 217	0.697	35.388	55.878	0.000	5.154	0.321	0.630
903 - 218	0.208	0.000	19.386	1.822	1.782	0.000	13.242
903 - 219	0.191	0.265	15.231	0.000	1.440	0.000	8.853
903 - 220	0.179	0.000	18.648	3.513	1.393	0.000	14.700
903 - 221	0.924	10.409	72.729	0.000	9.306	5.875	0.000
903 - 222	0.835	19.392	68.172	0.000	6.173	4.556	0.000
903 - 223	0.067	0.000	3.554	5.200	0.646	0.000	21.427
903 - 224	0.067	0.000	4.540	4.841	0.505	0.000	15.177
903 - 225	0.077	0.000	7.379	2.799	0.586	0.000	13.082
903 - 226	0.141	0.000	16.102	1.209	0.865	0.000	15.868
903 - 227	0.177	0.000	14.465	0.875	2.207	0.000	14.770
903 - 228	0.241	0.075	18.895	0.000	4.066	0.000	13.840
903 - 229	0.536	35.686	48.552	0.000	13.018	0.000	0.384
903 - 230	0.585	33.973	50.960	0.000	11.980	0.000	0.623
903 - 232	0.378	0.000	27.973	2.138	3.147	0.000	19.309
903 - 233	0.461	0.000	33.524	0.823	0.484	0.000	23.657
903 - 234	0.335	0.000	20.352	6.563	71.174	0.000	0.273
903 - 235	0.390	0.000	19.664	8.729	68.101	1.084	0.813
903 - 237	0.075	52.195	6.018	0.000	0.000	0.000	18.385
903 - 239	0.165	31.422	10.483	0.000	3.986	0.000	24.933
903 - 241	0.089	0.000	5.288	3.307	0.801	0.000	8.908
903 - 245	0.187	0.000	6.687	6.805	78.191	2.532	2.808
903 - 246	0.133	0.000	4.489	5.106	85.200	1.041	1.330
903 - 249	0.229	0.000	17.279	1.729	2.135	0.000	21.415
903 - 250	0.110	0.000	10.610	1.223	31.561	0.000	12.623
903 - 251	0.096	5.948	7.311	0.000	43.983	0.000	9.527
903 - 252	0.247	0.000	19.419	0.676	3.893	0.000	19.066
903 - 253	0.126	2.767	13.356	0.000	0.243	0.000	25.229
903 - 254	0.068	46.563	6.003	0.000	1.006	0.000	17.481
903 - 255	0.139	1.845	9.116	0.000	20.047	0.000	33.471
903 - 256	0.083	2.960	5.967	0.000	27.405	0.000	25.939
903 - 259	0.060	3.561	8.309	0.000	0.393	0.000	16.028
903 - 260	0.060	3.082	7.225	0.000	0.542	0.000	18.658
903 - 261	0.274	0.000	13.888	7.766	68.211	0.000	3.536
903 - 262	0.333	0.000	23.803	6.318	62.157	2.082	2.050
903 - 263	0.124	0.000	7.413	4.243	2.392	0.000	12.295
903 - 264	0.200	0.000	12.575	4.228	1.365	0.000	9.391
903 - 265	0.030	0.000	2.265	0.085	0.465	0.000	0.345
903 - 266	0.053	0.000	4.110	0.814	0.530	0.000	3.006
903 - 268	0.154	0.610	9.729	0.000	7.271	0.000	49.013
903 - 269	0.146	0.000	7.567	1.303	4.297	0.000	40.260
903 - 270	0.169	0.000	8.754	3.464	38.652	0.000	30.446
903 - 271	0.181	0.000	9.041	2.007	5.914	0.000	47.357
903 - 272	0.069	0.000	3.123	2.607	1.447	0.000	27.803
903 - 273	0.091	0.000	3.070	3.273	1.423	0.000	28.939
903 - 274	0.310	1.329	27.611	0.000	2.071	0.000	0.547
903 - 275	0.265	1.158	23.683	0.000	1.959	0.000	1.163
903 - 276	0.245	0.000	22.411	3.713	61.620	0.000	1.966
903 - 277	0.230	32.183	20.098	0.000	36.076	0.000	1.467
903 - 278	0.113	48.235	11.076	0.000	1.068	0.000	11.124
903 - 279	0.066	42.093	9.052	0.000	0.151	0.000	16.580
903 - 280	0.090	0.000	5.816	2.098	26.164	0.000	23.921
903 - 281	0.161	0.000	13.104	0.322	2.266	0.000	53.415
903 - 282	0.111	0.000	5.113	3.209	3.716	0.000	44.840
903 - 283a	0.111	0.000	5.195	2.600	0.944	0.000	66.519
903 - 283b	0.152	0.642	12.453	0.000	1.235	0.000	48.285
903 - 283c	0.156	0.000	5.286	6.151	1.372	0.000	52.042
903 - 283d	0.156	0.000	6.401	4.764	1.928	0.000	51.653
903 - 283e	0.166	0.000	4.765	6.638	1.517	0.000	52.567
903 - 284	0.179	0.000	6.364	5.447	7.881	0.000	18.404

Table V.1: Mineral normalization results from ores and rocks.

No.	Anatase	Quartz	Kaolinite	Gibbsite	Goethite	Hematite	Cryptomelane
903 - 285	0.160	0.000	4.615	5.675	1.470	0.000	50.565
903 - 286	0.170	0.000	6.029	5.365	6.617	0.000	16.572
903 - 287	0.173	0.000	5.274	6.980	12.475	0.000	9.948
903 - 290	0.121	0.000	5.379	2.652	2.114	0.000	23.742
903 - 291	0.140	0.000	6.494	1.142	1.813	0.000	0.860
903 - 292	0.163	0.102	11.501	0.000	3.890	0.000	0.622
903 - 293	0.139	0.080	8.470	0.000	2.053	0.000	0.392
903 - 294	0.183	0.205	9.617	0.000	2.537	0.000	1.603
903 - 295	0.092	6.848	10.163	0.000	80.612	0.000	0.152
903 - 296	0.238	1.136	24.305	0.000	46.651	0.000	0.952
903 - 297	0.190	1.145	18.415	0.000	2.180	0.000	3.365
903 - 298	0.128	1.936	8.629	0.000	1.578	0.000	50.324
903 - 299	0.162	0.185	7.756	0.000	1.972	0.000	49.283
903 - 300	0.097	0.913	6.220	0.000	3.215	0.000	0.563
903 - 301	0.125	0.070	7.058	0.000	1.689	0.000	0.756
903 - 302	0.147	0.017	7.918	0.000	2.395	0.000	0.825
903 - 303	0.113	7.557	9.036	0.000	1.150	0.000	8.065
903 - 304	0.122	24.656	9.713	0.000	0.942	0.000	6.688
903 - 305	0.127	11.398	11.522	0.000	1.271	0.000	7.742
903 - 306	0.238	6.231	19.013	0.000	1.743	0.000	8.012
903 - 307	0.124	0.539	14.000	0.000	0.570	0.000	8.197
903 - 308	0.104	0.000	10.839	0.212	0.675	0.000	7.603
903 - 309	0.187	0.881	17.682	0.000	0.963	0.000	7.168
903 - 310	0.246	1.583	20.707	0.000	1.439	0.000	7.736
903 - 311	0.141	1.489	14.338	0.000	0.886	0.000	8.571
903 - 312a	0.119	0.056	13.077	0.000	0.910	0.000	8.267
903 - 312b1	0.056	0.089	4.730	0.000	0.758	0.000	5.543
903 - 312b2	0.048	0.000	5.117	0.072	0.537	0.000	8.420
903 - 312b3	0.076	1.224	5.821	0.000	0.921	0.000	6.546
903 - 312b4	0.056	0.000	4.964	0.259	0.852	0.000	7.979
903 - 315b5	0.070	0.208	5.837	0.000	0.824	0.000	6.391
903 - 313	0.188	2.109	14.482	0.000	1.469	0.000	9.169
903 - 314	0.191	1.716	16.866	0.000	1.159	0.000	8.208
903 - 315	0.164	3.868	17.444	0.000	1.243	0.000	7.644
903 - 316	0.169	3.497	15.166	0.000	1.263	0.000	6.895
903 - 317	0.166	2.286	14.053	0.000	1.758	0.000	9.251
903 - 318	0.156	1.654	11.906	0.000	1.681	0.000	12.300
903 - 319	0.104	1.256	8.284	0.000	1.042	0.000	11.750
903 - 320	0.125	1.997	11.328	0.000	1.448	0.000	11.189
903 - 322	0.084	0.126	7.253	0.000	1.086	0.000	14.963
903 - 323	0.091	0.169	8.095	0.000	0.761	0.000	10.409
903 - 324	0.662	1.725	59.383	0.000	15.114	0.000	4.710
903 - 325	0.695	3.299	63.285	0.000	18.810	0.000	3.925
903 - 326a.	0.861	0.250	66.989	0.000	20.653	6.608	0.000
903 - 326b.	0.534	0.000	42.995	2.736	32.294	0.000	1.682
903 - 326c.	0.703	0.000	55.207	3.154	19.733	15.514	0.000
903 - 327	0.703	0.000	58.148	5.659	10.515	0.000	2.810
903 - 328	0.080	1.621	5.214	0.000	0.677	0.000	8.417
903 - 329	0.059	2.241	4.978	0.000	0.588	0.000	7.911
903 - 330	0.101	0.000	3.143	2.624	1.125	0.000	33.975
903 - 331	0.125	0.000	6.364	1.138	2.053	0.000	31.056
903 - 332	0.079	0.000	4.277	1.590	2.359	0.000	35.343
903 - 333	0.124	0.000	4.710	1.872	1.741	0.000	33.646
903 - 334	0.097	9.748	9.521	0.000	0.999	0.000	13.572
903 - 335	0.067	5.527	5.351	0.000	0.908	0.000	9.917
903 - 336	0.041	8.323	5.778	0.000	82.716	0.000	0.134
903 - 337	0.838	32.814	66.591	0.000	0.000	0.388	0.000
903 - 338	0.736	20.764	61.233	0.000	13.992	2.568	0.000
903 - 339	0.076	11.922	7.231	0.000	3.676	0.000	25.908
903 - 340a.	0.067	39.359	7.389	0.000	0.841	0.000	18.084
903 - 340b.	0.067	41.481	7.771	0.000	0.949	0.000	16.473
903 - 341a.	0.075	0.000	3.089	1.994	1.333	0.000	48.343
903 - 342a.	0.138	0.000	16.844	0.684	1.035	0.000	24.216
903 - 343	0.082	25.619	7.432	0.000	1.486	0.000	33.263
903 - 344	0.181	12.266	15.312	0.000	6.236	0.000	8.090
903 - A	0.082	0.000	5.567	0.266	15.012	0.000	36.210
903 - B	0.549	17.532	20.235	0.000	2.223	0.000	20.690
903 - B I.a	1.022	19.494	78.052	0.000	0.000	0.000	0.000
903 - B I.b	1.026	19.306	78.534	0.000	0.000	0.000	0.000

No.	Anatase	Quartz	Kaolinite	Gibbsite	Goethite	Hematite	Cryptomelane
903 - B I.c	1.018	19.848	77.435	0.000	0.000	0.000	0.000
903 - B I.d1	1.019	21.206	77.782	0.000	0.000	0.000	0.000
903 - B I.d2	1.013	20.351	78.341	0.000	0.000	0.000	0.000
903 - B I.d3	1.038	19.180	79.271	0.000	0.000	0.000	0.000
903 - B I.d4	1.027	19.411	79.205	0.000	0.000	0.000	0.000
903 - B I.e	0.966	21.303	73.627	0.000	0.000	0.000	0.000
903 - B II.a	0.074	0.000	5.730	5.187	0.462	0.000	11.056
903 - B II.b	0.073	0.000	5.441	5.344	0.466	0.000	11.406
903 - B II.c	0.074	0.000	5.520	4.957	0.473	0.000	11.250
903 - B II.d1	0.075	0.000	5.562	5.228	0.476	0.000	11.012
903 - B II.d2	0.074	0.000	5.546	5.447	0.475	0.000	11.088
903 - B II.d3	0.074	0.000	5.544	4.745	0.475	0.000	11.084
903 - B II.d4	0.075	0.000	5.331	5.214	0.486	0.000	11.172
903 - B II.e	0.073	0.000	4.971	5.071	0.483	0.000	11.063
903 - B III.	0.112	1.573	11.197	0.000	0.672	0.000	9.063
903 - B V.	0.133	0.000	12.010	2.612	0.808	0.000	3.776
903 - Mn 2	0.095	0.000	8.139	1.599	2.678	0.000	12.080

Table V.1: Mineral normalization results from ores and rocks.

No.	Romanechite	Todorokite	Pyrolusite	P2O5	Water	Sum
903 - 3	1.095	0.903	77.356	0.041	0.000	100.21
903 - 4	1.477	1.381	85.551	0.054	0.858	99.96
903 - 5a	8.649	1.093	44.683	0.046	2.650	99.44
903 - 5b	0.033	0.400	0.000	0.007	0.443	100.41
903 - 6	13.408	5.552	47.572	0.047	7.801	99.45
903 - 7	21.920	4.607	45.091	0.037	6.638	99.30
903 - 8	11.258	5.840	43.353	0.034	10.472	99.43
903 - 9	15.424	2.661	60.558	0.060	3.375	99.52
903 - 10	5.381	6.251	35.115	0.027	17.592	99.38
903 - 11	2.394	5.897	39.805	0.037	17.276	99.41
903 - 12	2.194	5.516	42.984	0.044	16.111	99.39
903 - 13	2.286	6.775	40.247	0.033	15.511	99.34
903 - 14	3.142	6.317	38.252	0.040	17.045	99.30
903 - 15	7.932	4.425	36.198	0.042	11.461	99.32
903 - 16	7.973	5.945	41.789	0.041	10.867	99.38
903 - 17	2.599	6.149	37.619	0.035	15.137	99.37
903 - 18	12.284	5.475	37.712	0.030	9.540	99.48
903 - 19	6.267	5.437	30.428	0.031	14.882	99.53
903 - 20	0.036	0.638	0.000	0.002	0.117	100.31
903 - 21	2.373	0.886	5.109	0.041	0.939	99.64
903 - 22	13.907	2.401	40.555	0.052	8.457	99.11
903 - 23	9.233	5.335	39.648	0.032	14.354	99.28
903 - 24	2.184	0.648	4.922	0.042	0.744	99.61
903 - 25	1.569	0.473	6.093	0.035	0.539	99.64
903 - 26	0.038	0.456	0.000	0.001	0.000	101.06
903 - 27	0.042	0.508	0.000	0.039	0.000	99.80
903 - 28a	0.150	0.452	0.689	0.014	0.000	99.84
903 - 28b	0.039	0.476	0.000	0.014	0.000	99.72
903 - 29	0.598	0.451	0.750	0.016	0.000	99.89
903 - 30	0.226	0.454	0.080	0.016	0.000	99.71
903 - 31a	0.073	0.439	0.000	0.005	0.367	100.22
903 - 31b	0.039	0.716	0.000	0.001	0.436	100.52
903 - 32	0.035	1.768	0.000	0.004	3.756	101.03
903 - 33	4.909	7.158	43.915	0.042	18.053	99.22
903 - 34	5.634	7.569	44.848	0.042	17.767	99.21
903 - 35	4.088	4.752	60.255	0.046	10.204	99.46
903 - 36	5.324	6.701	49.304	0.045	16.332	99.31
903 - 37	5.531	7.849	39.768	0.047	20.126	99.24
903 - 38	5.065	6.712	37.340	0.049	18.772	99.29
903 - 39	5.448	7.092	38.415	0.051	20.038	99.30
903 - 40	5.433	7.473	37.070	0.458	21.344	99.23
903 - 41	2.251	3.320	70.732	0.084	9.071	99.63
903 - 42	4.325	4.755	31.529	0.043	15.885	99.38
903 - 43	4.264	3.439	18.826	0.040	13.772	99.35
903 - 44	6.228	5.665	32.439	0.064	15.233	99.27
903 - 45	4.350	4.678	25.783	0.044	13.134	99.36
903 - 46	5.411	7.460	40.383	0.059	17.339	99.35
903 - 47	5.591	5.832	55.168	0.073	11.874	99.40
903 - 48	7.587	5.650	43.666	0.067	12.538	99.31
903 - 49	5.647	3.122	27.631	0.054	10.065	99.37
903 - 50	7.849	5.748	52.377	0.068	11.616	99.33
903 - 51	7.895	5.845	53.061	0.069	11.932	99.31
903 - 52	4.560	1.277	12.916	0.045	3.384	99.40
903 - 53	0.396	0.435	0.234	0.023	0.000	99.58
903 - 54	6.983	2.389	39.043	0.056	4.056	99.40
903 - 55	11.612	3.992	60.153	0.074	5.908	99.23
903 - 56	16.717	5.388	39.610	0.069	13.325	98.95
903 - 57	1.259	0.434	3.598	0.010	1.748	99.52
903 - 58	8.397	3.079	60.399	0.061	5.168	99.52
903 - 59	14.513	3.804	47.403	0.056	6.620	99.15
903 - 60	7.027	3.018	49.200	0.041	2.531	99.74
903 - 61	12.177	3.506	57.585	0.068	7.787	99.36
903 - 62	5.401	1.562	74.482	0.056	0.502	99.66
903 - 63	0.915	1.765	77.076	0.072	0.515	99.93
903 - 64	0.495	0.896	7.744	0.070	1.920	99.64
903 - 65a	0.701	0.693	7.448	0.051	0.808	99.59
903 - 65b	2.767	7.925	21.002	0.181	14.307	100.06
903 - 66	1.258	2.041	9.955	0.043	3.508	99.64
903 - 67	1.186	2.004	7.325	0.037	3.475	99.81

Table V.1: Mineral normalization results from ores and rocks.

No.	Romanechite	Todorokite	Pyrolusite	P2O5	Water	Sum
903 - 68a	6.803	2.583	45.829	0.049	6.035	99.49
903 - 68b	9.294	5.154	49.695	0.070	9.832	99.18
903 - 69	9.455	4.929	50.622	0.070	9.765	99.20
903 - 70	9.173	4.888	49.095	0.059	8.992	99.19
903 - 71	8.729	5.370	57.527	0.066	8.947	99.19
903 - 72	9.204	5.739	53.286	0.070	10.806	99.06
903 - 73	7.788	6.314	52.244	0.062	9.439	99.17
903 - 74	7.542	5.909	38.887	0.050	11.576	99.06
903 - 75	7.570	6.338	44.090	0.057	12.363	99.03
903 - 76	6.565	6.022	42.974	0.049	12.902	99.14
903 - 77a	6.122	6.827	52.810	0.070	11.382	99.07
903 - 77b	7.494	4.786	57.565	0.073	9.523	99.20
903 - 78	3.979	6.346	62.069	0.087	9.018	99.30
903 - 79	0.000	0.649	0.403	0.035	1.185	99.75
903 - 80	1.497	1.784	74.474	0.058	2.005	99.86
903 - 81	8.324	3.056	57.325	0.049	6.342	99.44
903 - 82	8.773	3.834	46.794	0.049	8.441	99.39
903 - 83	6.192	2.795	63.738	0.052	5.346	99.53
903 - 84	7.056	2.987	41.831	0.043	6.856	99.48
903 - 85	4.606	3.849	62.157	0.093	7.207	99.45
903 - 86	3.338	4.198	41.006	0.115	11.356	99.60
903 - 87	2.833	1.709	16.146	0.066	7.900	99.58
903 - 88	6.356	6.378	44.897	0.062	9.441	99.45
903 - 89	7.306	4.798	37.433	0.079	12.523	99.34
903 - 90	1.798	0.631	4.831	0.023	2.258	99.59
903 - 91	5.593	5.528	45.711	0.055	11.833	99.39
903 - 92	4.533	6.212	45.630	0.048	14.061	99.37
903 - 93	4.075	6.485	49.594	0.047	12.542	99.41
903 - 94	3.587	6.214	50.313	0.044	14.555	99.36
903 - 95	4.233	7.365	47.094	0.040	15.770	99.31
903 - 96	4.650	7.738	45.732	0.041	17.326	99.22
903 - 97	4.319	7.475	46.578	0.043	15.938	99.33
903 - 98	3.693	5.998	56.727	0.047	12.319	99.36
903 - 99	5.854	7.051	39.791	0.039	17.775	99.28
903 - 100	7.100	8.132	29.914	0.030	20.873	99.24
903 - 101	4.870	9.240	32.984	0.040	19.667	99.24
903 - 102	4.335	6.313	52.715	0.067	10.352	99.55
903 - 103	7.484	3.684	66.718	0.071	5.627	99.59
903 - 104	4.914	2.364	60.644	0.064	3.958	99.60
903 - 105	5.059	2.905	75.329	0.062	1.953	99.67
903 - 106	8.512	5.090	57.626	0.050	8.965	99.40
903 - 107	10.230	6.054	46.946	0.052	12.416	99.26
903 - 108	11.821	6.115	35.743	0.041	14.588	99.19
903 - 109	7.552	3.654	61.342	0.059	6.438	99.45
903 - 110	7.364	2.365	27.333	0.044	5.026	99.56
903 - 111	7.107	2.255	64.531	0.073	10.527	99.65
903 - 112	6.400	1.316	51.969	0.052	2.682	99.52
903 - 113	1.326	0.237	9.704	0.161	2.860	99.65
903 - 114	0.895	0.214	5.059	0.009	0.829	99.83
903 - 115a	0.000	0.217	0.346	0.006	0.020	99.90
903 - 115b	0.000	0.228	0.224	0.017	0.000	99.96
903 - 116a	2.012	2.135	16.077	0.089	9.476	99.79
903 - 116b	1.537	4.319	27.593	0.081	8.871	100.05
903 - 117b	0.565	12.952	32.053	0.049	9.796	100.67
903 - 118a	0.243	4.064	22.091	0.141	11.744	99.93
903 - 118b	0.036	0.633	5.052	0.013	0.348	99.75
903 - 119	0.073	9.782	26.675	0.146	12.678	100.41
903 - 120	0.107	6.192	49.789	0.070	2.652	100.24
903 - 121	0.218	6.031	59.189	0.090	3.549	100.25
903 - 122	0.360	5.125	48.941	0.064	3.798	100.14
903 - 123	0.180	8.067	53.470	0.083	6.712	100.36
903 - 124	0.828	1.623	13.609	0.010	5.570	99.62
903 - 125	0.752	1.216	11.649	0.012	3.201	99.57
903 - 126	0.756	1.026	11.075	0.007	1.727	99.55
903 - 127	0.839	0.858	7.962	0.011	0.000	100.56
903 - 128	0.364	0.440	5.725	0.005	0.000	100.43
903 - 129	0.289	0.435	4.615	0.009	0.000	101.05
903 - 130	0.415	1.032	14.300	0.010	1.591	99.57
903 - 131	0.454	0.621	12.085	0.005	0.175	99.53

No.	Romanechite	Todorokite	Pyrolusite	P2O5	Water	Sum
903 - 132	0.368	0.444	3.401	0.009	0.000	99.96
903 - 133	0.176	0.425	2.164	0.006	0.527	99.50
903 - 134	0.370	0.447	2.539	0.011	0.000	100.42
903 - 135	0.919	0.444	6.133	0.005	0.000	101.56
903 - 136	0.483	0.448	3.162	0.015	0.000	100.60
903 - 137	0.525	0.452	1.631	0.014	0.000	100.09
903 - 138	1.686	0.674	4.976	0.010	0.000	100.79
903 - 139	0.227	0.697	2.028	0.018	0.000	100.24
903 - 140	0.143	1.558	0.000	0.010	1.357	99.90
903 - 141a	0.000	0.401	0.020	0.004	0.052	100.37
903 - 141b	0.000	0.412	0.020	0.011	0.201	99.52
903 - 141c	0.000	0.411	0.020	0.007	1.216	99.56
903 - 141 B	0.003	0.580	0.000	0.005	0.064	100.43
903 - 142	0.142	6.426	48.088	0.040	8.982	100.13
903 - 143	0.141	9.453	46.790	0.033	7.943	100.39
903 - 144	0.433	8.231	55.229	0.044	6.605	100.22
903 - 145	0.356	4.957	65.758	0.047	4.484	100.12
903 - 146	0.358	7.038	45.286	0.063	8.864	100.23
903 - 147	0.255	5.663	56.048	0.074	7.350	100.14
903 - 148	1.629	7.393	45.718	0.126	7.935	100.20
903 - 149	0.294	7.345	34.359	0.069	7.883	100.25
903 - 150	0.293	4.264	73.942	0.038	2.105	100.11
903 - 151	0.287	5.607	50.946	0.060	5.981	100.11
903 - 152a	0.146	7.323	39.345	0.068	4.943	100.28
903 - 152b	0.152	7.183	37.162	0.129	7.771	100.23
903 - 153	2.444	5.873	32.267	0.099	11.658	100.03
903 - 154	0.499	6.485	42.787	0.075	7.506	100.19
903 - 155	1.160	5.543	25.211	0.169	10.278	99.96
903 - 156	0.120	0.229	1.616	0.143	0.000	100.34
903 - 157	0.086	0.491	3.084	0.410	4.175	99.89
903 - 158	0.164	0.234	0.664	0.329	1.382	99.83
903 - 159	0.163	0.493	3.847	0.373	3.969	99.77
903 - 160	0.258	0.677	77.932	0.082	0.000	100.65
903 - 161	0.219	0.673	51.020	0.083	1.542	99.92
903 - 162	0.187	3.908	2.522	0.040	11.228	99.90
903 - 164	0.548	3.461	2.710	0.087	17.307	99.64
903 - 168 B	0.371	8.188	43.400	0.039	5.889	100.30
903 - 169 B	0.330	6.246	56.186	0.040	4.217	100.22
903 - 170a	0.037	0.448	0.000	0.001	0.000	101.00
903 - 170b	0.081	0.488	0.000	0.005	0.441	100.64
903 - 171a	0.041	0.489	0.000	0.001	0.000	100.72
903 - 171b	0.037	0.442	0.000	0.001	0.000	100.55
903 - 172	0.038	0.455	0.000	0.001	0.112	100.58
903 - 173	0.037	0.447	0.000	0.002	0.000	100.96
903 - 174	0.151	0.455	0.000	0.005	0.710	100.38
903 - 175	0.112	0.451	0.000	0.003	0.663	100.50
903 - 176	0.219	0.440	0.000	0.006	0.571	100.09
903 - 177	0.386	0.466	0.000	0.013	1.056	100.07
903 - 178	2.447	0.441	9.712	0.069	8.202	99.71
903 - 179	0.047	0.564	0.000	0.255	2.377	100.28
903 - 180	0.239	0.576	1.559	0.657	1.758	99.90
903 - 181	0.724	0.805	8.995	0.615	3.433	99.88
903 - 182	1.032	1.145	80.936	0.077	0.000	100.30
903 - 183	1.196	1.541	80.423	0.090	0.000	100.39
903 - 184	1.030	1.354	82.031	0.097	0.000	101.20
903 - 185	0.050	0.597	0.341	0.664	0.000	100.04
903 - 186	0.052	0.626	0.000	0.606	0.000	100.28
903 - 187	0.091	0.546	0.000	0.688	0.000	101.56
903 - 188	0.633	4.398	24.904	0.068	14.984	99.88
903 - 189	0.598	2.536	2.302	0.058	0.000	100.31
903 - 191B	5.918	7.455	47.141	0.043	14.966	99.20
903 - 190	2.277	2.824	24.642	0.278	22.055	99.80
903 - 200	0.180	0.433	2.134	0.014	0.000	100.27
903 - 201	0.320	0.429	2.508	0.014	0.000	100.39
903 - 202	0.688	0.645	3.607	0.011	0.000	100.78
903 - 203	0.617	0.853	3.889	0.012	0.000	100.89
903 - 204	0.936	0.641	5.154	0.010	0.000	101.17
903 - 205	0.852	0.835	6.003	0.008	0.000	101.55
903 - 206	1.091	0.828	7.117	0.011	0.000	100.27

Table V.1: Mineral normalization results from ores and rocks.

No.	Romanechite	Todorokite	Pyrolusite	P2O5	Water	Sum
903 - 207	0.978	1.221	10.205	0.005	0.296	99.58
903 - 208	0.732	1.019	9.602	0.009	0.547	99.54
903 - 209	1.235	5.378	60.564	0.056	2.980	100.13
903 - 210	0.266	0.699	1.118	0.025	0.000	99.95
903 - 211	0.542	2.493	4.241	0.010	0.105	99.78
903 - 212	0.819	5.981	40.974	0.025	6.758	100.09
903 - 213	0.037	17.260	47.977	0.100	5.745	101.07
903 - 215	0.000	0.218	0.548	0.005	0.000	99.94
903 - 216	0.183	4.042	73.790	0.039	2.399	100.08
903 - 217	0.145	0.208	1.842	0.009	0.000	100.27
903 - 218	0.354	6.604	50.032	0.045	6.731	100.21
903 - 219	0.400	2.751	67.350	0.045	3.394	99.92
903 - 220	0.212	7.166	48.451	0.042	5.941	100.25
903 - 221	0.000	0.228	0.195	0.019	0.000	99.68
903 - 222	0.039	0.221	0.319	0.026	0.000	99.73
903 - 223	11.397	6.045	40.790	0.034	10.152	99.31
903 - 224	13.722	4.738	47.766	0.036	7.931	99.32
903 - 225	4.873	4.293	54.322	0.048	11.820	99.28
903 - 226	4.146	5.591	37.911	0.034	17.433	99.30
903 - 227	13.203	10.448	33.897	0.019	10.055	100.12
903 - 228	15.667	8.102	30.515	0.021	8.644	100.07
903 - 229	0.417	0.217	0.697	0.019	0.141	99.67
903 - 230	0.301	0.216	0.000	0.018	1.127	99.78
903 - 232	0.741	3.807	31.139	0.097	11.141	99.87
903 - 233	1.532	4.691	19.520	0.039	15.113	99.84
903 - 234	0.000	0.280	0.063	0.670	0.175	99.89
903 - 235	0.000	0.270	0.313	0.620	0.000	99.99
903 - 237	2.725	1.283	10.220	0.083	8.810	99.80
903 - 239	1.672	3.451	11.437	0.092	12.212	99.85
903 - 241	2.614	4.286	73.073	0.030	1.666	100.06
903 - 245	0.206	0.295	2.365	0.597	0.000	100.67
903 - 246	0.303	0.289	2.028	0.693	0.000	100.61
903 - 249	11.975	7.134	26.808	0.015	11.137	99.86
903 - 250	1.384	3.174	35.214	0.059	4.055	100.01
903 - 251	0.994	2.827	22.407	0.123	6.504	99.72
903 - 252	11.935	5.767	25.646	0.023	13.082	99.75
903 - 253	0.405	7.374	40.872	0.016	9.818	100.21
903 - 254	0.931	3.975	16.079	0.019	7.933	100.06
903 - 255	1.737	4.775	13.390	0.292	15.021	99.83
903 - 256	2.057	5.433	14.622	0.456	15.080	100.00
903 - 259	2.467	3.653	59.249	0.087	6.060	99.87
903 - 260	3.138	4.799	56.406	0.083	5.873	99.87
903 - 261	0.629	0.554	6.040	0.491	0.000	101.39
903 - 262	0.329	0.270	3.165	0.382	0.000	100.89
903 - 263	15.285	4.892	41.658	0.038	10.792	99.13
903 - 264	15.596	4.202	40.693	0.042	10.582	98.87
903 - 265	0.405	1.376	97.242	0.031	0.000	102.24
903 - 266	9.992	2.288	79.376	0.044	0.000	100.21
903 - 268	3.300	7.341	5.197	0.237	16.968	99.82
903 - 269	4.464	7.824	17.204	0.094	16.794	99.95
903 - 270	0.044	3.061	4.857	0.266	10.057	99.77
903 - 271	0.933	6.695	9.076	0.278	18.364	99.85
903 - 272	2.626	5.244	47.745	0.181	9.169	100.01
903 - 273	0.673	5.584	46.211	0.185	10.626	100.08
903 - 274	0.178	0.656	65.894	0.052	1.142	99.79
903 - 275	0.248	0.854	69.107	0.048	1.321	99.81
903 - 276	0.224	0.257	4.291	0.588	4.531	99.85
903 - 277	1.181	0.251	1.680	0.344	6.332	99.84
903 - 278	10.029	1.064	9.531	0.109	7.289	99.64
903 - 279	0.072	6.173	18.761	0.013	7.312	100.27
903 - 280	1.093	3.603	23.712	0.443	12.963	99.90
903 - 281	2.036	5.152	5.823	0.097	17.166	99.54
903 - 282	3.148	9.101	15.397	0.200	15.202	100.04
903 - 283a	1.857	4.773	0.356	0.143	16.863	99.36
903 - 283b	6.934	6.547	6.700	0.246	16.434	99.63
903 - 283c	7.160	6.698	6.192	0.240	14.345	99.64
903 - 283d	6.267	5.743	8.204	0.194	14.215	99.52
903 - 283e	8.689	6.488	5.739	0.241	12.773	99.58
903 - 284	32.448	2.500	19.524	0.247	6.165	99.16

No.	Romanechite	Todorokite	Pyrolusite	P2O5	Water	Sum
903 - 285	8.415	2.418	8.691	0.241	17.030	99.28
903 - 286	36.065	2.481	18.993	0.233	6.559	99.08
903 - 287	38.176	1.525	19.520	0.317	4.669	99.06
903 - 290	1.873	7.670	48.100	0.178	8.465	100.29
903 - 291	0.730	0.441	88.313	0.024	0.000	99.96
903 - 292	0.329	0.651	82.493	0.049	0.046	99.85
903 - 293	0.217	0.437	87.864	0.047	0.165	99.86
903 - 294	0.289	0.621	83.821	0.025	0.970	99.87
903 - 295	0.000	0.867	0.000	0.317	0.921	99.97
903 - 296	0.262	0.250	23.229	0.467	2.128	99.62
903 - 297	0.653	0.437	72.990	0.072	0.368	99.82
903 - 298	0.595	1.184	18.261	0.131	16.420	99.19
903 - 299	0.321	6.759	19.218	0.209	13.979	99.84
903 - 300	0.809	4.488	84.683	0.026	0.000	101.01
903 - 301	0.328	0.671	89.130	0.032	0.000	99.86
903 - 302	0.291	0.669	87.059	0.029	0.515	99.87
903 - 303	5.536	4.405	54.303	0.056	9.275	99.50
903 - 304	4.431	4.414	41.915	0.053	6.567	99.50
903 - 305	4.951	1.525	50.539	0.058	10.611	99.74
903 - 306	4.371	6.110	44.092	0.071	9.467	99.35
903 - 307	6.642	5.197	51.973	0.081	12.029	99.35
903 - 308	6.065	6.463	57.389	0.083	9.788	99.22
903 - 309	5.382	7.019	50.246	0.077	9.476	99.08
903 - 310	5.409	6.300	43.099	0.066	12.599	99.18
903 - 311	5.302	7.563	48.736	0.072	12.125	99.22
903 - 312a	4.557	7.704	55.517	0.092	9.129	99.43
903 - 312b1	2.727	6.236	70.273	0.076	8.920	99.41
903 - 312b2	2.279	9.887	61.378	0.085	11.657	99.48
903 - 312b3	2.029	6.824	66.120	0.101	9.855	99.52
903 - 312b4	2.524	7.672	64.460	0.095	10.647	99.51
903 - 315b5	1.931	6.624	67.570	0.089	9.930	99.47
903 - 313	5.114	7.117	48.623	0.101	11.053	99.42
903 - 314	5.333	6.758	47.297	0.077	11.734	99.34
903 - 315	4.092	5.374	47.966	0.065	11.534	99.39
903 - 316	3.276	6.116	54.967	0.066	8.008	99.42
903 - 317	3.521	8.454	49.424	0.052	10.506	99.47
903 - 318	3.834	7.467	49.337	0.047	10.964	99.34
903 - 319	3.666	6.468	52.942	0.045	13.783	99.34
903 - 320	3.703	6.513	50.850	0.045	12.135	99.33
903 - 322	5.884	7.766	48.036	0.040	13.968	99.21
903 - 323	4.156	5.525	59.039	0.051	11.119	99.42
903 - 324	1.281	1.288	9.058	0.043	6.335	99.60
903 - 325	0.890	0.933	7.291	0.037	0.406	99.57
903 - 326a.	0.980	0.244	4.428	0.047	0.000	101.06
903 - 326b.	2.763	0.229	11.797	0.070	4.490	99.59
903 - 326c.	1.064	0.277	5.925	0.052	0.000	101.63
903 - 327	3.409	1.093	15.330	0.031	1.793	99.49
903 - 328	2.911	3.175	70.757	0.089	6.535	99.48
903 - 329	1.708	2.356	74.602	0.092	5.056	99.59
903 - 330	3.906	9.897	33.123	0.171	12.216	100.28
903 - 331	2.831	8.080	38.796	0.065	9.665	100.17
903 - 332	2.463	9.088	34.654	0.108	10.253	100.21
903 - 333	4.745	8.792	31.855	0.144	12.514	100.14
903 - 334	0.775	2.817	58.200	0.056	4.086	99.87
903 - 335	0.848	3.025	71.752	0.060	2.476	99.93
903 - 336	0.000	0.293	0.285	0.359	2.000	99.93
903 - 337	0.000	0.198	0.170	0.005	0.000	101.01
903 - 338	0.000	0.224	0.192	0.027	0.000	99.74
903 - 339	1.794	6.718	31.053	0.144	11.604	100.12
903 - 340a.	2.384	3.472	18.825	0.086	9.456	99.96
903 - 340b.	3.115	2.807	19.408	0.069	7.750	99.89
903 - 341a.	1.355	4.620	27.383	0.076	11.428	99.70
903 - 342a.	11.975	5.931	29.569	0.054	9.352	99.80
903 - 343	1.475	6.974	7.344	0.304	16.123	100.10
903 - 344	1.693	1.667	39.225	0.491	14.715	99.88
903 - A	2.442	5.892	21.379	0.209	12.843	99.90
903 - B	0.035	14.574	11.734	0.014	13.096	100.68
903 - B I.a	0.033	0.401	0.000	0.003	1.409	100.41
903 - B I.b	0.034	0.411	0.000	0.004	1.075	100.39

No.	Romanechite	Todorokite	Pyrolusite	P2O5	Water	Sum
903 - B I.c	0.000	0.192	0.165	0.005	1.701	100.37
903 - B I.d1	0.000	0.194	0.166	0.005	0.004	100.38
903 - B I.d2	0.000	0.195	0.167	0.003	0.309	100.38
903 - B I.d3	0.000	0.192	0.017	0.008	0.691	100.40
903 - B I.d4	0.000	0.194	0.166	0.007	0.368	100.38
903 - B I.e	0.000	0.770	0.000	0.005	3.973	100.64
903 - B II.a	18.579	5.119	44.436	0.034	8.684	99.36
903 - B II.b	18.808	5.083	44.237	0.037	8.456	99.35
903 - B II.c	18.567	6.606	44.409	0.037	7.612	99.50
903 - B II.d1	18.781	4.939	46.137	0.038	7.054	99.30
903 - B II.d2	18.801	4.925	46.097	0.036	6.812	99.30
903 - B II.d3	18.832	4.923	46.367	0.038	7.232	99.32
903 - B II.d4	18.783	4.959	46.401	0.031	6.864	99.32
903 - B II.e	18.357	6.774	44.794	0.039	7.910	99.53
903 - B III.	7.572	4.703	51.394	0.061	12.817	99.16
903 - B V.	16.611	2.207	55.590	0.061	5.318	99.12
903 - Mn 2	7.683	4.677	53.062	0.055	9.510	99.58

Table V.2: Microbiological leaching of Mn ores from Groote Eylandt; after R. Varga and J. Madgwick. A V.2 - 1

Number	Ø leached	Ø Uptake	Ø Ox formed	Mn 31.1.86	Mn 7.2.86	Mn 14.2.86
3	20	6.5	2.6	15	12	11
4	19	6	1	16	16	18
5a.	38	8	4.3	24	19	20
6	22	6.5	3.2	19	19	19
7	23	4.5	2	17	17	18
8	25	5	2.3	22	18	19
9	25	5	3.3	18	18	17
10	27	10	2.7	15	18	18
11	30	15	6.9	19	22	17
12	25	4	3	17	17	17
13	23	7	5.1	21	18	18
14	24	10	5.7	18	13	19
15	24	12	5.8	15	13	16
16	24	12	5.6	16	18	20
17	23	5	5.6	16	18	19

Number	Mn 21.2.86	Mn 28.2.86	Mn 7.3.86	Mn 14.3.86	Mn 21.3.86	pH 21.3.86
3	14	18	23	31	19	5.83
4	15	15	30	31	17	5.76
5a.	18	21	24	30	17	5.54
6	17	16	28	32	19	6
7	20	24	28	26	17	5.94
8	17	24	41	37	20	5.95
9	16	22	24	37	22	6.05
10	15	13	25	40	27	5.62
11	17	25	32	44	24	6.01
12	17	21	35	36	25	5.8
13	18	16	35	30	17	5.91
14	14	21	31	28	19	6.21
15	18	17	27	28	17	5.41
16	24	19	34	32	18	5.87
17	21	16	32	30	20	5.7

Number	Mn 4.4.86	pH 4.4.86	Mn 11.4.86	pH 11.4.86	Mn 18.4.86	pH 18.4.86
3	22	5.89	31.2	5.99	20.2	5.96
4	21	6.15	29.5	6.15	20.4	5.93
5a.	26	5.98	34.6	5.86	21.9	5.72
6	19	5.98	30.1	5.74	18.9	5.62
7	22	6.1	31.3	5.76	18.8	5.61
8	25	6.23	32.4	5.81	18.4	5.7
9	24	6.08	29.6	5.91	19.6	5.91
10	26	6.16	33.3	5.88	18.4	5.94
11	24	6.2	35.5	5.89	15.6	6.01
12	21	6	33.7	5.96	19.4	5.88
13	23	6.12	31	5.73	18.9	5.78
14	21	6.21	32.8	5.83	20	5.89
15	16	5.33	22.6	5.45	12.1	5.02
16	23	5.81	26.7	5.5	16.7	5.38
17	23	5.72	25.1	5.82	16.5	5.47

Table V.2: Microbiological leaching of Mn ores from Groote Eylandt; after R. Varga and J. Madgwick. A V.2 - 2

Number	Mn 2.5.86	pH 2.5.86	Mn 9.5.86	pH 9.5.86	Mn 16.5.86	pH 16.5.86
3	14	5.61	13	5.68	13	4.92
4	15	5.62	17	5.68	15	5.2
5a.	17.5	5.62	17	5.61	12	4.94
6	12.5	5.4	10	5.21	9	4.72
7	13	5.39	12	5.18	10	4.68
8	13	5.4	14	5.3	11	4.82
9	12.9	5.32	13	5.24	11	4.88
10	15	5.79	14	5.41	12	4.97
11	12.7	6.12	15	6.08	17	5.24
12	13.5	5.41	15	5.45	10	4.74
13	14.4	5.42	13	5.41	10	4.82
14	15	5.61	15	5.42	14	5.02
15	10	4.86	12	4.92	8	4.68
16	9	5.36	11	5.1	10	4.85
17	10.5	5.08	12	5.16	12	4.86
Number	Mn 23.5.86	pH 23.5.86	Mn 30.5.86	pH 30.5.86	Mn 6.6.86	pH 6.6.86
3	11	4.86	12	4.51	11.5	2.98
4	9	5.59	13.5	5.17	12	3.02
5a.	7	5.11	13	4.82	10.6	2.76
6	6	4.86	10.5	4.51	11.8	2.46
7	5	4.72	10	4.49	10.5	2.84
8	5	4.88	11.7	4.57	12.6	2.82
9	6	4.92	12	4.6	11.7	3.12
10	7	4.99	13	4.58	12	2.87
11	10	4.96	11	4.62	16.5	2.93
12	8	4.81	10	4.53	10.3	2.45
13	8	4.98	12.6	4.62	9.8	2.78
14	9	4.99	12.5	4.71	13.1	2.93
15	6	4.81	10	4.49	10	2.92
16	7	4.78	11.2	4.5	10.6	3.03
17	8	4.87	13	4.5	10.8	2.63
Number	Mn 13.6.86	pH 13.6.86	Mn 20.6.86	pH 20.6.86		
3	15	2.8	10.5	4.63		
4	14.5	2.98	12.9	5.78		
5a.	14	2.8	13	5.2		
6	14	2.51	8.6	4.96		
7	13	2.8	8.5	5.35		
8	15	2.74	9.8	5.45		
9	14.4	3.2	9	5.07		
10	18	2.91	10	5.53		
11	16.5	3.01	10	5.62		
12	15.5	2.51	10	5.43		
13	11.5	2.82	9	5.22		
14	13.8	2.89	11	5.31		
15	12.5	2.87	9.5	5.23		
16	12.5	2.97	8	5.1		
17	13.5	2.76	9	5.11		

C.R.L. No.	MnO2	Fe2O3	SiO2	Al2O3	P2O5	K2O	CaO	SrO	BaO	TiO2	Na2O	MgO	LOI	Anatase	Quartz
38476B	53.30	1.70	1.90	3.60	0.08	0.52	0.07	0.35	3.11	0.15	0.13	0.27	15.00	0.10	0.00
38477B	54.20	1.20	1.50	2.70	0.10	1.51	0.06	0.22	2.90	0.11	0.17	0.32	12.00	0.08	0.00
38484/85B	55.50	1.80	3.20	2.30	0.09	1.22	0.18	0.06	0.15	0.12	0.11	0.09	15.00	0.08	0.42
38486B	53.30	2.60	4.40	3.00	0.08	0.86	0.12	0.06	0.38	0.14	0.19	0.14	15.00	0.09	0.74
38488B	54.80	1.40	1.30	2.20	0.04	0.43	0.06	0.18	3.87	0.10	0.07	0.37	15.00	0.06	0.00
38490B	51.00	1.70	1.20	2.90	0.04	0.48	0.10	0.25	6.09	0.15	0.09	0.73	11.00	0.11	0.00
38561B	53.10	2.00	2.60	1.90	0.11	0.65	0.10	0.41	1.61	0.12	0.11	0.60	11.00	0.09	0.35
38563B	54.00	1.40	1.90	2.00	0.10	0.87	0.08	0.34	1.29	0.11	0.17	0.70	11.00	0.08	0.00
38566B	55.80	1.30	1.80	1.50	0.07	0.52	0.09	0.40	0.89	0.12	0.08	0.45	13.00	0.08	0.03
38574B	53.70	2.30	2.80	2.50	0.08	0.27	0.06	0.21	2.09	0.12	0.03	0.31	15.00	0.08	0.00
38575B	52.10	3.00	4.20	3.40	0.07	0.24	0.04	0.16	1.64	0.16	0.03	0.18	16.00	0.10	0.16
38579B	53.90	1.50	1.30	2.00	0.09	0.91	0.10	0.37	1.13	0.11	0.21	0.79	10.00	0.08	0.00
38579/80B	53.50	1.70	2.10	2.10	0.10	0.81	0.09	0.40	1.21	0.13	0.17	0.70	10.00	0.10	0.00
38581B	56.30	1.30	1.50	1.50	0.08	0.56	0.09	0.39	0.98	0.12	0.10	0.49	14.00	0.08	0.00
38584/85B	44.50	6.40	6.60	5.50	0.07	0.46	0.07	0.36	1.12	0.25	0.06	0.34	12.00	0.18	0.11
38588B	56.70	1.20	2.00	1.60	0.07	0.26	0.06	0.24	1.66	0.09	0.05	0.30	15.00	0.06	0.10
38591B	55.10	1.80	2.40	2.30	0.06	0.29	0.05	0.19	1.87	0.10	0.02	2.00	17.00	0.06	0.00
38633	51.60	4.20	4.70	2.60	0.06	0.79	0.06	0.08	1.36	0.16	0.04	0.10	15.00	0.10	1.40
38634	56.40	1.30	4.00	1.50	0.07	0.32	0.04	0.10	1.13	0.14	0.02	0.11	15.00	0.09	1.89
38635	47.50	2.50	6.50	6.10	0.03	2.68	0.09	0.06	0.33	0.20	0.19	0.09	8.00	0.16	0.00
38636	44.10	4.80	12.10	4.50	0.04	2.18	0.05	0.04	0.13	0.14	0.17	0.03	9.00	0.11	6.97
38601/11B	51.40	2.50	2.40	3.20	0.07	0.86	0.08	0.36	1.48	0.13	0.09	0.75	10.00	0.10	0.00

Table V.3: Battery activity tests (after Swinkels and Williams, 1982), chemical analyses, and mineral norms of Mn oxide ores from Groote Eylandt.

C.R.L. No.	Kaolinite	Gibbsite	Goethite	Hematite	Cryptomelane	Psilomelane	Todorokite	Pyrolusite	P2O5	Water	Sum
38476B	4.18	4.05	1.46	0.00	7.73	10.00	3.82	51.22	0.07	17.03	99.64
38477B	3.60	3.17	1.11	0.00	17.36	10.17	4.75	44.87	0.09	14.30	99.50
38484/85B	5.86	0.00	1.47	0.00	11.57	0.47	5.60	56.45	0.07	18.21	100.20
38486B	7.67	0.00	2.16	0.00	8.23	1.21	5.86	57.46	0.07	16.69	100.17
38488B	2.85	2.23	1.21	0.00	5.47	12.42	2.51	54.77	0.03	17.82	99.38
38490B	3.04	4.41	1.73	0.00	7.54	22.54	4.25	45.57	0.04	9.43	98.66
38561B	5.58	0.00	1.94	0.00	10.70	5.87	4.60	60.60	0.10	9.40	99.23
38563B	4.73	0.89	1.33	0.00	12.36	4.69	5.39	60.23	0.09	9.37	99.17
38566B	4.10	0.00	1.15	0.00	8.62	3.02	3.49	65.53	0.06	13.41	99.50
38574B	6.14	0.25	1.95	0.00	4.13	6.70	1.77	61.64	0.07	16.79	99.52
38575B	8.53	0.00	2.45	0.00	3.25	5.11	1.32	60.50	0.06	18.21	99.69
38579B	3.36	2.15	1.54	0.00	13.63	4.27	6.94	61.01	0.09	6.07	99.14
38579/80B	5.41	0.76	1.69	0.00	12.72	4.56	5.81	61.78	0.10	6.24	99.17
38581B	3.37	0.47	1.13	0.00	8.65	3.22	3.75	63.09	0.07	15.67	99.49
38584/85B	15.89	0.00	6.16	0.00	7.77	4.02	2.82	53.01	0.07	9.45	99.48
38588B	4.09	0.00	0.98	0.00	4.30	5.27	2.12	66.11	0.06	16.52	99.61
38591B	4.85	0.49	1.39	0.00	3.85	5.53	1.27	59.55	0.05	20.49	97.54
38633	6.70	0.00	3.68	0.00	7.84	4.35	1.95	55.51	0.05	18.22	99.81
38634	3.80	0.00	1.07	0.00	3.65	3.55	1.16	68.35	0.06	16.20	99.81
38635	17.88	1.49	2.38	0.00	31.53	1.33	6.67	33.11	0.03	5.33	99.91
38636	13.85	0.00	4.89	0.00	24.27	0.50	4.93	35.61	0.04	8.83	99.99
38601/11B	6.23	2.80	2.56	0.00	12.96	5.62	3.88	58.88	0.07	5.77	98.87

Table V.3: Battery activity tests (after Swinkels and Williams, 1982), chemical analyses, and mineral norms of Mn oxide ores from Groote Eylandt.

C.R.L. No.	charge capacity 1400 mV	measured drain time	initial OCV mV
38476B	1.50	94.00	1529.00
38477B	1.70	92.00	1528.00
38484/85B	0.80	86.00	1502.00
38486B	0.80	90.00	1543.00
38488B	2.70	93.00	1562.00
38490B	3.60	101.00	1576.00
38561B	3.20	110.00	1554.00
38563B	4.50	113.00	1583.00
38566B	1.80	98.00	1508.00
38574B	0.80	93.00	1511.00
38575B	0.40	80.00	1513.00
38579B	4.80	109.00	1579.00
38579/80B	4.30	106.00	1582.00
38581B	2.40	100.00	1550.00
38584/85B	0.40	86.00	1475.00
38588B	1.80	96.00	1488.00
38591B	0.60	77.00	1440.00
38633	0.10	78.00	1444.00
38634	0.40	84.00	1486.00
38635	1.20	92.00	1506.00
38636	0.50	78.00	1545.00
38601/11B	2.90	102.00	1531.00

Table V.3: Battery activity tests (after Swinkels and Williams, 1982), chemical analyses, and mineral norms of Mn oxide ores from Groote Eylandt.

Appendix VI.

Table VI.1: Sampling Locations.

Table VI.2: Field Test Data; [ppm], [°C], [l/min].

Table VI.3: Chemical Analyses of Water Samples; [ppm].

Table VI.4: Rainfall Data; [mm].

Table VI.5: Correlation Matrix for Water Analyses.

Table VI.1: Water sample locations.

No.	Date	Location (river: km)
W 1	14.5.85	F3-Quarry, ore
W 2	14.5.85	F3-Quarry, sump near ore
W 3	15.5.85	F3-Quarry, laterite
W 4	15.5.85	F3-Quarry, sump near laterite
W 5	15.5.85	Angurugu River, bridge near mission, 6.8
W 6	16.5.85	Angurugu River, top crossing, 9.25
W 7	17.5.85	Nashe's Gash
W 8	17.5.85	Tailings Dam
W 9	17.5.85	Angurugu River, big river bend, 2.55
W 10	18.5.85	D-Quarry, ore
W 11	18.5.85	D-Quarry, ore
W 12	19.5.85	D-Quarry, laterite
W 13	18.5.85	Boat ramp, Milner Bay
W 14	19.5.85	Emerald River, bridge
W 15	20.5.85	D-Quarry, ore
W 16	21.5.85	F3-Quarry, laterite
W 17	21.5.85	F3-Quarry, laterite
W 18	21.5.85	F3-Quarry, laterite
W 19	21.5.85	F3-Quarry, laterite
W 20	21.5.85	F3-Quarry, laterite
W 21	30.5.85	F3-Quarry, ore
W 22	30.5.85	G-South Quarry
W 23	30.5.85	G-South Quarry
W 24	3.6.85	D-Quarry
W 25	7.6.85	G-South Quarry
W 26	10.6.85	Angurugu River, near sea, 1.65
W 27	10.6.85	Angurugu River, Rowel Highway, 4.6
W 28	12.6.85	D-Quarry, sump
W 29	14.6.85	Sea, near mouth of Angurugu River, 0
W 30	21.5.86	F3-Quarry, Mn-laterite
W 31	21.5.86	F3-Quarry, ore
W 32	21.5.86	Angurugu River, top crossing
W 33	21.5.86	Angurugu River,pumping station
W 34	21.5.86	Angurugu River, bridge near mission
W 35	21.5.86	Angurugu River, Rowell Highway Bridge
W 36	21.5.86	Angurugu River, big river bend
W 37	21.5.86	Angurugu River, near sea
W 38	26.5.86	Creek, 0.4 km south of highway bend
W 39	26.5.86	Creek, 2.6 km south of highway bend
W 40	26.5.86	Emerald River, bridge
W 41	29.5.86	Angurugu River, big river bend
W 42	29.5.86	Angurugu River, big river bend
W 43	1.6.86	Umbakumba, jetty
W 44	1.6.86	Bartalumba Bay, jetty
W 45	9.6.86	F3-Quarry, Mn-laterite
W 46	9.6.86	F3-Quarry, Mn-laterite
W 47	9.6.86	F3-Quarry, Mn-laterite
W 48	9.6.86	F3-Quarry, Mn-laterite
W 49	9.6.86	F3-Quarry, Mn-laterite
W 50	10.6.86	Angurugu River, pumping station
W 51	10.6.86	Angurugu River, pumping station
W 52	10.6.86	Angurugu River, pumping station
W 53	10.6.86	Angurugu River, pumping station
W 54	10.6.86	Angurugu River, pumping station
W 55	11.6.86	Angurugu River, big river bend
W 56	11.6.86	Angurugu River, big river bend
W 57	11.6.86	Angurugu River, big river bend
W 58	11.6.86	Angurugu River, big river bend
W 59	11.6.86	Angurugu River, big river bend
W 60	11.6.86	Angurugu River, big river bend
W 61	11.6.86	Angurugu River, big river bend
W 62	11.6.86	Angurugu River, big river bend
W 63	11.6.86	Angurugu River, big river bend
W 64	11.6.86	Angurugu River, big river bend
W 65	11.6.86	Angurugu River, big river bend
W 66	15.6.86	Amagula Pools
W 67	15.6.86	Amagula River, downstream
W 68	15.6.86	Sea, 3 km west of mouth Amagula River
W 69	10.9.86	D-Quarry, borehole
W 70	10.9.86	D-Quarry, borehole
W 71	10.9.86	D-Quarry, borehole
W 72	10.9.86	D-Quarry, borehole
W 73	10.9.86	D-Quarry, borehole
W 74	10.9.86	D-Quarry, borehole
W 75	10.9.86	D-Quarry, borehole
W 76	10.9.86	D-Quarry, borehole
J 1	5.9.86	Emerald River, bridge
J 2	5.9.86	Angurugu River, top crossing, 9.25
J 3	5.9.86	Angurugu River, pumping station, 7.7
J 4	5.9.86	Angurugu River, bridge near mission, 6.8
J 5	5.9.86	Angurugu River, Rowel Highway, 4.6
J 6	5.9.86	Angurugu River, big river bend, 2.55
J 7	5.9.86	Angurugu River, near sea, 1.65
J 8	5.9.86	Sea, near mouth of Angurugu River, 0
J 9	5.9.86	Boat ramp, Milner Bay
J 10	5.9.86	F3- Quarry, laterite
J 11	5.9.86	F3- Quarry, ore
J 12	5.9.86	F3- Quarry, sump
J 13	5.9.86	G-South Quarry, sump
J 14	5.9.86	D-Quarry, sump
J 15	14.11.86	F3-Quarry, laterite
J 16	14.11.86	F3-Quarry, ore
J 17	24.1.86	Emerald River, bridge
J 18	24.1.86	Angurugu River, top crossing, 9.25
J 19	28.1.86	Angurugu River, pumping station, 7.7
J 20	28.1.86	Angurugu River, bridge near mission, 6.8
J 21	28.1.86	Angurugu River, Rowel Highway, 4.6
J 22	28.1.86	Sea, near mouth of Angurugu River, 0
J 23	28.1.86	Angurugu River, big bend, 2.55
J 24	29.1.86	Boat ramp, Milner Bay
J 25	29.1.86	F3-Quarry, sump
J 26	29.1.86	G-Quarry, sump
J 27	29.1.86	D-Quarry, sump
T.D.	28.1.86	Tailings Dam

Table VI.2: Field tests of water samples.

No.	Temperature [°C]	pH	Oxygen [ppm]	Fe [ppm]	Mn [ppm]	flux rate [l/min]
W 1	29.8	3.98	4.2	0.00	0.10	7-8
W 2	28.0	4.91	6.5	0.00	0.20	n.d.
W 3	30.9	4.60	5.1	0.04	0.00	9-9
W 4	32.0	4.93	6.9	0.01	0.15	n.d.
W 5	29.0	5.78	6.5	0.30	0.15	n.d.
W 6	27.0	5.14	6.3	0.30	0.06	n.d.
W 7	n.d.	n.d.	n.d.	n.d.	n.d.	n.d.
W 8	23.5	4.25	7.1	0.01	0.25	n.d.
W 9	27.0	6.50	7.5	0.30	0.30	n.d.
W 10	30.0	4.83	2.0	0.00	0.06	11.15
W 11	30.0	4.87	4.1	0.15	0.03	0.60
W 12	29.5	n.d.	4.2	0.01	n.d.	0.3-0.4
W 13	28.0	7.89	5.8	0.10	0.25	n.d.
W 14	26.5	5.52	4.8	0.30	0.10	n.d.
W 15	30.5	4.96	3.6	0.02	0.06	2.74
W 16	30.0	4.58	4.7	0.00	0.00	3.45
W 17	30.0	n.d.	5.0	0.00	0.00	0.50
W 18	30.0	4.51	5.2	0.00	0.00	0.82
W 19	30.0	4.83	4.5	0.00	0.00	0.60
W 20	29.8	4.46	5.0	0.00	0.00	0.31
W 21	29.5	n.d.	n.d.	n.d.	0.10	n.d.
W 22	29.5	n.d.	4.8	0.00	0.06	4.30
W 23	29.5	n.d.	4.8	0.00	0.06	0.63
W 24	28.0	3.91	5.6	0.00	0.00	7.00
W 25	26.0	5.37	7.0	0.01	0.20	n.d.
W 26	27.0	6.79	7.2	0.15	0.10	n.d.
W 27	27.0	5.88	7.1	0.30	0.25	n.d.
W 28	28.0	5.52	6.0	0.02	0.06	n.d.
W 29	26.0	7.86	6.4	0.10	0.03	n.d.
W 30	29.2	4.62	1.1	0.00	0.60	5.00
W 31	29.0	4.14	2.5	0.00	0.60	14.00
W 32	3.0	5.18	7.5	0.25	0.03	n.d.
W 33	27.0	6.80	0.1	0.10	n.d.	n.d.
W 34	28.2	5.65	7.6	0.40	0.1-0.15	n.d.
W 35	29.0	6.25	6.3	0.25	0.20	n.d.
W 36	32.2	7.78	6.4	0.30	0.25	n.d.
W 37	30.2	7.36	6.9	0.25	0.30	n.d.
W 38	23.4	5.41	7.3	0.04	0.03	n.d.
W 39	25.2	5.74	7.1	0.10	0.03	n.d.
W 40	25.5	5.15	4.8	0.08	0.06	n.d.
W 41	25.5	7.20	4.6	0.50	0.50	n.d.
W 42	25.5	7.25	4.3	0.50	0.40	n.d.
W 43	27.8	8.16	6.2	0.04	0.00	n.d.
W 44	26.8	7.19	6.7	0.09	0.00	n.d.
W 45	29.0	4.35	1.0	0.01	0.15	~2
W 46	29.0	4.38	0.9	0.01	0.15	~2
W 47	29.0	4.42	0.9	0.01	0.10	~2
W 48	29.0	4.44	0.8	0.01	0.13	~2
W 49	29.0	4.43	1.0	0.01	0.13	~2
W 50	27.0	5.03	6.1	0.80	0.15	n.d.
W 51	27.2	5.04	6.4	0.70	0.13	n.d.
W 52	27.2	5.12	6.1	0.60	0.10	n.d.
W 53	27.0	5.12	6.1	>0.8	0.08	n.d.
W 54	27.2	5.10	6.8	n.d.	n.d.	n.d.
W 55	26.8	7.04	5.1	~0.9	0.40	n.d.
W 56	22.5	7.38	5.5	0.45	0.30	n.d.
W 57	24.3	7.54	4.6	0.25	0.30	n.d.
W 58	25.8	7.63	4.8	0.25	0.20	n.d.
W 59	26.2	7.98	5.4	0.25	0.15	n.d.
W 60	26.8	7.91	4.7	0.12	0.20	n.d.
W 61	27.6	7.85	5.6	0.15	0.20	n.d.
W 62	27.7	7.97	5.3	0.25	0.20	n.d.
W 63	28.5	7.67	5.6	0.15	0.25	n.d.
W 64	27.2	7.41	5.9	0.18	0.30	n.d.
W 65	26.1	7.65	6.4	0.15	0.25	n.d.
W 66	25.8	5.21	6.2	0.20	0.06	n.d.
W 67	23.5	6.03	8.2	0.35	0.10	n.d.
W 68	26.1	8.20	n.d.	n.d.	n.d.	n.d.
W 69	29.0	4.60	5.2	0.08	0.70	n.d.

n.d. = not determined

Table VI.2: Field tests of water samples.

No.	Temperature [°C]	pH	Oxygen [ppm]	Fe [ppm]	Mn [ppm]	flux rate [l/min]
W 70	29.0	4.77	6.1	0.08	0.50	n.d.
W 71	30.0	4.48	5.2	0.08	0.25	n.d.
W 72	30.0	4.68	6.3	0.25	0.15	n.d.
W 73	29.0	4.75	5.9	0.15	~0.1	n.d.
W 74	29.7	4.70	5.2	0.04-6	0.4-0.5	n.d.
W 75	29.0	4.71	5.5	0.25	~0.8	n.d.
W 76	30.2	4.71	5.4	0.08	~0.8	n.d.
J 1	26.0	5.30	5.5	0.25	0.10	n.d.
J 2	26.0	5.20	5.5	0.30	0.03	n.d.
J 3	27.0	5.30	7.5	0.30	0.10	n.d.
J 4	27.0	5.70	7.5	0.30	0.15	n.d.
J 5	27.0	6.00	7.0	0.32	0.20	n.d.
J 6	27.0	7.20	6.3	0.15	0.15	n.d.
J 7	29.0	7.60	4.3	0.32	0.20	n.d.
J 8	29.0	8.10	5.3	0.06	0.00	n.d.
J 9	24.0	8.00	5.0	0.01	0.00	n.d.
J 10	31.0	4.60	3.6	0.00	0.03	2.00
J 11	29.0	3.90	5.3	0.03	0.25	0.50
J 12	27.0	4.70	6.8	0.01	0.10	n.d.
J 13	30.0	4.90	5.8	0.01	0.60	n.d.
J 14	28.0	5.00	7.5	0.00	0.15	n.d.
J 15	30.0	4.60	6.0	0.00	0.00	2.00
J 16	29.0	4.40	7.5	0.00	0.15	1.00
J 17	30.0	5.40	5.5	0.20	0.10	n.d.
J 18	31.0	5.60	6.7	0.60	0.06	n.d.
J 19	30.0	5.10	6.3	0.30	0.10	n.d.
J 20	31.0	5.90	7.0	0.40	0.00	n.d.
J 21	34.0	6.50	6.8	0.30	0.30	n.d.
J 22	33.0	7.80	3.5	0.00	0.00	n.d.
J 23	35.0	7.70	6.5	0.00	0.30	n.d.
J 24	31.0	8.20	5.5	0.00	0.00	n.d.
J 25	30.0	5.20	7.0	0.00	0.15	n.d.
J 26	31.0	5.10	6.8	0.03	1.20	n.d.
J 27	33.0	5.20	6.8	0.00	0.20	n.d.
T.D.	32.0	4.60	7.3	0.00	1.00	n.d.

n.d. = not determined

Table VI.3: Chemical analyses of water samples (ICP). A VI.3 - 1

No.	Ag	Al	B	Ba	Be	C*	Ca	Cd	Ce	Cl*
W 1	0.002	0.211	0.030	0.003	0.003	1.70	0.802	0.001	0.030	8
W 2	0.002	0.211	0.016	0.002	0.003	1.10	0.003	0.001	0.030	8
W 3	0.002	0.155	0.012	0.007	0.002	2.46	0.003	0.001	0.030	11
W 4	0.002	0.166	0.008	0.004	0.000	1.64	0.003	0.001	0.030	9
W 5	0.002	0.131	0.007	0.004	0.000	2.20	0.003	0.001	0.030	10
W 6	0.002	0.129	0.006	0.002	0.000	3.63	0.003	0.001	0.030	10
W 7	0.002	0.167	0.010	0.000	0.000	n.d.	0.003	0.001	0.030	n.d.
W 8	0.002	0.150	0.012	0.003	0.000	n.d.	0.232	0.001	0.030	82
W 9	0.002	0.103	0.090	0.008	0.000	1.98	7.270	0.001	0.030	3091
W 10	0.002	0.219	0.005	0.000	0.000	2.75	0.003	0.001	0.030	15
W 11	0.002	0.251	0.004	0.000	0.002	1.64	0.003	0.001	0.030	11
W 12	0.002	0.224	0.004	0.000	0.000	3.71	0.003	0.001	0.030	9
W 13	0.017	0.017	0.004	0.007	0.000	4.42	484.8	0.011	1.632	n.d.
W 14	0.002	0.152	0.019	0.005	0.002	2.68	0.003	0.001	0.030	11
W 15	0.002	0.087	0.015	0.009	0.000	0.89	0.003	0.001	0.030	8
W 22	0.002	0.098	0.009	0.007	0.000	1.09	0.003	0.001	0.030	9
W 23	0.002	0.149	0.014	0.005	0.000	0.99	0.003	0.004	0.030	9
W 24	0.002	0.145	0.008	0.002	0.002	1.26	0.003	0.001	0.030	9
W 25	0.002	0.141	0.010	0.000	0.000	1.01	0.003	0.001	0.030	11
W 26	0.028	0.017	0.004	0.012	0.000	3.44	484.5	0.008	1.575	5318
W 27	0.002	0.092	0.039	0.009	0.001	1.81	0.421	0.001	0.030	15
W 28	0.002	0.117	0.014	0.001	0.000	1.38	0.003	0.001	0.030	10
W 29	0.024	0.017	0.004	0.012	0.000	2.92	438.3	0.023	1.494	17700
W 30	0.002	0.044	0.067	0.019	0.000	0.70	0.04	0.001	0.040	n.d.
W 31	0.002	0.148	0.044	0.015	0.000	0.90	0.65	0.003	0.035	n.d.
W 32	0.002	0.099	0.031	0.014	0.000	2.60	0.02	0.004	0.030	30
W 33	0.002	0.041	0.058	0.021	0.000	0.60	0.05	0.001	0.069	40
W 34	0.003	0.030	0.041	0.029	0.000	1.70	0.03	0.002	0.050	25
W 35	0.002	0.023	0.034	0.030	0.000	0.90	7.51	0.004	0.148	1450
W 36	0.008	0.017	0.251	0.044	0.000	5.30	107.5	0.008	0.772	4890
W 37	0.008	0.017	0.249	0.042	0.000	2.80	103.4	0.004	0.755	10520
W 38	0.002	0.287	0.030	0.008	0.000	2.70	0.21	0.002	0.030	15
W 39	0.002	0.246	0.025	0.009	0.000	2.70	0.00	0.001	0.030	15
W 40	0.002	0.109	0.011	0.017	0.000	3.50	0.14	0.002	0.030	20
W 41	0.003	0.017	0.328	0.064	0.000	2.40	265.0	0.004	0.518	9860
W 42	0.011	0.017	0.331	0.060	0.000	3.10	311.7	0.009	0.597	10780
W 43	0.018	0.017	0.259	0.021	0.001	24.60	530.7	0.016	0.365	19360
W 44	0.021	0.017	0.154	0.024	0.001	28.70	542.9	0.017	0.379	20070
W 45	0.003	0.056	0.004	0.017	0.000	0.90	0.11	0.017	0.071	15
W 46	0.004	0.067	0.004	0.026	0.000	0.60	0.09	0.009	0.082	15
W 47	0.003	0.220	0.057	0.021	0.000	2.10	0.06	0.009	0.065	15
W 48	0.002	0.265	0.004	0.028	0.000	9.00	0.05	0.004	0.060	15
W 49	0.002	0.276	0.057	0.017	0.000	7.30	0.03	0.004	0.043	15
W 50	0.002	0.206	0.055	0.021	0.000	0.80	0.10	0.008	0.047	20
W 51	0.002	0.161	0.048	0.022	0.000	2.60	0.08	0.005	0.046	15
W 52	0.002	0.136	0.045	0.019	0.000	1.40	0.09	0.006	0.030	15
W 53	0.002	0.142	0.043	0.023	0.000	0.50	0.03	0.005	0.030	15
W 54	0.002	0.119	0.037	0.018	0.000	2.00	0.09	0.006	0.056	15
W 55	0.013	0.017	0.275	0.056	0.000	2.40	244.4	0.016	0.661	8720
W 56	0.014	0.017	0.282	0.053	0.000	2.10	259.1	0.011	0.678	9430
W 57	0.018	0.017	0.321	0.050	0.001	2.10	355.5	0.013	0.575	12130
W 58	0.020	0.017	0.298	0.038	0.001	2.60	456.4	0.018	0.470	16170
W 59	0.020	0.017	0.187	0.032	0.001	1.70	512.9	0.015	0.330	18080
W 60	0.015	0.017	0.339	0.036	0.001	1.90	434.4	0.012	0.395	16380
W 61	0.013	0.017	0.298	0.038	0.001	1.90	402.6	0.011	0.411	13970
W 62	0.014	0.017	0.279	0.041	0.001	2.30	392.6	0.013	0.424	14250
W 63	0.014	0.017	0.297	0.043	0.000	2.80	339.1	0.014	0.477	12340
W 64	0.012	0.017	0.264	0.047	0.000	2.00	252.0	0.010	0.588	9360
W 65	0.012	0.017	0.273	0.047	0.000	1.70	245.5	0.014	0.587	8790
W 66	0.002	0.104	0.031	0.014	0.000	1.70	0.25	0.014	0.057	15
W 67	0.002	0.237	0.029	0.013	0.000	1.80	0.19	0.010	0.030	15
W 68	0.020	0.017	0.219	0.025	0.001	27.40	543.7	0.014	0.221	20000
W 69	0.002	0.017	0.046	0.002	0.000	n.d.	1.25	0.001	0.030	30
W 70	0.002	0.017	0.031	0.004	0.000	n.d.	1.06	0.001	0.030	20
W 71	0.002	0.017	0.004	0.002	0.000	n.d.	0.16	0.001	0.030	15
W 72	0.002	0.017	0.004	0.001	0.000	n.d.	0.18	0.002	0.030	20
W 73	0.002	0.017	0.004	0.000	0.000	n.d.	0.12	0.001	0.030	20
W 74	0.002	0.017	0.008	0.002	0.000	n.d.	0.39	0.001	0.030	15
W 75	0.002	0.017	0.004	0.007	0.000	n.d.	0.33	0.001	0.030	15

* denotes method other than ICP; n.d. = not determined

Table VI.3: Chemical analyses of water samples (ICP).

No.	Ag	Al	B	Ba	Be	C*	Ca	Cd	Ce	Cl*
W 76	0.002	0.017	0.013	0.006	0.000	n.d.	1.17	0.001	0.030	15
J 1	0.002	0.017	0.004	0.005	0.000	1.79	0.288	0.001	0.030	14
J 2	0.002	0.017	0.004	0.004	0.000	2.87	0.371	0.001	0.030	10
J 3	0.002	0.017	0.004	0.008	0.000	1.50	0.317	0.001	0.030	10
J 4	0.002	0.017	0.004	0.010	0.000	1.00	0.386	0.001	0.030	14
J 5	0.002	0.017	0.004	0.010	0.000	1.66	2.800	0.001	0.030	138
J 6	0.002	0.017	0.051	0.020	0.000	3.36	121.8	0.001	0.030	5430
J 7	0.002	0.017	0.085	0.016	0.000	1.85	124.6	0.001	0.030	5860
J 8	0.002	0.017	0.122	0.017	0.000	n.d.	395.6	0.011	1.364	18750
J 9	0.004	0.034	0.784	0.018	0.000	7.15	1003	0.022	1.247	19800
J 10	0.002	0.017	0.004	0.011	0.000	1.24	0.254	0.003	0.050	14
J 11	0.002	0.017	0.004	0.018	0.000	2.81	0.229	0.001	0.047	10
J 12	0.002	0.017	0.004	0.011	0.000	0.66	0.121	0.001	0.036	14
J 13	0.002	0.017	0.004	0.023	0.000	2.89	0.337	0.001	0.039	21
J 14	0.002	0.017	0.004	0.004	0.000	1.59	0.650	0.001	0.034	14
J 15	0.002	0.032	0.033	0.008	0.000	n.d.	0.099	0.001	0.030	n.d.
J 16	0.002	0.042	0.006	0.008	0.000	n.d.	0.003	0.001	0.030	n.d.
J 17	0.002	0.039	0.004	0.012	0.000	n.d.	0.132	0.001	0.030	n.d.
J 18	0.002	0.043	0.004	0.011	0.000	n.d.	0.118	0.001	0.030	n.d.
J 19	0.002	0.044	0.004	0.016	0.000	n.d.	0.138	0.001	0.030	n.d.
J 20	0.002	0.041	0.004	0.018	0.000	n.d.	0.219	0.001	0.030	n.d.
J 21	0.002	0.017	0.079	0.048	0.000	n.d.	57.4	0.001	0.268	n.d.
J 22	0.013	0.017	0.363	0.089	0.000	n.d.	377.4	0.001	1.425	n.d.
J 23	0.012	0.017	n.d.	0.073	0.000	n.d.	176.2	0.001	1.128	n.d.
J 24	0.023	0.017	0.004	0.105	0.000	n.d.	412.7	0.001	1.612	n.d.
J 25	0.002	0.034	0.004	0.012	0.000	n.d.	0.132	0.001	0.030	n.d.
J 26	0.002	0.017	0.004	0.004	0.000	n.d.	0.081	0.001	0.030	n.d.
J 27	0.002	0.017	0.004	0.007	0.000	n.d.	0.299	0.001	0.030	n.d.
T.D.	0.002	0.054	0.004	0.000	0.000	n.d.	0.003	0.001	0.030	n.d.

* denotes method other than ICP; n.d. = not determined

No.	Co	Cr	Cu	Eu	Fe	Ga	Gd	K	La
W 1	0.003	0.017	0.002	0.001	0.001	0.060	0.010	0.170	0.003
W 2	0.003	0.002	0.002	0.001	0.001	0.060	0.010	0.109	0.003
W 3	0.003	0.002	0.002	0.001	0.001	0.060	0.010	0.080	0.003
W 4	0.003	0.002	0.002	0.001	0.001	0.060	0.010	0.080	0.003
W 5	0.003	0.002	0.002	0.001	0.001	0.060	0.010	0.080	0.003
W 6	0.003	0.002	0.002	0.001	0.001	0.060	0.010	0.080	0.003
W 7	0.003	0.002	0.002	0.001	0.001	0.060	0.010	0.833	0.003
W 8	0.003	0.002	0.002	0.001	0.001	0.060	0.010	1.536	0.003
W 9	0.003	0.002	0.002	0.001	0.001	0.060	0.010	10.932	0.003
W 10	0.003	0.002	0.002	0.001	0.001	0.060	0.010	0.080	0.003
W 11	0.003	0.002	0.002	0.001	0.001	0.060	0.010	0.080	0.003
W 12	0.003	0.002	0.002	0.001	0.001	0.060	0.010	0.080	0.003
W 13	0.003	0.046	0.003	0.033	0.001	0.060	0.036	461.7	0.115
W 14	0.007	0.009	0.002	0.001	0.001	0.060	0.010	0.080	0.003
W 15	0.003	0.009	0.002	0.001	0.001	0.060	0.010	0.080	0.003
W 22	0.003	0.002	0.002	0.001	0.001	0.060	0.010	0.080	0.003
W 23	0.003	0.001	0.002	0.001	0.001	0.060	0.010	0.080	0.003
W 24	0.003	0.005	0.002	0.001	0.001	0.060	0.010	0.080	0.003
W 25	0.003	0.006	0.002	0.001	0.001	0.060	0.010	0.080	0.003
W 26	0.003	0.070	0.002	0.034	0.001	0.146	0.078	411.3	0.127
W 27	0.003	0.006	0.002	0.001	0.001	0.060	0.010	2.471	0.003
W 28	0.003	0.002	0.002	0.001	0.001	0.060	0.010	0.080	0.003
W 29	0.003	0.060	0.002	0.031	0.001	0.117	0.069	368.2	0.114
W 30	0.003	0.002	0.002	0.001	0.001	0.060	0.012	0.080	0.004
W 31	0.003	0.002	0.002	0.001	0.001	0.060	0.010	0.482	0.003
W 32	0.003	0.002	0.002	0.001	0.001	0.060	0.010	0.105	0.003
W 33	0.003	0.002	0.002	0.001	0.001	0.060	0.017	0.169	0.007
W 34	0.011	0.008	0.002	0.002	0.001	0.104	0.035	0.179	0.010
W 35	0.003	0.002	0.002	0.002	0.001	0.073	0.028	12.2	0.011
W 36	0.008	0.011	0.002	0.011	0.001	0.079	0.062	100.9	0.049
W 37	0.005	0.012	0.003	0.011	0.001	0.069	0.064	98.1	0.049
W 38	0.003	0.002	0.002	0.001	0.001	0.060	0.010	0.093	0.003
W 39	0.003	0.002	0.002	0.001	0.001	0.060	0.010	0.080	0.003
W 40	0.003	0.002	0.002	0.001	0.001	0.060	0.010	0.129	0.003
W 41	0.006	0.013	0.002	0.019	0.001	0.060	0.029	216.4	0.067
W 42	0.006	0.020	0.005	0.024	0.001	0.129	0.079	246.3	0.090
W 43	0.019	0.029	0.009	0.041	0.001	0.060	0.109	475.7	0.145
W 44	0.025	0.046	0.009	0.043	0.001	0.060	0.123	479.1	0.151
W 45	0.003	0.002	0.002	0.002	0.001	0.114	0.056	0.183	0.013
W 46	0.003	0.007	0.002	0.003	0.001	0.122	0.060	0.129	0.013
W 47	0.003	0.006	0.002	0.002	0.001	0.104	0.056	0.165	0.011
W 48	0.003	0.002	0.002	0.001	0.001	0.060	0.020	0.083	0.006
W 49	0.007	0.002	0.002	0.001	0.078	0.060	0.016	0.080	0.004
W 50	0.005	0.002	0.002	0.001	0.001	0.060	0.017	0.227	0.004
W 51	0.003	0.002	0.002	0.001	0.001	0.060	0.014	0.115	0.004
W 52	0.003	0.002	0.002	0.002	0.001	0.071	0.025	0.208	0.007
W 53	0.006	0.002	0.002	0.001	0.001	0.068	0.028	0.155	0.006
W 54	0.006	0.002	0.002	0.002	0.001	0.093	0.036	0.190	0.010
W 55	0.012	0.030	0.006	0.021	0.001	0.060	0.090	190.4	0.080
W 56	0.012	0.023	0.007	0.022	0.001	0.060	0.112	198.0	0.086
W 57	0.012	0.030	0.008	0.029	0.001	0.060	0.128	269.8	0.109
W 58	0.026	0.034	0.010	0.036	0.001	0.060	0.135	364.2	0.131
W 59	0.021	0.037	0.011	0.040	0.001	0.060	0.138	419.0	0.143
W 60	0.016	0.029	0.007	0.033	0.001	0.060	0.097	347.9	0.116
W 61	0.010	0.022	0.006	0.030	0.001	0.060	0.090	316.2	0.108
W 62	0.016	0.027	0.008	0.030	0.001	0.060	0.100	307.7	0.108
W 63	0.010	0.020	0.006	0.026	0.001	0.060	0.094	251.6	0.096
W 64	0.016	0.020	0.005	0.021	0.001	0.060	0.086	191.4	0.078
W 65	0.014	0.020	0.005	0.020	0.001	0.060	0.086	185.2	0.076
W 66	0.008	0.003	0.002	0.002	0.001	0.101	0.034	0.397	0.009
W 67	0.003	0.002	0.002	0.001	0.001	0.065	0.020	0.288	0.007
W 68	0.016	0.028	0.011	0.042	0.001	0.060	0.143	455.7	0.147
W 69	0.003	0.002	0.002	0.001	0.001	0.060	0.010	1.390	0.003
W 70	0.003	0.002	0.002	0.001	0.001	0.060	0.010	1.231	0.003
W 71	0.003	0.002	0.002	0.001	0.001	0.060	0.010	0.358	0.003
W 72	0.003	0.002	0.002	0.001	0.001	0.060	0.010	0.981	0.003
W 73	0.003	0.002	0.002	0.001	0.001	0.060	0.010	0.430	0.003
W 74	0.003	0.002	0.002	0.001	0.001	0.060	0.010	0.459	0.003
W 75	0.003	0.002	0.002	0.001	0.001	0.060	0.010	0.356	0.003

* denotes method other than ICP; n.d. = not determined

No.	Co	Cr	Cu	Eu	Fe	Ga	Gd	K	La
W 76	0.003	0.002	0.002	0.001	0.001	0.060	0.010	0.561	0.003
J 1	0.003	0.002	0.002	0.001	0.001	0.060	0.010	0.080	0.003
J 2	0.003	0.002	0.002	0.001	0.043	0.060	0.010	0.080	0.003
J 3	0.003	0.002	0.091	0.001	0.022	0.060	0.010	0.080	0.003
J 4	0.003	0.002	0.020	0.001	0.060	0.060	0.010	0.080	0.003
J 5	0.003	0.012	0.040	0.001	0.035	0.060	0.010	2.561	0.003
J 6	0.018	0.019	0.006	0.006	0.001	0.060	0.010	119.6	0.018
J 7	0.012	0.032	0.006	0.005	0.001	0.060	0.010	122.3	0.015
J 8	0.012	0.042	0.004	0.017	0.001	0.060	0.025	545.3	0.220
J 9	0.125	0.218	0.125	0.019	0.002	0.120	0.042	539.2	0.184
J 10	0.012	0.028	0.002	0.001	0.026	0.060	0.023	0.473	0.006
J 11	0.003	0.019	0.002	0.001	0.009	0.060	0.022	0.353	0.007
J 12	0.013	0.031	0.002	0.001	0.046	0.060	0.014	0.344	0.004
J 13	0.008	0.024	0.002	0.001	0.083	0.060	0.015	0.367	0.005
J 14	0.005	0.030	0.002	0.001	0.035	0.060	0.010	0.175	0.004
J 15	0.004	0.002	0.002	0.001	0.003	0.060	0.010	0.080	0.003
J 16	0.003	0.002	0.002	0.001	0.007	0.060	0.010	0.080	0.003
J 17	0.003	0.002	0.002	0.001	0.007	0.060	0.010	0.080	0.003
J 18	0.004	0.002	0.002	0.001	0.003	0.060	0.010	0.080	0.003
J 19	0.005	0.002	0.002	0.001	0.010	0.060	0.010	0.080	0.003
J 20	0.003	0.002	0.002	0.001	0.010	0.060	0.010	0.661	0.003
J 21	0.005	0.004	0.002	0.003	0.001	0.060	0.010	67.7	0.019
J 22	0.042	0.036	0.142	0.026	0.001	0.338	0.078	351.8	0.110
J 23	0.047	0.035	0.143	0.016	0.001	0.379	0.082	193.2	0.089
J 24	0.052	0.051	0.239	0.032	0.001	0.514	0.148	378.8	0.135
J 25	0.004	0.002	0.002	0.001	0.001	0.060	0.010	0.080	0.003
J 26	0.003	0.002	0.002	0.001	0.008	0.060	0.010	0.080	0.003
J 27	0.003	0.002	0.002	0.001	0.013	0.060	0.010	0.201	0.003
T.D.	0.003	0.002	0.002	0.001	0.002	0.060	0.010	0.080	0.003

* denotes method other than ICP; n.d. = not determined

No.	Li	Mg	Mn	Mo	Na	Nb	Ni	O2-sat. [%]*	P
W 1	0.017	0.421	0.082	0.030	6.220	0.110	0.004	55.80	0.040
W 2	0.017	0.498	0.134	0.030	5.952	0.110	0.004	83.90	0.040
W 3	0.017	0.615	0.009	0.030	8.242	0.110	0.004	68.60	0.040
W 4	0.017	0.546	0.102	0.030	6.987	0.110	0.004	94.30	0.040
W 5	0.017	0.521	0.175	0.030	6.043	0.110	0.004	85.10	0.040
W 6	0.017	0.415	0.026	0.030	5.382	0.110	0.004	80.20	1.238
W 7	0.017	4.906	0.303	0.030	57.223	0.110	0.004	n.d.	0.040
W 8	0.017	8.490	0.334	0.030	92.842	0.110	0.004	85.30	0.040
W 9	0.017	31.251	0.243	0.030	302.4	0.110	0.004	100.00	0.040
W 10	0.017	0.816	0.053	0.030	8.166	0.110	0.004	26.60	0.040
W 11	0.017	0.754	0.024	0.030	8.067	0.110	0.004	54.40	0.040
W 12	0.017	0.671	0.007	0.030	7.516	0.110	0.004	55.40	0.040
W 13	0.262	1749.9	0.041	0.244	16208.5	0.110	0.086	74.80	0.040
W 14	0.017	0.607	0.058	0.030	6.079	0.110	0.004	60.60	0.040
W 15	0.017	0.495	0.148	0.030	6.548	0.110	0.004	48.20	0.040
W 22	0.017	0.420	0.212	0.030	5.749	0.110	0.004	63.30	0.040
W 23	0.017	0.439	0.182	0.030	5.948	0.110	0.004	63.30	0.040
W 24	0.017	0.549	0.133	0.030	7.089	0.110	0.004	72.30	0.040
W 25	0.017	0.506	0.091	0.030	5.966	0.110	0.004	87.60	0.040
W 26	0.229	1613.5	0.245	0.316	14127	0.110	0.082	91.60	0.040
W 27	0.017	6.932	0.244	0.030	62.16	0.110	0.004	90.30	0.040
W 28	0.017	0.662	0.032	0.030	8.052	0.110	0.004	77.40	0.040
W 29	0.206	1416.8	0.073	0.243	12515.2	0.322	0.087	80.10	0.040
W 30	0.017	0.413	0.052	0.040	7.261	0.193	0.012	14.45	0.040
W 31	0.017	1.936	0.524	0.030	12.150	0.520	0.032	32.72	0.040
W 32	0.017	0.368	0.021	0.040	6.239	0.514	0.020	94.81	0.040
W 33	0.017	0.383	0.045	0.067	6.059	0.617	0.017	86.51	0.040
W 34	0.017	0.417	0.089	0.108	6.318	0.797	0.029	98.45	0.040
W 35	0.017	24.04	0.269	0.092	340.6	0.765	0.028	82.46	0.040
W 36	0.017	290.7	0.241	0.240	3081	1.226	0.058	87.67	0.040
W 37	0.017	280.8	0.290	0.232	2979	1.210	0.052	91.88	0.051
W 38	0.017	0.548	0.013	0.030	8.182	0.302	0.008	87.64	0.040
W 39	0.017	0.51	0.033	0.030	8.538	0.167	0.009	87.76	0.040
W 40	0.017	0.429	0.057	0.030	6.966	0.270	0.008	59.63	0.040
W 41	0.017	693.6	0.540	0.243	6683	0.110	0.063	57.14	0.040
W 42	0.017	825.6	0.438	0.424	n.d.	0.505	0.075	53.42	0.040
W 43	0.048	1699	0.029	0.613	n.d.	0.110	0.093	79.79	0.040
W 44	0.121	1729	0.039	0.649	n.d.	0.110	0.105	84.92	0.040
W 45	0.017	0.506	0.089	0.207	8.828	0.777	0.025	13.09	0.040
W 46	0.017	0.478	0.061	0.227	8.164	0.874	0.031	11.78	0.040
W 47	0.017	0.453	0.063	0.211	7.990	0.643	0.033	11.78	0.040
W 48	0.017	0.434	0.058	0.071	7.763	0.514	0.018	10.47	0.130
W 49	0.017	0.435	0.056	0.070	7.691	0.482	0.019	13.09	0.040
W 50	0.017	0.415	0.060	0.073	6.696	0.482	0.032	77.61	0.040
W 51	0.017	0.392	0.049	0.062	6.529	0.450	0.027	81.63	0.040
W 52	0.017	0.404	0.051	0.084	6.539	0.514	0.033	77.81	0.040
W 53	0.017	0.395	0.045	0.084	6.427	0.681	0.034	77.61	0.040
W 54	0.017	0.418	0.049	0.106	6.548	0.784	0.029	86.73	0.592
W 55	0.017	614.4	0.385	0.406	5998	0.716	0.088	64.64	0.040
W 56	0.017	649.9	0.376	0.466	6246	0.886	0.083	65.01	0.040
W 57	0.022	940	0.308	0.556	n.d.	0.880	0.093	56.03	0.040
W 58	0.027	1313	0.147	0.631	n.d.	0.563	0.096	59.93	0.040
W 59	0.030	1538	0.080	0.648	n.d.	0.374	0.106	67.84	0.040
W 60	0.032	1226	0.163	0.516	n.d.	0.313	0.084	59.57	0.040
W 61	0.018	1100	0.189	0.504	n.d.	0.379	0.085	71.89	0.040
W 62	0.017	1058	0.205	0.499	n.d.	0.537	0.086	68.12	0.040
W 63	0.017	857.6	0.229	0.467	n.d.	0.540	0.082	72.82	0.040
W 64	0.017	613	0.273	0.404	6055	0.753	0.074	75.25	0.040
W 65	0.017	591.2	0.257	0.396	5869	0.745	0.075	80.30	0.040
W 66	0.017	0.663	0.028	0.109	10.110	0.771	0.031	65.04	0.040
W 67	0.017	0.561	0.065	0.070	9.160	0.675	0.026	98.56	0.040
W 68	0.021	1650	0.020	0.729	n.d.	0.324	0.105	n.d.	0.040
W 69	0.017	1.115	0.235	0.030	20.020	0.110	0.029	68.06	0.209
W 70	0.017	0.793	0.226	0.030	13.440	0.110	0.008	79.84	0.149
W 71	0.017	0.632	0.149	0.030	11.000	0.110	0.004	69.06	0.047
W 72	0.017	0.73	0.097	0.030	12.380	0.110	0.004	83.67	0.361
W 73	0.017	0.695	0.048	0.030	10.670	0.110	0.004	77.23	0.040
W 74	0.017	0.629	0.107	0.030	12.050	0.110	0.004	68.78	0.040
W 75	0.017	0.628	0.672	0.030	11.330	0.110	0.010	71.99	0.115

* denotes method other than ICP; n.d. = not determined

Table VI.3: Chemical analyses of water samples (ICP).

No.	Li	Mg	Mn	Mo	Na	Nb	Ni	O2-sat. [%]*	P
W 76	0.017	0.493	0.551	0.030	11.310	0.110	0.010	71.90	0.092
J 1	0.017	0.621	0.073	0.030	4.360	0.110	0.004	68.84	1.437
J 2	0.017	0.520	0.034	0.030	3.720	0.110	0.004	68.84	1.288
J 3	0.017	0.652	0.072	0.030	4.676	0.110	0.004	95.42	0.451
J 4	0.017	0.595	0.106	0.030	4.094	0.110	0.004	95.42	0.222
J 5	0.017	9.353	0.209	0.030	6.962	0.110	0.009	95.42	1.256
J 6	0.076	378.5	0.132	0.077	4042	0.365	0.028	80.15	0.743
J 7	0.080	390.7	0.211	0.074	4019	0.196	0.028	56.28	1.383
J 8	0.366	1650	0.045	0.212	1754	2.974	0.204	69.37	0.041
J 9	0.572	1703	0.099	0.976	16748	2.466	0.344	60.61	7.491
J 10	0.017	0.790	0.026	0.088	10.683	0.176	0.023	48.52	1.767
J 11	0.017	0.685	0.126	0.057	7.694	0.306	0.039	69.37	1.850
J 12	0.017	0.807	0.162	0.041	7.244	0.228	0.029	86.51	1.302
J 13	0.017	0.795	0.621	0.040	7.781	0.222	0.048	77.03	0.805
J 14	0.017	0.964	0.108	0.037	6.432	0.137	0.022	96.77	2.545
J 15	0.017	0.609	0.033	0.030	14.319	0.110	0.004	79.70	0.562
J 16	0.017	0.296	0.072	0.030	6.683	0.110	0.004	98.20	0.475
J 17	0.017	0.537	0.051	0.030	7.956	0.110	0.004	73.00	0.374
J 18	0.017	0.485	0.059	0.030	6.959	0.110	0.004	90.30	0.367
J 19	0.017	0.476	0.074	0.030	7.215	0.110	0.004	83.70	0.239
J 20	0.017	0.573	0.245	0.030	8.919	0.110	0.004	94.30	0.040
J 21	0.020	178	0.519	0.030	2061	0.228	0.004	95.40	0.092
J 22	0.020	970	0.092	0.398	10747	1.001	0.024	48.50	0.925
J 23	0.020	493	0.382	0.350	5855	1.035	0.020	92.30	3.699
J 24	0.020	1063	0.019	0.517	11490	2.817	0.059	74.10	1.885
J 25	0.017	0.438	0.208	0.030	7.790	0.110	0.004	92.90	0.171
J 26	0.000	0.187	0.584	0.030	1.844	0.110	0.004	91.60	0.658
J 27	0.000	0.516	0.197	0.030	4.999	0.110	0.004	94.20	0.359
T.D.	0.000	0.009	0.001	0.030	0.030	0.110	0.004	99.70	0.288

* denotes method other than ICP; n.d. = not determined

Table VI.3: Chemical analyses of water samples (ICP).

No.	Pb	Si	Sm	Sr	Ti	V	Yb	Zn	Zr
W 1	0.030	3.333	0.020	0.000	0.004	0.003	0.002	0.003	0.003
W 2	0.030	3.049	0.020	0.000	0.004	0.003	0.002	0.019	0.003
W 3	0.030	4.336	0.020	0.001	0.004	0.003	0.004	0.034	0.003
W 4	0.030	3.618	0.020	0.000	0.004	0.003	0.001	0.001	0.003
W 5	0.030	5.154	0.020	0.000	0.004	0.003	0.001	0.001	0.003
W 6	0.030	4.679	0.020	0.000	0.004	0.003	0.004	0.001	0.003
W 7	0.030	5.025	0.020	0.049	0.004	0.003	0.007	0.001	0.003
W 8	0.030	5.274	0.020	0.062	0.004	0.003	0.001	0.001	0.003
W 9	0.030	5.274	0.020	0.203	0.004	0.003	0.001	0.029	0.003
W 10	0.030	5.099	0.020	0.000	0.004	0.003	0.001	0.001	0.003
W 11	0.030	5.015	0.020	0.000	0.004	0.003	0.001	0.001	0.003
W 12	0.030	5.064	0.020	0.000	0.004	0.003	0.001	0.001	0.003
W 13	0.030	1.127	0.070	8.429	0.004	0.089	0.001	0.540	0.009
W 14	0.030	5.803	0.020	0.001	0.004	0.020	0.001	0.052	0.003
W 15	0.030	3.682	0.020	0.000	0.004	0.003	0.001	0.012	0.003
W 22	0.030	4.031	0.020	0.000	0.004	0.003	0.001	0.029	0.003
W 23	0.030	4.276	0.020	0.000	0.004	0.023	0.005	0.049	0.003
W 24	0.030	3.941	0.020	0.000	0.004	0.003	0.002	0.027	0.003
W 25	0.030	4.555	0.020	0.000	0.004	0.003	0.001	0.001	0.003
W 26	0.030	1.258	0.140	7.816	0.025	0.012	0.003	0.585	0.034
W 27	0.030	5.514	0.020	0.036	0.004	0.006	0.001	0.011	0.003
W 28	0.030	5.778	0.020	0.000	0.004	0.003	0.001	0.001	0.003
W 29	0.030	1.642	0.116	7.207	0.004	0.117	0.002	0.471	0.026
W 30	0.030	3.40	0.020	0.006	0.007	0.003	0.003	0.037	0.003
W 31	0.030	4.45	0.020	0.029	0.006	0.003	0.001	0.021	0.003
W 32	0.030	4.04	0.020	0.002	0.005	0.003	0.001	0.014	0.003
W 33	0.030	4.36	0.023	0.003	0.006	0.003	0.001	0.01	0.003
W 34	0.030	4.58	0.041	0.004	0.009	0.006	0.001	0.022	0.005
W 35	0.030	4.52	0.028	0.207	0.007	0.003	0.001	0.019	0.003
W 36	0.071	4.08	0.074	2.220	0.014	0.036	0.001	0.049	0.014
W 37	0.030	4.46	0.074	2.117	0.012	0.037	0.001	0.055	0.013
W 38	0.030	3.89	0.020	0.003	0.004	0.003	0.001	0.027	0.003
W 39	0.030	3.27	0.020	0.001	0.004	0.003	0.001	0.018	0.003
W 40	0.030	5.82	0.020	0.005	0.004	0.003	0.001	0.055	0.003
W 41	0.030	3.50	0.068	4.591	0.006	0.045	0.001	0.554	0.003
W 42	0.030	3.21	0.072	5.291	0.017	0.066	0.001	0.096	0.016
W 43	0.053	0.50	0.129	9.520	0.023	0.103	0.001	0.15	0.022
W 44	0.030	0.55	0.151	9.782	0.028	0.114	0.022	0.169	0.028
W 45	0.052	3.56	0.048	0.007	0.013	0.003	0.001	0.039	0.007
W 46	0.030	3.58	0.050	0.007	0.013	0.012	0.001	0.028	0.007
W 47	0.030	3.61	0.043	0.006	0.010	0.005	0.001	0.02	0.005
W 48	0.030	3.55	0.020	0.006	0.008	0.009	0.001	0.021	0.003
W 49	0.030	3.53	0.020	0.006	0.006	0.003	0.001	0.017	0.003
W 50	0.030	4.53	0.020	0.004	0.008	0.003	0.001	0.017	0.003
W 51	0.030	4.46	0.020	0.004	0.008	0.003	0.001	0.012	0.003
W 52	0.030	4.48	0.020	0.004	0.010	0.003	0.001	0.011	0.003
W 53	0.030	4.44	0.020	0.003	0.008	0.003	0.001	0.011	0.003
W 54	0.030	4.56	0.031	0.004	0.010	0.003	0.001	0.009	0.006
W 55	0.073	3.50	0.074	4.322	0.018	0.065	0.001	0.078	0.021
W 56	0.046	3.41	0.094	4.498	0.021	0.068	0.001	0.082	0.026
W 57	0.156	2.71	0.117	6.108	0.025	0.085	0.001	0.1	0.030
W 58	0.030	1.59	0.137	7.984	0.029	0.106	0.001	0.121	0.031
W 59	0.030	1.01	0.152	9.041	0.029	0.104	0.001	0.142	0.032
W 60	0.030	1.82	0.104	7.549	0.021	0.087	0.001	0.121	0.021
W 61	0.030	2.13	0.091	6.964	0.019	0.076	0.001	0.109	0.019
W 62	0.030	2.28	0.100	6.783	0.021	0.079	0.001	0.11	0.022
W 63	0.069	2.59	0.089	5.738	0.019	0.068	0.001	0.111	0.020
W 64	0.073	3.42	0.071	4.288	0.018	0.061	0.001	0.076	0.019
W 65	0.061	3.44	0.072	4.204	0.017	0.060	0.001	0.072	0.020
W 66	0.030	5.12	0.030	0.006	0.009	0.004	0.001	0.034	0.004
W 67	0.030	4.73	0.020	0.005	0.007	0.003	0.001	0.068	0.003
W 68	0.030	0.52	0.156	9.720	0.028	0.108	0.001	0.179	0.029
W 69	0.030	6.86	0.020	0.016	0.004	0.003	0.001	0.905	0.003
W 70	0.030	6.81	0.020	0.011	0.004	0.003	0.001	0.239	0.003
W 71	0.030	7.11	0.020	0.005	0.004	0.003	0.001	0.407	0.003
W 72	0.030	8.94	0.020	0.006	0.004	0.003	0.001	0.135	0.003
W 73	0.030	9.99	0.020	0.006	0.004	0.003	0.001	0.109	0.003
W 74	0.030	6.83	0.020	0.011	0.004	0.003	0.001	0.24	0.003
W 75	0.030	6.31	0.020	0.013	0.004	0.003	0.001	0.302	0.003

* denotes method other than ICP; n.d. = not determined

No.	Pb	Sl	Sm	Sr	Tl	V	Yb	Zn	Zr
W 76	0.030	5.85	0.020	0.011	0.004	0.003	0.001	0.129	0.003
J 1	0.030	5.504	0.020	0.000	0.004	0.003	0.001	0.013	0.003
J 2	0.002	4.624	0.020	0.000	0.004	0.003	0.001	0.026	0.003
J 3	0.030	4.478	0.020	0.000	0.004	0.003	0.001	0.049	0.003
J 4	0.030	4.973	0.020	0.000	0.004	0.003	0.001	0.033	0.003
J 5	0.121	4.732	0.020	0.009	0.004	0.003	0.001	0.053	0.003
J 6	0.172	3.149	0.020	0.324	0.004	0.036	0.001	0.094	0.003
J 7	0.221	3.358	0.020	0.323	0.004	0.033	0.001	0.108	0.003
J 8	0.682	0.840	0.216	10.570	0.007	0.206	0.001	0.209	0.009
J 9	1.692	1.463	0.282	10.688	0.105	0.312	0.001	0.575	0.127
J 10	0.250	4.474	0.021	0.001	0.004	0.027	0.001	0.056	0.009
J 11	0.195	3.335	0.023	0.000	0.004	0.019	0.001	0.057	0.008
J 12	0.325	3.075	0.020	0.000	0.004	0.019	0.001	0.055	0.007
J 13	0.320	5.913	0.020	0.001	0.004	0.024	0.001	0.036	0.007
J 14	0.305	3.447	0.020	0.001	0.004	0.017	0.001	0.048	0.005
J 15	0.030	3.847	0.020	0.008	0.004	0.003	0.001	0.011	0.003
J 16	0.030	2.409	0.020	0.002	0.004	0.003	0.001	0.003	0.003
J 17	0.030	6.373	0.020	0.004	0.004	0.003	0.001	0.038	0.003
J 18	0.030	4.223	0.020	0.004	0.004	0.003	0.001	0.045	0.003
J 19	0.030	4.410	0.020	0.004	0.004	0.003	0.001	0.062	0.003
J 20	0.030	4.495	0.020	0.007	0.004	0.003	0.001	0.074	0.003
J 21	0.030	3.932	0.020	1.270	0.004	0.017	0.001	0.154	0.003
J 22	0.374	2.281	0.168	7.236	0.029	0.144	0.006	0.385	0.035
J 23	0.458	2.887	0.165	3.603	0.030	0.106	0.001	0.295	0.040
J 24	0.483	1.247	0.248	7.565	0.047	0.184	0.008	0.303	0.060
J 25	0.030	2.724	0.020	0.006	0.004	0.003	0.001	0.086	0.060
J 26	0.030	0.893	0.020	0.007	0.004	0.003	0.001	0.092	0.060
J 27	0.030	1.752	0.020	0.006	0.004	0.003	0.001	0.101	0.060
T.D.	0.030	0.008	0.020	0.000	0.004	0.003	0.001	0.001	0.060

* denotes method other than ICP; n.d. = not determined

Table VI.4: Annual and mean rainfall data [mm] from Angurugu Mission at Groote Eylandt. A VI.4 - 1

	1980/81	1981/82	1982/83	1983/84	1984/85	1985/86	1986/87	1987/88	mean: 1921-85
JUN	6	9	0	1	3	0	11	24	15
JUL	2	1	0	3	3	14	8	2	2
AUG	1	10	9	13	18	0	0	0	2
SEP	0	17	22	4	13	0	17	0	4
OCT	63	91	2	8	6	11	173	0	30
NOC	56	86	85	87	8	112	27	20	90
DEC	184	103	151	173	47	51	70		159
JAN	310	199	98	220	288	246	355		241
FEB	171	188	182	424	247	15	540		248
MAR	197	298	199	412	362	217	73		322
APR	53	95	119	34	203	119	112		159
MAY	52	9	96	8	18	31	37		41

	Ag	Al	B	Ba	Be	C	Ca	Cd	Ce	Cl	Co	Cr	Cu	Eu	Fe	Ga	Gd	K	La	Li	Mg
Ag	1.00	-0.36	0.25	0.37	-0.14	0.12	0.60	0.58	0.88	0.64	0.05	0.35	-0.03	0.91	-0.16	0.52	0.77	0.74	0.76	0.36	0.79
Al		1.00	-0.29	-0.39	0.36	0.19	-0.36	-0.20	-0.40	-0.44	-0.20	-0.32	-0.23	-0.44	-0.17	-0.20	-0.39	-0.41	-0.41	-0.20	-0.40
B			1.00	0.59	-0.14	0.37	0.80	0.55	0.59	0.79	0.81	0.72	0.55	0.57	-0.17	0.18	0.51	0.72	0.78	0.63	0.65
Ba				1.00	-0.33	0.16	0.35	0.45	0.43	0.53	0.13	0.10	-0.03	0.57	-0.11	0.09	0.73	0.41	0.49	-0.02	0.36
Be					1.00	-0.13	-0.15	-0.25	-0.17	-0.18	-0.09	-0.10	-0.10	-0.18	-0.15	-0.17	-0.24	-0.17	-0.18	-0.09	-0.16
C						1.00	0.39	0.18	0.32	0.31	0.40	0.38	0.26	0.21	0.13	0.10	0.07	0.35	0.34	0.42	0.33
Ca							1.00	0.67	0.86	0.89	0.79	0.91	0.57	0.81	-0.16	0.51	0.53	0.97	0.96	0.90	0.95
Cd								1.00	0.68	0.68	0.46	0.54	0.27	0.66	-0.23	0.63	0.73	0.67	0.74	0.53	0.66
Ce									1.00	0.85	0.42	0.66	0.27	0.94	-0.18	0.58	0.72	0.92	0.94	0.67	0.94
Cl										1.00	0.61	0.71	0.39	0.85	-0.20	0.35	0.63	0.91	0.91	0.68	0.88
Co											1.00	0.91	0.75	0.31	-0.02	0.31	0.17	0.64	0.65	0.86	0.58
Cr												1.00	0.68	0.54	0.00	0.48	0.29	0.82	0.80	0.96	0.79
Cu													1.00	0.15	0.09	0.20	0.01	0.44	0.44	0.67	0.39
Eu														1.00	-0.20	0.46	0.80	0.91	0.92	0.51	0.92
Fe															1.00	-0.19	-0.22	-0.18	-0.19	-0.09	-0.18
Ga																1.00	0.49	0.52	0.54	0.57	0.56
Gd																	1.00	0.61	0.72	0.21	0.61
K																		1.00	0.98	0.81	0.99
La																			1.00	0.77	0.97
Li																				1.00	0.80
Mg																					1.00
Mn																					
Mo																					
Na																					
Nb																					
Ni																					
O-sat																					
P																					
Pb																					
Si																					
Sm																					
Sr																					
Ti																					
V																					
Yb																					
Zn																					
Zr																					
Rain																					
pH																					
Fe*																					
Mn*																					

Table VI.5: Correlation matrix for water analyses.

	Mn	Mo	Na	Nb	Ni	O-sat	P	Pb	Si	Sm	Sr	Ti	V	Yb	Zn	Zr	Rain	pH	Fe*	Mn*
Ag	0.31	0.52	0.77	0.18	0.39	0.11	-0.10	-0.03	-0.56	0.58	0.76	0.25	0.34	0.27	0.60	0.38	0.00	0.57	0.09	0.14
Al	-0.50	-0.35	-0.41	-0.19	-0.32	-0.27	-0.31	-0.24	0.14	-0.34	-0.39	-0.19	-0.33	0.09	-0.35	-0.27	0.06	-0.49	-0.13	-0.39
B	0.39	0.89	0.69	0.77	0.87	-0.01	0.55	0.69	-0.38	0.81	0.75	0.84	0.85	-0.15	0.53	0.81	-0.02	0.66	0.17	0.28
Ba	0.64	0.57	0.39	0.52	0.40	-0.10	-0.11	0.01	-0.23	0.36	0.45	0.24	0.30	-0.25	0.27	0.20	0.06	0.55	0.43	0.64
Be	-0.13	-0.20	-0.16	-0.26	-0.21	-0.04	-0.14	-0.10	0.03	-0.16	-0.16	-0.13	-0.13	0.40	-0.14	-0.12	0.00	-0.31	-0.20	-0.17
C	-0.01	0.32	0.34	0.36	0.40	-0.30	0.32	0.36	-0.26	0.39	0.34	0.41	0.40	0.07	0.30	0.41	0.01	0.18	-0.18	-0.03
Ca	0.28	0.90	0.96	0.60	0.93	0.02	0.59	0.71	-0.65	0.96	0.96	0.86	0.91	0.10	0.85	0.92	-0.09	0.68	0.01	0.06
Cd	0.09	0.77	0.66	0.69	0.70	-0.21	0.22	0.35	-0.50	0.72	0.71	0.60	0.65	-0.04	0.51	0.62	-0.03	0.46	0.15	0.03
Ce	0.35	0.76	0.93	0.48	0.71	0.10	0.24	0.34	-0.64	0.86	0.94	0.58	0.67	0.20	0.81	0.69	0.03	0.70	0.06	0.14
Cl	0.41	0.83	0.90	0.58	0.80	0.06	0.39	0.50	-0.58	0.84	0.90	0.64	0.85	0.01	0.73	0.74	0.02	0.82	0.10	0.24
Co	0.05	0.78	0.61	0.72	0.90	-0.05	0.85	0.95	-0.39	0.80	0.63	0.94	0.91	-0.09	0.50	0.93	-0.14	0.39	-0.08	-0.09
Cr	0.13	0.79	0.80	0.60	0.93	0.00	0.83	0.91	-0.59	0.89	0.79	0.90	0.92	0.05	0.73	0.96	-0.08	0.45	-0.14	-0.07
Cu	-0.03	0.52	0.41	0.46	0.63	0.08	0.70	0.73	-0.24	0.58	0.43	0.71	0.66	-0.09	0.38	0.70	-0.21	0.26	-0.03	-0.13
Eu	0.46	0.74	0.91	0.36	0.63	0.07	0.10	0.20	-0.63	0.76	0.92	0.46	0.59	0.17	0.77	0.57	0.00	0.74	0.15	0.27
Fe	0.20	-0.19	-0.18	-0.18	-0.08	-0.01	0.17	0.12	0.13	-0.17	-0.17	-0.13	-0.08	-0.14	-0.10	-0.08	-0.09	-0.22	-0.17	0.22
Ga	-0.07	0.50	0.54	0.47	0.48	-0.22	0.18	0.27	-0.49	0.63	0.51	0.48	0.36	0.16	0.56	0.49	-0.03	0.17	-0.14	-0.17
Gd	0.41	0.74	0.61	0.56	0.50	-0.14	-0.07	0.04	-0.46	0.60	0.67	0.39	0.41	-0.01	0.36	0.41	-0.01	0.54	0.19	0.33
K	0.35	0.85	1.00	0.51	0.84	0.05	0.44	0.55	-0.69	0.92	0.98	0.73	0.82	0.14	0.88	0.82	-0.07	0.74	0.05	0.13
La	0.37	0.91	0.97	0.61	0.88	0.02	0.42	0.55	-0.66	0.95	0.99	0.77	0.84	0.11	0.82	0.84	-0.04	0.73	0.07	0.16
Li	-0.01	0.72	0.81	0.56	0.87	0.00	0.75	0.83	-0.58	0.88	0.77	0.87	0.87	0.13	0.76	0.93	-0.13	0.44	-0.14	-0.21
Mg	0.33	0.80	1.00	0.45	0.80	0.06	0.39	0.50	-0.70	0.89	0.97	0.68	0.78	0.18	0.89	0.78	-0.06	0.72	0.04	0.10
Mn	1.00	0.31	0.34	0.09	0.25	0.15	-0.04	0.07	-0.06	0.24	0.37	0.09	0.19	-0.14	0.31	0.12	-0.03	0.48	0.20	0.90
Mo		1.00	0.83	0.81	0.93	-0.14	0.52	0.66	-0.57	0.93	0.88	0.89	0.87	-0.05	0.63	0.89	-0.08	0.62	0.08	0.17
Na			1.00	0.48	0.82	0.05	0.42	0.53	-0.70	0.91	0.98	0.70	0.80	0.16	0.89	0.80	-0.07	0.74	0.05	0.12
Nb				1.00	0.80	-0.14	0.46	0.61	-0.33	0.73	0.53	0.80	0.71	-0.23	0.29	0.73	0.01	0.43	0.12	0.06
Ni					1.00	-0.04	0.71	0.84	-0.56	0.94	0.85	0.95	0.95	-0.05	0.69	0.96	-0.08	0.56	0.05	0.10
O-sat						1.00	0.00	-0.03	0.12	-0.04	0.05	-0.09	-0.04	0.08	0.03	-0.03	0.16	0.35	0.29	0.11
P							1.00	0.93	-0.31	0.59	0.41	0.74	0.74	-0.04	0.41	0.76	-0.03	0.18	-0.19	-0.14
Pb								1.00	-0.37	0.71	0.53	0.86	0.85	-0.09	0.47	0.87	-0.08	0.27	-0.19	-0.06
Si									1.00	-0.62	-0.65	-0.47	-0.52	-0.21	-0.63	-0.54	-0.07	-0.31	0.19	0.09
Sm										1.00	0.93	0.90	0.90	0.08	0.79	0.95	-0.05	0.61	-0.02	0.04
Sr											1.00	0.74	0.82	0.14	0.86	0.83	-0.03	0.71	0.07	0.15
Ti												1.00	0.89	-0.03	0.57	0.97	-0.13	0.42	-0.02	-0.05
V													1.00	-0.05	0.66	0.94	-0.06	0.58	-0.04	0.04
Yb														1.00	0.19	0.03	0.00	-0.10	-0.14	-0.25
Zn															1.00	0.66	-0.01	0.55	0.00	0.09
Zr																1.00	-0.11	0.49	-0.08	-0.06
Rain																	1.00	0.04	-0.06	-0.01
pH																		1.00	0.30	0.35
Fe*																			1.00	0.26
Mn*																				1.00

Table VI.5: Correlation matrix for water analyses.

Appendix VII.

Table VII.1: pH and mV Data.

Table VII.2: Hydrochemical Analyses of Experiments; [ppm].

Table VII.3: Geochemical Analyses of Solids from Experiments; [ppm].

Table VII.1: pH and mV data of battery experiment (89 days). A VII.1 - 1

Time [days]	pH	mV	Time [days]	pH	mV	Time [days]	pH	mV
0.00	4.90	310	13.75	4.32	425	23.85	4.20	474
0.08	5.05	350	13.96	4.31	420	24.15	4.20	474
0.17	5.00	360	14.67	4.30	450	26.73	4.20	540
0.33	5.00	375	14.79	4.30	443	26.90	4.20	535
0.50	4.90	380	14.88	4.39	435	27.27	4.20	535
0.58	4.85	380	15.00	4.38	430	28.90	4.20	563
0.63	4.90	376	15.17	4.28	436	28.90	4.15	579
0.85	4.80	373	15.17	4.23	442	30.60	4.20	595
0.88	4.68	369	15.27	4.25	448	30.60	4.25	601
1.04	4.65	365	15.27	4.28	454	31.73	4.25	606
2.10	4.62	382	15.79	4.30	460	32.02	4.23	587
2.17	4.60	375	15.79	4.23	457	32.27	4.20	583
2.25	4.57	370	15.92	4.23	455	33.08	4.20	585
2.40	4.54	382	16.29	4.23	460	33.08	4.15	588
2.71	4.51	390	16.50	4.23	468	33.29	4.15	590
2.92	4.48	375	16.50	4.27	475	33.29	4.20	593
3.25	4.46	382	16.79	4.27	483	33.83	4.20	595
3.33	4.43	375	16.79	4.23	480	34.02	4.17	592
4.50	4.40	385	16.88	4.23	478	34.02	4.15	593
4.58	4.37	375	17.21	4.23	478	34.21	4.15	593
5.65	4.35	377	17.38	4.23	482	34.21	4.20	599
5.65	4.40	377	17.38	4.26	487	34.81	4.23	605
5.83	4.40	377	17.67	4.28	491	35.23	4.23	590
5.83	4.35	377	17.67	4.24	496	35.69	4.23	593
6.15	4.35	367	17.79	4.28	500	35.77	4.23	570
6.25	4.35	367	17.79	4.20	495	35.85	4.23	550
6.44	4.35	373	18.04	4.20	490	35.94	4.23	538
6.44	4.50	379	18.17	4.21	490	36.02	4.23	533
6.81	4.50	385	18.67	4.22	510	36.19	4.23	530
6.81	4.35	380	18.67	4.26	510	36.52	4.23	538
7.23	4.32	377	18.77	4.26	508	36.60	4.23	533
7.52	4.30	380	18.77	4.20	505	36.69	4.23	520
7.52	4.35	387	19.27	4.20	502	36.94	4.23	490
7.81	4.40	395	19.73	4.20	515	37.10	4.23	490
7.81	4.30	390	19.81	4.20	595	37.60	4.23	505
8.10	4.33	387	19.90	4.20	585	37.69	4.22	497
8.58	4.35	393	20.19	4.20	480	37.85	4.22	470
8.58	4.33	398	20.31	4.20	487	38.02	4.22	455
8.69	4.33	404	20.31	4.25	456	38.19	4.21	455
8.69	4.37	409	20.81	4.25	425	38.60	4.21	475
8.81	4.37	415	20.81	4.20	420	38.73	4.20	475
8.81	4.35	415	20.94	4.20	415	38.94	4.19	458
9.15	4.35	415	20.94	4.25	412	39.06	4.19	458
10.48	4.35	423	21.04	4.25	410	39.15	4.18	461
10.48	4.32	432	21.04	4.20	408	39.15	4.15	465
10.73	4.32	440	21.19	4.20	407	39.19	4.15	468
10.73	4.37	449	21.25	4.20	416	39.19	4.18	472
10.81	4.37	457	21.25	4.25	426	39.31	4.18	475
10.81	4.32	455	21.77	4.26	435	39.31	4.15	479
10.90	4.32	453	21.90	4.26	433	40.06	4.18	482
11.19	4.32	453	22.13	4.26	439	40.06	4.13	486
11.31	4.32	457	22.13	4.20	445	40.25	4.13	489
11.31	4.37	461	22.25	4.20	451	40.25	4.20	493
11.38	4.37	465	22.25	4.25	457	40.65	4.20	496
11.96	4.37	410	22.77	4.27	463	40.77	4.20	485
12.21	4.37	405	22.77	4.20	461	41.02	4.20	460
12.38	4.37	412	22.94	4.20	460	41.10	4.20	457
12.92	4.37	405	23.48	4.20	467	41.10	4.12	457
13.08	4.35	400	23.48	4.25	475	41.21	4.12	457
13.19	4.27	397	23.77	4.25	482	41.21	4.20	464
13.19	4.33	411	23.77	4.20	478	41.52	4.20	470
41.69	4.20	460	51.33	4.13	509	62.71	4.20	413
41.94	4.20	432	51.33	4.20	513	63.00	4.20	407
42.06	4.20	425	51.77	4.20	518	63.00	4.15	407
42.19	4.20	425	51.85	4.15	515	63.23	4.15	408
42.73	4.20	457	52.31	4.12	512	63.23	4.22	410
43.69	4.20	475	52.38	4.12	514	63.44	4.23	412
43.98	4.20	462	52.38	4.18	516	63.44	4.17	409
44.27	4.20	465	52.79	4.20	518	64.00	4.17	407

Table VII.1: pH and mV data of battery experiment (89 days).

Time [days]	pH	mV	Time [days]	pH	mV	Time [days]	pH	mV
45.69	4.20	490	52.79	4.13	517	64.00	4.14	404
45.85	4.20	477	53.10	4.13	515	64.31	4.14	401
46.02	4.20	420	54.85	4.13	540	64.31	4.20	398
46.27	4.20	420	55.23	4.13	465	64.73	4.20	396
46.38	4.20	441	55.42	4.15	453	64.73	4.15	393
46.38	4.15	461	55.42	4.20	441	65.71	4.16	390
46.60	4.18	482	55.81	4.20	429	66.71	4.18	400
46.69	4.18	477	55.81	4.12	417	66.71	4.15	403
46.77	4.18	465	56.40	4.13	405	67.79	4.20	405
47.02	4.18	430	56.44	4.15	405	67.79	4.15	406
47.02	4.15	427	56.44	4.20	406	68.85	4.20	408
47.15	4.15	425	56.77	4.20	407	68.85	4.15	409
47.19	4.10	425	59.29	4.20	393	69.33	4.18	411
47.31	4.15	430	59.29	4.15	395	69.33	4.12	412
47.77	4.18	460	59.52	4.18	397	69.54	4.17	414
48.19	4.10	478	59.77	4.20	400	69.79	4.20	415
49.73	4.10	495	61.00	4.15	400	70.13	4.13	400
49.73	4.15	496	61.00	4.10	400	70.58	4.16	390
49.79	4.15	497	61.67	4.10	400	70.58	4.12	387
49.79	4.10	501	61.67	4.15	400	71.88	4.17	385
50.38	4.10	505	61.77	4.15	400	71.88	4.15	383
50.38	4.10	508	61.77	4.10	400	72.21	4.15	382
50.77	4.20	512	61.98	4.10	400	72.73	4.20	390
50.83	4.17	509	62.19	4.14	400	73.21	4.15	385
50.83	4.12	507	62.29	4.14	405	88.96	4.13	394
51.19	4.13	505	62.29	4.20	409			

Sample	Ag [ppm]	Al [ppm]	B [ppm]	Ba [ppm]	Be [ppm]	Ca [ppm]	Cd [ppm]	Ce [ppm]
BW 1a	0.002	0.104	0.008	0.014	0.000	0.118	0.001	0.030
BW 1b	0.002	0.563	1.056	1.303	0.000	18.929	0.001	0.106
BW 2b†	0.010	0.315	0.217	0.185	0.002	11.23	0.002	0.030
BW 3a	0.002	0.017	0.004	0.004	0.000	0.00	0.001	0.030
BW 3b	0.002	0.017	0.004	0.003	0.000	0.00	0.003	0.030
BW 3c	0.002	0.017	0.016	0.007	0.000	0.00	0.001	0.030
BW 3d	0.002	0.017	0.008	0.006	0.000	0.00	0.003	0.030
BW 5a^	0.026	0.017	0.248	0.005	0.000	466.4	0.007	0.030

Sample	Cl [ppm]*	Co [ppm]	Cr [ppm]	Cu [ppm]	Eu [ppm]	Fe [ppm]	Ga [ppm]	Gd [ppm]
BW 1a	n.d.	0.003	0.002	0.002	0.001	0.001	0.060	0.010
BW 1b	n.d.	0.044	0.002	0.007	0.001	0.001	0.060	0.010
BW 2b†	n.d.	0.021	0.002	0.013	0.001	0.001	0.060	0.010
BW 3a	n.d.	0.003	0.002	0.002	0.001	0.001	0.060	0.010
BW 3b	n.d.	0.003	0.002	0.002	0.001	0.005	0.060	0.012
BW 3c	n.d.	0.003	0.002	0.002	0.001	0.001	0.060	0.010
BW 3d	n.d.	0.003	0.002	0.002	0.001	0.001	0.060	0.010
BW 5a^	16800	0.011	0.006	0.007	0.012	0.001	0.060	0.043

Sample	K [ppm]	La [ppm]	Li [ppm]	Mg [ppm]	Mn [ppm]	Mo [ppm]	Na [ppm]	Nb [ppm]
BW 1a	0.080	0.003	0.017	0.662	0.123	0.030	8.278	0.110
BW 1b	248.1	0.003	0.032	13.27	26.76	0.030	41.31	0.129
BW 2b†	97.54	0.008	0.017	9.256	5.681	0.030	35.61	0.662
BW 3a	0.122	0.003	0.017	0.188	0.129	0.030	1.215	0.110
BW 3b	0.203	0.003	0.017	0.173	0.128	0.030	1.321	0.118
BW 3c	0.137	0.003	0.017	0.126	0.114	0.030	1.740	0.110
BW 3d	0.084	0.003	0.017	0.124	0.189	0.030	1.610	0.110
BW 5a^	269.2	0.023	0.529	1502	0.001	0.209	6430	0.110

Sample	Ni [ppm]	O-sat.[%]*	P [ppm]	Pb [ppm]	Si [ppm]	Sm [ppm]	Sr [ppm]	Ti [ppm]
BW 1a	0.004	95.62	0.040	0.030	3.12	0.020	0.005	0.004
BW 1b	0.427	49.14	0.349	0.030	31.34	0.020	0.966	0.004
BW 2b†	0.179	25.23	0.040	0.030	25.64	0.020	0.860	0.004
BW 3a	0.004	98.17	0.040	0.030	5.08	0.020	0.005	0.004
BW 3b	0.008	95.57	0.097	0.030	6.26	0.020	0.005	0.004
BW 3c	0.004	94.26	0.040	0.030	7.49	0.020	0.004	0.004
BW 3d	0.009	88.71	0.040	0.030	7.34	0.020	0.004	0.004
BW 5a^	0.048	91.59	0.040	0.030	0.34	0.023	0.779	0.019

Sample	V [ppm]	Yb [ppm]	Zn [ppm]	Zr [ppm]
BW 1a	0.003	0.001	0.001	0.003
BW 1b	0.003	0.001	0.206	0.003
BW 2b†	0.004	0.001	0.260	0.003
BW 3a	0.003	0.001	0.009	0.003
BW 3b	0.004	0.001	0.012	0.003
BW 3c	0.003	0.001	0.025	0.003
BW 3d	0.003	0.001	0.118	0.003
BW 5a^	0.068	0.003	0.107	0.016

* analyses other than ICP
† BW 2a: distilled water; O-sat.=89.73 %
^ BW 5b: not analyzed

Table VII.3: Geochemical analyses of solids from experiments, [ppm].

No.	Al2O3	As	B	BaO	CaO	Ce	Co	Cr	Cu	Eu
B I.a	29.1	2	6.97	0.01	0.01	41.14	14.58	29.39	19.31	0.44
B I.c	28.6	n.d.	1.09	n.d.	n.d.	32.94	13.39	28.84	21.76	0.44
B I.d1	28.5	n.d.	1.62	n.d.	n.d.	39.35	14.03	29.40	21.67	0.48
B I.d2	28.5	n.d.	5.50	n.d.	n.d.	39.81	13.65	28.68	21.63	0.50
B I.d3	29.3	n.d.	109.59	n.d.	n.d.	41.31	13.81	43.25	22.44	0.53
B I.d4	29.0	n.d.	9.09	n.d.	n.d.	34.83	13.74	29.28	21.00	0.38
B I.e	27.9	n.d.	1.54	n.d.	0.01	35.77	12.59	28.66	22.19	0.39
B II.a	4.2	31	39.53	5.10	0.05	73.08	70.16	14.11	74.40	2.52
B II.c	4.0	n.d.	44.00	5.06	0.04	80.83	72.43	14.40	78.99	2.53
B II.d1	4.1	n.d.	48.79	5.08	0.03	84.86	71.85	13.40	78.32	2.48
B II.d2	4.2	n.d.	20.62	5.10	0.03	77.55	73.06	13.46	79.50	2.23
B II.d3	3.9	n.d.	21.91	5.11	0.03	83.66	73.39	14.49	79.30	2.51
B II.d4	4.0	n.d.	19.00	5.06	0.03	81.49	74.95	13.72	79.91	2.57
B II.e	3.9	n.d.	24.59	5.05	0.05	82.18	73.72	16.15	79.61	2.63

No.	Fe	Gd	K2O	La	LOI	MgO	Mn	Mo	Na2O	Nd
B I.a	1.0	0.00	0.12	12.98	11.0	0.01	0.1	4.1	0.01	9.88
B I.c	0.8	0.00	0.14	13.62	10.9	0.01	0.2	n.d.	0.01	10.85
B I.d1	0.8	0.00	0.12	14.15	10.3	0.01	0.2	n.d.	0.01	13.08
B I.d2	0.8	0.56	0.12	14.09	10.4	0.01	0.2	n.d.	0.01	13.64
B I.d3	0.8	0.52	0.12	14.75	10.8	0.01	0.1	n.d.	0.01	14.86
B I.d4	0.8	0.01	0.12	14.27	10.6	0.02	0.2	n.d.	0.01	12.42
B I.e	0.8	0.00	0.13	12.80	11.5	0.01	0.1	n.d.	0.03	11.29
B II.a	0.6	11.87	0.93	46.50	11.0	0.34	52.0	41.0	0.19	41.31
B II.c	0.6	12.82	0.94	48.19	10.7	0.33	52.4	n.d.	0.27	44.06
B II.d1	0.6	12.72	0.91	13.43	10.5	0.36	52.3	n.d.	0.20	46.76
B II.d2	0.6	11.72	0.92	46.74	10.5	0.36	52.5	n.d.	0.20	42.28
B II.d3	0.6	12.91	0.92	48.40	10.5	0.35	52.7	n.d.	0.20	43.42
B II.d4	0.6	13.05	0.92	48.52	10.4	0.35	52.4	n.d.	0.20	44.00
B II.e	0.6	13.15	0.94	48.02	10.9	0.33	52.9	n.d.	0.27	43.10

No.	Ni	P	Pb	Sc	SiO2	Sm	Sr	SrO	Th	TiO2
B I.a	0.00	30	12	14.2	56.1	0.00	0.00	0.01	15	1.52
B I.c	216.61	60	n.d.	n.d.	55.7	0.00	0.00	n.d.	n.d.	1.50
B I.d1	0.00	60	n.d.	n.d.	56.9	0.00	0.00	n.d.	n.d.	1.49
B I.d2	0.00	30	n.d.	n.d.	55.8	0.00	0.00	n.d.	n.d.	1.47
B I.d3	6.41	90	n.d.	n.d.	55.8	0.00	0.00	n.d.	n.d.	1.53
B I.d4	0.00	80	n.d.	n.d.	55.5	0.00	0.00	n.d.	n.d.	1.50
B I.e	0.16	60	n.d.	n.d.	57.1	0.00	0.00	0.01	n.d.	1.46
B II.a	62.60	360	25	7.4	2.3	10.41	2587.69	0.14	4	0.10
B II.c	74.65	390	n.d.	n.d.	2.2	11.10	2728.30	0.14	n.d.	0.10
B II.d1	69.90	390	n.d.	n.d.	2.2	11.08	2676.26	0.14	n.d.	0.10
B II.d2	71.42	370	n.d.	n.d.	2.2	9.91	2658.12	0.14	n.d.	0.10
B II.d3	68.85	400	n.d.	n.d.	2.2	11.17	2707.60	0.14	n.d.	0.10
B II.d4	73.03	320	n.d.	n.d.	2.1	11.18	2685.99	0.14	n.d.	0.10
B II.e	82.85	410	n.d.	n.d.	2.0	11.11	2680.86	0.13	n.d.	0.10

No.	U	V	W	Yb	Zn	Zr
B I.a	3	11.95	10	0.45	39.82	279.51
B I.c	n.d.	13.71	n.d.	0.44	39.07	276.86
B I.d1	n.d.	12.93	n.d.	0.64	39.53	279.23
B I.d2	n.d.	12.51	n.d.	0.63	39.46	280.02
B I.d3	n.d.	13.09	n.d.	0.71	40.38	280.00
B I.d4	n.d.	12.80	n.d.	0.80	38.99	274.36
B I.e	n.d.	11.64	n.d.	0.41	39.18	278.92
B II.a	11	170.95	75	3.10	74.55	18.17
B II.c	n.d.	183.76	n.d.	3.23	73.94	18.69
B II.d1	n.d.	181.46	n.d.	3.23	74.28	18.78
B II.d2	n.d.	182.72	n.d.	3.08	74.39	18.10
B II.d3	n.d.	184.74	n.d.	3.28	73.40	19.51
B II.d4	n.d.	184.99	n.d.	2.53	73.45	19.51
B II.e	n.d.	181.19	n.d.	3.23	74.23	18.48

n.d. = not determined